Kahle

Martinsried

6.MARTINSRIEDER ZYTOMETRIEKURS

GESELLSCHAFT FÜR ZYTOMETRIE

UND ESACP

1.-5.3.1993

ORGANISATION:

Prof.Dr.G.Valet, S.Klingel, T.Elsherif, G.Shankar, H.Kahle

Arbeitsgruppe Zellbiochemie

Max-Planck-Institut für Biochemie

8033 Martinsried

Für die finanzielle Unterstützung des Kurses durch folgende Firmen sei an dieser Stelle vielmals gedankt:

Becton Dickinson, Heidelberg
Boehringer, Mannheim
LAMBDA Fluor.Technologie, Graz
PARTEC, Münster
Photometrics, München
SERVA, Heidelberg

6.MARTINSRIEDER ZYTOMETRIEKURS

PROGRAMM

Sonntag, 28.2.:

12.00-19.00h	Registration im Kurssaal des Institutes

Montag, 1.3.: Instrumentation, Immunsystem

9.00- 9.45h	**V.Kachel:** Prinzipien durchflußzytometrischer Instrumentation
9.45-10.05h	**A.Raffael:** BD Zytometer und Zellsorter
10.05-10.25h	**R.Böngeler:** PARTEC Zytometer und Zellsorter
10.25-10.45h	Pause
10.45-11.05h	**W.Pfanhauser:** Photometrics Kamerasystem zur digitalen Fluoreszenzbildanalyse
11.05-11.50h	**A.Radbruch:** Immunsystem, Immunfluoreszenz und Zellsortierung
11.50-13.30h	Mittagessen
13.30-18.00h	Praktische Arbeit im Kurssaal

Dienstag, 2.3.: Immunsystem, DNA, Molekularbiologie

9.00- 9.45h	**A.Raffael:** Lymphozytenphänotypisierung, monoklonale AK und Datenverarbeitung
9.45-10.30h	**W.Göhde**: Hochauflösende Flowcytometrie und Sortierung menschlicher Tumorzellen
10.30-10.50h	Pause
10.50-11.35h	**F.Otto**: Methodik und Anwendung durchflußzytometrischer Chromosomenanalyse
11.35-12.10h	**Th.Cremer**: Fluoreszente in-situ Hybridisierung I
12.10-13.30h	Mittagessen
13.30-18.00h	Praktische Arbeit im Kurssaal

10.20-10.40h	Pause
10.40-11.25h	**M.Kubbies**: Zelluläre Wachstumsfaktoren
11.25-11.55h	**E.Koller**: Neue Fluoreszenzfarbstoffe und potentielle Anwendungsmöglichkeiten in der Zytometrie (LAMBDA/SERVA)
11.55-12.25h	**NN:** Reagenzien für die Zytometrie und in-situ Hybridisierung (Boehringer)
12.25-14.00h	Mittagspause
14.00-18.00h	Praktische Arbeit im Kurssaal

Donnerstag, 4.3.: Zellbiologie, Plankton, Zellfunktion

9.00- 9.45h	**M.Poot**: Zellproliferation
9.45-10.30h	**M.Nüsse:** Mikronukleibildung und Nachweis zellulärer Schädigung
10.30-10.50h	Pause
10.50-11.10h	**V.Kachel**: Planktonanalyse
11.10-11.55h	**G.Valet**: Zellfunktion, Klinische Diagnostik und Datenanalyse
11.55-13.30h	Mittagessen
13.30-18.00h	Praktische Arbeit im Kurssaal

Freitag, 5.3.:

9.00-12.00h	Praktische Arbeit im Kurssaal
12.00h	Mittagessen und Abfahrt

- **Frühstück**: 7-8.30h für Gästehausbewohner in der Cafeteria des Instituts bzw. im Hotel bei Hotelunterkunft
- **Mittagessen**: 11.30-13.30h für alle Teilnehmer, Referenten, Mitarbeiter und Firmenangehörige
- **Abendessen/Brotzeit**: 18h für alle Teilnehmer, Referenten, Mitarbeiter, und Firmenangehörige
- Die Mahlzeiten werden in der **Cafeteria** des Instituts eingenommen (bitte die ausgegebenen **Essensmarken** verwenden).

Kurseinteilung

Gruppe 1:
Bocker
Chaffard
Endl
Fiala

Gruppe 2:
Glantz
Habermehl
Härtel
Hauler

Gruppe 3:
Hexel
Irmer
Kayser
Kellner

Gruppe 4:
Koenigsmann
Krause
Molks
Müller

Gruppe 5:
Plath
Papadimitriou
Rhein
Russ

Gruppe 6:
Schenck
Schmitz
Seier
Spring
Steinbach

Gruppe 7:
Viergutz
Vogelsang
Wagner
Weigerstorfer

Einteilung für Montag, den 1.3.1993:

Referenten:	Gruppen:	Themen:
Beisker/Nüsse	1	Chromosomen,in-situ Hybridisierung in Bakterien Mikronuklei und zelluläre Toxizität
Göhde/Böngeler	2	hochauflösende DNS Zytometrie an Tumorzellen
Kachel	3	Instrumentation, Planktonanalyse
Otto	4	Chromosomenpräparation, h`ochaufl. DNS-Zytometrie
Radbruch/Mechtold	5	Immunzytometrie, Zellsortierung mit MACS und FACS
Raffael	6	Immunphänotypisierung, Datenverarbeitung
Valet/Kahle	7	Funktionszytometrie, Datenverarbeitung

Die Gruppeneinteilung gilt **nur** für Montag, danach bitte entsprechend dem eigenen Interesse auf die einzelnen Referenten verteilen. Vormerkblätter für die verschiedenen Kurstage liegen auf dem vorderen Labortisch beim Kurssaaleingang auf. Je Referent und Tag bitte **nicht mehr** als 6 Teilnehmer eintragen.

Nachstehende Themen werden nur an folgenden Tagen behandelt:

Referenten:	Themen:	Tage:
Cremer/Scherthan	in-situ Hybridisierung	Di,Mi
Kubbies	Wachstumsfaktoren	Mi
Poot	Zellproliferation	Di-Do

6.MARTINSRIEDER ZYTOMETRIEKURS

REFERENTEN:

1. **Beisker**, Dr.W.
   GSF-Inst.f.Biophysikalische
   Strahlenforschung
   Ingolstädter Landstr.1
   8042 Neuherberg
   Fax: 089/3187-2842
   Tel: 089/3187-3349

2. **Böngeler**, Dr.R.
   PARTEC GmbH
   Otto-Hahn-Str.32
   4400 Münster
   Fax: 02534/5270
   Tel: 02534/8588

3. **Cremer**, Prof.Dr.Th.
   Institut für Humangenetik
   der Universität
   Im Neuenheimer Feld 328
   6900 Heidelberg 1
   Fax: 06221/56-3834
   Tel: 06221/56-5332

4. **Göhde**, Prof.Dr.W.
   Klinik- u.Poliklinik für Strahlen-
   therapie der Universität
   Albert-Schweitzer-Str.33
   4400 Münster
   Fax: 0251/83-5310
   Tel: 0251/83-5281

5. **Kachel**, PD Dr.Ing.V.
   Arb.Gruppe Zellmeßtechnik
   Max-Planck-Inst.f.Biochemie
   Am Klopferspitz 18a
   8033 Martinsried
   Fax: 089/8578-2571
   Tel: 089/8578-3777

6. **Kubbies**, Dr.M.
   Boehringer Mannheim GmbH
   Forschungszentrum Penzberg
   Nonnenwald 2
   8122 Penzberg
   Fax: 08856/60-2786
   Tel: 08856/603068

7. **Nüsse**, Dr.M.
   GSF Inst.f.Biophysikalische
   Strahlenforschung
   Ingolstädter Landstr.1
   8042 Neuherberg
   Fax: 089/3187-2842
   Tel: 089/3187-3349

8. **Otto**, Dr.F.
   Fachklinik Hornheide
   Experimentelle Tumorforschung
   Dorbaumstr.300
   4400 Münster
   Fax: 0251/3287-651
   Tel: 0251/3287-299

9. **Poot**, Dr.M.
   Institut für Humangenetik
   der Universität
   Biocenter am Hubland
   8700 Würzburg
   Fax: 0931/888-4084
   Tel: 0931/888-4069

10. **Radbruch**, Prof.Dr.A.
    Institut für Genetik
    der Universität
    Weyertal 121
    5000 Köln 41
    Fax: 0221/470-3419
    Tel: 0221/470-5185

6.MARTINSRIEDER ZYTOMETRIEKURS

REFERENTEN:

11. **Raffael**, Dr.A.
    Becton Dickinson GmbH
    Immunzytometriesysteme
    Tullastr.8-12
    6900 Heidelberg
    Fax: 06221/305-201
    Tel: 06221/303-798

12. **Scherthan**, Dr.H.
    Institut für Humangenetik
    der Universität
    Im Neuenheimer Feld 328
    6900 Heidelberg 1
    Fax: 06221/56-3834
    Tel: 06221/56-5332

13. **Valet**, Prof.Dr.G.
    Arb.Gruppe Zellbiochemie
    Max-Planck-Institut für Biochemie
    Am Klopferspitz 18a
    8033 Martinsried
    Fax: 089/8578-2518
    Tel: 089/8578-2563

14. **Wallner**, Dr.G.
    GSF-Inst.f.Biophysikalische
    Strahlenforschung
    Ingolstädter Landstr.1
    8042 Neuherberg
    Fax: 089/3187-2842
    Tel: 089/3187-3349

6.MARTINSRIEDER ZYTOMETRIEKURS

FIRMEN:

1. **Becton Dickinson GmbH**
   Dr.A.Raffael
   Immunzytometriesysteme
   Tullastr.8-12
   6900 Heidelberg
   Fax: 06221/305-201
   Tel: 06221/303-798

2. **Boehringer Mannheim GmbH**
   Dr.Fiala
   Abt.GB-MSP1
   Postfach 310120
   6800 Mannheim 31
   Fax: 0621/759-8550
   Tel: 0621/759-8830

3. **LAMBDA**
   Fluoreszenztechnologie
   Dr.E.Koller
   Grottenhofstr.3
   A-8053 Graz
   Fax: 0043/316/295681252
   Tel: 0043/316/295769

4. **PARTEC GmbH**
   Dr.R.Böngeler
   Otto-Hahn-Str.32
   4400 Münster
   Fax: 02534/5270
   Tel: 02534/8588

5. **Photometrics GmbH**
   W.Pfanhauser
   Sollnerstr.61
   8000 München 71
   Fax: 089/799580
   Tel: 089/799715

6. **SERVA Feinbiochemica GmbH**
   Kayser
   Postfach 105260
   6900 Heidelberg 1
   Fax: 06221/502-0
   Tel: 06221/502143

6.MARTINSRIEDER ZYTOMETRIEKURS

TEILNEHMER:

1. **Bocker**, T.
   Institut für Pathologie
   der Universität
   Franz-Josef-Strauß-Allee 11
   8400 Regensburg
   Fax: 0941/944-6601
   Tel: 0941/944-6602

2. **Chaffard**, R.
   Institut für Pathologie
   der Universität
   Holbeinstr.40
   CH-4003 Basel
   Fax: 0041/61/2652525
   Tel: 0041/61/2653194

3. **Endl**, Dipl.Phys.E.
   Institut für Pathologie
   der Universität
   Franz-Josef-Strauß-Allee 11
   8400 Regensburg
   Fax: 0941/944-6601
   Tel: 0941/944-6602

4. **Fiala**, Dr.
   Boehringer Mannheim GmbH
   Abt.GB-MSP1
   Postfach 310120
   6800 Mannheim 31
   Fax: 0621/759-8550
   Tel: 0621/759-8830

5. **Glantz**, R.
   Inst.f.Biophysik u.Strahlenbiologie
   der Universität
   Martinistr.52
   2000 Hamburg 20
   Fax: 040/4717-2353
   Tel: 040/4717-5139

6. **Habermehl**, P.
   Kinderklinik u.Poliklinik
   der Universität
   Langenbeckstr.1
   6500 Mainz
   Fax: 06131/17-3327
   Tel: 06131/222332

7. **Härtel**, W.
   Hoechst AG
   GE-AI/H780
   Postfach 800320
   6230 Frankfurt/M 80
   Fax: 069/305-15122
   Tel: 069/305-16354

8. **Hauler**,
   Fa.Thomae Biotechn.Produktion
   Verfahrensentwicklung
   Postfach 1755
   7950 Biberach a.d.Riss 1
   Fax: 07351/54-4813
   Tel: 07351/54-5102

9. **Hexel**, K.
   Institut für Immunol.u.Genetik
   DKFZ
   Im Neuenheimer Feld 280
   6900 Heidelberg 1
   Fax: 06221/42-3740
   Tel: 06221/401629

10. **Irmer**, Dipl.Biol.U.
    Biologisches Institut
    der Universität
    Pfaffenwaldring 47
    7000 Stuttgart 80
    Fax: 0711/685-5022
    Tel: 0711/685-5096

6.MARTINSRIEDER ZYTOMETRIEKURS

TEILNEHMER:

11. **Kayser**,
Fa.SERVA GmbH
Postfach 105260
Carl-Benz-Str.7
6900 Heidelberg
Fax: 06221/502-0
Tel: 06221/502-143

12. **Kellner**, R.
Innere Klinik und Poliklinik
Universitätsklinikum
Hufelandstr.55
4300 Essen 1
Fax: 0201/723-2000
Tel: 0201/723-5924

13. **Koenigsmann**, Dr.M.
Klinikum Steglitz der FU
Abt.Innere Medizin
Hindenburgdamm 30
1000 Berlin 45
Fax: 030/798-3779
Tel: 030/8349894

14. **Krause**, J.
Robert-Bosch-Krankenhaus
Auerbachstr.110
7000 Stuttgart 50
Fax: 0711/810-1721
Tel: 0711/810-1790

15. **Molks**, M.
Klinikum Steglitz der FU
Abt.Innere Medizin
Hindenburgdamm 30
1000 Berlin 45
Fax: 030/798-3779
Tel: 030/8349894

16. **Müller**, Dr.S.
Inst.f.Experim.Immunologie
der Universität
Deutschhausstr.1
3550 Marburg
Fax: 06421/
Tel: 06421/286966

17. **Plath**, Th.
Deutsches Rheumaforschungs-
zentrum Berlin
Nordufer 20
1000 Berlin 20
Fax: 030/454-2060
Tel: 030/454-2090

18. **Papadimitriou**, Dr.Ch.
Klinikum Steglitz der FU
Abt.Innere Medizin
Hindenburgdamm 30
1000 Berlin 45
Fax: 030/798-3779
Tel: 030/8349894

19. **Rhein**, Dr.A.P.
Akademie des Sanitäts- und
Gesund-
heitswesens der Bundeswehr
Neuherbergstr.11
8000 München 45
Fax: 089/3168-3293
Tel: 089/3168-3395

20. **Russ**, S.
Dr.Karl Thomae GmbH
Biotechnische Produktion
Postfach 1755
7850 Biberach der Riss 1
Fax: 07351/54-4811
Tel: 07351/54-5102

6.MARTINSRIEDER ZYTOMETRIEKURS

TEILNEHMER:

21. **Schenck**, Dipl.Biol.C.
Urologische Klinik
Klinikum Großhadern
Marchioninistr.15
8000 München 70
Fax: 089/7095-3446
Tel: 089/7095-8890

22. **Schmitz**, Dr.J.
Bernhard Nocht Institut
für Tropenkrankheiten
Bernhard Nocht Str.74
2000 Hamburg 36
Fax: 040/3118-2455
Tel: 040/3118-2400

23. **Seier**, Dipl.Biol.M.
Labor Centrum Nordhorn
Postfach 2180
Jahnstr.7-9
4460 Nordhorn
Fax: 05921/789-0
Tel: 05921/789-44

24. **Spring**, K.
Fa.MERLIN
Ges.f.Mikrobiol.Diagnostik
5303 Bornheim 2
Fax: 02222/82055
Tel: 02222/82050

25. **Steinbach**, Dr.P.
Institut für Pathologie
der Universität
Franz-Josef-Strauß-Allee 11
8400 Regensburg
Fax: 0941/944-6601
Tel: 0941/944-6602

26. **Viergutz**, Dipl.Ing.T.
Forsch.Inst.Biologie
Landwirtsch.Nutztiere
Wilhelm-Stahl-Allee 2
O-2551 Dummerstorf
Fax: 038208/7487
Tel: 038208/7494

27. **Vogelsang**, Dr.H.
Chirurg.Klinik d.TU Station 1/12
Klinikum r.d.Isar
Ismaningerstr.22
8000 München 80
Fax: 089/4140-2161
Tel: 089/4180-5185

28. **Wagner**, Dr.B.
Abt.Klinische Hämostaseologie
der Universität
Univ.Kliniken i.Landeskrankenhaus
6650 Homburg/Saar
Fax: 06841/16-2530
Tel: 06841/16-2556

29. **Weigerstorfer**, Dr.O.
Inst.f.Histologie
u.Embryologie d.Universität
Müllerstr.59
A-6020 Innsbruck
Fax: 0043/512/507-2360
Tel: 0043/512/507-2543

DNA ANALYSE UND FLUORESZENTE IN-SITU HYBRIDISIERUNG BEI BAKTERIEN

Dr.W.Beisker, Dr.G.Wallner

GSF-Inst.f.Biophysikalische Strahlenforschung
8042 Neuherberg
Lehrstuhl für Mikrobiologie der TU München

FLOW CYTOMETRY OF MICROBIAL CELLS

W. Beisker[1] and G. Wallner[2]

(1) GSF - Inst. f. Biophysikalische Strahlenforschung
Ingolstädter Landstrasse 1, D-8042 Neuherberg, FRG
(2) Lehrstuhl für Mikrobiologie, Technische Universität München,
Arcisstrasse 21, D-8000 München 2, FRG

Experiment 1

Title: **In situ hybridization of microbial cells with rRNA-targeted fluorescent oligonucleotide probes.**

Literature: Wallner, G., R. Amann, and W. Beisker: Optimizing fluorescent in situ hybridization with rRNA-targeted oligonucleotide probes for flow cytometric identification of microorganisms. Cytometry 14: 136-143, 1993.

Amann, R. I., B. J. Binder, R. J. Olson, S. W. Chisholm, R. Devereux, and D. A. Stahl: Combination of 16S rRNA-targeted oligonucleotide probes with flow cytometry for analyzing mixed microbial populations. Appl. Environ. Microbiol. 56: 1919-1925, 1990.

DeLong, E. F., G. S. Wickham, N. R. Pace: Phylogenetic stains: ribosomal RNA-based probes for the identification of single cells. Science 243: 41-44, 1989.

Introduction: Fluorescent oligonucleotide probes complementary to short sequence elements within the naturally amplified 16S and 23S rRNA can identify microbial cells at different phylogenetic levels by in situ hybridization ("phylogenetic stain"). By targeting more conserved regions of the rRNA molecule larger groups of microorganisms can be stained. More variable regions are specific at genus or species level. The hybridized cells can be analysed by fluorescence microscopy or flow cytometry.

In this experiment we use probes complementary to highly conserved regions: "EUB" is specific for Bacteria and will stain E. coli, "EUK" is specific for Eucarya and will stain S. uvarum.

Cells: Escherichia coli and Saccharomyces uvarum cells were fixed in 4% paraformaldehyd, washed, and resuspended in 1 Vol. PBS (130 mM NaCl, 30 mM sodium phosphate buffer, pH 7.2) plus 1 Vol. of absolute ethanol. The final concentration is approximately 10^6 to 10^8 cells per ml.

Hybridization buffer:

0.9 M NaCl, 0.1 % SDS, 20 mM Tris/HCl, pH 7.2

Fluorescent oligonucleotide probes:

Oligodeoxynucleotides (length 15 to 25 nucleotides) were chemically synthesized. Via a 5' amino-linker the fluorescent dye 5(6)-Carboxyfluorescein-N-hydroxysuccinimidester (FLUOS, Boehringer Mannheim) was attached to the probe.

Hybridization: 5 µl of cells and 5 µl of oligonucleotide probe (10 ng/µl; final conc. 1 ng/µl) are added to 40 µl of hybridization buffer.

After two hours of incubation at 46°C the sample is diluted by 500 µl of ice-cold PBS and measured in a flow cytometer.

Flow cytometry:

Excitation: 488 nm, 500 mW (argon laser)

Emission: 530 nm band pass filter

Experiment 2

Title: **Determination of guanine-plus-cytosine content of bacteria.**

Literature: Van Dilla, M. A., R. G. Langlois, D. Pinkel, D. Yajko, and W. K. Hadley: Bacterial characterization by flow cytometry. Science 220: 620-622, 1983.

Sanders, C. A., D. M. Yajko, W. Hyun, R. G. Langlois, P. S. Nassos, M. J. Fulwyler, and W. K. Hadley. Determination of guanine-plus-cytosine content of bacterial DNA by dual-laser flow cytometry. J. Gen. Microbiol. 136: 359-365, 1990.

Introduction: Bacterial species vary widely in DNA base composition: %G+C values range between 25 and 70 percent of the total number of base pairs present in the DNA. Double fluorescent DNA staining of bacterial cells by Chromomycin A3, having guanine-cytosine (GC) binding preference, and Hoechst 33258, having adenine-thymine (AT) binding preference, provides information on the DNA base composition.

Cells: Cells of Escherichia coli, Staphylococcus aureus, and Micrococcus luteus were fixed in 70% ethanol at a concentration of 10^6 to 10^8 per ml.

Staining: 10 μl of Chromomycin A3 (CA3; 1 mM = 1.2 mg/ml) and 10 μl of Hoechst 33258 (HOE; 0.3 mM = 0.16 mg/ml) are added to 1 ml of TMS-buffer (150 mM NaCl, 1.5 mM $MgCl_2$, 10 mM TRIS/HCl, pH 7.2), containing 10 μl of cell suspension.

Flow Cytometry:

Excitation: 457 nm, 160 mW (argon laser; CA3), and
360 nm, 250mW (argon laser; HOE)

Emission: 424 nm band pass filter (CA3), and
500 nm long pass filter (HOE)

Experiment 3

Title: **Effect of chloramphenicol-treatment on the DNA content of E. coli cells.**

Literature: Steen, H. B., E. Boye, K. Skarstad, B. Bloom, T. Godal, and S. Mustafa: Applications of flow cytometry on bacteria: cell cycle kinetics, drug effects, and quantitation of antibody binding. Cytometry 2: 249-257, 1982.

Introduction: Chloramphenicol inhibits protein synthesis and - as de novo protein synthesis is required for it - initiation of chromosome replication and cell division.

In fast growing E. coli cells the cell division rate is faster than the chromosome replication rate. Therefore these cells initiate replication of a chromosome before the previous round of replication has been completed. Chloramphenicol blocks chromosome initiation and cell division, whereas DNA synthesis, that is replication of chromosomes which had already initiated when the antibiotic was given, continues. This results in cells containing DNA amounts equivalent to two or four complete chromosomes.

Cells: Escherichia coli cells were harvested at various times after chloramphenicol (100 μg/ml) had been added, and were fixed in 70% ethanol.

Staining: 25 μl of 4,6-Diamidino-2-phenylindole (DAPI; 0.2 mM = 0.075 mg/ml) are added to 1 ml of PBS (130 mM NaCl, 30 mM sodium phosphate buffer, pH 7.2), containing 10 μl of cell suspension.

Flow cytometry:

Excitation: 360 nm, 250 mW (argon laser)

Emission: 424 nm band pass filter

© 1993 Wiley-Liss, Inc.

Cytometry 14:136–143 (1993)

Optimizing Fluorescent In Situ Hybridization With rRNA-Targeted Oligonucleotide Probes for Flow Cytometric Identification of Microorganisms

Günter Wallner, Rudolf Amann, and Wolfgang Beisker
Lehrstuhl für Mikrobiologie, Technische Universität München, 8000 München 2 (G.W., R.A.) and GSF-Institut für Biophysikalische Strahlenforschung, Neuherberg, (W.B.), Germany

Received for publication April 7, 1992; accepted July 21, 1992

A combination of fluorescent rRNA-targeted oligonucleotide probes ("phylogenetic stains") and flow cytometry was used for a high resolution automated analysis of mixed microbial populations. Fixed cells of bacteria and yeasts were hybridized in suspension with fluorescein- or tetramethylrhodamine-labeled oligonucleotide probes complementary to group-specific regions of the 16S ribosomal RNA (rRNA) molecules. Quantifying probe-conferred cell fluorescence by flow cytometry, we could discriminate between target and nontarget cell populations. We critically examined changes of the hybridization conditions, kinetics of the hybridization, and posthybridization treatments. Intermediate probe concentrations, addition of detergent to the hybridization buffer, and a posthybridization washing step were found to increase the signal to noise ratio. We could demonstrate a linear correlation between growth rate and probe-conferred fluorescence of *Escherichia coli* and *Pseudomonas cepacia* cells. Oligonucleotides labeled with multiple fluorochromes showed elevated levels of nonspecific binding and therefore could not be used to lower the detection limits, which still restrict studies with fluorescing rRNA-targeted oligonucleotide probes to well-growing microbial cells. Two probes of different specificities—one labeled with fluorescein, the other with tetramethylrhodamine—could be applied simultaneously for dual color analysis. © 1993 Wiley-Liss, Inc.

Key terms: Identification, bacteria, flow cytometry, yeast, ribosomal RNA, oligonucleotide probes, in situ hybridization

Individual microbial cells often lack the morphological complexity needed to identify them as members of a defined genus or species. Whereas botanists and zoologists readily identified and enumerated their organisms of interest in situ, microbiologists had to use indirect approaches prone to obvious inaccuracies to analyze mixed microbial samples. Microorganisms had to be isolated in pure culture prior to an identification based on physiological characteristics. This is not only tedious and time-consuming, but also hardly results in the detection and identification of all microorganisms. In samples from many ecosystems, only a minor fraction of the viable cells grows to visible colonies on solid medium. Direct microscopy reveals cell counts that may exceed the numbers of colonies derived from plating by several orders of magnitude (12). Some of these "missing cells" might not be viable, but many microorganisms cannot be cultured on the standard media used to determine viable counts (7); others may in principle be culturable but occur in a physiological state in which the cells are viable but nonculturable (8).

In contrast to lack of morphological diversity, the molecular diversity of proteins and nucleic acids of microorganisms is very high. Therefore, a natural classification of microorganisms could be achieved through a comparative sequence analysis of informative macromolecules, most notably of the ribosomal RNA molecules (24). Today, two highly specific tools can be used to identify individual microbial cells by molecular

This study was presented in part at the XV Congress of the International Society for Analytical Cytology, Bergen, Norway.

Address reprint requests to Dr. Rudolf Amann, Lehrstuhl für Mikrobiologie, TU München, Arcisstr. 21, D-8000 München 2, Germany.

characteristics: (1) antibodies recognize and bind to specific (surface) epitopes and (2) single-strand nucleic acid probes hybridize specifically to complementary strands of target nucleic acid (either DNA or RNA).

Throughout this study, we have used rRNA-targeted, fluorescently labeled oligonucleotides. Probes of this type have only recently been applied to single cell identification (1,9). Compared to the immunofluorescence approach and to nucleic acid probes with other target molecules, these synthetic nucleic acid probes have several significant advantages: (1) Large rRNA sequence data bases are publicly available (14). Comparative sequence analyses allow identification of target regions on the rRNA molecules specific for certain phylogenetic groups ranging from subspecies (1) to kingdom level (11). (2) Specific target sequences for a nonculturable microorganism can be revealed by molecular techniques without prior cultivation (19). (3) The rRNA molecules are naturally amplified target molecules. A single *Escherichia coli* cell from an exponentially growing culture contains between 10^4 to 10^5 copies of 5S, 16S, and 23S rRNA, which allows detection of individual cells with oligonucleotide probes that direct only one fluorescent dye molecule to each target. (4) The cellular rRNA content is not constant for a certain species but directly correlated with the growth rate of the microbial cells (9). This could be exploited to gain insights into the physiological activity of individual cells, but in natural ecosystems it often means that cells have not enough rRNA to be detected at all. Methods to increase the sensitivity of rRNA-targeted oligonucleotides are therefore required and are under development (25).

After hybridization, fluorescence conferred by rRNA-targeted oligonucleotide probes can be analyzed by epifluorescence microscopy (1,9) or flow cytometry (2). For the analysis of suspended cells, the latter approach offers the advantages of easy quantification of the hybridization signal emitted from an individual cell and rapid, automated analysis of many cells. Here we used these characteristics of the flow cytometer to optimize systematically the in situ hybridization of fluorescent oligonucleotides to rRNA in fixed, suspended microbial cells. Similar combinations of flow cytometry and rRNA-detection by in situ hybridization have been reported for leukemia cells (4,15) and yeast cells (5). However, in those studies biotin-labeled polynucleotide transcripts were applied as probes and detected indirectly with FITC-labeled streptavidin. Compared to the directly end-labeled oligonucleotides, these longer probes have a higher sensitivity (directing more than one label to each target), but by binding to conserved as well as variable regions of the rRNA molecules, they would likely lack the specificity necessary for an analysis of mixed microbial samples.

Flow cytometric analyses employing DNA-dyes to determine the cellular DNA base composition (17,22) or mixed dyes to achieve "fingerprint" staining patterns (13,18) are applicable for the differentiation and identification of microorganisms only in selected cases. Immunofluorescent identification has been successfully combined with flow cytometry (10,16,21,23). However, antibody specificity is in general restricted to the species or subspecies level and their production requires previous cultivation of the target organism. Since a combination of fluorescent, rRNA-targeted oligonucleotide probes, and flow cytometric analysis promises to become a powerful tool for high resolution, rapid, automated identification of microorganisms, we tried to optimize this technique.

MATERIAL AND METHODS

Cell Growth and Fixation

The bacterial and yeast strains used were all grown aerobically in YT-broth (gl^{-1}: tryptone, 10; yeast extract, 5; glucose, 5; sodium chloride, 5; pH 7.2): *Escherichia coli* (DSM 30083 T; DSM = Deutsche Sammlung von Mikroorganismen und Zellkulturen GmbH, Braunschweig, FRG; T = type strain), *Pseudomonas cepacia* (DSM 50181) and *Saccharomyces carlsbergensis* (Institut für Brauereitechnologie und Mikrobiologie, Technical University Munich, strain 66) at 30°C. The cells were harvested during exponential growth and fixed with fresh, cold paraformaldehyde: three volumes of 4% paraformaldehyde in phosphate-buffered saline (PBS; 130 mM sodium chloride, 10 mM sodium phosphate buffer, pH 7.2) were mixed with one volume of cell suspension and incubated at 4°C for 16 h. The cells were pelleted by centrifugation in an Eppendorf microcentrifuge (8,000 g, 2 min), washed with PBS solution, and resuspended in one volume of PBS and one volume of absolute ethanol at a concentration of 10^8–10^9 cells per ml. The fixed cells could be stored at −20°C for several months without apparent change in light scatter or fluorescence intensity after hybridization.

Fluorescent Oligodeoxynucleotide Probes

The following probes were used in this study: EUB338, a probe complementary to a 16S rRNA region conserved for all bacteria (5′-GCTGCCTCCCGTAGGAGT-3′; ref. 1); NON338, an oligonucleotide complementary to the probe EUB338, serving as a negative control for nonspecific binding (5′-ACTCCTACGGGAGGCAGC-3′); and a probe specific for Eucarya, Euk516 (5′-ACCAGACTTGCCCTCC-3′; ref. 1). The oligodeoxynucleotides were synthesized with a primary amino group at the 5′-terminus [5′-Amino-Modifier C6: 6-(4-monomethoxytritylamino)hexyl-(2-cyanoethyl)-(N,N-diisopropyl)-phosphoramidite; Glen Research, Sterling, VA]. For internal or multiple labeling an "Amino-Modifier-dT" [5′-dimethoxytrityl-5-(N-(trifluoroacetylaminohexyl)-3-acrylamido)-2′-deoxyuridine, 3′((2-cyanoethyl)-(N,N-diisopropyl))-phosphoramidite;Glen Research] was used to create primary amine side chains at thymidine sites within the oligonucleotides. The fluorescent dyes TRITC [tetramethylrhodamine-5-(and-6-)-isothiocyanate; Molec-

ular Probes, Eugene, OR] or FLUOS [5(6)-carboxyfluorescein N-hydroxysuccinimide ester; Boehringer Mannheim, Germany) were coupled to these amino groups, and the dye-oligonucleotide conjugates were purified by exclusion chromatography, polyacrylamide gel electrophoresis, and reverse phase chromatography as described elsewhere (1). The probes were dissolved in double-distilled water and stored at −20°C.

Hybridization of Fixed Cells with Fluorescent Probes

Cells (10^5–10^6) were added to 50 μl of prewarmed hybridization solution containing 0.9 M sodium chloride, 20 mM Tris/HCl (pH 7.2), 0.1% sodium dodecyl sulfate (SDS), and usually 1 to 5 ng/μl probe in a 1.6 ml Eppendorf tube. The tube was transferred to a 46°C dry incubator. After 2 h, the hybridization was stopped by adding 500 μl of cold PBS solution (pH 8.4; 0°C). Samples could be stored on ice for several hours without significant loss of fluorescence intensity.

If a washing step followed the hybridization, the cells were pelleted by centrifugation (8,000 g, 2 min), washed in 100 μl of hybridization buffer (48°C, 20 min), and resuspended in 500 μl PBS solution (pH 8.4) for flow cytometric analysis.

Flow Cytometry and Data Analysis

A FACStar PLUS flow cytometer (Becton Dickinson (BD), Mountain View, CA), equipped with two argon-ion lasers (Innova; Coherent, Palo Alto, CA) was used to measure forward angle light scatter (FSC), right angle light scatter (SSC), and fluorescence of the microbial cells. These parameters were acquired as pulse height signals (four decades in logarithmic scale) in list mode for 5,000 or 10,000 events at a rate of ~ 200 cells per second. The samples were analyzed using the standard stream-in-air configuration, usually triggered on FSC as threshold parameter. The lasers were tuned to 488 nm and/or 514 nm at a power output of 500 mW each. TRITC and FLUOS were excited at 514 nm and 488 nm, emission was measured with a 575 nm band pass filter (BD 575 DF 26), and a 530 nm band pass filter (BD 530 DF 30; both Becton Dickinson), respectively.

During two-color measurements, the emission light, excited sequentially by the two lasers, was split by the standard half-mirror (BD) and fed to the respective photomultiplier tube. For further wavelength selection, a 530 nm long pass (OG 530; Schott, Mainz, Germany) and a 530 nm band pass filter (BD 530 DF 30) were combined for FLUOS detection in order to exclude scattered light of the 514 nm excitation line. A 570 nm long pass filter (OG 570; Schott) was used for TRITC detection.

The recorded list-mode data files were transfered by FASTFILE-software (BD) to an IBM-compatible PC-system. Data analysis and graphics were performed using the DAS-software package (DAS = Data Analysis Software (DAS V 4.03), designed by W. Beisker).

RESULTS AND DISCUSSION

Most of the results presented below were obtained by analyzing mixtures of fixed cells of rapidly growing *E. coli* and *S. carlsbergensis* after hybridization with probes specifically binding to Bacteria (EUB338 to *E. coli*) or Eucarya (EUK516 to *S. carlsbergensis*). This system has the advantage that fluorescence by both specific and nonspecific binding can clearly be quantified as the two cell types can easily be distinguished by another independent parameter (forward angle light scatter). However, various other probes and bacteria gave similar results (e.g., *Pseudomonas fluorescens, P. putida, P. cepacia, Comamonas testosteroni, Enterobacter cloacae*). Using fast-growing cells of these species, the mean fluorescence values of target cells (specifically stained) were about one order of magnitude higher than those of nontarget (nonspecifically stained) ones. That means that despite the broad variation of fluorescence intensities within populations of equally treated cells (CV = 30 − 40%; CV = coefficient of variation = standard deviation/mean) target and nontarget cells could readily be distinguished.

Problems occurred with very small cells (e.g., *Pseudomonas diminuta*) or *E. coli* cells harvested in late stationary phase due to their low ribosome content. Certain Gram-positive cells (e.g., *Bacillus subtilis, Lactococcus lactis*) showed limited probe accessibility, which could be improved by a lysozyme/EDTA treatment (25). In both cases target cells with a weak fluorescence signal resulting from low cellular ribosome contents or restricted cell permeability may be misinterpreted as nontarget cells.

Probe Concentration and Incubation Time

Subsamples taken at different times after starting the hybridization with various probe concentrations confirmed that high probe concentrations increase the velocity of hybridization, whereas the maximum specific signal is constant over a broad range of concentrations. Maximum fluorescence values were reached after ~ 1, 2, 3, 5 hours, 1, and 2 days for 20, 5, 1, 0.3, 0.1, and 0.01 ng/μl probe concentration, respectively. These maxima were practically the same for probe concentrations between 0.1 and 5 ng/μl as they are determined by the number of ribosomes per cell as long as probe is in excess (part of the underlying data sets are shown in Fig. 1).

At a probe concentration of 0.01 ng/μl, the number of probe molecules is not sufficient to bind to all available ribosomes and the mean fluorescence per cell decreases. In contrast, too high probe concentrations (like 20 ng/μl) increase nonspecific staining. That means that both target and nontarget cells show elevated fluorescence, but the crucial ratio of specific to nonspecific signal declines at too high probe concentrations. Therefore an optimal signal to noise ratio is obtained using intermediate probe concentrations (Fig. 2). As the specific signal also strongly depends on the incubation

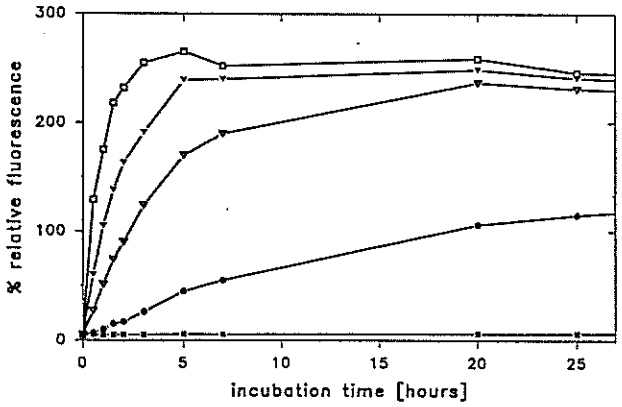

FIG. 1. Dependence of probe-conferred fluorescence on probe concentration and incubation time. Subsamples of *E. coli* cells hybridized with different probe concentrations were taken at certain times. After a washing step, the mean fluorescence values of the cells were determined relative to calibration beads (100% = mean fluorescence of doublets of 0.5 μm diameter "polychromatic" beads; Polysciences, Warrington, PA). 1 (hollow square), 0.3 (filled triangle), 0.1 (hollow triangle), and 0.01 ng/μl (filled circle) of the bacterial probe EUB338, 1 ng/μl of the eukaryotic probe EUK516 (filled square; negative control), all labeled with FLUOS.

time, especially at low probe concentrations, and the nonspecific signal on post-hybridization washing, these conditions also have to be considered for determining the optimal probe concentration. Accordingly, probe concentrations of about 1 ng/μl and incubation times of at least 2 h are recommended if a washing step follows the hybridization, lower concentrations, and longer incubation times if washing is omitted.

Nonspecific Staining

If no washing step is involved, part of the "nonspecific staining" corresponds to the increased fluorescence noise caused by dye-oligonucleotide conjugate freely dissolved in the sample suspension. The fluorescence values of the nonspecifically stained cell population lie within the elevated background noise. However, washed samples with background fluorescence close to the instrument noise level or relatively strong nonspecific staining of yeast or aggregates of many bacterial cells above the fluorescence noise level prove that probe is actually bound nonspecifically to all cells, especially at high probe concentrations.

There are several indications that this nonspecific staining is not caused by mispairing of the probe to nontarget sequences but is due to binding of the conjugated dye molecules to other cell components, possibly on the cell surface: (1) without permeabilizing the cells with detergent they show the same fluorescence level with positive and negative control probes (Fig. 3); (2) probes with different nucleotide sequences used as negative controls cause similar nonspecific staining; (3) attaching more than one dye molecule to each oligonucleotide increases nonspecific binding significantly (Table 1). A possible reason for irreversible nonspecific binding could be unreacted dye molecules not efficiently removed during the probe purification and covalently binding to proteins by their aminoreactive groups.

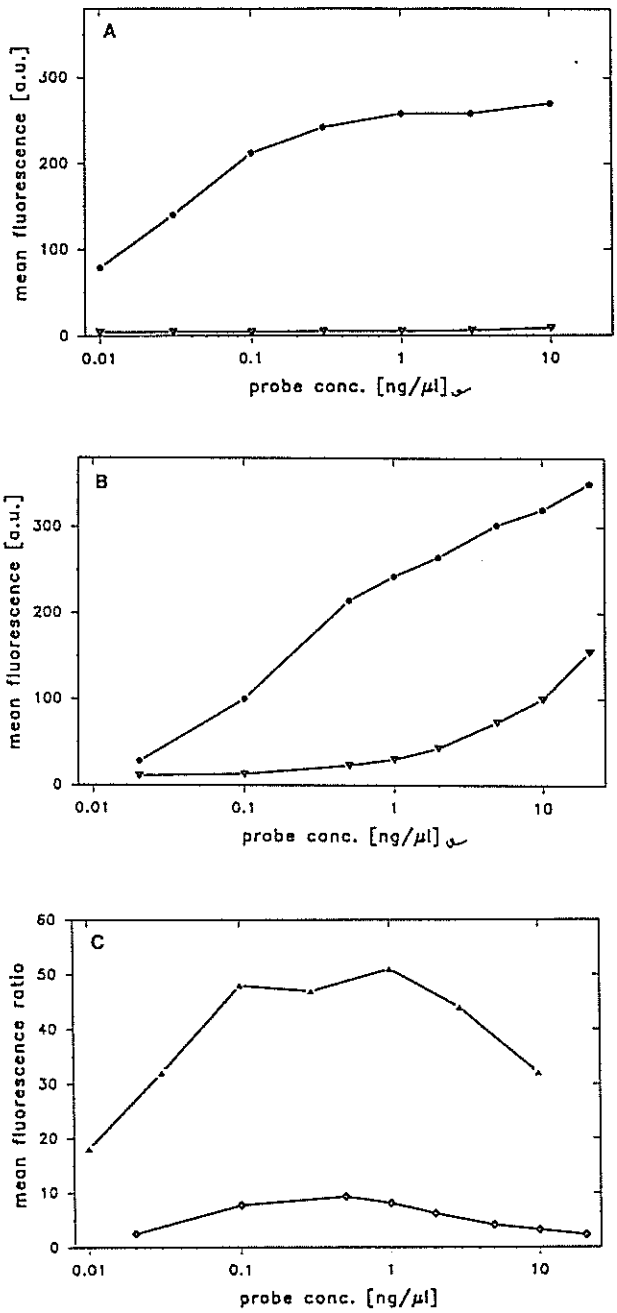

FIG. 2. Fluorescence per cell (arbitrary units) as a function of probe concentration. Mean fluorescence of *E. coli* cells after hybridization with different concentrations of the FLUOS-labeled bacterial (filled circles; EUB338) and eukaryotic (hollow triangle; EUK516) probes. A. 16 h incubation time, posthybridization washing. B. 2 h incubation time, no washing step. C. The ratios of specific (EUB338) to nonspecific (EUK516) signal were calculated from the data shown in A (filled triangle) and B (hollow diamond). The maximum ratio is much higher if a washing step is employed, but in both cases it is highest at intermediate probe concentrations.

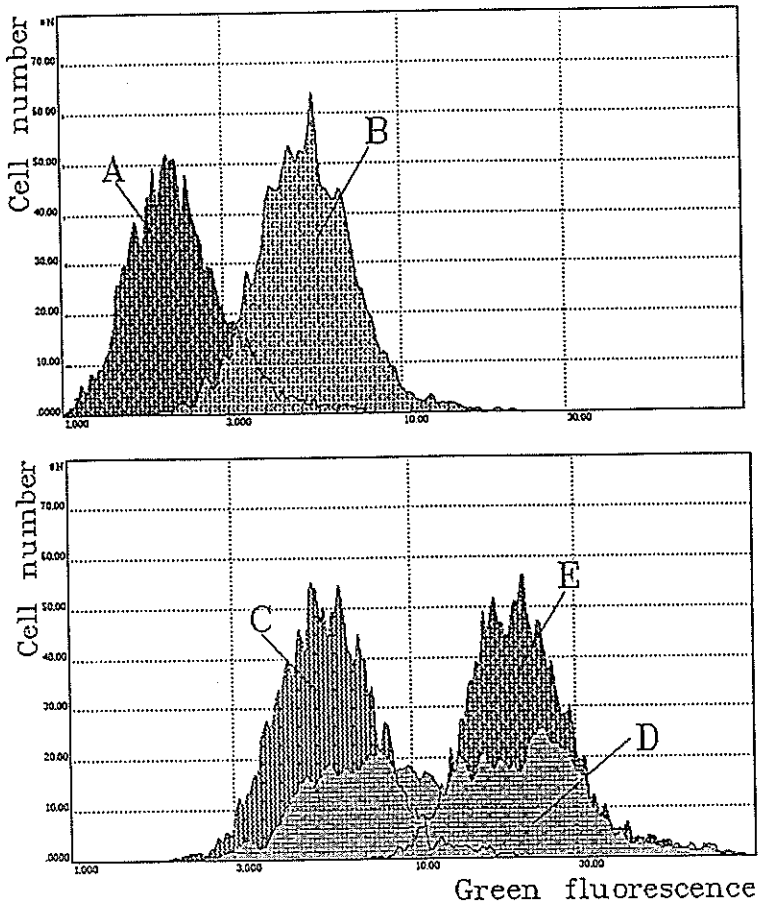

FIG. 3. Addition of detergent to the hybridization buffer. Histograms showing the distribution of green fluorescence (a. u.) of *E. coli* cells after hybridization with FLUOS-labeled probes (5 ng/μl probe concentration, 2 h incubation time, no posthybridization washing). A. No probe, 0.1% SDS. B. NON338 (control for nonspecific staining), 0.1% SDS. C. EUB338, no SDS. D. EUB338, 0.01% SDS. E. EUB338, 0.1% SDS. Detergent is essential for maximum specific staining of all cells.

Blocking reagents added to the hybridization buffer could not reduce nonspecific staining. Standard blocking reagents tested were (final concentrations): 10x Denhardt Solution (0.2% bovine serum albumine, 0.2% ficoll, 0.2% polyvinylpyrrolidon), 0.005% and 0.05% heparin, 0.2% bovine serum albumine, and 0.1% polyadenylic acid.

As shown above, nonspecific staining is strongly dependent on probe concentration. A washing step as described in Materials and Methods can reduce the fluorescence of nontarget cells to instrument noise level if the probe concentration is not higher than about 5 ng/μl. At higher concentrations, nonspecifically bound probe is not sufficiently removed by this washing procedure. A washing treatment can improve the maximum ratio of specific to nonspecific signal by up to one order of magnitude. However, cells may be lost during the washing procedure. If absolute or relative numbers of certain microorganisms are to be assessed, it seems more appropriate to omit any step employing centrifugation.

Hybridization Buffer

The standard hybridization solution contained 0.9 M sodium chloride, 0.1% sodium dodecyl sulfate (SDS), and 20 mM Tris/HCl (pH 7.2; final concentrations). The addition of detergent is essential for access of probe molecules to their intracellular targets. If hybridizations with specific probes were carried out without any detergent, cell fluorescence was as low as with negative control probes (only nonspecific staining). At higher SDS-concentrations all cells were specifically stained (same fluorescence level at different SDS-concentrations above about 0.05%), whereas at low concentrations of SDS cells showed a broad range of fluorescence intensities with two main populations, one representing maximally specifically, the other only nonspecifically stained cells (Fig. 3). Triton X-100 or Tween 20 gave similar results.

The stringency of hybridization is strongly influenced by the incubation temperature (hybridization and washing) and the concentration of monovalent cat-

Table 1.
Multiple Labeling of Probe EUB338

(a) Probe sequences and positions of labels

Names	Sequence (5'-3')[a,b]
X(1t)	XGCTGCCTCCCGTAGGAGT
Z(2i)	GCTGCCTCCCGTAGGAGT
Z(2e)	TAAATGCTGCCTCCCGTAGGAGT
Z(3i)	GCTGCCTCCCGTAGGAGT
Z(3e)	TATATATATATATATAGCTGCCTCCCGTAGGAGT

(b) Hybridization results with multiply labeled probes[c]

Probe	Number of Labels	*E. coli* (specific)	*S. carlsbergensis* (nonspecific)
X(1t)	1	22	22
Z(2i)	2	22	67
Z(2e)	2	4	36
Z(3i)	3	9	88
Z(3e)	3	31	190
NON338	1	2	10
no probe	0	2	10

[a]X = 5'-Aminomodifier (standard labeling).
[b]T = Aminomodifier-dT.
[c]Mean fluorescence intensities (relative values) after hybridization with 1 pmol/µl of TRITC-labeled probe and a subsequent washing step.

ions in the buffer (e.g., 20). For the probes tested in this study, the buffer composition and temperatures as described above were sufficiently stringent to rule out mispairing as a source of nonspecific binding. However, since the dissociation temperature of an oligonucleotide probe is also dependent on its length and base composition, hybridization conditions have to be optimized for each individual probe.

Signal Amplification

Multiple labeling of each probe molecule with several dye molecules via aminolinkers within the hybridizing sequence or within an added oligo-dA/T tail did not improve the specific signal (in some cases it was even much weaker) but increased nonspecific binding (Table 1). Similar observations using epifluorescence microscopy were made with multiple labeling by tailing probes with terminal deoxynucleotidyltransferase (D.A. Stahl and R. Amann, unpublished). This is supposedly caused by nonspecific binding of dye moieties to cell components.

Simultaneous application of several probes of the same specificity and carrying the same fluorochrome but binding to different regions of the target rRNAs, was shown to increase the specific signal (2). However, the increase was less than additive and could be partially attributed to nonspecific binding resulting from the increased total probe concentration.

Indirect signal amplification should be possible using hapten-labeled probes and antibodies conjugated with several dye molecules. Digoxigenin-labeled probes could be detected inside fixed cells by fluorescent antibodies, but the fluorescence signals were not significantly stronger compared to directly labeled probes (25). Higher numbers of dye molecules per antibody and better permeabilization of cells for antibodies might, however, favour this approach.

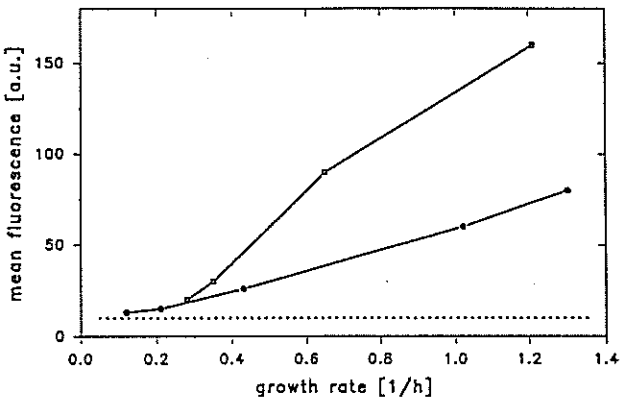

FIG. 4. Probe-conferred fluorescence per cell (a. u.) as a function of growth rate. Mean fluorescence intensities of *E. coli* (filled circle) and *P. cepacia* (hollow square) cells after hybridization with the FLUOS-labeled bacterial probe EUB338 are shown as a function of their growth rates. Cells were grown at 37°C (*E. coli*) or 30°C (*P. cepacia*) aerobiacally and were harvested during exponential growth in media that supported different growth rates (see below). As there is one probe binding site per ribosome and the ribosome and rRNA content of the cells is proportional to growth rate over a wide range, probe-conferred fluorescence is well correlated to growth rate. Very slowly growing cells have rRNA-contents close to the detection limit of this technique (dotted line: fluorescence background level). Media used (ref. 9); resulting growth rates [h^{-1}] for *E. coli*/*P. cepacia* are given in brackets (/): mineral salt medium (42 mM Na_2HPO_4, 22 mM KH_2PO_4, 9.5 mM NaCl, 19 mM NH_4Cl, 2 mM $MgSO_4$, 0.1 mM $CaCl_2$) containing 0.2% acetate (0.12/0.35), 0.2% pyruvate (0.21/−), 0.2% glucose (0.43/0.26), 0.2% glucose and 0.2% casein (1.02/0.65); YT-broth (see Materials and Methods; 1.30/1.21).

Growth Rate and Ribosome Content

The ribosome and, accordingly, the rRNA content of microorganisms is proportional to growth rate over a wide range (6,9). As there is exactly one target region on every ribosome for each oligonucleotide probe, the probe-conferred fluorescence should be directly proportional to the ribosome content. The hybridization of *E. coli* and *P. cepacia* cells harvested during exponential growth in media that determine different growth rates (see Fig. 4; ref. 9) confirmed these correlations. As expected, cells harvested in stationary phase showed much lower fluorescence intensities than those fixed during exponential growth from the same culture. Probe-conferred fluorescence of very slowly growing or starving cells was in some cases at background level and therefore below the detection limit.

Dual-Color Analysis

For the simultaneous application of two different probes, the combination of fluorochromes, excitation wavelengths, and emission filters that were available to us and yielded the best results are described in Materials and Methods. The ratio of mean fluorescence intensities of target to nontarget cells was up to 10 for

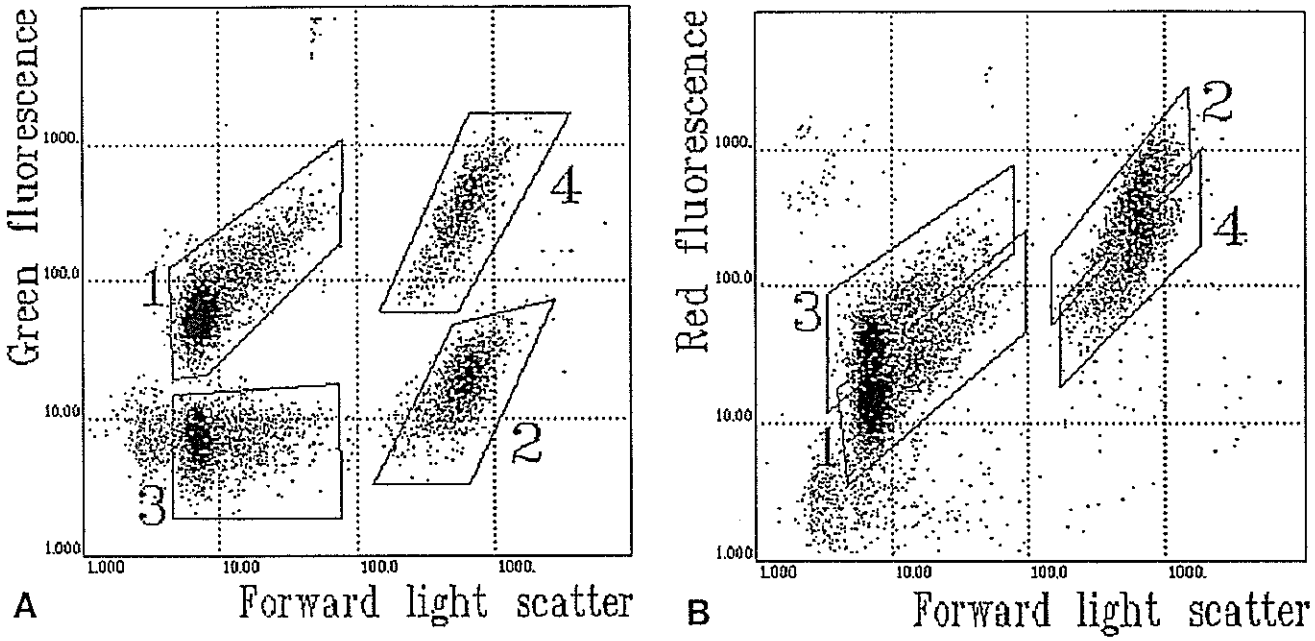

FIG. 5. Dual-color analysis of *E. coli* and yeast cells hybridized simultaneously with two rRNA-targeted oligonucleotide probes of different specificity and labeled with different fluorochromes. Dot plots showing green (A) and red (B) fluorescence per cell (a. u.) vs. forward light scatter. Overlay of two experiments, allowing the direct comparison of specific and nonspecific signals. *E. coli* (gates #1 and #3) and *S. carlsbergensis* (#2 and #4) cells were hybridized simultaneously with two different probes: In one experiment (gates #1 and #2) the bacterial probe EUB338 that binds specifically to *E. coli* cells was labeled with FLUOS (green fluorescence), the eukaryotic probe EUK516, staining *S. carlsbergensis* specifically, was conjugated to TRITC (red fluorescence). In the other experiment (#3 and #4) EUB338 was labeled with TRITC, and EUK516 with FLUOS. The ratio of specific to nonspecific signal is much higher for FLUOS- than for TRITC-labeled probes as a result of several problems discussed in the text.

FLUOS-labeled probes, but only up to 3 for TRITC (Fig. 5). These values are much lower than for single-color (and single laser) conditions and result from the following problems: (1) The absorption of TRITC at the 514 nm line of the argon ion laser is far below its maximum, whereas the 488 nm line is almost at the absorption maximum of FLUOS. Accordingly, in single-color analyses the signal to noise ratios also were higher for FLUOS—(up to 50) than for TRITC-labeled probes (up to 10). (2) A 530 nm long pass filter had to be added to the 530 nm band pass filter in front of the detector for green fluorescence. It largely (but not completely) excluded scattered light from the 514 nm excitation line, but also reduced the FLUOS signal. (3) Crosstalk from the "red tail" of FLUOS into the photomultiplier tube for TRITC detection increased the background for red fluorescence. It could not be "cut off" by appropriate filters without diminishing the TRITC signal.

Therefore, it was easily possible for FLUOS-, but hardly for TRITC-labeled probes to distinguish definitively target from nontarget cells in dual-label experiments under the given conditions. Changing from TRITC to a fluorochrome with excitation and emission maxima at longer wavelengths and to an appropriate dye laser should give much better results in combination with FLUOS and the 488 nm argon laser line.

CONCLUSIONS

In this study we varied the in situ hybridization parameters of buffer composition, probe concentration, incubation time, or posthybridization washing in order to optimize signal to noise ratios. We were able to distinguish clearly between target and nontarget cells in most cases. Sensitivity problems occurred with very small, slowly growing or stationary phase cells due to their low cellular ribosome content. Since attempts for significant signal amplification failed we tried to improve the simultaneous use of two probes labeled with different dyes. Such dual-label analyses can be used not only for enumeration of two distinct populations simultaneously but also allow combination of a specific and a universal rRNA-targeted probe. The universal probe is complementary to a sequence region that all organisms tested have in common and can be applied as a positive control to quantify the cell content of accessible ribosomes. Possibly false negative results of target cells that show weak fluorescence signals due to low ribosome content or limited cell permeability can then be excluded from analysis. In addition, the universal probe can be used to determine for each cell the ribosome content that is correlated to growth rate and is a measure of physiological activity (ref. 9; this study).

Epifluorescence microscopy studies indicated that fluorescently labeled, rRNA-targeted oligonucleotide probes can reliably identify microbial cells in natural ecosystems without prior cultivation in the laboratory (1,3,19). Based on the systematic optimization of fluorescent in situ hybridization and flow cytometry described in this work, we have recently been able to enumerate specific groups of bacteria directly in fixed waste water samples (Wallner et al., in preparation). The combination of flow cytometric analysis and hybridization definitely shows potential for high resolution automated microbial identification. However, this only applies to samples in which most of the microbial cells are free-living rather than associated with surfaces. In attached microbial communities (biofilms), the number and exact spatial distribution of specific populations will be best analyzed by a combination of fluorescent in situ hybridization with epifluorescence microscopy (3), which can be combined with image analysis if quantification of fluorescence is required.

ACKNOWLEDGMENTS

This work was financially supported in part by the Commission of the European Communities, High Resolution Automated Microbial Identification (HRAMI) programme, contract BIOT-CT91-0294.

LITERATURE CITED

1. Amann RI, Krumholz L, Stahl DA: Fluorescent-oligonucleotide probing of whole cells for determinative, phylogenetic, and environmental studies in microbiology. J Bacteriol 172:762–770, 1990.
2. Amann RI, Binder BJ, Olson RJ, Chisholm SW, Devereux R, Stahl DA: Combination of 16S rRNA-targeted oligonucleotide probes with flow cytometry for analyzing mixed microbial populations. Appl Environ Microbiol 56:1919–1925, 1990.
3. Amann R, Stromley J, Devereux R, Key R, Stahl DA: Molecular and microscopic identification of sulfate-reducing bacteria in multispecies biofilms. Appl Environ Microbiol 58:614–623, 1992.
4. Bauman JGJ, Bentvelzen P: Flow cytometric detection of ribosomal RNA in suspended cells by fluorescent in situ hybridization. Cytometry 9:517–524, 1988.
5. Bertin B, Broux O, Van Hoegaerden M: Flow cytometric detection of yeast by in situ hybridization with a fluorescent ribosomal RNA probe. J Microbiol Methods 12:1–12, 1990.
6. Bremer H, Dennis PP: Modulation of chemical composition and other parameters of the cell by growth rate. In: Escherichia coli and Salmonella typhimurium, Cellular and Molecular Biology, Neidhardt FC et al. (eds.). ASM, Washington DC, 1987, pp 1527–1542.
7. Brock TD: The study of microorganisms in situ: Progress and problems. In: Symposium of the Society for General Microbiology Fletcher M. et al. (eds). Cambridge University Press, Cambridge, UK, 1987, pp. 1–17.
8. Colwell RR, Brayton PR, Grimes DJ, Roszak DR, Huq SA, Palmer LM: Viable but nonculturable Vibrio cholerae and related pathogens in the environment: implications for the release of genetically engineered microorganisms. Biotechnology 3:817–820, 1985.
9. DeLong EF, Wickham GS, Pace NR: Phylogenetic stains: Ribosomal RNA-based probes for the identification of single cells. Science 243:1360–1363, 1989.
10. Donnelly CW, Baigent GJ: Method for flow cytometric detection of Listeria monocytogenes in milk. Appl Environ Microbiol 52: 689–695, 1986.
11. Giovannoni SJ, DeLong EF, Olsen GJ, Pace NR: Phylogenetic group-specific oligodeoxynucleotide probes for identification of single microbial cells. J Bacteriol 170:720–726, 1988.
12. Jannasch HW, Jones GE: Bacterial populations in seawater as determined by different methods of enumeration. Limnol Oceano 4:128–139, 1959.
13. Miller JS, Quarles JM: Flow cytometric identification of microorganisms by dual staining with FITC and PI. Cytometry 11: 667–675, 1990.
14. Olsen GJ, Larsen N, Woese CR: The ribosomal RNA data base project (RDP). Nucleic Acids Res 19, Suppl: 2017–2021, 1991.
15. Pajor L, Bauman JGJ: Flow cytometric measurement of rRNA levels detected by fluorescent in situ hybridization in differentiating K-562 cells. Histochemistry 96:73–81, 1991.
16. Sahar E, Lamed R, Ofek I: Rapid identification of Streptococcus pyogenes by flow cytometry. Eur J Clin Microbiol 2:192–195, 1983.
17. Sanders CA, Yajko DM, Hyun W, Langlois RG, Nassos PS, Fulwyler MJ, Hadley WK: Determination of guanine-plus-cytosine content of bacterial DNA by dual-laser flow cytometry. J Gen Microbiol 136:359–365, 1990.
18. Shelly DC, Warner IM, Quarles JM: Characterization of bacteria by mixed-dye fluorometry. Clin Chem 29:290–296, 1983.
19. Spring S, Amann R, Ludwig W, Schleifer KH, Petersen N: Phylogenetic diversity and identification of nonculturable magnetotactic bacteria. System Appl Microbiol 15:116–122, 1992.
20. Stahl DA, Amann RI: Development and application of nucleic acid probes. In: Nucleic Acid Techniques in Bacterial Systematics, Stackebrandt E and Goodfellow M (eds). John Wiley and Sons, Chichester, 1991, pp 205–248.
21. Tyndall RL, Hand RE, Mann RC, Evans C, Jernigan R: Application of flow cytometry to detection and characterization of Legionella spp. Appl Environ Microbiol 49:852–857, 1985.
22. Van Dilla MA, Langlois RG, Pinkel D, Yajko D, Hadley WK: Bacterial characterization by flow cytometry. Science 220:620–622, 1983.
23. Völsch A, Nader WF, Geiss HK, Nebe G, Birr C: Detection and analysis of two serotypes of ammonia-oxidizing bacteria in sewage plants by flow cytometry. Appl Environ Microbiol 56:2430–2435, 1990.
24. Woese CR: Bacterial evolution. Microbiol Rev 51:221–271, 1987.
25. Zarda B, Amann R, Wallner G, Schleifer KH: Identification of single bacterial cells using digoxigenin-labelled, rRNA-targeted oligonucleotides. J Gen Microbiol 137:2823–2830, 1991.

Bacterial Characterization by Flow Cytometry

Abstract. *Bacteria were analyzed in a dual-beam flow cytometer after double staining with the fluorescent dyes chromomycin A3 and Hoechst 33258, which bind preferentially to DNA that is rich in guanine-cytosine and adenine-thymine, respectively. The measurements were indicative of the cellular DNA content and base composition, cell concentration, and proliferative state of the population. The ratio of the chromomycin A3 signal to the Hoechst 33258 signal increased with the guanine-cytosine content of the cellular DNA for the six cultured species measured, following expectation. Bacteria in urine from patients with urinary tract infections were characterized without interference from host cell DNA, debris, or other particulates.*

Flow cytometry, which has been applied extensively to mammalian cells and chromosomes (*1*), offers many possibilities for microbial measurement. The techniques of quantitative fluorescence cytochemistry make it possible to determine important structural and functional properties of individual cells with high precision at rates of 10^3 cells per second. More than one cellular property can be measured simultaneously. The objectives of the limited number of microbiological applications of flow cytometry have included the determination of ploidy levels, state of proliferation, state of protozoan infection, or glycoprotein cell wall composition in the case of yeast cells (*2, 3*). Fluorescent stains for the cellular content of DNA, total nucleic acid, or protein were used, sometimes in combination: fluorescein-coupled lectins were used in the yeast cell wall studies (*3*).

We report here the application of a double fluorescent DNA staining method to bacteria. Originally developed for use with mammalian chromosomes (*4*), the technique uses chromomycin A3, having guanine-cytosine (GC) binding preference, and Hoechst 33258, having adenine-thymine (AT) binding preference. This stain combination provides information on the DNA base composition (that is, the proportion of GC and AT base pairs) as well as the DNA content. Bacterial species vary widely in base composition: GC values range between 25 and 70 percent of the total number of base pairs present in the DNA. We have analyzed six cultured bacterial species of clinical importance that differ in base composition and show that they can be distinguished on this basis. The flow cytometric ranking of the GC percentage strongly correlates with the biochemically determined GC percentages reported in the literature. We also show that bacteria in infected human urine can be measured in the same way without interference by host cellular and particulate material.

Cultured bacteria were collected by centrifugation and resuspended in 70 percent ethanol at concentrations of the order of 10^8 organisms per milliliter. Urine from patients with urinary tract infections was centrifuged and the bacterial pellet was resuspended in an equal volume of 70 percent ethanol. Fixed suspensions can be stored at 4°C for several months with no apparent degradation. For flow analysis, small portions of fixed bacterial suspension were added to a staining solution containing 3 μM Hoechst 33258, 10 μM chromomycin A3, 10 mM tris (pH 7.2), 150 mM NaCl, and 1.5 mM $MgCl_2$. Bacterial concentrations were typically 2×10^7 cells per milliliter in the final stained suspension, but variations in concentration from 10^7 to 10^8 cells per milliliter had no effect on the observed staining intensities.

Fluorescence from the doubly stained bacteria was measured with a dual-beam flow cytometer (*5*). The bacteria suspended in staining solution flow single file through a flow chamber and sequentially intersect a pair of laser beams, focused to elliptical spots of dimensions 150 by 20 μm spaced ~ 200 μm apart. The Hoechst 33258 was excited with 500 mW of the 337- to 356-nm lines from a Spectra-Physics 171-01 krypton ion laser, and the chromomycin A3 was excited with 500 mW of the 458-nm line of a Spectra-Physics 171-18 argon laser. The two fluorescence flashes emitted as a cell passes through the beams were collected with an f/1.0 lens and imaged through a Corning 3-71 filter (transmits above 480 nm) onto separate photomultipliers (EMI 9798 B). The resultant electrical pulses were amplified, processed, digitized, and stored in the memory of a two-parameter multichannel analyzer. Since the flow velocity is the same for all cells, the two signals from each cell are associated by their time separation. The 3-71 filter transmits almost all the chromomycin A3 fluorescence and about half the Hoechst 33258 fluorescence. Thus the photomultiplier focused on the 458-nm beam yields a signal (C) proportional to the

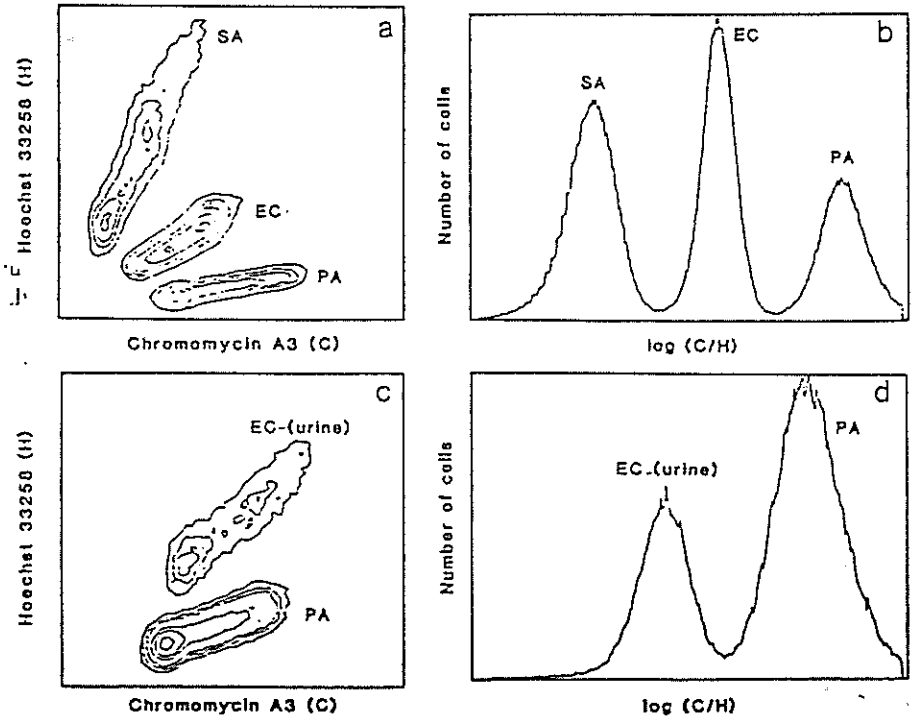

Fig. 1. (a) Bivariate contour plot of the fluorescence signals from a mixture of cultured *Staphylococcus aureus* (*SA*), *Escherichia coli* (*EC*), and *Pseudomonas aeruginosa* (*PA*) after double DNA staining with Hoechst 33258 (H) and chromomycin A3 (C). The peak height (number of cells) is indicated by the contours. (b) Distribution of the ratio of the two fluorescent signals, C/H, over the cell population of (a). (c) Bivariate contour plot of the fluorescence signals from *E. coli* from an infected urine sample after double DNA staining with Hoechst 33258 and chromomycin A3. Cultured *P. aeruginosa* was added as an internal standard. (d) Distribution of C/H over the cell population of (c).

chromomycin A3 content. The other photomultiplier, focused on the ultraviolet beam, measures about half the Hoechst 33258 fluorescence light that is collected plus the chromomycin A3 fluorescence stimulated by energy transfer from excited Hoechst 33258 molecules; this signal (H) is approximately proportional to the Hoechst 33258 content. Data were recorded at ~ 10^3 cells per second with a Nuclear Data model 6600 computer, which also generated both a real-time isometric display of the number of particles versus the two fluorescence signals and a display of the number of cells as a function of the ratio of the two fluorescence signals.

For quantitative measurements, standard aliquots of a reference suspension (*Escherichia coli* or *Pseudomonas aeruginosa*) were added to the stained sample so that fluorescence ratios could be determined relative to the reference strain independent of instrumental gain settings. The concentration of the strain being tested could also be determined directly by comparison of the peak volumes of the test strain and the reference strain.

The measurements on a mixture of three cultured bacterial species are shown in Fig. 1. In the bivariate contour plot (Fig. 1a) each bacterial species forms a distinct cluster which carries several pieces of information. The radial coordinate is roughly proportional to the cellular DNA content. The radial extension of the cluster reflects increasing DNA content due to chromosome replication, incompletely separated cells, and possibly clumping. The angular displacement of a cluster from the vertical (H) axis is a function of the GC percentage. The three clusters are ordered as expected on the basis of the published values of GC percentages listed in Table 1. The cluster volumes are proportional to the bacterial concentrations. In Fig. 1b the distribution of the ratio of the two fluorescence signals, C/H, is shown. Information on DNA content is absent in this display, since all cells on a radial line of the contour plot have the same C/H ratio. The distribution is plotted as a function of the logarithm of C/H to show more clearly that the shapes and coefficients of variation of the three peaks (15 to 20 percent) are comparable. The three peaks are well separated, an indication that these three species with widely differing GC percentages are easy to resolve in a mixture.

The data for all six species are tabulated in Table 1, along with data on GC values found in *Bergey's Manual* (6).

Table 1. Bacterial species analyzed by dual-beam flow cytometry after staining with Hoechst 33258 and chromomycin A3.

Bacterial species	Description	GC (%)†	GC/AT‡	(C/H)§
Pseudomonas aeruginosa	Gram-negative rods	67	1.00	1.00
Klebsiella pneumoniae	Gram-negative rods	52–56	0.58	0.45
Escherichia coli	Gram-negative rods	50–51	0.50	0.31–0.41¶
*Escherichia coli**	Gram-negative rods	50–51	0.50	0.43–0.44 ‖
Escherichia coli	Gram-negative rods	50–51	0.50	0.40–0.42#
Streptococcus pyogenes	Gram-positive cocci	35–40	0.30	0.18
Streptococcus pneumoniae	Gram-positive cocci	39–42	0.33	0.13
Staphylococcus aureus	Gram-positive cocci	31–39	0.27	0.11

*All isolates were obtained from clinical specimens at the Microbiology Division, San Francisco General Hospital, San Francisco, except for these two *E. coli* samples obtained from the Meat Science Research Laboratory, Department of Agriculture. †Range found in *Bergey's Manual* (6). ‡As calculated from the midpoint of the range of values in *Bergey's Manual* (6) and normalized to unity for *P. aeruginosa*. §Fluorescence signal ratio normalized to unity for *P. aeruginosa*. Replicate measurements indicate a precision of approximately ± 10 percent (standard deviation/mean). ¶Range of values of four strains. ‖ Values for two strains. #Values for two infected urine specimens analyzed directly from patient urine sediment.

The value of C/H increases with increasing GC/AT percentages, as would be expected from the preference of chromomycin A3 for GC-rich DNA and Hoechst 33528 for AT-rich DNA. The fact that C/H increases faster than the GC/AT percentages is the result of the mechanism of stain binding (stretches of three base pairs are optimal) and energy transfer (4). Some details are not yet understood. We observe significant differences in C/H values among the strains of *E. coli* listed in Table 1. Although individual strains of *E. coli* differ slightly in GC percentage, it is possible that strain-to-strain differences in other biochemical characteristics may have some effect on C/H. The correlation of C/H and GC/AT values for *Streptococcus pyogenes*, *S. pneumoniae*, and *Staphylococcus aureus* is not clear-cut because of the wide range of literature values of GC percentages for these species.

Bacterial infection of urine specimens can be detected with a flow cytometer. The measured results on a urine specimen infected with *E. coli* (about 10^9 per milliliter) are shown in Fig. 1, c and d. A sample of cultured *P. aeruginosa* was added to the urine specimen to provide an internal calibration. The bacteria stain well and nonspecific staining of other particles or debris in the urine is minimal. The C/H of 0.42 (normalized to *P. aeruginosa*) falls within the range of values obtained from cultured strains of *E. coli* (Table 1). The coefficient of variation of the *E. coli* peaks in Fig. 1, b and d, are equal (14 to 15 percent). This shows comparable measurement resolution of *E. coli* from urine and cultured strains.

Our new flow cytometric method for bacterial characterization that is sensitive to DNA base composition adds a new dimension of specificity to flow cytometric methods for determining the cellular content of total nucleic acids, protein, and DNA. It has potential for the rapid counting and identification of bacteria in clinical, food, and environmental samples. The ability to measure mixtures of species may allow direct determination of the relative concentration and proliferative state of each species without the perturbations induced by methods dependent on culturing, which would be important in studies of microbial competition (7). The measurement of genome size and base composition of unknown strains may facilitate determination of phylogenetic relations. Specificity for bacterial identification may be further enhanced by the use of other optical probes such as fluorescent antibodies to surface antigens, fluorogenic substrates for proteases and other enzymes, fluorescent probes for total protein, fluorescein-conjugated lectins, and the scattering of linearly or circularly polarized light.

M. A. VAN DILLA
R. G. LANGLOIS
D. PINKEL

Biomedical Sciences Division, Lawrence Livermore National Laboratory, University of California, Livermore 94550

D. YAJKO
W. K. HADLEY

Department of Laboratory Medicine, University of California, San Francisco, and Microbiology Division, San Francisco General Hospital, San Francisco 94110

References and Notes

1. M. Melamed, P. Mullaney, M. Mendelsohn, *Flow Cytometry and Sorting* (Wiley, New York, 1979); P. K. Horan and L. L. Wheeless, Jr., *Science* 198, 149 (1977).
2. K. Hutter and H. Eipel, *J. Gen. Microbiol.* 113, 369 (1979); J. E. Bailey, J. Fazel-Madjlessi, D. N. McQuitty, L. Y. Lee, J. C. Allred, J. A. Oro, *Science* 198, 1175 (1977); A. Paau, J. Oro, J.

Cowles, *Plant Physiol.* 63, 402 (1979); R. Howard, F. Battye, G. Mitchell, *J. Histochem. Cytochem.* 27, 803 (1979); H. Steen, E. Brye, K. Skarstad, B. Bloom, T. Godal, S. Mustafa, *Cytometry* 2, 249 (1982).
3. R. Douglas and C. Ballou, *J. Biol. Chem.* 255, 5979 (1980).
4. R. Langlois, A. Carrano, J. Gray, M. Van Dilla, *Chromosoma* 77, 229 (1980).
5. P. Dean, in *Flow Cytometry*, O. Laerum, T. Lindmo, E. Thorud, Eds. (Universitetsforlaget, Oslo, 1980), vol. 4, pp. 41–44; P. Dean and D. Pinkel, *J. Histochem. Cytochem.* 26, 622 (1978).
6. *Bergey's Manual of Determinative Bacteriology*, R. Buchanan and N. Gibbons, Eds. (Williams and Wilkins, Baltimore, ed. 8, 1974).
7. A. G. Fredrickson and G. Stephanopoulos, *Science* 213, 972 (1981).
8. This work was performed under the auspices of the Department of Energy by the Lawrence Livermore National Laboratory under contract W-7405-ENG-48.

28 June 1982; revised 30 November 1982

Interrelated Striated Elements in Vestibular Hair Cells of the Rat

Abstract. *Unusual fixation procedures revealed a series of interrelated striated organelles in type I and type II vestibular hair cells of the rat; these organelles seemed to be less well developed in cochlear hair cells. The findings suggest that contractile elements may play a role in sensory transduction in the inner ear, particularly in the vestibular system.*

Actin is present in the hair cells of vestibular (*1, 2*) and auditory (*3, 4*) receptors. By S-1 myosin decoration methods (*5*), actin has been found in the stereocilia and their rootlets, the cuticular plate, and the electron-opaque material that forms the junctional complexes of the reticular lamina. Because myosin also has been found in apical parts of hair cells of the organ of Corti (*6*), it might be expected that actin and myosin are organized into contractile elements that take part in signal processing in the inner ear. Generally, however, S-1 myosin decoration has failed to demonstrate highly organized actin filaments in the cuticular plate (*1–4*). Only Slepecky and her colleagues (*7*) have illustrated an infracuticular, striated element containing actin (*4*). Lowenstein and Osborne (*8*) earlier described ribbonlike striated elements in vestibular hair cells of ammocoetes larvae of the lamprey extending from the cuticular plate to the cell membrane basally and ending close to synaptic sites. Their results, obtained by conventional transmission electron microscopy, prompted them to hypothesize that such striated material might be involved in transduction. Other investigators have also reported finding isolated laminated, or striated, elements in the basal part of the cuticular plate, or below it, in hair cells of both normal (*9–14*) and pathological (*9, 15*) inner ears in many species. Striated material was also abundant in hair cells of old monkeys (*12*) and elderly humans (*12, 16*), and in drug-treated animals (*13, 17*). The apparently increased incidence of such bodies under pathological conditions and as a consequence of aging seems to have overshadowed findings in normal material, and laminated bodies have generally come to be regarded as pathological entities. Nevertheless, several investigators have emphasized that striated elements are normal constituents of vestibular (*8, 10–12*) and cochlear (*7, 14*) hair cells.

We now describe our ultrastructural finding of a series of interrelated striated elements in apical parts of vestibular hair cells of the rat. Included in the series are the cuticular plate and its basal attachments to the hair cell margins, the connections of the strut array of the kinociliary basal body (*18*) to the cuticular plate, and striated organelles associated with the plasma membrane and extending below the apical junctional complexes. The latter organelles are more extensive in type I than in type II hair cells. In contrast, rat cochlear hair cells seem to lack similar striated organelles associated with the plasma membrane and to have less robust striations in the cuticular plate. Our findings indicate a broader distribution of striated elements in vestibular hair cells than was found previously. They support the concept that contractile elements may play a role in transduction in the inner ear (*7, 8, 19*), particularly in the vestibular system.

Fig. 1. (A) Striations in the substance of the cuticular plate (*CP*) of a type I utricular hair cell. (B) Striations along the lower face of the circular plate of a type II utricular hair cell. The three arrows indicate opposite electron-opaque stripes and an intermediate line. Magnification: ×43,000.

Our results were obtained in specific-pathogen-free, young adult, Sprague-Dawley rats (Charles River) during an effort to determine an optimal method for preserving inner ear tissue collected under space-flight conditions. Osmium tetroxide could not be used, because of its toxicity; tissues, once collected, might have to be stored for as long as 5 days before further processing could take place. The following method resulted in unexpected preservation of the striated organelles in hair cells. Temporal bones were rapidly removed from decapitated rats, and the oval and round windows of the cochleas were opened immediately upon immersion in 2.5 percent glutaraldehyde in 0.1*M* sodium phosphate buffer (*p*H 7.4). After fixation for 2 hours at room temperature, the tissues were stored in fresh fixative in vials at 4°C for 5 days. The tissues were then washed in buffer, fixed in 1.0 percent osmium tetroxide in 0.1*M* sodium phosphate buffer (*p*H 7.4) for 1 hour, then washed again, microdissected, and prepared by standard methods for transmission electron microscopy. Subsequent experiments demonstrated that the striated organelles were well preserved when prolonged storage was omitted. The organelles were not seen, however, after fixation in Karnovsky's (*20*) 4 percent paraformaldehyde–5 percent glutaraldehyde solution.

The striated organelles of hair cells have a repeating pattern of alternating electron-opaque stripes and broader, more electron-lucent bands. The bands are intersected by narrow, electron-opaque, intermediate lines (Figs. 1 and 2). This pattern is organizationally similar to that of striated rootlets of the kinociliary basal body in the hair cells themselves, and particularly to that described for contractile rhizoplasts in the flagellate *Platymonas subcordiformis* (*21*). It is also comparable to the pattern commonly reported for isolated laminat-

FLUORESZENTE IN-SITU HYBRIDISIERUNG

IN CHROMOSOMEN UND INTERPHASENKERNEN

Prof.Dr.Th.Cremer, Dr.H.Scherthan

Institut für Humangenetik und Anthropologie
der Universität Heidelberg

From: Human Cytogenetics - A practical approach Vol. I (2nd edition) D.E. Rooney and B.H. Czepulkowski, eds. IRL Press, Oxford (1992)

6

Chromosome analysis by non-isotopic *in situ* hybridization

P. LICHTER and T. CREMER

1. Introduction

In situ hybridization provides the most direct way to study the chromosomal localization of DNA sequences. Based on the early work of Gall and Pardue in 1969 (1), routine isotopic *in situ* hybridization protocols were established in many laboratories during the 1970s. In 1981 Gerhard *et al.*, Malcolm *et al.*, and Harper *et al.* were the first to demonstrate the possibility of localizing single-copy sequences cloned from individual genes by isotopic *in situ* hybridization (2–4). A protocol for isotopic chromosomal localization of DNA probes is described elsewhere in this *Practical Approach* series (5). This chapter is devoted to non-isotopic *in situ* hybridization techniques, in particular, fluorescence *in situ* hybridization protocols. Based on the developments in the early 1980s (for review, see ref. 6), this approach has become increasingly popular over the last few years. A number of reasons account for this development (for discussion, see refs 7–8), notably an increase in speed, improved signal resolution, the development of *in situ* suppression hybridization protocols, advanced optical equipment for 2-D and 3-D analyses of labelled specimens, and in particular the ability to combine several techniques for simultaneous multicolour detection of different nucleic acid targets within the same preparation. *Figure 1* illustrates schematically the principles of this method.

Non-isotopic *in situ* hybridization using chromosome specific DNA probes provides a powerful tool for the analysis of numerical and structural chromosome aberrations not only in metaphase, but also directly in the interphase nucleus, an approach which has been termed *interphase cytogenetics* (9) (for review, see ref. 8). This is of great significance in cases where metaphase chromosome spreads cannot be prepared in sufficient quality or quantity (e.g. as is the case with many tumours), or not at all as in non-cycling cells.

The first applications of non-isotopic *in situ* hybridization to clinical cytogenetics took advantage of tandemly repeated, chromosome specific DNA elements, such as alphoid DNA sequences, which are present in the heterochromatin of most human chromosomes (for review, see ref. 8). A procedure

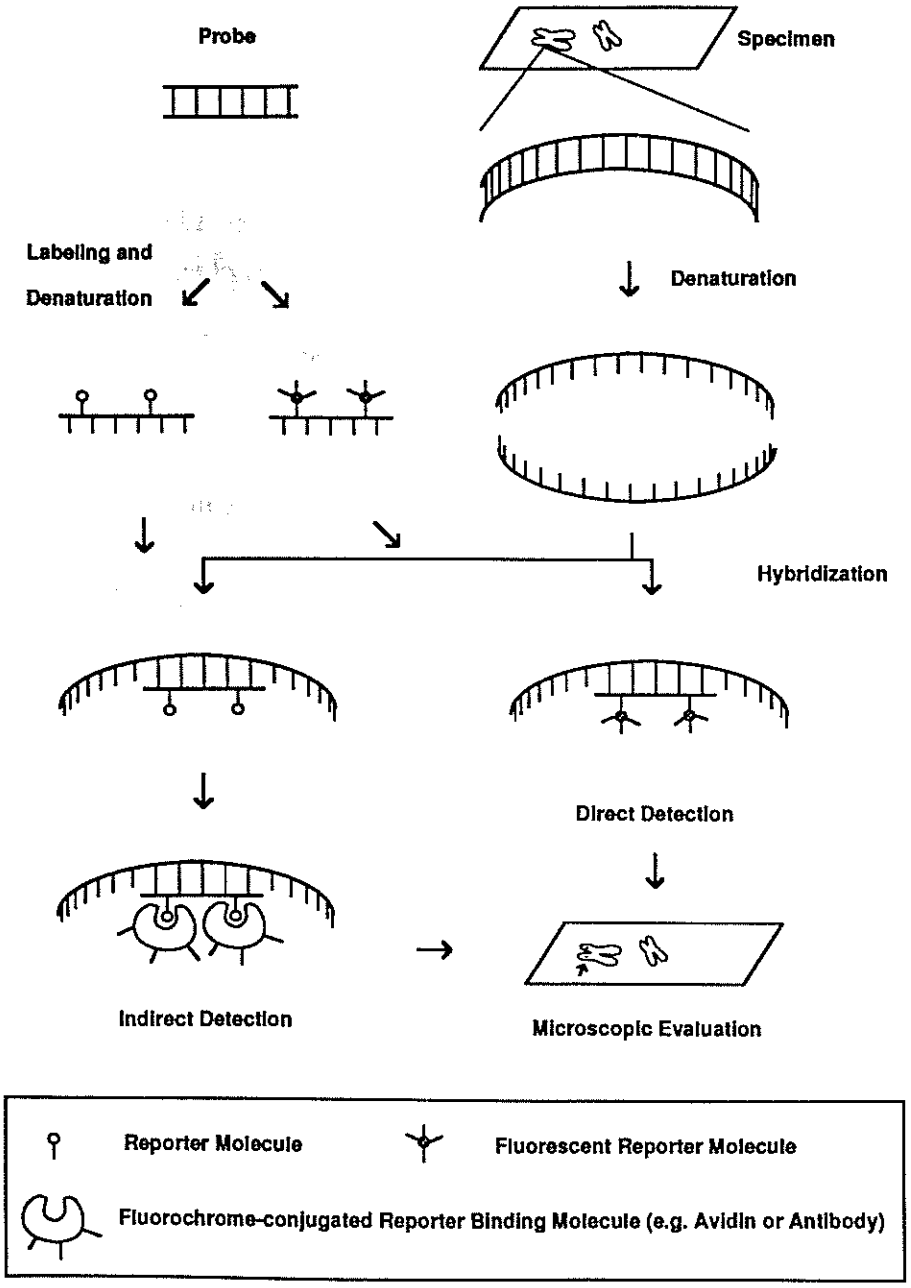

Figure 1. Schematic illustration of fluorescence *in situ* hybridization.

useful for such purposes is given below (*Protocols 3–6*). Since the target region is considerably large, expanding up to many hundred kilobases in length, it is easy to detect after *in situ* hybridization with a single repeated element or even part of it used as a probe. Recently, oligomeres defining highly specific sub-sequences of the repeated element have been introduced as probes. The latter approach, however, requires special protocols of oligomere synthesis or enzymatic tailing in the presence of chemically modified nucleotides, which are beyond the scope of this chapter.

Typical probes for mapping to human chromosomes are either cDNAs or cloned genomic DNA fragments. Most cDNAs consist only of single-copy sequences whereas the vast majority of cloned genomic fragments contain, in addition to unique sequences, interspersed repetitive sequences (IRS), such as SINEs (small interspersed repetitive elements, e.g. Alu-elements) and LINEs (large interspersed repetitive elements, e.g. L1-elements). For cDNAs and genomic fragments known to be entirely single-copy the standard procedure (*Protocols 3–6*) can be used. Parameters influencing the quality of non-isotopic *in situ* hybridization signals have been optimized and more precisely defined by a number of groups (e.g. refs 10–15). All this knowledge has contributed to the standard procedure described.

When interspersed repetitive elements are present in a probe, application of the standard procedure results in hybridization signals distributed over the whole chromosome complement due to the ubiquitous presence of IRS throughout the genome. Since the most abundant repetitive DNA is the Alu-repeat family, which is preferentially located within R-bands (16), usually an R-banding-like staining pattern results. Protocols have been developed by which the portion of the signal caused by IRS within a given probe can be suppressed, while a highly specific signal is produced by the target site specific single-copy (or low-copy repeat) sequences (17–19). The principle of this method, which has been called *chromosomal* in situ *suppression* (CISS) *hybridization* (18), is illustrated in *Figure 2*. The labelled probe fragments are denatured together with an excess of unlabelled competitor DNA. Thereafter, pre-annealing is allowed for a given period of time. During this time, IRS elements of the probe will hybridize rapidly with the excess IRS of the competitor DNA, while most of the much less abundant chromosome specific sequences remain single-stranded. Accordingly, the resulting double-stranded IRS elements in the pre-annealed probe can no longer hybridize to their chromosomal DNA targets. In addition, a second competition effect is likely to contribute to the suppression of IRS signals. Remaining single-stranded IRS elements will hybridize to chromosomal IRS targets during the subsequent *in situ* hybridization. Again, unlabelled IRS elements of the competitor DNA would be in excess, and hybridization of remaining, single-stranded probe IRS elements would be prevented (see bottom of *Figure 2*). Any source of human DNA containing a sufficiently high concentration of IRS may serve as competitor DNA. Routinely, we use total genomic DNA (e.g. placental

DNA). In this case, too much competitor DNA is disadvantageous since chromosome site specific signals might also become significantly suppressed in addition to IRS signals. This risk can be avoided by using the *CotI* fraction of human genomic DNA, since the latter consists largely of rapidly annealing repetitive elements. *CotI* fractions have recently become commercially available. Salmon sperm DNA is added to the pre-annealing reaction in order to adjust the total DNA concentration. When there is still considerable staining of the chromosomes after *in situ* hybridization caused by IRS sequences, the experiment should be repeated with more competitor. However, some IRS banding can be helpful for chromosome identification. A protocol for CISS hybridization is given below (*Protocol 8*).

There is a fairly good correlation of labelling efficiency and size of targeted DNA. Cosmids commonly contain 25–40 kb of cloned insert DNA and are very efficient probes which almost all yield highly specific signals on metaphase chromosomes. Usually more than 90% of all metaphases show signals on both chromatids of both chromosome homologues (see *Figure 3*) with virtually no background spots. Therefore, the need for statistical analysis is greatly reduced and the efficiency is high enough to use such probes for diagnosis of chromosomal aberrations such as trisomies (see *Figure 3*) (20), translocations (21–23), inversions (24), and deletions (23, 25, 26). When the size of the target DNA detected by a given probe decreases (e.g. using probe fragments cloned in phage or plasmid vectors), the percentage of successfully delineated target sites also decreases. With probes containing approximately 2 kb single-copy sequences, a maximum of 40 to 50% of all target sites can presently be detected. Although we and others have successfully mapped single-copy DNA fragments of about 1 kb by fluorescence *in situ* hybridization, the discrimination of weak specific signals against background dots is likely to require statistical analysis based on the time-consuming evaluation of many metaphases. The development of very powerful camera systems which are more sensitive than the human eye promises to improve the detection of very weak hybridization signals significantly (see Section 6). Alternatively, it may be advisable to first isolate a larger probe for physical mapping, for instance, by screening a cosmid library.

The mapping of yeast artificial chromosomes (YACs) can also be carried out applying CISS hybridization (23, 27). Total genomic DNA of yeast cultures containing YACs with human DNA fragments has been successfully used as a probe. In this case, the amount of probe DNA has to be increased due to the small percentage of YAC DNA in yeast cells, while the concentration of human competitor DNA remains constant. Total yeast DNA can be added as competitor but is not essential. The quality of *in situ* hybridizations with YAC probes is often increased when YAC DNA purified after pulsed field gel electrophoresis is used. An alternative technique for generating YAC DNA probe sequences is described below (see Section 7).

In order to stain whole chromosomes or larger chromosomal regions,

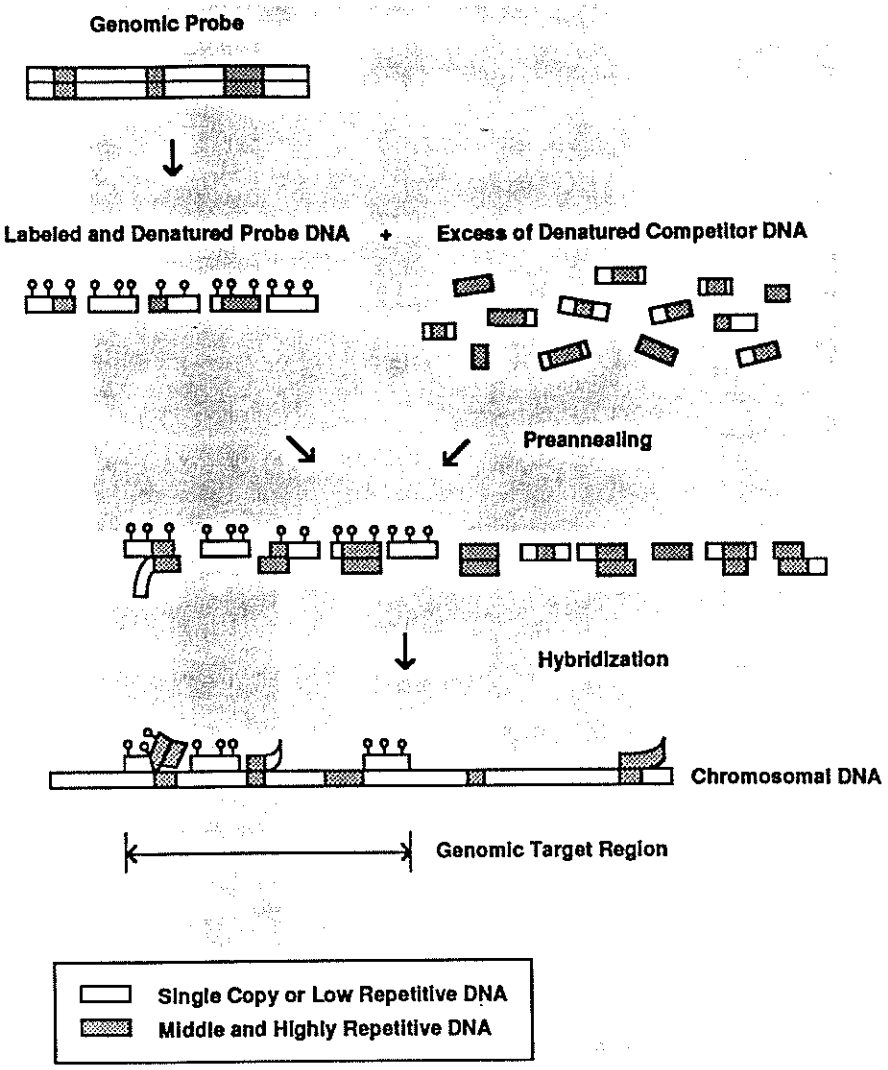

Figure 2. Schematic illustration of chromosomal *in situ* suppression (CISS) hybridization. For explanation see text.

different kinds of probe sets can be used. Entire chromosomes are specifically delineated using the DNA from sorted human chromosomes as a pool (18, 19). This procedure has also been termed 'chromosome painting' (19). The libraries used are either cloned in lambda phage vectors (28) or in pBS plasmid vectors (29). The latter are generally easier to use since the portion of vector sequences is small compared to most of the presently available recombinant lambda libraries. Accordingly, background problems which may arise

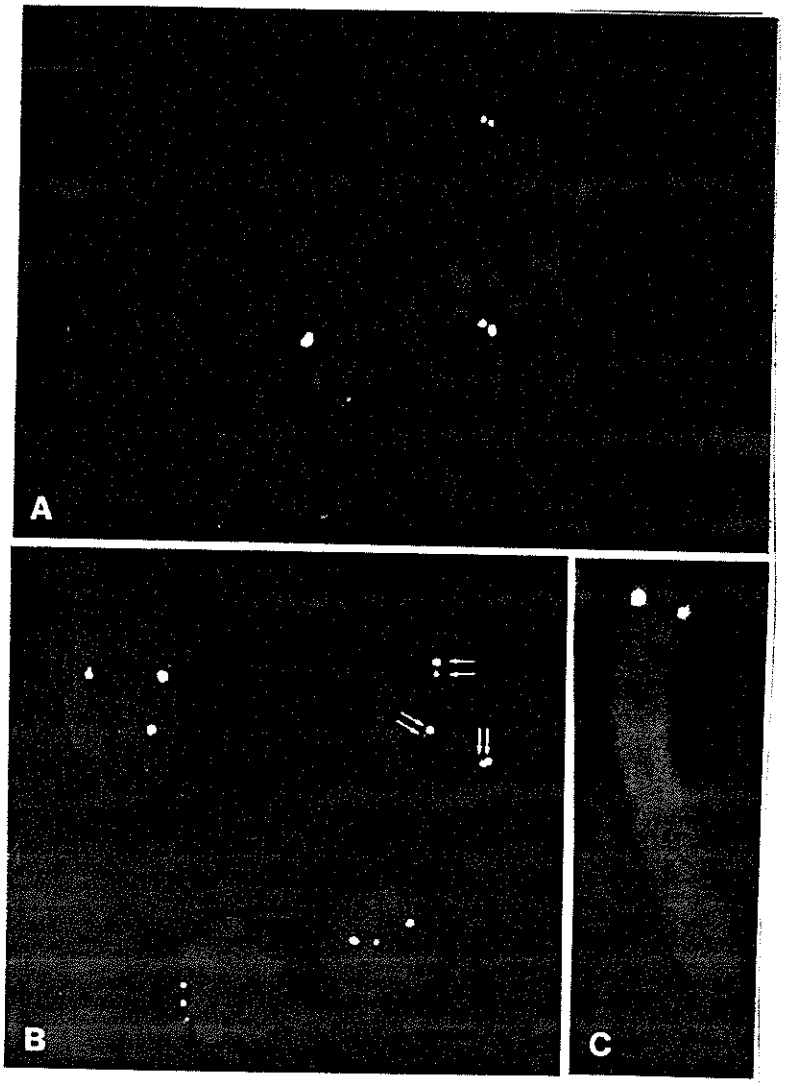

from high amounts of labelled vector can be eliminated. This problem could otherwise be overcome by isolating the library inserts (18). *Figure 6*A (p. 186) shows a chromosome 5 of *Macaca fuscata* specifically painted with total bacteriophage library DNA derived from human chromosome 5. Painting of the complete homologous *Macaca* chromosome 5 indicates the high level of evolutionary conservation of these chromosomes in human and *Macaca fuscata* for at least twenty million years.

Probe sets for the specific staining of subchromosomal regions can be generated in several ways. These include the pooling of single clones from

Figure 3. Chromosomal *in situ* suppression hybridization with cosmid DNA probes. (A and B) Cosmid c512 mapping to 21q22.3 hybridized to a metaphase spread (A) and nuclei (B) of lymphocytes from a Down's syndrome patient. The biotin labelled probe was detected with avidin–FITC; chromosomes and nuclei were counterstained with propidium iodide. Note the highly specific labelling, allowing a rapid diagnosis of trisomy 21 (20). On the metaphase in panel A the signals are visible on both chromatids (all signals are doublets) of all three chromosomes 21. Correspondingly three signals are seen in the nuclei (B). Note that the signals in the nuclei are doublets also (depicted, for example, by the small arrows in the upper right nucleus), indicating the G_2 stage of these nuclei. The doublets are not always visible simultaneously in G_2 nuclei, since part of the fluorescence spots are not in the imaged focal plane. (C) Cosmid K40 containing the human haemoglobin beta gene cluster localized on the short arm of chromosome 11 (42). Note the pale background R-banding pattern by propidium iodide in A and C. (A–C) These digitized images were obtained by using a confocal laser scanning microscope and after applying image processing for better illustration (see Section 6).

a particular region (30), regional specific DNA libraries established from microdissected chromosomal material (31, 32) (*Figure 6*C), as well as genomic DNA of somatic cell hybrids containing pieces of human chromosomes (e.g. 'radiation induced hybrids') (33, 34). Alternatively, species-specific polymerase chain reaction (PCR) amplification products from such hybrids constitute probe sets of high quality (see also Section 7).

2. Specimen preparation

A number of specimen preparation techniques are compatible with fluorescence *in situ* hybridization. For specimen preparation for more specialized applications (such as studies of numerical and structural chromosome aberrations in tissue sections from solid tumours and three-dimensional chromosome analysis directly in the cell nucleus) the reader is referred to the literature (35–37). Painting procedures and mapping of DNA probes on metaphase chromosomes can be carried out using conventional methanol/acetic acid fixed metaphase spreads (see Chapter 2, Section 2). After chromosome spreading, the air-dried preparations are dehydrated in the following way:

(a) Put slides through a series of 70%, 90%, and 100% ethanol (10 min each) at room temperature.

(b) Air-dry again.

(c) Put slides in containers and keep at room temperature for short-term use.

or

Seal the containers in bags containing drierite and keep at −70°C (or −20°C) for long-term storage. In our experience slides can be stored at −70°C for at least one year without affecting their quality for *in situ* hybridization. Once a container has been thawed do not refreeze the slides.

Slides can also be stored in 70% ethanol for up to several weeks. Although it is generally believed that slides should age several days before performing an *in situ* hybridization, we have achieved good results with slides prepared the same day. However, in these cases baking of the slides for 2–3 h at 50–60 °C has been proved to better conserve chromosome morphology.

3. Labelling procedures

A number of sensitive non-isotopic labelling and detection procedures are available (for review see refs 6, 8). Because of their high sensitivity and commercial availability two techniques are routinely used in many laboratories: probe labelling with either biotin or digoxigenin as reporter molecules and indirect detection of hybridized probe via avidin or antibodies, (see right half of *Figure 1*). As nucleotides conjugated directly with fluorescent dyes are becoming commercially available, the *in situ* hybridization and direct detection of fluorochromated probes (see left half of *Figure 1*) provides an alternative procedure, which is particularly useful when large regions are targeted, i.e. for staining of repetitive DNA or for chromosome painting. Recently, several suppliers have started to offer chromosome specific probes labelled with biotin or fluorochromes. The commercial availability of probes for chromosomes and chromosomal sub-regions of interest in combination with commercial *in situ* hybridization and detection kits will facilitate the introduction of the new staining procedures even in cytogenetic laboratories which are not generally equipped for molecular cytogenetics.

Although a vast majority of vector sequences in a pool of probes can cause an increase in background, in the case of single probes there is usually no need for insert isolation. In our experience, the isolation of inserts from plasmid vectors, for example, prior to the labelling does not improve the results. It has been postulated that some vector sequences within a probe will facilitate the formation of a network of probe fragments at the site of hybridization and thus increase the signal intensity.

Labelling by enzymatic incorporation of modified nucleotides is much more efficient than labelling by incubation with reactive compounds, such as photobiotin. Prokaryotic polymerases used for different nucleic acid labelling procedures accept unmodified nucleotides better than they accept modified nucleotides. Therefore they incorporate modified nucleotides only up to a certain level. In our experience, the non-isotopic labelling efficiency of primer extension (38) and nick-translation (see *Protocol 1*) is comparable. Another important requirement for a good *in situ* hybridization probe is the size of the probe molecules obtained after the labelling reaction. The molecules should be between 100 and 500 nucleotides in length. This size range can be easily obtained by adjusting the DNase concentration in a nick-translation reaction. Therefore, we prefer nick-translation for labelling, especially because long

genomic fragments as template in a primer extension reaction often result in probe molecules of a higher size-range.

3.1 Biotinylation by nick-translation

This protocol is based on the work of Langer *et al.* (39). Since labelled probes can be stored for long periods (at −20°C) without affecting the probe quality, large probe amounts can be labelled at one time. A standard reaction is carried out with 2 μg template DNA in 100 μl volume. The solution with the prepared DNA template should be free of RNA. During the establishment of the labelling procedure in a laboratory, when new reagents are prepared, or when no *in situ* hybridization signal can be found, it is advisable to perform a dot-blot assay to test the biotin labelling (*Protocol 2*).

Protocol 1. Nick-translation

Materials

- 10 × buffer containing 0.5 M Tris–HCl pH 8.0, 50 mM $MgCl_2$, 0.5 mg/ml BSA.
- 0.1 M β-mercaptoethanol. Dilute 0.1 ml of β-mercaptoethanol with 14.4 ml double-distilled water.
- 10 × nucleotide stock containing 0.5 mM dATP, 0.5 mM dGTP, 0.5 mM dCTP and 0.5 mM biotin-11-dUTP.[a]
- DNase I solution. Dissolve 3 mg DNase I in 0.5 ml 0.3 M NaCl, add 0.5 ml glycerol, store at −20°C. Dilute 1 μl of this stock solution in 1 ml of ice-cold water *immediately* before use.[b]
- Column buffer containing 10 mM Tris–HCl pH 8.0, 1 mM EDTA and 0.1% SDS.
- Resin for spin column. Disperse 30 g of Sephadex G-50 (medium) in 300 ml of column buffer containing 0.1% SDS[c] and incubate for several hours at 95°C or autoclave.

Method

1. Combine:
   - RNA-free DNA solution containing 2 μg DNA
   - 10 μl of 10 × buffer
   - 10 μl of 0.1 M β-mercaptoethanol
   - 10 μl 10 × nucleotide stock
   - tested volume of DNase I solution[b]
   - 20 units *Escherichia coli* DNA polymerase I

   adjust to 100 μl with double-distilled water (enzymes should be added last)

Protocol 1. *Continued*

2. Incubate the reaction for 2 h in a 15°C water bath.
3. Put the reaction on ice, and keep it on ice until the actual size of the probe molecules is determined.
4. Take an aliquot of 7 μl, add gel loading buffer to the aliquot, denature it by incubation in a boiling water bath for 3 min, put the tube on ice for 3 min, load the aliquot on a standard 2% agarose minigel along with a suitable size marker, quickly run the gel (e.g. 15 volts per centimetre for 30 min) to avoid renaturation of the probe in the gel, visualize DNA in the gel, e.g. by staining in 0.5 μg/ml ethidium bromide, and take photographs during UV illumination.
5. The probe molecules will be visible as a smear. This should contain only fragments smaller than 500 nt and larger than 100 nt. A peak intensity at 250–300 nt seems optimal.
   (a) If the DNA is between 100–500 nt, proceed to step 6;
   (b) if the probe is larger, add more DNase I to the reaction kept on ice, incubate further at 15°C (usually higher concentrations of DNase are added for a further 30 min incubation) and repeat the previous step 4;
   (c) if the DNA is not or almost not digested, purify probe and repeat again starting from step 1;
   (d) if part of the DNA is smaller than 100 nt, repeat starting from step 1 using less volume of DNase I dilution;
   (e) if all the DNA is smaller than 100 nt, purify probe from possible contaminating DNase and repeat again starting from step 1.
6. For enzyme inactivation add 3 μl of 0.5 M EDTA (15 mM final concentration), 1 μl 10% SDS (0.1% final concentration), and heat for 15 min at 68°C.
7. Separate labelled probe from unincorporated nucleotides by gel filtration using a spin column.
   (a) Take a 1-ml syringe; remove the stamp; put a plug of silanized glass wool (2–3 mm high) at the bottom of the syringe.
   (b) Pack the syringe with buffered Sephadex G-50 resin to the 1-ml mark.
   (c) Put the column in a 15-ml tube and spin in a clinical centrifuge at 1600 *g* for 5 min.
   (d) Remove flow through, pack again to the 1-ml mark when necessary, spin as before,
   (e) Load 100 μl column buffer and spin again.
   (f) Repeat this step two more times.
   (g) The flow through after the third wash of the column should have the same volume as the loaded buffer, i.e. 100 μl. Put a small reaction tube in the 15-ml tube underneath the syringe, load the sample, and spin as before. The flow through now contains the labelled probe at a

concentration of approximately 20 ng/μl. In this form the labelled probe is ready to use or can be frozen for long-term storage.

Biotinylated DNA should not be subjected to phenol extraction, since the DNA will be lost in the phenol phase or the phenol/water interphase due to the hydrophobicity of biotin.

[a] There are also biotinylated nucleotides other than biotin-11-dUTP commercially available. Linker arms longer than 11 (e.g. biotin-14-dXTP or biotin-16-dXTP) are also appropriate to label *in situ* hybridization probes. When the modified nucleotide is different, e.g. biotinylated dATP, substitute the 0.5 mM dATP with 0.5 mM biotinylated dATP, and 0.5 mM biotin-11-dUTP with 0.5 mM dTTP, respectively.

[b] The volume of the diluted stock that is used in the nick-translation reaction must be tested for each new batch of DNase I stock solution. Carry out a series of digestions with 2 μg of a probe DNA, 10 μl 10 × buffer, 10 μl β-mercaptoethanol, and 1 μl, 2.5 μl, 5 μl or 10 μl of the DNase I dilution, respectively, in a volume of 100 μl. Incubate for 2 h at 15°C. Thereafter, take an aliquot of 7 μl and test the size of the digested DNA as described (step 4 in *Protocol 1*). Choose the volume of DNase that resulted in probe fragments of 100–500 nt in length for the nick-translation reaction (see step 1 in *Protocol 1*). The DNase stock should be diluted (1:1000) immediately before applying to the nick translation reaction. Discard the remainder of the dilution.

[c] SDS has to be included because the biotinylated probe might otherwise stick in the column due to the hydrophobic biotin groups.

Protocol 2. Dot-blot assay to test biotin labelling

This simple colorimetric assay is designed to test the quality of biotinylation of a probe. Commercial kits for this dot-blot assay are available.

Materials

- DNA dilution buffer containing 0.1 mg/ml sheared salmon sperm DNA and 6 × SSC (1 × SSC: 0.15 M NaCl, 0.015 M Na_3 citrate, pH 7.0).
- Prepare a series of dilutions of biotinylated standard DNA (purchased standard or previously used, well-labelled probe) in DNA dilution buffer (see above) resulting in solutions of 0, 1, 2, 5, 10, and 20 pg/μl standard DNA.
- AP 7.5 buffer containing 0.1 M Tris–HCl pH 7.5, 0.1 M NaCl and 2 mM $MgCl_2$.
- AP 9.5 buffer containing 0.1 M Tris–HCl pH 9.5, 0.1 M NaCl and 50 mM $MgCl_2$.
- Blocking buffer containing 3% BSA (fraction V) in AP 7.5 buffer.
- TE buffer containing 10 mM Tris–HCl pH 7.5 and 1 mM EDTA.
- Prepare or buy 75 mg/ml nitroblue tetrazolium in 70% dimethylformamide and 50 mg/ml 5-bromo-4-chloro-3-indolyl phosphate in dimethylformamide.

Method

1. Prepare a series of dilutions of biotinylated test DNA in DNA dilution

Protocol 2. *Continued*

buffer (see above) resulting in solutions of 0, 1, 2, 5, 10, and 20 pg/μl test DNA.

2. Spot 1-μl aliquots of the different concentrations of test DNA in parallel with 1-μl aliquots of the same concentrations of the standard DNA on a small piece of nitrocellulose filter (e.g. 3 × 4 cm).
3. Bake the filter for 30–60 min at 80°C.
4. Wash the filter with AP 7.5 buffer for 1 min at room temperature in a dish.
5. Seal the filter in a plastic bag together with 5–10 ml blocking buffer, and incubate for 30–60 min at 37°C.
6. Open the bag at one end, squeeze out the blocking buffer, fill in a freshly prepared solution of streptavidin-conjugated alkaline phosphatase (dilute streptavidin-conjugated alkaline phosphatase to 1 μg/ml in AP 7.5 buffer), seal the bag again and incubate for 30 min at 37°C.
7. Take the filter out of the bag and wash at room temperature in a dish with AP 7.5 buffer 2 × for 5 min followed by a wash with AP 9.5 buffer for 10 min (agitate).
8. Seal the filter in a plastic bag together with 7.5 ml substrate buffer *freshly* prepared in the following way: Add 33 μl of nitroblue tetrazolium (NBT) to 7.5 ml AP 9.5 buffer, mix gently, add 25 μl of 5-bromo-4-chloro-3-indolyl phosphate (BCIP) and mix gently again (do not vortex!). Incubate in the dark at 37°C or, alternatively, at room temperature (to slow down the reaction) until colour development is suitable. Usually 15–60 min is sufficient whereas longer incubation often results in higher background.
9. To stop the reaction, take the filter out of the bag and wash at room temperature (agitate) in a dish with TE buffer followed by air-drying.
10. Evaluate the colour signals. In order to be suitable for *in situ* hybridization, the spotted test probe should give signals of similar intensities as the spotted standard DNA of the corresponding concentrations. If the labelling was good and the assay worked well even 1 pg of labelled probe is visible.

3.2 Digoxigenin-labelling by nick-translation

For simultaneous hybridization/dual colour detection usually biotin labelled probes are combined with alternatively labelled probes. A very popular alternative non-isotopic technique is the digoxigenin based detection system (40). Digoxigenin labelling of DNA probes is carried out exactly the same

way as biotinylation by nick-translation (see *Protocol 1*) with one exception: 10 × nucleotide stock contains:

- 0.5 mM dATP
- 0.5 mM dGTP
- 0.5 mM dCTP
- 0.375 mM dTTP, and
- 0.125 mM digoxigenin-11-dUTP

Furthermore, when the dot-blot assay is carried out to test the labelling with digoxigenin, *Protocol 2* is used, but anti-digoxigenin antibody-conjugated alkaline phosphatase is used instead of streptavidin-conjugated alkaline phosphatase (step 6).

4. *In situ* hybridization and detection

4.1 Standard protocol for *in situ* hybridization

This procedure, comprising *Protocols 3–6*, is used when all the sequences of a probe should contribute to the hybridization signal, such as chromosome specific repetitive DNA probes, unique c-DNAs or genomic DNA fragments without IRS sequences. In the following the protocol is given for a 10 μl hybridization volume. This can be conveniently used when a 18 mm^2 coverslip is applied to cover the hybridization mixture on the slide. When larger areas are to be hybridized, scale up the solutions accordingly.

4.1.1 Probe mixture and probe denaturation

When very small volumes of DNA solutions (1 or 2 μl) are added, the DNA can be lyophilized before resuspension in formamide. With increasing volumes of DNA solution, we usually get less background in the hybridizations when precipitating the DNA before resuspension in formamide.

Protocol 3. Probe mixture and probe denaturation

Materials

- 3 M sodium acetate pH 5.0.
- Deionize formamide (several batches from several sources should be tested) using ion exchange resin (e.g Dowex XG8).
- Hybridization buffer containing 4 × SSC and 20% dextran sulphate. Prepare 20 × SSC and 50% dextran sulphate solutions. Dissolve dextran sulphate thoroughly, then autoclave it or filter it through a nitrocellulose filter. Combine 200 μl of 20 × SSC and 400 μl of 50% dextran sulphate with 400 μl of double-distilled water. Store at 4°C. Pipette carefully because dextran sulphate is very viscous.

Protocol 3. *Continued*

Method

1. Lyophilize 10–20 ng of labelled probe of a chromosome specific repeat cluster.

   or

   precipitate 20–60 ng of labelled single-copy DNA[a]. Add 1/20th vol. of 3 M sodium acetate and 2 vol. of ethanol, mix well, incubate at −70°C for 30 min, spin in Eppendorf centrifuge for 15 min; discard the supernatant (in most cases the small pellets are visible); wash the pellet by adding 400 μl 70% ethanol; spin for 5 min; discard the supernatant; lyophilize.
2. Resuspend in 5 μl of deionized formamide by vortexing or vigorously shaking for several minutes. Note that biotinylated DNA dissolves better in formamide than in water.
3. Add 5 μl of hybridization buffer and mix well. During this step, proceed with chromosome denaturation (see *Protocol 4*).
4. Denature the probe DNA by incubation at 75°C for 5 min followed by chilling on ice for approximately 5 min. Apply to denatured chromosomes (see *Protocol 4*).

[a] As an option 5 μg of sheared salmon sperm DNA can be added as carrier to any of these probes and could be co-lyophilized or co-precipitated with the probe.

Protocol 4. Chromosome denaturation

Materials

- Denaturation solution containing 70% deionized formamide and 2 × SSC. Check the pH value and adjust it to approximately pH 7.0, if necessary.
- 70% ice-cold ethanol.
- 90% ice-cold ethanol.
- 100% ice-cold ethanol.

Method

1. Label the area to be hybridized on the slide by scratching on the under side of the slide with a diamond pen.
2. Pre-warm the slides to 50–60°C in an incubator in order to prevent dropping of the temperature when the slides are put into the denaturation solution.

3. Add denaturation solution into a Coplin jar and heat it in a water bath to 70°C. Check temperature with a thermometer inside (!) the Coplin jar (the temperature should not drop below 68°C).
4. Put pre-warmed slides into the denaturation solution and incubate for *exactly* 2 min.
5. Transfer the slides to a Coplin jar (on ice) with cold 70% ethanol; incubate for 3 min.
6. Transfer the slides to a Coplin jar (on ice) with cold 90% ethanol; incubate for 3 min.
7. Transfer the slides to a Coplin jar (on ice) with cold 100% ethanol; incubate for 3 min.
8. Air-dry the slides.

When chromosomes are over-denatured, they usually look fuzzy when counterstained with propidium iodide or DAPI. Very bright staining with these dyes might be an indication of insufficient chromosomal denaturation.

Protocol 5. Hybridization

Method

1. Add 10 μl hybridization mixture with denatured probe to denatured chromosome preparation.
2. Put an 18 mm^2 coverslip on the hybridization mixture droplet. Avoid air bubbles!
3. Seal the edges of the coverslip with rubber cement.
4. Transfer the slides into a wet chamber (lidded dish with wet paper towels at the bottom and a frame to put slides on) and incubate at 37°C overnight.

Protocol 6. Detection

During the whole procedure the slides should never get dry.

Materials

- Washing solution A containing 50% formamide (does not need to be deionized) and 2 × SSC, pre-warmed to 42°C.

Protocol 6. *Continued*

- Washing solution B consisting of 1 × SSC (this concentration can vary according to the stringency for a particular probe; see below), pre-warmed to 60°C.
- Blocking solution containing 4 × SSC and 3% BSA (fraction V). Alternatively, dry fat milk (supplied as powder) can be used instead of BSA.
- Detection cocktail containing 4 × SSC, 1% BSA, and 0.1% Tween 20.
- Washing solution C containing 4 × SSC and 0.1% Tween 20, pre-warmed to 42°C.
- Counterstaining solution containing 2 × SSC and 200 ng/ml propidium iodide, or 200 ng/ml DAPI, or 200 ng/ml of both counter-stains.[a]
- Washing solution D containing 2 × SSC and 0.05% Tween 20.
- Antifade-mounting medium. Dissolve 0.233g 1,4-diazobicyclo (2.2.2) octane (DABCO) in 800 μl double-distilled water, add 200 μl 1 M Tris–HCl pH 8.0, add 9 ml glycerol and mix by inverting. Store in the dark at 4°C. By applying this solution the bleaching of fluorochromes after excitation is considerably decreased (41).

Method

1. Take the slides out of the wet chamber and carefully remove the rubber cement using forceps.
2. Transfer the slides into a Coplin jar containing washing solution A pre-warmed to 42°C, agitate in shaking water bath for 10–15 min (until the coverslips slide off).
3. Transfer the slides, without coverslips, into a new Coplin jar with washing solution A and agitate for 5 min.
4. Change the pre-warmed washing solution A twice more and shake for 5 min each.
5. Change three times into pre-warmed (60°C) washing solution B and shake for 5 min each.
6. Take the slides out of the Coplin jar, drain them as efficiently as possible by absorbing solution from the slide edges with a paper towel, and add 200 μl blocking solution. Cover with a 22 × 40 mm coverslip.
7. Transfer the slides into a wet chamber and incubate for 30 min at 37°C.
8. Lift up each slide and let the coverslip slide off, drain excess fluid as described above, and add 200 μl detection cocktail containing fluorochrome-conjugated detection reagent.[b] Cover with a 22 × 40 mm coverslip.[c]

   Higher signal intensities of digoxigenin labelled probe can be achieved by an indirect immunofluorescence detection (42). In this case substitute step 8 by the following procedure:

i. Lift up the slide to let the coverslip slide off, drain it as thoroughly as possible by absorbing solution from the slide edges with a paper towel, and add 200 μl detection cocktail containing 3 μg/ml sheep anti-digoxigenin antibody.

ii. Lift up the slide to let the coverslip slide off, and put it in a Coplin jar with pre-warmed washing solution C. Agitate at 42°C for 5 min.

iii. Change the washing solution twice more and shake for 5 min at 42°C.

iv. Take each slide out of the Coplin jar, drain it as described above and add 200 μl detection cocktail containing 3 μg/ml fluorochrome-conjugated anti-sheep antibodies. Cover with a 22 × 40 mm coverslip.

9. Transfer the slides into a wet chamber and incubate for 30 min at 37°C.

10. Lift up each slide and let the coverslip slide off, and put it in a Coplin jar with pre-warmed washing solution C. Agitate at 42°C for 5 min.

11. Change the washing solution twice more and shake for 5 min at 42°C.

12. Put into a Coplin jar (wrapped with aluminium foil) containing counterstaining solution and agitate at room temperature for 15 min.

13. Exchange counterstaining solution with washing solution D and incubate for 1 min (room temperature).

14. Take each slide out of the Coplin jar, drain excess fluid with a paper towel, and add 30 μl anti-fade solution. Cover with a 22 × 40 mm coverslip, avoiding air bubbles. Drain the edges of the coverslip and put the slide into a dark container. Short-term storage is carried out at room temperature and long-term storage at 4°C.[d]

[a] When rhodamine or Texas red is used for probe detection propidium iodide cannot be used as counterstain due to overlapping emission spectra of the fluorochromes. For the same reason AMCA and DAPI cannot be combined. In standard reactions, we detect a probe with FITC and counterstain with propidium and DAPI simultaneously (see also Section 5).

[b] For probe detection of biotinylated probe usually 5 μg/ml avidin-FITC is used. However, when different fluorochromes are to be applied, the same concentration of avidin–rhodamine, avidin–AMCA, etc., can be used. For detection of digoxigenin labelled probe 3 μg/ml of FITC-conjugated (or rhodamine-conjugated) anti-digoxigenin antibody is used. When biotin and digoxigenin labelled probes were hybridized simultaneously, both detection reagents, e.g. avidin–rhodamine and FITC-conjugated anti-digoxigenin, can be added simultaneously to the detection cocktail.

[c] Keep slides in the dark as much as possible after fluorochrome reagents have been applied.

[d] After microscopic inspection, the slides can be subjected to a signal amplification procedure (see Section 4.3).

In order to obtain specific signals from sequences with homologies to other chromosomal regions, it might be necessary to vary the stringency of the procedure. This is especially true for chromosome specific alphoid DNA repeats. Practically, the stringency can be increased best by decreasing the

salt concentration (e.g. 2 × SSC instead of 4 × SSC in the hybridization buffer in *Protocol 3*) or increasing the formamide concentration (e.g. from 50 to 70%) during the *in situ* hybridization. Furthermore, the post-hybridization washes (*Protocol 6*, step 5, can be carried out at higher stringencies by using lower salt concentrations (0.3 × SSC or even 0.1 × SSC as washing solution B).

4.1.2 Detection by a colorimetric assay

Commercial kits are available for a number of detection assays using alkaline phosphatase or horse-radish peroxidase conjugated to the detection reagent (avidin or antibodies). For visualization various substrates for the enzymes are used, which are converted by the enzymatic activity to products forming coloured precipitates. The procedures are very similar for the various combinations of enzymes and substrates. *Note*: most substrates of these enzymes, including 3,3-diaminobenzidine-tetrahydrochloride (DAB), are hazardous; use gloves and take care of the waste material. A protocol for using horse-radish peroxidase as enzyme and DAB as substrate is given below. The procedure corresponds to the above detection procedure (*Protocol 6*) until step 6.

Protocol 7. Detection by a colorimetric assay

Materials

- Blocking solution containing phosphate-buffered saline (PBS) (137 mM NaCl, 2.7 mM KCl, 8.5 mM Na_2HPO_4 and 1.5 mM KH_2PO_4, pH 7.0) and 3% BSA (fraction V).
- Detection solution containing PBS, 1% BSA and 0.1% Tween 20.
- Washing solution containing PBS and 0.1% Tween 20, pre-warmed to 42°C.
- DAB/H_2O_2 staining solution. Combine 3 ml PBS, 30 μl DAB stock solution (50 mg DAB per millilitre of water), and 15 μl H_2O_2 immediately before use.

Method

1. Perform post-hybridization washes as described in *Protocol 6*, steps 1 to 5.
2. Take the slides out of the Coplin jar, drain as efficiently as possible by absorbing solution from the slide edges with a paper towel, and add 200 μl blocking solution. Cover with a 22 × 40 mm coverslip.
3. Transfer the slides into a wet chamber and incubate for 30 min at 37°C.
4. Lift up each slide and let the coverslip slide off, drain excess fluid as

described above, and add 200 μl detection solution containing 5 μg/ml of streptavidin. Cover with a 22 × 40 mm coverslip.[a]

5. Transfer the slides into a wet chamber and incubate for 30 min at 37°C.
6. Lift up each slide and let the coverslip slide off, and put it in a Coplin jar with pre-warmed washing solution. Agitate at 42°C for 5 min.
7. Change the washing solution twice more and shake for 5 min at 42°C.
8. Take each slide out of the Coplin jar, drain excess fluid as described above, and add 200 μl detection solution containing 3 μg/ml biotinylated horse-radish peroxidase. Cover with a 22 × 40 mm coverslip.
9. Transfer the slides into a wet chamber and incubate for 30 min at 37°C.
10. Lift up each slide and let the coverslip slide off, and put it in a Coplin jar with pre-warmed washing solution. Agitate at 42°C for 5 min.
11. Change the washing solution twice more and shake for 5 min at 42°C.
12. Incubate in the dark with DAB/H_2O_2 staining solution for 10–20 min, or until sufficient substrate precipitate has accumulated, at room temperature.
13. Wash briefly in PBS, counterstain if necessary and mount as described in *Protocol 6*.
14. Evaluate the precipitated DAB product by transmission light microscopy.[b]

[a] Note that some suppliers offer a complex of streptavidin and biotinylated horse-radish peroxidase. In this case steps 6 to 9 are omitted. However, this complex may penetrate insufficiently into nuclei.
[b] For combination with chromosome banding (*Figure 7*) see Section 5.3.

4.2 Chromosomal *in situ* suppression (CISS) hybridization

This protocol is used when genomic DNA fragments (generally all genomic probes) or cDNAs containing IRS sequences are used as probe. The general difference to the standard protocol is the combination of probe and competitor DNA and an additional pre-annealing step after probe denaturation. Again the protocol is given for a 10 μl hybridization volume.

Depending on the complexity of the probe or target sequences, different concentrations of labelled probe are used. The following guide-lines have proved to be useful for determining the probe amount. Amounts below are given for 10 μl hybridization volumes:

- Single cosmids, plasmids, or phages — 20–60 ng
- Band specific probe pools — 100–200 ng
- Gel-purified single YACs — 50 ng
- Total yeast DNA containing a YAC — 1 μg

• Isolated inserts of a library derived from individual sorted human chromosomes		50–250 ng
e.g.	F- and G-group chromosomes	50 ng
	C-group chromosomes	150–200 ng
	A-group chromosomes	250 ng
• Total DNA from a library derived from individual sorted human chromosomes		
when vector to insert ratio is ~1:1		150–500 ng
e.g.	F- and G-group chromosomes	150 ng
	C-group chromosomes	300–350 ng
	A-group chromosomes	500 ng
when vector to insert ratio is ~10:1		0.5–2 μg
e.g.	F- and G-group chromosomes	0.5 μg
	C-group chromosomes	1–1.5 μg
	A-group chromosomes	2 μg

Protocol 8. Chromosomal *in situ* suppression hybridization

Materials

- 1 μg/μl salmon sperm DNA sheared or DNase digested to a size of approximately 500 nt (commercially available).
- 1 μg/μl human placental DNA digested with DNase to a size of 200–500 nt (digestion as described in *Protocol 1*, or 1 μg/μl *Cot1* fraction of human DNA with the same size range (commercially available)).
- Solutions to be prepared for the *Protocols 3–6*.
- Labelled probe as above.

Method

1. Combine the labelled probe DNA with 1–3 μg human competitor DNA (total human or *Cot1* fraction) and add salmon sperm DNA to adjust to a total amount of 10 μg DNA.
2. Add 1/20th vol. of 3 M sodium acetate and 2 vol. of ethanol, mix well, incubate at −70°C for 30 min, spin in Eppendorf centrifuge for 15 min, discard supernatant, wash the pellet by adding 400 μl 70% ethanol, spin for 5 min, discard the supernatant, and lyophilize.
3. Resuspend the pellet (which is visible in most cases) in 5 μl of deionized formamide by vortexing or vigorously shaking for several minutes.
4. Add 5 μl of hybridization buffer (*Protocol 3*) and mix well. During this step proceed with chromosome denaturation (see *Protocol 4*).
5. Denature the DNA by incubation at 75°C for 5 min. During this step start

pre-warming the slides with the denatured chromosomes (see *Protocol 4*) to 42°C (heat a plate or use a metal tube in a water bath).

6. Transfer the tubes from 75°C quickly to 37°.
7. Incubate for 5–15 min to allow pre-annealing.
8. Apply the pre-annealed DNA solution to denatured chromosomes on pre-warmed slides.
9. Continue as described in *Protocols 5* and *6*.

4.3 Signal amplification

Some laboratories routinely use signal amplification procedures in order to detect fluorescence signals. The principle of this method is illustrated in *Figure 4*. The technique is based on binding of antibodies directed against the previously used detection reagent (avidin or antibody). The procedure can be either direct (left half of *Figure 4*) using one layer of fluorescently labelled antibodies, or indirect (right half of *Figure 4*) using one layer of antibodies conjugated with a reporter group and a second layer of fluorescent reagents directed against the reporter groups. In case of indirect amplification, usually the last detection reagent is the same as the one used for the primary detection; this procedure is therefore also referred to as sandwich amplification. It allows several cycles of amplification by using only two different reagents. Occasionally, we apply one cycle of sandwich amplification when probes are very small, resulting in weak signals. However, the amplification is not linear: while the signal intensity is increasing, the signal-to-noise ratio is decreasing. We recommend that signal amplification is performed only when slides are low in background. The protocol below, designed for the signal amplification of biotin labelled probes, is based on the work by Pinkel *et al.* (14).

Protocol 9. Signal amplification

Materials

- Washing solution C containing 4 × SSC and 0.1% Tween 20, pre-warmed to 42°C.
- Detection cocktail containing 4 × SSC, 1% BSA, and 0.1% Tween 20.

Method

1. Carefully remove the coverslip from the mounted slide (see Section 4.1).
2. Put the slides in a Coplin jar containing washing solution C, which is pre-warmed in a 42°C shaking water bath. Gently agitate for 10 min.
3. Change the washing solution C three more times and shake in 42°C for 10 min each.

Protocol 9. *Continued*

4. Take the slide out of the Coplin jar, drain it as thoroughly as possible by absorbing solution from the slide edges with a paper towel, and add 200 μl detection cocktail containing 1–5 μg/ml biotinylated anti-avidin antibodies. Cover with a 22 × 40 mm coverslip.
5. Transfer the slide into a wet chamber and incubate for 30 min at 37°C.
6. Lift up the slide to let the coverslip slide off, and put it in a Coplin jar with pre-warmed washing solution C. Agitate at 42°C for 5 min.
7. Change the washing solution twice more and shake for 5 min at 42°C.
8. Take the slide out of the Coplin jar, drain it as described above, and add 200 μl detection cocktail containing 5 μg/ml avidin-conjugated fluorochrome (e.g. avidin–FITC). Cover with a 22 × 40 mm coverslip.
9. Repeat washing as before, see steps 6 and 7.
10. Counterstain chromosomes and mount as described above (*Protocol 6*).

5. Chromosome counterstaining and banding

The rapid and precise relative mapping of fluorescently labelled probes along counterstained chromosomes has been demonstrated (42). By a combination of *in situ* hybridization to prometaphase chromosomes with digital imaging microscopy (see Section 6) numerous probes can be ordered using mapping coordinates defined in the following way: the distance between the signal and a reference point is given as the fraction of the length of the total chromosome or a sub-chromosomal region. For example, an 'FLpter' value is the fractional length of a chromosome with reference point pter. It should be noted that the ISCN banding ideograms (43) are not normalized relative to the fractional length of chromosomes. Therefore, mapping coordinates defined by fractional length values cannot be extrapolated from the ISCN ideograms in order to define them as a band locus. However, this approach is very useful to map the relative chromosomal position of multiple probes (for further discussion see ref. 8).

To verify a chromosome assignment, co-hybridization with a probe or probe set known to map to the target chromosome of interest can be easily performed (preferably by a dual colour experiment). In order to express mapping data in terms of classical cytogenetic terminology, banding methods can be combined with non-isotopic *in situ* hybridization protocols. Fluorescence banding with a fluorochrome that emits in a range different to the fluorochrome used for probe detection is advantageous since it does not require a relocation of chromosomes. Banding by quinacrine, Hoechst 33258 chromomycin A_3 or DAPI (see Chapter 4 and ref. 44) can easily be

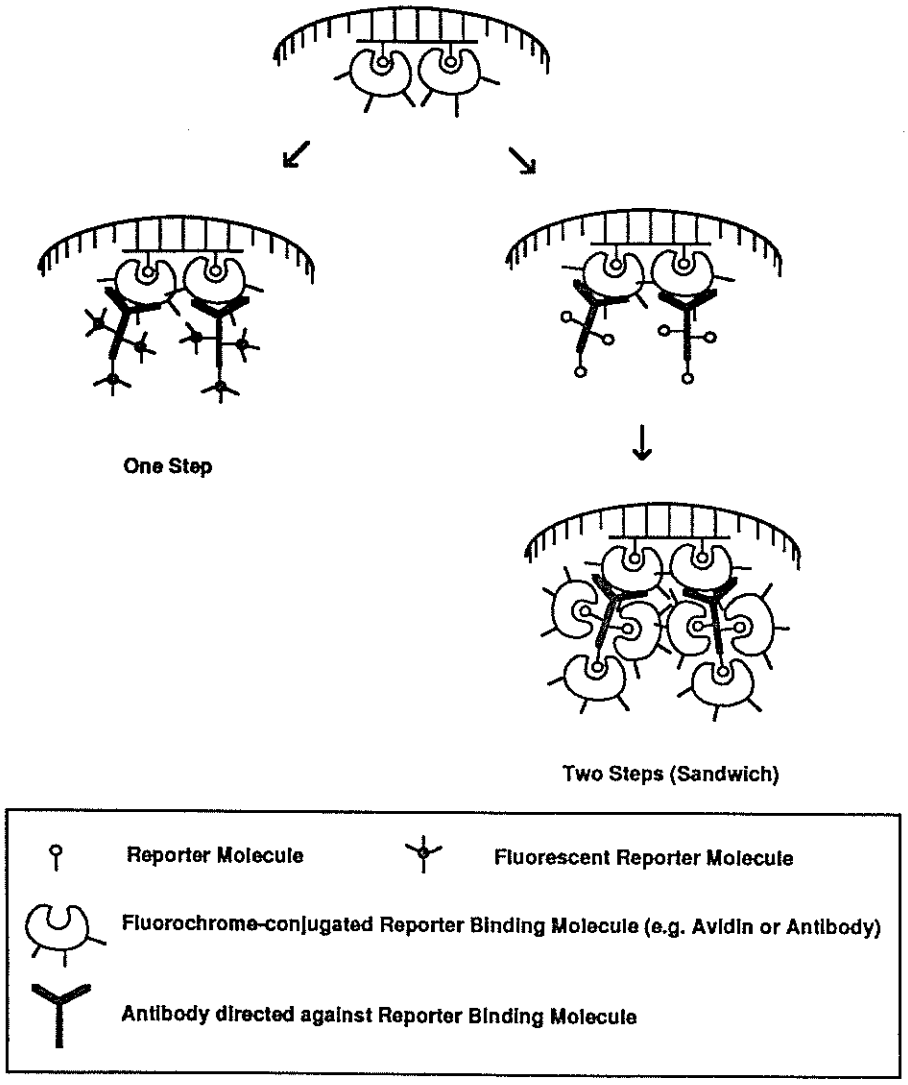

Figure 4. Schematic illustration of a signal amplification procedure. For further explanation see text.

performed after the hybridization/detection procedure (*Protocol 6*, step 6). On heat-denatured chromosomes, staining with DAPI alone, i.e. without additional stains such as actinomycin or distamycin, results in a differential Q-banding-like pattern of good quality (see *Figure 5*, panel B; see also ref. 45). However, differences in the staining pattern of heterochromatin by DAPI and quinacrine should be noted. Unfortunately, it is often difficult to document DAPI-banding by conventional photography. Due to the heat

denaturation of the chromosomes, a differential staining is also achieved with propidium iodide, resulting in an R-banding-like pattern. This banding is often pale (see *Figure 3*, A and C) and in our hands the quality has been very variable. Propidium iodide staining in combination with fluorescent replication banding (see *Protocol 11*), however, results in high quality banding (46, 47).

5.1 Alu-banding

Distinct chromosomal banding patterns can be produced by *in situ* hybridization with DNA probes for interspersed repetitive elements (IRS). Co-hybridization of a DNA probe with IRS sequence(s) causes a simultaneous *in situ* hybridization banding profile (42, 48). For human chromosomes Alu repeats are very useful, generating an R-banding like banding pattern. Both cloned Alu sequences and sequences generated by IRS-PCR (see Section 7) have been reported as co-hybridization probes (42, 49). An example of a cosmid mapping in combination with Alu-banding is shown in *Figure 5*, panels A and C.

Protocol 10. Alu-banding

1. Prepare a 10-μl probe mixture and perform probe denaturation as described in *Protocol 3* (without competition) or *Protocol 8* (with competition), depending on the characteristics of the probe. When CISS hybridization is performed, use only 1 μg competitor DNA per 10 μl volume.
2. Prepare a 5 μl probe mixture with 100–300 ng Alu-enriched DNA (e.g. a cloned fragment containing Alu elements; see ref. 42) and perform denaturation as described in *Protocol 3*.
3. Combine mixtures from steps 1 and 2 prior to application on to slides with denatured chromosomes (*Protocol 4*).
4. Proceed as described in *Protocol 5*.

5.2 GTG-banding

Well-established banding techniques may be preferred. These techniques can be performed with fluorescence *in situ* hybridization prior (pre-banding) or after *in situ* hybridization (post-banding). In experienced hands, both approaches give excellent results. Pre-banding has the advantage that any interference of chromosomal heat denaturation with banding quality can be avoided. A disadvantage is the fact that metaphase spreads have to be relocated and photographed twice. For pre-banding we have followed the protocol described by Klever *et al.* (50). Two examples are shown in *Figure 6*. After routine trypsin–Giemsa (GTG) banding (see Chapter 4) the preparations are treated as shown in *Protocol 11*.

Protocol 11. De-staining and post-fixation of GTG-banded chromosomes

1. Embed the preparations in Eukitt.
2. Locate metaphases and take photographs.
3. Remove the embedding material and Giemsa stain by the following washes in Coplin jars:
   - xylol for 1 min
   - xylol/ethanol (1:1, v/v) for 1 min
   - methanol/acetic acid (3:1, v/v), two times for 5 min
4. Air-dry the slides.
5. Transfer the slides in a Coplin jar containing 3.7% formaldehyde in phosphate-buffered saline (PBS, pH 7), incubate for 10 min.
6. Wash in PBS, twice more for 5 min.
7. Air-dry again.
8. Proceed as described in *Protocol 4*.

The additional fixation results in improved preservation of chromosomal morphology during heat denaturation.

5.3 Replication banding

For post-banding we can recommend replication banding procedures performed after 5-bromo-2′-deoxyuridine (BrdU) incorporation during S-phase. For details see refs 51 and 52.

Protocol 12. Fluorescent replication banding

1. Add BrdU and fluorodeoxyuridine (FdU) in a final concentration of 10 μg/ml and 0.5 μg/ml, respectively, to PHA-stimulated lymphocyte cultures from peripheral blood (see Chapter 2) after 65 h of cultivation.
2. Six hours later add colcemid to a final concentration of 0.05 μg/ml and cultivate cells for 30 min more.
3. Prepare metaphase spreads (see Chapter 2) and proceed with *in situ* hybridization as described above.
4. In the case of fluorescence *in situ* hybridization, the incorporated BrdU can be detected by simultaneous indirect immunofluorescence using monoclonal mouse-anti-BrdU antibodies for the first step and FITC- or TRITC-conjugated anti-mouse IgG antibodies for the second step. For this, proceed as described in *Protocol 6* (*indirect immunofluorescence* described under step 8 *i* to *iv*) with antibody concentrations according to the recommendations of the suppliers.

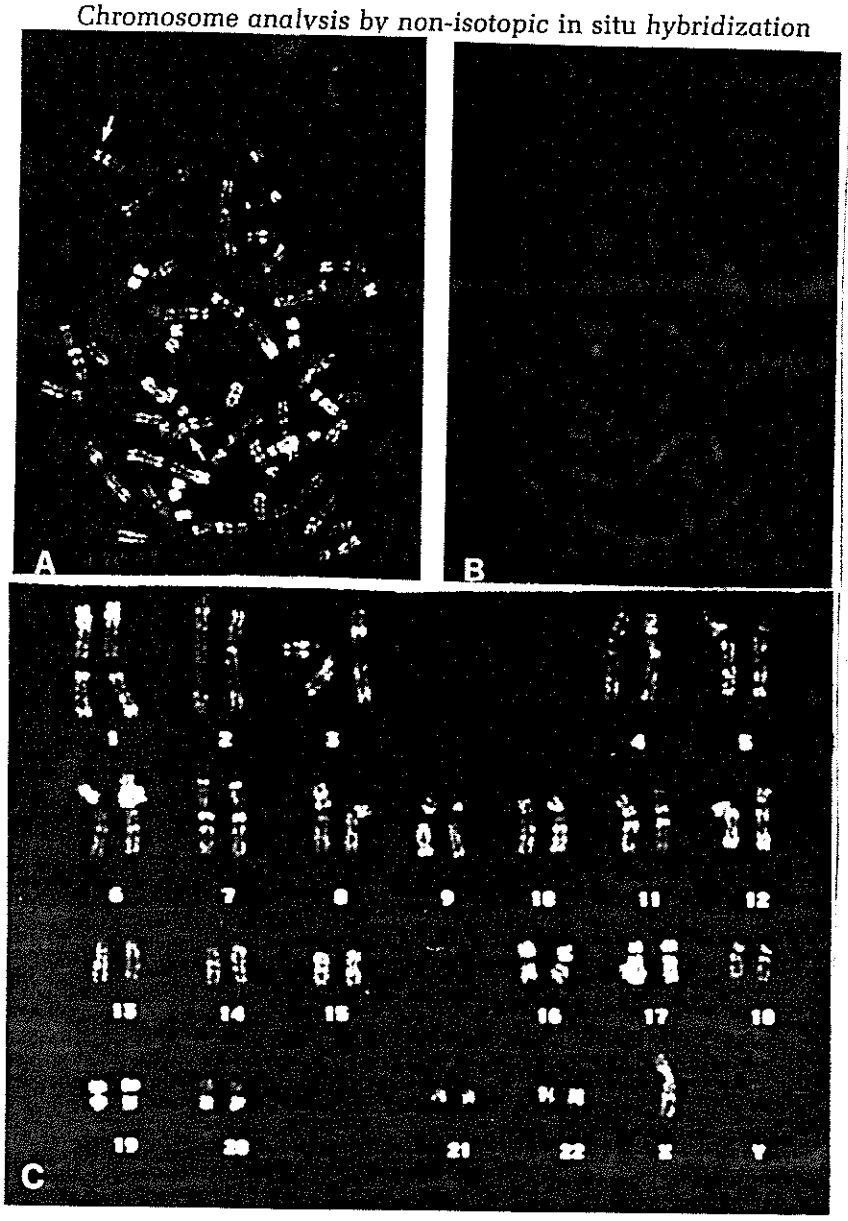

Figure 5. Simultaneous visualization of fluorescently labelled cosmid probe and Alu-banding. (A) Digoxigenin-labelled cosmid probe J1-2 (see ref. 42) and a biotin-labelled DNA probe containing four Alu-repeats were cohybridized and detected via rhodamine and FITC, respectively. Note the R-banding like pattern of the Alu probe signal. Chromosome identification and band assignment can easily be performed by using the Alu-banding. Cosmid J1-2 had been mapped by determining the fractional distance of the chromosome length (see text) to a chromosome region corresponding to 11p11.2. This is indeed the cytological map position, as the signal is within the brightly stained band 11p11.2 (see arrows). (B) DAPI-stain of the metaphase shown in A. Note, that the DAPI

If permanent staining is preferred, the Hoechst 33258–Giemsa technique can be applied to BrdU pulsed chromosome complements (53). This procedure has been used for isotopic techniques as well as non-isotopic techniques using permanent alkaline phosphatase or peroxidase (see Section 4.1.2) signal detection procedures (54, 55). Examples are shown in *Figure 7*. For a good banding quality it is important to adjust the pH of the solution used for heat denaturation of the chromosomes (see *Protocol 4*) to a range between pH 6 and pH 7, since a higher pH (>8) may result in massive swelling of the chromosomes (A. Brückner, unpublished observations). After signal detection, the slides are treated as described in *Protocol 13*.

Protocol 13. Permanent replication banding

Materials

- 33258 Hoechst-staining solution. Dissolve 5 mg of 33258 Hoechst in 100 ml 'Latt' buffer containing 0.15 M NaCl, 0.03 M KCl, 0.01 M phosphate (pH 7). Keep this stock solution in the dark at 4°C. Dilute in Latt buffer 1:200 just prior to use (final concentration 0.25 μg/ml).
- Giemsa solution. Combine 30 ml 67 mM KH_2PO_4, 30 ml 67 mM Na_2HPO_4, and 3 ml Gurr's–Giemsa stain R66.

Method

1. Perform steps 1–3 as described in *Protocol 12*.
2. Incubate the slides in a Coplin jar in the dark with 33258 Hoechst staining solution at room temperature for 15 min.
3. Briefly wash with water.
4. Put the slides into a dish, cover them with a thin layer of 2 × SSC just sufficient to prevent air-drying, and expose them to the light of a UV-mercury lamp.[a]
5. Incubate in 2 × SSC at 60°C for 90 min.

Figure 5 *cont.*
stain produces a Q-banding-like pattern in heat denatured chromosomes, even without further treatment (such as actinomycin). Whereas Alu-probes do not label centromeres and several pericentromeric regions, the DAPI-counterstain reveals the full chromosome continuum (compare panels A and B). (C) Complete karyotype of the Alu-banded metaphase in panel C (46,XY). Note, that the quality of the Alu-banding is superior to the DAPI-banding.
(Reprinted by permission of the publisher from Lichter, Boyle, Cremer, and Ward, *Genetic Analysis Techniques and Applications*, 8(4), pp. 24–35. Copyright 1991 by Elsevier Science Publishing Co., Inc.)

Protocol 13. *Continued*

6. Stain the slide with Giemsa solution for approximately 20 min or until a good differentiation is visible.
7. Air-dry and embed in Eukitt.

[a] For example, the authors use a 30 W lamp at a distance of 20 cm for 30 min.

6. Microscopy

Signals from painted whole chromosomes, stained sub-chromosomal regions, or localized single probes are generally visible when an epifluorescence microscope is used. Examples of photographs taken on a standard microscope are shown in *Figure 6*. Counting signals in interphase nuclei can easily be carried out with a standard equipment. Potential users who are inexperienced in the field of fluorescence microscopy should seek expert advice before they buy their own system. It is very important to have appropriate objectives and filter sets for the visualization of the essential fluorochromes. The most commonly used fluorochromes are (a) blue colour: DAPI (chromosome staining) and AMCA (conjugated to avidin, antibody, or nucleotides); (b) green colour: quinacrine (chromosome staining), FITC or bidopy (both conjugated); (c) red colour: propidium iodide (chromosome staining), rhodamine or Texas red (both conjugated). Filter sets for various fluorochromes are described elsewhere in this book (see Chapter 8). For some applications a filter set may be used which is very selective for a given fluorochrome, while in other applications filter sets may be used which allow the simultaneous detection of two fluorochromes, such as FITC for signal detection and propidium iodide for chromosome-staining (see *Figure 3*). Double band-pass filter sets have become available, which allow the simultaneous recording of fluorochromes, such as FITC and rhodamine. Such filter sets may become very important in two colour mapping experiments, when the geometric relation of two distinctly coloured sites have to be recorded as accurately as possible. A change of filter sets generally leads to more or less pronounced shifts, detectable for example after double exposure of photographic films (registration problem).

In order to exploit the full potential of multicolour fluorescence *in situ* hybridization in clinical and tumour cytogenetics, quantitative digital fluorescence microscopy is clearly needed. Digitized images are not only easier to handle but can also be subject to powerful image processing. Digital filtering procedures can facilitate the analysis considerably; for instance, by enhancing signal to noise ratios. When digital images (taken with different filter sets from the same object) are electronically overlayed, the registration problem is again evident. At present a perfect solution to this problem is not available. It is advisable to ask the commercial supplier for a special align-

ment of the emission filters of the different filter sets. In addition, internal reference points may be included in a specimen by point-like particles carrying the various fluorescent dyes. This could greatly facilitate the automated correction of misalignments by appropriate software.

Different camera systems allow the generation of digitized images. The currently most sensitive system is the cooled CCD (charged coupled device) camera. Examples of images generated by using a cooled CCD camera are shown in *Figure 5*. This device allows photon counting, and with longer integration times fluorescence signals can be detected which are not visible to the observer's eyes. This might improve the analysis of fluorescence *in situ* hybridization with probes smaller than 2 kb (see Section 1). For the recording of chromosome painting images less expensive camera systems will be sufficient.

Digitized images can also be generated using a confocal laser scanning microscope. Examples are shown in *Figure 3*. In contrast to CCD or video-camera systems, the confocal laser microscope can greatly reduce the out-of-focus fluorescence allowing generation of high quality optical sections through the labelled specimen. Therefore, if three-dimensional recording of fluorescent cellular specimens is needed, a laser confocal scanning microscope is the instrument of choice. Although at present this device is not as sensitive as the current cooled CCD systems, signals visible to the observer's eyes by conventional epifluorescence microscopy can be nicely imaged. The registration problem can be overcome by parallel excitation/emission of different fluorochromes in the dual channel mode. However, using the confocal laser scanning microscope, one is limited to the use of the fluorochromes which can be excited by the lasers available in the instrument. Most instruments today allow excitation of one or two fluorochromes (green and red fluorochromes) in the standard set-up. Additional laser equipment for three colour detection (i.e. an additional UV-laser for blue fluorochromes) is very costly. When only

Figure 6. (Overleaf). Combination of CISS hybridization and GTG-banding (A) CISS-hybridization of biotinylated human chromosome 5 specific bacteriophage DNA library sequences to a fibroblast metaphase spread from *Macaca fuscata*. The probe delineates the entire homologue macaque chromosome except for the centromeric heterochromatin. Lack of labelling may be due to rapid divergence in heterochromatic sequences during primate evolution (J. Wienberg, A. Jauch, R. Stanyon, and T. Cremer, unpublished observation). Note the visualization of the two chromosome 5 domains in the cell nucleus. (B) GTG banding of the *Macaca fuscata* metaphase spread shown in (A). (C) FITC-signals detected on a human lymphocyte metaphase spread after CISS-hybridization of biotinylated microlibrary DNA derived from 37 microdissected human chromosomes 8 (bands 8q23-8q24.1) kindly provided by B. Horsthemke. Big arrows indicate the labelled subregion on chromosome 8, small arrows point to a weak signal on chromosome 9q33. This minor signal could be explained by an occasional error made during the microdissection procedure. (Courtesy of C. Lengauer; for details see ref. 32). (D) GTG-banding of the metaphase spread shown in (C).

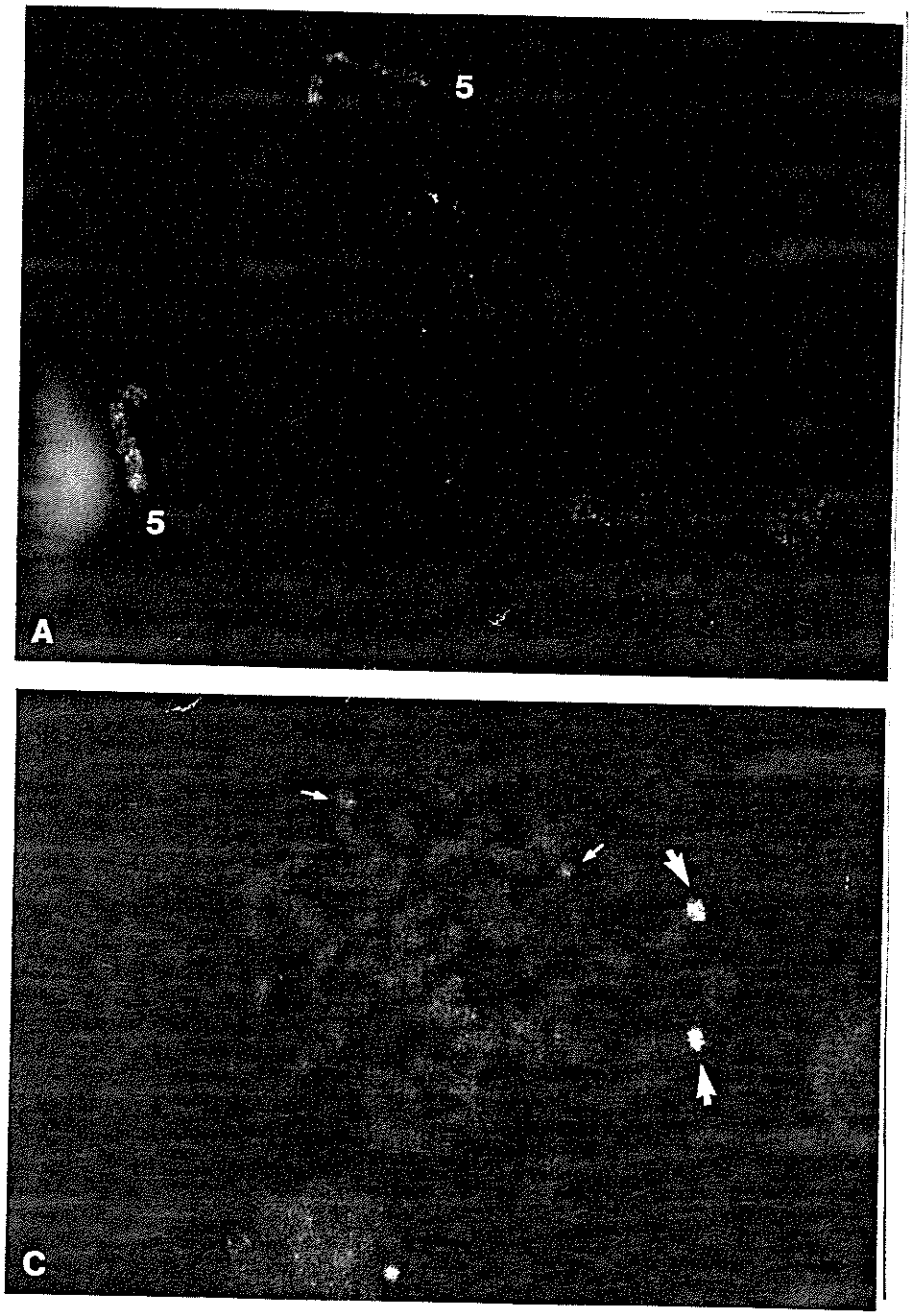
5
5
A
C

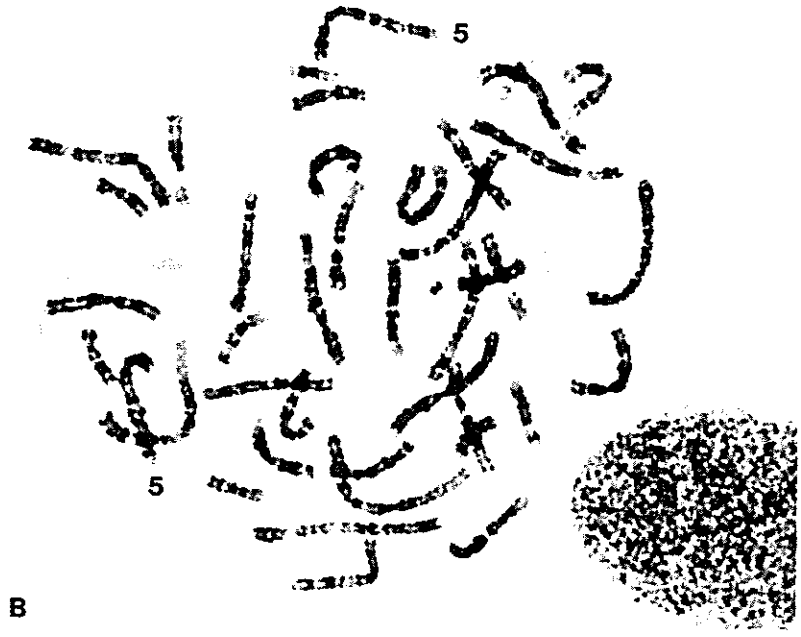

B

D

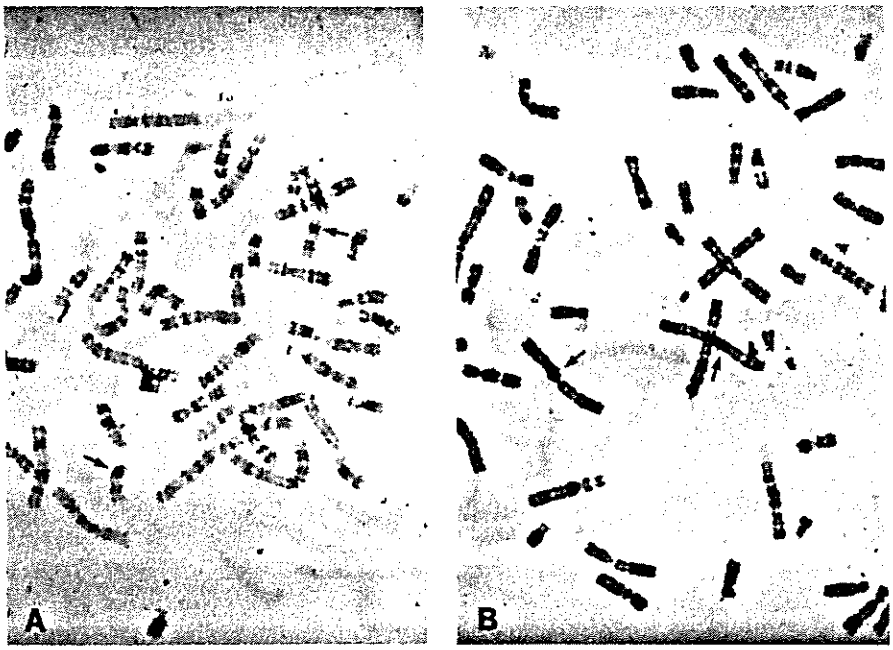

Figure 7. Combination of non-isotopic *in situ* hybridization and permanent replication banding. Male human lymphocyte metaphase chromosomes after Hoechst 33258–Giemsa replication banding and *in situ* hybridization with biotinylated probes L1.84 (A) and pUC1.77 (B) Colorimetric probe detection was carried out using horse-radish peroxidase. Arrows indicate the heterochromatic band 1q12 delineated by pUC1.77 and the pericentromeric heterochromatin of chromosome 18 delineated by L1.84. (Courtesy of A. Brückner.)

two-dimensional work is carried out, such as mapping of signals on metaphase chromosomes, the much cheaper CCD camera systems seem preferable.

When purchasing equipment for digital imaging microscopy, special attention should be paid to the computer hardware, in particular to memory and storage capacity, as well as software capability for specialized applications.

7. Advanced techniques and applications

Polymerase chain reaction (PCR) provides a rapid and easily applicable alternative means of generating DNA probes useful for the specific delineation of chromosomal regions. Oligonucleotide primers can be used to generate probes for chromosome specific sequences, such as chromosome specific DNA repeats (56, 57). IRS-PCR (interspersed-repetitive sequence – polymerase chain reaction) protocols have been applied to generate human DNA

probes from human-rodent somatic hybrid cells (58, 59) which are useful for chromosome painting (60, 61). This approach is based on oligonucleotide primers that anneal specifically to human specific subsequences within IRS, e.g. within Alu- or L1-elements. During the PCR, human sequences between appropriately located human Alu- or L1-elements are amplified. In this way, probes can be generated for human chromosome sub-regions of interest contained in hybrid cells or YACs.

The potential of almost all applications of *in situ* hybridization is greatly enhanced by multicolour detection of simultaneously hybridized probes. This is particularly useful when structural chromosome aberrations involving different chromosomal regions are to be diagnosed, or when several numerical aberrations should be detected in parallel. Three fluorochrome colours can be easily distinguished, and by combinations of three different labelling/detection procedures—i.e. by labelling single probes with one, two or three colours—an even higher number of targets can be distinguished (62). The advent of commercially available nucleotides directly conjugated with fluorochromes will improve the ability to combine multiple colours in one experiment. These nucleotides can be incorporated into DNA probes by nick-translation resulting in directly fluorochrome labelled DNA probes. Wiegant *et al.* (63) have demonstrated the feasibility of such an approach for rapid cosmid mapping. While the sensitivity of detection is somewhat reduced as compared to indirect detection procedures, background problems seem also considerably reduced.

Non-isotopic *in situ* hybridization to prometaphase chromosomes has become a powerful tool in the investigation of the linear order of DNA sequences located on a given metaphase or prometaphase chromosome (42). The maximum resolution which has been achieved in this way depends on the localization of the two target sites, e.g. in G- or R-bands, but targets which are considerably closer to each other than 1 Mb can generally not be ordered. To further improve the mapping resolution, chromosomal DNA can be analysed in more de-condensed states as, for example, in interphase nuclei. The average distance which can be measured between two point-like cosmid signals in interphase nuclei has been shown to increase linearly from 30 kb up to a distance of about 1 Mb (64, 65). Therefore, average distances between multiple probes could allow the indirect ordering of closely spaced probes.

An interesting alternative approach to *in situ* hybridization (as described in this chapter) is hybridization of oligonucleotide primers to cellular nucleic acids followed by primer extension in the presence of labelled nucleotides (66, 67). Although the general sensitivity of this assay has to be proven, it may allow the detection of allelic differences *in situ*. Choosing the appropriate primer or primer combination, sequence differences or small deletions could be detected by the presence or absence of signals.

Acknowledgements

We thank our colleagues Andreas Brückner, Anna Jauch, Johannes Wienberg, and Christoph Lengauer who have contributed unpublished material for illustrations to this chapter. We are grateful to David Ward for stimulating discussions.

References

1. Gall, J. G. and Pardue, M. L. (1969). *Proc. Natl. Acad. Sci. USA,* **63,** 378.
2. Gerhard, D. S., Kawasaki, E. S., Bancroft, F. C., and Szabo, P. (1981). *Proc. Natl. Acad. Sci. USA,* **78,** 3755.
3. Harper, M. E., Ullrich, A., and Saunders, G. F. (1981). *Proc. Natl. Acad. Sci. USA,* **78,** 4458.
4. Malcolm, S., Barton, P., Murphy, C., and Ferguson-Smith, M. A. (1981). *Ann. Hum. Genet.,* **45,** 135.
5. Buckle, V. J. and Craig, I. W. (1986). In *Human Genetic Diseases, A Practical Approach* (ed. K. E. Davies), p. 85. IRL Press, Oxford.
6. Raap, A. K., Dirks, R. W., Jiwa, N. M., Nederlof, P. M., and van der Ploeg, M. (1990). In *Modern Pathology of AIDS and Other Retroviral Infections* (ed. P. Racz, A. T. Haase, and J. C. Gluckman), p. 17. Karger, Basel.
7. Lichter, P. and Ward, D. C. (1990). *Nature,* **345,** 93.
8. Lichter, P., Boyle, A. L., Cremer, T., and Ward, D. C. (1991). *Genet. Anal. Techn. Appl.,* **8,** 24.
9. Cremer, T., Landegent, J., Brückner, A., Scholl, H. P., Schardin, M., Hager, H. D., *et al.* (1986). *Hum. Genet.,* **74,** 346.
10. Manuelidis, L. (1985). *Focus,* **7,** 4.
11. Lawrence, J. B. and Singer, R. H. (1985). *Nucleic Acids Res.,* **13,** 1777.
12. Lawrence, J. B., Villnave, C. A., and Singer, R. H. (1988). *Cell,* **52,** 51.
13. Albertson, D. G. (1985). *EMBO J.,* **4,** 2493.
14. Pinkel, D., Straume, T., and Gray, J. W. (1986). *Proc. Natl. Acad. Sci. USA,* **83,** 2934.
15. Raap, A. K., Marijnen, J. G. J., Vrolijk, J., and van der Ploeg, M. (1986). *Cytometry,* **7,** 235.
16. Manuelidis, L. and Ward, D. C. (1984). *Chromosoma,* **91,** 28.
17. Landegent, J. E., Jansen in de Wal, N., Dirks, R. W., Baas, F., and van der Ploeg, M. (1987). *Hum. Genet.,* **77,** 366.
18. Lichter, P., Cremer, T., Borden, J., Manuelidis, L., and Ward, D. C. (1988). *Hum. Genet.,* **80,** 224.
19. Pinkel, D., Landegent, J., Collins, C., Fuscoe, J., Segraves, R., Lucas, J., and Gray, J. W. (1988). *Proc. Natl. Acad. Sci. USA,* **85,** 9138.
20. Lichter, P., Jauch, A., Cremer, T., and Ward, D. C. (1990). In *Molecular Genetics of Chromosome 21 and Down Syndrome* (ed. D. Patterson), p. 69. Alan R. Liss, New York.
21. Arnoldus, E. P. J., Wiegant, J., Noordemeer, I. A., Wessels, J. W., Beverstock, G. C., Grosveld, G. C., *et al.* (1990). *Cytogenet. Cell Genet.,* **54,** 108.

22. Tkachuk, D., Westbrook, C., Andreef, M., Donlon, T., Cleary, M., Suranarayan, K., *et al.* (1990). *Science,* **250,** 559.
23. Rowley, J. D., Diaz, M. O., Espinosa III, R., Patel, Y. D., van Melle, E., Ziemin, S., *et al.* (1990). *Proc. Natl. Acad. Sci. USA,* **87,** 9358.
24. Dauwerse, J. G., Kievits, T., Beverstock, G. C., van der Keur, D., Smit, E., Wessels, H. W., *et al.* (1990). *Cytogenet. Cell Genet.,* **53,** 126.
25. Lux, S. E., Tse, W. T., Menninger, J. C., John, K. M., Harris, P., Shalev, O. *et al.* (1990). *Nature,* **345,** 736.
26. Ried, T., Mahler, V., Vogt, P., Blonden, L., van Ommen, G. J. B., Cremer, T., and Cremer, M. (1990). *Hum. Genet.,* **85,** 581.
27. Wada, M., Little, R. D., Abidi, F., Porta, G., Labella, T., Cooper, T., Della Valle, G., D'Urso, M., and Schlessinger, D. (1990). *Am. J. Hum. Genet.,* **46,** 95.
28. van Dilla, M. A., Deaven, L. L., Albright, K. L., Allen, N. A., Aubuchon, M. R., Bartholdi, M. F., *et al.* (1986). *Biotechnology,* **4,** 537.
29. Fuscoe, J. C., Collins, C. C., Pinkel, D., and Gray, J. W. (1989). *Genomics,* **5,** 100.
30. Lichter, P., Cremer, T., Tang, C. C., Watkins, P. C., Manuelidis, L., and Ward, D. C. (1988). *Proc. Natl. Acad. Sci. USA,* **85,** 9664.
31. Lengauer, C., Eckelt, A., Weith, A., Endlich, N., Ponelies, N., Lichter, P., *et al.* (1991). *Cytogenet. Cell Genet.,* **56,** 27.
32. Lengauer, C., Wienberg, J., Cremer, T., Lüdecke, H.-J., and Horsthemke, B. (1991). *Hum. Evol.,* **6,** 67.
33. Kievits, T., Devilee, P., Wiegant, J., Wapenaar, M. C., Cornelisse, C. J., van Ommen, G. J. B., and Pearson, P. L., (1990). *Cytometry,* **11,** 105.
34. Boyle, A. L., Lichter, P., and Ward, D. C. (1990). *Genomics,* **7,** 127.
35. Manuelidis, L. and Borden, J. (1988). *Chromosoma,* **96,** 397.
36. Emmerich, P., Jauch, A., Hofmann, M.-C., Cremer, T., and Walt, H. (1989). *Lab. Investigation,* **61,** 235.
37. Popp, S., Scholl, H. P., Loos, P., Jauch, A., Stelzer, E., Cremer, C., and Cremer, T. (1990). *Exp. Cell Res.,* **189,** 1.
38. Feinberg, A. P. and Vogelstein, B. (1984). *Anal. Biochem.,* **137,** 266.
39. Langer, P. R., Waldrop, A. A., and Ward, D. C. (1981). *Proc. Natl. Acad. Sci. USA,* **78,** 6633.
40. Kessler, C., Höltke, H. J., Seibl, R., Burg, J., and Mühlegger, K. (1990). *Biol. Chem. Hoppe-Seyler,* **371,** 917.
41. Johnson, G. D., Davidson, R. S., McNamee, K. C., Russell, G., Goodwin, D., and Holborow, E. J. (1982). *J. Immunol. Methods,* **55,** 231.
42. Lichter, P., Tang, C. C., Call, K., Hermanson, G., Evans, G. A., Housman, D., and Ward, D. C. (1990). *Science,* **247,** 64.
43. Harnden, D. G., Path, F. R. C., and Klinger, H. P. (1985). *ISCN 1985. An International System for Human Cytogenetic Nomenclature.* Karger, Basel.
44. Verma, R. S. and Babu, A. (1989). *Human Chromosomes, Manual of Basic Techniques.* Pergamon Press, New York.
45. Cremer, T., Lichter, P., Borden, J., Ward, D. C., and Manuelidis, L. (1988). *Hum. Genet.,* **80,** 235.
46. Cherif, D., Julier, C., Delattre, O., Derré, J., Lathrop, G. M., and Berger, R. (1990). *Proc. Natl. Acad. Sci. USA,* **87,** 6639.

47. Takahashi, E., Hori, T., O'Connell, P., Leppert, M., and White, R. (1990). *Hum. Genet.*, **86**, 14.
48. Boyle, A. L., Ballard, S. G., and Ward, D. C. (1990). *Proc. Natl. Acad. Sci. USA*, **87**, 7757.
49. Baldini, A. and Ward, D. C. (1991). *Genomics*, **9**, 770.
50. Klever, M., Grond-Ginsbach, C., Scherthan, H., and Schroeder-Kurth, T. M. (1991). *Hum. Genet.*, **86**, 484.
51. Latt, S. A. (1973). *Proc. Natl. Acad. Sci. USA*, **70**, 3395.
52. Vogel, W., Autenrieth, M., and Speit, G. (1986). *Hum. Genet.*, **72**, 129.
53. Perry, P. and Wolff, S. (1974). *Nature*, **251**, 156.
54. Devilee, P., Cremer, T., Slagboom, P., Bakker, E., Scholl, H. P., Hager, H. D., *et al.* (1986). *Cytogenet. Cell Genet.*, **41**, 193.
55. Bhatt, B., Burns, J., Flannery, D., and McGee, J. O. (1988). *Nucleic Acids Res.*, **16**, 3951.
56. Dunham, I., Lengauer, C., Cremer, T., and Featherstone, T. (1991). *Hum. Genet.*, in press.
57. Weier, H.-U.G., Kleine, H.-D., and Gray, J. W. (1991). *Hum. Genet.*, **87**, 489.
58. Nelson, D. L., Ledbetter, S. A., Corbo, L., Victoria, M. F., Ramirez-Solis, R., Webster, T. D., *et al.* (1989). *Proc. Natl. Acad. Sci. USA*, **86**, 6686.
59. Ledbetter, S. A., Nelson, D. L., Warren, S. T., and Ledbetter, D. H. (1990). *Genomics*, **6**, 475.
60. Lengauer, C., Riethman, H., and Cremer, T. (1990). *Hum. Genet.*, **86**, 1.
61. Lichter, P., Ledbetter, S. A., Ledbetter, D. H., and Ward, D. C. (1990). *Proc. Natl. Acad. Sci. USA*, **87**, 6634.
62. Nederlof, P. M., van der Flier, S., Wiegant, J., Raap, A. K., Tanke, H. J., Ploem, J. S., and van der Ploeg, M. (1990). *Cytometry*, **11**, 126.
63. Wiegant, J., Ried, T., Nederlof, P., van der Ploeg, M., Tanke, H. J., and Raap, A. K. (1991). *Nucleic Acids Res.* (In press.)
64. Trask, B., Pinkel, D., and van den Engh, G. (1989). *Genomics*, **5**, 710.
65. Lawrence, J. B., Singer, R. H., and McNeil, J. A. (1990). *Science*, **249**, 928.
66. Koch, J. E., Kølvraa, S., Petersen, K. B., Gregersen, N., and Bolund, L. (1989). *Chromosoma*, **98**, 259.
67. Weier, H.-U., Zitzelsberger, H. F., and Gray, J. W. (1991). *Biotechniques*, **10**, 498.

[CANCER RESEARCH 52, 2590–2596, May 1, 1992]

Metaphase and Interphase Cytogenetics with Alu-PCR-amplified Yeast Artificial Chromosome Clones Containing the *BCR* Gene and the Protooncogenes c-*raf-1*, c-*fms*, and c-*erbB-2*[1]

Christoph Lengauer,[2] Harold C. Riethman, Michael R. Speicher, Masafumi Taniwaki, David Konecki, Eric D. Green, Reinhard Becher, Maynard V. Olson, and Thomas Cremer

Institut für Humangenetik u. Anthropologie, Universität Heidelberg, Im Neuenheimer Feld 328, 6900 Heidelberg, Germany [C. L., M. R. S., M. T., D. K., T. C.]; The Wistar Institute, Philadelphia, Pennsylvania 19104 [H. C. R.]; Department of Genetics, Washington University School of Medicine, St. Louis, Missouri 63110 [E. D. G., M. V. O.]; and Innere Klinik und Poliklinik (Tumorforschung), Universitätsklinikum Essen, Hufelandstrasse 55, 4300 Essen 1, Germany [R. B.]

ABSTRACT

A human yeast artificial chromosome (YAC) library was screened by polymerase chain reaction with oligonucleotide primers defined for DNA sequences of the *BCR* gene and the protooncogenes c-*raf-1*, c-*fms*, and c-*erbB-2*. Alu-PCR-generated human DNA sequences were obtained from the respective YAC clones and used for fluorescence *in situ* hybridization experiments under suppression conditions. After chromosomal *in situ* suppression hybridization to GTG-banded human prometaphase chromosomes, seven of nine initially isolated YAC clones yielded strong signals exclusively in the chromosome bands containing the respective genes. Two clones yielded additional signals on other chromosomes and were excluded from further tests. The band-specific YACs were successfully applied to visualize specific structural chromosome aberrations in peripheral blood cells from patients with myelodysplasia exhibiting del(5)(q13q34), chronic myeloid leukemia and acute lymphocytic leukemia with t(9;22)(q34;q11), acute promyelocytic leukemia (M3) with t(15;17)(q22;q21), and in a cell line established from a proband with the constitutional translocation t(3;8)(p14.2;q24). In addition to the analysis of metaphase spreads, we demonstrate the particular usefulness of these YAC clones in combination with whole chromosome painting to analyze specific chromosome aberrations directly in the interphase nucleus.

INTRODUCTION

Specific chromosomal anomalies play a role in initiation and progression of neoplastic diseases. The unequivocal diagnosis of such aberrations using chromosome banding techniques, however, often suffers from a lack of mitotic tumor cells. In addition, the quality of chromosome spreads is often not sufficient for detailed cytogenetic analyses of the affected chromosomes, and it remains doubtful whether the results of such analyses are representative for the whole tumor cell population. Recent improvements of fluorescence *in situ* hybridization have provided a tool to visualize chromosome aberrations of interest in tumor cells at all stages of the cell cycle. Libraries from sorted human chromosomes have been used for CISS[3] hybridization to "paint" whole chromosomes in tumor cells (1–3), while individual DNA clones have been applied to delineate breakpoint regions with high resolution (4–8). YAC clones (9), which span several hundred kilobases within a chromosome region of interest, provide an ideal tool for such studies (10–13). Recently, Alu-PCR (14) has been applied as a rapid means to amplify human DNA sequences from YAC clones with complexities which generally yield strong signals both on metaphase spreads and in interphase nuclei (15). General use of such clones in tumor cytogenetics, however, is still limited by a lack of appropriate YACs.

In this study we have screened a YAC library for clones containing the *BCR* gene and the human protooncogenes c-*raf-1*, c-*fms*, and c-*erbB-2*. Nine clones were isolated which contained the expected sequences from the respective genes. After CISS hybridization seven of these clones showed signals exclusively within the expected bands of GTG-banded prometaphase chromosomes. We demonstrate that these clones can be used with high reliability for the detection of structural chromosome aberrations in patients with various hematological diseases and constitutive chromosome translocations, respectively, at all stages of the cell cycle. Double color CISS hybridization of YAC clones in combination with whole chromosome painting libraries was used to facilitate the mapping of clones with respect to the localization of the breakpoint in individual tumors.

MATERIALS AND METHODS

Human Cells. Metaphase spreads and interphase nuclei were prepared from phytohemagglutinin-stimulated normal male and female human blood lymphocytes, from Epstein-Barr virus-transformed lymphocytes of a proband carrying the translocation t(3;8)(p14.2;q24), and from nonstimulated lymphocytes of patients with various hematological diseases, including CML and ALL with t(9;22)(q34;q11), acute promyelocytic leukemia (M3) with t(15;17)(q22;q21), and myelodysplasia with del(5)(q13q34). Metaphase chromosome spreads were prepared using standard techniques of Colcemid treatment, hypotonic treatment, and methanol/acetic acid fixation. Conventional chromosome analyses were performed in GTG-banded metaphase spreads. For high resolution mapping, prometaphase chromosomes were obtained by the methotrexate synchronization technique described by Yunis (16). Preparations were stored in 70% ethanol at 4°C until use. Prometaphase chromosome spreads were GTG banded, photographed with a black and white film (AgfaOrtho), and postfixed as described by Klever *et al.* (17) prior to use in CISS hybridization experiments.

DNA Library Probes. Bacteriophage libraries from sorted human chromosomes were obtained from the ATCC (chromosome 3, LA03NS02; chromosome 5, LA05NS01) (18). The plasmid library from sorted human chromosomes 17 was a generous gift from Dr. Joe Gray, University of California, San Francisco (19). Bacteriophage libraries were amplified in liquid culture using *Escherichia coli* LE 392 as the bacterial host. DNA from bacteriophage and plasmid libraries was purified as described by Maniatis *et al.* (20).

PCR Screening of Human YAC Clone Library. Oligonucleotide primers defined for the amplification of DNA sequences of the protooncogenes c-*raf-1* (21), c-*fms* (22), and c-*erbB-2* (23) and for an intron-exon junction region of the *BCR* gene (24) were used for PCR

Received 11/5/91; accepted 2/26/92.

The costs of publication of this article were defrayed in part by the payment of page charges. This article must therefore be hereby marked *advertisement* in accordance with 18 U.S.C. Section 1734 solely to indicate this fact.

[1] This work was supported by grants from the Deutsche Forschungsgemeinschaft (Cr 59/10-1) and the Deutsche Krebshilfe (W23/90/Cr1). C. L. has been the recipient of a scholarship from the Konrad-Adenauer-Stiftung. H. R. was supported by an NIH postdoctoral fellowship (DHHS 1 F32 G11-12884). E. D. G. is a Lucille P. Markey Scholar, and his work was supported in part by a grant from the Lucille P. Markey Charitable Trust.

[2] To whom requests for reprints should be addressed.

[3] The abbreviations used are: CISS, chromosomal *in situ* suppression; YAC, yeast artificial chromosome; CML, chronic myeloid leukemia; ALL, acute lymphatic leukemia; PCR, polymerase chain reaction; PFGE, pulsed field gel electrophoresis; ATCC, American Type Culture Collection; FITC, fluorescein isothiocyanate; TRITC, tetramethylrhodamine isothiocyanate; DAPI, 4,6-diamidino-2-phenylindole dihydrochloride; APL, acute promyelocytic leukemia.

screening of the Washington University human YAC library as described previously (25).

c-*raf-1*

RAF1: 5′ AGA GGT GAT CCG AAT GCA GGA 3′
RAF2: 5′ TCA ATG GAA GAC AGG ATC TGA 3′
Predicted length of amplification product, 611 base pairs

c-*fms*

FMS1: 5′ TTC TGC TGA GGA GTT GAC GAC 3′
FMS2: 5′ CTT GGT GTG GCC AGC CAA TGC 3′
Predicted length of amplification product, 690 base pairs

c-*erbB-2*

ERB1: 5′ GAC ACC TAC GGC AGA GAA CCC 3′
ERB2: 5′ GTA CAA AGC CTG GAT ACT GAC 3′
Predicted length of amplification product, 510 base pairs

BCR gene

BCR1: 5′ GAC ACT GGC TTA CCT TGT GC 3′
BCR2: 5′ GAC GAT GAC ATT CAG AAA CC 3′
Predicted length of amplification product, 183 base pairs

PCR of human genomic DNA with these primer pairs showed specific amplification products of the predicted length. Clones identified in the appropriate filters by colony hybridization were grown and confirmed by colony PCR (26).

Molecular Characterization of YAC Clones. Methods for the growth of YAC-containing yeast strains, the preparation of DNA for conventional and PFGE, and Southern analysis of DNA have been described previously (9, 27). PCR products to be used as probes were purified using polyacrylamide gel electrophoresis as described previously (25). DNA probes for RAF-1, BCR, FMS, and ERBB2 were obtained from the ATCC (Accession nos. 41050, 59120, 41017, and 57584, respectively). The DNA probes were labeled radioactively (^{32}P) using the random-hexamer priming method of Feinberg and Vogelstein (28).

Alu-PCR Amplification of YAC Clones, CISS Hybridization, and Probe Detection. For CISS hybridization human sequences were generated by Alu-PCR amplification from the YAC clones as described in detail elsewhere (15). Briefly, agarose plugs prepared for pulsed field gel electrophoresis containing individual YAC clones were equilibrated in PCR buffer [10 mM Tris-HCl (pH 8.4), 50 mM KCl, 1.5 mM $MgCl_2$, 0.001% gelatin]. After careful equilibration, plugs were melted for 5 min at 70°C, and an aliquot equivalent to approximately 100 ng of genomic YAC clone DNA was added to the Alu-PCR assay using the primer pair as follows: CL1: 5′ TCC CAA AGT GCT GGG ATT ACA G 3′; CL2: 5′ CTG CAC TCC AGC CTG GG 3′ (15). Each primer was used at a concentration of 0.25 μM in a total volume of 100 μl of PCR buffer containing 250 μM of each of the four nucleotides and 2.5 units of *Taq* polymerase (Perkin Elmer/Cetus). After initial denaturation at 96°C for 3 min, 30 cycles of PCR were carried out with denaturation at 96°C for 1 min, annealing at 37°C for 30 s, and extension at 72°C for 6 min. Ten-μl aliquots of amplified DNA sequences were fractionated by gel electrophoresis. Alu-PCR amplification products were labeled with biotin-11-dUTP using standard nick translation procedures (29). DNA library probes (see above) were nick translated with digoxigenin-11-dUTP.

Chromosome preparations were pretreated with RNase A and pepsin, postfixed for 10 min in 3% paraformaldehyde, and stored in 70% ethanol overnight (8). CISS hybridization and detection of YAC probes with FITC conjugated to avidin were carried out as described previously (30) with the following modifications. For hybridization, 100 to 150 ng of the Alu-PCR-amplified YAC DNA were used as a probe after preannealing with various amounts (30 to 100 μg) of an unlabeled Cot1 DNA fraction (BRL/Life Technologies; Catalogue No. 5279SA). The signals were amplified once (31). In two-color CISS hybridization experiments with biotinylated YAC probes and digoxigenin-labeled library probes, the latter were detected by indirect immunofluorescence using mouse antidigoxin (Sigma) and goat anti-mouse Ig-TRITC (Sigma). After FITC signal detection, cells were counterstained with 1 μg/ml of DAPI and 0.2 μg/ml of propidium iodide. In two-color CISS hybridization experiments DAPI was used as the only counterstain. Cells were mounted in fluorescence antifading buffer (1 mg of *p*-phenylendiamine in 1 ml of glycerine buffer, pH 8.0) and evaluated with a Zeiss Photomicroscope III or a Zeiss Axiophot equipped with a double band pass filter (Zeiss). Microphotographs were taken with AGFACHROM 1000 RS or Kodak Ektachrome 400 color slide films.

RESULTS

Isolation and Molecular Characterization of YAC Clones for the *BCR* Gene and the Protooncogenes c-*raf-1*, c-*fms*, and c-*erbB-2*

Nine YAC clones containing the *BCR* gene or the protooncogenes c-*raf-1*, c-*fms*, or c-*erbB-2*, respectively, were isolated by PCR screening of the Washington YAC library established from human genomic DNA. Each of the nine isolated YAC strains was checked for the presence of expected gene-specific sequences by Southern blot analysis of digested DNA samples. The amplified PCR products and previously characterized oncogene sequences from the cloned region [obtained from ATCC (see "Materials and Methods")] were used as DNA hybridization probes for these analyses. Each isolated YAC carried the expected sequences (data not shown), although two clones which contained c-*erbB-2* sequences (A153G3 and B217G7) were later found to contain additional DNA from chromosomal regions apparently unrelated to the c-*erbB-2* gene (see the CISS hybridization experiments described below). PFGE of three of the nine clones (A230A7, D107B4, and A168H4) showed minor YAC bands which were related to the major YAC band of the respective clone as indicated by Southern blot hybridization with the respective oncogene probes. The seven oncogene-bearing YAC clones which apparently contain DNA only from the expected human genomic regions are listed in Table 1.

Alu-PCR amplification from an aliquot of melted agarose plugs containing 100 ng of YAC clone DNA yielded numerous bands of 0.1 to at least 4 kilobases in length for each clone (Fig. 1). The size and intensity of individual bands were found to be specific and reproducible for each YAC clone. YAC clones which were isolated for the same genomic site all showed some bands with apparently identical position and intensity, while other bands were distinctly different. These results confirm that PCR screening of the YAC library yielded different YAC clones for the *BCR* gene and the protooncogenes c-*raf-1* and c-*erbB-2*.

High Resolution Mapping of Alu-PCR-amplified YAC Clones

Alu-PCR-amplified probes obtained for each of the nine isolated YAC clones were used for CISS hybridization on

Table 1 *YAC clones with DNA only from expected human genomic regions*

YAC clone	Gene	Size (kilobases)
B99E1	*BCR*	115
D107F9	*BCR*	215
D73A7	c-*fms*	205
D122A5	c-*erbB-2*	500
A230A7	c-*erbB-2*	115 (135)[a]
A168H4	c-*raf-1*	550 (420)
D107B4	c-*raf-1*	240 (210)

[a] Numbers in parentheses, secondary YAC band of the indicated size, related to the primary YAC band (both contain the expected sequences), also present in the YAC-bearing yeast strain.

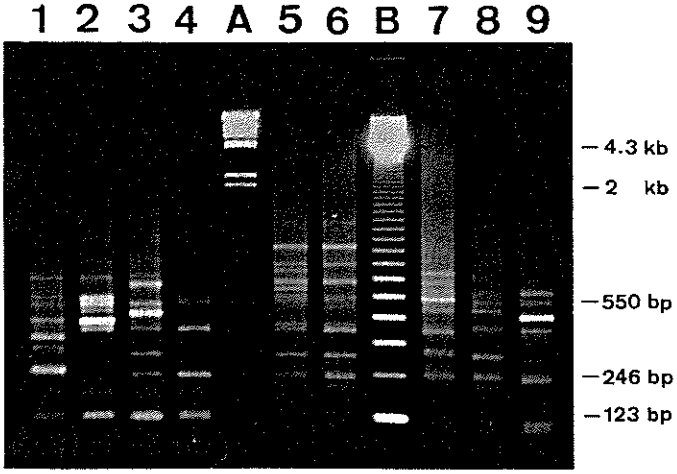

Fig. 1. Agarose gel (1.2%) of Alu-PCR-amplified YAC clone DNA. *Lanes 1* to *4*, c-*erbB-2* YAC clones A153G3, B217G7, D122A5, and A230A7; *Lanes 5* and *6*, *BCR* YAC clones D107F9 and B99E11; *Lanes 7* and *8*, c-*raf-1* YAC clones A168H4 and D107B4; *Lane 9*, c-*fms* YAC clone D73A7; marker *Lane A*, λ/*Hind*III; marker *Lane B*, 123-base pair ladder.

normal human metaphase and prometaphase spreads (46, XY, approximately 800 to 1000 band level) (Fig. 2). Prometaphase chromosome spreads were GTG banded prior to CISS hybridization. For each YAC clone, at least 50 metaphase spreads and 25 prometaphase spreads were evaluated, and the localization of the signals was compared with the localizations of the respective genes reported elsewhere (32–34). Fig. 2, *E* to *L*, shows examples of the high resolution mapping of site-specific YAC clones. The two *BCR* YACs mapped to 22q11, the two c-*raf-1* YACs mapped to 3p25, the c-*fms* YAC mapped to 5q33, and two of the c-*erbB-2* clones (D122A5 and A230A7) mapped exclusively to 17q12–21.1 (see Fig. 2, *A* to *D*, for examples). However, two of the four YAC clones obtained for the c-*erbB-2* protooncogene (A153G3 and B217G7) showed additional band-specific signals on other autosomes (data not shown). These clones were excluded from further experiments.

Application of Alu-PCR-amplified YAC Clones in the Analysis of Structural Chromosome Aberrations

Analysis of Metaphase Spreads. The Alu-PCR-amplified YAC clones were used to delineate specific deletions and translocations (Fig. 3). In each case a minimum of 50 tumor metaphase spreads was evaluated. Even metaphase spreads with very poor spreading could be easily evaluated.

Fig. 3*A* shows a metaphase spread from a patient with 5q− syndrome after two-color CISS hybridization with a human chromosome 5 genomic DNA library and the biotinylated c-*fms* YAC probe D73A7. The hybridization signal of the c-*fms* YAC clone is visible only on the normal chromosome 5. In the other chromosome 5 the signal is lost because of an interstitial deletion involving the c-*fms* protooncogene (32).

Fig. 3*D* shows a metaphase spread with t(9;22)(q34;q11) from a patient with CML after CISS hybridization with the *BCR* YAC clone D107F9. The normal chromosome 22, the Philadelphia (Ph^1) chromosome, and the der(9) are clearly labeled. These results were obtained with both *BCR* YAC clones D107F9 and B99E1 in three CML patients and in one patient with ALL carrying the Ph^1 chromosome (data not shown). These results demonstrate that both clones span the breakpoint cluster region on chromosome 22 involved in these patients. Notably, the relative signal intensities observed on the der(9) differed for the two clones; *i.e.*, the signals obtained with B99E1 were considerably weaker than with D107F9.

Fig. 3*F* shows a metaphase spread from a patient with APL carrying the translocation t(15;17)(q22;q21). Two-color CISS hybridization was performed with a human chromosome 17 genomic library and the c-*erbB-2* YAC clone A230A7. The hybridization signal of the YAC clone is visible on the normal chromosome 17 and the translocation chromosome (17pter→17q21::15q22→15qter). The same result was obtained with the c-*erbB-2* clone D122A5 (data not shown). These findings confirm directly that the breakpoint in APL is distal to the c-*erbB-2* sequences contained in these clones (35).

Fig. 3*G* shows a metaphase spread from an individual carrying the constitutional translocation t(3;8)(p14.2;q24). Two-color CISS hybridization was performed with a chromosome 3 genomic library and the c-*raf-1* YAC clone A168H4. The hybridization signal of the YAC clone is visible on the normal chromosome 3 and the translocation chromosome (8pter→8q24::3p14.2→3pter). As expected, the breakpoint in 3p is proximal to the c-*raf-1* sequences contained in these clones.

Analysis of Interphase Nuclei. Alu-PCR-generated probes from YAC clones yielded specific signals in interphase nuclei. The intensity of these signals varied with different clones, but was generally comparable to signals obtained from chromosome-specific alphoid probes. For example, Fig. 4 shows the result of CISS hybridization of the c-*raf-1* YAC probe A168H4 to normal lymphocyte nuclei. Table 2 shows the results of interphase cytogenetics performed with the seven band-specific YAC clones both in normal lymphocytes and in cells with the specific structural aberrations described above. These data were fully consistent with the conclusions obtained by the analysis of metaphase spreads. Interphase nuclei carrying the t(3;8)(p14.2;q24) translocation showed two signals after CISS hybridization with the c-*raf-1* YAC clone A168H4. Additional painting of chromosome 3 showed large and small domains both carrying a c-*raf-1* YAC-specific signal, while a third medium-sized domain did not (Fig. 3*I*). CISS hybridization of the c-*fms* YAC clone D73A7 to lymphocyte interphase nuclei of three patients with 5q− syndrome showed one distinct green signal only in most nuclei (Table 2), which was located within one of the two red-painted chromosome 5 domains (compare Fig. 3, *B* and *C*). Interestingly, Patient 1 showed only 2 of 200 interphase nuclei with a normal painting pattern; *i.e.*, two chromosome 5 domains both carrying the c-*fms* YAC clone signal, while 24% and 35% normal nuclei, respectively, were observed in Patients 2 and 3. For comparison, Patient 1 showed only metaphase spreads carrying the del(5q) ($n = 34$), while Patient 2 and Patient 3 showed 9% ($n = 46$) and 34% ($n = 21$) normal metaphase spreads. The differences between the percentages of normal and aberrant metaphase spreads and interphase nuclei in Patient 2 suggest that metaphase cell populations are not necessarily representative of the heterogeneity of normal and tumor cells present in the interphase cell population. CISS hybridization of the *BCR* YAC clone D107F9 to tumor interphase nuclei of a patient with CML showed that most nuclei contained three signals, as expected from a clone overlapping the breakpoint region in 22q11 (Fig. 3*E*).

DISCUSSION

In this study we have screened a human YAC library for YAC clones containing the *BCR* gene and the protooncogenes c-*raf-1*, c-*fms*, and c-*erbB-2*. Seven YAC clones contained sequences from these genes and showed signals exclusively within the bands to which the respective genes have been previously mapped. The localization of the two c-*erbB-2* clones could be

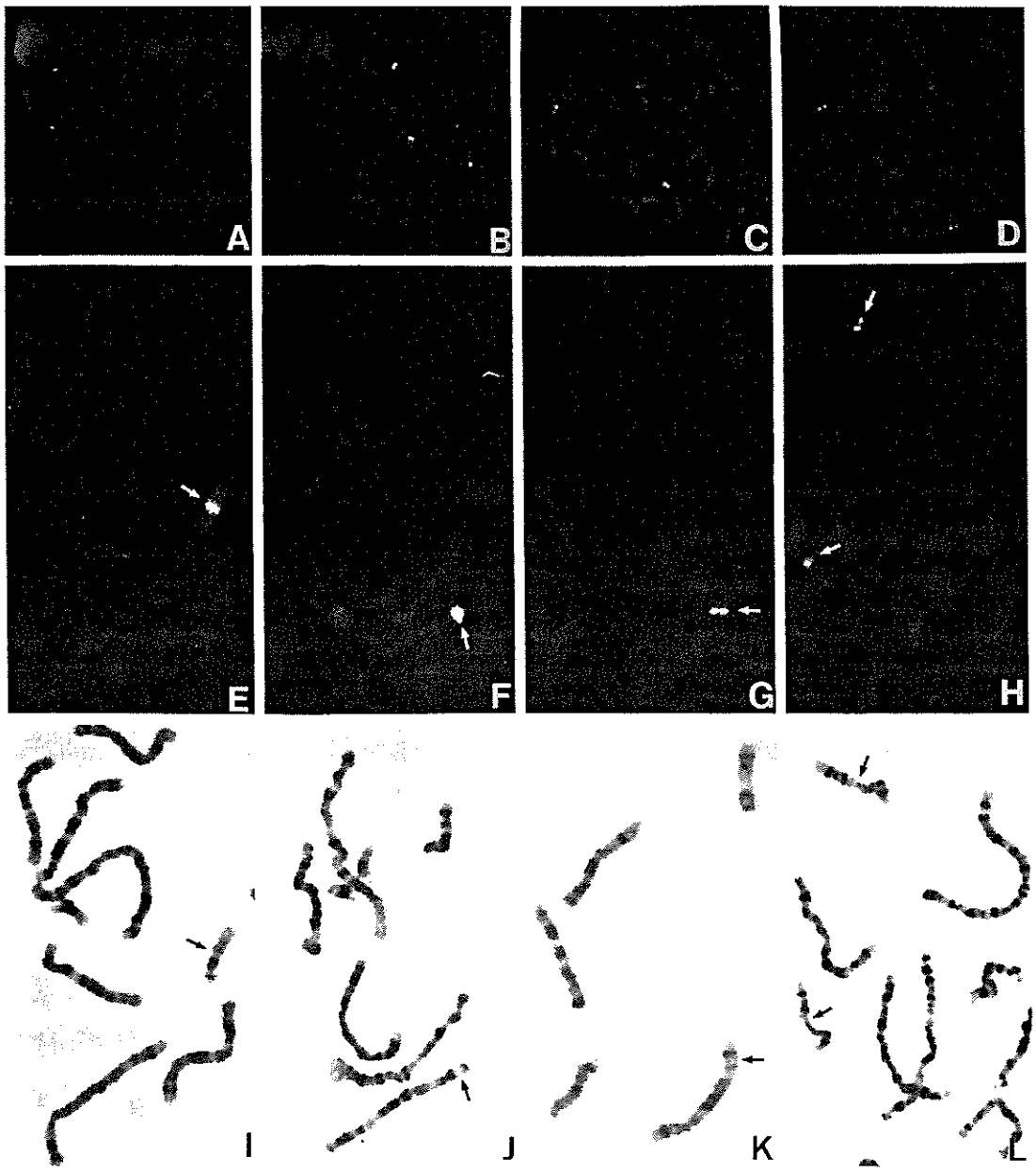

Fig. 2. Whole metaphase spreads after CISS hybridization of Alu-PCR-amplified probes from the *BCR* YAC D107F9 (*A*), the c-*raf-1* YAC A168H4 (*B*), the c-*fms* YAC D73A7 (*C*), and the c-*erbB-2* YAC D122A5 (*D*). Biotinylated probes were detected with avidin-FITC. Chromosomes were counterstained with propidium iodide. *E* to *L*, high-resolution mapping of Alu-PCR-amplified YAC clones. Prometaphase chromosomes were GTG banded (Fig. 3, *I* to *L*) and used for CISS hybridization after destaining. Biotin-labeled probes were detected with avidin-FITC. Chromosomes were counterstained with propidium iodide (Fig. 3, *E* to *H*). *E* and *I*, partial prometaphase with chromosome 22 indicating the localization of the *BCR* YAC clone D107F9 on 22q11 (*arrow*). *F* and *J*, partial prometaphase with chromosome 3 indicating the localization of the c-*raf-1* YAC clone A168H4 on 3p25 (*arrow*). *G* and *K*, partial prometaphase with chromosome 5 indicating the localization of the c-*fms* YAC clone D73A7 on 5q33 (*arrow*). *H* and *L*, partial prometaphase with two chromosomes 17 indicating the localization of the c-*erbB-2* YAC clone A230A7 on 17q12–21.1 (*arrows*).

narrowed down to 17q12–q21.1. The signals obtained with Alu-PCR-amplified YAC clones in metaphase spreads and interphase nuclei are clearly superior to signals which can generally be obtained with individual bacteriophage or cosmid clones. These strong signals, combined with a low background, make these probes ideal for tumor interphase cytogenetics and allow analyses using conventional fluorescence microscopy.

Recently, it has been demonstrated that interphase cytogenetics can also be applied to paraffin-embedded sections from solid tumors (36–38). We are presently exploiting the possibilities of using the c-*raf-1* YAC clones to diagnose deletions of 3p in several solid tumors, such as renal cell carcinomas (39) and small cell carcinomas of the lung (40). In addition, the c-*erbB-2* YACs may provide a useful tool to study the possible amplification of this region in patients with breast cancer (41, 42).

As demonstrated for the two *BCR* YAC clones in the case of CML and ALL cells with t(9;22)(q34;q11), small populations of interphase tumor cells carrying a specific translocation can be easily distinguished from normal interphase cell populations with YAC clones spanning the breakpoint region of interest. Similarly, tumor cell populations carrying a specific deletion can be discriminated from normal cells as exemplified for the c-*fms* YAC clone in several cases with the 5q− syndrome. The ability to diagnose specific chromosome aberrations at the single cell level makes interphase cytogenetics particularly useful to study heterogeneous cell populations. The unequivocal classification of individual nuclei, however, may be complicated

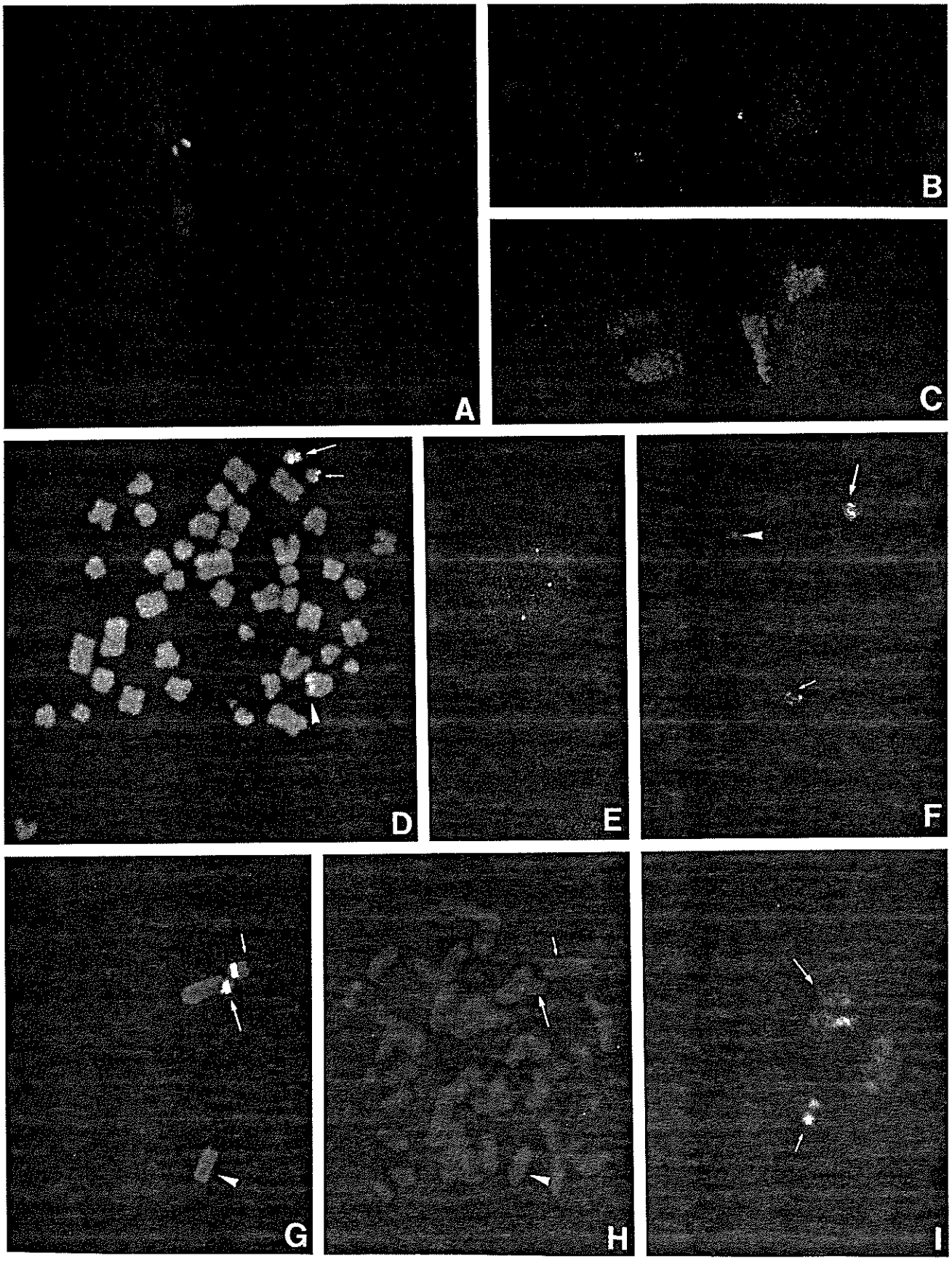

Fig. 3. Metaphase spread (*A*) and interphase nuclei (*B* and *C*) of a patient with 5q− syndrome after two-color CISS hybridization with a biotinylated Alu-PCR-amplified probe of c-*fms* YAC clone D73A7 (detection with avidin-FITC, green) and with a digoxigenin-labeled bacteriophage library from sorted human chromosomes 5 (detection with TRITC-conjugated antibodies, red). In *A*, the normal chromosome 5 shows strong specific labeling with the c-*fms* YAC on both chromatids, while the signal is missing on the deleted chromosome 5. In *B*, two nuclei exhibit one signal of the c-*fms* YAC clone only. In *C*, the same nuclei show two chromosome 5 domains. Note that the c-*fms* signal shown in *B* colocalizes with one domain. Metaphase spread (*D*) and interphase nucleus (*E*) of a patient with CML exhibiting the

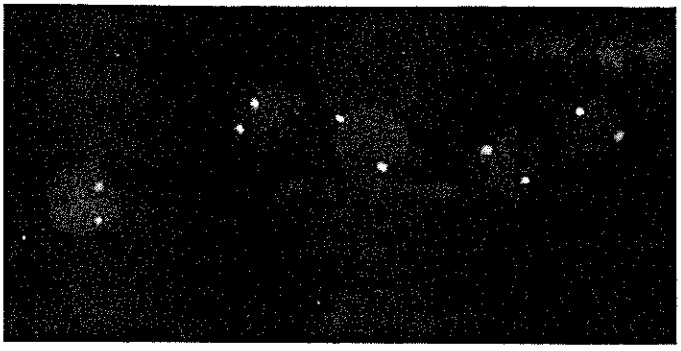

Fig. 4. Five normal lymphocyte nuclei with two signals each obtained after CISS hybridization with the c-*raf-1* YAC A168H4. Alu-PCR-generated, biotinylated probes were detected with avidin-FITC. Nuclei were counterstained with propidium iodide.

Table 2 *Results of interphase cytogenetics performed with the seven band-specific YAC clones*

The number of evaluated nuclei was 200 to 400.

YAC clone	Chromosome status	No. of signals in interphase nuclei (%)				
		0	1	2	3	4
c-*raf-1*						
D107B4	Normal diploid	1	1	97	1	0
A168H4	Normal diploid	0	3	97	0	0
A168H4	t(3;8)	0	2	95	2	1
c-*erbB-2*						
D122A5	Normal diploid	1	3	86	10	0
A230A7	Normal diploid	1	8	89	2	0
A230A7	t(15;17)	1	7	91	1	0
c-*fms*						
D73A7	Normal diploid	1	3	93	3	0
D73A7	del(5q); Patient 1	1	98	1	0	0
D73A7	del(5q); Patient 2	0	76	24	0	0
D73A7	del(5q); Patient 3	0	65	35	0	0
BCR						
B99E11	Normal diploid	0	5	93	2	0
D107F9	Normal diploid	1	3	90	6	0
D107F9	t(9;22)	2	6	28	62	2

by incomplete hybridization of a fraction of nuclei resulting in an underestimation of the true number of specific targets present in these cells (false negatives) or by artifactual fluorescent spots in nuclei which are counted as true signals (false positives). In cell populations containing both normal cells and tumor cells, false negatives would simply result in an underestimate of the fraction of tumor cells. A definitive decision, however, of whether or not the cell population would contain tumor cells could still be reached by a sufficiently large sample size. In contrast, false positives could lead to the erroneous diagnosis that a small percentage of tumor cells were still present within a large majority of normal cells. A strategy to discriminate artifactual from true signals could be based on multiple-color *in situ* hybridization experiments (8, 43, 44). For example, the discrimination of background spots from true hybridization signals can be facilitated by simultaneous painting of the target chromosome to which the respective YAC clone maps. In this case, interphase signals are counted only if they are found within the corresponding chromosome domain. Alternatively, false positives could be avoided by applying multiple-color *in situ* hybridization of probes which span the breakpoint of interest and flank it on both sites (8). Obviously, the chance of side-by-side localization of differently colored artifactual spots should be a rare event. Evaluation of such multiple-color *in situ* hybridization experiments will be very much facilitated by recent developments in digital fluorescence microscopy (45). In particular, the intriguing prospects of the automated evaluation of cells with specifically painted chromosome aberrations using digital image analysis could result in a tremendous reduction of the human workload (46). Direct labeling of DNA probes with fluorochromes has recently become possible and will further facilitate the application of multiple-color *in situ* hybridization (8, 43).

ACKNOWLEDGMENTS

We thank Brigitte Schoell for expert technical assistance and Angelika Wiegenstein for photographic work. We are grateful to Dr. G. Kovacs and A. Kovacs for providing metaphase spreads from the lymphoblastoid cell line with t(3;8)(q14.2;q24) and to Dr. Lore Zech for discussions.

REFERENCES

1. Cremer, T., Lichter, P., Borden, J., Ward, D. C., and Manuelidis, L. Detection of chromosome aberrations in metaphase and interphase tumor cells by *in situ* hybridization using chromosome-specific library probes. Hum. Genet., *80:* 235–246, 1988.
2. Lichter, P., Cremer, T., Borden, J., Manuelidis, L., and Ward, D. C. Delineation of individual human chromosomes in metaphase and interphase cells by *in situ* suppression hybridization using recombinant DNA libraries. Hum. Genet., *80:* 224–234, 1988.
3. Pinkel, D., Landegent, J., Collins, J., Fuscoe, J., Segraves, R., Lucas, J., and Gray, J. W. Fluorescence *in situ* hybridization with human chromosome specific libraries: detection of trisomy 21 and translocation of chromosome 4. Proc. Natl. Acad. Sci. USA, *85:* 9138–9142, 1988.
4. Arnoldus, E. P. J., Wiegant, J., Noordermeer, I. A., Wessels, J. W., Beverstock, G. C., Grosveld, G. C., van der Ploeg, M., and Raap, A. K. Detection of the Philadelphia chromosome in interphase nuclei. Cytogenet. Cell Genet., *54:* 108–111, 1990.
5. Tkachuk, T. C., Westbrook, C. A., Andreeff, M., Donlon, T. A., Cleary, M. L., Suryanarayan, K., Homge, M., Redner, A., Gray, J., and Pinkel, D. Detection of *bcr-abl* fusion in chronic myelogeneous leukemia by *in situ* hybridization. Science (Washington DC), *250:* 559–561, 1990.
6. Goa, J., Erickson, P., Gardiner, K., Le Beau, M. M., Diaz, M. O., Patterson, D., Rowley, J. D., and Drabkin, H. A. Isolation of a yeast artificial chromosome spanning the 8;21 translocation breakpoint t(8;21)(q22;q22.3) in acute myelogenous leukemia. Proc. Natl. Acad. Sci. USA, *88:* 4882–4886, 1991.
7. Selleri, L., Hermanson, G. G., Eubanks, J. H., Lewis, K. A., and Evans, G. A. Molecular localization of the t(11;22)(q24;q12) translocation of Ewing sarcoma by chromosomal *in situ* suppression hybridization. Proc. Natl. Acad. Sci. USA, *88:* 887–891, 1991.
8. Ried, T., Lengauer, C., Cremer, T., Wiegant, J., Raap, A. K., van der Ploeg, M., Groitl, P., and Lipp, M. Specific metaphase and interphase detection of the breakpoint region in 8q24 of Burkitt lymphoma cells by triple color

translocation t(9;22)(q34;q11) after CISS hybridization with the biotinylated Alu-PCR-amplified *BCR* YAC D107F9 detected with avidin-FITC. In *D*, note signals on both chromatids of the normal chromosome 22 (*large arrow*), the Ph[1] chromosome (*small arrow*), and the derivative chromosome 9 (9pter→9q34::22q11→22qter) (*arrowhead*). Chromosomes are counterstained with propidium iodide. In *E*, in correspondence with the result obtained in the metaphase spreads, the interphase nucleus clearly exhibits three signals. *F*, metaphase spread with a translocation t(15;17)(q22;q21) obtained from a patient with APL after two-color CISS hybridization with the biotinylated Alu-PCR-amplified c-*erbB-2* YAC A230A7 (green signals) and with a digoxigenin-labeled plasmid library from sorted human chromosomes 17 (red). Signals from the c-*erbB-2* YAC can be observed on both chromatids of the normal chromosome 17 (*large arrow*) and the derivative chromosome 17 (*small arrow*). The *arrowhead* points to the translocated chromosome 17 material on the derivative chromosome 15. Metaphase spread (*G*) and interphase nucleus (*I*) of a proband carrying the constitutional translocation t(3;8)(p14.2;q24) after two-color CISS hybridization with the biotinylated Alu-PCR-amplified c-*raf-1* YAC A168H4 (green signals) and with a digoxigenin-labeled bacteriophage library from sorted human chromosomes 3 (red). Signals of the c-*raf* YAC clone can be observed on both chromatids of the normal chromosome 3 (*large arrow*) and the derivative chromosome 8 together with the translocated chromosome 3 material (*small arrow*). In the derivative chromosome 3, the chromosome 3 material (3p14.2→3qter) is painted red (*arrowhead*). *H*, DAPI picture of the same metaphase as shown in *G*. In *I*, the corresponding interphase nucleus is weakly outlined by background red fluorescence and shows three bright red domains representing the normal chromosome 3 and the two translocation chromosomes with chromosome 3 material. Note that only the large normal chromosome 3 domain (*large arrow*) and the small domain (3p14.2→3pter) contained in the derivative chromosome 8 (*small arrow*) show colocalization with green c-*raf-1* signals.

fluorescence *in situ* hybridization. Genes Chromosomes Cancer, *4:* 69–74, 1992.
9. Burke, D. T., Carle, G. F., and Olson, M. V. Cloning of large segments of exogenous DNA into yeast by means of artificial chromosome vectors. Science (Washington DC), *236:* 806–812, 1987.
10. Rowley, J. D., Diaz, M. O., Espinosa, R., Patel, J. D., van Melle, E., Ziemin, S., Taillon-Miller, P., Lichter, P., Evans, G. A., Kersey, J. H., Ward, D. C., Domer, P. H., and Le Beau, M. M. Mapping chromosome band 11q23 in human acute leukemia with biotinylated probes: identification of 11q23 translocation breakpoints with a yeast artificial chromosome. Proc. Natl. Acad. Sci. USA, *87:* 9358–9362, 1990.
11. Wada, M., Little, R. D., Abidi, F., Porta, G., Labella, T., Cooper, T., Della Valle, G., D'Urso, M., and Schlessinger, D. Human Xq24–Xq28: approaches to mapping with yeast artificial chromosomes. Am. J. Hum. Genet., *46:* 95–106, 1990.
12. Heitz, D., Rousseau, F., Devys, D., Saccone, S., Abderrahin, H., Le Paslier, D., Cohen, D., Vincent, A., Toniolo, D., Della Valle, G., Johnson, S., Schlessinger, D., Oberlé, I., and Mandel, J. L. Isolation of sequences that span the fragile X and identification of a fragile X-retarded CpG island. Science (Washington DC), *251:* 1236–1239, 1991.
13. Montanaro, V., Casamassimi, A., D'Urso, M., Yoon, J. Y., Freije, W., Schlessinger, D., Muenke, M., Nussbaum, R. L., Saccone, S., Maugeri, S., Santoro, A. M., Motta, S., and Della Valle, G. *In situ* hybriiization to cytogenetic bands of yeast artificial chromosomes covering 50% of human Xq24–Xq28 DNA. Am. J. Hum. Genet., *48:* 183–194, 1991.
14. Nelson, D. L., Ledbetter, S. A., Corbo, L., Victoria, M. F., Ramirez-Solis, R., Webster, T. D., Ledbetter, D. H., and Caskey, C. T. Alu polymerase chain reaction: a method for rapid isolation of human-specific sequences from complex DNA sources. Proc. Natl. Acad. Sci. USA, *86:* 6686–6690, 1989.
15. Lengauer, C., Green, E. D., and Cremer, T. Fluorescence *in situ* hybridization of YAC clones after Alu-PCR amplification. Genomics, in press, 1992.
16. Yunis, J. J. High resolution of human chromosomes. Science (Washington DC), *191:* 1268–1270, 1976.
17. Klever, M., Grond-Ginsbach, C., Scherthan, H., and Schroeder-Kurth, T. Chromosomal *in situ* suppression hybridization after Giemsa banding. Hum. Genet., *86:* 484–486, 1991.
18. van Dilla, M. A., Deaven, L. L., Albright, K. L., Allen, N. A., Aubuchon, M. R., Bartholdi, M. F., Brown, N. C., Campbell, E. W., Carrano, A. V., Clark, L. M., Cram, L. S., Crawford, B. D., Fuscoe, J. C., Gray, J. W., Hildebrand, C. E., Jackson, P. J., Jett, H. J., Longmire, J. L., Lozes, C. R., Luedemann, M. L., Martin, J. C., McNinch, J. S., Meincke, L. J., Mendelsohn, M. L., Meyne, J., Moyzis, R. K., Munk, A. C., Perlman, J., Peters, D. C., Silva, A. W., and Trask, B. J. Human chromosome-specific DNA libraries: construction and availability. Biotechnology, *4:* 537–552, 1986.
19. Collins, C. C., Kuo, W. L., Segraves, R., Fuscoe, J. C., Pinkel, D., and Gray, J. W. Construction and characterization of plasmid libraries enriched in sequences from single human chromosomes. Genomics, *11:* 997–1006, 1991.
20. Maniatis, T., Fritsch, E. F., and Sambrook, J. Molecular Cloning: A Laboratory Manual. Cold Spring Harbor, NY: Cold Spring Harbor Laboratory, 1982.
21. Bonner, T. I., Kerby, S. B., Sutrave, P., Gunnell, M. A., Mark, G., and Rapp, U. R. Structure and biological activity of human homologs of the *raf/mil* oncogene. Mol. Cell Biol., *5:* 1400–1407, 1985.
22. Coussens, L., Van Beveren, C., Smith, D., Chen, E., Mitchell, R. L., Isacke, C. M., Verma, I. M., and Ullrich, A. Structural alteration of viral homologue of receptor proto-oncogene *fms* at carboxyl terminus. Nature (Lond.), *320:* 277–280, 1986.
23. Yamamoto, T., Ikawa, S., Akiyama, T., Semba, K., Nomura, N., Miyajima, N., Saito, T., and Toyoshima, K. Similarity of protein encoded by the human c-*erb-B-2* gene to epidermal growth factor receptor. Nature (Lond.), *319:* 230–234, 1986.
24. Heisterkamp, N., Stam, K., Groffen, J., de Klein, A., and Grosveld, G. Structural organization of the *bcr* gene and its role in the Ph[1] translocation. Nature (Lond.), *315:* 758–761, 1985.
25. Green, E. D., and Olson, M. V. Systematic screening of yeast artificial chromosome libraries by use of the polymerase chain reaction. Proc. Natl. Acad. Sci. USA, *87:* 1213–1217, 1990.
26. Huxley, C., Green, E. D., and Dunham, I. Rapid assessment of *S. cerevisiae* mating type by PCR. Trends Genet., *6:* 236, 1990.
27. Chu, G., Vollrath, D., and Davis, R. W. Separation of large DNA molecules by contour-clamped homogeneous electric fields. Science (Washington DC), *234:* 1582–1588, 1986.
28. Feinberg, A. P., and Vogelstein, B. A technique for radiolabeling DNA restriction endonuclease fragments to high specific activity. Anal. Biochem., *137:* 266–267, 1984.
29. Langer, P. R., Waldrop, A. A., and Ward, D. C. Enzymatic synthesis of biotin-labeled polynucleotides: novel nucleic acid affinity probes. Proc. Natl. Acad. Sci. USA, *78:* 6633–6637, 1981.
30. Lichter, P., Tang, C. J. C., Call, K., Hermanson, G., Evans, G. A., Housman, D., and Ward, D. C. High resolution mapping of human chromosome 11 by *in situ* hybridization with cosmid clones. Science (Washington DC), *247:* 64–69, 1990.
31. Pinkel, D., Gray, J. W., Trask, B., van den Engh, G., Fuscoe, J., and van Dekken, H. Cytogenetic analysis by *in situ* hybridization with fluorescently labeled nucleic acid probes. Cold Spring Harbor Symp. Quant. Biol., *51:* 151–157, 1986.
32. Le Beau, M., Westbrook, C. A., Diaz, M. O., Larson, R. A., Rowley, J. D., Gasson, J. C., Golde, D. W., and Sherr, C. J. Evidence for the involvement of GM-CSF and FMS in the deletion (5q) in myeloid disorders. Science (Washington DC), *231:* 984–987, 1986.
33. Groffen, J., Stepenson, J. R., Heisterkamp, N., de Klein, A., Bartram, C. R., and Grosveld, G. Philadelphia chromosomal breakpoints are clustered within a limited region *bcr* on chromosome 22. Cell, *36:* 93–99, 1984.
34. Bonner, T., O'Brien, S. J., Nash, W. G., Raap, C. R., Morton, C. C., and Leder, P. The human homologs of the *raf* (*mil*) oncogene are located on human chromosomes 3 and 4. Science (Washington DC), *223:* 71–74, 1984.
35. Borrow, J., Goddard, A. D., Sheer, G., and Solomon, E. Molecular analysis of acute promyelocytic leukemia breakpoint cluster region on chromosome 17. Science (Washington DC), *259:* 1577–1580, 1990.
36. Emmerich, P., Jauch, A., Hofman, M. C., Cremer, T., and Walt, H. Interphase cytogenetics in paraffin embedded sections from testicular germ cell tumor xenografts and in corresponding cultured cells. Lab. Invest., *61:* 235–242, 1989.
37. Walt, H., Emmerich, P., Cremer, T., Hofman, M. C., and Bannwart, F. Supernumary chromosome 1 in interphase nuclei of atypical germ cells in paraffin-embedded human seminiferous tubulus. Lab. Invest., *61:* 527–531, 1989.
38. Hopman, A. H. N., Poddighe, P. J., Smeets, W. A. G. B., Moesker, O., Beck, J. L. M., Vooijs, G. P., and Ramaekers, F. C. S. Detection of numerical chromosome aberrations in bladder cancer by *in situ* hybridization. Am. J. Pathol., *135:* 1105–1117, 1989.
39. Kovacs, G., Erlandsson, R., Boldog, F., Ingvarsson, S., Muller-Brechlin, R., Klein, G., and Sumegi, J. Consistent chromosome 3p deletion and loss of heterozygosity in renal cell carcinoma. Proc. Natl. Acad. Sci. USA, *85:* 1571–1575, 1988.
40. Brauch, H., Tory, K., Kotler, F., Gazdor, A. F., Pettengill, O. S., Johnson, B., Graziano, S., Winton, T., Buys, C. H. C. M., Sorenson, G. D., Poiesz, B. J., Minna, J. D., and Zbar, B. Molecular mapping of deletion sites in the short arm of chromosome 3 in human lung cancer. Genes Chromosomes Cancer, *1:* 247–255, 1990.
41. Slamon, D. J., Clark, G. M., Wong, S. G., Levin, W. J., Ullrich, A., and McGnire, W. L. Human breast cancer: correlation of relapse and survival with amplification of the *HER-2/neu* oncogene. Science (Washington DC), *235:* 177–182, 1987.
42. McCann, A. H., Dervan, P. A., O'Regan, M., Codd, M. B., Gullick, W. J., Tobin, B. M. J., and Carney, D. N. Prognostic significance of c-*erbB-2* and estrogene receptor status in human breast cancer. Cancer Res., *51:* 3296–3303, 1991.
43. Wiegant, J., Ried, T., Nederlof, P. M., van der Ploeg, M., Tanke, H. J., and Raap, A. K. *In situ* hybridization with fluoresceinated DNA. Nucleic Acids Res., *19:* 3237–3241, 1991.
44. Nederlof, P. M., van der Flier, S., Wiegant, J., Raap, A. K., Tanke, H. J., Ploem, J. S., and van der Ploeg, M. Multiple fluorescence *in situ* hybridization. Cytometry, *11:* 126–131, 1990.
45. Lichter, P., Boyle, A. L., Cremer, T., and Ward, D. C. Analysis of genes and chromosomes by non-isotopic *in situ* hybridization. Genet. Anal. Tech. Appl., *8:* 24–35, 1991.
46. Cremer, T., Remm, B., Kharboush, I., Jauch, A., Wienberg, J., Stelzer, E., and Cremer, C. Non-isotopic *in situ* hybridization and digital image analysis of chromosomes in mitotic and interphase cells. Revue Europeene de Technologie Biomedicale, *13:* 50–54, 1991.

Proc. Natl. Acad. Sci. USA
Vol. 89, pp. 8611–8615, September 1992
Evolution

Reconstruction of genomic rearrangements in great apes and gibbons by chromosome painting

(primates/phylogeny/comparative cytogenetics/chromosome aberrations/chromosome-specific staining)

A. JAUCH*†, J. WIENBERG‡, R. STANYON§, N. ARNOLD‡, S. TOFANELLI¶, T. ISHIDA‖, AND T. CREMER*

*Institut für Humangenetik und Anthropologie, Universität Heidelberg, Heidelberg, Federal Republic of Germany; ‡Institut für Anthropologie und Humangenetik, Universität München, Munich, Federal Republic of Germany; §Istituto di Antropologia fisica, Università di Genova, Genoa, Italy; ¶Istituto di Antropologia, Università di Firenze, Florence, Italy; and ‖Department of Anthropology, University of Tokyo, Tokyo, Japan

Communicated by Frank H. Ruddle, May 29, 1992

ABSTRACT **The homology between hylobatid chromosomes and other primates has long remained elusive. We used chromosomal *in situ* suppression hybridization of all human chromosome-specific DNA libraries to "paint" the chromosomes of primates and establish homologies between the human, great ape (chimpanzee, gorilla, and orangutan), and gibbon karyotypes (*Hylobates lar* species group, $2n = 44$). The hybridization patterns unequivocally demonstrate the high degree of chromosomal homology and synteny of great ape and human chromosomes. Relative to human, no translocations were detected in great apes, except for the well-known fusion-origin of human chromosome 2 and a 5;17 translocation in the gorilla. In contrast, numerous translocations were detected that have led to the massive reorganization of the gibbon karyotype: the 22 autosomal human chromosomes have been divided into 51 elements to compose the 21 gibbon autosomes. Molecular cytogenetics promises to finally allow hylobatids to be integrated into the overall picture of chromosomal evolution in the primates.**

The origin of human and great ape chromosomes is well understood from comparative chromosome-banding analysis and has been widely confirmed by gene mapping (1–4). Yet the lesser apes, which are classified with great apes and human in the same primate superfamily Hominoidea, apparently show no karyological relationship with any other primate species (5–7). Only very few gibbon chromosomes appear to have a similar banding pattern compared with other catarrhine chromosomes. Even within hylobatids very few chromosome homologies can be found between species differing in diploid number ($2n = 38$, 44, 50, and 52), and there is little gene-mapping data supporting chromosome homologies between human and gibbon species (8). Gene-mapping data for the *Hylobates lar* species group ($2n = 44$) has, to our knowledge, not yet been reported. In contrast to the highly heterogeneous karyotypes, the hylobatids are fairly homogeneous in most other biological characteristics that also reveal their close relationship to great apes and humans (9–13). Molecular studies place gibbon divergence from pongids and humans at 16–23 million years, whereas orangutans diverged 12–16 million years ago, and human and African apes diverged ≈5–10 million years ago (13, 14).

Recently, chromosomal *in situ* suppression (CISS) hybridization (15–17) has been applied to establish homologies between human and primate chromosomes (18–21). In contrast to previous comparative gene-mapping experiments that have been restricted to single-copy sequences, this approach provides an overall comparison of DNA sequence homologies for complete chromosomes and extended chromosome subregions. In the present study phage or plasmid libraries derived from all 24 flow-sorted human chromosomes were hybridized to chromosome preparations of chimpanzee, gorilla, orangutan, and three of the 44-chromosome gibbon species (*H. lar*, *Hylobates moloch*, and *Hylobates klossii*).

MATERIALS AND METHODS

Cell Lines and Sample Preparation. Metaphase chromosome spreads for *in situ* hybridization experiments were prepared and stored as reported (18). Great ape chromosome preparations were obtained from lymphocyte or fibroblast cultures established from material provided by the Heidelberg Zoo (courtesy of H. Wiesner, Munich, and A. Poley, Heidelberg). Gibbon chromosomes were prepared from lymphoblastoid cell lines HylE-7, HylE-5, and HykE-1 established from a male *H. lar*, a female *H. moloch*, and a female *H. klossii*, respectively. Cell lines were immortalized with Epstein–Barr virus derived from the B95-8 cell line. (For further information about the origin of the individuals write to T.I.). The G-banded karyotypes of all three cell lines are the same and appeared to be normal diploid ($2n = 44$), including a polymorphism for chromosome 8. These hylobatids are known to be polymorphic within and between species for this chromosome (22). For gibbon chromosome 8 the following karyotypes were found: 8b/8c, 8a/8c, and 8b/8b. Chromosome banding before CISS hybridization was done as described (23).

DNA Probes and *in Situ* Hybridization. CISS hybridization of DNA library probes to human and primate chromosomes was done as described (15, 16). Briefly, DNA prepared from chromosome-specific human bacteriophage libraries (American Type Culture Collection nos. LA01NS01, LL02NS01, LA03NS02, LA04NS02, LA05NS01, LL06NS01, LA07NS01, LL08NS02, LL09NS01, LL10NS01, LL11NS01, LA12NS01, LL13NS02, LL14NS01, LL15NS01, LL16NS03, LL17NS02, LL18NS01, LL19NS01, LL20NS01, LA21NS01, LL22NS01, LA0XNS01, and LL0YNS01) or plasmid libraries (pBS1 to pBS4, pBS6 to pBS22, pBSX, and pBSY) were used as probes. The plasmid libraries were provided by J. Gray (University of California, San Francisco) and are described in detail by Collins *et al.* (24). In some experiments human genomic DNA obtained from the blood of a male individual (46,XY) was hybridized to gibbon chromosome preparations.

Library DNA was labeled with either biotin or digoxigenin by standard nick-translation assays. CISS hybridization was done as described in detail elsewhere (16). Briefly, 10 μl of the hybridization mixture [50% (vol/vol) formamide/1× stan-

The publication costs of this article were defrayed in part by page charge payment. This article must therefore be hereby marked "*advertisement*" in accordance with 18 U.S.C. §1734 solely to indicate this fact.

Abbreviations: AMCA, 7-amino-4-methylcoumarin-3-acetic acid; CISS, chromosomal *in situ* suppression; FITC, fluorescein isothiocyanate; *PTR*, *Pan troglodytes* (chimpanzee); *GGO*, *Gorilla gorilla*; *PPY*, *Pongo pygmaeus* (orangutan).

†To whom reprint requests should be addressed at: Institut für Humangenetik und Anthropologie, 6900 Heidelberg, Im Neuenheimer Feld 328, F.R.G.

dard saline citrate/10% (wt/vol) dextran sulfate] containing 1–2 μg of labeled phage library DNA or 300–500 ng of labeled plasmid library DNA, 4–8 μg of human genomic competitor DNA, and 10 μg of salmon sperm DNA was heated 5 min at 75°C. The denatured DNA was allowed to preanneal for 20 min at 37°C before the hybridization mixture was dropped on heat-denatured primate chromosome preparations and covered with 18 mm × 18 mm coverslips. After hybridization and washing of the slides, biotinylated DNA probes were detected with fluorescein isothiocyanate (FITC) coupled with avidin (Vector Laboratories). In double-hybridization experiments digoxigenin-labeled probes were detected with FITC-conjugated mouse anti-digoxigenin antibodies (Boehringer Mannheim), whereas biotin-labeled probes were detected with avidin coupled with AMCA (7-amino-4-methylcoumarin-3-acetic acid; Vector Laboratories). AMCA signals were amplified once as previously described for FITC signals (25).

RESULTS

We analyzed the hybridization pattern of all 24 human chromosome-specific libraries in chimpanzee (*Pan troglodytes; PTR*), gorilla (*Gorilla gorilla; GGO*), orangutan (*Pongo pygmaeus; PPY*) and in gibbons (*H. lar, H. klossii*, and *H. moloch*). The resulting hybridization pattern is summarized in Table 1.

Painting of Great Ape Chromosomes. In all great apes the human chromosome 2 library painted two chromosome pairs. The only other translocation found was a reciprocal translocation between chromosomes homologous to human chromosomes 5 and 17 (Fig. 1 *a* and *b*; for further details see ref. 21). Other interchromosomal rearrangements that have been proposed (for review see ref. 26) could be ruled out. In particular, no hybridization signals were observed that could be expected from the proposed translocation in the orangutan between chromosomes homologous to human chromosomes 8 and 20 (3) (Fig. 1 *c* and *d*). Still very small interstitial or terminal translocations may only be identified with appropriate, subregional DNA probes.

Libraries from acrocentric human chromosomes showed occasional cross hybridization to the short arms of other acrocentric human and great ape chromosomes, possibly due to sequence homologies in nuclear organizer regions and/or pericentric heterochromatin (24). In addition, several other chromosomal subregions in hominoid chromosomes remained unlabeled. These regions include telomeric heterochromatin in the chimpanzee and gorilla, Y chromosome heterochromatin in gorilla and orangutan, and an interstitial heterochromatic band on chimpanzee chromosome 14. Intriguingly, reduced hybridization was noted on the heterochromatic short arms of chimpanzee chromosomes 12 and 13, suggesting loss of some genetic material during the formation of human chromosome 2.

Painting of Gibbon Chromosomes. All three 44-chromosome gibbon species analyzed showed the same G-banded karyotype and the same hybridization pattern with the human chromosome libraries, except for gibbon chromosome 8. In contrast to the stability of great ape karyotypes the human libraries detected many translocations in the gibbon karyotypes (for examples, see Fig. 1 *f–j*). For all libraries, the classical G-banding was done before *in situ* hybridization; photographs were taken and compared thereafter to the CISS hybridization patterns. Fig. 2 shows the identification of four gibbon chromosome segments homologous to the human chromosome 1 library. Only gibbon chromosomes labeled with human chromosome libraries 11, 14, 20, X, and Y were not involved in interchromosomal rearrangements (for example, see Fig. 1*e*). Chromosomes homologous to human chromosomes 7, 13, 15, 18, 21, and 22 were translocated to another gibbon chromosome (for examples, see Fig. 1 *f* and *g*). Other hylobatid chromosomes showed multiple translocations composed of up to five different human chromosome segments (mode = 2) (for examples, see Fig. 1 *h–j*). Accordingly, the 22-autosomal human chromosomes could be divided into 51 segments to compose the 21 gibbon autosomes (Table 1).

CISS hybridization with the human chromosome 5 library showed a heterozygous pericentric inversion of gibbon chromosome 8 (type 8c) in cell line HylE-7 (Fig. 1*j*) as previously described in *H. lar* individuals. Instead, type 8a (found in cell line HykE-1 from the *H. klossii* individual) hybridization indicated a translocation between gibbon chromosomes 8 and 13 (data not shown).

Table 1. Chromosome homologies between human and hominoids (chimpanzee, gorilla, orangutan, and gibbons) revealed by chromosome painting with human chromosome-specific DNA libraries

Human chromosome-specific DNA library	Homologies detected in hominoid species			
	Chimpanzee	Gorilla	Orangutan	Gibbon*
Chromosome				
1	*PTR* 1	*GGO* 1	*PPY* 1	*HLA* 5q; 7q; 9p; 19
2	*PTR* 12; 13	*GGO* 12; 11	*PPY* 12; 11	*HLA* 1p; 10p; 12p; 16p; 16q
3	*PTR* 2	*GGO* 2	*PPY* 2	*HLA* 4p; 7q; 10q; 12q
4	*PTR* 3	*GGO* 3	*PPY* 3	*HLA* 2q; 3q; 18q
5	*PTR* 4	*GGO* 4q; 19p; 19q	*PPY* 4	*HLA* 6p; 6q; 8p or 8q†; 18p
6	*PTR* 5	*GGO* 5	*PPY* 5	*HLA* 3p; 3q 20
7	*PTR* 6	*GGO* 6	*PPY* 10	*HLA* 1p; 1q
8	*PTR* 7	*GGO* 7	*PPY* 6	*HLA* 7q; 9p; 9q
9	*PTR* 11	*GGO* 13	*PPY* 13	*HLA* 8q; 13q
10	*PTR* 8	*GGO* 8	*PPY* 7	*HLA* 2p; 2q; 3q
11	*PTR* 9	*GGO* 9	*PPY* 8	*HLA* 11
12	*PTR* 10	*GGO* 10	*PPY* 9	*HLA* 7p; 7q; 10p; 10q; 14p; 14q
13	*PTR* 14	*GGO* 14	*PPY* 14	*HLA* 4q
14	*PTR* 15	*GGO* 18	*PPY* 15	*HLA* 17
15	*PTR* 16	*GGO* 15	*PPY* 16	*HLA* 15p; 15q
16	*PTR* 18	*GGO* 17	*PPY* 18	*HLA* 6p; 6q; 8p
17	*PTR* 19	*GGO* 4p; 4q; 19q	*PPY* 19	*HLA* 8q; 13p; 16p; 16q
18	*PTR* 17	*GGO* 16	*PPY* 17	*HLA* 5p
19	*PTR* 20	*GGO* 20	*PPY* 20	*HLA* 10p; 14p; 14q; 16q
20	*PTR* 21	*GGO* 21	*PPY* 21	*HLA* 21
21	*PTR* 22	*GGO* 22	*PPY* 22	*HLA* 15q
22	*PTR* 23	*GGO* 23	*PPY* 23	*HLA* 8p; 8q
X	*PTR* X	*GGO* X	*PPY* X	*HLA* X
Y	*PTR* Y	*GGO* Y	*PPY* Y	*HLA* Y

Assignment of great ape chromosomes was made by simultaneous 4′,6-diamidino-2-phenylindole (DAPI) banding (data not shown); assignment of gibbon chromosomes was achieved by G-banding before CISS hybridization (compare Fig. 2 and text). Great ape and gibbon chromosomes or chromosome arms with complete or partial homology to specific human chromosomes are indicated. Many gibbon chromosome arms are painted with more than one library. For details of the extension of the homologies, see Fig. 3. *HLA*, *H. lar*.

**Hylobates* sp. ($2n = 44$).

†Gibbon chromosome 8 is polymorphic (see text).

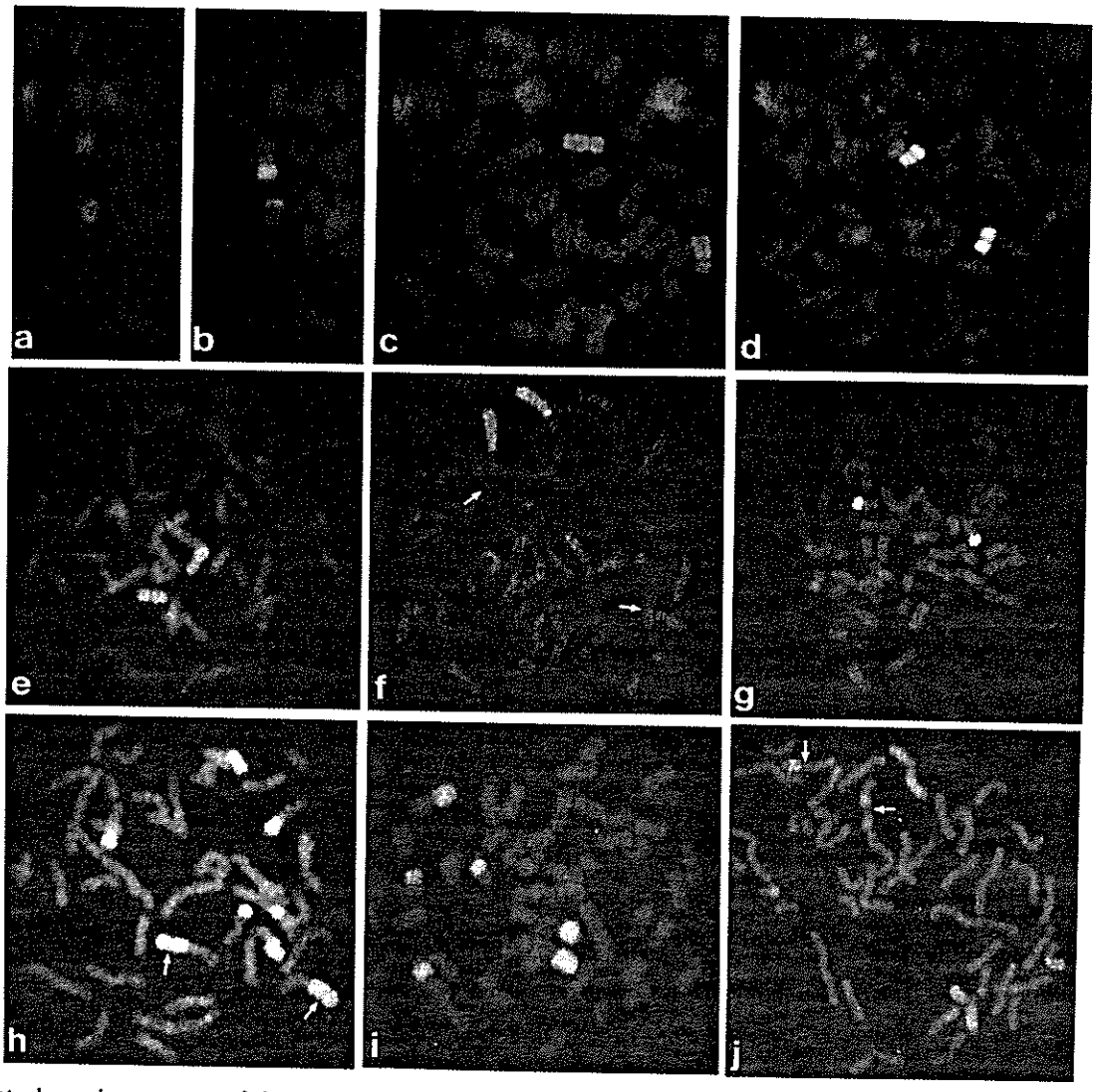

FIG. 1. Metaphase chromosomes of *GGO* (*a* and *b*), *PPY* (*c* and *d*) and *H. lar* (*e–j*) painted with biotin- or digoxigenin-labeled human chromosome-specific phage or plasmid DNA libraries. Hybridization sites were detected with FITC-conjugated antibodies against digoxigenin (*a*), avidin conjugated with 7-amino-4-methylcoumarin-3-acetic acid (*b*), or avidin-conjugated with FITC (*c–j*). Chromosomes were counterstained with propidium iodide. For chromosome identification G-banding was done before CISS-hybridization (data not shown). (*a* and *b*) Partial metaphase spread from *GGO* after two-color CISS-hybridization with libraries for human chromosomes 5 (*a*) and 17 (*b*), respectively. Note the reciprocal translocation detected by these libraries on gorilla chromosomes 4 and 19. (*c* and *d*) Orangutan chromosomes 6 and 21 painted with human chromosome 8 and 20 libraries, respectively. (*e*) Human chromosome 11 DNA library delineates gibbon chromosome 11. Painting with human chromosome 7 (*f*) and chromosome 21 DNA libraries (*g*) indicates that the entire homologous chromosomes were translocated to gibbon chromosomes 1 and 15, respectively. Note that the nuclear organizer region (*f*, arrows) on gibbon chromosome 12 was not labeled by any of the human DNA libraries hybridized under suppression conditions. (*h–j*) Painting with human DNA libraries from chromosome 3 (*h*), chromosome 4 (*i*), and chromosome 5 (*j*) demonstrates the occurrence of multiple reciprocal translocations. In *h* the arrows point to a small unlabeled subregion in gibbon chromosome 4. In *j* arrows indicate a heterozygous pericentric inversion in gibbon chromosome 8 after painting with the human chromosome 5 library. Note that the painted region is located on the short arm of one homolog and on the long arm of the other.

For identification of the apparent breakpoints a comparison of G-banding and CISS hybridization patterns was done in 5–10 metaphase spreads for each human library and investigated 44-chromosome gibbon species. An idiogram summarizing all detected breakpoints is provided in Fig. 3. Still the localization of these breakpoints should be considered approximate for several reasons. (*i*) The banding resolution of the lymphoblastoid samples was limited to ≈300–400 bands. (*ii*) The borders of painted versus nonpainted chromosome regions were occasionally somewhat fuzzy, probably due to the denaturation of chromosomes. (*iii*) Some swelling of the chromosomes was noticed after the *in situ* hybridization procedure that also slightly impaired a precise overlay of the pictures from a given chromosome after G-banding and subsequent painting.

Notably, cross-hybridization events as found with libraries from human acrocentric chromosomes in great apes (see above) were not apparent when these libraries were hybridized to gibbon chromosomes. Furthermore, the single nuclear organizer region of the "marker chromosome" (gibbon chromosome 12) (Fig. 1*f*), as well as several pericentromeric and interstitial bands in the gibbons, remained unlabeled when hybridized under suppression conditions with any of the human chromosome-specific DNA libraries (Fig. 3) or total human DNA. In contrast, in the absence of competitor DNA at least some of these regions, especially the nuclear organizer region, became strongly painted with human genomic DNA.

DISCUSSION

In the great apes our results mostly confirm chromosome homologies previously suggested by chromosome banding and gene mapping (1–4). Conflicting hypotheses concerning particular interchromosomal rearrangements were resolved.

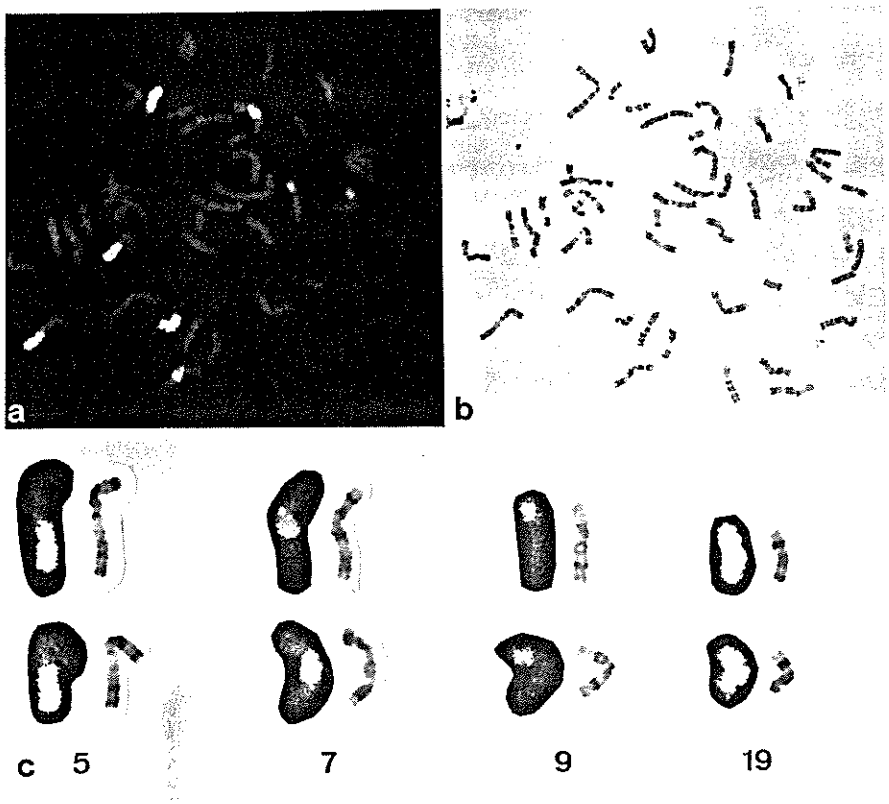

FIG. 2. Identification of painted chromosome regions on G-banded chromosomes from *H. lar*. (*a*) Metaphase spread painted with a plasmid DNA library from flow-sorted human chromosomes 1. (*b*) Same metaphase spread after G-banding. (*c*) Painted chromosomes shown side by side with G-banded chromosomes at higher magnification. The gibbon chromosome number is indicated below each pair (compare with Fig. 3).

In addition to the well-known fusion-origin of human chromosome 2, the evolutionary-derived reciprocal translocation in the gorilla between chromosomes homologous to human chromosomes 5 and 17 was confirmed (18, 21), whereas other previously proposed translocations were rejected.

Our results show that translocations have played a major role in the massive karyotypic reorganization in hylobatids. With exception of gibbon chromosome 8, the consistency of the translocation patterns in lymphoblastoid cell lines derived from three different gibbon species indicates that artifacts of cell transformation and *in vitro* cultivation can be ruled out. Although the CISS hybridization technique with human chromosome-specific libraries is ideally suited to identify translocations of homologous chromosome segments, its potential to detect intrachromosomal changes is limited. In spite of this limitation, our present data indicate the occurrence of numerous intrachromosomal rearrangements. To match the banding patterns of human autosome segments homologous with gibbon counterparts, intrachromosomal rearrangements have often to be assumed (data not shown). In several gibbon chromosomes—i.e., no. 6 (Figs. 1*j* and 3), 14 (Fig. 3), and 16 (Fig. 3), two chromosomal subregions painted by one human autosome library were interrupted by a region homologous to another human autosome. The assumption of a single translocation followed by a pericentric inversion appears to be the easiest explanation for these findings. It is likely that other intrachromosomal rearrangements have occurred in the gibbons but have not been identified so far. In the future a reliable estimate of the magnitude of such effects may be obtained by using multiple-color *in situ* hybridization with subregional probes.

Balanced inversion and translocation polymorphisms have been reported for different gibbon species (5, 6, 22, 27). Inversions were previously hypothesized to account for the three forms—a, b, and c—of gibbon chromosome 8 (22). Our data support this hypothesis for chromosome forms 8b and 8c. In contrast, the data suggest that a reciprocal translocation of gibbon chromosomes 8 and 13 led to form 8a. However, we cannot exclude the possibility that rearrangements restricted to one of the three lymphoblastoid gibbon cell lines investigated so far have occurred *in vitro*. Additional gibbon specimens must be analyzed with *in situ* hybridization to rule out this possibility.

Although some subregions in hominoid chromosomes remained unlabeled with chromosome-specific DNA libraries, hybridization experiments with human whole-genomic DNA labeled all chromosome regions. One explanation is that formerly unhybridized regions contain repetitive sequences that are suppressed in CISS-hybridization experiments.

The data support the hypothesis that changes in the gibbon karyotype are characterized by an extremely high evolutionary rate compared with other primates (7, 28). Papionini karyotypes (macaques, baboons, mandrills, and cercocebus monkeys) are conservative and nearly identical in all these species (29). These karyotypes have frequently been used as an "outgroup" for determining the direction of chromosomal rearrangements in hominoid species. Recently, we applied chromosome painting with all 24 human chromosome-specific DNA libraries to chromosome preparations of *Macaca fuscata* (20). Only three macaque chromosomes were each hybridized by two separate human libraries. Even though Papionini are evolutionarily more distant from humans than hylobatids, all other libraries painted an entire homologous counterpart in the macaque karyotype.

The mechanism of the rapid rate of chromosomal evolution in gibbons remains to be explained. It is not clear whether gibbons have a higher chromosomal mutation rate or whether chromosomal mutations have occurred at a normal rate but were more easily fixed, or both. Molecular data show that the evolutionary rate seen in the gibbon genome is within the range of other primates (13). Rates of chromosomal rearrangements and molecular evolution, however, may be independent.

It is generally argued that the heterozygotes for chromosomal rearrangements (especially translocations) should have drastically reduced fertility due to the loss of genetically unbalanced offspring (30, 31). Population bottlenecks and inbreeding have been proposed to explain the rapid fixation of

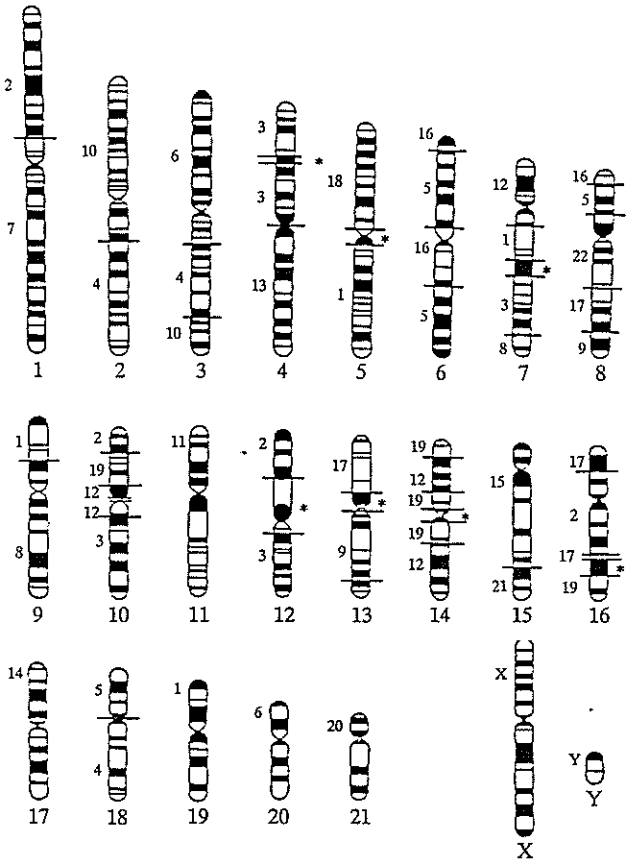

FIG. 3. Idiogramatic summary of the hybridization patterns of human chromosome-specific DNA libraries to G-banded chromosomes of *H. lar* [idiogram after Stanyon and Chiarelli (7)]. Gibbon chromosome numbers are given below each chromosome. The nuclear organizer region-bearing chromosome, which so far has been referred to as "marker chromosome" and not included into the numbering system, is designated here as chromosome 12. Numbers at left of each chromosome indicate the subregions painted with the respective human chromosome-specific library. Bars indicate the tentative translocation breakpoints identified by superimposition of G-banded chromosomes with the same chromosomes after CISS hybridization (≈300- to 400-band stage). Some chromosomal subregions indicated by asterisks remained unlabeled with any human library.

such rearrangements (32, 33). On the one hand, a rapid fixation may have been favored by gibbon social structure and ecology, including monogamous matings, nuclear family units, and an arboreal lifestyle. In contrast, the chromosomally conservative Papionini live in large terrestrial groups with multiple male and multiple female matings (28, 29). On the other hand, the reduction of fitness due to chromosomal rearrangements may be less drastic than normally proposed. Even though very few gibbons have been karyotyped, most species have chromosome polymorphisms. Apparently, all 44-chromosome gibbon species share such polymorphisms (22), indicating that they are not transient but have even survived speciation events. These findings argue against drastic bottlenecks during the divergence of the various 44-chromosome gibbon species. Other gibbon species have probable translocation polymorphisms (5, 6) or subspecies with different karyotypes (34), suggesting that the process of karyological transformation is still underway. CISS hybridization analysis of larger sample sizes, especially of free-ranging lesser apes, could provide further insight into the possible role of chromosome polymorphisms during speciation events.

The three other karyomorphs in hylobatids remain to be fully studied with the CISS hybridization technique. Preliminary data on *Hylobates syndactylus* ($2n = 50$) show translocations not present in the *H. lar* species group and *H. klossii*. For example, the human chromosome 7 library paints segments on three different chromosomes in *H. syndactylus* (18), in contrast to the 44-chromosome gibbon species, where only one chromosome is painted. These studies promise to help resolve the evolutionary relationships within hylobatids and with other primates and will finally allow hylobatids to be integrated into the overall picture of chromosomal evolution in the primates.

We gratefully acknowledge Dr. H. Wiesner for providing us with the great ape samples, B. Schoell and F. Bigoni for technical assistance, and A. Wiegenstein for photographic work. We thank T. M. Schroeder-Kurth for her support and encouragement. This work was supported by grants from the Deutsche Forschungsgemeinschaft, the Land Baden-Württemberg, the Italian Ministry for Universities and Scientific Research, and a Consiglio Nationale delle Ricerche grant.

1. Dutrillaux, B. (1979) *Hum. Genet.* **48**, 255–296.
2. Seuànez, H. (1979) *The Phylogeny of Human Chromosomes* (Springer, Berlin).
3. Yunis, J. & Prakash, O. M. (1982) *Science* **215**, 1525–1529.
4. O'Brien, S. J. & Marshall Graves, J. A. (1990) *Cytogenet. Cell Genet.* **55**, 406–433.
5. Couturier, J., Dutrillaux, B., Turleau, C. & de Grouchy, J. (1982) *Ann. Genet.* **25**, 5–10.
6. Van Tuinen, P. & Ledbetter, D. H. (1983) *Am. J. Phys. Anthropol.* **61**, 453–466.
7. Stanyon, R. & Chiarelli, B. (1983) *J. Hum. Evol.* **12**, 305–315.
8. O'Brien, S. J. & Marshall Graves, J. A. (1991) *Cytogenet. Cell Genet.* **58**, 1124–1152.
9. Bruce, E. J. & Ayala, F. J. (1979) *Evolution* **33**, 1040–1056.
10. Haimoff, E. H., Chivers, D. J., Gittins, S. P. & Whitten, T. (1982) *Folia Primatol.* **39**, 213–237.
11. Darga, L. L., Baba, M. L., Weiss, M. L. & Goodman, M. (1984) in *The Lesser Apes*, eds. Preuschoft, H., Chivers, D. J., Brockelman, W. Y. & Creel, N. (Edinburgh Univ. Press, Edinburgh), pp. 448–466.
12. Cronin, J. E., Sarich, V. M. & Ryder, O. (1984) in *The Lesser Apes*, eds. Preuschoft, H., Chivers, D. J., Brockelman, W. Y. & Creel, N. (Edinburgh Univ. Press, Edinburgh), pp. 467–485.
13. Sibley, G. & Ahlquist, J. E. (1987) *J. Mol. Evol.* **26**, 99–121.
14. Caccone, A. & Powell, J. (1989) *Evolution* **43**, 925–942.
15. Cremer, T., Lichter, P., Borden, J., Ward, D. C. & Manuelidis, L. (1988) *Hum. Genet.* **80**, 235–246.
16. Lichter, P., Cremer, T., Borden, J., Manuelidis, L. & Ward, D. C. (1988) *Hum. Genet.* **80**, 224–234.
17. Pinkel, D., Landegent, J., Collins, C., Fuscoe, J., Segraves, R., Lucas, J. & Gray, J. W. (1988) *Proc. Natl. Acad. Sci. USA* **85**, 9138–9142.
18. Wienberg, J., Jauch, A., Stanyon, R. & Cremer, T. (1990) *Genomics* **8**, 347–350.
19. Lengauer, C., Lüdecke, H.-J., Wienberg, J., Cremer, T. & Horsthemke, B. (1991) *Hum. Evol.* **6**, 67–71.
20. Wienberg, J., Stanyon, R., Jauch, A. & Cremer, T. (1992) *Chromosoma* **101**, 265–270.
21. Stanyon, R., Wienberg, J., Romagno, D., Bigoni, F., Jauch, A. & Cremer, T. (1992) *Am. J. Phys. Anthropol.*, in press.
22. Stanyon, R., Sineo, L., Chiarelli, B., Camperio Ciani, A. S., Haimoff, A. H., Mootnick, A. R. & Suturman, D. R. (1987) *Folia Primatol.* **48**, 56–64.
23. Klever, M., Grond-Ginsbach, C., Scherthan, H. & Schroeder-Kurth, T. (1991) *Hum. Genet.* **86**, 484–487.
24. Collins, C., Kuo, W. L., Segraves, R., Fuscoe, J., Pinkel, D. & Gray, J. W. (1991) *Genomics* **11**, 997–1006.
25. Pinkel, D., Gray, J. W., Trask, B., van den Engh, G., Fuscoe, J. & van Dekken, H. (1986) *Cold Spring Harbor Symp. Quant. Biol.* **51**, 151–157.
26. Seuànez, H. N. (1987) in *The Chromosomes of Man: Evolutionary Considerations*, eds. Obe, G. & Basler, A. (Springer, Berlin), pp. 65–89.
27. Tantravahi, R., Dev, V. G., Firschein, I. L., Miller, D. A. & Miller, O. J. (1975) *Cytogenet. Cell Genet.* **15**, 92–102.
28. Marks, J. (1983) *Cytogenet. Cell Genet.* **34**, 261–264.
29. Stanyon, R., Fantini, C., Camperio-Ciani, A., Chiarelli, B. & Ardito, G. (1988) *Am. J. Primatol.* **16**, 3–17.
30. Stam, P. (1979) *Genetica* **50**, 149–158.
31. Chesser, R. K. & Baker, R. J. (1986) *Evolution* **40**, 625–632.
32. Lande, R. (1979) *Evolution* **33**, 234–251.
33. Larson, A., Prager, E. M. & Wilson, A. C. (1979) *Chromosomes Today* **8**, 215.
34. Couturier, J. & Lernould, J.-M. (1991) *Folia Primatol.* **56**, 95–104.

SHORT COMMUNICATION

Fluorescence *in Situ* Hybridization of YAC Clones after *Alu*–PCR Amplification

CHRISTOPH LENGAUER,* ERIC D. GREEN,† AND THOMAS CREMER*

*Institut für Humangenetik u. Anthropologie, Universität Heidelberg, Im Neuenheimer Feld 328, 6900 Heidelberg, Federal Republic of Germany; and †Department of Genetics, Washington University School of Medicine, Saint Louis, Missouri 63110

Received November 5, 1991; revised February 10, 1992

***Alu*–PCR protocols were optimized for the generation of human DNA probes from yeast strains containing yeast artificial chromosomes (YACs) with human inserts between 100 and 800 kb in size. The resulting DNA probes were used in chromosome *in situ* suppression (CISS) hybridization experiments. Strong fluorescent signals on both chromatids indicated the localization of specific YAC clones, while two clearly distinguishable signals were observed in ≥90% of diploid nuclei. Signal intensities were generally comparable to those observed using chromosome-specific alphoid DNA probes. This approach will facilitate the rapid mapping of YAC clones and their use in chromosome analysis at all stages of the cell cycle.** © 1992 Academic Press, Inc.

Yeast artificial chromosomes (YACs) (2) containing a variety of human inserts have recently been mapped by fluorescence *in situ* hybridization (FISH) using either total yeast clone DNA or YAC DNA isolated from pulsed-field gels [for review see (9, 13)]. However, the hybridization efficiency of YACs was generally less than satisfactory in metaphase spreads, while interphase nuclei could not be evaluated at all. To overcome these problems, we have tested whether the *Alu*–PCR approach first described by Nelson *et al.* (10) would allow the amplification of human DNA sequences from YACs with complexities sufficient for FISH experiments. *Alu* primer 517 (nt positions 220 to 236 of the consensus *Alu* repeat) (10), which was successfully used to amplify human sequences from rodent × human hybrid cell lines (5, 8), did not yield DNA probes useful for *in situ* hybridization when applied to YAC clones (data not shown). It appeared necessary to search for an *Alu* primer pair and to define PCR conditions that would allow the specific amplification of human sequences between *Alu* blocks in all possible orientations with optimized yields from YAC clones.

For this purpose we designed two primers, CL1 and CL2, chosen from the most conserved regions of the *Alu* repeat family, which are located close to the 5′ and 3′ ends of the approx 300-bp-long *Alu* block, respectively (4): CL1, 5′ TCC CAA AGT GCT GGG ATT ACA G 3′ (nt positions 23 to 44 of the consensus Alu repeat); CL2, 5′ CTG CAC TCC AGC CTG GG 3′ (nt positions 244 to 260). Primer 278 described by Nelson *et al.* (10) is partially identical with primer CL1 but contains 11 additional bases at the 5′ end. Due to the orientation of these primers, *Alu*–PCR-amplified sequences would contain only very brief *Alu* segments. This may facilitate the effective suppression of labeled *Alu* sequences in FISH experiments. For comparison, several other primers were derived from regions located more interior within the *Alu* block, including primers CL3, 5′ GTT GGC CAG GCT GGT CT 3′ (nt positions 82 to 98); and TC 65 (nt positions 220 to 236) (10), as well as primer A1 (nt positions 268 to 285) (1), located at the extreme 3′ end of the *Alu* repeat.

Under a variety of amplification conditions, the primer pairs CL1/CL2, CL1/TC65, CL1/A1, CL3/CL2, CL3/TC65, and CL3/A1 were tested for their ability to amplify a maximum amount of human sequences from YAC clones; amplification products from yeast DNA should be avoided. For *PCR* experiments, 100 ng of purified genomic yeast clone DNA was used. Alternatively, agarose plugs prepared for pulsed-field gel electrophoresis containing the respective yeast cells and stored in 0.5 *M* EDTA were equilibrated two times, 30 min each, in 1 *M* Tris–HCl (pH 8.0) and 30 min in PCR buffer (10 m*M* Tris–HCl, pH 8.4, 50 m*M* KCl, 1.5 m*M* $MgCl_2$, 0.001% gelatin) at room temperature. Afterwards the plugs were stored overnight in PCR buffer at 4°C. The plug was melted for 5 min at 70°C, and an aliquot equivalent to approx 100 ng of genomic yeast cell DNA was added to the *Alu*–PCR assay. For rapid testing we were also able to pick a small amount of yeast cells (just visible on a sterile pipet tip) directly from clones grown on plates. After dilution of the cells in 1.5 ml distilled water, aliquots of up to 20 μl were added to the PCR assay without any further pretreatment. This latter approach, however, provided fewer reproducible amplification yields.

In the PCR assay, each primer was used at a concentration of 0.25 μ*M* in a total volume of 100 μl PCR buffer containing 250 μ*M* of each of the four dNTPs and 2.5 units of *Taq* polymerase (Perkin–Elmer/Cetus). After initial denaturation at 96°C for 3 min, 30 cycles of PCR were carried out with denaturation at 96°C for 1 min and extension at 72°C for 6 min. The annealing time was 30 s, while the annealing temperature was varied between 55 and 37°C. Ten-microliter aliquots of amplified DNA sequences were fractionated by electrophoresis in a 1.5%

GENOMICS 13, 826–828
0888-7543/92 $5.00
Copyright © 1992 by Academic Press, Inc.
All rights of reproduction in any form reserved.

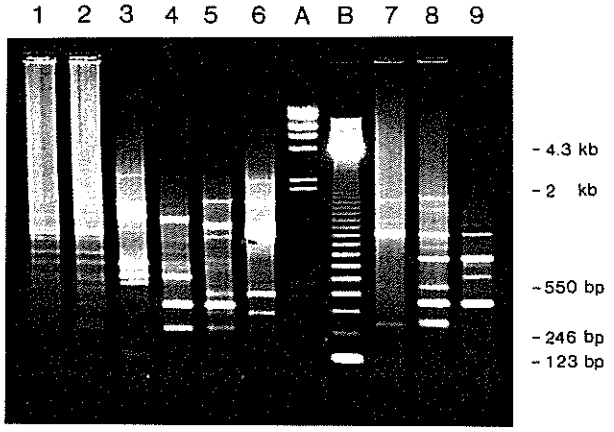

FIG. 1. Agarose gel (1.2%) of *Alu*–PCR-amplified YAC clones of the CF contig (3). Lanes **1, 2:** two independent *Alu*–PCR amplifications of a melted agarose plug containing the YAC yCF-1/7/5-R (790 kb). Lanes **3–9:** *Alu*–PCR-amplified YAC clone DNA, yKM19-3 (150 kb); yCF-10 (240 kb); yCF-7 (240 kb); yCF-5 (280 kb); yW30-5 (260 kb); yJ311-3 (340 kb); yJ311-1 (350 kb); marker lane A, λ/*Hin*dIII; marker lane **B;** 123-bp ladder. Overlapping YAC clones show bands with apparently identical position and intensity, while other bands are distinctly different.

agarose gel in 1× TAE (0.04 *M* Tris–acetate, 0.001 *M* EDTA). The highest yield of amplification products was obtained at the lowest annealing temperature (37°C) (data not shown). In particular, at decreasing annealing temperature a smear of amplification products ranging up to 8 kb became more prominent. Primer combinations CL1/CL2 and CL3/CL2 showed the best yield of amplification products. Figure 1 shows a typical agarose gel with *Alu*–PCR-amplified sequences obtained with CL1/CL2 from eight YAC clones containing human inserts between 150 and 790 kb, which belong to a YAC contig previously established from the cystic fibrosis gene at band 7q31 (3). The size and intensity of the individual bands were highly reproducible for each YAC clone. None of the combinations of primer pairs chosen in these experiments yielded specific amplification products from genomic yeast DNA, although combinations containing primer CL3 showed a band <50 bp indicating the formation of primer dimers. Accordingly, we decided to test amplification products obtained with primer pair CL1/CL2 for their suitability as FISH probes.

PCR products were ethanol precipitated, resuspended in double-distilled water, and used for nick translation with biotin–11-dUTP. Alternatively, biotin–11-dUTP was directly incorporated during the PCR. Note that the size of the labeled probes should range between some 100 and 400 bp for efficient FISH with low background. In the case of PCR labeling, the amplification products should be post-treated with appropriate concentrations of DNase I. Chromosome preparations prepared from phytohemagglutinin (PHA)-stimulated human blood lymphocytes using standard techniques were pretreated with RNase A and pepsin, postfixed in 1% acid-free, buffered formaldehyde, and stored in 70% ethanol overnight according to the protocol described by Ried *et al.* (12). Chromosomal *in situ* suppression (CISS) hybridization and probe detection with fluorescein isothiocyanate (FITC) conjugated to avidin were carried out as described previously (7) with the following modifications: For hybridization 100–150 ng of the *Alu*–PCR-amplified YAC DNA was used as a probe after preannealing with titrated amounts (30–100 μg) of unlabeled C_0t 1 DNA (BRL/Life Technologies, Cat. No. 5279SA). The signals

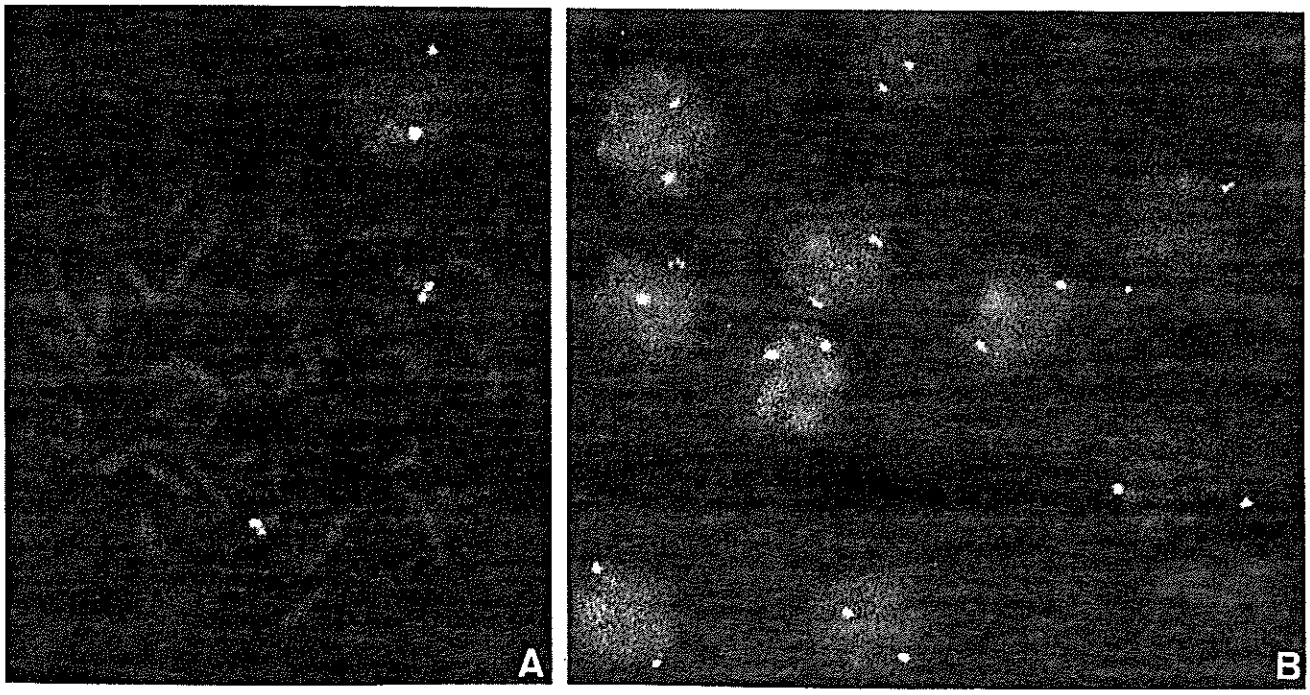

FIG. 2. Metaphase spread (A) and interphase nuclei (A, B) after CISS hybridization of the *Alu*–PCR-amplified YAC clone yCF-1/7/5-R and detection of the biotinylated probe with avidin FITC. Chromosomes counterstained with propidium iodide.

TABLE 1

YAC clone	Number of signals in interphase nuclei (%)			
	0	1	2	3
yCF-1/7/5-R	1	4	95	0
yCF-10	3	5	90	2
yCF-7	1	3	92	4
yCF-5	2	4	91	3
yW30-5	0	1	97	2

Note. Number of evaluated nuclei: 200.

were amplified once (11). Cells were counterstained with 1 μg/ml 4,6-diamidino-2-phenylindole-dihydrochloride (DAPI) and 0.2 μg/ml propidium iodide, mounted in fluorescence antifading buffer (1 mg *p*-phenylendiamine in 1 ml glycerine buffer, pH 8.0), and evaluated with a Zeiss Photomicroscope III.

Figure 2A shows the result of CISS hybridization of *Alu*–PCR-amplified sequences from YAC clone yCF-1/7/5-R to a normal male human metaphase spread. Chromosome identification was performed after DAPI banding or after simultaneous hybridization with a chromosome 7 alphoid repeat probe (data not shown). In 100 subsequent metaphase spreads, which were analyzed on two slides, strong signals with the expected localization on the long arm of chromosome 7 were seen on both chromatids. Figure 2B demonstrates that the *Alu*–PCR probe obtained from this YAC clone also yielded strong specific signals in interphase nuclei. Table 1 shows the results of signals counted in interphase nuclei of normal lymphocytes after CISS hybridization with *Alu*–PCR-amplified probes obtained from five YAC clones. For each clone, 90% or more of randomly evaluated nuclei showed two clearly separated signals.

Possible limitations of this approach should be taken into consideration. The efficiency of probe generation by *Alu*–PCR depends on the number of adequately spaced *Alu* elements that flank site-specific sequences in each individual YAC. Therefore, YAC clones derived from parts of the genome with a particularly low content in *Alu* sequences may not be used effectively. Up to now we have tested more than 60 YAC clones containing some 100 to 800 kb of human insert from various regions of the human genome, including both R- and G-bands. Each of these clones yielded clearly detectable metaphase and interphase signals using the protocol described in this report. While many clones showed signals restricted to one specific chromosome band, others showed signals on different chromosome subregions indicating that these clones either detected sequence homologies within the respective subregions or contained a chimeric YAC or several different YACs. *Alu*–PCR-generated probes from chromosome band-specific YAC clones provide ideal tools for the analysis of specific numerical and structural chromosome aberrations at any stage of the cell cycle (6).

ACKNOWLEDGMENTS

We thank Angelika Wiegenstein for photographic work. This work was supported by grants from the Deutsche Forschungsgemeinschaft (Cr 59/10-1). C.L. is the recipient of a scholarship from the Konrad-Adenauer-Stiftung. E.D.G. is a Lucille P. Markey Scholar, and his work was supported in part by a grant from the Lucille P. Markey Charitable Trust.

REFERENCES

1. Brooks-Wilson, A. R., Goodfellow, P. N., Povey, S., Nevanlinna, H. A., de Jong, P. J., and Goodfellow, P. J. (1990). Rapid cloning and characterization of new chromosome 10 DNA markers by Alu element-mediated PCR. *Genomics* **7:** 614–620.
2. Burke, D. T., Carle, G. F., and Olson, M. V. (1987). Cloning of large segments of exogenous DNA into yeast by means of artificial chromosome vectors. *Science* **236:** 806–812.
3. Green, E. D., and Olson, M. V. (1990). Chromosomal region of the cystic fibrosis gene in yeast artificial chromosomes: A model for human genome mapping. *Science* **250:** 94–98.
4. Kariya, Y., Kato, K., Hayashizaki, Y., Himeno, S., Tarui, S., and Matsubara, K. (1987). Revision of consensus sequence of human *Alu* repeats—A review. *Gene* **53:** 1–10.
5. Lengauer, C., Riethman, H. C., and Cremer, T. (1990). Painting of human chromosomes with probes generated from hybrid cell lines by PCR with Alu and L1 primers. *Hum. Genet.* **86:** 1–6.
6. Lengauer, C., Riethman, H. C., Speicher, M. R., Taniwaki, M., Konecki, D., Green, E. D., Becher, R., Olson, M. V., and Cremer, T. (1992). Metaphase and interphase cytogenetics with Alu-PCR amplified YAC clones containing the BCR-gene and the protooncogenes c-raf-1, c-fms, c-erbB-2. *Cancer Res.* **52:** 2590–2596.
7. Lichter, P., Cremer, T., Borden, J., Manuelidis, L., and Ward, D. C. (1988). Delineation of individual human chromosomes in metaphase and interphase cells by in situ suppression hybridization using recombinant DNA libraries. *Hum. Genet.* **80:** 224–234.
8. Lichter, P., Ledbetter, S. A., Ledbetter, D. H., and Ward, D. C. (1990). Fluorescence in situ hybridization with Alu and L1 polymerase chain reaction probes for rapid characterization of human chromosomes in hybrid cell lines. *Proc. Natl. Acad. Sci. USA* **87:** 6634–6638.
9. Lichter, P., Boyle, A. L., Cremer, T., and Ward, D. C. (1991). Analysis of genes and chromosomes by non-isotopic in situ hybridization. *Genet. Anal. Technol. Appl.* **8:** 24–35.
10. Nelson, D. L., Ledbetter, S. A., Corbo, L., Victoria, M. F., Ramirez-Solis, R., Webster, T., Ledbetter, D. H., and Caskey, C. T. (1989). Alu polymerase chain reaction: A method for rapid isolation of human-specific sequences from complex DNA sources. *Proc. Natl. Acad. Sci. USA* **86:** 6686–6690.
11. Pinkel, D., Gray, J. W., Trask, B., van den Engh, G., Fuscoe, J., and van Dekken, H. (1986). Cytogenetic analysis by in situ hybridization with fluorescently labeled nucleic acid probes. *Cold Spring Harbor Symp. Quant. Biol.* **51:** 151–157.
12. Ried, T., Lengauer, C., Cremer, T., Wiegant, J., Raap, A. K., van der Ploeg, M., Groitl, P., and Lipp, M. (1992). Specific metaphase and interphase detection of the breakpoint region in 8q24 of Burkitt lymphoma cells by triple color fluorescence in situ hybridization. *Genes, Chrom. Cancer* **4:** 69–74.
13. Selleri, L., Hermanson, G. G., Eubanks, J. H., and Evans, G. A. (1991). Chromosomal in situ hybridization using yeast artificial chromosomes. *Genet. Anal. Technol. Appl.* **8:** 59–66.

Eur. J. of Histochem.
36, 15-25, 1992
© Luigi Ponzio e figlio - Editori in Pavia

Analysis of chromosomes in molecular tumor and radiation cytogenetics: approaches, applications, perspectives.

C. Cremer[1 2] and T. Cremer[3]

[1]Institute of Applied Physics, University of Heidelberg, Albert-Ueberle-Str. 3-5, D-6900 Heidelberg, Germany; [2]Interdisciplinary Centre for Scientific Computing (IWR), University of Heidelberg, Im Neuenheimer Feld 368, D-6900 Heidelberg; [3]Institute of Human Genetics and Antrophology, University of Heidelberg, Im Neuenheimer Feld 328, D-6900 Heidelberg

Accepted 3/9/1991

Limitations of conventional cytogenetics

For the study of pathological processes the analysis of chromosomes has become of ever growing importance. Today, entire journals are dedicated to this task; thousands of publications so far have shown a close correlation between chromosome aberrations and malignancy (Dal Cin and Sandberg, 1989). Presently, information is available on more than 14,000 neoplasms with an abnormal karyotype (Mitelman *et al.,* 1990). Accordingly, one should have expected that cytogenetics would play a central role not only in tumor research but also in clinical pathology of tumors, as well as therapy planning and control. This, however, until now has not been the case. A major reason for this may be the practical difficulties of conventional chromosome diagnostics:

1) Using chromosome banding procedures, the human workload is too high for extensive applications in a clinical environment.
2) Due to the limitations of microscopic banding analysis, tumorrelevant changes can be detected only if the alterations exceed approximately 2000 to 4000 kilobasepairs (kb) of DNA. Thus, tumorrelevant small alterations (e.g. small translocations, amplifications below a certain amount; submicroscopic deletions; viral integration sites, Doerfler, 1989) cannot be detected in this way.
3) Tumor cells are often difficult to cultivate; even then, they may contain only a few analysable metaphase spreads; it remains unclear whether these few metaphase spreads are representative for the entire tumor cell population.
4) A detailed diagnosis is possible only with metaphase spreads, NOT with interphase nuclei. In particular, specific chromosome aberrations cannot be simultaneously diagnosed in tissue sections viewed by pathologists.

Similar limitations are encountered in the use of conventional staining procedures for the study of chromosome aberrations induced by ionizing irradiation. Translocations may be particularly useful to monitor the effects of a single exposure even many years after such an event has taken place, as well as cumulative effects of multiple or chronic exposures. Since in a variety of cases, malignant tumors are correlated with specific translocations, the correlation with dose of the amount of such translocations in irradiated cells might contribute to better risk estimates for the induction of malignant tumors by ionizing radiation. However, due to the statistical requirements (numbers of cells to be evaluated), the human workload is too high to routinely allow biological dosimetry, particularly in the most important low dose range. Again, a diagnosis of specific aberrations is possibile only with metaphase spreads (e.g. from cultured peripheral lymphocytes), NOT with interphase nuclei. This makes it difficult to analyse the clastogenic effects of *a local* irrradiation exposure of tissues which cannot easily be cultivated *in vitro*.

Attempts to apply automatic image analysis of banded chromosomes (Piper and Lundsteen, 1987; Piper and Granum, 1989; Lundsteen and Piper, 1989) to translocation monitoring in tumor and radiation cytogenetics, so far have met with considerable problems.

New Approaches: General Strategy

To overcome the problems outlined above, a new strategy has been proposed for a rapid and efficient chromosome analysis: only the chromosomes or chromosome subregions relevant for the solution of a given specific problem are highlighted. This approach has been applied not only to metaphase spreads but also to interphase nuclei. Its realization depended on two important technical developments of the last decade, namely the invention of highly sensitive non-isotopic *in situ* hybridization protocols and the generation of numerous human chromosome specific DNA clones (for review see Lichter *et al.,* 1991). The latter development was largely facilitated by the generation of DNA libraries for individual human chromosome types using fluorescence activated chromosome sorting. Quantitative sorting and cloning was first performed with the human sex chromosomes (Davies *et al.,* 1981; Cremer C., *et al.,* 1982, 1984) and later applied to all human chromosome types (Van Dilla *et al.,* 1990). The concept of interphase cytogenetics (Cremer T. *et al.,* 1986) was based on evidence that chromosomes occupy distinct territories (chromosome domains) in the cell nucleus (Cremer C., *et al.,* 1980; Cremer T., *et al.,* 1982; Schardin *et al.,* 1985; Manuelidis, 1985). If only a few chromosome regions of interest are decorated, automated image analysis may be greatly facilitated. With few exceptions, such a strategy has not been feasible using conventional dyes; recently, however, selective "painting" of whole human chromosomes or of chromosomal subregions has become possible. In this new approach DNA probes with a suitable sequence are chemically labelled, e.g. with biotin, aminoacetylfluorene, mercury or digoxigenin; then they are hybridized *in situ* to the complementary sequences of the chromosomal DNA (*in situ* hybridization, ISH). To visualize the binding sites, absorbing dyes, or fluorescence techniques (fluorescence-*in situ*-hybridization, FISH) may be used.

Using conventional fluorescence microscopy, unique DNA-targets as small as 1kb can be detected (for review see Lichter *et al.,* 1991).

In situ suppression (CISS-) hybridization protocols ("chromosome painting") have been designed to suppress the signals of interspersed repetitive sequences which in addition to site specific sequences are present in many cloned DNA probes (Landegent *et al.*, 1987; Cremer T. *et al.*, 1988a; Lichter *et al.*, 1988a; Lengauer *et al.*, 1991; Pinkel *et al.*, 1988; Ried *et al.*, 1990). This achievement makes it possible to use cloned DNA sequences from the human genome, e.g. plasmid, bacteriophage-, cosmid- or yeast artificial chromosome (YAC-) clones either individually or in appropriate combinations for site specific *in situ* hybridization without the need of elaborate subcloning schemes in order to remove unwanted interspersed repetitive elements from these probes. In this way it has become possible to specifically "paint" entire individual chromosomes or chromosome subsets, individual chromosome arms or chromosome band, down to the level of individual genes and intragenic regions (for review see Lichter *et al.*, 1991).

Applications

In the following, a few examples shall be discussed for the application of this new concept in molecular tumor cytogenetics and radiation cytogenetics.

I. Molecular Tumor Cytogenetics

In recent years chromosome specific tandem repetitive sequences located in the constitutive heterochromatin have been cloned for most human chromosomes (Willard and Waye, 1987). Such clones have provided useful tools in FISH-experiments to define specific numerical chromosome aberrations. For example, specific repetitive DNA sequences for human chromosomes 1, 7 and 18 were used to study numerical aberrations of these chromosomes in human glioma cell lines both in metaphase cells and in interphase nuclei (Cremer T. *et al.*, 1988a, b). The majority of these glioma cell nuclei was observed to have three or more hybridization "spots" for each chromosome type, whereas in normal diploid cells, only two hybridization spots were detected in the majority of cases. Such a rapid assessment of numerical aberrations in interphase nuclei has already been applied to a variety of other malignant tumors (Devilee *et al.*, 1988; Hopman *et al.*, 1988, 1991; Anastasi *et al.*, 1990; Van Dekken *et al.*, 1990; Kolluri *et al.*, 1990; Poddighe *et al.*, 1991) including paraffin embedded tissue sections (Emmerich *et al.*, 1989a). An automated image analysis of numerical aberrations should be straightforward if an appropriate contrast can be achieved between the gray level value of the hybridized spot-regions and the gray level values of the surrounding nuclear areas.

To test the feasibility of a threshold oriented automated classification, images of female human lymphocyte nuclei following FISH with an alphoid DNA probe specific for the pericentromeric region on the X chromosomes were analysed. Our preliminary results (Cremer C. *et al.*, 1992) suggest that a rapid and reliable automated classification may indeed be feasible (one to a few seconds per nucleus using a 80386 microprocessor).

For a more general application of ISH methods in the detection of malignancy, it is important to identify also tumorrelevant translocations at all stages of the cell cycle. For this purpose entire human chromosomes have been decorated by CISS-hybridization and applied for the detection of chromosome aberrations in metaphase

and interphase tumor cells (Cremer T. *et al.*, 1988a, 1990). Interphase nuclei with a reciprocal translocation including a segment of the painted chromosome show three domains, i.e. the domain of the unaffected chromosome and two domains reflecting the painted chromosome material in the resulting two translocation chromosomes. The relative sizes of these domains reflect the relative size of the painted chromosomes and chromosome segments in metaphase spreads. Image analysis provides a means to correctly segment the painted chromosome domains by gray-level thresholding (Cremer T. *et al.*, 1988a and our unpublished data). In cases where the painted interphase chromosome domains appear inhomogeneously stained or less compact or where the domains overlap each other a correct determination of the number and size of the painted domains may not be possible. This problem can be greatly reduced by painting exclusively the specific breakpoint regions of interest. For this purpose probes are useful which either span the breakpoint or flank it at both sites. The specificity of this approach was further enhanced by painting the two sites in different colors (Arnoldus *et al.*, 1990; Trask *et al.*, 1991; Lichter *et al.*, 1991). Recently, Ried *et al.*, (1991) have developed a triple color *in situ* hybridization protocol for the specific metaphase and interphase detection of translocations in Burkitt lymphoma cells with breakpoints in 8q24. In addition to the painting of the entire chromosome 8 in blue color using a chromosome 8 specific library, individual clones flanking the breakpoint were used to paint both sites in green and red, respectively. In normal nuclei the green and red signals are colocalized in the normal two blue chromosome 8 domains. In Burkitt tumor cell nuclei, however, this colocalization is only observed in the remaining normal chromosome 8 domain, while the other green and red signal becomes clearly separated by the translocation event. This example may suffice to illuminate the possibilities of a highly specific breakpoint analysis in interphase nuclei. Criteria such as the number, color, size and relative positioning of painted chromosome regions can be used to distinguish tumor nuclei unequivocally from normal nuclei. In principle, an automated, rapid classification should become feasible also in these cases by digitizing the different color images separately; from this, the number, size and relative location of the differently colored spots may be obtained. It will be an important task of automated molecular tumor cytogenetics to set up reliable and rapid automated classification algorithms of multicolored interphase nuclei. The possibility to combine chromosome painting with immunophenotyping of tumor cells (Tiainen *et al.*, 1991) adds another important aspect which may help to improve classification schemes for various tumors in the future.

II. Molecular Radiation Cytogenetics

The recent developments of fluorescence *in situ* hybridization procedures have also opened new perspectives for a rapid classification of irradiation-induced translocations in human cells (Pinkel *et al.*, 1986; Lucas *et al.*, 1989; Cremer T. *et al.*, 1990; Popp *et al.*, 1990a, 1992). Using probes from chromosome specific DNA libraries established by flow sorting of human chromosomes, selective staining of whole human metaphase chromosomes was performed following ^{60}Co-γ-irradiation of stimulated human lymphocytes (Cremer T. *et al.*, 1990). In this way, quadratic dose-effect curves for translocations were obtained by microscopic observation. By counting the number of hybridized interphase chromosome domains, nuclear dose

response curves were obtained which again suggested a quadratic dependence on dose of aberrations of the specific chromosomes painted. As a first clinically relevant application, chromosome aberrations were detected by "painting" procedures in lymphocyte metaphase spreads of patients which had incorporated the radioactive X-ray contrast medium "Thorotrast" about 40 years ago (Popp *et al.,* 1990a). Thorotrast contains the radioisotope ^{232}Th and is permanently stored within the reticulo endothelial system. It decays mostly with α-emission. In two patients studied so far, about 2% of the painted lymphocyte chromosomes were aberrant (translocations; deletions; insertions). In two age matched controls treated at the same time in the same hospital without receiving a Thorotrast injection, however, only about 0.3% of the painted chromosomes showed alterations. A rapid automated detection of radiation-induced chromosome translocations is feasible in appropriately painted metaphase spreads, using simple thresholding procedures. The evaluation is based on the assumption that (in the case of one chromosome type painted) a normal metaphase spread exhibits two painted areas whereas an aberrant metaphase spread containing translocation(s) involving painted chromosome material shows more than two. From the number of recognized signals and their size, the metaphase spreads are classified as "normal" or "aberrant". This approach has the particular advantage that instead of 46 (or more) objects in a metaphase spread, only a few have to be segmented. The results so far indicate a false classification rate of a few percent obtained in this way (Cremer C. *et al.,* 1992). In the future a system can be envisaged which combines automated digital fluorescence microscopy with an automated metaphase finder to relocate the metaphase classified as "abnormal" for the further visual inspection by an experienced cytogeneticist. The workload of the cytogneticist could thus be greatly reduced in particular in the low dose range, where the frequency of aberrant metaphase spreads is low. The accuracy of such a system will then largely depend on the rate of false negatives, i.e. metaphase spreads which are classified as "normal" by the system and are therefore not reviewed although they contain a translocation detectable by the cytogeneticist. A low rate of false negative could probably be achieved by defining strict criteria for the automated classification of "normal" cells, thus accepting a higher rate of false positives, i.e. cells classified "abnormal" by the system but normal by the reviewing cytogeneticist.

A preliminary analysis of lymphocyte nuclei following irradiation and chromosome painting, suggests that threshold segmentation procedures may be used for a classification of chromosome aberrations also in interphase nuclei, if a sufficient contrast between hybridized and non-hybridized areas can be realized (Cremer C. *et al.,* 1992).

In cases where chromosomes can be isolated in suspension, e.g. from human peripheral lymphocytes, a considerable further speed up of automated chromosome analysis may become possible by a laser-technological approach, called Slit-Scan Flow Cytometry (Lucas *et al.,* 1991). In this technique, oriented chromosomes very rapidly pass one after another a focused laser beam. As a result, one obtains time resolved fluorescence profiles (presently up to about 1,000 per second). These profiles may be different for normal and aberrant chromosomes. In case of homogeneous staining for example, a normal chromosome is represented by a bimodal profile with one significant dip (1 centromere), while a dicentric chromosome is represented by a

profile with two significant dips (Cremer C. *et al.*, 1989). To improve the reliability of dicentric detection, the centromeric regions may be highlighted by FISH in suspension (Celeda *et al.*, manuscript in preparation). Fluorescence hybridization of entire chromosomes in suspension (Dudin *et al.*, 1987) may eventually allow the rapid slit scan monitoring of chromosome translocations (Hausmann *et al.*, 1991).

Perspectives

1. The recent development of molecular cytogenetics has already largely closed the gap which so far existed between the analysis of chromosome changes at the light microscopic level and at the DNA level (Ferguson-Smith, 1991). The cytogenetic "resolution" (in terms of the minimum amount of a specific piece of chromosomal DNA identifiable in an individual cell) has been increased a thousand times as compared with conventional cytogenetics (a few kb as compared to a few Mb of DNA contained within a small chromosome band). With image intensifier systems, it might become possible to detect even unique DNA segments smaller than 1 kb routinely (H. Tanke and D.C. Ward, personal communications). In metaphase spreads, these approaches will facilitate the accurate identification of small translocations and deletions. In interphase nuclei as well as in nuclei of terminally differentiated cells they make possible for the first time a cytogenetic analysis of specific numerical and structural aberrations of any chromosome. Multicolor *in situ* hybridization procedures (Nederlof *et al.*, 1990; Trask, 1991) will help to test individual cells simultaneously for a variety of numerical and structural aberrations. In this way tests can be developed which are optimized for the particular needs of a cytogenetic analysis, for example in prenatal diagnosis or in certain types of tumors. More simple and rapid protocols for multicolor *in situ* hybridization are urgently required to speed up the implementation of the new possibilities in routine clinical and tumor cytogenetic laboratories. Individual bacteriophage and cosmid DNA probes directly labelled with fluoresceine have already successfully been used in FISH-experiments (Wiegant *et al.*, 1991; Ried *et al.*, 1991). The commercial availability of fluorochrome labelled probes at moderate costs for specific diagnostic purposes will be of great importance for cytogenetic laboratories who do not have the equipment and expertise presently required for the successful performance of molecular cytogenetics experiments. Various groups are concerned wiht the use of polymerase chain reaction (PCR) to amplify probes (e.g. Lengauer *et al.*, 1990; Lichter *et al.*, 1990; Weier *et al.*, 1990; Celeda *et al.*, 1992; Dunham *et al.*, 1992). In this way more elaborate cloning procedures for probe generation can be avoided.

2. The preliminary results obtained so far suggest that rapid, automated image analysis procedures for painted chromosomes may be feasible and may contribute to a considerable reduction of the human workload. Highly sensitive, fast registration devices suitable for multi-color-fluorescence imaging have to be developed together with appropriate software. For some applications digital transmittance light microscopy of permanently colored *in situ* hybridization specimens will be advantageous. It should, however, be taken into consideration that multicolor analyses will only become feasible in the fluorescent mode. For

example, a chromosome painted in one color, may be banded simultaneously in another color, the colocalization of two colors at a given ratio may distinguish a chromosome target from other targets which are only painted in a single color, as well as from another target painted with these two colors at a distinctly different ratio etc. We expect that in the not too distant future, the possibilities to detect specific genes, mRNAs and proteins simultaneously in the same cell using multicolor fluorescence approaches will not only be of great importance in research laboratories but also become more and more important in many diagnostic settings. In the light of these considerations the development of appropriate systems for digital fluorescence microscopy at a reasonable price appears to be a challenge for the optical and computer industry.

3. So far chromosomal *in situ* suppression hybridization and image analysis has been largely applied to human cells. However, this approach opens new avenues also in animal tumor and radiation research as soon as appropriate DNA probes become available. In this respect the establishment of chromosome specific libraries using fluorescence activated flow sorting from mouse and rat appears as an important goal. In addition to the applications discussed in this review, a wide spectrum of other applications has already been started or can be foreseen in human, animal and plant cytogenetics. Some of these applications, such as the physical mapping of genes both on mitotic chromosomes and in interphase nuclei (Landegent *et al.*, 1987; Lawrence *et al.*, 1988; Trask *et al.*, 1989; Lichter *et al.*, 1990; for review see Lichter *et al.*, 1991), studies of chromosome evolution (Wienberg *et al.*, 1990), as well as studies of the threedimensional structure and arrangements of chromosomes in nuclei of various cell types (Borden and Manuelidis, 1988; Manuelidis and Borden, 1988; Van Dekken *et al.*, 1989; Emmerich *et al.*, 1989b; Popp *et al.*, 1990b; Geiger *et al.*, 1991; Cremer T. *et al.*, 1991; Bradl *et al.*, 1992) will likely improve our understanding of fundamental biological processes. Questions to which extent cell type specific threedimensional arrangements of chromatin may exist in the cell nucleus and whether such arrangments may change during malignant transformation provide research topics of particular interest for which appropriate tools have now been developed in our and other laboratories. Other applications concerning improved cytogenetic analyses of domestic animals and economic plants will likely provide great practical benefits.

ACKNOWLEDGEMENTS

The work of the authors has been supported by the Deutsche Forschungsgmeinschaft, the Deutsche Krebshlife (Mildred Scheel Stiftung) and the Land Baden-Württemberg.

REFERENCES

Anastasi J., Le Beau M.M., Vardiman J.W., and Westbrook C.A.: Detection of numerical chromosomal abnormalities in neoplastic hematopoietic cells by *in situ* hybridization with a chromosome-specific probe. Am. J. Pathol. *136*, 131-139, 1990.

Arnoldus E.P.J., Wiegant J., Noordermeer I.A., Wessels J.W., Beverstock G.C., Grosveld G.C., van der Ploeg M., and Raap A.K.: Detection of the Philadelphia chromosome in interphase nuclei. Cytogenet. Cell Genet. *54,* 108-111, 1990.

Borden J., and Manuelidis L.: Movement of the X chromosome in Epilepsy. Science *242,* 1687-1691, 1988.

Bradl J., Hausmann M., Ehemann V., Komitowski D., and Cremer C.: Towards a three-dimensional axio-tomographical microscopy of human interphase nuclei, submitted, 1992.

Celeda D., Bettag U., and Cremer C.: PCR amplification and simultaneous digoxigenin incorporation of long DNA probes for fluorescence *in situ* hybridization. Biotechniques, in press, 1992.

Cremer C., Cremer T., Fukuda M., and Nakanishi K.: Detection of laser-uv-microirradiation induced DNA photolesions by immunofluorescent staining. Hum. Genet. *54,* 107-110, 1980.

Cremer C., Gray J.W., and Ropers H.H.: Flow cytometric characterization of a Chinese hamster x man hybrid cell line retaining the human Y chromosome. Hum. Genet. *60,* 262-266, 1982.

Cremer C., Rappold G., Gray J.W., Müller C.A., and Ropers H.H.: Preparative dual beam sorting of the human Y chromosome and *in situ* hybridization of cloned DNA probes. Cytometry *5,* 572-579, 1984.

Cremer C., Hausmann M., Zuse P., Aten J.A., Barths J., and Bühring H.J.: Flow cytometry of chromosomes: principles and applications in medicine and molecular biology. Optik *82,* 9-18, 1989.

Cremer C., Remm B., Bischoff A., Vollweller T., Popp S., and Cremer T.: Automated detection of radiation-induced chromosome aberrations following fluorescence *in situ* hybridization. J. Radiat. Res. (Japan), in press, 1992.

Cremer T., Cremer C., Baumann H., Luedtke E.-K., Sperling K., Teuber V., and Zorn C.: Rabls model of the interphase chromosome arrangement tested in Chinese hamster cells by premature chromosome condensation and laser uv-microbeam experiments. Hum. Genet. *60,* 46-56, 1982.

Cremer T., Landegent J.E., Brückner H., Scholl H.P., Schardin M., Hager H.D., Devilee P., Pearson P.L., and Vand der Ploeg M.: Detection of chromosome aberrations in the human interphase nucleus by visualization of specific target DNAs with radioactive and non-radioactive *in situ* hybridization techniques. Diagnosis of trisomy 18 with probe L1.84. Hum. Genet. *74,* 346-352, 1986.

Cremer T., Lichter P., Borden J., Ward D.C., and Manuelidis L.: Detection of chromosome aberrations in metaphase and interphase tumor cells by *in situ* hybridization using chromosome specific library probes. Hum. Genet. *80,* 235-246, 1988a.

Cremer T., Tesin D., Hopman A.H.N., and Manuelidis L.: Rapid interphase and metaphase assessment of specific chromosomal changes in neuroectodermal tumor cells by *in situ* hybridization with chemically modified DNA probes. Exp. Cell Res. *176,* 199-220, 1988b.

Cremer T., Popp S., Emmerich P., Lichter P., and Cremer C.: Rapid metaphase and interphase detection of radiation-induced chromosome aberrations in human lymphocytes by chromosomal suppression *in situ* hybridization. Cytometry *11,* 110-118, 1990.

Cremer T., Remm B., Kharboush I., Jauch A., Wienberg J., Stelzer E., and Cremer C.: Non-isotopic *in situ* hybridization and digital image analysis of chromosomes in mitotic and interphase cells. Rev. Eur. Technol. Biomed. *13,* 50-54, 1991.

Dal Cin P., and Sandberg A.A.: Chromosomal Aspects of Human Oncogenesis. Critical Reviews in Oncogenesis *1,* 113-126, 1989.

Davies K., Young B., Elles R., Hill M., and Williamson R.: Cloning of a representative genomic library of the human X chromosome after sorting by flow cytometry. Nature *293,* 374-376, 1981.

Devilee P., Thierry R.F., Kievits T., Kolluri R., Hopman A.H.N., Willard H.F., Pearson P.L., and Cornelisse C.J.: Detection of chromosome aneuploidy in interphase nuclei from human primary breast tumors using chromosome-specific repetitive DNA probes. Cancer Res. *48,* 5825-5830, 1988.

Doerller W.: Malignant transformation of cells by DNA viruses Adenovirus. DNA integration in the mammalian genome. Critical Reviews in Oncogenesis *1,* 21-219, 1989.

Dudin G., Cremer T., Schardin M., Hausmann M., Bier F., and Cremer C.: A method for nucleic acid hybridization to isolated chromosomes in suspension. Hum. Genet. *76,* 290-292, 1987.

Dunham I., Lengauer C., Cremer T., and Featherstone T.: Rapid generation of chromosome specific alphoid DNA probes using the polymerase chain reaction. Hum. Genet., in press, 1992.

Emmerich P., Jauch A., Hofmann M.C., Cremer T., and Walt H.: Interphase cytogenetics in paraffin embedded sections from human testicular tumor xenografts and in corresponding culture cells. Lab. Invest. *61* (2), 235-242, 1989a.

Emmerich P., Loss P., Jauch A., Hopman A.H.N., Wiegand J., Higgins M., White B.N., Vand der Ploeg M., Cremer C., and Cremer T.: Double *in situ* hybridization in combination with digitized image analysis. A new approach to study interphase chromosome topography. Exp. Cell Res. *181,* 126-140, 1989b.

Ferguson-Smith M.A.: Putting the genetics back into cytogenetics. Am. J. Hum. Genetics *48,* 179-182, 1991.

Geiger B., Komitowski D., Jauch A., Hausmann M., and Cremer C.: Optical sectioning and 3d-image reconstruction to determine the volume of specific chromosome regions in human interphase cell nuclei. Optik (Stuttgart) *86,* 113-119, 1991.

Hausmann M., Dudin G., Aten J.A., Heilig R., Diaz E., and Cremer C.: Slit scan flow cytometry of isolated chromosomes following fluorescence hybridization. An approach on online screening for specific chromosomes and chromosome translocations. Z. Naturf. *46c,* 433-441, 1991.

Hopman A.H.N., Ramaekers F.C.S., Raap A.K., Beck J.L.M., Devilee P., Van der Ploeg M., and Voojis G.P.: *In situ* hybridization as a tool to study numerical chromosome aberrations in solid bladder tumors. Histochemistry *89,* 307-312, 1988.

Hopman A.H.N., Moesker O., Smeets W.G.B., Pauwels R.P.E., and Vooijs G.P.: Numerical chromosomes 1, 7, 9 and 11 aberrations in bladder cancer detected by *in situ* hybridization. Cancer Res. *51,* 644-651, 1991.

Kolluri R.V., Manuelidis L., Cremer T., Sait S., Gezer S., and Raza A.: Detection of monosomy 7 in interphase cells for patients with myeloid disorders. Am.J. Hematol. *33(2),* 117-122, 1990.

Landegent J.E., Jansen in de Wal, N., Dirks R.W., Baas F., and van der Ploeg, M.: Use of whole cosmide cloned genomic sequences for chromosomal localization by non-radioactive *in situ* hybridization. Hum. Genet. *73,* 354-357, 1987.

Lawrence J.B., Vilnave C.A., and Singer R.H.: Cell *52,* 51-61, 1988.

Lengauer C., Riethman H., and Cremer T.: Painting of human chromosomes with probes generated from hybrid cell lines by PCR with Alu and L1 primers. Hum. Genet. *86,* 1-6, 1990.

Lengauer C., Eckelt A., Weith A., Endlich N., Ponelies N., Lichter P., Greulich K.O., and Cremer T.: Painting of defined chromosomal regions by *in situ* suppression hybridization of libraries from laser-microdissected chromosomes. Cytogenetc. Cell Genet. *56,* 27-30, 1991.

Lichter P., Cremer T., Borden J., Manuelidis L., and Ward D.C.: Delineation of individual human chromosomes in metaphase and interphase cells by *in situ* suppression hybridization using recombinant DNA libraries. Hum. Genet. *80,* 224-234, 1988a.

Lichter P., Cremer T., Tang C.C., Watkins P.C., Manuelidis L., and Ward D.C.: Rapid detection of human chromosome 21 aberrations by *in situ* hybridization. Proc. Natl. Acad. Sci. USA *85,* 9664-9668, 1988b.

Lichter P., and Ward D.C.: Is non-isotopic *in situ* hybridization finally coming of age? Nature (London) *345,* 93-95, 1990.

Lichter P., Boyle A.L., Cremer T., and Ward D.C.: Analysis of genes and chromosomes by non-isotopic *in situ* hybridization. Genet. Anal. Techn. Appl. *8,* 24-35, 1991.

Lucas J.N., Tenjin T., Straume T., Pinkel D., Moore D., Litt M., and Gray J.W.: Rapid human chromosome aberration analysis using fluorescence *in situ* hybridization. Int. J. Radiat. Biolog. *56* (1), 35-44, 1989.

Lucas J.N., Mullikin J.C., and Gray J.W.: Dicentric chromosome frequency analysis using slit-scan flow cytometry. Cytometry *12*, 316-322, 1991.

Lundsteen C., and Piper J. (eds): Automation of cytogenetics. Springer Verlag, Berlin, 1989.

Manuelidis L.: Individual interphase domains revealed by *in situ* hybridization. Hum. Genet. *71*, 288-293, 1985.

Manuelidis L., and Borden J.: Reproducible compartimentalization of individual chromosome domains in human CNS cells revealed by *in situ* hybridization and three-dimensional reconstruction. Chromosoma (Berl). *96*, 397-410, 1988.

Mitelman F., Kaneko Y., and Trent J.M.: Report of the committee on chromosome changes in neoplasia. Cytogen. Cell Genet. *55*, 358-396, 1990.

Nederlof P.M., Van der Flier S., Wiegant J., Raap A,K., Tanke H.J., Ploem J.S., and Van der Ploeg M.: Multiple fluorescence *in situ* hybridization. Cytometry *11*, 126-131.

Pinkel D., Straume T., and Gray J.W.: Cytogenetic analysis using quantitative, high sensitive, fluorescence hybridization. Proc. Natl. Acad. Sci. USA *83*, 2934-2938, 1986.

Pinkel D., Landegent J., Collings C., Fuscoe J., Segraves R., Lucas J., and Gray J.W.: Fluorescence *in situ* hybridization with human chromosome-specific libraries. Detection of trisomy 21 and translocations of chromosome 4. Proc. Natl. Acad. Sci. USA *85*, 9138-9142, 1988.

Piper J., and Lundsteen C.: Human chromosome analysis by machine. Trends Genet. *3*, 309-313, 1987.

Piper J., and Granum E.: On fully automatic feature measurement for banded chromosome classification. Cytometry *10*, 242-255, 1989.

Poddighe P.J., Moesker O., Smeets D., Awwad B.H., Ramaekers F.C.S., and Hopman A.H.N.: Interphase cytogenetics of hematological cancer: comparison of classical karyotyping and *in situ* hybridization using a panel of eleven chromosome specific DNA probes. Cancer Res. *51*, 1959-1967, 1991.

Popp S., Remm B., Hausmann M., Luhrs H., Van Kaick G., Cremer T., and Cremer C.: Towards a cumulative biological dosimeter based on chromosome painting and digital image analysis. Kerntechnik *55*, 204-210, 1990a.

Popp D., Scholl H.P., Loos P., Jauch A., Stelzer E., Cremer C., and Cremer T.: Distribution of chromosome 18 and X centric heterochromatin in the interphase nucleus of cultures human cells. Exp. Cell Res. *189*, 1-12, 1990b.

Popp S., Jauch A., Qiu J.Y., Smialek B., Cremer T., and Becher R.: Translocation t(8, 21) in acute non lymphocytic leukemia delineated by chromosomal *in situ* suppression hybridization. Cancer Genet. Cytogenet., in press, 1991.

Popp S., and Cremer T.: Development of a biological dosimeter for translocation scoring based on twocolor fluorescence *in situ* hybridization of chromosome subsets. J. Radiat. Res. (Japan), in press, 1992.

Ried T., Mahler V., Vogt P., Blonden L., Van Ommen G.J.B., Cremer T., and Cremer M.: Carrier detection by *in situ* suppression hybridization with cosmid clones of the Duchenne/Becker muscular dystrophy (DMB/BMD) locus. Hum. Genet. *85*, 581-586, 1990.

Ried T., Lengauer C., Cremer T., Wiegant J., Raap A.K., van der Ploeg M., Grotl P., and Lipp M.: Specific metaphase and interphase detection of the breakpoint region in 8.24 of Burkitt lymphoma cells by triple color fluorescence *in situ* hybridization. Genes, Chromosomes and Cancer, in press, 1991.

Schardin M., Cremer T., Hager H.D., and Lang M.: Specific staining of human chromosomes in Chinese hamster x man hybrid cell lines demonstrates interphase chromosome territories. Hum. Genet. *71*, 281-287, 1985.

Tiainen M., Popp S., Parlier V., Emmerich P., Bellomo M.J., Ruutu T., Cremer T., and Knuutila S.: Chromosomal *in situ* suppression hybridization of immunologically classified mitotic cells in hematological malignancies. Genes, Chromosomes and Cancer, in press, 1991.

Trask B., Pinkel D., and van den Engh G.: Genomics *5*, 710-717, 1989.

Trask B.: Fluorescence *in situ* hybridization. Application in cytogenetic and gene mapping. Trends Genet. *7,* 149-154, 1991.

Van Dekken H., Pinkel D., Mulliken J., Trask B., Van den Engh G., and Gray J.: Three-dimensional analysis of the organization of human chromosome domains in human and human-hamster hybrid interphase nuclei. J. Cell Science *94,* 299-306, 1989.

Van Dekken H., Pizzolo J.G., Reuter V.E., and Melamed M.R.: Cytogenetic analysis of human solid tumors by *in situ* hybridization with a set of 12 chromosome-specific DNA probes. Cytogenet. Cell Genet. *54,* 103-107, 1990.

Van Dilla M.A., and Deaven L.L.: Construction of gene libraries for each human chromosome. Cytometry *11,* 208-218, 1990.

Weier H.-U., Segraves R., Pinkel D., and Gray J.W.: Synthesis of Y chromosome-specific labeled DNA probes by *in vitro* DNA amplification. J. Histochem. Cytochem. *38,* 421-426, 1990.

Wiegant J., Ried T., Nederlof P.M., van der Ploeg M., Tanke H.J., and Rapp A.K.: *In situ* hybridization with fluoresceinated DNA. Nucleic Acids Res., *19,* 3237-3241, 1991.

Willard H.F., and Waye J.S.: Chromosome specific subsets of human alpha satellite DNA: analysis of sequence divergence within and between chromosomal subsets and evidence for an ancestral pentameric repeat. J. Mol. Evol. *25,* 207-214, 1987.

Wienberg J., Jauch A., Stanyon R., and Cremer T.: Molecular cytotaxonomy of primates by chromosomal *in situ* suppression hybridization. Genomics *8,* 347-350, 1990.

J. RADIAT. RES., 33: SUPPLEMENT, 61–70 (1992)

Development of a Biological Dosimeter for Translocation Scoring Based on Two-Color Fluorescence in Situ Hybridization of Chromosome Subsets

S. POPP AND T. CREMER

Institute of Human Genetics and Anthropology, University of Heidelberg,
Im Neuenheimer Feld 328, D-6900 Heidelberg,
Federal Republic of Germany

biological dosimetry/chromosomal aberrations/multicolor fluorescence in situ hybridization/chromosome painting

Recently fluorescence in situ hybridization protocols have been developed which allow the paining of individual chromosomes using DNA-libraries from sorted human chromosomes. This approach has the particular advantage that radiation induced chromosome translocations can be easily detected, if chromosomes of distinctly different colors take part in the translocation event. To enhance the sensitivity of this approach two metaphase chromosome subsets A and B (A: chromosomes 1, 2, 4, 8, 16; B: 3, 5, 9, 10, 13) were simultaneously painted in green and red color. Counterstaining of the chromosomes with DAPI resulted in a third subset which exhibited blue fluorescence only. Green-red, green-blue and red-blue translocation chromosomes could be easily detected after irradiation of lymphocyte cultures with ^{137}Cs-γ-rays. Analyses of painted chromosomes can be combined with conventional GTG-banding analyses. This new biological dosimeter should become useful to monitor both long term effects of single irradiation events and the cumulative effects of multiple or chronic irradiation exposures. In contrast to translocation scoring based on the analysis of banded chromosomes, this new approach has the particular advantage that a rapid, automated scoring of translocations can now be envisaged.

INTRODUCTION

Scoring of chromosomal aberrations in lymphocytes of peripheral blood can serve as a sensitive biological dosimeter of radiation exposures [1]. The usefulness of a biological dosimeter in the low dose range requires that scoring can be performed easily and rapidly in large numbers of cells. For this purpose the evaluation of either micronuclei derived from acentric chromosome fragments [2–4] or of dicentric chromosomes (for review see [5]) has become particulary useful. Dicentric chromosomes can be detected easily in homogeneously stained metaphases and procedures for the automated scoring of dicentrics have been developed [6, 7]. False positives and false negatives, however, impair the accuracy of such analyses particularly at the low dose range. In particular, the distinction between true dicentrics and composites of two normal chromosomes touching or overlapping end to end can be difficult. A more comprehensive analysis of structural chromosome aberrations performed on banded chromosome complements is time consuming and requires skilled personel. A fully automated evaluation of banded

chromosome complements for structural chromosome aberrations has not been possible so far [8].

The formation of micronuclei or dicentrics may lead to cell death. Accordingly, a biological dosimeter based on such aberrations is useful for the detection of acute irradiation effects. Its value, however, is limited in cases where long term biological dosimetry is needed. Such a dosimeter can be based on the detection of reciprocal translocations in irradiated cell populations. By and large cells, such as stem cells of the red bone marrow, with reciprocal translocations would retain the same proliferative potential as normal stem cells. Accordingly, the progeny of red bone marrow stem cells with reciprocal translocations can be detected in the peripheral blood with undiminished frequency even many years after such an event has taken place [9]. In rare cases a specific genetic imbalance may lead to a growth advantage of the affected cell and finally give rise to a tumor cell population [10].

Fluorescence in situ hybridization has become a suitable new tool for the rapid detection of structural chromosome aberrations in metaphase spreads obtained from irradiated cell populations [11, 12]. In particular, "painting" of entire human chromosomes based on chromosomal in situ suppression (CISS-) hybridization protocols [13, 14] in combination with digital image analysis can be applied for the rapid evaluation of translocation chromosomes composed of differently colored chromosome segments [15–20]. Using this approach, we have evaluated chromosome translocations in patients who had received an intravascular injection of Thorotrast more than fourty years ago [17]. This X-ray contrast medium contains ^{232}Thorium which decays mainly under emission of alpha-particles. The percentage of translocations was found to be significantly higher in exposed patients than in controls.

In the studies mentioned above, a single chromosome type, e.g. chromosome 1, occasionally two chromosome types, e.g. chromosome 1 and 2, were painted in each cell. In the present study we have painted two subsets, each comprising five chromosome pairs, simultaneously in green and red color. In this way, the number of translocations which can be simultaneously scored in each metaphase spread can be increased. It is our aim to develop a new, sensitive biological dosimeter able to detect the long term effects of single radiation exposures, as well as the cumulative effects of repeated or chronic irradiation at the low dose range.

MATERIALS AND METHODS

Cell Material

10 ml of blood was obtained from a female donor (46, XX) and irradiated at room temperature with 8 Gy of ^{137}Cs-γ-rays (662 keV). Lymphocytes were isolated, stimulated with phytohemagglutinin (PHA) to divide and cultured for 72 hours using standard techniques [21]. Colcemid arrested metaphase spreads were obtained after hypotonic treatment (0.075 M KCl) and fixation with methanol/acetic acid (3:1, vv). For control experiments 10 ml of blood was obtained from a male donor (46, XY) and cultivated as described above.

Pretreatment of slides

Prior to CISS-hybridization experiments slides were pretreated according to the following standard protocol with modifications described below. Slides were digested with RNase A (100 μg/ml 2×SSC) for 1 h at 37°C, washed three times, 5 min. each, in 2×SSC, digested with pepsin (50 mg/ml in 0.01 M HCl) for 10 min. at 37°C, washed 2×5 min. in phosphate buffered saline (PBS) and 5 min. in PBS containing 50 mM $MgCl_2$ and then postfixed for 10 min. at room temperature in 1% formaldehyde (Merck) in PBS containing 50 mM $MgCl_2$. After another washing step in PBS slides were dehydrated in 70%, 90% and 100% ethanol.

In some experiments chromosomes were banded prior to in situ hybridization using a standard protocol for GTG-banding [22] and photographed with Agfa ortho 16 DIN black and white negative films. The oil was removed by xylene and xylene/ethanol (1:1), 5 min. each. Slides were then destained in methanol/acetic acid (3:1, vv), 2×5 min. After an ethanol series with descending concentrations (100%, 90% and 70% ethanol, 3 min. each) and 5 min. washing in PBS slides were postfixed for 10 min. at room temperature in PBS containing 3.7% formaldehyde [23]. After washing steps in PBS and in 2×SSC slides were digested with RNase A and pepsin and postfixed in 1% formaldehyde as described above.

DNA libraries and CISS-hybridization

Bacteriophage libraries from sorted human chromosomes 3 (LA03NS02), 5 (LA05NS01), 9 (LL09NS01) were obtained from the American Type Culture Collection. Plasmid libraries from sorted human chromosomes 1, 2, 4, 8, 10, 13, 16 were kindly provided by Dr. Joe Gray [24]. Amplification of these libraries and isolation of bacteriophage and plasmid DNA were carried out according to standard protocols [25]. Library DNAs from several sorted chromosomes were mixed to generate two probe sets A and B. Probe set A contained the library DNAs for chromosomes 1, 2, 4, 8 and 16, probe set B contained the DNAs for chromosome 3, 5, 9, 10 and 13. Optimum DNA amounts for each chromosome were determined empirically in order to achieve painting with a roughly similar intensity on all chromosomes of a given subset. For example, in our present experiments one μg DNA of probe set A contained 170 ng+240 ng +110 ng+240 ng+240 ng of plasmid DNA from chromosome libraries 1, 2, 4, 8, 16, respectively. One μg DNA of probe set B contained 240 ng bacteriophage DNA each from the chromosome libraries 3, 5, 9, 120 ng plasmid DNA from chromosome library 10 and 160 ng plasmid DNA from chromosome library 13. These DNA amounts should be taken as a hint and may have to be modified for the particular needs of other laboratories. Nicktranslation of the probe sets was carried out either with biotin-11-dUTP (Sigma) or digoxigenin-11-dUTP (Boehringer Mannheim) using standard protocols [26]. 10 μl of hybridization mixture contained 0.5 to 1 μg of each probe set, 25 μg human Cot 1-DNA (BRL) and 25 μg sonicated salmon sperm DNA (Sigma). CISS-hybridization was carried out as described [13, 26]. Biotin-labeled probes were detected using avidin conjugated to rhodamine isothiocyanate (XRITC) (Vector Laboratories). Signals were amplified once [11] using biotin-conjugated antibodies against avidin (Vector Laboratories) followed by another rhodamine-avidin step. Digoxigenin-labeled probes were detected by indirect immunofluorescence using a mouse monoclonal antibody against digoxigenin (Boehringer Mannheim) and an anti mouse lgG

conjugated with fluorescein isothiocyanate (FITC) made in sheep (Sigma). Signal amplification was obtained with anti-sheep IgG conjugated with FITC made in donkey (Sigma). Cells were counterstained with 0.2 μg/ml 4',6-diamidino-2-phenylindole-dihydrochloride (DAPI) and mounted in fluorescence antifading buffer [27]. Cells were viewed with a Zeiss photomicroscope Axiophot equipped for epifluorescence using a Plan-Neofluar 100×/1.3 oil objective. Filter combinations used were as follows: FITC: BP 450–490, FT 510, LP 515–565 or LP 520; XRITC: BP 546, FT 580, LP 590; DAPI: BP 365, FT 395, LP 397. For microphotographs with double and triple exposures a double band pass filter for the simultaneous FITC- and rhodamine-detection (Corl Zeiss, Oberkochen, Germany) was used. Microphotographs were taken on Agfachrome 1000 ASA color slide films.

RESULTS

Two color CISS-hybridization with two probe sets A and B was applied to metaphase spreads prepared from normal human lymphocyte cultures and cultures irradiated with 8 Gy of ^{137}Cs-γ-rays. Probe set A painted the human chromosomes 1, 2, 4, 8 and 16, probe set B chromosomes 3, 5, 9, 10 and 13. After detection of the hybridized chromosomes with the fluorochromes FITC or rhodamine a green and a red chromosome subset could be easily distinguished (Fig. 1a, b). Counterstaining of the whole chromosome spread with DAPI (Fig. 1c) results in a third chromosome subset exhibiting blue fluorescence only (compare Fig. 1c with 1d). In the following this subset is briefly referred to as blue chromosome subset although the red and green painted chromosomes were simultaneously stained with the blue DAPI fluorochrome. Accordingly, any translocation occuring between chromosomes of differently colored subsets could easily be scored in the irradiated cell sample, including green-red, green-blue, red-blue translocation chromosomes, even when the amount of translocated chromosome material was small (see Fig. 2a-f, k-p, for examples). GTG-banding was performed prior to CISS-hybridization and allowed conventional chromosome banding analyses in addition to the analyses of painted chromosomes (Fig. 2m, p, s, v). While the unequivocal identification of aberrant chromosomes was often difficult or even impossible when based solely on chromosome banding, the contribution of chromosome material from each of the three distinctly colored

Fig. 1. Peripheral human lymphocyte metaphase spread (46, XY) after two-color CISS-hybridization with probe set A (biotin-labeled DNA from human chromosome libraries 1, 2, 4, 8, 16) and probe set B (digoxigenin-labeled DNA from human chromosome libraries 3, 5, 9, 10, 13).

a: Chromosome pairs 3, 5, 9, 10 and 13 painted with fluoresceine isothiocyanate (FITC, green fluorescence).

b: Chromosomes 1, 2, 4, 8 and 16 painted with rhodamine isothiocyanate (red fluorescence).

c: Metaphase after counterstaining with DAPI (blue fluorescence).

d: Same metaphase after triple exposure. Note the three subsets of chromosomes painted green, red or blue only.

chromosome subsets to aberrant chromosomes, such as translocation chromosomes (see above), ring chromosomes (Fig. 2g, h, t-v), chromosome fragments (Fig. 2q-s), as well as to micronuclei (Fig. 2i, j) could be unequivocally determined.

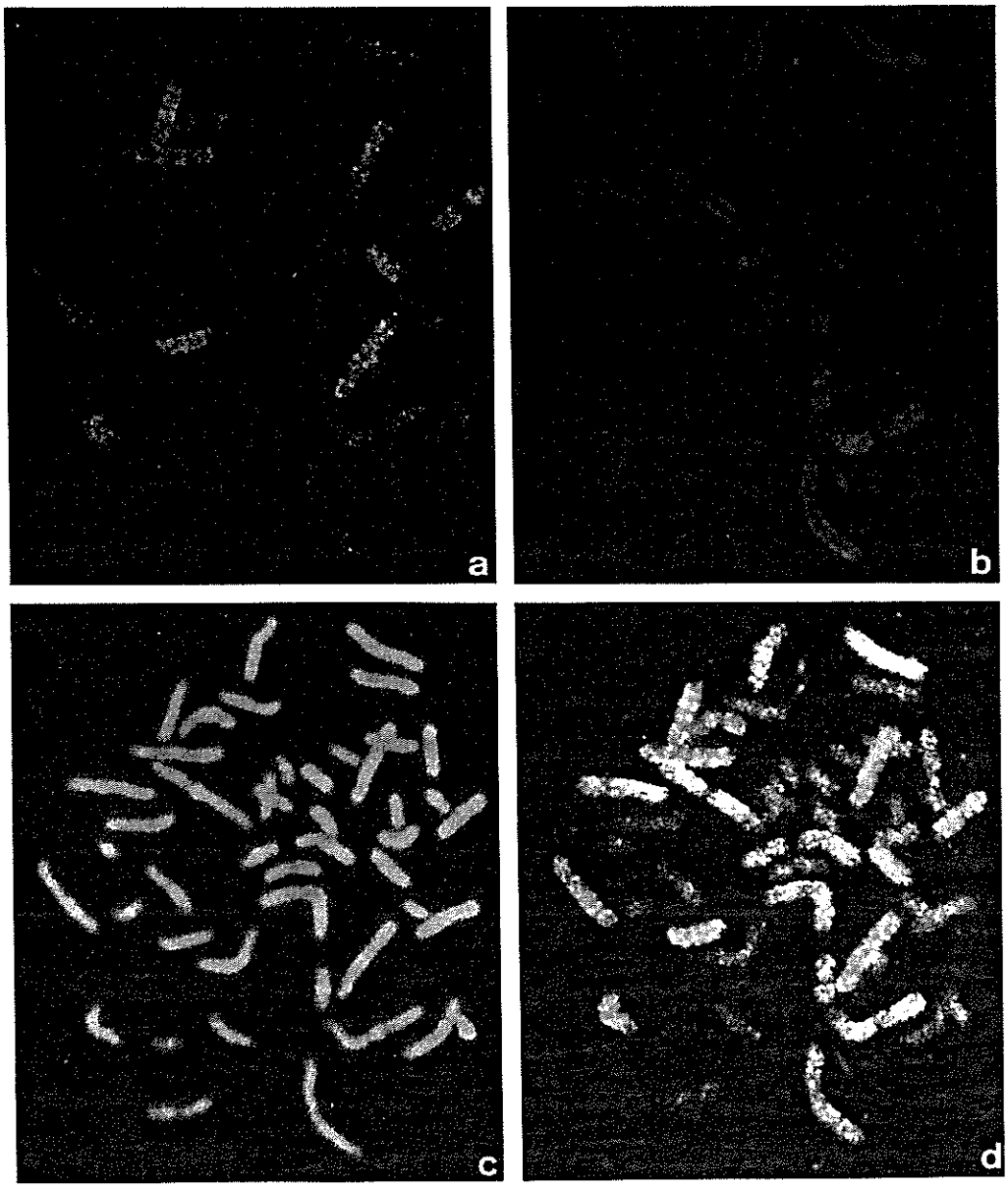

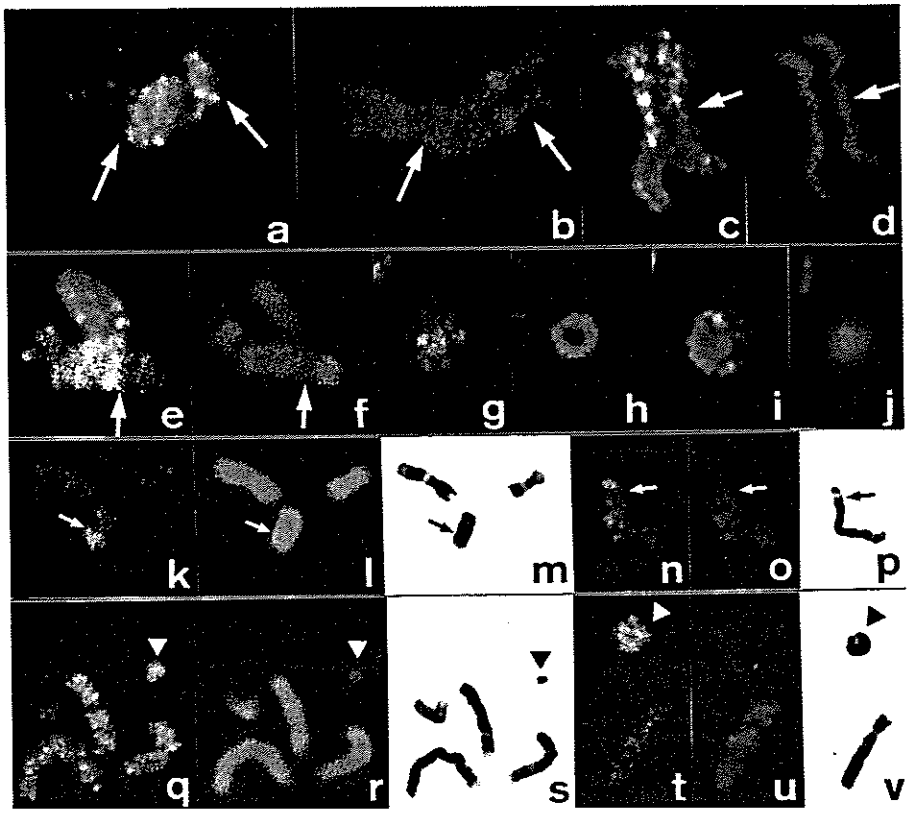

Fig. 2. Metaphase chromosome spreads with multiple chromosome aberrations obtained from a peripheral human lymphocyte culture (46, XX) irradiated with 8 Gy of ^{137}Cs-γ-rays after two-color CISS-hybridization with DNA probe set A (human chromosome libraries 1, 2, 4, 8, 16) and probe set B (human chromosome libraries 3, 5, 9, 10, 13). a, b, g-j: probe set A labeled with digoxigenin and detected with FITC-conjugated antibodies (green fluorescence); probe set B labeled with biotin and detected with rhodamine-conjugated avidin (red fluorescence); c-f, k-v: probe set A labeled with biotin (red fluorescence); probe set B labeled with digoxigenin (green fluorescence).

a, b) Translocation chromosome with green painted chromosome material (a) counterstained with DAPI (b). Arrows point to the breakpoint regions.

c, d) Endoreduplicated translocation chromosome detected with probe set A (red) and probe set B (green) (c) and counterstained with DAPI (d). Arrow points to the breakpoint region.

e, f) Partial metaphase spread shows two painted chromosomes and one non-painted chromosome (e) all counterstained with DAPI (f). An acrocentric chromosome (#13) is painted entirely green. Part of a submetacentric translocation chromosome is painted red, while the other part is exclusively stained with DAPI. Arrow points to the breakpoint region. A small metacentric chromosome (left) is stained with DAPI. Note that very small translocations may not be distinguished from background. For example, two red fluorescent dots on this chromosome are considered as background dots.

g, h) Ringchromosome entirely painted with probe set B (red fluorescence; g), counterstained with DAPI (h).

DISCUSSION

This study demonstrates that two-color fluorescence in situ hybridization of chromosomal subsets can be used to develop a biological dosimeter based on translocation scoring. Two chromosomal subsets (combining chromosomes 1, 2, 4, 8, 16 and 3, 5, 9, 10, 13, respectively) were detected with green and red fluorochromes in different combinations. A third subset comprising the non-hybridized chromosomes exhibited blue fluorescence only after counterstaining with DAPI. With this approach any translocation of at least a few megabase size between chromosomes of different color can be easily detected. Painting of chromosome subsets can be combined with conventional chromosome banding analysis (e.g. [23, 26]). Translocation scoring based on a distinct change of color along an individual chromosome should provide a new and particulary useful possibility for automation. Sensitive color CCD-cameras are presently being developed and may be used to digitize images from multicolored chromosome spreads for further analyses. It can be expected that such an approach will also help to facilitate the automated image analysis of overlapping chromosomes painted in different colors. Additional labelling of centromeric and telomeric chromosomal subregions can be used to distinguish between true di- or multicentric chromosomes and composite chromosomes (false positives). In conclusion, multicolor painting of chromosome subsets should result in a long term biological dosimeter with considerably improved sensitivity as compared to the routine evaluation of dicentric chromosomes.

The general applicability of the biological dosimeter described in this report is presently limited by the requirements of multicolor chromosome painting in routine cytogenetic laboratories. Limitations due to the difficulties of probe generation, labeling and detection protocols, however, will likely be overcome in the near future when painting probes directly conjugated with appropriate fluorochromes become commercially available. In addition, digital fluoresc-

---

i, j) Micronucleus derived from chromosome material detected with both probe sets A and B (i), counterstained with DAPI (j).

k-m) Partial metaphase spread shows two normal chromosomes 11 and 17 and an aberrant chromosome after CISS-hybridization (k), counterstaining with DAPI (l) and GTG-banding (m). The aberrant chromosome shows a small translocation painted green with probe set B (arrow). The rest of this chromosome is stained with DAPI. The two normal chromosomes are also not painted.

n-p) Translocation chromosome composed of two chromosome subregions painted with probe sets A (n) and B (o) after GTG-banding (p). Arrows point to the breakpoint region.

q-s) Partial metaphase spread shows four chromosomes and a small chromosome fragment (arrowhead) after two-color CISS-hybridization (q), counterstaining with DAPI (r) and GTG-banding (s). Two normal chromosome 9 homologs and the fragment are painted green, while a normal chromosome 4 is painted red. A normal chromosome 19 is exclusively stained with DAPI.

t-v) Partial metaphase spread shows two chromosomes with GTG-banding (v), a green painted ring chromosome (t) and a red painted chromosome 4 (u).

ence microscopy will help to increase the number of useful fluorochromes. For example, even fluorochromes emitting in the infrared can be included. In addition, painting probes may be labeled with two fluorochromes simultaneously. In this way chromosomes with colocalization of two fluorochromes can be easily distinguished from other chromosomes which show fluorescence from a single fluorochrome only [28]. When designing improved versions of a biological dosimeter based on multicolor chromosome painting, one has to weigh the potential benefit of more sophisticated painting protocols which also require more sophisticated hardware and software for automated evaluation against the practicability of such protocols. Our goal is to increase the sensitivity of the translocation scoring to an extent which is useful for dosimetry in the low-dose range. This approach could also be applied to study the effects of ageing on the frequency of interchromosomal rearrangements in various cell types of a normal population.

The approach described in this paper should also be useful to define the composition of marker chromosomes in clinical and tumor cytogenetics which cannot be analyzed by classical banding procedures alone. Using multicolor CISS-hybridization with probes for several chromosomal subsets the chromosomal origin of a marker chromosome can be narrowed down rapidly to a few candidate chromosomes. Additional multicolor CISS-hybridization experiments with individual chromosome libraries and chromosome band specific DNA probes can then be defined to pinpoint the exact origin of the marker chromosome.

As compared to translocation scoring by conventional banding analyses the requirements for chromosome spreading are less demanding in multicolor chromosome painting experiments. In the latter approach translocations can be easily detected even in metaphase spreads with poor spreading. Furthermore, overlapping chromosomes of different color can be more easily segmented with appropriate filtering (our unpublished data). Still, the requirement of mitotic cells for translocation scoring provides a major obstacle for the application of a biological dosimeter, for example in cases of local irradiation of tissues from which metaphase spreads cannot easily be prepared in sufficient numbers. Therefore, it would be highly desirable, if a biological dosimeter could be developed for chromosome aberration scoring directly in cell nuclei of irradiated tissues. In contrast to the painting of individual chromosomes which has been supplied successfully for the scoring of chromosome translocations in the interphase nucleus [15], [16], nuclear painting patterns derived from the painting of chromosomal subsets as described in this paper are not suitable for such interphase cytogenetic analyses. The sensitivity and accuracy with which chromosome translocations can be detected in interphase nuclei after multicolor painting of individual chromosome domains and the potential of such an approach for automated analyses provides an important field for future investigations. Region specific probes are generally more useful for interphase cytogenetics than whole chromosome paint libraries. The number of such probes useful for the interphase detection of specific numerical or structural chromosome aberrations is rapidly increasing. Using such probes, it may become possible to detect specific subpopulations of interphase cells containing irradiation induced preneoplastic or neoplastic chromosome aberrations, for example in the bone marrow of an irradiated patient.

ACKNOWLEDGEMENTS

We thank Dr. Masafumi Taniwaki for advice in chromosome banding procedures, Brigitte Schoell for the preparation of probe DNAs, Dorothea Schwarz, Verona Weickardt and Angelika Wiegenstein for photographic work, the German Cancer Research Center, Heidelberg, for the possibility to use a ^{137}Cs-γ-ray source, and the Land Baden-Württemberg for financial support. Part of the costs of the color figures were generously covered by the Carl Zeiss company, Oberkochen, Germany.

REFERENCES

1. W. G. Eisert and M. L. Mendelsohn (1984) Biological dosimetry, cytometric approaches to mammalian systems. Springer Verlag, Berlin.
2. H. J. Evans, C. J. Neary, F. S. Williamson (1959) The relative biological efficiency of single doses of fast neutrons and gamma rays on Vicia faba roots and the effect of oxygen, Part II. Chromosome damage: The production of micronuclei. Int. J. Radiat. Biol., **3**: 216–229.
3. M. Fenech and A. A. Morley (1986) Cytokinesis-block micronucleus method in human lymphocytes: Effect of in vivo ageing and low dose X-irradiation. Mut. Res., **161**: 193–198.
4. J. S. Prosser, J. E. Moquet, D. C. Lloyd, A. A. Edwards (1988) Radiation induction of micronuclei in human lymphocytes. Mut. Res., **199**: 37–45.
5. D. C. Lloyd (1984) An overview of radiation dosimetry by conventional cytogenetic methods. Biological dosimetry (Eds. W. G. Eisert and M. L. Mendelsohn). Springer Verlag, Berlin. pp. 3–14.
6. T. Lörch, C. Wittler, G. Stephan, J. Bille (1989) An automated chromosome aberration scoring system. Automation of cytogenetics (Eds. C. Lundsteen and J. Piper). Springer Verlag, Berlin. pp. 19–30.
7. C. Cremer, M. Hausmann, P. Zuse, J. A. Aten, J. Barths, H. J. Bühring (1989) Flow cytometry of chromosomes: principles and applications in medicine and molecular biology. Optik, **82**: 9–18.
8. J. Piper, E. Granum (1989) On fully automatic feature measurement for banded chromosome classification. Cytometry, **10**: 242–255.
9. A. A. Awa, T. Sofuni, T. Honda, M. Itoh, S. Neriishi, M. Otake (1978) Relationship between the radiation dose and chromosome aberrations in atomic bomb survivors of Hiroshima and Nagasaki. J. Radiat. Res., **19**: 126–140.
10. Y. Kano, A. J. Grosovsky, J. B. Little (1987) Interrelationships among X-ray-induced anchorage independence mutagenesis and chromosomal rearrangements in human diploid fibroblasts. Int. J. Cancer, **40**: 64–68.
11. D. Pinkel, T. Straume. J. W. Gray (1986) Cytogenetic analysis using quantitative, high sensitive, fluorescence in situ hybridization. Proc. Natl. Acad. Sci. USA, **83**: 2934–2938.
12. J. N. Lucas, T. Tenjin, T. Straume, D. Pinkel, D. Moore, M. Litt, J. W. Gray (1989) Rapid human chromosome aberration analysis using fluorescence in situ hybridization. Int. J. Radiat. Biol., 56, **1**: 35–44.
13. P. Lichter, T. Cremer, J. Borden, L. Manuelidis, D. C. Ward (1988) Delineation of individual human chromosomes in metaphase and interphase cells by in situ suppression hybridization using recombinant DNA libraries. Hum. Genet., **80**: 224–234.
14. D. Pinkel, J. Landegent, C. Collins, J. Fuscoe, R. Segraves, J. Lucas, J. W. Gray (1988) Fluorescence in situ hybridization with human chromosome-specific libraries: detection of trisomy 21 and translocations of chromosome 4. Proc. Natl. Acad. Sci. USA, **85**: 9138–9142.

15. T. Cremer, P. Lichter, J. Borden, D. C. Ward, L. Manuelidis (1988) Detection of chromosome aberrations in metaphase and interphase tumor cells by in situ hybridization using chromosome-specific library probes. Hum. Genet., **80**: 235–246.
16. T. Cremer, S. Popp, P. Emmerich, P. Lichter, C. Cremer (1990) Rapid metaphase and interphase detection of radiation-induced chromosome aberrations in human lymphocytes by chromosomal suppression in situ hybridization. Cytometry, **11**: 110–118.
17. S. Popp, B. Remm, M. Hausmann, H. Lührs, G. van Kaick, T. Cremer, C. Cremer (1990) Towards a cumulative biological dosimeter based on chromosome painting and digital image analysis. Kerntechnik, 55, **4**: 204–210.
18. T. Cremer, B. Remm, I. Kharboush, A. Jauch, J. Wienberg, E. Stelzer, C. Cremer (1991) Non isotopic in situ hybridization and digital image analysis of chromosomes in mitotic and interphase cells. Proceedings of the First European Conference on Biomedical Engineering. Nice, February 1991, RBM, **13**: 50–54.
19. C. Cremer, B. Remm, A. Bischoff, T. Vollweiler (1992) Automated detection of radiation-induced chromosome aberrations following fluorescence in situ hybridization J. Radiat. Res., inpress.
20. J. W. Evans, J. A. Chang, A. J. Giaccia, D. Pinkel, J. M. Brown (1991) The use of fluorescence in situ hybridization combined with premature chromosome condensation for the identification of chromosome damage. Br. J. Cancer, **63**: 517–521.
21. H. G. Schwarzacher (1970) Präparation von Mitose-Chromosomen. Methoden in der medizinischen Cytogenetik (Eds. H. G. Schwarzacher, U. Wolf). Springer-Verlag, Berlin. pp. 55–66.
22. R. S. Verma and A. Babu (1989) Human chromosomes. Manual of basic techniques. Pergamon press, Inc., New York. pp. 47–49.
23. M. Klever, C. Grond-Ginsbach, H. Scherthan, T. M. Schroeder-Kurth (1991) Chromosomal in situ suppression hybridization after giemsa banding. Hum. Genet., **86**: 484–486.
24. C. Collins, W. L. Kuo, R. Segraves, J. Fuscoe, D. Pinkel, J. W. Gray (1991) Construction and characterization of plasmid libraries enriched in sequences from single human chromosomes. Genomics, **11**: 997–1006.
25. T. Maniatis, E. F. Fritsch, J. Sambrook (1982) Molecular cloning. A laboratory manual. Cold Spring Harbor Laboratory, New York.
26. P. Lichter and T. Cremer (1991) Chromosome analysis by non-isotopic in situ hybridization. Human Cytogenetics, Vol. 1: A practical approach (Eds. D. E. Rooney and B. H. Czepulkowski). 2nd edition. IRL Press, Oxford, in press.
27. G. D. Johnson and G. M. de C. Nogueira Araujo (1981) A simple method of reducing the fading of immunofluorescence during microscopy. J. Immunol. Methods, **43**: 349–350.
28. P. Nederlof, S. van der Flier, J. Wiegant, A. K. Raap, H. J. Tanke, J. S. Ploem, M. van der Ploeg (1990) Multiple fluorescence in situ hybridization. Cytometry, **11**: 126–131.

HOCHAUFLÖSENDE FLOWCYTOMETRIE UND SORTIERUNG MENSCHLICHER TUMORZELLEN

Prof.Dr.W.Göhde

Klinik und Poliklinik für Strahlentherapie
der Universität
4400 Münster

Hochauflösende DNS- und Protein-Durchflußzytophotometrie und Sortierung menschlicher Tumorzellen

W.Göhde

1. Einleitung

Die DNS-Durchflußzytophotometrie fand in den letzten Jahren wieder mehr Interesse, weil sich das DNS-Histogramm als vergleichsweise zuverlässiger Tumormarker erwies: die überwiegende Mehrzahl aller soliden Tumore ist aneuploid. Während der Nachweis von Aneuploidien bei Spontantumoren mit klassischen zytogenetischen Methoden zeitaufwendig (Kultivierung) und häufig unsicher ist (nicht alle Tumorzellinien liefern mit gleicher Sicherheit auswertbare Metaphasen), gelingen Ploidiebestimmungen mit Hilfe der Zytophotometrie und der Durchflußzytophotometrie heute auch in der täglichen klinischen Routine.

Als klinisch verwertbare Informationen werden u.a. angestrebt:

1. Hinweise über die Prognose
2. Absicherung der Diagnose
3. Verlaufskontrolle nach Behandlung

zu 1: Der Wert der DNS-Histogramme für die Vorhersage des weiteren Krankheitsverlaufs (Prognose) wird noch immer diskutiert. Meist beschränkt sich diese Diskussion auf den Vergleich der klinischen Daten der diploiden mit denen der aneuploiden oder multiklonalen Fälle. Die Zuordnung der einzelnen zytometrischen Befunde zu einer dieser drei Gruppen hängt in hohem Maße von der Art der Probenaufbereitung und der Meßgenauigkeit ab: je besser die erzielte Auflösung ist, desto mehr Fälle lassen sich als aneuploid (Abb.1) oder multiklonal (Abb.2) einordnen.

zu 2:

A) Aneuploidie ist ein sicherer Tumormarker (Abb.1). Ein aneuploider Befund sollte stets als Neoplasie angesehen werden; in der überwiegenden Zahl der Fälle bedeutet das Malignität. Nicht endgültig bewiesen ist, ob Aneuploidie immer zu maligner Entartung (ein "klinischer" Befund) führt.

B) Die Bedeutung des Auftretens einzelner abnormer Zellen für die Diagnose und prognostische Einschätzung einer Erkrankung wird noch diskutiert: z.B. Häufigkeit von Zellen mit mehr als 5c-DNS-Gehalt (Auer). Einzelzellzytophotometrie und Flow-Zytophotometrie werden gleichermaßen bemüht, um hier klinisch verwertbare Antworten zu finden.

C) Es wird in der Literatur zunehmend darüber berichtet, daß funktionelle Parameter von hohem diagnostischem und prognostischem Wert sein können. Ein solcher funktioneller Parameter ist die proliferative Aktivität bzw. der Anteil der Zellen in der DNS-Synthesephase.

S-Phase Anteile lassen sich unmittelbar aus den DNS-Histogrammen abschätzen oder durch zusätzliche Antikörpermarkierung (nach BUdR-Einbau) quantifizieren. Man erhält dadurch eine Information, die dem 3H-Thy-Markierungsindex entspricht.

Da Tumorbiopsien Mischkollektive unterschiedlicher Zellinien sind, werden auch hier höchste Anforderungen an die Meßtechnik gestellt.

D) Ein weiterer in der Pathologie geläufiger Parameter zur Charakterisierung unterschiedlicher Zellarten ist die "Kern-Plasma-Relation", als deren biochemisches Äquivalent das DNS-Protein-Verhältnis angesehen werden kann (Abb.3). Inwieweit die simultane Messung des DNS- und Proteingehaltes zur noch besseren Erkennung unterschiedlicher Zellarten in Tumorbiopsien herangezogen werden kann, soll im Laufe des Kurses ebenfalls erprobt und diskutiert werden.

E) Die on line-Zellsortierung hat bisher kaum Eingang in die klinische Routine gefunden; dafür gibt es eine Reihe von Gründen. Als ein Beispiel für den Wert der Zellsortierung sei die Bearbeitung "diploider" bzw. fraglicher zytophotometrischer Befunde genannt. Die Zellsortierung, d.h. die Anreicherung bestimmter und ggf. sehr seltener Zellen schlägt hier eine Brücke zur Zytomorphologie bzw. Einzelzellzytophotometrie.

zu 3: Über Verlaufskontrollen nach Behandlung von Malignomen wurde gelegentlich berichtet. Dabei wurden insbesondere die Veränderungen der Häufigkeit aueuploider Zellen bzw. deren Wiederauftreten als Ankündigung eines Rezidivs und die behandlungsbedingte Beeinflussung des Ablaufs der Zellteilung ausgewertet.

2. Geräte

FCM: Für den Kurs stehen Geräte zur Verfügung, die Fluoreszenzanregungen bis zum kurzwelligen UV erlauben. Für die hochauflösenden DNS-Messungen eignen sich besonders kovalent bindende Farbstoffe wie DAPI und Hoechst. CV's von menschlichen Zellen und den meisten Tumorzellen im Bereich deutlich unter 2% sollten damit auch in der klinischen Routine möglich sein.

Sortierung: Hochauflösende DNS-Durchflußzytophotometrie und Sortierung erfordern neue Konzepte für die Datenacquisition. Real-time display, Vermeidung von interrupts und die freie Wahl von Sortierfenstern (bis zu 1 Kanal Breite bei 1-Parameter-Sortierung und über den Rechner kontrollierte Sortierfenster beliebiger Form bei 2-Parameter-Sortierung) sind bei Tumoren oft Voraussetzung für die effektive Sortierung. Abb.4 zeigt das Sortierprinzip schematisch.

3. Protokolle

DNS-Messung: Den Teilnehmern werden alle gängigen Möglichkeiten der DNS-Fluoreszenzmessung angeboten (DAPI, Hoechst, PJ, EB, MMC etc.). Im Vordergrund steht ein modifiziertes Otto-Protokoll: Damit erhält man sehr gute DNS-Verteilungen bei weitgehender Vermeidung von Zellaggregaten.

DNS-Protein-Messung: Für die 2-Parametermessungen werden die Zellen mit DAPI und SR 101 fluorochromiert (Stöhr und Goerttler). Die Anregung beider Fluorochrome kann mit UV-Licht erfolgen.

Zellsortierung: Für die Zellsortierung steht ein Sorter zur Verfügung, der ein geschlossenes Flüssigkeits-System aufweist (siehe beiliegende Abb.). Das System erlaubt input-Raten von 15 000 Zellen pro Sekunde (Mehrparameter-Sortierung) bis über 20 000 Zellen pro Sekunde (Einparameter-Sortierung), wobei die output Rate von bis zu 300 Zellen pro Sekunde noch gute Reinheit der Sortierfraktion garantiert.

Datenverarbeitung: Für die Acquisition bei real-time-Darstellung und mit list mode wird ein Mortorola 68020-Prozessor verwendet. Spezielle Auswertungen können z.B. off line mit IBM Rechnern erfolgen (z.B. DPAC, Multicycl,).

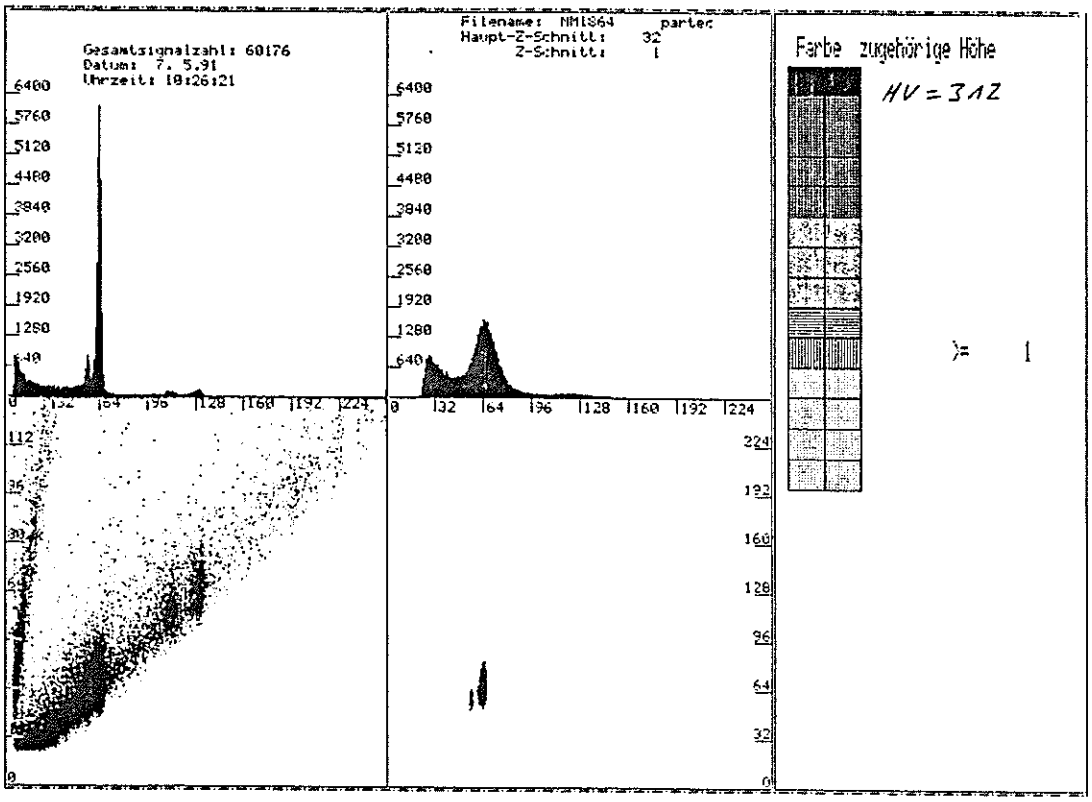

Abb. 1
DNS- und Protein-Histogramm eines Mamma Carcinoms.
oben links : DNS-Histogramm
oben rechts: Protein-Histogramm
unten : zwei unterschiedliche Z-Schnitte des DNS-Protein-Histogramms.

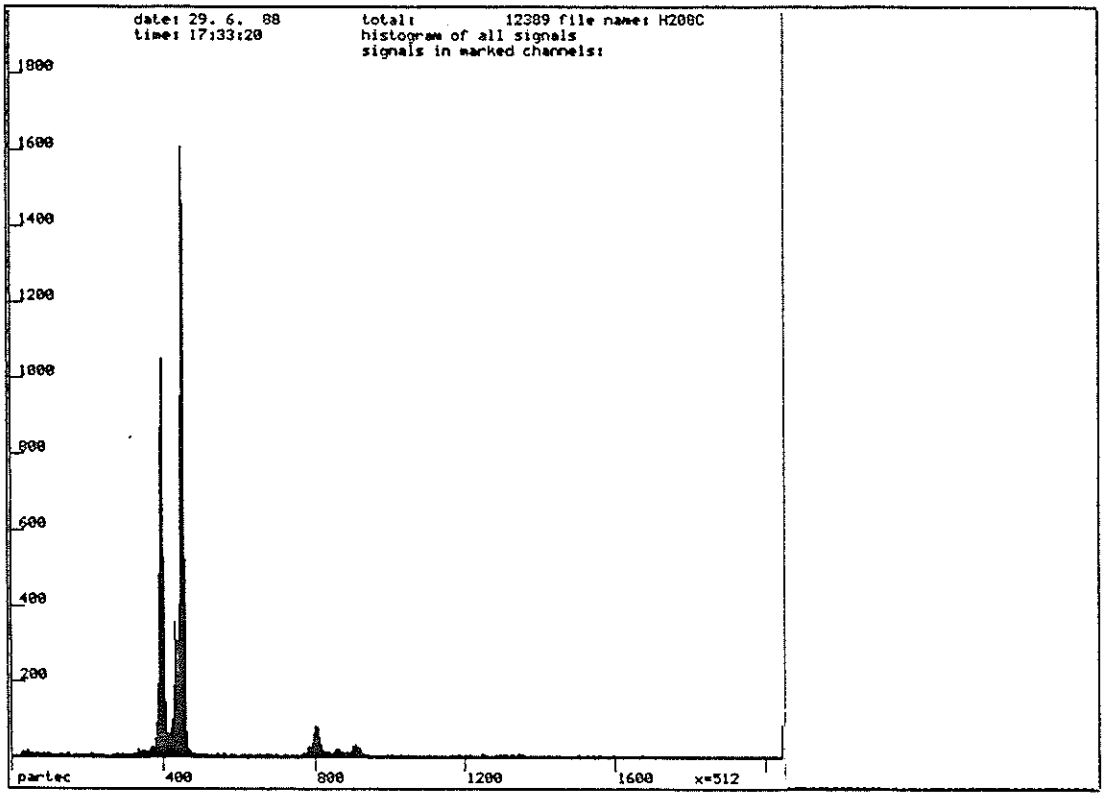

Abb. 2
DNS-Histogramm eines Malignen Melanoms
mit 2 Tumorzellinien

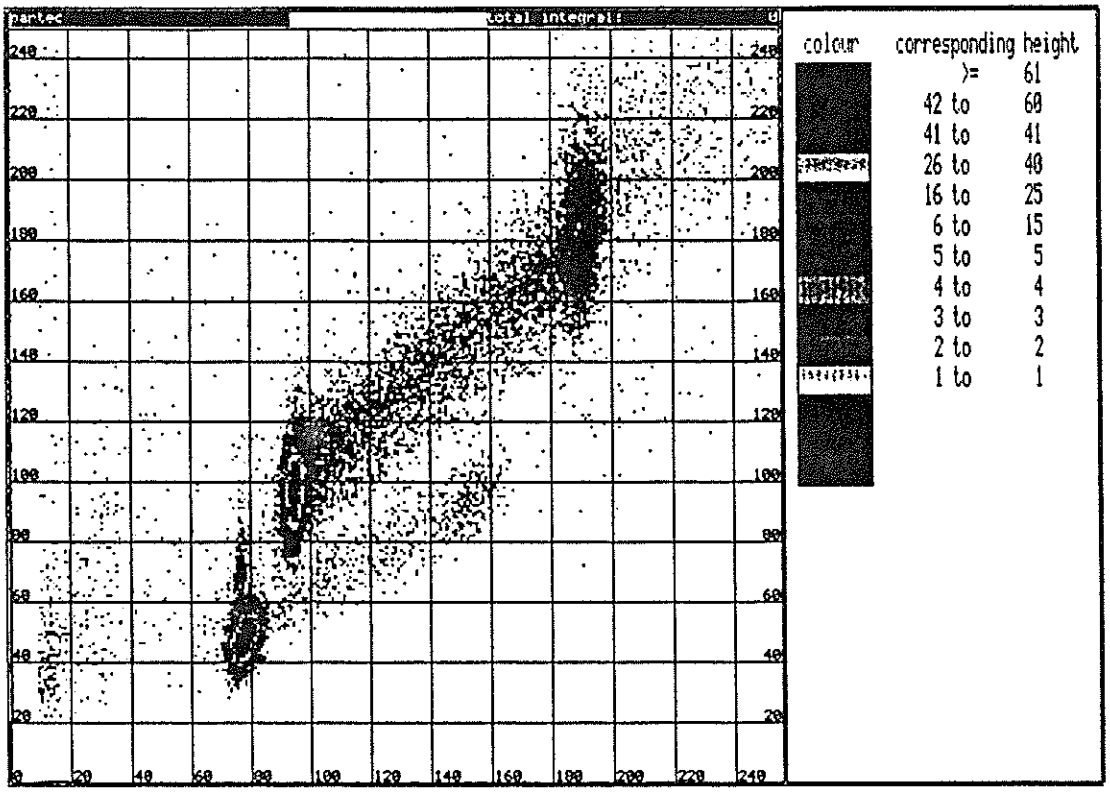

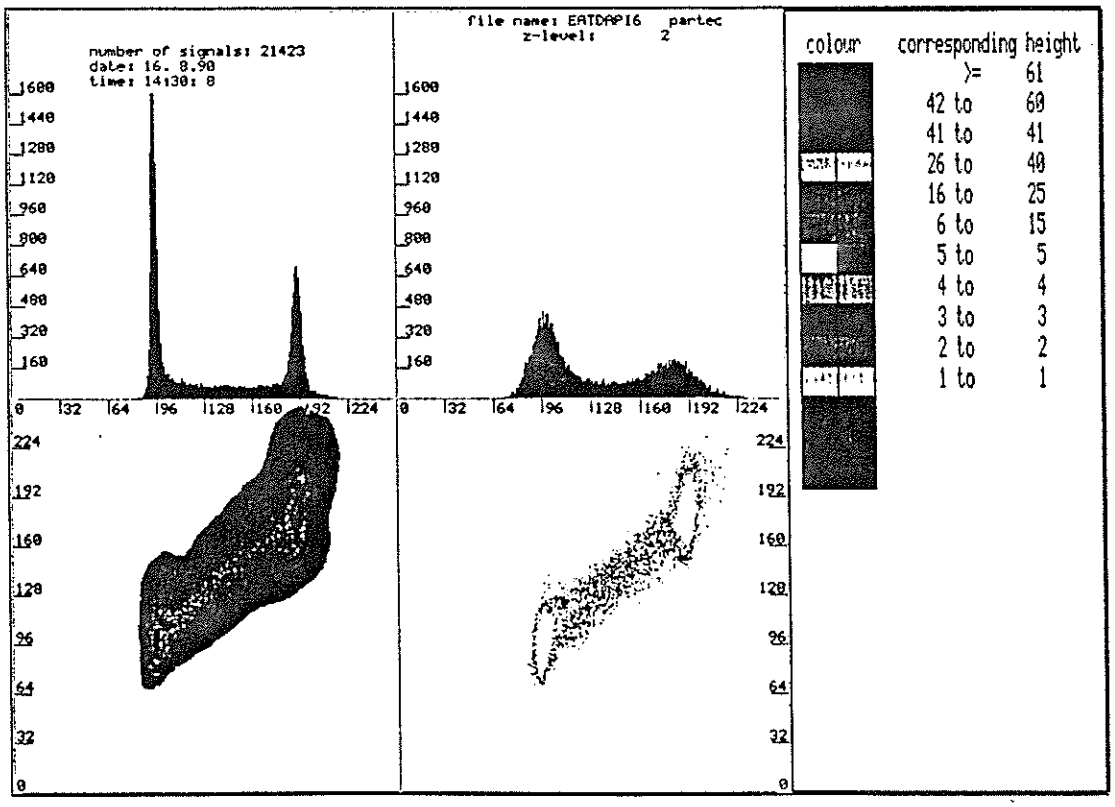

Abb. 3
oben: DNS-Protein-Histogramm von EAT-Zellen in vivo. Der Anteil normaler Zellen (Leukozyten, Epithelzellen) weist niedrigere Werte für den DNS- und Proteingehalt auf.
unten: Durch ein in seiner Form freiwählbares Gate-Fenster "bereinigtes" DNS-Protein Histogramm der Tumorzellen.

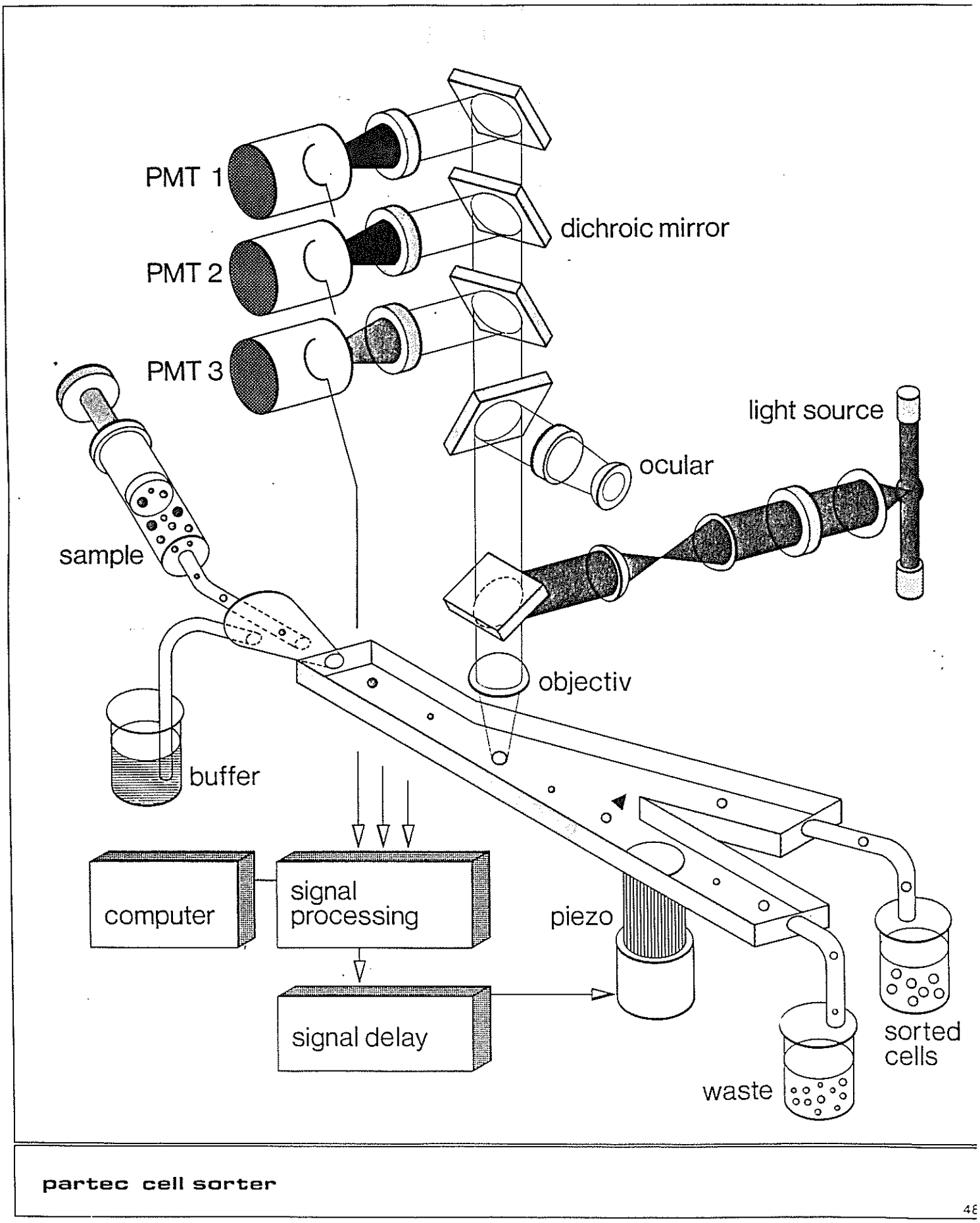

Abb. 4
Schematische Darstellung des Zell-Sorters. Die Zellen werden durch ein geschlossenes Kanalsystem bewegt; während der Sortierung kann man gleichzeitig die Meßstelle und die Kanalverzweigung im Okular oder auf einem TV-Monitor sehen. Die Ablenkung der zu sortierenden Zellen erfolgt durch eine von einem Piezo-Kristallsystem verursachte Druckwelle. Die Ablenkung jeder sortierten Zelle ist visuell kontrollierbar; das Einstellen der richtigen Signal-Verzögerung ist daher problemlos.

ANTICANCER RESEARCH *10:* 1555-1562 (1990)

Two-Wavelength Mercury Arc Lamp Excitation for Flow Cytometric DNA-Protein Analyses

T. HEIDEN[1], W. GÖHDE[2] and B. TRIBUKAIT[1]

[1]*Department of Medical Radiobiology, Karolinska Institute, S:10401 Stockholm, Sweden;*
[2]*Department of Radiotherapy-Radiooncology, University of Münster, 4400 Münster, F.R.G.*

Abstract. *Correlated DNA- and protein-determinations were performed using flow cytometry and DAPI-sulforhodamine 101 (SR101) staining. Two-wavelength UV-green excitation using a single HBO lamp was found to be superior to single wavelength UV excitation, since it resulted in a higher specificity in the SR101 measurements. The effects of overlapping in the emission spectra and of energy transfer from DAPI to SR101 were minimised. Different staining conditions and the specificity of SR101 staining were examined. No binding of SR101 to DNA and RNA could be detected. Good reproducibility was achieved in the protein measurements using human lymphocytes as an internal reference. Examples are given of the analysis of mixed cell populations with different cellular protein contents and different growth and metabolic activities. Correlated measurements of DNA and protein appear to be useful for further analysis of tumor cell populations.*

Correlated measurements of the DNA- and the total protein-contents of individual cells are useful both in monitoring the growth and the metabolism of cell populations and in analysing heterogeneous samples containing cell populations with different cellular protein contents.

The first two-parameter analyses of DNA and protein content of mammalian cells by flow cytometry were made by Göhde and Dittrich in 1970 (1). Since then, several methods of correlated DNA-protein analyses have been described using different dye combinations and various optical configurations for the flow cytometers (2-9).

In most cases, flow cytometers with excitation by a single laser beam or by monochromatic light from a mercury arc lamp have been used for DNA-protein analyses (1, 2, 9, 10). Such optical configuratons imply that the protein and the DNA dye are measured simultaneously. This may result in incorrect quantitative measurements. For example when using the DNA-and protein-stains DAPI-sulforhodamine101 (SR101), there are problems with overlapping emission spectra and/or energy transfer from one dye to the other. In such cases the two measured fluorescence intensitites do not correspond exactly to the amounts of the corresponding dyes bound in the cell. The influences of energy transfer and of overlapping emission spectra can be minimised by the sequential excitation of the dyes with two lasers as it was introduced by Stöhr, Eipel, Goerttler and Vogt-Schaden in 1977 (5). This double-laser system has been used for DNA- and protein-analyses of cells stained with DAPI and SR101, which was introduced by Stöhr *et al* (7).

The aim of this study was to measure the cellular DNA and protein content with high specificity using a simple and, compared with double-laser systems, inexpensive two-wavelength system equipped only with a single mercury arc lamp. The two-wavelength optical system has been described earlier by Göhde (11). The DAPI-SR101 staining was chosen for this study because it is fast and straightforward and the dye solutions are stable for a long time (7), and because in addition it provides a high precision in the DNA analysis. The staining conditions, the binding specificity of SR101 and the internal standardisation using human lymphocytes were all investigated.

Materials and Methods

Cells and preparation. Mouse Ehrlich *Ascites* Tumor (EAT) cells, which were passaged by intraperitoneal injection into NMRI mice, were washed with Tris buffer pH 7.5 (0.1 M Tris, 0.07 M NaCl, 0.005 M EDTA, pH 7.5) and fixed in ice-cold 95% ethanol.

Human bladder tumor tissue was gently squeezed through nylon gauze of 90 μm width and rinsed with Tris buffer pH 7.5. After centrifugation (215 g, 5 min) the cell pellet was fixed in ice-cold 95% ethanol.

Human ascites tumor cells, taken from three patients with ovary cancer [illegible] washed with HBSS and separated in a percoll density gradient (1.02-1.14 g/ml). Nine parts of the percoll stock solution (Pharmacia, Sweden, No. 170891-01) were diluted with one part of 1.5 M NaCl. Four parts of this solution were mixed with six parts of 0.9% saline and sodium methyl cellulose was added to a final concentration of 0.2%. The

Correspondence to: Prof. Bernhard Tribukait, Department of Medical Radiobiology, Karolinska Institute, Box 60212, S:10401 Stockholm, Sweden.

Key Words: Two-wavelength excitation, flow cytometry, DNA-protein analysis, DAPI-SR101.

0250-7005/90 $2.00+.40

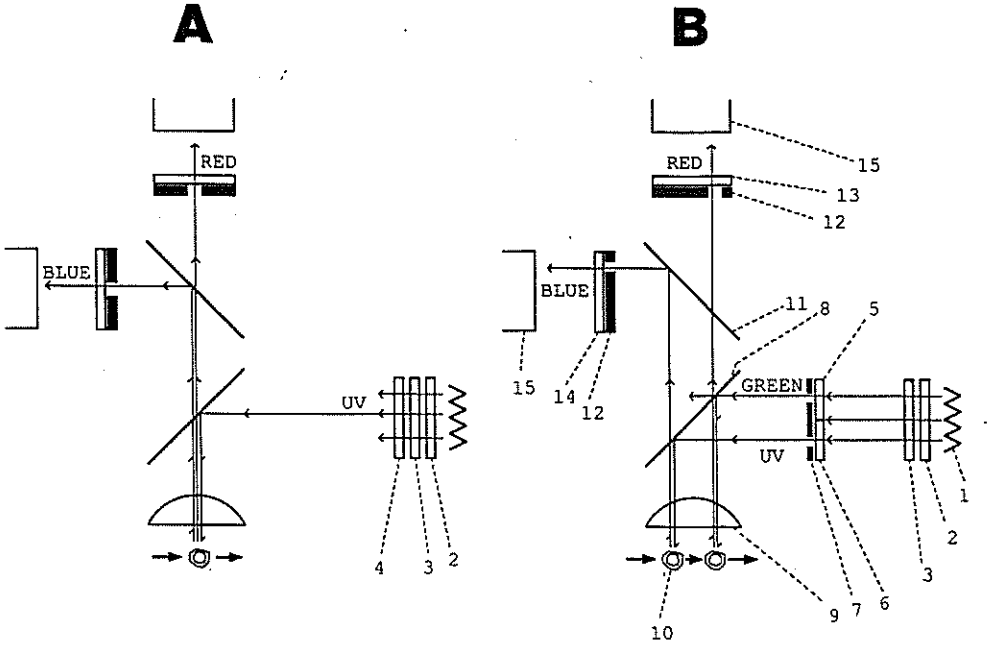

Figure 1. *Schematic representation of the conventional UV-excitation optics (A) and the two-wavelength UV-GREEN-excitation optics (B). The latter method makes it possible to make different excitations and measurements in two spatially separated regions.*
HBO100 arc (1), heat protection filters KG1 (2) and BG38 (3), UV-filter UG1 (4), double filter consisting of a bandpass green filter KP560 (5) and of UG1 (6), double slit field diaphragm (7), dichroic mirror TK 420 (8), 1.3 numerical aperture objective (9), flowing cell (10), dichroic mirror TK 500 (11), measuring field diaphragms (12), barrier filters RG630 (13) and GG435 (14), photomultipliers (15). The thin lines with arrows indicate schematically the light paths. All lenses except the objective front lense have been omitted.

osmolality was 300 mosmol/l. To create the density gradient, the tubes were centrifuged at 15,000 rpm for 15 min using a JA-10 Beckman rotor head at 4°C. Three different bands were harvested, and the cells were fixed in ice-cold 95% ethanol.

Human lymphocytes were isolated from peripheral blood using a ficoll density gradient. A layer of 4 ml heparinized blood was carefully pipetted onto 3 ml ficoll in a tube (Ficoll-Paque, Pharmacia, Sweden, No. 10-a-001-07). Centrifuging was performed at 500 g for 10 min, the band of lymphocytes was removed, the cells were washed in Tris buffer pH 7.5 and then fixed in ice-cold 95% ethanol. Stimulated human lymphocytes were kindly supplied by Dr. Marjanovic, while stimulation was performed as described by Marjanovic *et al* (20).

Staining. Staining was performed using DAPI (Serva 18860) or DNA and Sulforhodamine 101 (SR101, Aldrich Chemie 28491-2) for protein according to Stöhr *et al* (7). The procedure was slightly modified: a mixture of both dyes (8 μM DAPI, 50 μM SR101, 100 mM Tris, 70 mM NaCl, pH 7.5, 300 mosmol/l) was used instead of sequentially staining first with SR101 and then additionally with DAPI. One drop of cell sediment from the fixed sample, stored in the refrgerator, was suspended in 1 ml of staining solution. The suspension was passed twice through a 21 gauge needle and then filtered through a 90 μm nylon mesh. For examination of the staining conditions the staining time was varied between 5 and 60 min, the SR101 concentration between 1.5 and 62.5 μM, and the cell concentration between 0.06 and $1.5*10^6$ cells/ml.

Internal standardisation. Internal standardisation was carried out by adding unstimulated lymphocytes immediately after suspending cells of the sample in the staining solution.

Incubation with pepsin, RNAse, or DNAse. For the examination of the binding specificity of SR101, EAT cells were incubated in pepsin- or DNAse-solution and then washed with Tris buffer ph 7.5 prior to staining with DAPI-SR101. RNAse incubation was performed directly in the staining solution.

Pepsin incubation: 0.416 g pepsin (1200 E/g, Merck 7180) per 100 ml 0.055 n HCl was used. The cells were incubated for 10 min at 37°C.

DNAse incubation: 1mg DNAse I (Sigma D-4527) per ml Tris buffer pH 6.5 (0.25 M sucrose, 5 mM $MgCl_2$, 20 mM Tris, pH 6.5) was used. The incubation time was 1 h at 37°C.

RNAse incubation: 0.1 mg RNAse-A type III (Sigma R-5125) per ml DAPI-SR101 staining solution was used. The incubation time was 30 min at room temperature. The enzyme activity was controlled using ethidium bromide staining of treated and untreated EAT cells.

Spectrophotometric analyses. Measurements of excitation and emission spectra were performed using a Perkin Elmer LS-5 Luminescence Spectrophotometer. Solutions of 8 μM DAPI and 50μM SR101 in Tris buffer pH 7.5 (100 mM Tris, 70 mM NaCl, pH 7.5) were analysed. The energy spectrum of the mercury arc lamp HBO100 was kindly supplied by Osram (BRD). Calculations of filtered lamp spectra were performed using data from the Farb- und Filterglas Katalog (Schott, BRD). The thickness of the color glasses KG1, BG38 and UG1 was 3 mm. The transmission of the bandpass filter KP560 was measured using a Varian spectrophotometer.

Flow cytometry. A Partec Flow Cytometer and sorter PASII (Partec AB, Münster, BRD), equipped with a HBO 100 Mercury arc lamp and an 1.3 aperture objective, was used.

Two optical configurations were compared (Figure 1). The first uses UV excitation and simultaneous measurement of blue and red fluorescence, the second uses successively UV excitation/blue emission measurement and green excitation/red emission measurement, which is based on the two-wavelength principle developed by Göhde (11). This implies two spatially separated regions of excitation. Each cell crosses both regions

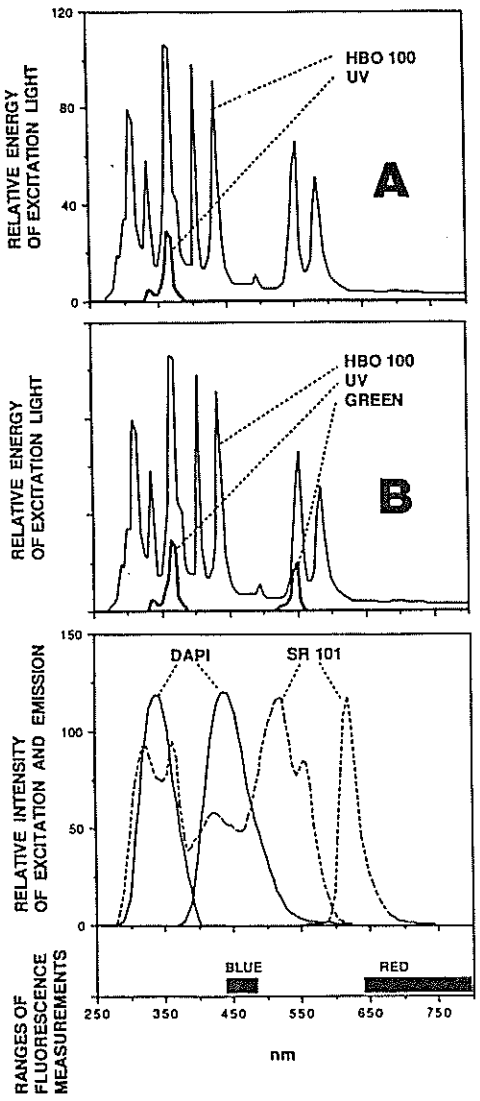

Figure 2. *Spectra of excitation light for conventional UV (A) and UV-GREEN (B) excitation; energy spectrum of the mercury arc lamp HBO100 before passing (HBO100) and after passing the filters KG1, BG38, and UG1 (UV) and KG1, BG38, and KP560 (GREEN) respectively. Fluorescence excitation and emission spectra of DAPI (DAPI) and SR101 (SR101) and ranges of fluorescnece detection are shown in the lower part of Figure 2.*

In addition to the measurement of DAPI, the two-wavelength excitation method (B and Figure 1 B) makes it possible to make a separate excitation and measurement just of the SR101 fluorescence.

sequentially in time and generates two pulses of emission fluorescence, which can be correlated with each other.

Results

Comparison between UV and UV-GREEN excitation. The excitation and emission spectra of DAPI and SR101 as well as the ranges of fluorescence detection of the single and two wavelength measurements are shown in Figure 2. The two parameter histograms of double-stained cells, which were analysed using only UV and two-wavelengths UV-GREEN excitation, show different patterns (Figure 3). The histograms of cells only stained with DAPI make it easier to explain this difference.

Overlapping emission spectra: When single UV excitation and simultaneous measurement of blue and red fluorescence are used, a problem which arises is that part of DAPI fluorescence is measured in the red channel due to the overlapping emission spectra of DAPI and SR101. The control measurement of cells stained only with DAPI, which was performed at the same gain setting as the measurement of DAPI-SR101 stained cells, shows that about 15% of the red fluorescence of double-stained cells is contributed by DAPI (Figure 3a). Of course this percentage also depends on the amount of DAPI and SR101 bound in the cell. It is expected to be higher, for example, in the analysis of human lymphocytes or isolated nuclei with a low protein content relative to the DNA content. At first glance the extent to which the emission spectra overlap does not seem to be high (Figure 2), but the significant contribution of DAPI fluorescence in the red obviously depends on the high fluorescence intensity of DAPI in relation to SR101.

Two-wavelength UV-GREEN excitation and sequential measurements of blue and red fluorescence result in an artificial contribution in the red channel of only about 2% (Figure 3b), probably due to the extremely weak DAPI excitation by green light.

Energy transfer: The effect of energy transfer on the SR101 measurement can be seen after substracting the contribution of DAPI in the red, caused by the overlapping of the emission spectra, and then calculating the ratio of the protein peak positions of G2 cells in relation to G1 cells. This value is 1.65 in the case of single UV excitation and 1.53 in the case of two-wavelength UV-GREEN excitation. This difference can be explained by energy transfer from DAPI to SR101, which influences the SR101 measurement, when the single UV excitation is applied. Besides UV light, SR101 also absorbs part of the DAPI fluorescence, which enhances the SR101 fluorescence intensity depending on the DAPI fluorescence. The difference between the G2/G1 ratios is assumed to imply that the SR101 fluorescence is excited more strongly in G2 than in G1 cells due to an additional excitation by energy transfer from DAPI when single UV excitation is applied and both dyes are measured at the same time.

The sequential measurement of UV-excited DAPI and green-excited SR-101 minimises the effect of energy transfer from DAPI to SR101 on the analysis of SR101, since the excitation of DAPI by green light s extremely weak.

The influence of the energy transfer from DAPI to SR101 on the measurement of DAPI is obviously very small. An example of this is illustrated in Figure 7, which shows the DAPI-SR101 analysis of a human bladder tumor. Alla the G1 cells in this tissue, which cover a wide range of different protein values, show the same DNA value (CV 1.1), and no

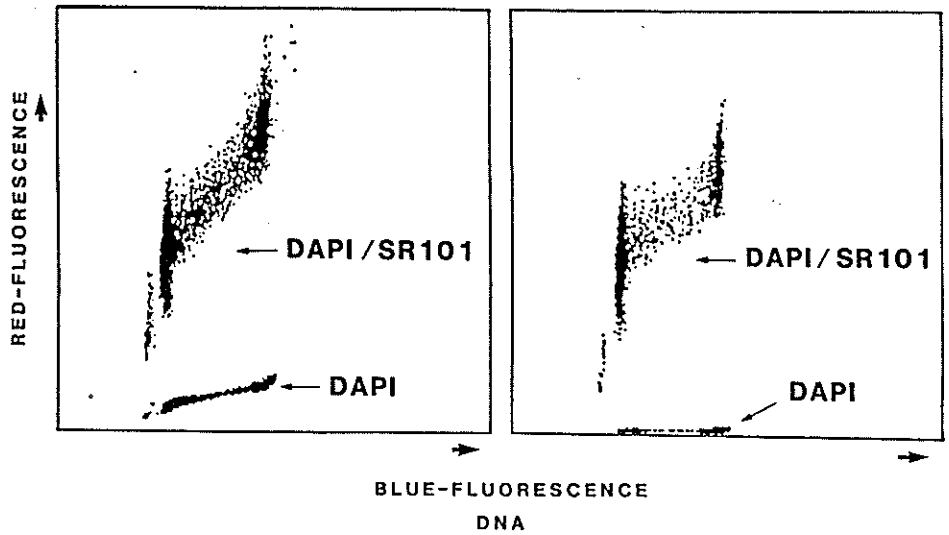

Figure 3. *Correlated measurements of blue and red fluorescence in EAT cells using the conventional UV (A) and the two-wavelength UV-GREEN (B) excitation optics.*
The cells were stained with DAPI/SR101 and for the control analyses only with DAPI. Staining conditions: 30-60 min staining time, about 800.000 cells/ml. 8 μM DAPI, 50 μM SR101 and no SR101 respectively. The control measurements (bottom of Figure 3 A and B) were performed at the same gain settings as the corresponding analyses of double-stained cells. The gain settings of the analyses in A and B were chosen so that the maxima of G1 SR101-peaks of double-stained cells were in the same channel.

skewness of the G1 population in the two-parameter histogram can be seen.

In summary, the application of two-wavelength excitation provides a more correct measurement of the SR101 fluorescence since the influences of overlapping emission spectra and of energy transfer are minimised. The precision of the DNA measurement is not affected.

Examination of staining conditions. The influences of different staining times, cell concentrations, and SR101 concentrations on the analysis of EAT cells were studied.

Figure 4 (left) shows the effect of the staining time on the measurement of DAPI and SR101 at fixed concentrations of 8 μM and 50 μMN respectively. The DAPI fluorescence intensity increased by only about 8% during one hour, while the SR101 fluorescence decreased by about 15%. The increase in the DAPI fluorescence probably indicates that the staining slowly approached saturation within the 1 h staining time. The decrease in the SR101 fluorescence may have been caused by loss of proteins.

The SR101 concentration was studied in the range of 1.6 to 75 μM with a constant staining time of 30-60 min (Figure 4 centre). With increasing SR101 concentration, the fluorescence intensity reached a maximum value at 25μM. At higher concentration the fluorescence decreased slightly. The decrease in the SR101 fluorescence intensity might be the result of dye-dye interactions or of auto-absorption.

Increasing SR101 concentration correlated with a decrease in the DAPI fluorescence intensity by about 32%, which coincides with an increase in the accuracy of the DNA measurement, as seen from the CV. The CV decreased from 4.4 ± 0.6 to 2.3 ± 0.2 (mean value ± SD). Both may be caused by a blockage of DAPI-protein binding sites by SR101. The decrease in the DAPI fluorescence may also result from an increasing absorption of UV-excitation light by SR101.

A staining time of 30-60 min and a SR101 concentration of 50 μM were chosen when the cell concentration was varied between $0.06*10^6$ and $2*10^6$ cells/ml (Figure 4 right). Over this range a roughly constant SR101 fluorescence intensity was observed, while the DAPI fluorescence intensity gradually decreased with increasing cell concentration. Above $1*10^6$ cells/ml the CV increased markedly to more than 4.

As a result of these experiments a staining time of 30-60 min and, in agreement with Stöhr *et al* (7), concentrations of 8 μM DAPI and 50 μm SR101 were regarded as useful in order to achieve reliable quantitative measurements.

Specificity of SR101 staining. After pepsin treatment of the cells for 10 min the SR101 fluorescence decreased by about 85% (Figure 5). Since microscopic examination showed that the cytoplasm was completely removed by pepsin digestion, this experiment only allows us to draw the conclusion that SR101 binds as well in the nucleus as in the cytoplasm of cells. It is an open question whether the SR101 fluorescence remaining after pepsin treatment is due to unspecific staining or to staining of residual nuclear proteins.

The binding specificity was further examined by incubation of the cells with DNAse and RNAse. As shown in Table I and Figure 6, no binding of SR101 to DNA or RNA could

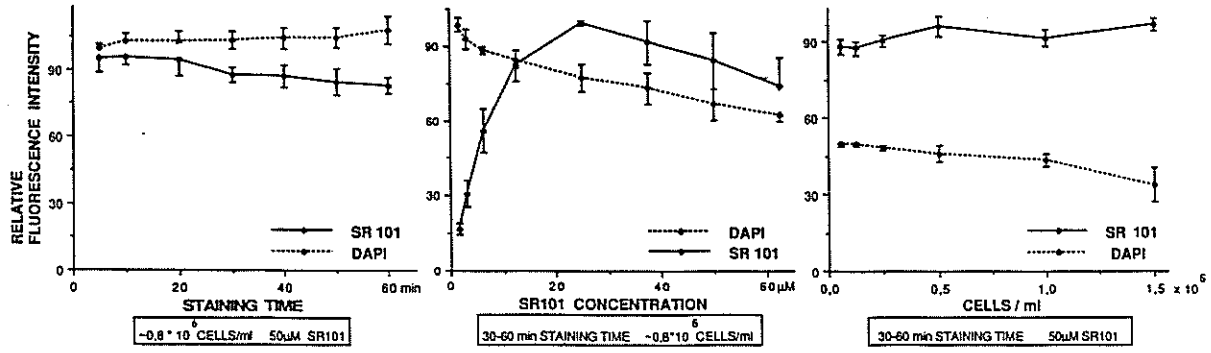

Figure 4. *DAPI- and SR101-fluorescence intensities in EAT cells with different staining conditions analysed with the two-wavelength excitation system. The peak channel numbers for the G1 cells were determined, mean values ± SD are shown for different staining times (n=6), SR101 concentrations (n=5), and cell concentrations (n=4). All measurements for each of the three experiments were performed at the same gain settings.*

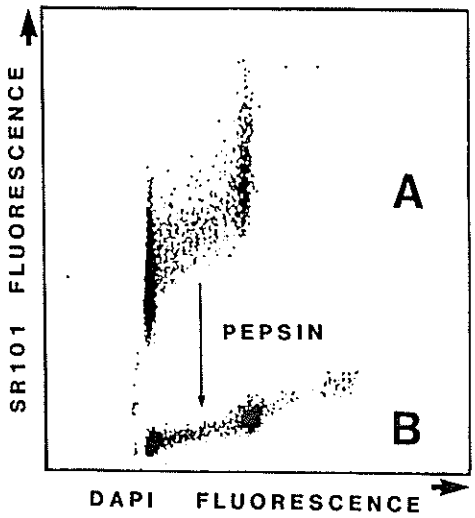

Figure 5. *DAPI-SR101 fluorescence distributions of EAT cells with (B) and without (A) pepsin treatment. Both measurements were performed at the same gain setting. Staining and measurement conditions: 8 µM DAPI, 50 µM SR101, staining time 30-60 min, cell concentration up to 1×10⁶ cells/ml. The two wavelengths system was applied.*

be detected. Since acid dyes like SR101 react predominantly with amino groups and since removal of DNA and RNA did not change the fluorescence of SR101, good speicificity of SR101 for proteins can be assumed.

Internal standardisation. Internal standardisation can be performed with human lymphocytes for the determination of both DNA and protein. For example Figure 7 shows the analysis of a human bladder tumor with and without added lymphocytes. The reproducibility of the protein determinations was investigated. Five aliquots from one sample of a seven-day old EAT tumor were prepared and measured after internal standardisation with lymphocytes. A mean value of 4.84 ± 0.36 SD was found.

Table I. *Effect of RNAse- and DNAse-treatment on the SR101 fluorescence of EAT cells.*

	Control	+RNAse	Control	+DNAse
Relative SR101 fluorescence intensity*	100±2.0	98±3.3	100±6.5	99±3.9

* The mean values of SR101-fluorescence intensity distributions were determined. The measurements were performed at the same gain settings. Mean value ± SD (N=3).

Analysis of stimulated lymphocytes and of density gradient separated human ascites tumor cells. Two examples of analysis of mixed cell populations were chosen exhibiting different growth or metabolic activities. An analysis was made of human lymphocytes after concanavalin A stimulation and of percoll density gradient-separated human *ascites* tumor cells from three patients with ovary cancer.

The histogram of stimulated lymphocytes (Figure 8) shows substantially the same patterns as those obtained from DNA-RNA analyses using acridine orange or H33342-pyronine Y (12, 13). This suggests that DNA-protein measurements using DAPI-SR101 can also be used, for example, to analyse stimulated cells in mixed populations of quiescent and proliferating lymphocytes.

The examples of the histograms for density gradient separated human *ascites* tumor cells (Figure 9) are representative of all the three analysed *ascites* tumors. Three bands of cells were separated in the gradients (1.02-1.14 g/ml). Increasing density in the bands correlated with a decrease in the proportion of cells with a high protein content. The fraction with the highest density contained only cells with a low protein content (Figure 9a), whereas the lowest density fraction (Figure 9c) contained cells with both high and low protein contents. Obviously cells exceeding a certain protein content belong to the group of low density cells irrespective

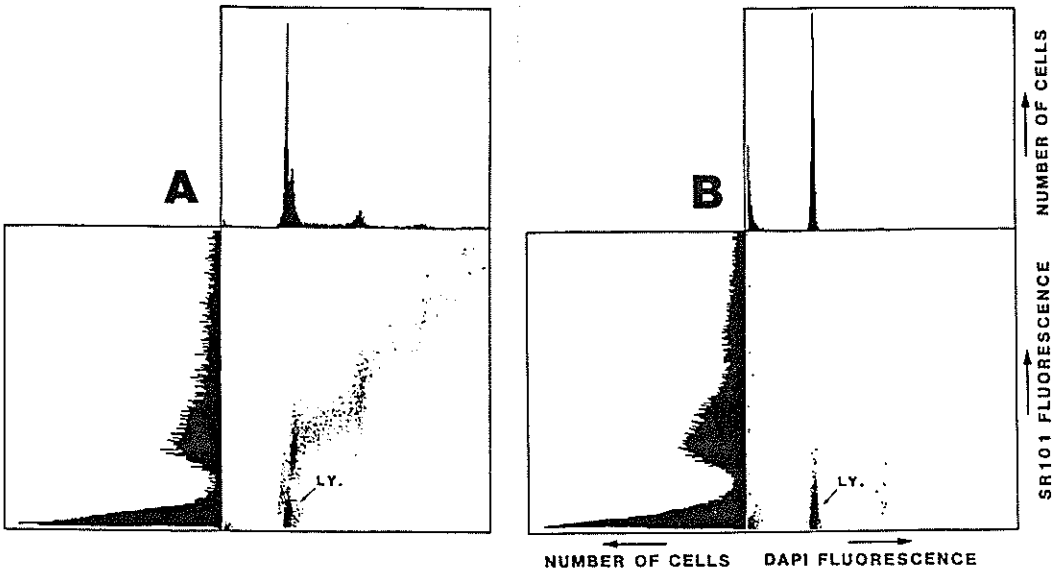

Figure 6. *One and two dimensional distributions of DAPI- and SR101-fluorescence intensities in EAT cells with (B) and without (A) DNAse treatment. Human lymphocytes, which were not treated with DNAse, were added to both samples. Staining and measurement conditions as described in Figure 5.*

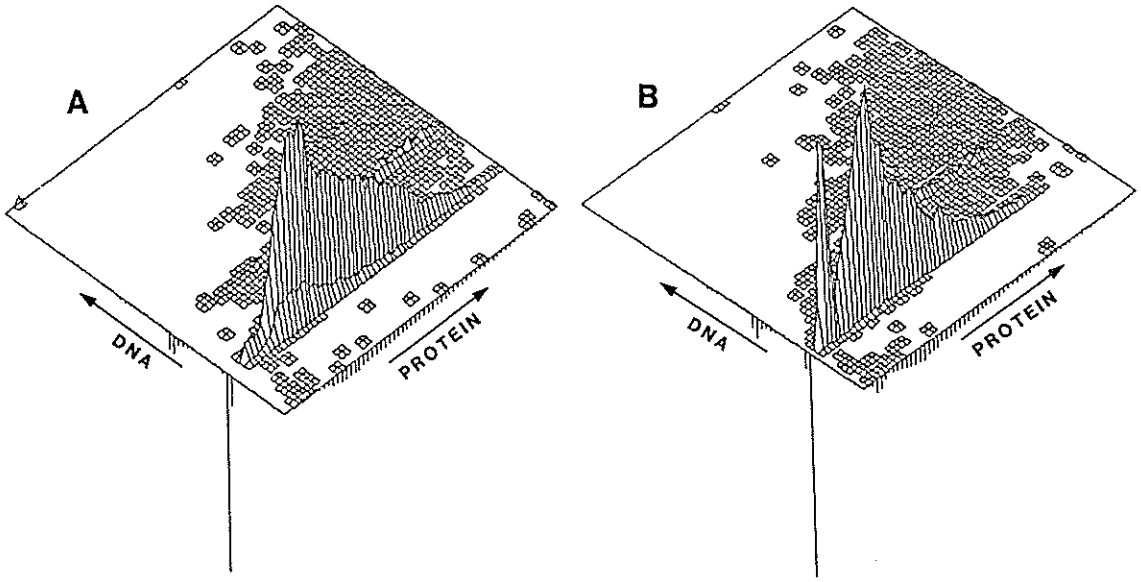

Figure 7. *DNA-protein distribution for cells of a diploid bladder tumor without (A) and with (B) internal lymphocyte standardsation. Staining and measurement conditions as described in Figure 5.*

of whether they are measured in unseparated or density gradient separated samples. A number of studies on tumor cells have shown that low density correlates with higher viability, as determined by due exclusion and plating efficiency tests (14-17). Decreasing density can also correlate with progressive maturation, as shown for keratinocytes by Goldenhersh *et al* (18).

Discussion

The aim of this study was to study the effects of various experimental conditions when making correlated cellular DNA-protein measurements using the fluorochromes DAPI and SR101 in order to obtain a high specificity and reliability of the analyses.

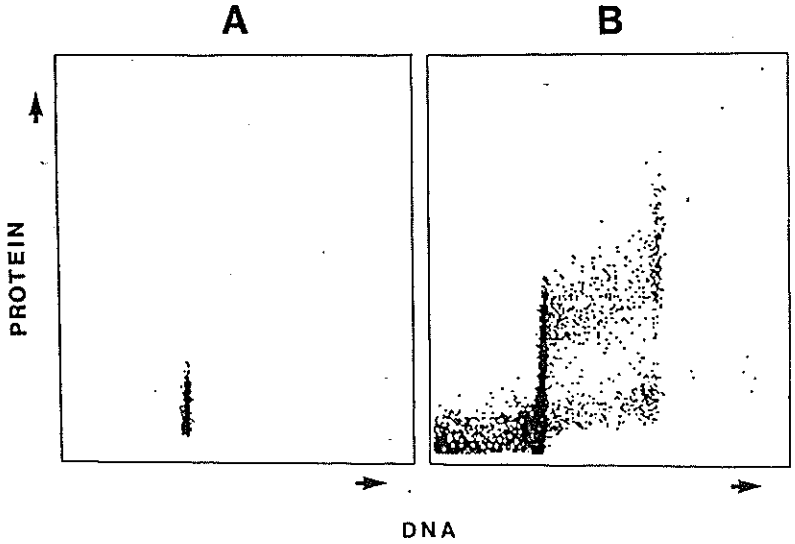

Figure 8. *DNA-protein measurements of unstimulated (a) and concanavalin A stimulated (B) lymphocytes. Staining and measurement conditions as described in Figure 5.*

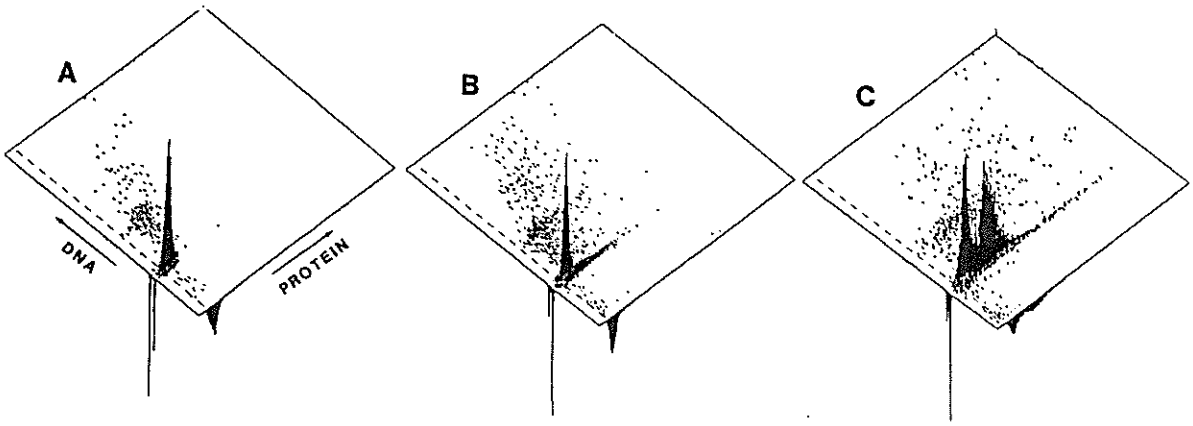

Figure 9. *DNA-protein measurements of density gradient separated human ascites tumor cells. The cells were harvested in gradients of 1.02 to 1.14 g/ml; low (A), medium (B), and high (C) density. The lines indicate the protein content of human lymphocytes. Staining and measurement conditions as described in Figure 5.*

In their first studies Stöhr *et al* (7), who introduced Dapi-SR101 staining, used a dual laser configuration to excite the fluorochromes separately, employing the 351 nm line of a krypton laser and the 488 nm line of an argon laser. Subsequently, Goerttler and Stöhr (9) used single laser excitation of both dyes using the 363 nm line of an argon laser.

In this study a comparison was made between two different optical configurations, both using a single mercury arc lamp. Successive UV- and green-excitation in two spatially separated regions, based on the two-wavelength excitation principle of Göhde (11), proved to be superior to conventional excitation using only UV light. By applying the two-wavelength principle, the artificial effects caused by the overlapping emission spectra and by energy transfer processes can be minimised. This allows more precise measurements of the cellular protein content without reducing the precision of the DNA analysis. The introduction of this optical configuration does not involve excessive expense and effort. It can also be applied to other types of analysis.

Our studies on the staining conditions showed that the concentrations of 50 μM SR101 and 8 μM DAPI, as described by Stöhr *et al* (7), cell concentrations of up to 1×10^6 cells/ml and a staining time of 30 - 60 min were appropriate for reliable SR101 measurements; this was confirmed by the analysis of internally standardised EAT cells. The internal lymphocyte standardisation showed good reproducibility in the protein estimations. The SD for 5 protein analyses of the same sampale was 7.4% of the mean value.

It was shown in a previous report that DAPI staining for single DNA measurements of human lymphocytes and bladder tumor cells, incubated with pepsin, resulted in a lower staining intensity of lymphocytes compared with diploid

tumor cells (19). Ongoing studies on bladder carcinomas using the double staining protocol as described in this paper have not shown such artificial differences between lymphocytes and diploid tumor cells. One possible reason for this difference might be that pepsin digestion causes differences in stainability with DAPI, which do not occur when staining is performed without enzymatic treatment. Another explanation might be that additional staining with SR101 blocks DAPI-protein binding sites and thus enhances the specificity of DAPI binding to DNA, increasing the precision of the ploidy determinations.

The two examples of DAPI-SR101 analyses of stimulated lymphocytes and density gradient-separated human *ascites* tumor cells show that combined DNA-protein measurements are useful and that they make it possible to achieve better characterisation of cellular growth and metabolic activity, particularly in tumor cell populations.

Acknowledgements

This research was supported by the Heinrich Warner Foundation and the King Gustav V Jubilee Foundation.

References

1 Göhde W and Dittrich W: Simultane Impulsfluorimetrie des DNS- und Proteingehaltes von Tumorzellen. Z Anal Chem *252:* 328-330, 1970.
2 Crissman HA and Steinkamp JA: Rapid simultaneous measurement of DNA, protein, and cell volume in single cells from large mammalian cell populations. J Cell Biol *59:* 766-771, 1973.
3 Hutter KJ, Göhde W and Emeis CC: Untersuchungen über die DNS-, RNS- und Proteinsynthese ausgewählter Mikroorganismenpopulationmen mit Hilfe der Impulscytophotometie. I. Mitteilung. Methodische Untersuchungen über geeignete Fluoreszenzfarbstoffe und Färbeverfahren. Chem Mikrobiol Technol Lebensm *4:* 29-32, 1975.
4 Freeman DA and Crissman HA: Evaluation of six fluorescent protein stains for use in flow microfluorometry. Stain Technol *50:* 279-284, 1975.
5 Stöhr M, Eipel H, Goerttler K and Vogt-Schaden M: Extended application of flow microfluorometry by means of dual laser excitation. Histochem *51:* 305-313, 1977.
6 Stöhr M, Goerttler K and Futterman G: Multi-line laser excitation. Third Int Symp Pulse Cytophotometry, Vienna: 23-29, 1978.
7 Stöhr M, Vogt-Schaden M, Knobloch M, Vogel R and Futterman G: Evaluation of eight fluorochrome combinations for simultaneous DNA-protein flow analyses. Stain Technol *53:* 205-215, 1978.
8 Stöhr M and Goerttler K: The Heidelberg flow analyzer and sorter (HEIFAS) approach on the prescreening of uterine cancer. J Histochem Cytochem *27:* 564-566, 1979.
9 Goerttler K and Stöhr M: Quantitative cytology of the positive region in flow sorted vaginal smears. J Histochem Cytochem *27:* 567-572, 1979.
10 Hutter KJ and Eipel HE: Simultaneous measurement of DNA and protein content of microorganisms by flow cytometry. European J Appl Microbiol Biotechnol *6:* 223-231, 1979.
11 Göhde W: United States Patent 4.255.229, 1980.
12 Shapiro HM: Flow cytometric estimations of DNA and RNA content in intact cells stained with Hoechst 33342 and Pyronin Y. Cytometry *2:* 143-150, 1981.
13 Darzynkiewicz Z, Traganos F and Melamed M: New cell cycle compartments identified by multiparameter flow cytometry. Cytometry *1:* 98, 1980.
14 Grdina DJ, Medistrich MI and Withers HR: Separation of clonogenic cells from stationary phase cultures by density gradient centrifugation. Exptl Cell Res *85:* 15-22, 1985.
15 Mackillop WJ, Stewart SS and Buick RN: Density/volume analysis in the study of cellular heterogeneity in human ovarian carcinoma. Br J Cancer *45:* 812-820, 1982.
16 Sonka J, Stöhr M, Vogt-Schaden M and Volm M: Isopycnic density-gradient centrifugation- a separation parameter which improves flow cytometric measurements on heterogeneous tumors. cytometry *4:* 141-149, 1983.
17 Mavligit GM, Gutterman JU and Hersh EM: Separation of viable from non-viable tumor cells using ficoll-hypaque density solution. Immunol Communic *2:* 463-472, 1973.
18 Goldenhersh MA, Good RA, Sarkar NH and Safai B: Separation of epidermal cells by density gradient centrifugation on a continuous colloidal silica (percoll) gradient. Analyt Biochem *119:* 246-252, 1982.
19 Heident T, Strang P, Stendahl U and Tribukait B: The reproducibility of flow cytometric analyses in human tumors. Methodological aspects. Anticancer Res. *10:* 49-54, 1990.
20 Marjanovic S, Wielburski A and Nelson BD: Effect of phorbol myristate acetate and concanavalin A on the glycolytic enzymes of human peripheral lymphocytes. Biochim Biophys Acta *970:* 1-6, 1988.

Received June 5, 1990
Accepted August 3, 1990

partec

protocol 1

Hochauflösende DNS-Flow Cytometrie mit DAPI

DR. FRIEDRICH OTTO

Abt. für Experimentelle Tumorforschung
Fachklinik Hornheide
Westfälische Wilhelms-Universität
4400 Münster

Partec GmbH
Hüfferstraße 73-79 · 4400 Münster
Telefon 0251 / 80078 · Telefax 0251 / 82979

Partec AG
Sonnenweg 7 · CH-4144 Arlesheim
Telefon 061 / 727755 · Telefax 061 / 727768

4/88

Filterschema DAPI

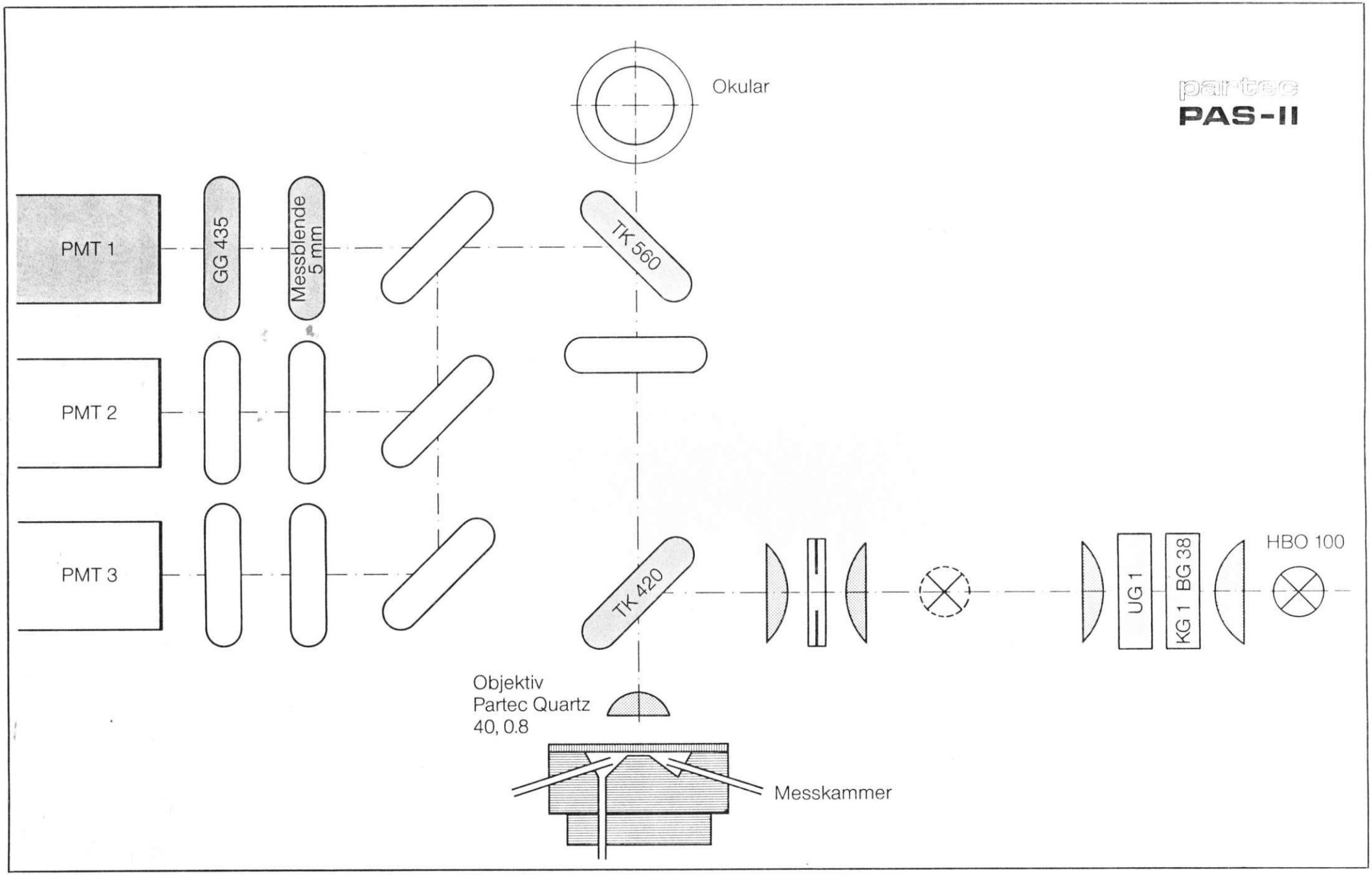

Literaturangaben:

1. Göhde, W., Dittrich, W.: Impulsfluorometrie - ein neuartiges Durchflußverfahren zur ultraschnellen Mengenbestimmung von Zellinhaltsstoffen.
XIII. Ges. Histochem., Graz 1969.

2. Van Dilla, M.A., Trujillo, T.T., Mullaney, P.F., Coulter, J.R.: Cell microfluorometry: A method for rapid fluorescence measurements.
Science 163: 1213-1214, 1969.

3. Otto, F.J., Oldiges, H., Göhde, W., Jain, V.K.: Flow cytometric measurement of nuclear DNA content variations as a potential in vivo mutagenicity test.
Cytometry 2: 189-191, 1981.

4. Göhde, W., Schumann, J., Zante, J.: The use of DAPI in pulse cytophotometry.
In: Lutz, D. ed: Pulse Cytophotometry: 229-232, Ghent 1978.

Abb. 1: Durchflußzytometrische DNS-Histogramme menschlicher Lymphozyten;
oben: Lymphozyten eines Mannes (CV = 0,75 %)
unten: Lymphozyten von Mann und Frau gemischt.

Abb. 2: Durchflußzytometrische DNS-Histogramme menschlicher Haut;
oben: normale Haut (CV = 1,07 %)
unten: Primärtumor eines malignen Melanoms, bei dem die hochauflösende Messung die Existenz zweier Tumorstammlinien nachweist.

Abb. 1

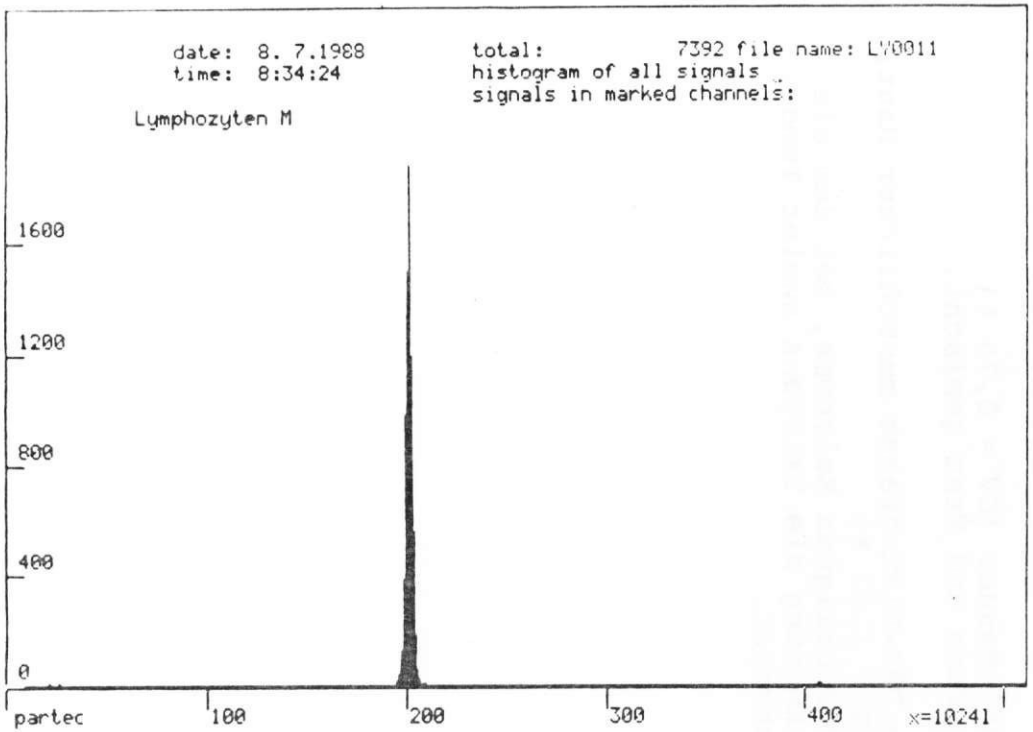
date: 8. 7.1988
time: 8:34:24
total: 7392 file name: LV0011
histogram of all signals
signals in marked channels:
Lymphozyten M
1600
1200
800
400
0
partec
100
200
300
400
x=10241

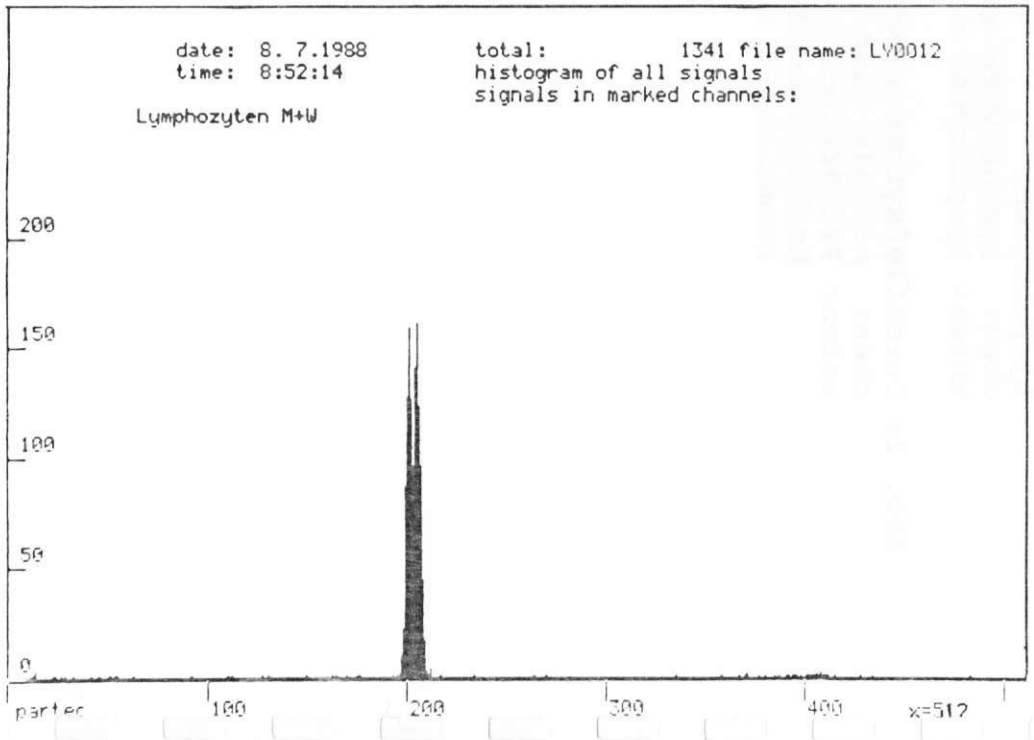
date: 8. 7.1988
time: 8:52:14
total: 1341 file name: LV0012
histogram of all signals
signals in marked channels:
Lymphozyten M+W
200
150
100
50
0
partec
100
200
300
400
x=512

Abb. 2

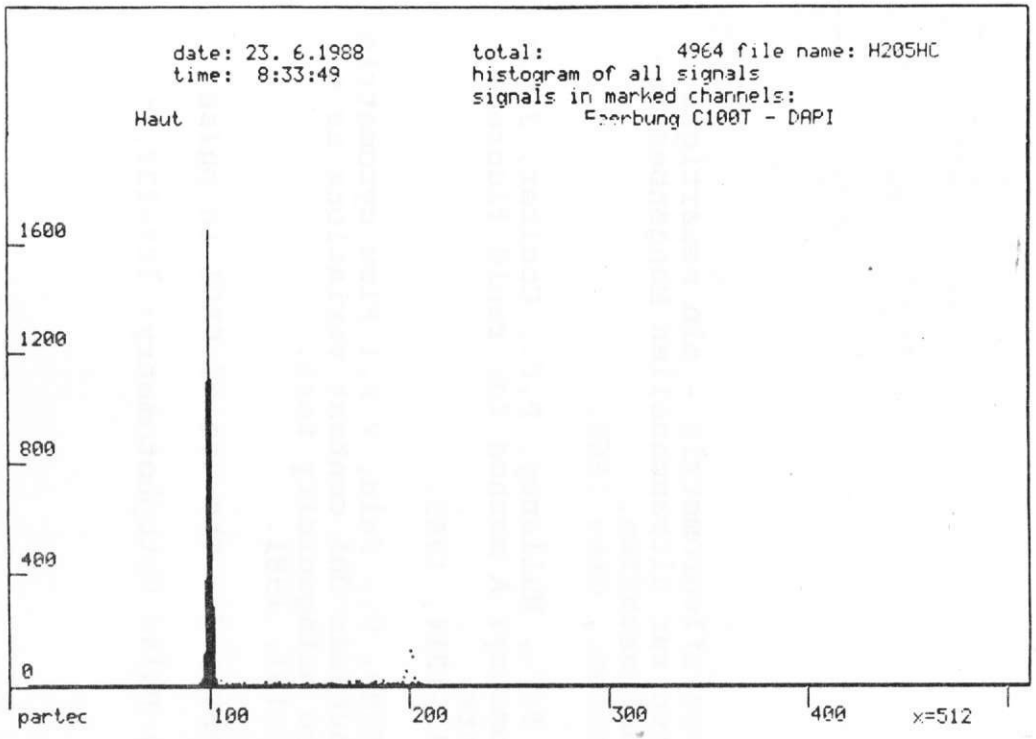
date: 23. 6.1988
time: 8:33:49
total: 4964 file name: H205HC
histogram of all signals
signals in marked channels:
Faerbung C100T - DAPI
Haut
1600
1200
800
400
0
partec
100
200
300
400
x=512

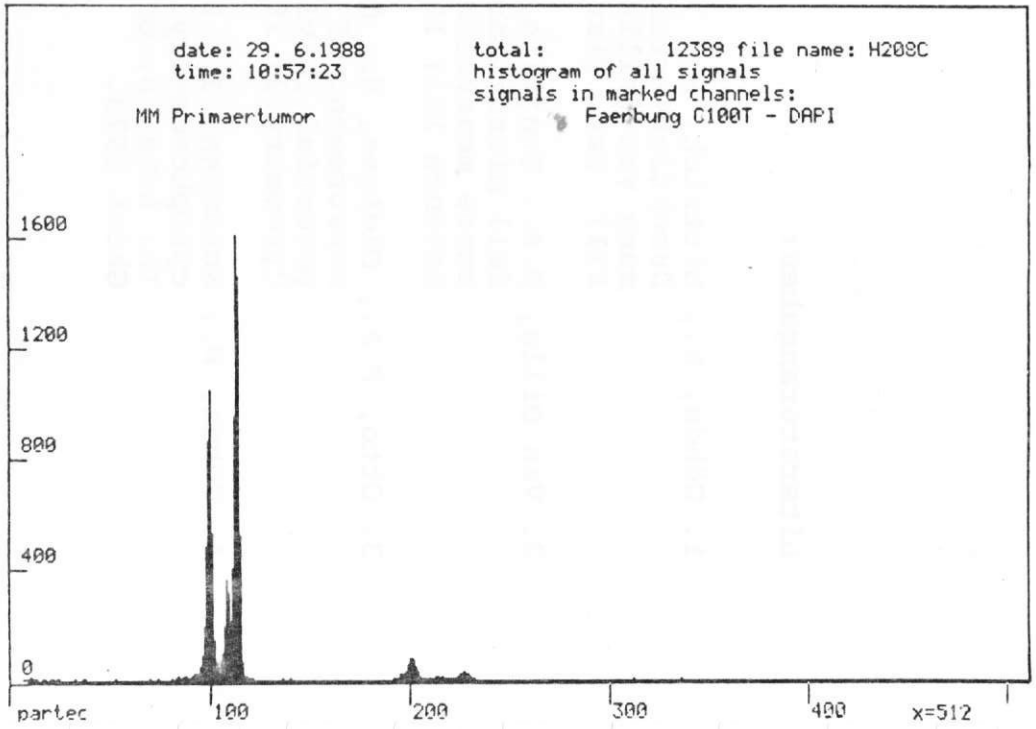
date: 29. 6.1988
time: 10:57:23
total: 12389 file name: H208C
histogram of all signals
signals in marked channels:
Faerbung C100T - DAPI
MM Primaertumor
1600
1200
800
400
0
partec
100
200
300
400
x=512

Einleitung:

Mit der Einführung der Durchflußzytometrie (1,2) gewann die Messung der zellulären DNS neue Bedeutung. Die Genauigkeit der DNS-Messung wurde durch Fortschritte der instrumentalen Technik und Weiterentwicklung der Färbemethoden ständig gesteigert. Mit der zunehmenden Meßgenauigkeit wuchsen Anwendungsmöglichkeiten und Aussagefähigkeit des Verfahrens.
Als ein wichtiges Einsatzgebiet der durchflußzytometrischen DNS-Messung erwies sich die Tumorforschung. Eine hohe Meßgenauigkeit und Auflösung ist notwendig, um aneuploide Zellinien, deren DNS-Gehalt oft nur wenig von dem normaler Zellen abweicht, sicher zu erkennen.
Die hier beschriebene Methode beruht auf der Vereinzelung der Zellkerne mit Zitronensäure und einem Detergenz (3) und der Färbung der DNS mit 4',6-Diamidino-2-phenylindol (DAPI). DAPI wurde von Göhde et al.(4) in die Durchflußzytometrie eingeführt und hat sich auf Grund seiner hohen Spezifität und Fluoreszenzintensität sehr bewährt.

Präparation und Färbung:

a) Gewebe mit Skalpell oder Schere zerschneiden,
b) mit Lösung Zitronensäure/Tween 20 bei Raumtemparatur 20 Minuten inkubieren, leicht schütteln oder rühren,
c) 10 Minuten bei 100 x g zentrifugieren, Überstand entfernen,
d) Zellen in 70%igem Äthanol fixieren.
   Die fixierten Zellen können gekühlt mehrere Monate aufbewahrt werden.
e) 10 Minuten bei 200 x g zentrifugieren, Fixiermittel vollständig entfernen,
f) Zellen mit 1 ml Zitronensäure/Tween 20 resuspendieren, 10 Minuten inkubieren, leicht schütteln,
g) 5 ml Lösung Phosphat/DAPI zugeben.
   Die gefärbten Zellen sind 24 bis 48 Stunden haltbar.

Messung:

Zur Messung mit dem Durchflußzytometer PAS II (Partec GmbH) werden folgende Filter verwendet:
KG 1 und BG 38 als Wärmeschutzfilter,
UG 1 als Anregungsfilter,
TK 420 als dichroischer Spiegel,
GG 435 als Sperrfilter.
(siehe Filterschema)

Reagenzien:

1.Lösung Zitronensäure/Tween 20

Zitronensäure H O.....2,1 g
Tween 20.....0,5 g
entionisiertes Wasser.....100 ml

2. Lösung Phosphat/DAPI

Na HPO 2 H O.....7,1 g
Stammlösung DAPI.....0,5 ml
entionisiertes Wasser.....100 ml

3. Stammlösung DAPI

4',6-Diamidino-2-phenylindol..3,5 mg
entionisiertes Wasser.....10 ml

Die Lösungen 1 und 2 sind bei Raumtemparatur 1 bis 2 Wochen haltbar. Die Stammlösung DAPI kann gekühlt und dunkel mehrere Monate aufbewahrt werden.

Ergebnisse

Durch die Behandlung mit Zitronensäure/Tween 20 werden die Zellen aus dem Gewebe gelöst und die Zellkerne isoliert. Durch die Zugabe von Phosphat/DAPI wird der ph-Wert angehoben und die DNS gefärbt.
Dieses Verfahren liefert durchflußzytometrische Histogramme des nukleären DNS-Gehalts von ausgezeichneter Reproduzierbarkeit und Auflösung. Variationskoeffizienten von 1 % und darunter können routinemäßig erreicht werden. Dies ermöglicht die Auflösung von Zellpopulationen, die sich im DNS-Gehalt um weniger als 2 % unterscheiden (Abb. 1). In der Tumorforschung wird die Erfassung aneuploider Zellinien wesentlich erleichtert (Abb. 2).
Das Verfahren ist bei einer Vielzahl von Zelltypen anwendbar. Gute Erfahrungen liegen vor bei menschlichen und tierischen Fibroblasten, Leukozyten, Knochenmarkzellen, Thymozyten, Lungen-, Leber-, Haut- und Testeszellen, verschiedenen Tumoren, bei Hühner- und Forellenerythrozyten sowie einer Reihe von Kulturzellen.

Es ist allerdings darauf hinzuweisen, daß DAPI bevorzugt AT-reiche DNS färbt. Daher ist die Färbung streng genommen nicht geeignet, absolute DNS-Mengen zu bestimmen oder Zellen mit unterschiedlichen AT-Anteilen zu vergleichen. Trotz dieser Einschränkung ist es möglich, Hühner- oder Forellenerythrozyten als inneren Standard zu benutzen, um die relative Peakposition oder den Variationskoeffizienten einer bestimmten Zellart zu ermitteln.

Zusätzliche Literatur

1. Bartkowiak D., J.Schumann, F.J.Otto, A.Lippold, H.Drepper: (1991) DNA flow cytometry in the prognosis of primary malignant melanoma. Oncology **48**, 39-43

2. Bartkowiak D., F.Otto, J.Schumann, A.Lippold, H.Drepper: (1991) Sequential DNA flow cytometry in metastatic malignant melanoma. Oncology **48**, 154-157

DURCHFLUSSZYTOMETRISCHE INSTRUMENTANTION

FÜR PLANKTONANALYSE

PD Dr.Ing.V.Kachel

Max-Planck-Institut für Biochemie
Arb.Gruppe Zellmeßtechnik
Martinsried

MACRO FLOW PLANKTOMETER

EUROMAR PROJEKTVORHABEN MAROPT EU 413
BORDTAUGLICHES MACRO FLOW PLANKTOMETER ZUR MULTIPARAMETRIGEN VERMESSUNG MIT INTEGRIERTER BILDSPEICHERUNG VON MEERESPLANKTON UND FISCHBRUT

V. Kachel, R. Hüller, E. Glossner, S. Schmidlechner,
J. Weingärtner, S.Schaub, P.Hummel
Max-Planck-Institut für Biochemie, 8033 Martinsried bei München

ZIELSETZUNG

Entwicklung eines Meßsystems zur automatisierten Erfassung der Eigenschaften von Plankton >100um und Fischlarven im Durchflußverfahren.

Geräteeigenschaften:

Berührungsloses Bestimmen der Organismusgröße und von Fluoreszenzeigenschaften verbunden mit meßwertgetriggerter Aufnahme von Bildern ausgewählter Organismen. Einfach handhabbares Tischgerät, verwendbar auch in Schiffslabors, Verwendung preiswerter Personal Computer.

Anwendungen:

Vermessung großer Populationen empfindlicher Organismen in lebendem Zustand ohne deren Lebensprozesse wesentlich zu beeinflussen, z.B. Zählung von Bevölkerungsdichten oder Überlebensraten, Bestimmung von Körpervolumen, Körperlängen, Volumenzunahme oder der Ausbildung innerer und äußerer Körpermerkmale, Quantifizierung von (fluoreszierenden) Darminhalten für Rückschlüsse auf Freßaktivitäten und Freßgewohnheiten.

ALLGEMEINE SYSTEMEINGESCHAFTEN

Das Macro Flow Planktometer (MFP) mißt als Basis das Volumen von Organismen nach dem elektrischen Widerstandsänderungsprinzip. Eine simultane Fluoreszenzmessung kann durch die Erkennung z.B. der natürlichen Fluoreszenz von Chl a zur Charakterisierung von Phytoplankton oder zur Bestimmung der Freßaktivitäten von Zooplankton und Fischlarven eingesetzt werden. Zusätzlich kann ein Absorptions- und Streulichtsensor in die Meßkammer eingebaut werden. Durch ein von der Durchflußanalyse gesteuertes elektronisches Bildaufnahmesystem wird die abstrakte Eigenschaftsanalyse mit einer bildlichen Darstellung ausgewählter Organismen kombiniert, die zusätzlich detaillierte morphologische Erkenntnisse über die jeweils selektierte Organismengruppe liefert.

Das Gerät ist für die Untersuchung von Zooplankton, Phytoplankton, Fischlarven und Fischeiern in See- und Süßwasser verwendbar.

KOOPERIERENDE PARTNER

Die technische Entwicklung wurde in der Arbeitsgruppe ZELLMESSTECHNIK des MAX-PLANCK-INSTITUTES für Biochemie durchgeführt. Die Gruppe arbeitet eng mit den Abteilungen für PLANKTOLOGIE (Prof.Dr. J. Lenz) und FISCHEREIBIOLOGIE (Prof. Dr. D. Schnack) des INSTITUTES FÜR MEERESKUNDE der Universität Kiel zusammen, welche die biologischen Zielsetzungen maßgeblich beeinflußt haben. Die Gruppe des MPI stellt ihr technisches Know How auch für die Entwicklung der in-situ Recording Systeme zur Verfügung, die im MAROPT Projekt unter Federführung der Partner des IFM entwickelt werden. Europäischer Partner des MAROPT Projektes ist die Firma HYTEC in Montpellier, Frankreich. Der Partner zur industriellen Weiterentwicklung des Macro Flow Planktometers ist seit 1991 die Firma SYSTEMTECHNIK NORD in Bremen (STN).

SYSTEMBESCHREIBUNG

Das Makro Flow Planktometer besteht aus Bausteinen, die zu einem dem Verwendungszweck angepaßten Gesamtsystem zusammengefügt werden:

(A) MESSKAMMER MIR DURCHFLUSSYSTEM UND SENSORIK
(B) ANALOGE ELEKTRONISCHE SPEISUNG UND SIGNALAUFBEREITUNG
(C) RECHNERSYSTEM ZUR DIGITALEN STEUERUNG UND DATEN-UND BILDAUFNAHME
(D) PROGRAMME ZUR SYSTEMSTEUERUNG, DATEN-UND BILDAUFNAHME, AUSWERTUNG

Diese vier Bausteine sind in jedem MFP notwendig. Sie sind modulär aufgebaut und können je nach zu erfassenden Eigenschaften der Meßproben erweitert werden. Die Eigenschaften werden an jedem durchfließenden Einzelorganismus gemessen.

Folgende Funktionsmodule können miteinander kombiniert werden:

ELEKTRISCHE KÖRPERVOLUMENMESSUNG
QUANTITATIVE MESSUNG FLUORESZIERENDER STOFFE IN DEN ORGANISMEN(ANR. 488nm)
STREULICHTMESSUNG
MESSWERGETRIGGERTE BILDAUFNAHME VON EINZELORGANISMEN.

Für Plankton und Fischlarven wird jeweils ein spezielles Meßkammersystem verwendet. Fischlarven erfordern ein räumlich größeres Kammersystem mit einem horizontal durchströmten Meßkammertrakt und einer Treibvorrichtung. Plankton dagegen wird in einer kleineren, vertikal durchströmten Anlage gemessen.

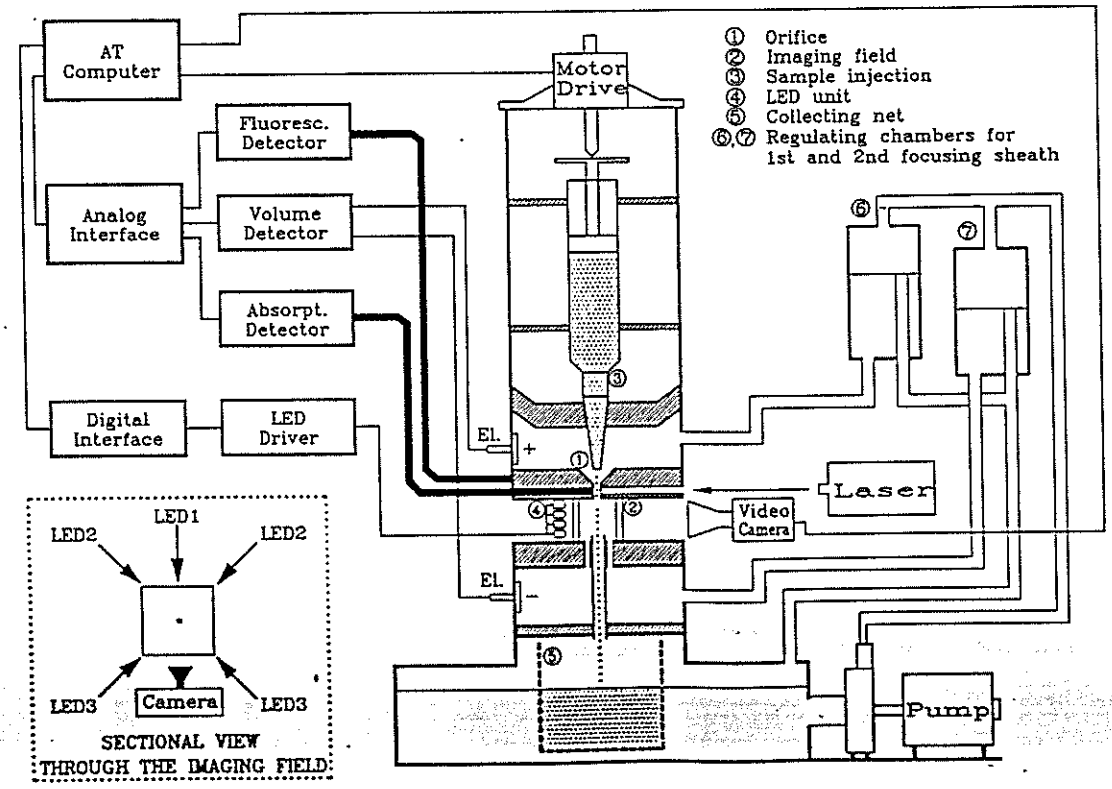

Abb.1 Prinzipieller Aufbau des Plankton-Meßkammersystems

Abb. 1 zeigt den prinzipiellen Aufbau der Planktonversion, Abb.2 die Ausführung des Prototypen. Das Flußsystem wird über eine Pumpe aus dem allgemeinen Vorrats- und Auffangbehälter gespeist. Der erste Hüllstrom wird aus dem Behälter 6 zugeführt, dessen Höhe hydrostatisch einen bestimmten Druck festlegt. Der erste Hüllstrom bündelt die aus der Zuführungsspitze der Spritze 3 austretenden Meßobjekte auf den achsennahen Bereich der Meßöffnung 1. Das Feld für die Bildaufnahme befindet sich unmittelbar hinter der Meßöffnung, in der neben der elektrischen Volumenmessung auch die laserangeregten Fluoreszenz- und Absorptionsmessungen durchgeführt werden. Der zweite Hüllstrom, der hinter dem Abbildungsraum aus dem Behälter 7 in die Kammer eingeführt wird, sorgt dafür, daß die Meßobjekte auf ihrer eng begrenzten Bahn bleiben. Nach Durchlaufen des Abbildungsfeldes werden sie vom anschließenden Fangrohr aufgefangen und in den Auffangbehälter 5 transportiert, ohne daß ein Teil davon in den Elektrodenraum gelangt.
Die elektrische Volumenmessung wird nach dem Coulter Verfahren zwischen den beiden eingezeichneten Elektroden durchgeführt. Jedes die Meßöffnung passierende Objekt erzeugt einen elektrischen Impuls, dessen Höhe ein Maß für das Volumen des gemessenen Teilchens ist. Innerhalb der Meßöffnung können die Meßobjekte von einem durch einen Lichtleiter zugeführten Argon-Laserstrahl beleuchtet werden. Dieses Anregungslicht erzeugt in Vorwärtsrichtung ein Absorptions- und Streulichtsignal und in 90°- Richtung ein Fluoreszenzsignal, wenn entsprechende fluoreszierende Substanzen in den Meßobjekten vorhanden sind. Die pulsförmigen Fluoreszenzsignale werden durch Lichtleiter zu den Detektoren und lichtelektrischen Wandlern geleitet. Nach Verstärkung im Analog-Interface stehen die Signale zur Analog-Digital-Wandlung im PC bereit. Durch logische Verknüpfung der Signalamplituden mit vom Benutzer festgelegten Fenstern wird über ein digitales Interface nach einer Laufzeitverzögerung die Bildaufnahme ausgelöst, wenn vom Computer Signale innerhalb des Auswahlfensters festgestellt werden.
Der Schrittmotor der Probeneinführungs-Spritze wird vom Computer gesteuert.
Bei einer vereinfachten motorlosen Prozedur zur Probeneingabe wird der Kolben der Spritze entfernt und nach Füllen der Spritze diese mit einem Deckel mit Belüftungsventil verschlossen. Die Kammern 6 und 7 werden so eingestellt, daß

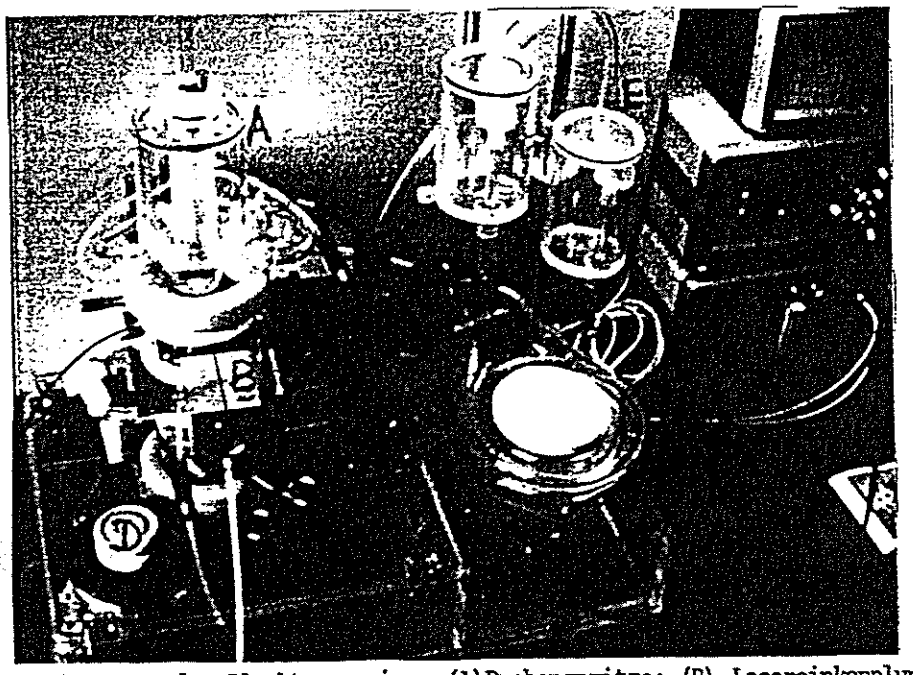

Abb.2: Durchflußsystems der Planktonversion: (A) Probenspritze; (B) Lasereinkopplung durch Lichtleiter; (C) CCD Kamera; (D) Entnahme der gemessenen Proben; (E) hydrostatische Druckregelung;

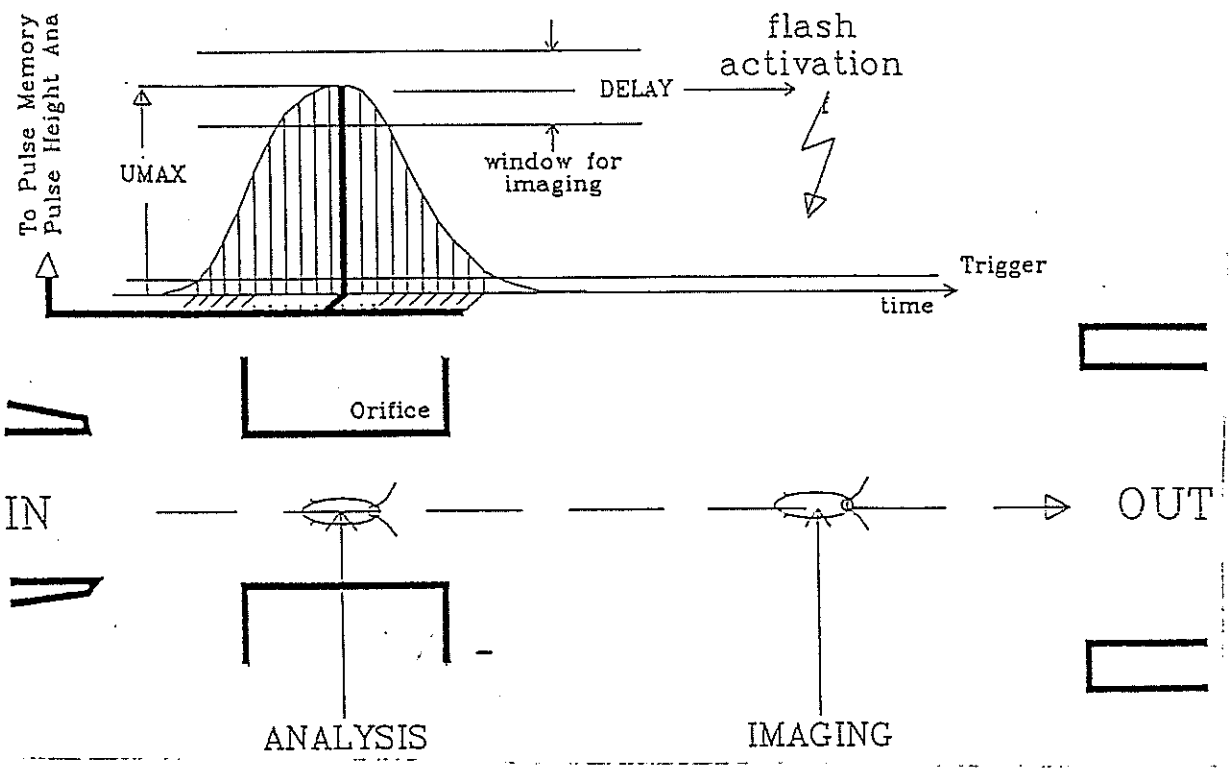

Abb.3: Prinzip der digitalen Pulshöhenanalyse und Bildtriggerung. Die Organismen treten von links in das System ein. Lag die Maximalamplitude im Bildfenster, dann wird eine Bildaufnahme ausgelöst.

in der Spritze Unterdruck herrscht. Durch entsprechendes Justieren des Belüftungsventils der Spritze läuft die Probe langsam in das Meßsystem ein. Die Histogramme der gemessenen Eigenschaftsverteilungen sind während und nach der Messung auf dem Bildschirm verfügbar.

Abb. 3 zeigt ein Schema der Amplitudenauswertung und Bildaufnahmetriggerung. Die Meßobjekte bewegen sich mit Geschwindigkeiten von ca.1 m/s, sie können also nur durch eine sehr kurzzeitige Belichtung scharf abgebildet werden. Es werden hier Bündel von mehreren rotleuchtenden "high brightness" Leuchtdioden verwendet, die mit 1 - 2 us Dauer gepulst werden. Eine CCD Kamera nimmt die Bilder auf, die von dort in eine Bildspeicherkarte des PC übertragen werden. Sie können vom Benutzer auf einem eigenen Bildschirm sofort betrachtet werden und/oder auf Magnetplatten oder -Bändern archiviert werden. Es ist geplant, sie auch in automatischen Bildverarbeitungssystemen zu analysieren.

In Abb.4 ist ein Blockschaltbild der Elektronik des Meß- und Bilderfassungssystems dargestellt.

Die Meßkammer für Fischlarven weist einige Modifikationen auf: Die Strömungsrichtung im Meßtrakt ist horizontal, weil sich Fische wie Larven im wesentlichen horizontal bewegen wollen. Das Kammersystem ist größer dimensioniert und der Probenzuführungsbehälter hat einen geregelten Wasserstand. Während der Messung wird der Aufenthaltsraum der Larven allmählich durch einen langsam absinkenden Treibkolben eingeengt, um sie zum Eintritt in das Meßsystem zu veranlassen.
Folgende Entwicklungsprobleme sind besonders zu erwähnen:
Die Strömungskanäle des Systems sind so groß, daß turbulente Strömung auftreten kann. Mit Testpartikeln wurde jedoch nachgewiesen, daß mit einem sorgfältig konstruierten Strömungskanal auch im turbulenten Strömungsbereich reproduzierbare Größenmessungen durchgeführt werden können.

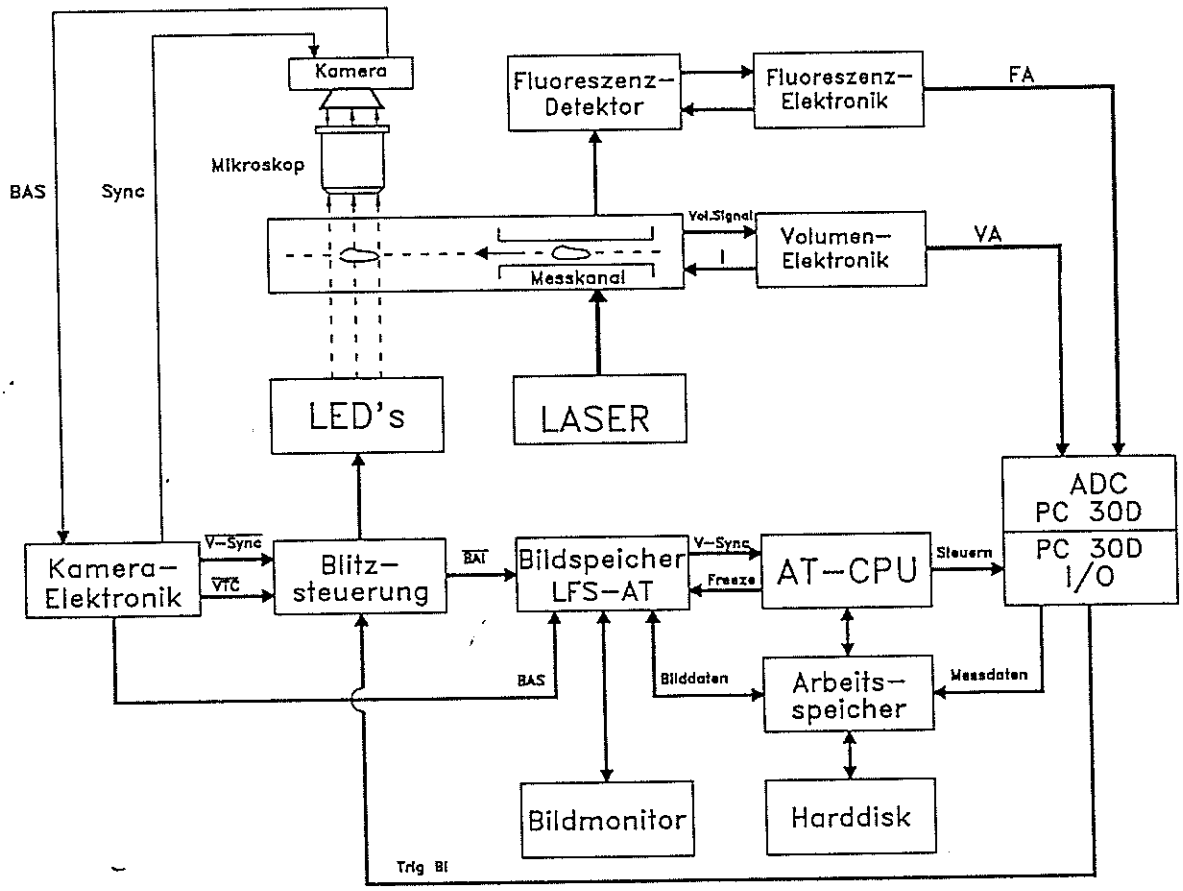

Abb.4: Blockschaltbild der Elektronik des Meß- und Bildsystems

Das Fischlarvensystem erfordert Durchflußvolumina von bis zu 10 l/min., die sich jedoch durch Rezirkulation des Wassers beherrschen lassen. Es muß darauf geachtet werden, daß über die Flüssigkeitskanäle kein undefinierter Kurzschluß der elektrischen Volumensignale erfolgt.
Schiffsbewegungen können die Flüssigkeiten in den Behältern des Systems in unerwünschte Bewegung bringen. Durch bremsende Lamelleneinsätze kann diese vermindert werden.
Ein wesentliches Problem stellt die hohe, von äußeren Einflüssen und "Erlebnissen" beeinflußbare Eigenbeweglichkeit der Fischlarven dar. Es wurde deshalb auf eine schonende Behandlung der Larven während des Meßvorganges besonders geachtet.

Das gesamte Meß- und Bildaufnahmesystem wird von einem IBM-AT kompatiblen Rechner gesteuert, der folgende Aufgaben erfüllen muß:

1. Abtasten und Abspeichern der Meßimpulse für eine spätere Rekonstruktion der Impulsform.
2. Erfassen und Klassifizieren der Maximalamplituden der Meßimpulse.
3. Darstellung, Auswertung und Abspeicherung der Ein- und Mehrparameter Eigenschaftshistogramme.
4. Festlegung von Triggerfenstern für die Aktivierung der Bildaufnahme
5. Feststellung, ob die einlaufenden Impulse mit ihren Amplituden in das Triggerfenster fallen.
6. Aktivierung des Beleuchtungsblitzes nach einer definierten Verzögerungs-

zeit, wenn ein Impulsmaximum in das Triggerfenster fiel.

7. Einfrieren des stroboskopischen Kamerabildes auf der digitalen Bildkarte des Computers, Darstellung der Bilder auf dem Bildmonitor.
8. Übertragung der digitalen Videobilder in Datenfiles auf der Festplatte
9. Rücklesen von Videobildern von der Festplatte in die Bildkarte und Darstellung der Bilder auf dem Bildmonitor.

Das modulär gegliederte Programm wurde in Assemblersprache geschrieben. Folgende Funktionsmodule sind verfügbar:

1. Aufnahme von 1 bis 3 Eigenschaften (Parameter) in unklassiertem LIST-MODE. Die Amplituden werden mit einer Auflösung von 4096 Kanälen gewandelt und dann als Datenliste auf der Harddisk gespeichert. Aus den unklassierten Daten können bei der Nachbearbeitung mit Hilfe der klassierenden Module Auswertehistogramme erstellt werden.

2. Klassierende Aufnahme und Darstellung von einem Parameter, Auflösung 128 Kanäle. Transientenspeicherung der Impulsformen. Software Peakdetektion. Fenstererzeugung zur Bildtriggerung. Bildabspeicherung, Bilddarstellung, Numerische Histogrammauswertung, Klassierung aus LIST MODE Daten.

3. Klassierende Aufnahme und Darstellung von 2 Parametern, Auflösung 128x 128 Kanäle. Software Peakdetektion. Fenstererzeugung zur Bildtriggerung und numerischen Auswertung. Bildtriggerung, Bildabspeicherung, Rückprojektion in den Einparameterbereich. Klassierung aus LIST MODE Daten.

4. Klassierung von 3-Parameter LIST MODE Daten in ein kubisches Displayfeld. Auflösung 64 x 64 x 64 Kanäle.

ANWENDUNGSBEISPIELE DES MACRO FLOW PLANKTOMETERS

Im Juli 1990 wurde der Prototyp des Systems erstmals auf einer Forschungsreise des RV Alkor in der Ostsee erfolgreich für Planktonmessungen eingesetzt. Abb.5 zeigt Volumenverteilungskurven von jeweils ca. 920 Kopepoden, die an Bord gemessen wurden. Die Kurve A stammt von unfixierten Kopepoden, die 3 Std. nach dem Fang aus einer Tiefe von 60-110 m (Apsteinnetz, 300um Maschenweite) gemessen wurden. (Meßlochlänge 3 mm, Durchmesser 2 mm; Meßstrom 1,7 mA; V=4 log.) Die Volumenverteilung B stammt unter identischen Meßbedingungen von der gleichen Probe von Kopepoden, aber nach deren Fixierung in 5% Formalin. Die Kurve B ist als Folge der Fixierung um ein Stück auf der logarithmischen Volumenachse zu kleineren Werten hin verschoben.

Abb. 6 zeigt Volumenmessungen von Renkenlarven aus dem Starnberger See. (Meßlochlänge 35 mm, Durchmesser 8,7 mm; Meßstrom 0,2 mA, V=1 log; Wassertemperatur 16°C). Die Verteilungen A und B wurden am 2.7.1991 aufgenommen. Die im logarithmischen Maßstab aufgenommenem Verteilungen zeigen eine gute Übereinstimmung. Die Kurve C zeigt eine Volumenverteilungskurve der gleichen Population nach 16 Tagen Fütterung unter gleichen Meßbedingungen. Das Wachstum der Larven kann auf diese Weise quantifiziert werden. Die Kalibriermessungen mit einem Kalibrierkörper von 10 mm Länge und 1,65 mm Durchmesser (V=21,4 mm^3) waren während der Messungen konstant (Kurven D am 5.7. und E am 18.7.). Die Bilder der Renkenlarven stammen von einer Bilderserie, die volumengetriggert am 25.4.1991 elektronisch gespeichert wurden. Auf den Bildern können zahlreiche Details der Larven erkannt werden.

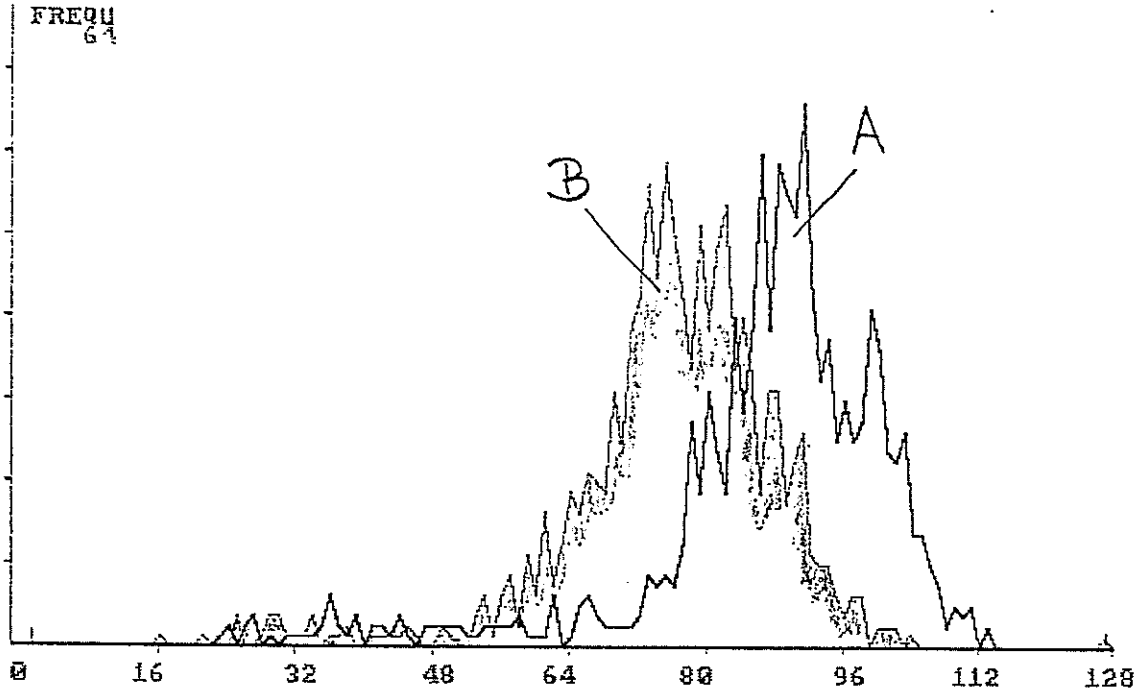

Abb.5: Volumenverteilungskurven von Kopepoden aus der Ostsee; A native Probe; B Probe nach Fixation mit 5% Formalin. (Meßlochlänge 3 mm, ML-Durchmesser 2 mm; Meßstrom 1,7 mA; V=4 log.

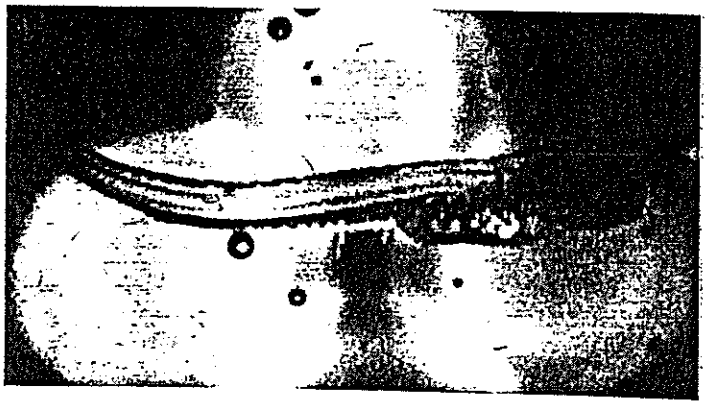

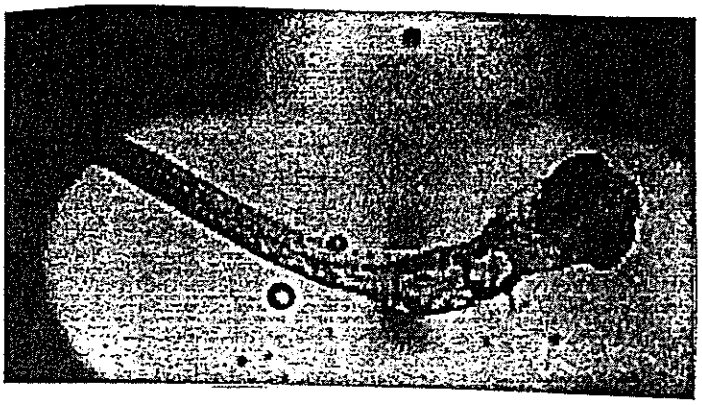

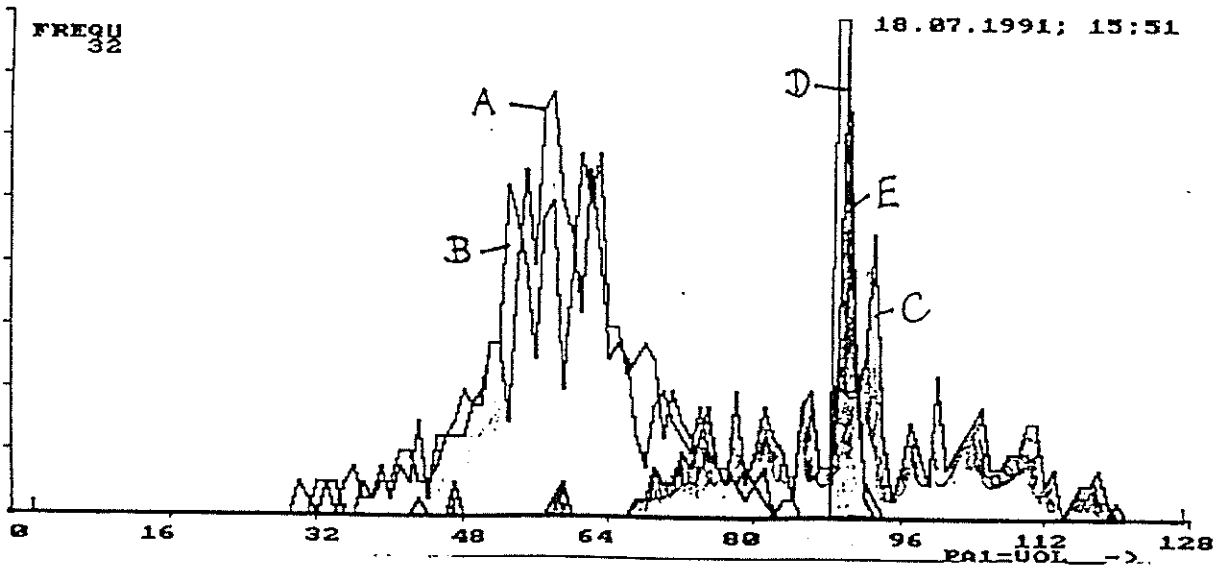

RENKENLARVEN STARNBERGER SEE, Fütterung
VOLUMENMESSUNG LD-8,7mm, LL 35mm, I 0,2mA
V=1 LOG; Wassertemp. 16°C
CALIB: D=1,65mm, L=10mm, V=21,4mm3

A	2.7.91	N=384;	M=58,54,	CV=15,95%	RENK
B	2.7.91	N=391;	M=58,96,	CV=16,11%	RENK
C	18.7.91	N=239;	M=91,51,	CV=14,88%	RENK
D	5.7.91	N=100;	M=89,68,	CV= 0,87%	CALIB
E	18.7.91	N= 50;	M=90,10,	CV= 0,74%	CALIB

Abb.6: Volumenverteilungskurven und volumengetriggerte Bilder von Renkenlarven

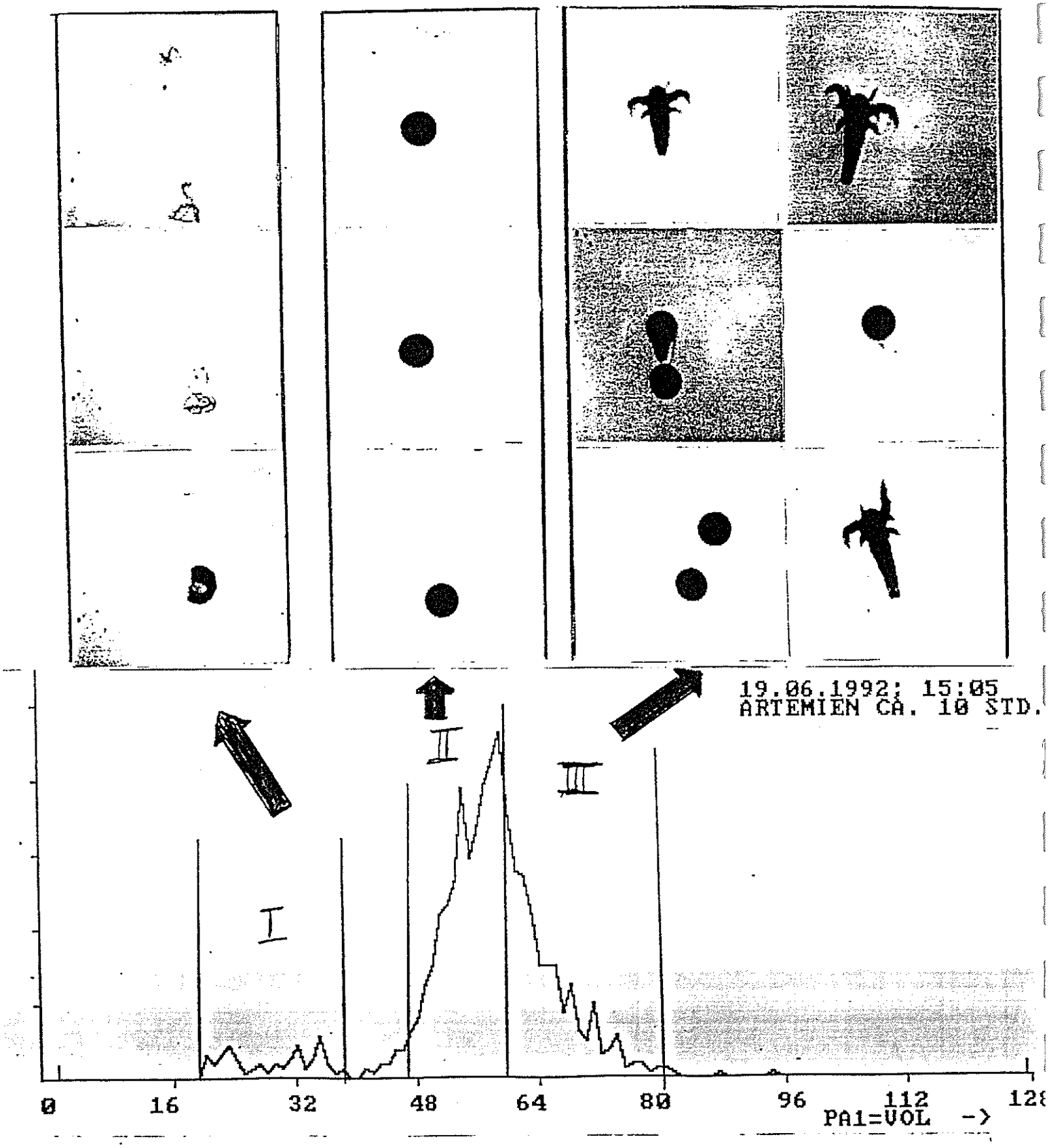
19.06.1992; 15:05
ARTEMIEN CA. 10 STD.
I
II
III
0
16
32
48
64
80
96
112
128
PA1=VOL ->
TOT= 992 MW= 56.40CHN C:\CYTDATA\ARTEMI02.P11

Abb. 7

WI7= 00

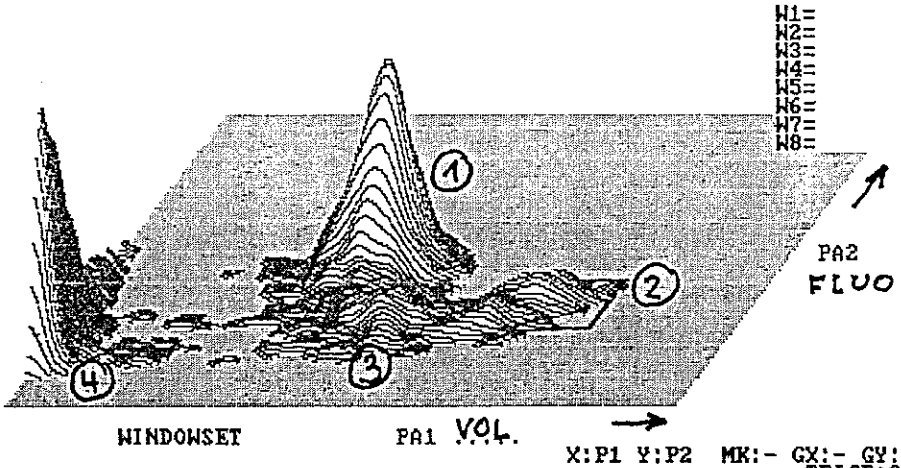

X:P1 Y:P2 MK:- GX:- GY:-
TRIGP:2
C:\CYTDATA\LIST0000
C:\CYTDATA\WINART02.W8:
22.06.1992; 15:41

!! HISTOGRAMM IS SMOOTHED !!

Abb. 8

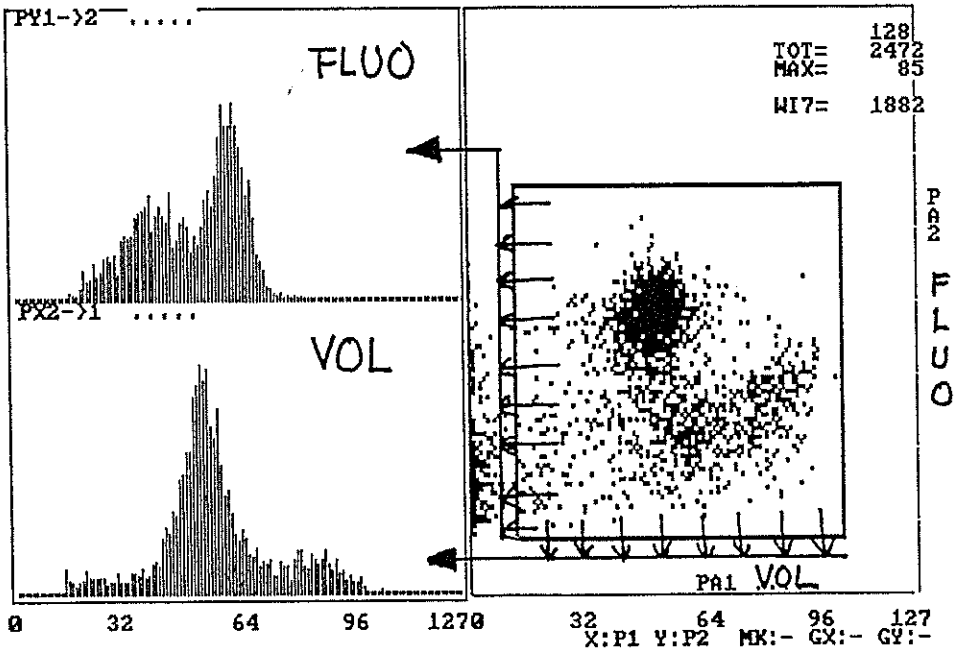

X:P1 Y:P2 MK:- GX:- GY:-

>S<=STORE PROJX00.P11/PROJY00.P11;ANY=ESC;>B<=STORESCR

C:\CYTDATA\WIARTVAL.W8:

Abb. 9

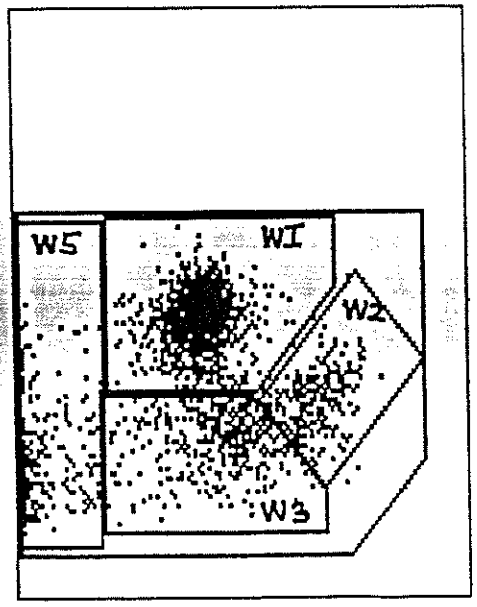

TOT= 2472
MAX= 28

W1=	1127	45.59 % of W8	1
W2=	245	9.91 % of W8	2
W3=	436	17.63 % of W8	3
W4=	00	0.00 % of W8	
W5=	656	26.53 % of W8	4
W6=	00	0.00 % of W8	
W7=	00	0.00 % of W8	
W8=	2472	100.00 % of W8	Tot

Abb. 10

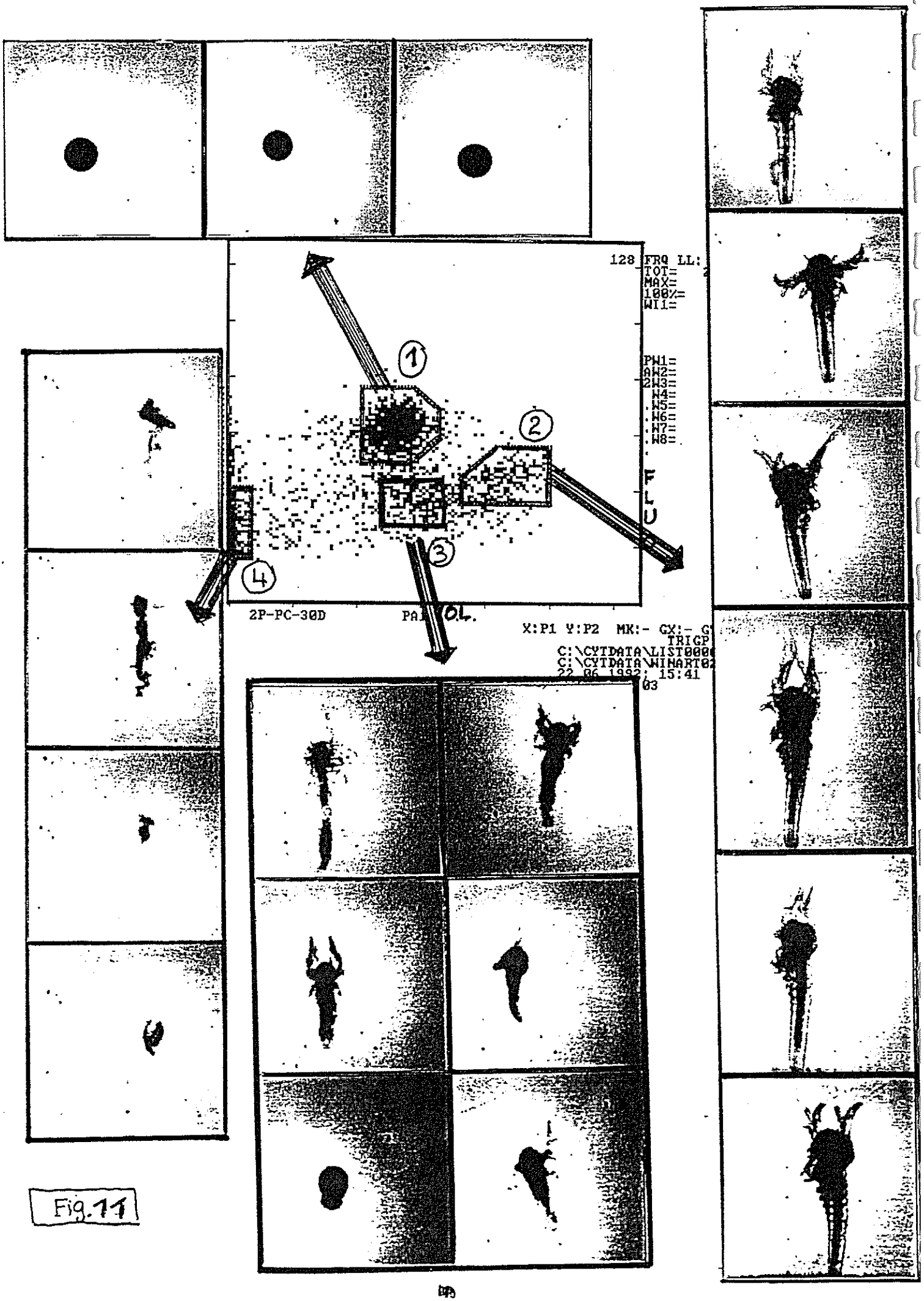
128 FRQ LL:
TOT=
MAX=
100%=
WI1=
PW1=
AW2=
2W3=
W4=
.W5=
.W6=
.W7=
.W8=
1
2
3
4
2P-PC-30D
X:P1 Y:P2 MK:- GX:-
TRIGP
C:\CYTDATA\LIST000
C:\CYTDATA\WIHART02
22 06 1992 15:41
03

Fig.11

Abb.7 zeigt eine Volumenverteilungskurve von Artemieneiern und Artemien, die ca. 10 Std. nach dem Schlüpfen der ersten Artemien am 19.6.1992 aufgenommen wurde. Über die mit I,II und III bezeichneten Bildfenster wurden während der Messung selektiv die diesen Meßbereichen zuzuordnenden Objekte abgebildet.
Die Bildreihen zeigen charakteristische Bilder der Objekte: Bereich I (kleine Volumina): Eihäute, Bruchstücke von Eiern; Bereich II (mittleres Volumen): Artemieneier; Bereich III (große Volumina): Geschlüpfte Artemien, große Eier und Doppeldurchtritte.

Die Abbildungen 8 bis 11 zeigen verschiedene Varianten einer Zweiparametermessung von Artemieneiern und Artemien, die am 22.6.1992 aufgenommen wurde. Die Eier dieser Probe waren am 19.6. zum Schlüpfen angesetzt worden. Es wurde im Fluoreszenzmikroskop festgestellt, daß Artemieneier und Artemien bei Anregung mit 488 nm eine gelbliche Fluoreszenz emittieren. Dies wird zur Demonstration des Fluoreszenzsystems des MFP benutzt. Das Fluoreszenzlicht wurde durch einen Langpaß LP530 vom Laser Anregungslicht abgetrennt.
In Abb.8 ist das Zweiparameterfeld mit der Häufigkeit auf der Z-Achse isometrisch dargestellt. In der Mitte des Feldes wird ein ausgeprägter Peak (1) beobachtet, der nach unten und rechts in die Bereiche (2) und (3) ausläuft. Links auf der Fluoreszenzachse beobachtet man einen Peak(4), der durch geringe Volumensignale charakterisiert ist.

Durch Projektionen auf die Volumen bzw. Fluoreszenzachse (Abb.9) lassen sich aus dem Zweiparameterhistogramm die entsprechenden Volumen- und Fluoreszenz-Einparameterverteilungskurven gewinnen. Die aus der Projektion gewonnene Einparameter-Volumenverteilungskurve der Abb.9 links unten ist der Kurve von Abb.7 ähnlich. Der zweite den Artemien zuzuordnende Peak ist allerdings ausgeprägter und weiter zu größeren Körpervolumina hin verschoben, weil die Artemien schon weiter entwickelt sind.

In Abb.10 ist eine numerische Auswertung des Zweiparameterfeldes mit den Fenstern W1, W2, W3 und W5 dargestellt. Die Messung umfaßt insgesamt 2472 Ereignisse, davon fallen 45,59% in den Bereich W1, 9,91% in W2, 17,63% in W3 und 26,53% im Bereich W5. Die Messung der 2472 Objekte dauerte ca. 4 Minuten, die Auswertung mit Graphik ist, wenn die Fenster vorhanden sind, nach ca. 2 Sekunden verfügbar.

Abb. 11 zeigt schließlich, wie durch Bildtriggerung über verschiedene Zweiparameter-Bildfenster die den Bereichen (1) bis (4) zuzuordnenden Objekte aus dem Durchfluß heraus bildlich dargestellt werden können. Im Bildfenster (1) wurden fast ausschließlich Artemieneier gefunden. Die Bilder aus Bildfenster (2), meßtechnisch charakterisiert durch großes Volumen und reduzierte Fluoreszenz, zeigen dagegen ausschließlich gut entwickelte Artemien. Im Fenster (3) aus dem Volumenbereich knapp oberhalb des Volumens der Arte-mieneier von Fenster (1), aber mit auch gegenüber Fenster (2) weiter reduzierter Fluoreszenz, findet man im wesentlichen denaturierte, meist wohl tote Artemien aus jüngeren Entwicklungsphasen. Im Fenster (4), charakterisiert durch sehr geringe Volumenwerte, findet man vor allem Bruchstücke von Organismen, Eihüllen u.a. Die Bilder wurden aus dem Computerspeicher durch einen Video-Printer ausgedruckt.

<u>Schlußfolgerung:</u>
Am vorliegenden Beispiel wird demonstriert, daß mit dem Macro Flow Planktometer Planktoneigfenschaften im vorgesehenen Größenbereich schneller, vielseitiger und genauer analysiert werden können als mit bisher angewendeten konventionellen Methoden.

Literatur:

Burkill P.H.: Analytical Flow Cytometry and its Application to Marine Microbial Ecology aus: Microbes in the Sea ed. S.Leigh, Ellis Horwood, Chichester, England, 1987

Farrenkopf Ch: Entwicklung und Realisierung einer ADC-Karte zur Impulshöhenmessung für den Einsatz in PCs. Diplomarbeit, Technische Universität München, 1992

Hüller R., Päffgen W., Glossner E., Hummel P., Kachel V.: A PC-AT based Video Device for Flow Cytometrically triggered Cell Imaging in Flow. Computerized Medical Imaging and Graphics 15:85-91,1991

Hüller R., Schmidlechner S., Glossner E., Schaub S., Kachel V.: A Macro Flow Planktometer for Analysis of Large Marine Plankton Organisms. CYTOMETRY Suppl.5:55,1991

Kachel V.: Electrical Resistance Pulse sizing: Coulter Sizing; in: Flow Cytometry and Sorting, 2.Edition Hrsg.M.R.Melamed, T.Lindmo, M.L.Mendelsohn, Wiley-Liss, New York, 1990

Kachel V,. Fellner-Feldegg H., Menke E.: Hydrodynamic Properties of Flow Cytometry Instruments. in flow Cytometry and Sorting, 2.Edition Hrsg.M.R.Melamed, T.Lindmo, M.L.Mendelsohn, Wiley-Liss, New York, 1990

Kachel V.,Kiemle Ch., Rembold H., Eichmeier J., Messerschmied Th., Flüchter J.: A Computerized Analyzer for Size Measurement of Fish Larvae and Young Fishes. PROCEEDINGS OF THE WORKSHOP OF NEW TRENDS IN ICHTYOLOGY, Neuherberg, in press

Peleska P.: Verbesserung der Meßempfindlichkeit der elektrischen Zellvolumenmessung in einem Durchflußzytometer. Diplomarbeit, Technische Universität München, 1992

Schmidlechner St.: Elektronische, mechanische und strömungstechnische Optimierung eines Durchflußplanktometers zur Messung von Großplankton und Fischbrut. Duiplomarbeit Fachhochschule München, 1989

Weingärtner J.: Realisierung der Fluoreszenz- und Streulichtmessung im Macro Flow Planktometer. Diplomarbeit, Fachhochschule München, 1992

Proceedings of the Conference:
Optics Within Life Sciences II
Münster, 4.-9.Oct. 1992, in press

OPTICAL AND ELECTRICAL METHODS FOR THE ANALYSIS OF SINGLE AQUATIC PARTICLES AND ORGANISMS

V. Kachel[a], R. Hüller[a], E. Glossner[a], P. Burkill[b], G. Tarran[b]
[a]Max-Planck-Institut für Biochemie, D-8033 Martinsried, Germany
[b]Plymouth Marine Laboratory, Plymouth, UK

INTRODUCTION

In the latter half of the twentieth century it has become apparent that the biological processes in the marine environment are of global importance. Much of this biological activity is attributed to tiny (<20 µm) single celled micro-organisms, known as phytoplankton. Although tiny, these organisms are very important as biological regulators of our climate and as contributors to the cycling of carbon [1,2].

Relatively little is known about phytoplankton. Of primary interest are studies of size distributions, abundances and population structure, in terms of the species present, understanding of basic physiological processes and detection of potentially dangerous species. It is also important to know how these factors vary in space and time[2], how they are influenced by environmental conditions and how phytoplankton influence those conditions.

The traditional method for plankton analysis has been absorption and fluorescence microscopy which has involved taxonomic recognition and enumeration of the many different species of plankton by an expert. This is both tedious and time consuming owing to the small size of plankton organisms and their normally low concentration in seawater.

More recently, automated microscopy with computer aided image analysis has been developed. For this to be effective and to speed up identification and enumeration, the samples have to be concentrated on filters, a lengthy procedure involving several handling steps. Many of the delicate cells in such samples are destroyed or become disfigured beyond recognition which causes uncertainties in evaluation.

The need for fast, accurate methods for analysing phytoplankton and other particles in seawater has led to the use of flow cytometry. This technology used widely at present in biomedical research and for medical diagnosis is also a valuable tool for plankton analysis[3,4]. Light sensitive pigments of phytoplankton fluoresce when excited by light of a particular wavelength. Optical sensors are used to detect fluorescent light as well as light reflected from particles, both of which are useful for identifying phytoplankton. Using the conductivity of seawater in which phytoplankton live cell volume and size can be electrically measured. Optical and electrical methods can be combined to provide multiparametric analysis with accurate results at high speed.

This paper introduces the principles of different sensors and the way in which they are integrated into a functioning flow cytometer. This is followed by a description of new technology combining analytical flow cytometry and video imaging of macro plankton called imaging in flow.

FLUORESCENCE ANALYSIS

The setup of optical sensors relative to the light source and fluorescent object is shown in Fig. 1. Either a monochromatic laser or a broad band lamp with an optical filter for wavelength selection illuminates the cell stream and excites natural or artificial fluorochromes in the cells. The emitted fluorescence light pulse is taken up by light collection optics, where, if several fluorochromes in the cells are excited simultaneously,

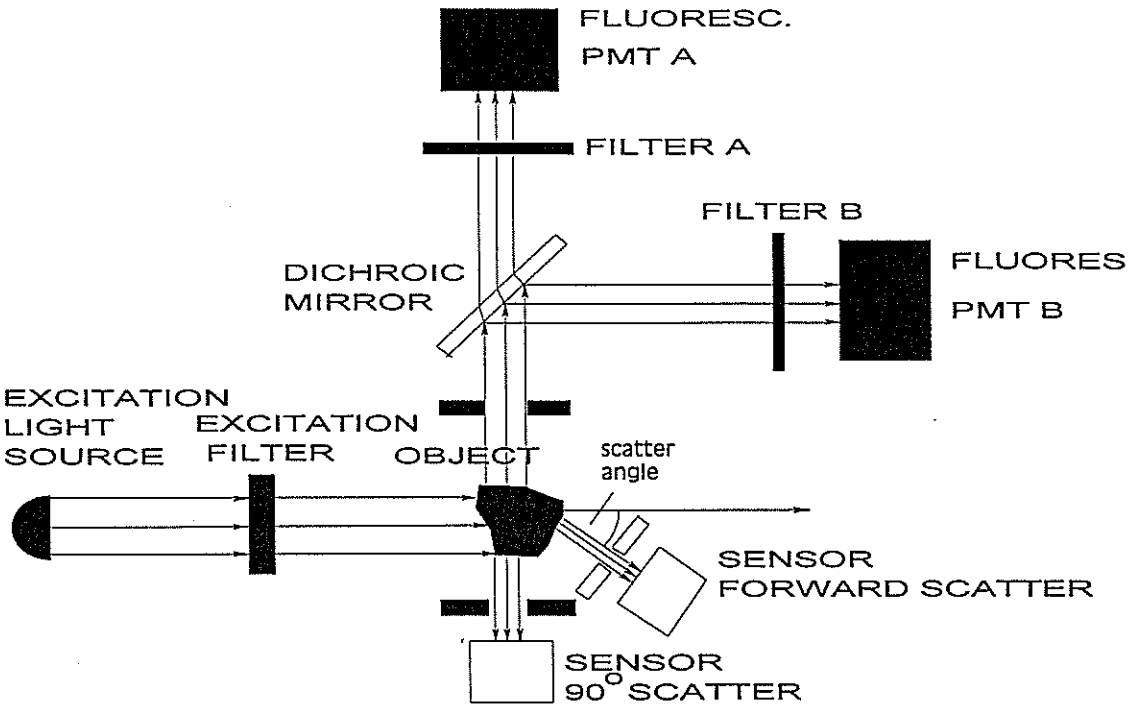

Fig.1: Fundamental setup of the optical sensors in a flow cytometer. The fluorescence in the object is excited by a light source. Two or more fluorescence wavelength ranges can be separated by filters and collected by separate photomultiplier tubes (PMT). The light scatter sensors evaluate the scattered original light of the light source.

optical filters separate the emitted light pulses into wavelength bands which are converted by photomultiplier tubes into electrical pulses.

Two main techniques are in use which mainly depend on whether a laser or an arc-lamp is used for excitation. Epi- illumination is usually provided by a high pressure arc lamp shone through an objective of high numerical aperture (Fig. 2a). The fluorescence is collected by the same objective in an axial direction to the sample stream. With radial light pick up (Fig. 2b) a laser illuminates the sample stream radially and the fluorescence is collected at 90 degrees to the direction of the laser illumination.

With radial pick up the plane of focus and the cell stream have to be exactly adjusted because minimal fluctuations in the particle path may cause considerable signal changes. With axial pick up, however, the particles always pass through the plane of focus which means fluorescence sensitivity is always constant. The numerical aperture of the collecting system plays an important role in the sensitivity of the fluorescence system. The amount of collected fluorescence light is dependent on the square of the numerical aperture A of the collection system.

For high sensitivity the light arriving at the PMTs has to be restricted to the light emitted from the cells. This is done by limiting the optical path in an intermediate image plane by a diaphragm, a pinhole or a slit.

The normally used argon lasers and high pressure mercury arc lamps have different features and optical characteristics:

Argon lasers providing a monochromatic coherent light can easily be focused to extremely small spots. If equipped with a Littow prism a restricted range of lines can be tuned. Ion lasers with output power of Watts are very expensive. They need a three phase power supply and water cooling. Modern air cooled low and medium power ion lasers are less

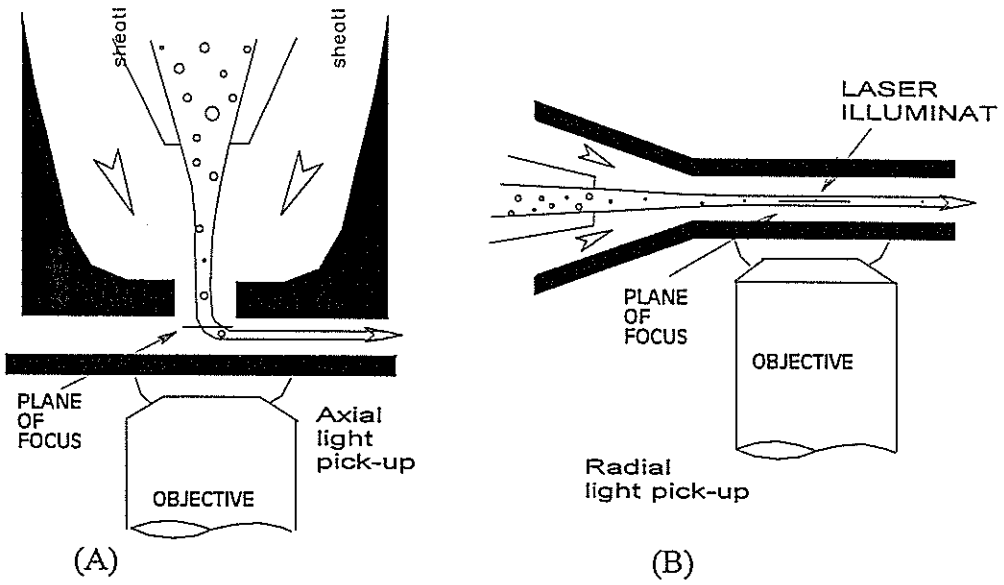

Fig.2: Two fundamental principles of illumination and light pick up. (A) The particle stream is illuminated along its axis and the illuminating objective is also the receiver of the fluorescence light (epi- illumination principle). The particles must pass through the plane of focus. (B) The particle stream is radially illuminated. The plane of focus of the objective taking up the fluorescence light is along the axis of the particle stream, making the system sensitive to local fluctuations of the beam. Concentrating the particle stream by hydrodynamic forces of a sheath flow is called Hydrodynamic Focusing.

expensive and work with domestic power. Lasers have long lifetimes between 2000 h and 10000 h.

Arc lamps provide excitation light in the whole visible range up to UV, with strong lines at distinct wavelengths and a broad band continuum. Efficient illumination optics are more complicated. Excitation wavelength ranges have to be selected using optical filters. Arc lamp systems are relatively small sized and cheap and work with domestic power supply. The lifetime of a lamp is only between 50 and 150 h and each new lamp has to be individually adjusted.

CELL VOLUME ANALYSIS

Optical small angle forward light scatter signals can be used to provide a relative measure of cell size. Unfortunately scatter signals are strongly influenced by cell shape, surface and internal structures, making their interpretation difficult [5,6]. Using the electrical resistance pulse sizing method (Coulter principle[7]) it is possible to more accurately measure cell volume.

Fig.3 shows the principle of a Coulter cell volume analyser. Non conducting particles suspended in an electrically conducting fluid are transported through a narrow orifice, across which a constant electric current flows, producing a strong electric field. The particle generates a resistance change which is transformed into an electrical voltage pulse. Its amplitude is used as a measure to calculate the particle volume. For a homogeneous field an analytical function can be derived for the dependence of the pulse height on the particle volume [7]:

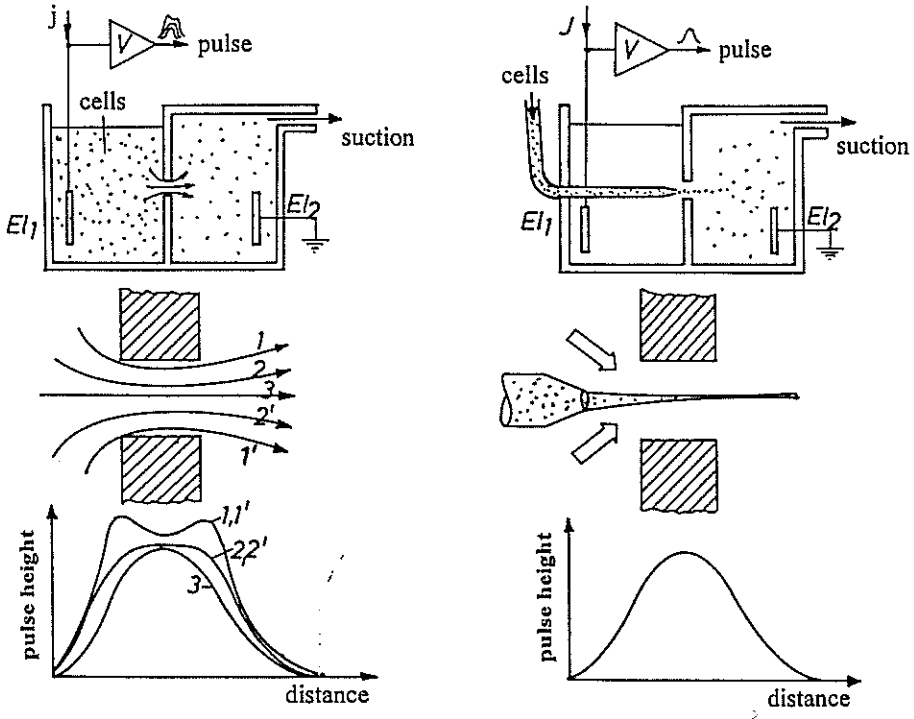

(A) (B)

Fig.3: The principle of electrical sizing. (A) The basic Coulter principle. The particles are passing on arbitrary paths through the orifice producing resistance change pulses of different shape and amplitude. Such differences are caused by the inhomogeneities of the electric field. The pulses are generated by Ohms law between the electrodes El1 and El2.

(B) Coulter system improved by hydrodynamic focusing. The particles injected through the outlet of a tube are concentrated by hydrodynamic focusing on a path along the axis of the orifice. All particles are evaluated on the same path producing uniformly shaped pulses.

$$\Delta V = \frac{\Delta U \cdot q^2 \cdot f_k}{\rho_1 \cdot i \cdot f_p}$$

ρ_1 = resistivity of medium
ρ_2 = resistivity of particles
ΔV = particle volume
ΔU = pulse height
i = orifice current
q = orifice cross section
f_p = shape+conductivity factor
f_k = orifice factor

For a homogeneous electric field: $f_k = 1$

Shape and conductivity factors:

for conducting spheres: $f_p = \frac{3(1-\rho_2/\rho_1)}{\rho_2/\rho_1 + 2}$

for non conducting spheres: $f_p = 3/2$

for prolate ellipsoids of revolution: $f_p = \frac{2(1-\rho_2/\rho_1)}{2 + ab^2 \cdot La(\rho_2/\rho_1 - 1)}$

In practice, calibration is performed by measuring reference particles of known features.

HYDRODYNAMIC FOCUSING

As the term flow cytometry implies, measurements are made on particles in a flowing medium. To obtain precise measurements it is essential that the particles in a sample are accurately aligned with respect to the sensors.

This is particularly important in the case of determining the volume of cells by the Coulter principle. The determination of volume and size is derived from the electrical pulse height as a particle passes through the orifice of the sensing zone [7]. As the electric field in the cylindrical orifices normally used is not fully homogeneous, measurements are only accurate if all particles are evaluated in the same electrical field. This can be achieved by restricting the particles to the axis of the sensing orifice by hydrodynamic focusing [8]. The particle stream is surrounded by a stream of sheath fluid aligning the particles to a thin thread in the sensor area (see Fig.3). Hydrodynamic focusing also improves the precision of fluorescence measurements as particles can be restricted to a limited field where the excitation light is homogeneously distributed.

Another advantage of hydrodynamic focusing is that non spherical particles pass the sensing zone oriented lengthwise. This reduces influences of particle shape so that identical shape factors can be applied for volume calculations.

INSTRUMENT SETUP

Fig.4 is a schematic diagram of an instrumental setup for three parameter measurements. It is different from a typical laser based system in so far as the fluorescence excitation is based on an arc lamp and electrical volumetry and fluorescence analysis are combined. For the concentration measurements a fixed volume of sample is analysed. This is achieved by injecting sample into the sensing zone in a syringe, attached to a computer controlled stepping motor which regulates the sample flow.

A vacuum pump moves the suspension through the transducer system. Analog electronics provide the current for the Coulter system, the high voltages for the photomultipliers and the lin/log amplification of the pulses. Analog pulse outputs are connected to a peak- detector and trigger interface which prepares the pulses for analog to digital conversion in the PC and for storing and graphical display of the resulting histograms [9].

Each of the parameters is able to work as the leading trigger responsible for initiating the uptake of signals from a particle or organism. If the leading trigger has no pulse, a self-clearing device is present which clears the peak detector, even if the cell or organism was not registered.

The data are either directly classified into histograms which provide a graphical representation of the data and their correlation or they are stored in list mode i.e. in the form of an unclassified list of data. Each cell in the list mode data is represented by an abstract group of data which normally has to be resolved into histograms for evaluation and recognition of its content.

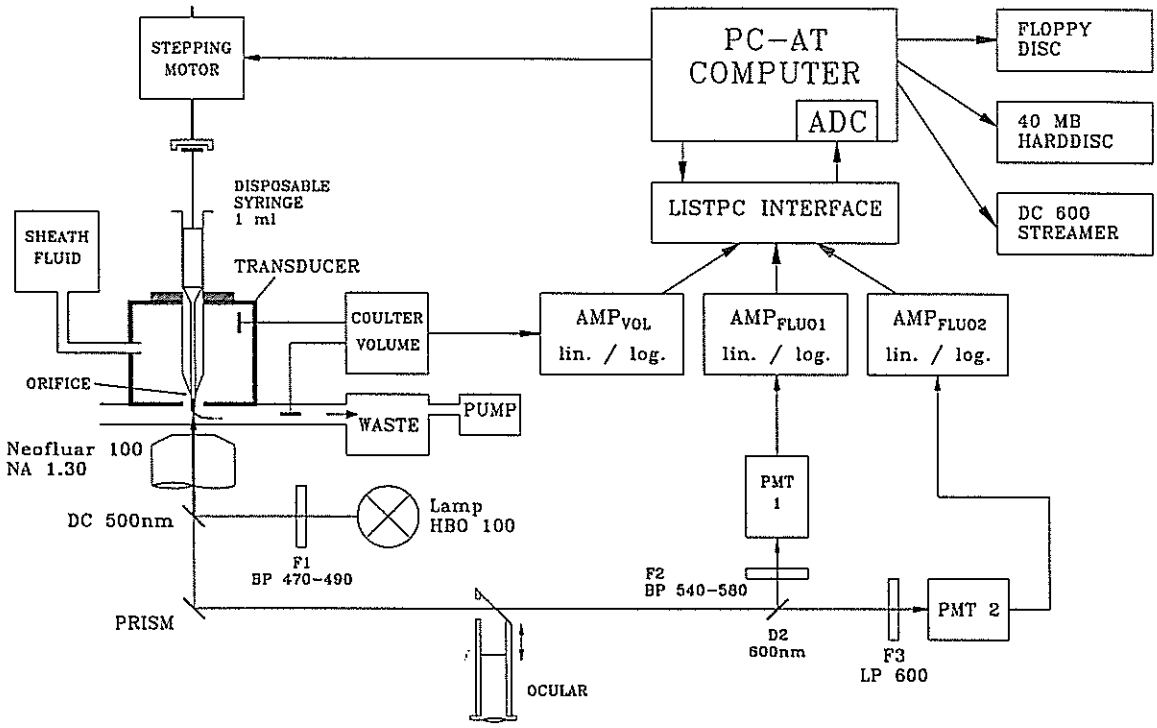

Fig.4: Instrumental setup for three parameter flow cytometric measurements (Fluvo system). The system combines particle counting, electrical volumetry and arc lamp based fluorescence analysis.

Data sets with more than 3 parameters have to be evaluated by gating procedures or by more abstract and complex methods like cluster analysis.

NEW DEVELOPMENTS

The methods and instruments described so far are only able to analyse organisms below a size of 100µm. Recently, however, a new instrument called the MACRO FLOW PLANKTOMETER(MFP) was developed within the EUROMAR project MAROPT which is capable of analysing plankton organisms in the millimetre size range, including fish larvae 5mm wide and 20mm - 30mm in length [10]. The measuring principles applied in this instrument are the same as described above. A major development has been the incorporation of an imaging in flow device, which is able to take video images of organisms directly from the flow stream. The imaging process is triggered by criteria based on the results of previous analysis performed in the same transducer [11].

Fig.5 shows the principle of the MFP. A pump feeds the recirculating flow from the supply vessel at the bottom. The first sheath flow supplied from vessel 6 concentrates the organisms which enter the sensor from the syringe vessel 3 into the axial path of the sensor orifice. The volume of the organisms is measured inside orifice 1 by the resistance pulse principle (Coulter).

In order to perform fluorescence measurements the organisms are illuminated by an Argon ion laser beam inside the orifice. Fluorescent substances like photosynthetic pigments emit fluorescence light as they pass through the excitation beam. The fluorescence pulses are captured by fibre optics and conducted to a PMT detector. The pulses are amplified in an analog interface, digitized, stored and processed in a personal computer. Imaging of an organism in the flow stream is triggered if the results of its analysis matched user-defined trigger windows.

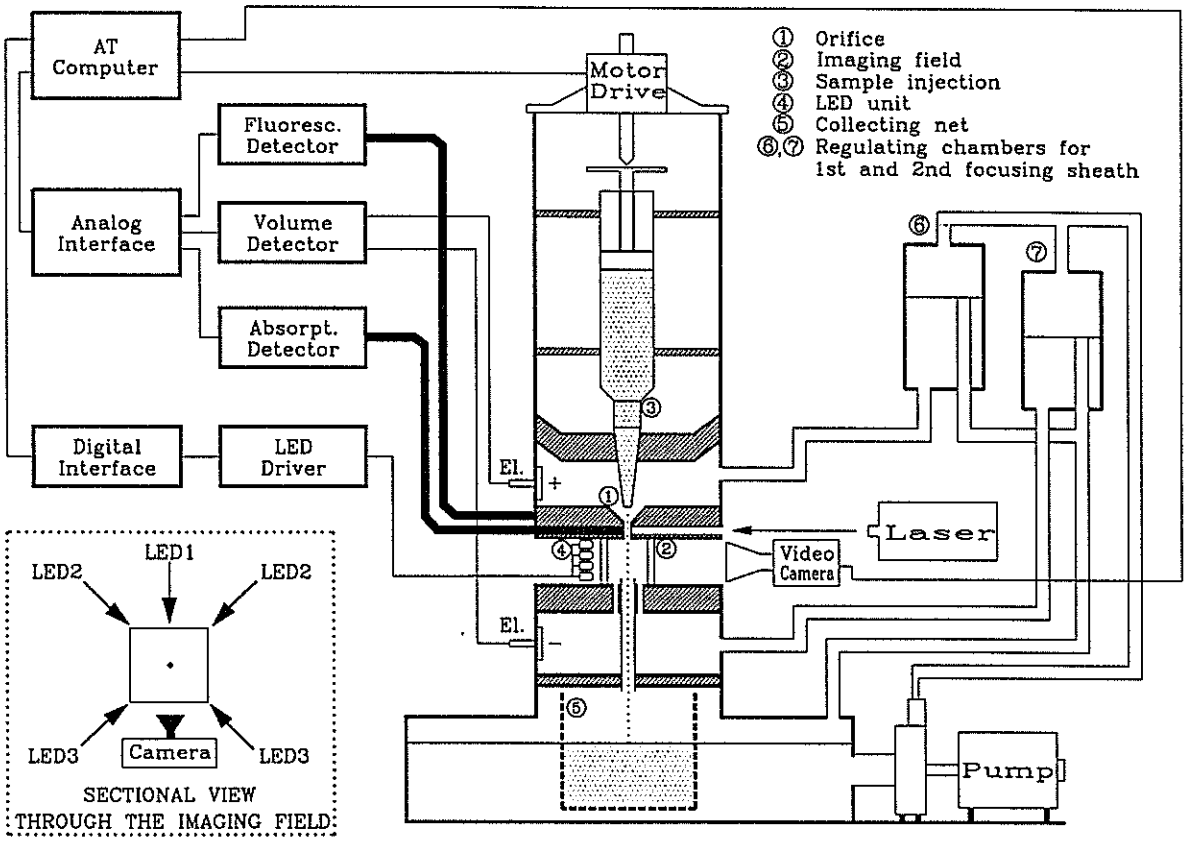

Fig. 5: The instrumental setup of the Macro Flow Planktometer for analysis of macro plankton and fish larvae. The flow system uses circulating sheath water. The analytical part can be equipped with optical and electrical sensors and can be combined with a triggered video imaging module.

The organisms move with a speed of about 1 m/s. To obtain a clear image, red high brightness light emitting diodes (LED) are pulsed for about 2 µs in order to flash the image onto the target of a CCD camera. From there the image can be directly shown on a monitor or be stored as an electronic data set on disk or tape [12].

Imaging in-flow improves the potential for analysing plankton accurately and rapidly. For example, Fig.6 shows a volume distribution curve of plankton fixed in formaldehyde from a lake near Munich measured in an orifice of 2mm diameter and a current 0.86 mA. The window ranges I and II were defined on the volume distribution curve for imaging. The images in the upper panel belong to range II, restricted to channels 82- 104 on the upper end of the volume distribution. The images show large *Daphnia* sp and *Bosmina* sp. If the image trigger is restricted to window range I the smaller organisms shown in the lower panel are imaged. The images contain a lot of morphological details which can be used to determine the species.

The MFP has also been used to investigate stages in the life cycle of the Brine Shrimp *Artemia* sp.(Fig.7). The sample was taken from *Artemia* eggs that had been allowed to hatch and grow over three days. The flow analysis represented by the histogram shows 4 main regions of interest. From the analysis alone clusters and their quantities can be determined but by using imaging in-flow the species within the clusters can actually be visualised as shown in Fig. 7. The images are digitally stored and printed by a video printer.

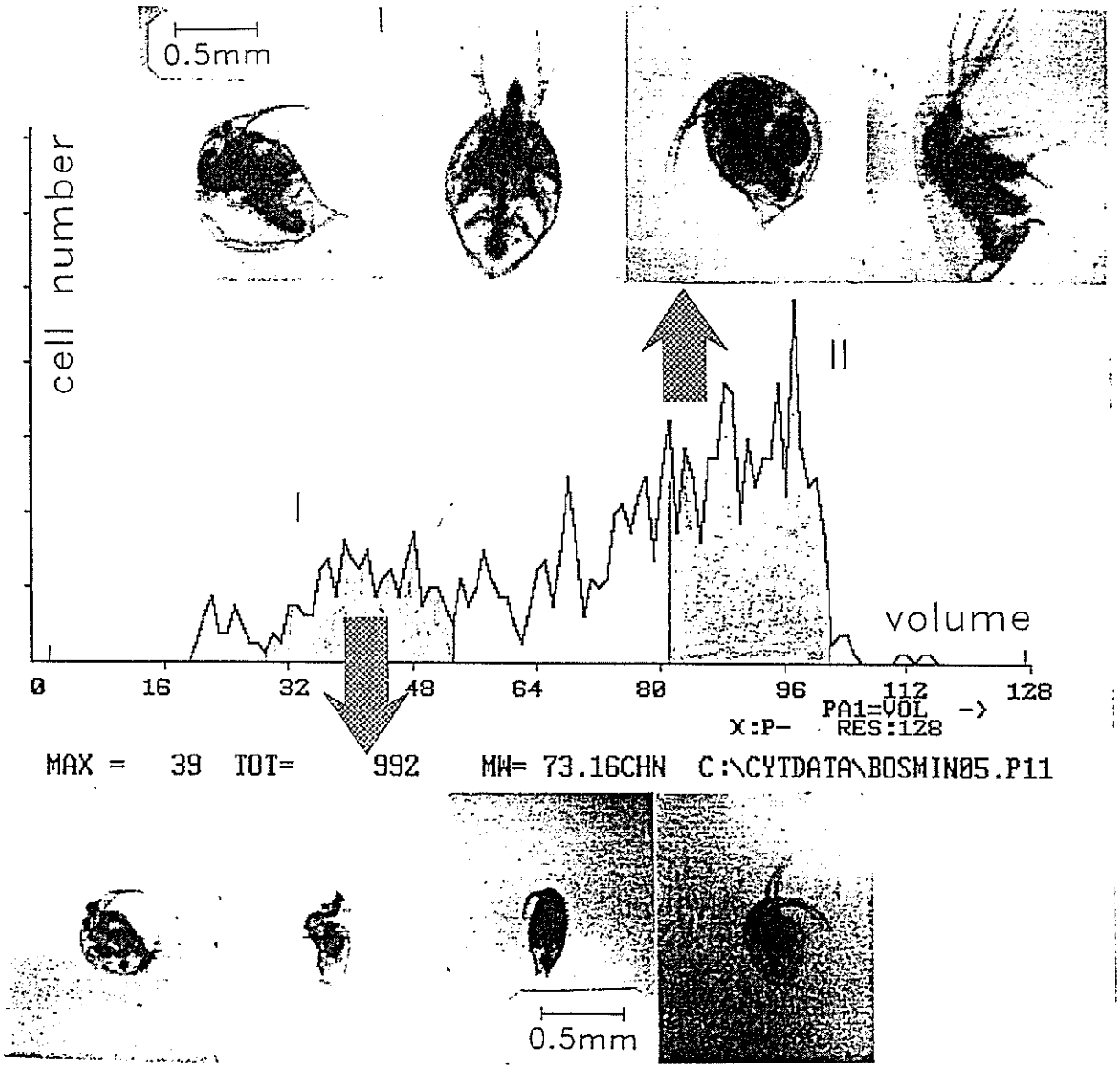

Fig. 6: Volume distribution curve of a sample of fresh water plankton measured with the MFP (log. scale). The upper panel shows images of organisms selectively triggered from the marked volume range at the high volume end of the volume distribution curve. Mainly large Daphnia sp and Bosminasp are found. The lower panel shows images of smaller individuals of the same species triggered from the low volume part of the distribution curve.

The main peak of window 1 contains eggs. The objects of window 2, characterised by large volume and reduced fluorescence are well developed *Artemia*. The images taken from window 3 with volume signals higher then those of the eggs and compared with window 2 more reduced fluorescence show denatured and mostly dead *Artemia*. In window 4 are images of parts of broken and dead *Artemia* or eggs cases.
The examples demonstrate the advantages of the new instrument compared with the use of microscopy, previously the only method for the inspection and analysis of samples. Counting, sizing, fluorescence analysis and imaging of large samples is done in a short time with automated documentation in the computer.

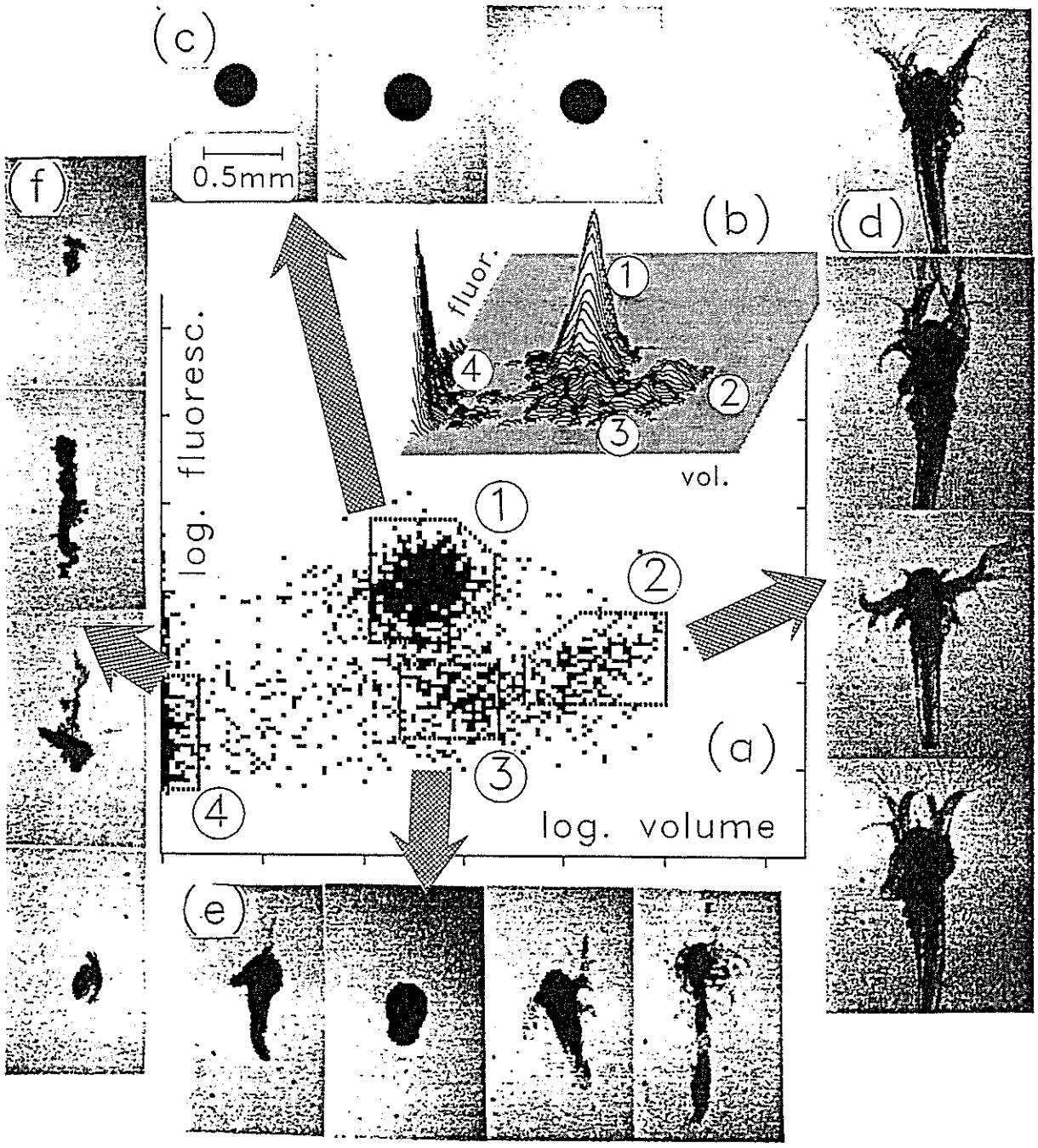

Fig.7 : Analysis of stages in the life cycle of the brine shrimp, Artemia. The two dimensional scatter plot, a., was used to define trigger criteria (1-4) for the taking of video images in c-f. Window 1 and c: Artemia eggs; window 2 and d: well developed Artemia; window 3 and d: denatured and dead Artemia; window 4 and f: cases of eggs and broken Artemia. insert b: Three dimensional representation of the two parameter scatter plot.

CONCLUSIONS

Flow cytometers are invaluable for plankton analysis. Development of new instruments such as the MFP, with its imaging in-flow system illustrate how the technology is improving our ability to discriminate the different species present in seawater. However, a great deal more work is required to provide technology for the specific needs of marine science e.g. systems have to be made more light-weight for better transportation and

shipboard use. A project in that sense is the international MAST project EUROPA dedicated to the development of a modular plankton analyser with acquisition, sorting, imaging and highly developed data analysis capabilities.

ACKNOWLEDGEMENT
Funding of Euromar MAROPT Förderkennzeichen 03F0054A is gratefully acknowledged.

REFERENCES

1 Burkill P.H.: Analytical flow cytometry and its application to marine microbial ecology. in: Microbes in the sea. ed: Ellis Horwood Ltd, Chichester, England, pp. 139-166, 1987
2 Tarran G.A., Burkill P.H., Kachel V.: Ocean monitoring: the application of flow cytometry for analysing single aquatic particles. (this book).
3 Steen H.: Flow cytometric instrumentation. in: Particle Analysis in Oceanography, ed. S.Demers, Springer, Berlin Heidelberg, pp.3-30, 1991
4 Olson R.J., Zettler E.R., Chisholm S.W., Dusenberry J.A.: Advances in oceanography through flow Cytometry. in: Particle Analysis in Oceanography, ed. S.Demers, Springer Berlin, Heidelberg, pp.351-402, 1991
5 Cunningham A., Buonaccorsi G.A.: Narrow-angle forward light scattering from individual algal cells: implications for size and shape discrimination in flow cytometry. Journal of Phytoplankton, in press
6 Salzman G.C., Brito Singham S., Johnston R.G., Bohren C.F.: Light scattering properties of cells. in: Particle Analysis in Oceanography, ed. S.Demers, Springer, Berlin Heidelberg, pp.189-212, 1991
7 Kachel V.: Electrical resistance pulse sizing:Coulter sizing. Flow Cytometry and Sorting, ed. M.R. Melamed, T. Lindmo, L. Mendelsohn; 2nd ed. Wiley- Liss, New York, pp 45-80, 1990
8 Kachel V., Fellner-Feldegg H., Menke E.: Hydrodynamic properties of flow cytometric instruments. Flow Cytometry and Sorting, ed. M.R. Melamed, T. Lindmo, L. Mendelsohn; 2nd ed., Wiley- Liss, New York, pp 27-44, 1990
9 Kachel V., Messerschmidt R., Hummel P.: Eight-parameter PC-AT based flow cytometric data system. Cytometry 11:805-812, 1990
10 Hüller R., Schmidlechner S., Glossner E., Schaub S., Kachel V.: A Macro Flow Planktometer for analysis of large marine plankton organisms. Cytometry Suppl.5:55,1991
11 Kachel V., Benker G., Weiss W., Gloßner E., Valet G., Ahrens O.: Problems of fast imaging in flow. CYTOMETRY IV, Universitetsforlaget Bergen, pp 49-55, 1980
12 Hüller R., Päffgen W., Gloßner E., Hummel P., Kachel V.: A PC AT based video Device for flow cytometrically triggered cell imaging in flow. Computerized Medical Imaging and Graphics 15:85-91,1991

Proceedings of the Conference:
Optics Within Life Sciences II
Münster, 4.-9.Oct. 1992, in press

Ocean monitoring: the application of flow cytometry for analysing single aquatic particles.

G. A. Tarran[a], P. H. Burkill[a] and V. Kachel[b]

[a]Plymouth Marine Laboratory, Prospect Place, West Hoe, Plymouth, PL1 3DH, United Kingdom

[b]Max Planck Institute fur Biochemie, D-8033 Martinsried, Germany

INTRODUCTION

The seas and oceans cover over 70% of the Earth's surface [1] and average over 4km in depth. They are our greatest natural asset, being very important as regulators of our planet's climate through cloud formation, as a sink for atmospheric gases such as carbon dioxide (the major greenhouse gas) and as a major heat sink [2]. Seawater also provides a medium for living organisms whose sizes span many orders of magnitude (Fig. 1). Over the last 20 years it has been realised that the tiny (1-200µm) microscopic organisms known as the plankton are very important to the health of the seas and oceans [3, 4]. They form the starting point of the food chain which is of fundamental importance to humans as consumers at the top end of the food chain (Fig. 1).

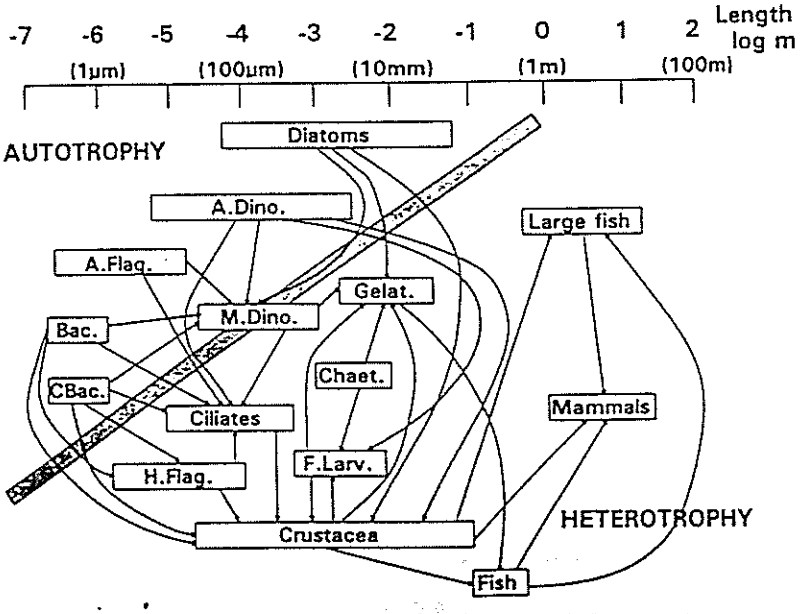

Figure 1. Trophic interactions within the pelagic food web. A.Dino., autotrophic dinoflagellates; A.Flag., autotrophic flagellates; Bac., bacteria; CBac., cyano-bacteria; Chaet., chaetognaths; F.Larv., fish larvae; Gelat., gelatenous zooplankton; H.Flag., heterotrophic flagellates; M.Dino., mixotrophic dinoflagellates.

Phytoplankton are also major contributors to the cycling of carbon. This is achieved through their photosynthetic activity, a biogenically mediated process that transforms carbon dioxide dissolved in seawater into complex organic molecules. These processes are carried out by the phytoplankton, the single-celled plants living in seawater, which, although microscopic in size are responsible for activity on a scale comparable to that found in the terrestrial environment. In addition to the utilisation of carbon dioxide some phytoplankton produce globally significant amounts of dimethyl sulphide, a gas responsible for the formation of acid rain.

In comparison with the plants in the terrestrial environment our knowledge of the phytoplankton is scarce. Details of community structure, distributions and concentrations of phytoplankton are poor. Such work in the past has only been possible using laborious microscopic techniques for identifying and counting plankton samples [5, 6].

Within the last decade flow cytometry, a technology designed originally for biomedical research and the diagnosis of human disease, has begun to be used successfully in marine research [7, 8]

TECHNOLOGY

Flow cytometry, is, at its simplest a method for measuring cell and particle characteristics present in a sample stream. In the context of analysing aquatic particles, optical measurements of light scatter and fluorescence are recorded simultaneously for each particle as it passes the focus of a high intensity light source such as a laser. Figure 2 shows the general principle of an optically based flow cytometer for the analysis of plankton. Initially, a hydrodynamically focused sample

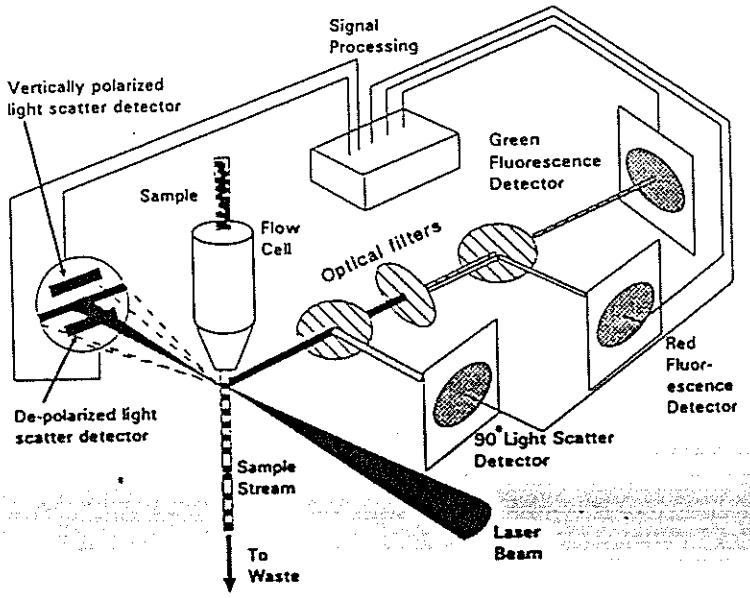

Figure 2. A schematic diagram of single cell analysis by flow cytometry

stream passes through the focus of the light source such as a laser. As the particles in the stream pass the beam they scatter light in all directions and may also fluoresce, if they contain autofluorescent pigments or artificial fluorescent molecules. Scattered light and fluorescence is picked up simultaneously by light collection systems; spectrally filtered using filters and mirrors and then detected by photomultiplier tubes where the quantity of light is converted to an electrical signal. This signal is then amplified, digitized and stored on computer or disk for later analysis. In addition to using optical sensors there are flow cytometers that can also make measurements of particle volume and diameter using electrical methods. The technology of flow cytometry, using both optical and electrical methods is further explained by Kachel *et al* [9] elsewhere in this book.

PLANKTON ANALYSIS

The history of flow cytometry in marine science goes back about 10 years when a group of marine scientists realised that this biomedical technique could be applied to marine science. In particular, they realised that the autofluorescence of chlorophyll, the pigment present in all plant cells could be measured by flow cytometry. They gathered at the Bermuda Biological Station for Research to assess the capabilities of flow cytometry for the analysis of phytoplankton [10]. For the first time marine scientists analysed natural seawater samples by flow cytometry. They obtained results similar to those in Figure 3 in which two dimensional maps or scatter plots are shown. On the left of Figure 3, red fluorescence, attributed to chlorophyll is on the X axis and forward light scatter, attributed to size is on the Y axis. Two populations are

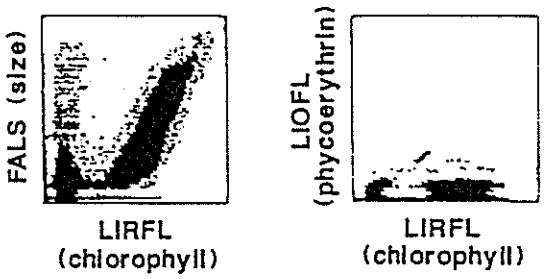

Figure 3. Two parameter scatter plots of a natural plankton sample from the North Atlantic Ocean. Left- Log red fluorescence (LIRFL) derived from chlorophyll vs. Forward angle light scatter (FALS), a measure of size. Right- LIRFL derived from chlorophyll vs. Log orange fluorescence (LIOFL) derived from phycoerythrin.

visible. To the left are non-fluorescing particles with a wide range of size which is made up of detritus and cells lacking chlorophyll. To the right is a red fluorescent population made up of phytoplankton. As flow cytometry collects

multiple parameters it is possible to visualise different combinations of dual parameters in two dimensions. In Figure 3b the X axis is again red fluorescence but this time orange/green fluorescence is on the Y axis which is due to another autofluorescent algal pigment, phycoerythrin. Phycoerythrin is only possessed in any significant quantities by certain groups of phytoplankton such as cyanobacteria and cryptomonads. In this case it is possible to identify three groups of phytoplankton, two which contain both phycoerythrin and chlorophyll and one which only contains chlorophyll.

These primary investigations provided a catalyst for a whole new area of development for marine science and the analysis of particles in the marine environment.

The role of phytoplankton in the cycling of carbon is now well established [11]. In the late 1980's and early 1990's a United Kingdom funded project known as the Biogeochemical Ocean Flux Study undertook a number of cruises into the North Atlantic Ocean to better understand the physical and biological processes involved in the cycling and fate of carbon. Flow cytometry was used to investigate various aspects of phytoplankton dynamics, including the fate of phytoplankton due to grazing by protozoa, single-celled grazing organisms and the temporal and spatial variations in the distribution and abundance of phytoplankton [12, 13].

Phytoplankton community composition varies in a spatial sense. This is clearly illustrated in Figure 4 which represents particle distributions at two latitudes in the North Atlantic, taken three days apart in early summer along

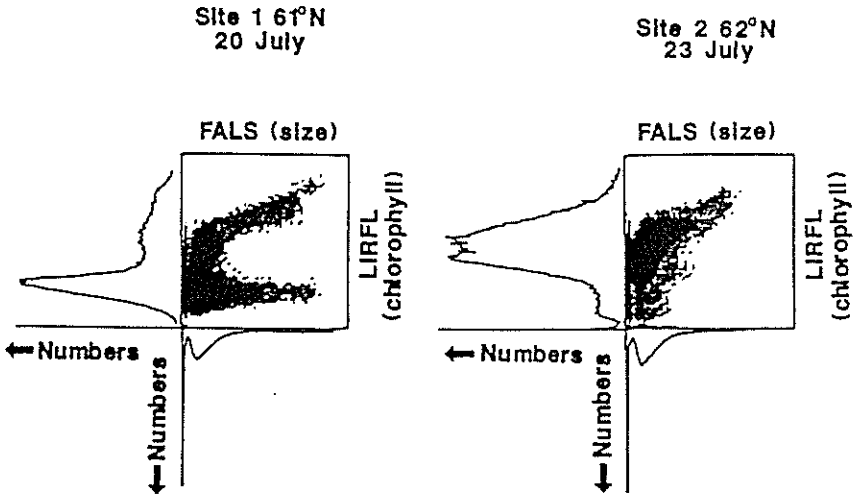

Figure 4. Distributions of phytoplankton and other particles along the 20° W meridian at 61° N and 62° 19' N in July 1991. Two dimensional scatter plots of log red fluorescence (LIRFL) derived from chlorophyll and log forward angle light scatter (FALS) with single parameter projections of LIRFL and FALS. Redrawn from G. A. Tarran and P. H. Burkill (in press) [2]

the 20°W meridian. The site at 61°N is characterised by a wide size range of particles and multiple phytoplankton populations. In addition, there is a lot of non-fluorescent material which is largely composed of detritus. This represents a community after the spring bloom. At 62°N the spring bloom had not yet started and the community is characterised by a population smaller in size and fluorescence characteristics and without any detritus.

Plankton distributions also vary greatly with depth over only a few tens of metres as shown in Figure 5. On the X axis is red fluorescence derived from chlorophyll and on the Y axis is orange/green fluorescence derived from phycoerythrin. It is interesting to note that there is a sub-surface chlorophyll maximum between 40-60m. Further analysis of the same cytometric data (Fig 6) provides information on the abundance of total phytoplankton as well as the sub-populations in which phycoerythrin is present or absent.

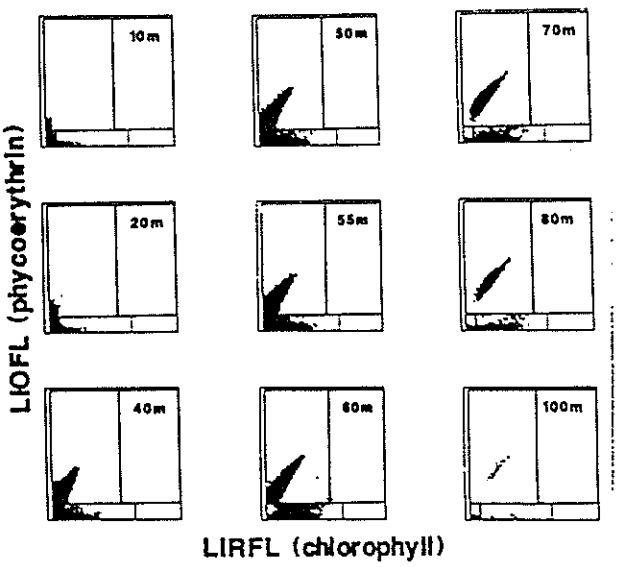

Figure 5. Dual fluorescence scatter plots of seawater samples from 33° N 22° W, showing how chlorophyll and phycoerythrin-containing cells vary with depth.

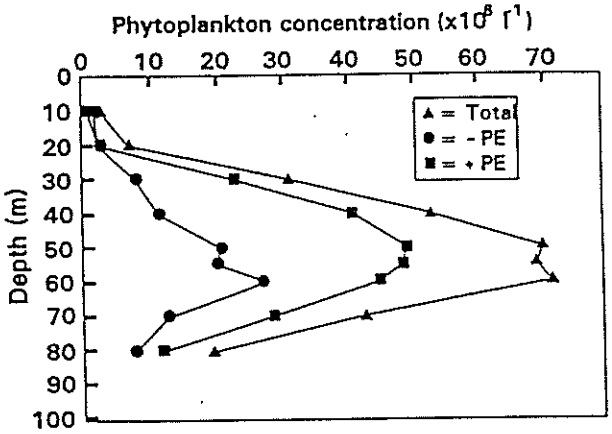

Figure 6. Vertical distribution of total phytoplankton and phytoplankton with and without pycoerythrin from 33° N 22° W. PE-, phytoplankton containing only chlorophyll; PE+, phytoplankton containing both phycoerythrin and chlorophyll.

COCCOLITHOPHORES

The phytoplankton consists of a wide range of species from many different groups. Using flow cytometry it has been possible to discriminate some of the different groups for specific studies. One important group of phytoplankton is called the coccolithophores. This single group of microscopic phytoplankton is particularly important in the cycling of carbon. Like other phytoplankton, they take up carbon dioxide dissolved in seawater for photosynthesis. They also form calcite plates which cover their bodies through the process of calcification. The relative importance of these two processes in the net flux of carbon is not fully understood (Fernandez, pers. comm) as calcification is intermittant and results in a net increase in pCO_2 in the water. However, the plates or coccoliths are very important in terms of the export of particulate carbon from the upper ocean to deep ocean sediments.

Coccolithophores regularly bloom during the spring in temperate regions. Satellite images of surface reflectance have revealed that coccolithophore blooms can cover areas in excess of 10,000 square kilometres [13], often consisting of a single dominant species of coccolithophore called *Emiliania huxleyi* (Fig. 7). At present, satellites cannot provide us with information about

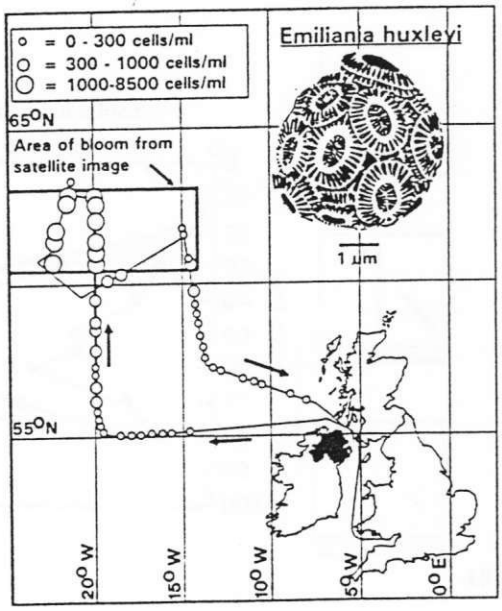

Figure 7. Surface abundance of the coccolithophore *Emiliania huxleyi during* cruise 60/91 of the RRS Charles Darwin in June 1991

the abundance of organisms present so research still needs to be carried out at surface level to provide sea-truth data.

Flow cytometry has recently been used to uniquely discriminate coccolithophores from other phytoplankton because the coccoliths depolarize

light, giving a relatively high horizontally polarized light signal when exposed to a vertically polarized light source. Using this property, in conjunction with fluorescence measurements it has been possible to carry out studies on their abundance in and out of blooms (Figure 7) and also on their fate, in terms of grazing by microzooplankton for the first time.

OTHER GROUPS

In addition to coccolithophores, other smaller groups of phytoplankton are being investigated using flow cytometry, effectively extending the analysis range of flow cytometers to below 1µm. For example, in 1988 it was reported that a new group of sub-micron sized prokaryotic phytoplankton, containing a chlorophyll *a* analog, di-vinyl chlorophyll had been discovered using flow cytometry [14]. This group who's size was between 0.4-0.8µm was called the prochlorophytes. They had been overlooked using traditional microscopic methods because their cell pigments were rapidly bleached by epifluorescence light sources. Using flow cytometry, however, exposure to light was reduced to a few microseconds and so the fluorescence signals could be successfully recorded. Prochlorophytes have been found in many areas of the world at high concentrations [14, 15], ranging from 5,000-100,000 cells ml^{-1}. They are now considered important in terms of their contribution to primary production, especially in the lower euphotic zone where the highest concentrations have been found.

Other prokaryotic groups that have been studied are the bacteria and cyanobacteria. Within the last 10-15 years they have been found to be important in recycling both dissolved and particulate organic carbon which is produced by the other plankton. The bacteria. are then consumed by other plankton creating a cycle termed the microbial loop [4, 7]

The smallest particles that have been resolved by flow cytometry are viruses, one tenth of a micron in size [16]. Viruses are a new group in terms of marine research, only having been studied in any detail during the last couple of years.

Recently, some flow cytometers have been developed outside the biomedical industry and are capable of analysing much larger organisms than phytoplankton. Kachel [9] constructed a flow cytometer capable of counting and sizing the brine shrimp *Artemia* sp. at differnt stages of its life cycle from eggs to adult. Work has also been carried out on fish larvae which are a few millimetres in length. The technique, therefore has potential for studying larger organisms in the open ocean.

ECOLOGICAL STUDIES

The monitoring of the health of the oceans through the analysis of plankton by research ships is constrained by time and money. In order to better understand the interactions between phytoplankton and other organisms it is necessary to conduct laboratory studies to compliment work carried out at sea. Such studies include investigations on the ability of protozoa and other, multi-

cellular grazers to select particular phytoplankton species as food [17, 18, 19]. Figure 8 shows an example of an experiment in which the grazer, a marine dinoflagellate was offered a mixture containing equal numbers of inert beads and a phytoplankton organism of equal size. Using flow cytometry it was possible to visualise four populations simultaneously. The fluorescent phytoplankton, non-fluorescent beads, starved grazers and grazers that had eaten fluorescent phytoplankton. Over 6 hours the phytoplankton were completely grazed whereas the beads remained at the same concentration, indicating that the grazer was able to select in favour of the phytoplankton, even though it was the same size as the beads. These experiments demonstrate that herbivorous zooplankton can be selective in what they eat and that there are factors other than size of food that determine selection of food. Such studies are important in our understanding of how food chains work and the manner in which the different groups interact, both in terms of their role as food for higher animals and as pathways for the flux of carbon on a global scale.

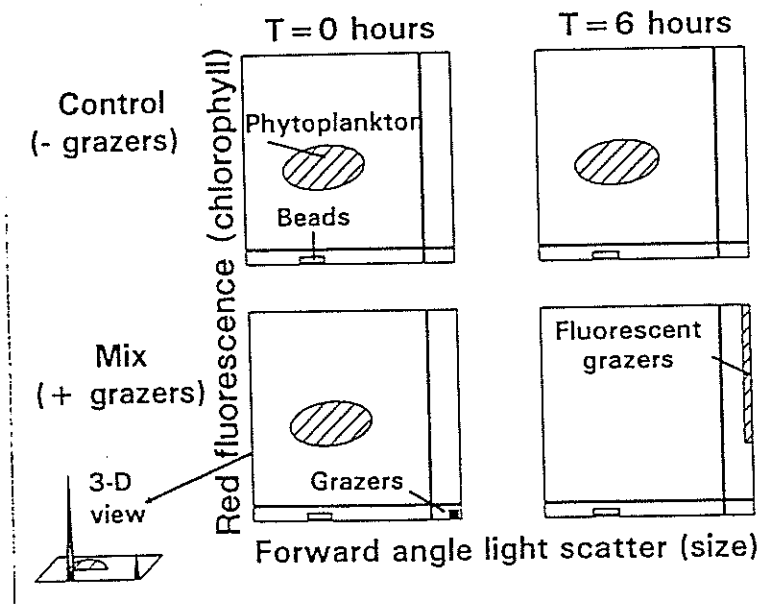

Figure 8. Prey selection in protozoa. In the absence of the protozoan grazer, phytoplankton and beads do not change over six hours (control). When protozoan grazers are added to a mixture of phytoplankton and beads over a six hour time course the phytoplankton are completely grazed whereas the beads remain at their original concentration.

THE FUTURE

Molecular techniques are becoming well established as tools for taxonomy and systematics. These techniques use comparisons of nucleic acid or amino acid sequences. One component that has been found to be very useful is ribosomal RNA. It is possible to find sequences of ribosomal RNA that are unique to particular taxa and species of organisms. The development of

fluorescently labelled probes that bind to specific sequences of ribosomal RNA are providing opportunities for the identification of particular phytoplankton by flow cytometry. There is a great deal of potential for these techniques in ecological studies, to help with the further discrimination of plankton and the routine analysis of seawater samples as well as studying the temporal and spatial variability of particular organisms such as nuisance algae that are responsible for the formation of toxic red tides.

A lot of work is still required on fundamental research. This includes further studies on the distributions and abundance of phytoplankton, as well as other aquatic particles such as detritus, bacteria, cyanobacteria, prochlorophytes and viruses.

There are also non-biological applications which have potential for analysis by flow cytometry. Preliminary work has been carried out to trace the passage of fluorescent particles that mimic sediment as they travel along rivers [20]. These studies have been carried out to better understand the role of sediment in the transport of pollutants such as heavy metals adsorbed onto the surfaces of sediment particles. There is also potential for expanding this sort of study to the marine environment as rivers discharge their waters into the sea.

Flow cytometry produces large multi-parametric data sets that require complex data analysis techniques to get the most from the data. Until now the data analysis capability of flow cytometers has been extremely limited. Multivariate statistical approaches and neural networks are now being developed to provide greater analytical power to help further identify phytoplankton and other aquatic particles.

As has happened many times in the past marine scientists have made use of existing technology used in biomedicine and industry. Projects are now underway to improve on the biomedically based technology. One project is the European Optical Plankton Analyser (EUROPA), a European Community funded project which is developing a new flow cytometer for the more specific needs of phytoplankton research.

In conclusion, flow cytometry is an exciting and powerful tool for the analysis of single aquatic particles. Many applications towards monitoring the health of the oceans and its inhabitants are already being used and further applications are being developed for the future.

ACKNOWLEDGEMENTS

The research was funded by the Natural Environment Research Council Biogeochemical Ocean Flux Study (BOFS) and the European Community MAST II project EUROPA.

REFERENCES

1 Burkill PH, Mantoura RFC. Phil Trans R Soc Lond A. 1990; 333: 99-112.
2 Tarran GA, Burkill PH. In: Lloyd DA, ed. Flow Cytometry in Microbiology. Springer-Verlag London (in press).
3 Pomeroy LR. Bioscience 1974; 24: 499-504.

4 Azam F, Fenchel T, Field JG, Gray JS, et al. Mar Ecol Prog Ser 1983; 10: 257-263.
5 Colebrook JM. Bull Mar Ecol 1960; 5: 51-62.
6 Colebrook JM. In: Nichols D ed. Monitoring the Marine Environment. Institute of Biology. London. 1979.
7 Olson RJ, Chisholm SW, Zettler ER, Armbrust EV. Deep Sea Res 1988; 35: 425-440.
8 Platt T. Cytometry 1989; 10: 500.
9 Kachel V, Hüller R, Gloßner E, Burkill PH, Tarran GA. (this book).
10 Yentsch CM, Horan PK, Muirhead K, Dortch Q, et al. Limnol Oceanogr 1983; 28: 1275-1280
11 Fenchel T. Ann Rev Ecol Syst 1988; 19: 19-38.
12 Tarran GA. In: Harris RP. Cruise report for RRS Charles Darwin cruise 61/91. Plymouth Marine Laboratory UK.
13 Holligan P. 1991. Cruise report for RRS Charles Darwin cruise 60/91. Plymouth Marine Laboratory UK.
14 Chisholm SW, Olson RJ, Zettler ER, Goericke R, et al. Nature 1988; 334: 340-343.
15 Frankel SL, Binder BJ, Chisholm SW. Limnol Oceanogr 1990; 35: 1156-1164.
16 Hercher M, Mueller W, Shapiro H. J Histochem Cytochem 1979; 27: 350-352.
17 Poulet SA, Marsot P. Science 1978; 200: 1403-1405.
18 Tarran GA. PhD Thesis. Southampton University UK.
19 Rassoulzadegan F, Fenaux L Strathmann RR Limnol Oceanogr 1984; 29: 357-361.
20 Marsh JK, Bale AJ, Uncles RJ Dyer KR. In: Proceedings of the Transport of Suspended Sediments and its Mathematical Modelling. International Association for Hydraulic Research. Florence (in press).

© 1990 Wiley-Liss, Inc.

Cytometry 11:805–812 (1990)

Eight-Parameter PC-AT Based Flow Cytometric Data System[1,2]

Volker Kachel,[3] Roger Messerschmidt, and Peter Hummel
Max-Planck-Institut für Biochemie, D-8033 Martinsried, Federal Republic of Germany

Recieved for publication December 18, 1989; accepted April 26, 1990

An 8-parameter flow cytometric data system is described using an IBM-AT compatible personal computer (PC) and a commercial analog to digital conversion (ADC) board. A dedicated pulse processing interface adapts the flow cytometric pulses to the ADC board and controls the number of parameters to be taken up and the trigger conditions. The trigger thresholds are automatically held at a level immediately above the noise level. For the timing of kinetic measurements a linear voltage ramp of adjustable rise time is available. A built-in precision voltage source can be used for an overall calibration. The data system is operated by software written in assembly language. Data may be collected and processed in 1–8-parameter listmode or 1–3-parameter histogram mode. Functions are available for graphical color displays, numerical integration, multiparameter gating, and printing.

Key terms: Multiparameter, personal computer, cytometry, hardware, software, pulse processing, data processing

Multiparameter flow cytometric data acquisition and processing requires data systems of considerable performance. Traditional systems are based on expensive minicomputers (1,5,6). Other specially designed systems are also expensive and difficult to reproduce (2–4). Modern IBM-AT compatible personal computers (PC) provide the required high performance for extremely low cost, and so it is desirable to make PCs applicable for flow cytometric (FCM) pulse height collection and processing. Add-in boards are on the market which can be used for data uptake, analog to digital conversion, or system control purposes.

For FCM pulse height analysis, commercial PC hardware cannot be directly used. A dedicated interface is required that holds the pulse amplitudes constant for the analog to digital conversion and controls triggering, priority selection, and interaction of the parameters. For operation of the system dedicated software is required.

THE COMMERCIAL PC SYSTEM COMPONENTS

The FCM data system described was built with a 12 Mhz clocked IBM-AT clone (Schmitt Computersysteme, Müchen, FRG) equipped with an 80286 CPU, a floppy disk, a 40 MB hard disk of 35 ms mean access time, an 80287 arithmetic coprocessor, an EGA color graphics board with color monitor, and the usual serial and parallel input/output interfaces. The operating system is MS-DOS. For data uptake either a DT 2821 F (Data Translation [DT], Marlboro, MA) or a PC30D (Meilhaus Electronik [MH], Puchheim, FRG) ADC add-in board can be used. Both can be programmed to scan up to 16 analog input voltages for 12 bit AD conversion. The throughput to the PC memory is 150,000(DT) or 200,000(MH) words/s. For higher speed requirements a DT 2821 G version is available with an acquisition time of 2.5 μs/channel and a throughput to memory of 250,000 words/s.

THE PULSE PROCESSING INTERFACE

The multiparameter pulse processing interface was specially tailored. It contains the trigger circuits, the peak detectors, a timer, and a precision voltage calibrator. A modular structure allows configurations for uptake of 2, 4, 6, or 8 parameters (Figs. 1,2). The main functions of the interface are controlled by software.

Peak Detector

A flow cytometer delivers pulses of a few microseconds' duration which load the peak detectors up to the

[1]This work was supported by the Deutsche Krebshilfe e.V.

[2]Presented in part at the XIIth and XIIIth meetings of the Society for Analytical Cytology in Cambridge, UK, 1987, and Breckenridge, USA, 1988.

[3]Address reprint requests to Dr. Ing. Volker Kachel, Max-Planck-Institut für Biochemie, D-8033 Martinsried, FRG

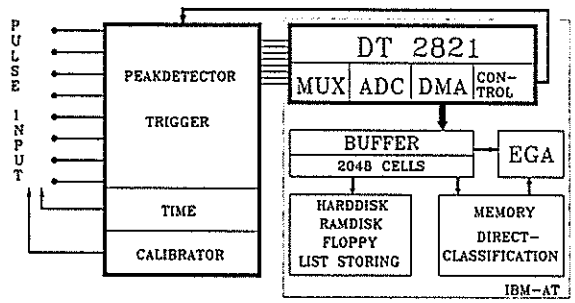

FIG. 1. Block diagram of the hardware of the PC data system. The incoming analog pulses are first handled by the peak detector/trigger interface. The pulse peak voltages are scanned by the multiplexer (MUX), converted (ADC), and transferred by DMA into the buffer memory. These functions and control of the interface are performed by the DT 2821 card. The buffer data blocks are either classified in the histogram memory or copied into listfiles on disk. Displays are shown on the EGA monitor.

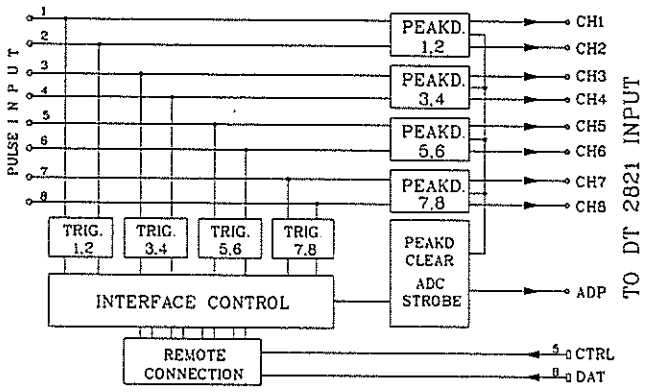

FIG. 2. The function blocks of the pulse interface. The trigger and peak detector modules for each two parameters are on separate plug in boards. The timer output can be connected to any of the pulse inputs. The remote control is operated by the digital I/O lines of the DT2821 board.

peak voltages which are held constant for the time the ADC needs for digitizing. In a multiplexed system, the AD converter is successively connected by an electronic switch to the input lines of the parameters to be measured. A peak hold time of the peak detectors of $7.7(n+1)$ μs (DT2821) or $5(n+1)$ μs (PC30D) is required. n is the number of cell parameters acquired. The peak voltage drop during the maximum hold time is below 0.1% of the maximum output voltage. After the end of the AD conversion the peak detectors have to be cleared for uptake of new pulses.

In multiparameter systems with prioritized trigger conditions, the peak detector clearance is essential. An incorrectly cleared peak detector holds its amplitude for longer time and disturbs the accurate processing of

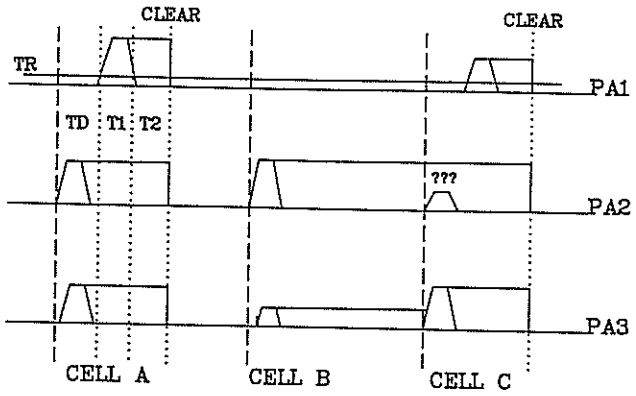

FIG. 3. Trigger problems in a system without auxiliary clear. PA1 is the trigger parameter. The parameters PA2 and PA3 do not trigger and are not able to initiate clearing of their peak detectors if no pulse of the triggering parameter was present. The small pulse of PA2 of cell C will be masked by the remaining high peak voltage of cell B resulting in a wrong pulse height evaluation. The peak voltage of PA3 of cell C exceeds the remaining peak voltage of cell B enabling a correct pulse height analysis.

subsequent pulses. Such distortion problems are explained in Figure 3. A wanted cell (A) of the triggering parameter passes through the transducer without problem. The trigger circuit reacts, initiates the AD conversion and finally clears the peak detectors. If, however, an unwanted cell (B) lacking a pulse of the triggering parameter PA1 occurs, no trigger reaction is initiated. The peak detectors of the parameters PA2 and PA3 are loaded but not cleared. That has consequences for the next ordinarily triggered cell (C) in that the small amplitude of the pulse of parameter PA2 is masked by the uncleared peak detector voltage of cell (B). The remaining pulse-peak of cell B is evaluated instead of that of the new cell (C). If the peak voltage of cell (C) exceeds the stored voltage of cell (B), the peak detector voltage is increased up to the new peak and, as shown with PA3, the amplitude of cell (C) is correctly measured. Such peak detector errors must be prevented by the trigger device.

Trigger Level and Priority

The trigger device of the interface has a simple basic structure. Assuming that the trigger signals of all parameters overlap these signals are logically ORed. The end of the OR signal indicating that the cell has left the sensing zone, starts the ADC conversion. The trigger device has a key function within a pulse processing system by accepting or rejecting pulses and discriminating between wanted cell pulses and noise. Usually, the trigger threshold is adjusted by the user. Each pulse going beyond that threshold starts an AD conversion. In principle, with multiparameter applications, as many trigger devices are present as parameters are measured. In most practical applications, only one leading parameter is selected for triggering or gating and only cells with a signal in that gating param-

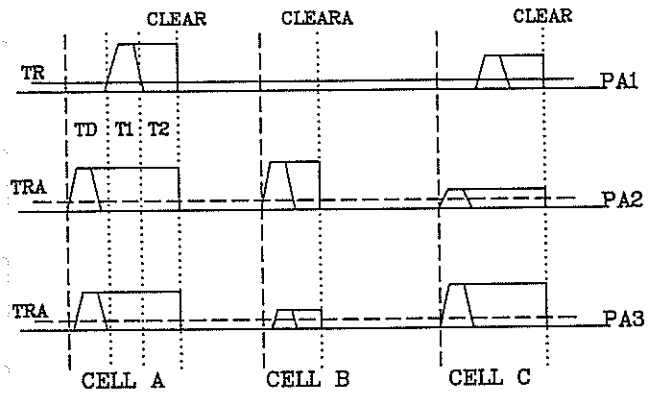

FIG. 4. Triggering with auxiliary clear. The parameters not used for triggering produce an auxiliary clear pulse (CLEARA) to clear the peak detectors if no pulse in the triggering parameter was present.

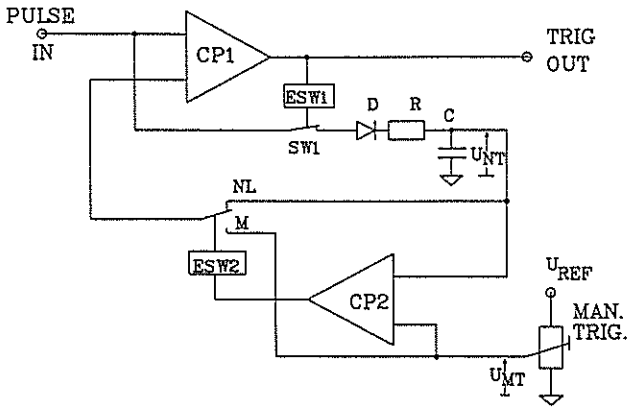

FIG. 5. The principle of generating an automatic trigger level from noise. The noise dependent trigger voltage U_{NT} is compared with the manual trigger level U_{MT}. If U_{MT} is below U_{NT}—i.e., the user has adjusted his manual trigger threshold in the noise—the comparator CP2 activates the electronic switch ESW2 that switches from the manual threshold U_{MT} to the "automatic threshold U_{NT}" derived from the peak noise. Otherwise the manual trigger level UMT is valid. the switch SW1 is opened as long as the trigger comparator CP1 detects a wanted cell pulse which should not contribute to the noise level evaluation.

eter are evaluated. The clearance problem of the non gating peak detectors occurs when the absent trigger does not clear the nonpriority peak detectors. In that case an additional self-clearance circuit of each nonpriorized parameter is necessary to abolish the peak detector voltages if no pulse of the leading parameter was present. Figure 4 explains the principle of the auxiliary clear function, which is initiated from the auxiliary trigger levels TRA of the nonleading parameters. The TRA triggers are disabled by the interface control from generating the ADC strobe pulse. The self-clearance procedure requires that the TRA trigger levels also be correctly adjusted above the noise level.

In order to facilitate the multiparameter trigger adjustment, an automatic trigger threshold adjustment device was developed, which prevents erroneous trigger conditions, particularly with noisy signals (Fig. 5). With the threshold in the noise the system may be blocked by overwhelming trigger signals. The automatic noise level trigger voltage U_{NT} is derived from the peak noise level of each parameter if there is no pulse present. The incoming noise is rectified by the diode D and smoothed by the RC circuit. The comparator CP2 compares the peak noise voltage level U_{NT} with the manual trigger voltage U_{MT}. If $U_{NT}>U_{MT}$ the Electronic Switch 2 (ESW2) is switched by CP2 to NL; i.e., the rectified noise peak voltage U_{NT} is taken as the basis for triggering even if the user has adjusted the manual trigger threshold in the noise. If a manual threshold U_{MT} above the noise peaks is adjusted, that threshold is taken for triggering. The comparator CP1 generates a trigger signal if the incoming pulse or noise exceeds the threshold voltage. During the trigger time, the output of the comparator CP1 identifies a pulse by going high and the Electronic Switch 1 (ESW1) opens SW1 in order to minimize the contribution of the wanted pulse amplitude onto the noise peak voltage level U_{NT}.

Timer and Voltage Reference

Flow cytometric applications cover also the measurement of cell changes lasting seconds and minutes. For that purpose a digitally generated linear voltage ramp can be connected to any of the interrogated input lines. It is released when the data uptake begins and each group of cell data obtains a time stamp in the form of a definite voltage value from the ramp. The time can be evaluated in the same way as the normal cell feature parameters (Figs. 8, 9).

The offset and gain stability of the interface and the ADC circuitry can be checked by means of built-in precision reference voltage sources of 2.5 V and 6.9 V. Figure 6 shows the interface unit with the cover of the housing removed.

SOFTWARE

The software provides tools for acquisition, storing, processing, and printing of multiparameter data. Listmode data can be acquired with up to 8 parameters and stored on disk without restriction in length. One- and two-parameter histograms can be directly measured and 1-, 2-, and 3-parameter cube histograms put together from any combination of the listmode data. Color is used for displaying either the time course of a measurement or for showing frequency contour lines of multiparameter histograms. The software together with a controller board is able to control a stepmotor-driven syringe input of the cell samples which allows input volumes from 1/32 up to 1/4 ml for cell counting. In the following a few particular features of the software are explained.

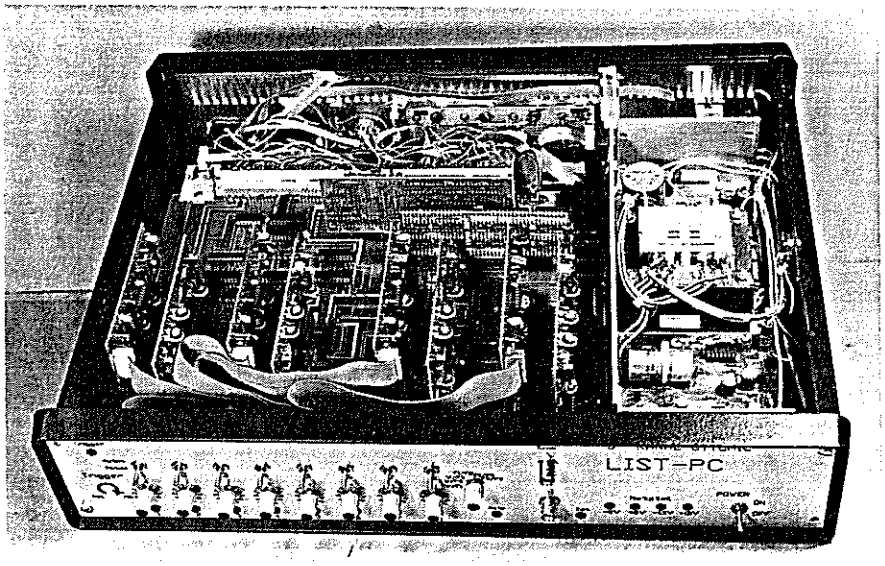

FIG. 6. The 8-parameter interface. For every two parameters a plug in board for the peak detectors and the automatic triggers is required. In this way the hardware may be set up for 2, 4, 6, or 8 parameters.

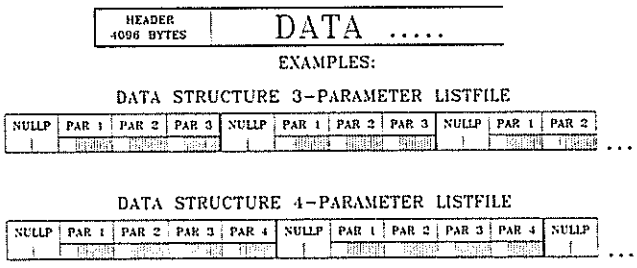

FIG. 7. The data structure of LIST-PC listfiles. The file begins with the ASCII header of 4,096 bytes. Each data group of a cell begins with a zero parameter for testing of the data integrity.

Program Modules

The program package consists of modules written in assembly language, which provides high execution speed. Modules are available for—

- Listmode data acquisition and storing
- 1-Parameter histogram acquisition and processing (128,256,512 channels)
- 2-Parameter histogram acquisition and processing (64 × 64, 128 × 128 channels)
- 3-Parameter histogram display from list data (64 × 64 × 64 channels)
- Snapshot storing and redisplay of graphical screens

Data Structure

The maximum resolution of the ADC circuits is 12 bit (4,096 channels). In listmode the data are collected with the full 12 bit resolution and stored in binary

FIG. 8. The pattern on the screen after finishing a 3-parameter listmode uptake with time as the third parameter. A cell population is simulated which divides after a while into two clusters. Full scale time was selected as 68 s from the timer of the interface. Each block of 2,048 cells is shown by a dedicated color. The number of cells and the sequence of colors can also be seen from the scale at bottom of the screen.

FIG. 9. A color for time cube histogram showing the same data set as in Figures 8 and 12. Time is parameter PA3 on the z-axis. This kind of display shows the full correlation of the three parameters and not only the projections. The color scale indicating the total number of cells is rebuilt at the bottom of the screen.

FIG. 10. Example of the EGA screen with a 128 × 128 channel hidden line two parameter histogram. The violet and red areas mark the fields of the integrating or gating windows 4 and 5. At the right-hand side there is the actual menu for operating the program.

FIG. 11. Example of making projections within a window. Top view onto the histogram of Figure 10 with color display of frequency at the right hand side. The window trace is shown in blue color. At left is shown the y (upper) and x (lower) projections of the field inside the window.

FIG. 12. Example of gating a 2-parameter histogram from another 2-parameter histogram based on a listfile. The gating histogram of the parameters 1 and 2 are shown in the right field. Only the cells with the parameters PA1 and PA2 inside the gating window are accepted for building the histogram of the parameters PA2 and PA3 shown in the left field. The accepted cells are shown in yellow, the others outside the gating window are in blue.

FIG. 13. Three-parameter histogram, 64 × 64 × 64 channels, with frequency identification by color. Each of ten colors marks a 10% frequency range according to the color scale at the right-hand side of the cube. The colors are selected such that generally increased brightness is correlated with higher frequencies. The 100% frequency value for display can be individually chosen. Areas with a content above that value are shown in white.

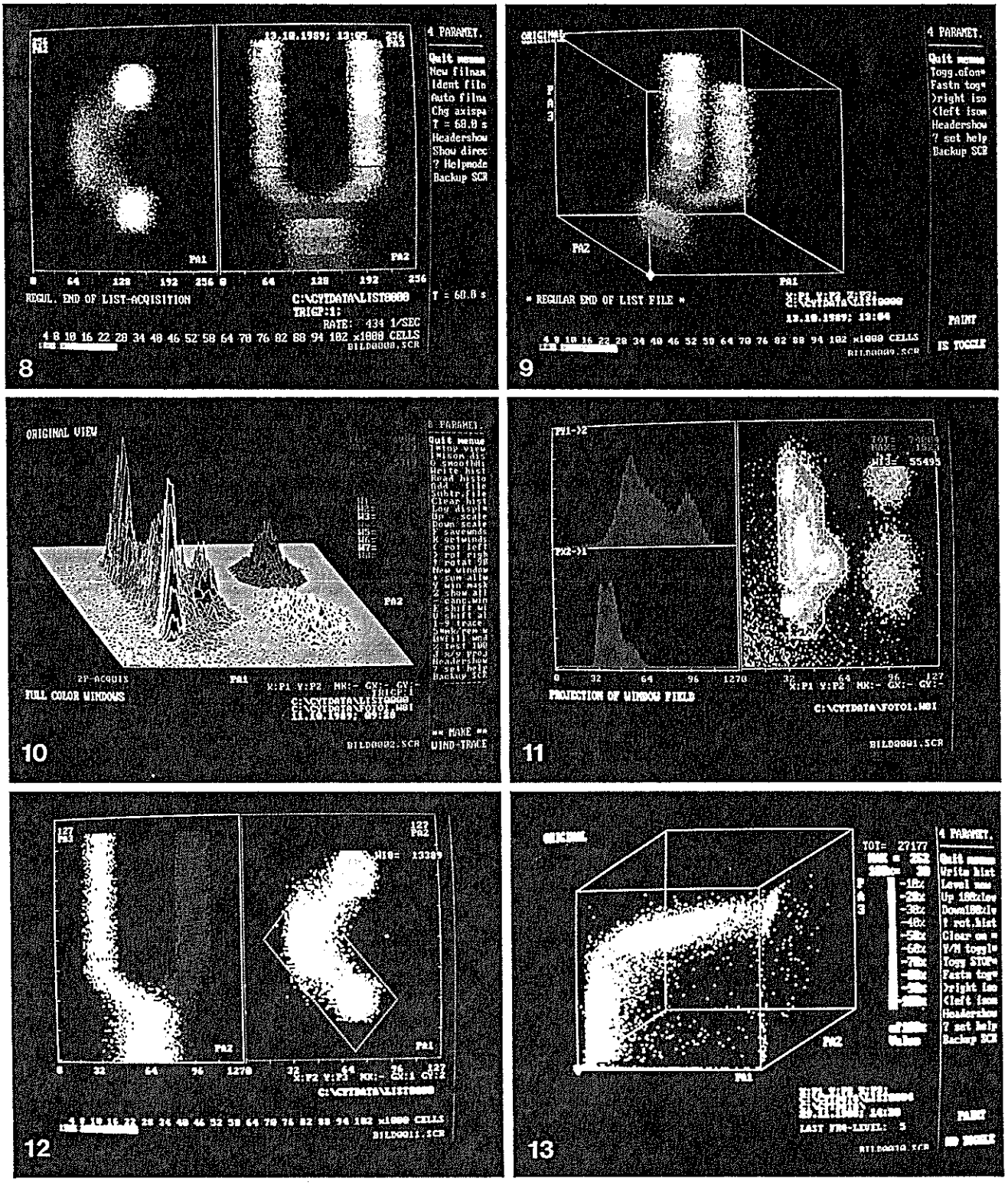
8
9
10
11
12
13
4 PARAMET.
REGUL. END OF LIST-ACQUISITION
* REGULAR END OF LIST FILE *
ORIGINAL VIEW
FULL COLOR WINDOWS
PROJECTION OF WINDOW FIELD
ORIGINAL

FIGS. 8–13.

format. The four most significant bits are not used (Fig. 7).

The data blocks of 2,048 cells, 2,048 × (2n+2) bytes (n=number of parameters), are first transferred via DMA (direct memory access) from the ADC board into a buffer memory. The variable number of parameters requires a variable buffer length. For histogram acquisition, the data blocks collected in the buffer are immediately classified into 1-, 2-, or 3-parameter histograms.

Data Integrity and Transfer

The data acquisition boards do not provide a means for testing the integrity of data groups belonging to a measured cell. If the subsequently stored data are only recognized by their position in the list, the loss of a single byte may have dramatic consequences in disordering the correlation of the data and cell features. The four unused most significant bits of each ADC data word are not accessible on the ADC board for labelling the parameters.

For testing data integrity, an additional gap-parameter, clamped to zero, is taken up as the first value in the data block of each cell (Fig. 7). It is done by always collecting n+1 parameters with the first ADC channel wired to ground. The input of the second channel is wired to the first parameter of the flow cytometer, etc. A quick software check of the zero-values of the gap words discloses disorders of the data structure before appending the buffer content to the data file on disk or classifying histograms. This method works with the given DMA structure, but requires an increased memory.

The list DMA data uptake is controlled by polling since with interrupt controlled disk transfer of high cell rates system crashes occurred. When one of the two buffer memories contains the values of 2,048 cells, the DMA transfer is stopped and reinitiated for transfer into the second buffer memory. The data integrity in the filled buffer is tested, and its content appended to the actual list file concurrently to collecting new data in the other buffer. Thus the only limitation for the size of the list data set is the data capacity of the disk. During the short pauses for buffer change the data of a few cells are lost. Real time histogram uptake is done concurrently to interrupt controlled DMA data acquisition. Here a circular buffer is used which is successively evaluated up to the actual DMA addresses.

With 8-parameter measurements with the computer described and pulse rates of up to 2,500 l/s, data transfer losses below 0.1% have been observed, if the data are collected on the hard disk or directly classified into single histograms (DT2821F board). If 4-parameter data are collected the transfer loss is below 1.5% for rates up to 4,000 l/s. With an 80386 system (25 Mhz clock, harddisk of 20 ms access time) 8-parameter list and histogram acquisition up to 5,000 cells/s was performed with data losses below 0.1%. The transfer loss was measured with fixed frequency pulses and calculated from comparing the number of collected events with the count of an independent counter of the trigger pulses. The transfer loss does not include the deadtime and coincidence loss caused by the unsynchronous appearance of cells in the transducer.

File Structure

Each data set begins with a header in ASCII followed by the binary data. The file header automatically stores the most important characteristics of the actual measurement. If histogram files are made from list files, the main block of the list header is copied into the histogram header defining the origin of the basic data. One hundred eighty characters of text are provided for individual comments. For routine use a user determined comment-file with a descriptive text mask can be copied into the comment field of the header. The first 15 letters of the comment are always shown in the graphical display.

The structure of the bodies of the filenames is free. Ordering numbers at the left end of the names, however, simplify the uptake and processing of a large number of successive samples. Six dedicated file extensions help to discriminate and order the different types of histogram files. When reading histogram files from disk, only the files of the actual type are accepted.

Color Graphics

During data uptake, the actual data are monitored on the screen in the form of scatterplots. A special feature of these dot histograms is that each block of 2,048 cells is marked on the screen by a distinct color. The sequence of colors is shown in a scale at the bottom of the screen.

With a stable measurement the subsequently appearing colors cover each other and no definitely colored area remains in the histogram. With drifting signals either from unstable measurements or kinetic experiments, as shown in Figures 8 and 9, a trace of colors corresponding with the acquired data blocks remains on the screen. Time sequence histograms can also be repeated from the listmode data.

Window fields or window limits for integration or gating within the 2-parameter histograms can be identified by characteristic colors (Figs. 10–12). Overlapping window areas are shown in white. Within the 2-parameter scatterplots and 3-parameter cube histograms the cell frequency contours are displayed by 10 colors. Each color covers 10% of the total frequency

FIG. 14. Color printout of a 2-parameter window evaluation. Up to 8 windows marked by color are simultaneously available. The windows are evaluated by absolute content and relative content related to window 8, which can be positioned anywhere in the field.

FIG. 15. Color printout of the 3-parameter cube histogram of Figure 11. The colors are converted for a good contrast against the white background.

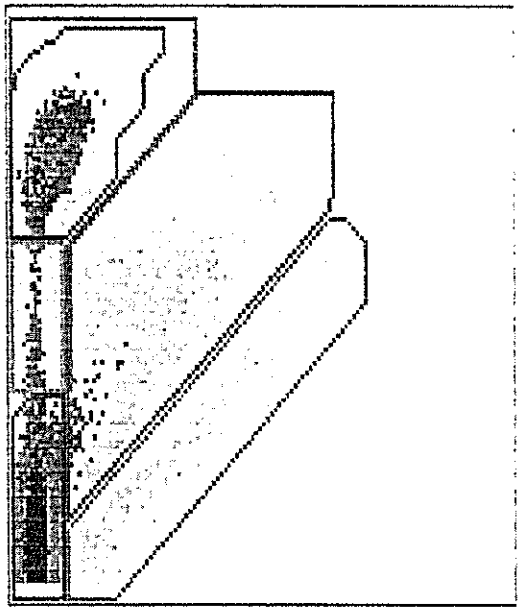

TOT= 32694
MAX= 243

W1=	23513	264.99 % of W8
W2=	218	2.45 % of W8
W3=	1274	14.35 % of W8
W4=	7551	85.10 % of W8
W5=	1991	22.43 % of W8
W7=	00	0.00 % of W8
W8=	8873	100.00 % of W8

X:P2 Y:P3 MK:- GX:- GY:-

EVALUATION 8 WINDOWS

C:\CYTDATA\LIST0004
C:\CYTDATA\WIN1.W8I
23.11.1989; 17:33

14

BILD0007.SCR

ORIGINAL

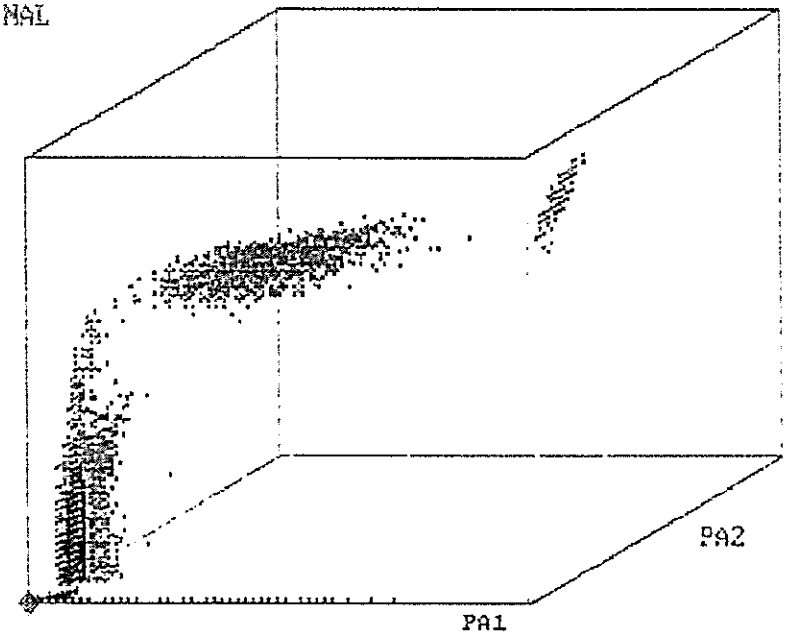

TOT= 27177
MAX = 252
100%= 31

P
A
3

-20%
-30%
-40%
-50%
-60%
-70%
-80%
-90%
-100%

of 100%
Value

X:P1 Y:P2 Z:P3:
C:\CYTDATA\LIST0004
29.11.1988; 14:28
LAST FRQ-LEVEL: 8

15

BILD0004.SCR

FIGS. 14–15.

range. The colors are selected such that channels with more content also appear with more brightness (Figs. 11, 13).

Within the pseudo-three-dimensional cube histograms in some cases a large number of points are superimposed, complicating the identification of clouds. The cube on the screen is normally rotating repeatedly back and forth through a small angle to facilitate recognizing whether a cloud is in the foreground or background of a cube.

Text and graphical displays of the screen can be printed by the commercial PIZAZZ program (Application Techniques Inc., Pepperell, USA) on most standard black-and-white and color printers. A different color scale is used for printout on white paper than is used on the screen with black background (Figs. 14, 15).

DISCUSSION

A dedicated data system based on a PC has some general advantages: The low-cost commercial hardware is available from a large number of suppliers. Most users are already familiar with the operating system, and the basic system can also be used for running standard software.

The data transfer loss can be neglected even if the stepping motor controlled cell counting device is used. Moreover, this data loss has no statistical relevance for the distribution curves since its occurrence is independent of the measured values. There are, however, also compromises to be made: in a multiplexed ADC system values are successively converted. The deadtime between the subsequent acquisition of two cells depends consequently on the number of parameters acquired. For cell rates above 1,000 l/s and a higher number of parameters, an additional data loss from the deadtime has to be expected. The deadtime loss depends also on the transducers used, e.g., the pulse lengths or pulse delays if the cells are interrogated at different locations. The immediate block transfer to disk allows acquisition without overflow as long as space is available on disk. No extended memory is required and the data file on disk is ready immediately after ending the acquisition.

It is theoretically possible that the data integrity test may be misleading if there are parameters measured with many zero values. In practice, however, the 12 bit readings of an input with even very low noise of 0.1% of the maximum pulse height can be clearly discriminated from the readings of the directly grounded gap input.

The graphics software is tailored for quick response. With the AT clone mentioned the generation of a 128×128 channel isometric hidden line display from a 30,000 cell list file requires about 6 s. For composing a 3-parameter cloud histogram of 262,144 channels from list data like that shown in Figure 13, about 15 s are required.

The data system has been used without problems on five different AT clones with different EGA compatible video cards and monitors, including an 80386 system.

The system stores the list values with a resolution of 12 bits, i.e., 4,096 channels. With very few exceptions such a high resolution is senseless for resolving typical cell distributions of coefficients of variation of >10%. It makes sense, however, to store cell data linearly converted in the increased number of channels instead of making a primary logarithmic compression which is difficult to reconvert into a linear scale.

For archive recording the gap words in the list files can be removed and replaced by numbering the free leading bits in the list data words.

The present file header is not compatible with the proposed FCM file standard. The files may, however, be converted into the file standard by a conversion program. That seems to be the best way of combining historically grown file structures with the FCM standard, which is required and very welcome for out-of-house data exchange. It is desirable that in future also a common data interchange medium will be defined.

The software modules have been developed for covering the elementary requirements of data collection and data handling. Means for building data bases, etc., are not included. For such purposes standard software can be used.

LITERATURE CITED

1. Hiebert RD, Jett JH, Salzman GC: Modular electronics for flow cytometry and sorting: The LACEL system. Cytometry 1:337–341, 1981.
2. Kachel V, Schneider H, Schedler K: A new flow cytometric pulse height analyzer offering microprocessor controlled data acquisition and statistical analysis. Cytometry 1:175–192, 1980.
3. Kachel V, Schneider H: Online three parameter data uptake, analysys and display module for flow cytometry. Cytometry 7:24–40. 1986.
4. Stewart SS, Price GB: Realtime acquisition, storage and display of correlated three-parameter flow cytometric data. Cytometry 7:82–88, 1986.
5. Van den Engh G, Stokdijk W: Parallel processing data acquisition system for multilaser flow cytometry and Cell sorting. Cytometry 10:282–293, 1989.
6. Voet L, Kurmann FJ, Hannig K: Data acquisition and control system for multiparameter cell sorting based on DEC LSI-11 microprocessor. Cytometry 2:383–389, 1982.

ZELLULÄRE WACHSTUMSFAKTOREN

Dr.M.Kubbies

Boehringer Forschungszentrum
Penzberg

9 High-Resolution Cell Cycle Analysis: The Flow Cytometric Bromodeoxyuridine-Hoechst Quenching Technique

M. Kubbies

9.1 Background

Cell cycle analysis of in vitro cell cultures is of relevance in basic and clinical research in various fields of immunology, cell biology and oncology. Historically cell proliferation has been studied using cell-counting techniques or radioactive thymidine labeling of S phase cells. With the advent of single cell analysis via flow cytometry interphase G_1, S, and G_2M cells were discernible. In addition, immunocytochemical techniques have been introduced selectively to label cycling $G_1/S/G_2M$ phase cells (proliferation markers such as like proliferating cell nuclear antigen (PCNA) monoclonal antibodies, mAbs) or proliferating, BrdU-labeled S phase cells (BrdU mAbs)[1].

However, none of biochemical or cytometric techniques mentioned above is able to resolve the complete history of cell proliferation of synchronous (e.g., initially resting lymphocytes) or asynchronous cell populations (e.g., tumor cell lines) or the heterogeneity of the proliferative status of cell populations. Even in clonally derived cell populations the duration of the cell cycle in different cells is heterogenous, and normal diploid cell fractions always exhibit a fraction of noncycling G_0/G_1 cells. To reveal the complexity of the proliferative status, cell cycle distribution, and kinetics of in vitro cell cultures, continuous labeling of cells is required. The most common labeling technique is the substitution of thymidine in DNA by BrdU. In contrast to the BrdU pulse labeling, BrdU mAb technique, however, the flow cytometric BrdU-Hoechst quenching analysis is a continuous BrdU labeling procedure [2–4]).

The cells are cultivated in the presence of BrdU, and during the observation period the DNA becomes unifilarily labeled in the first cell-cycle, and uni-and bifilarily in the second, third, and subsequent cell cycles [5]. Theoretically the maximum rate of the substitution of thymidine by BrdU corresponds to 50%, 75%, 87.5%, and so on for the first, second, third, and subsequent cell cycles, respectively. After BrdU labeling the cells are permeabilized and stained with the DNA-specific fluorochromes Hoechst 33258 or 33342. In the presence of BrdU the fluorescence intensity of DNA-bound Hoechst fluorochromes is decreased significantly (quenching effect) [6]. The more the cells are labeled with BrdU the more the Hoechst fluorescence intensity decreases. To achieve a better resolution of the different cell cycles, cells are counterstained with BrdU-non-sensitive

fluorochromes ethidium bromide (EB) or propidium iodide (PI). The fluorochrome-labeled cells are excited with UV light, and the analysis of the emitted blue (Hoechst) and red fluorescence (EB or PI) via flow cytometry routinely reveals up to three subsequent cell cycles (sometimes the fourth cell cycle is recognized) [3].

Due to this high-resolution cell kinetic analysis of cells in the first, second, and third cell cycles the dilution effect of non- or slowly cycling cells by rapidly proliferating populations can be calculated. For the first time, the BrdU-Hoechst quenching technique enables the quantitation of the true numbers of cells of the initial population remaining either in the noncycling G_0/G_1,compartment or the cycling/dividing cells in the various cell cycles [3]. In addition, harvests and BrdU-Hoechst analysis of cells at short intervals after culture setup enables quantitative exit kinetic/cell cycle analysis of cells from all cell cycles/compartments: percentages of noncycling cells, mean and shortest cell cycle/compartment durations (Smith and Martin exit kinetic model) [3,4,7].

The BrdU-Hoechst quenching technique is applicable to initially synchronous or asnychronous cell cultures [8]. It has been used for cell kinetic analysis of numerous normal diploid cell systems [e.g., peripheral blood lymphocytes (PBLs; T and B), fibroblasts, amniotic fluid cells] and various permanent cell lines (e.g., HL60, MOLT3, Jurkat, NIH3T3, MPCll plasmacytoma, cytotoxic T lymphocyte line (CTLL)) of human and murine origin, and other species. Due to the low BrdU substitution rate in vivo and due to the detection limit of the quenching effect, however, this analysis is not useful for in vivo BrdU labeling procedures. Finally, the BrdU-Hoechst quenching technique is a mild DNA staining procedure which enables unlimited use of immunocytochemical labeling of other intracellular or surface membrane epitops of interest [9]. In addition, due to the simplicity of cytochemistry there is only little loss of cells during the DNA staining procedure.

9.2 Material

- Synchronous, asynchronous cell cultures (adherent, suspension).
- Flow cytometer with UV excitation capability (BrdU-Hoechst only). Optional dual laser UV and 488-nm excitation for subpopulation specific BrdU-Hoechst analysis. No special requirements for data acquisition. Direct cytogram storage and data transfer capability to PC/AT computers is preferred. Software for data analysis should enable framing of regions of interest of cytograms, rotation, x- and y-axis projection, and storage of projected histograms.

Filters – **Optical filters (laser based flow cytometer):**
UV scatter light is selected by a beamsplitter DC 375 longpass (Omega) and UG11 bandpass (Schott); the 488-nm scatter light by a neutral beamsplitter 8/90 (Oriel) and a 488/10-nm bandpass (Omega).

- **Emission filters (DNA only, single laser):**
  Blue (Hoechst): K 45 bandpass (Balzers)
  Red [PI, EB, 7-aminoactinomycin D (7-AAD), LDS 751]: RG 630 longpass (Schott)
  Beamsplitter blue/red: DC 560 longpass (Omega)
- **Emission filters [DNA and fluorescein (FITC), dual laser]:**
  Blue (Hoechst): K 45 bandpass (Balzers)
  Red (PI, EB, 7-AAD, LDS 751): RG 630 longpass (Schott)
  Green (FITC): DF 530/30 bandpass (Omega)
  Beamsplitter #1 green-blue: DR 510 longpass (Omega)
  Beamsplitter #2 green-red: DR 595 longpass (Omega)
- **Emission filters [DNA and FITC/phycoerythrin (PE), dual laser]:**
  Blue (Hoechst): K 45 bandpass (Balzers)
  Red (7-AAD, LDS 751): RG 630 longpass (Schott)
  Green (FITC): DF 530/30 bandpass (Omega)
  Orange (PE) DF 580/20 bandpass (Omega)
  Beamsplitter #1 1st/2nd laser: half mirror
  Beamsplitter #2 green-orange: DR 560 shortpass (Omega)
  Beamsplitter #3 blue-red: DC 650 longpass (Omega)
- **Optical filters (arc lamp based flow cytometer):**
- Excitation filters:
  KG1, BG 38, UG1, beamsplitter LP 450 longpass (Schott)
- **Emission filters:**
  Blue (Hoechst): K 45 bandpass
  Red (PI, EB, 7-AAD): full mirror (Schott), RG 630 longpass
  Beamsplitter blue/red: beamsplitter LP 510 longpass (Schott)

DNA staining

- Bovine serum albumin (BSA; Boehringer Mannheim)
- RNAse A (Boehringer Mannheim)
- Trizma base (Sigma)
- Sodium chloride (Merck)
- Magnesium chloride (Merck)
- Calcium chloride (Merck)
- Non-idet P40 (NP40; Boehringer Mannheim)
- Hoechst 33258 (Boehringer Mannheim)
- PI (Sigma)
- EB (Boehringer Mannheim)
- 7-AAD (Serva)
- LDS 751 (Exciton)

Cell culture, cell harvest

- BrdU (Boehringer Mannheim)
- Deoxycytidine (DC; Sigma)
- Dimethylsulfoxide (DMSO; Sigma)
- Cell culture media (Boehringer Mannheim)
- Fetal calf serum (FCS; Boehringer Mannheim)
- 25 and 75 cm^2 cell culture flasks (Falcon)
  15-ml centrifuge tubes (Falcon)

Miscellaneous
- Minifuge (Heraeus)
- MPLUS software for data analysis (Phoenix Flow Systems)

9.3 Method

Cell culture

1. Cultivate cells at cell densities of 1–5x10^5 cells/ml (suspension culture) or 1–5x10^5 cells/25 cm^2 flask using routine cell culture techniques.
2. Supplement medium with 8x10^{-5} *M* BrdU and DC and protect cells from light during cultivation.
3. Harvest cells at room temperature by centrifugation at 400 *g* for 10 min (avoid direct exposure by intense light; low light level acceptable).
4. Cells may be stained directly for flow cytometric analysis. For short- or long-term storage cells are frozen in freezing medium at -20^{0}C (basal culture medium, 10% FCS, 10% DMSO).

DNA staining

Fluorochrome stock solutions (1 mg/ml) are prepared in sterile aqua dest (PI, EB), methanol (LDS 751) or 10% DMSO (7-AAD), protected from direct light exposure and stored at 4°C. Stock solutions may be used up to 1 year. Inactivate residual DNAse activity in RNAse A by heating of RNAse stock solution for 2 h at 80°C or use DNAse free RNAse preparations.

1. Thaw frozen cells or use freshly isolated cells, and centrifuge at room temperature at 400 *g* for 10 min.
2. Resuspend cell pellet at 1–5x10^5 cells/ml in DNA-staining buffer (100 m*M* Tris 7.4, 154 m*M* NaCl, 1 m*M* $CaCl_2$, 0.5 m*M* $MgCl_2$, 0.2% BSA, 0.1% NP40) supplemented with 10 U/ml RNAse A and 1.2 µg/ml Hoechst 33258.
3. Incubate at 4°C for 15 min in the dark.
4. Add BrdU-nonsensitive fluorochromes to final concentrations of: 2 µg/ml PI or EB, 10 µg/ml 7-AAD, or 40 µg/ml LDS 751 (use 7-AAD or LDS 751 only with FITC- and PE-labeled cells).
5. Incubate cells at least for a further 15 min at 4°C in the dark, and analyze sample within 8 h.

Subpopulation specific DNA staining

1. Use freshly isolated cells and label cells with mAbs via direct or indirect FITC and/or PE immunofluorescence.
2. Resuspend pellet in 50 µl PBS vortex cells and add 1 ml 1% paraformaldehyde (4°C).
3. Fix cells for 30–60 min at 4°C.
4. Centrifuge cells at 400 *g* for 10 min at 4°C and resuspend pellet at 1–5x10^5 cells/ml in PBS/0.01% Tween 20.

5. Add Hoechst 33258 (1.2 µg/ml; final concentration) and proceed according DNA staining step 3. Use PI or EB if cells are FITC labeled only. Use 7-AAD or LDS 751 with PE-labeled cells.
6. Final incubation time prior flow cytometric analysis should be at least 2h.

Flow cytometric analysis

1. Select UV light in arc lamp based flow cytometers by using the excitation filters as indicated in Sect. 9.2 (HBO 100-W/2 arc lamp). In laser-based instruments use either UV-capable ion argon lasers (tune to 351/364 nm and 50 mW) or HeCd lasers (325 nm and 10 mW miniumum) for excitation. Gate on DNA or scatter signal.
   For subpopulation-specific BrdU-Hoechst analysis in laser-based instruments use an argon laser additionally tuned at 488 nm and 50 mW for FITC and PE excitation. Delay both lasers for 30–60 µs. First/second laser adjustment depends on optical configuration of instrument. Gate on DNA or scatter signal.
2. Run samples at 300–1000 cells/s at room temperature (wait 30 s before data recording).
3. Record blue Hoechst fluorescence and red PI, EB, 7-AAD, or LDS 751 fluorescence using the optical filters indicated in the Sect. 9.2.
4. Depending on the complexity of the bivariate BrdU-Hoechst PI cytogram (or EB, 7-AAD, or LDS 751) analyze at least $2x10^4$ cells. Analyze at least $5x10^4$ cells in subpopulation-specific BrdU-Hoechst analysis.
5. Store data preferentially as single cytograms. In subpopulation-specific analysis store data in list mode for subsequent gating procedures.

Data analysis

1. Quantitate cell cycle distributions by extracting individual first, second, and third cell cycles from the bivariate BrdU-Hoechst PI cytograms, and perform G_1,-S-G_2M DNA histogram analysis of individual cell cycles (e.g., use MPLUS software for both procedures; $G_0/G_1 + S + G_2M = 100\%$).
2. Quantitation of real data (represents cell culture status): Calculate the relative percentages of cells in the first, second, and third cell cycles, and multiply by the percentages of the G_1, S and G_2M compartments of individual cell cycles from step 1. This gives the percentages of cells in individual compartments of the various cell cycles.
3. Quantitation of original data (representing true numbers of cycling or non-dividing cells; dilution effect of rapidly proliferating cells exerted on slowly or nonproliferating populations is taken into account): Take data from step 2; calculate „dilution factor" (DF):

$$DF = 100 /[(G_0G_1+S+G_2M) + (G_1'+S'+G_2M')/2 + (G_1''+S''+G_2M'')/4].$$

In the case of a fourth cell cycle the percentages of real data are divided by 8 and added to the denominator as shown above.

first cycle:	% orig. G_0/G_1	= % real G_0/G_1	x DF
	% orig. S	= % real S	x DF
	% orig. G_2M	= % real G_2M	x DF
second cycle:	% orig. G_1'	= % real $G_1'/2$	x DF
	% orig. S'	= % real S'/2	x DF
	% orig. G_2M'	= % real $G_2M'/2$	x DF
third cycle:	% orig. G_1''	= % real $G_1''/4$	x DF
	% orig. S"	= % real S"/4	x DF
	% orig. G_2M''	= % real $G_2M''/4$	x DF

The „percentage increased cell number" corresponds to:
% inc. cells = DF x 100
The calculation of the „Smith and Martin exit kinetic curves" of the individual cell cycle compartments requires specialized computer software. The formulas for calculation of the minimum and mean duration of cell cycle compartments, and the fractions of noncycling cells are shown in [3] and [10].

9.4 Example

The complexity of the cell kinetics of human PBLs is revealed only by the BrdU-Hoechst quenching technique. Typical examples of 48 and 72 h harvests of phytohemagglutinin stimulated, human PBLs are shown in Figure 1 (panels A and B). Two days after polyclonal activation the majority of PBLs are still in the noncycling G_0/G_1 compartment, and some cycling cells are found in the first (S, G_2M) and second cycle (G_1', S', G_2M'). The power of the flow cytometric BrdU quenching technique is shown by the fact that even the very small fraction 0.3% of third cycle G_1'' phase cells is significantly resolved. The nuclear decay lane represents dead cells of the G_0/G_1 population.

Three days after stimulation most of the PBLs have left the noncycling G_0/G_1 compartment. The culture now consists of cells in the first, second and third (G_1'', S", G_2M'') cell cycles. The fact that there are still PBLs in the S phase of the first cell cycle indicates that the process of cell activation and recruitment is still going on in the G_0/G_1 population. To display the quantitative distribution of the PBLs the isometric plots of panels A and B are shown below the bivariate BrdU-Hoechst PI dot plots. The corresponding framed regions of the individual first, second and third cell cycles in panels A and B are shown as one-parametric DNA-histograms.

Table 1 displays the dilution effect of fast proliferating, dividing cells (normally overestimated) exerted on slow cycling or nonproliferating cell populations (normally underestimated). Data are calculated from Figure 1

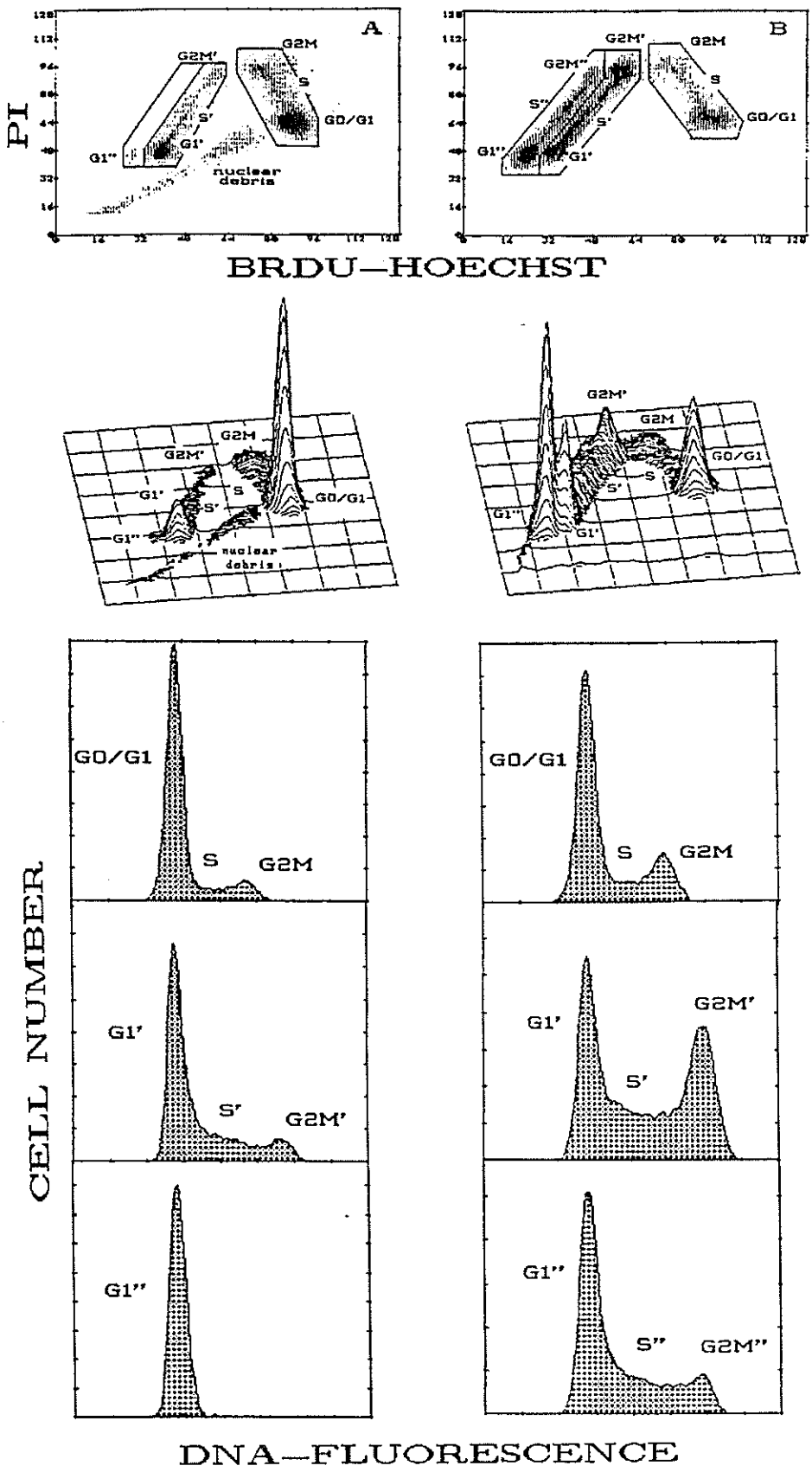

Figure 1. Bivariate BrdU-Hoechst Pl cytograms of phytohemagglutinin-stimulated PBLs harvested 48 (A) and 72 h (B) after activation. Due to the quenching effect of BrdU exerted on the DNA-bound Hoechst fluorochromes the lanes of subsequent cell cycles *(framed areas)* are left to the previous one. From the top to the bottom the data are displayed as bivariate dot plot, isometric plot, and projected first, second, and third cell cycle DNA histograms.
First cell cycle: G_0/G_1, S, G_2M.
Second cell cycle: G_1', S', G_2M'.
Third cell cycle: G_1'', S", G_2M''.

panel A (72 h harvest). With the knowledge of the number of cells in different, subsequent cell cycles the true percentages of cycling and nonactivated cells can be calculated.

A PBL subpopulation specific, multiparameter BrdU-Hoechst analysis is shown in Figure 2. PBLs from patients with Fanconi's anemia display a significant slowing of cell proliferation due to a slowing of G_2 phase progression and G_2 phase arrest in the first and second cell cycle. However, cell activation of G_0/G_1 cells is not affected [11]. From panels A and B it is obvious that almost all $CD8^+$ T cells have left the G_0/G_1 compartment. A significant number of G_0/G_1 cells are present only in the $CD4^-/CD8^-$ population (mainly B cells, panel B). The G_2 phase arrested populations of $CD8^+$ and $CD8^-$ cells are indicated by arrows.

Table 1. Calculation of the real data (cell culture status) and original data (true percentages of cycling/noncycling cells of the original population of the cell cycle distribution from the accompanying figure).

	First cell cycle			Second cell cycle			Third cell cycle		
	G_0/G_1	S	G_2M	G_1'	S'	G_2M'	G_1''	S"	G_2M''
Real (%)	14.3	4.8	3.3	8.3	20.8	6.7	18.5	21.5	1.8
Original (%)	28.2	9.4	6.4	8.2	20.6	6.6	9.0	10.6	0.9

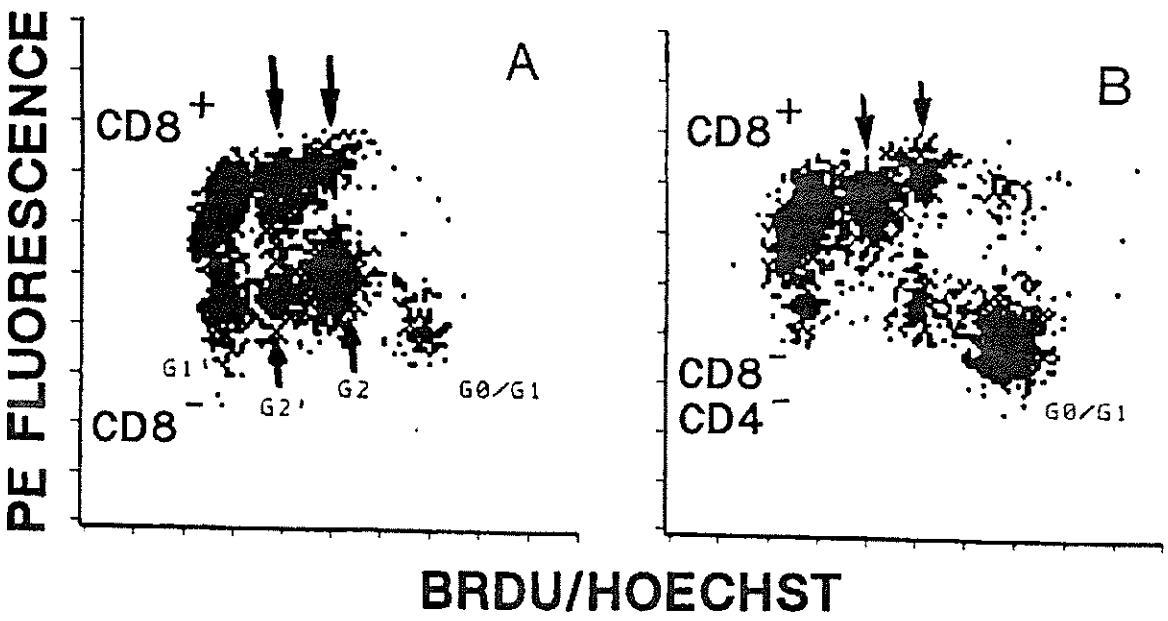

Figure 2. T cell subpopulation specific, high-resolution cell kinetic BrdU-Hoechst analysis of Fanconi's anemia cells 72 h after phytohemagglutinin-activation. Gating of CD4-FITC and CD8-PE labeled, and BrdU/Hoechst stained PBLs is on the $CD8^+$ and $CD8^-$ fractions (includes $CD4^+$ T cells; A) and on the $CD8^+$ and $CD4^-/CD8^-$ populations (B)

9.5 Modifications

Instead of detergent lysis of cells for DNA staining methanol (90%) or ethanol (70%) fixation procedures can be used for the bivariate BrdU-Hoechst PI cell cycle analysis. The latter fixation techniques additionally enable multiparameter analysis of intracellular epitops. Cells should be fixed for at least 1 h at -20°C prior to subsequent immunofluorescence labeling (depending on the antibody permeabilization by 0.05%–0.1% NP40/PBS, Tween 20/PBS, or Triton X100/PBS may be required). DNA staining is performed thereafter as described above for the paraformaldehyde fixation technique used for surface marker labeling.

9.6 Tips, Tricks, and Troubleshooting

Fluorodeoxyuridine

The BrdU-Hoechst quenching is dependent on a variety of cell biological, biochemical, biophysical, and technical factors [3]. For example, it is species (AT/GC ratio) and cell type dependent (intracellular thymidine pool), and might even depend on the serum lot used for cell culture (thymidine content). In order to block thymidine incorporation into DNA and therefore increase the amount of BrdU in DNA, fluorodeoxyuridine can be used as inhibitior for deoxythymidylate synthetase. However, technical and cellular parameters should be optimized first instead of using a potentially toxic inhibitor.

Hoechst, EB, and PI concentration range

Without significant alteration of the quenching effect the Hoechst and EB or PI concentrations can vary between 1.0–1.5 and 1.5–2.5 µg/ml, respectively.

BrdU concentration

Depending on the cell type and optical instrument configuration the range of the BrdU concentration for optimal quenching is $2–10 \times 10^{-5}$ *M*. At higher concentrations inhibition of cell activation and cell cycle progression may (but does not necessarily) occur. Equimolar concentrations of deoxycytidine should be added as medium supplemented to avoid possible adverse proliferative effects due to disturbance of the intracellular nucleotide pool.

Cell concentration

Cell densities significantly above 5×10^5 cell/ml in the staining buffer can decrease the quenching effect.

Fixed cells

Alcohol- or paraformaldehyde-fixed DNA-stained cells can be stored for several days with loss of resolution of the bivariate BrdU-Hoechst PI cytogram.

7-AAD and LDS 751

7-AAD and LDS 751 are recommended as BrdU nonsensitive counterstains using PE-labeled cells.

HeCd lasers The first cell cycle G_2M/G_1 fluorescence ratio is decreased below 2.0 due to overlapping effects of red fluorochrome (e.g. PI) excitation via the UV light source and from energy transfer from the Hoechst fluorochromes. This phenomenon is lacking with 325-nm excitation from a HeCd laser.

Filter selection The optical filter for blue (Hoechst) and red (PI, EB, etc.) fluorescence analysis in Sect. 9.2 are recommodations only. The blue and red fluorescence should be recorded at 400–500 nm and above 580 nm, respectively. The 50% value of the dichroic beamsplitter should be in the range between 510–570 nm.

Aggregates All DNA staining procedures induce cell clumping and increase the G_2M phase fractions artificially (depending on cell type, e.g., adherent cells). This is more significant using alcohol fixation procedures. To avoid cell clumping the „peak versus area" gating procedure is recommended for the sensitive, high-resolution cell kinetic BrdU-Hoechst technique.

Acknowledgement. The Fanconis anemia cells were kindly provided by Dr. D. Schindler from the Department of Human Genetics University of Wurzburg, FRG.

References

1. Gray JW Darzynkiewcz Z, (eds.): Techniques in cell cycle analysis. Humana Press, Clifton, NJ, 1987.
2. Kubbies M, Rabinovitch PS: Flow cytometric analysis of factors which influence the BrdU-Hoechst quenching effect in cultivated human fibroblasts and lymphocytes. Cytometry 3:276,1983.
3. Kubbies M, Hoehn H, Schindler D, Chen YC, Rabinovitch PS: Cell cycle analysis via BrdU-Hoechst flow cytometry: principles and applications. In: Flow Cytometry (Volume ll), Yen A (ed), CRC- Press, Florida, p. 5,1989.
4. Poot M, Kubbies M, Hoehn H, Grossmann A, Chen Y, Rabinovitch PS: In vitro cell cycle analysis using continuous BrdU labeling and bivariate Hoechst 33258-EB flow cytometry. In: Methods in cell biology, 33, Darzynkiewcz Z, et al (eds); Academic Press, NY, pp. 186,1990.
5. Kubbies M, Friedl R: Flow cytometric correlation between BrdU-Hoechst quench effect and base pair composition in mammalian cell nuclei. Histochemistry 83:133, 1985.
6. Latt SA, Wohlleb JC: Optical studies of the interaction of 33258 Hoechst with DNA, chromatin and the interphase chromosome. Chromosoma 52:297, 1975.
7. Rabinovitch PS: Regulation of human fibroblast growth rate by both non-cycling cell fraction and transition probability is shown by growth in BrdU followed by Hoechst 33258 flow cytometry. PNAS 80:2951,1983.
8. Omerod MG, Kubbies M: Cell cycle analysis of asynchronous cell populations by flow cytometry using bromodeoxyuridine label and Hoechst-propidium iodide staining. Cytometry, in press, 1992.
9. Kubbies M: High resolution multiparameter cell cycle analysis by BrdU/ Hoechst flow cytometry. In: Progress in cytometry: flow and image. Reports from the 3rd European cytometry users conference 1989 in Ghent, Belgium. Becton Dickinson (eds), p. 30,1990.

10. Kubbies M: Alteration of cell cycle kinetics by reducing agents in human PBL's from adult and aged donors. Cell Proliferation, 25:157,1992.
11. Kubbies M, Schindler D, Hoehn H, Schinzel A, Rabinovitch PS: Endogenous blockage and delay of the chromosome cycle despite normal recruitment and growth phase explain poor proliferation and frequent endomitosis in Fanconi anemia cells. Am J Hum Genet 37: 1007,1985.

10 Cell Activation: Indo-1 Ratiometric Analysis of Intracellular Ionized Calcium

M. KUBBIES

10.1 Background

Intracellular ionized calcium (Ca^{2+}) regulates various metabolic processes and is involved in signal transduction and cell activation. The intracellular concentration of Ca^{2+} in resting cells (100–200 n*M*) is far below the concentration of the extracellular environment. Most of the intracellular calcium, however, is bound in its nonionized form in the endoplasmic reticulum, mitochondria, cytosol, and cell memebrane. Influx of Ca^{2+} into cells occurs through the action of voltage gated channels after membrane depolarization or by the action of receptor-gated channels. The excess of Ca^{2+} is pumped out of the cells by the action of a membrane-bound Ca^{2+} ATPase (for review see [1,2]).

An increase in intracellular Ca^{2+} by extracellular binding of agonists to receptors initiates the activation cascade of the phosphoinositol pathway [3,4]. After binding to the receptor phospholipase C is activated, which cleaves phosphatidylinositol-4,5-bisphosphate into both second messengers diacylglycerol and inositol-1,4,5-trisphosphate. The latter binds to receptors of the endoplasmic reticulum, and as a first step Ca^{2+} is released from this intracellular compartment. Subsequently Ca^{2+} influx occurs from the extracellular environment. Although it remains open to debate whether intra- and/or extracellular influx of Ca^{2+} is sufficient for cell activation, a subsequent cascade of still unknown events triggers the cell activation process toward proliferation of the cells. However, there is evidence that cell proliferation can occur in the absence of a continuous increase in intracellular Ca^{2+} [5,6]. It remains to be shown whether small local changes or oscillations in intracellular Ca^{2+} are sufficient for cell activation [7].

Historically, intracellular Ca^{2+} was analyzed by microelectrode techniques and loading of cells by $^{45}Ca^{2+}$. Since then, various Ca^{2+}-binding fluorochromes have been developed, changing either the fluorescence intensity (quin-2, fluo-3), absorption spectrum (fura-2), or emission spectrum (indo-1) upon binding of ionized calcium (for review see [1]). Analysis of the Ca^{2+}-dependent alteration in fluorescence intensity requires simpler technical flow cytometric equipment. Recently fluo-3 has been developed to enable excitation at 488 nm. However, inhomogeneity of dye loading and different cell sizes may result in a rather high coefficient of variation (CV) of the fluo-3 histogram [8]. These limitations are circumvented using ratio

analysis of fluorescence signals of cells loaded with Ca^{2+}-sensitve fluorochromes. Ratio analysis yields results independent of biological (cell size), cytochemical (dye loading), or technical variations (drift in excitation light intensity). Whereas alteration in the absorption spectrum is ideally suited for microscopic digital ratio imaging (dual wavelength excitation, single wavelength emission analysis, fura-2), changes in the emission spectrum are optimal for flow cytometric analysis (single wavelenght excitation, dual wavelenght emission analysis, indo-1) [8-10].

Indo-1 exhibits a Ca^{2+}-independent emission of fluorescence intensity at the isobestic point around 450 nm (355 nm excitation). Binding of Ca^{2+} to indo-1 decreases the blue fluorescence intensity above 450 nm, whereas the intensity of the violet fluorescence below 450 nm increases [11]. Therefore, the ratio of violet/blue fluorescence increases even more compared to the increase in violet fluorescence intensity only. It has been shown that the indo-1 ratio varies with the emission wavelength recorded. Maximum ratios are obtained collecting light around or below 400 nm (violet) and above 500 nm (blue) [9]. Additionally, due to ratio imaging, the CV of the ratio distribution of the violet and blue fluorescence of a nonactivated resting cell population is significantly smaller. This improvement in flow cytomtric resolution enables detection of even small releases of intracellular Ca^{2+} from endoplasmic stores after buffering of the extracellular Ca^{2+} by ethyleneglycoltetraacetic acid (EGTA) [9,12].

The calcium-sensitive fluorochromes are membrane impermeable. Loading of viable cells is performed using indo-1 prepared as acetoxymethyl (AM) esters. These AM esters become hydrolyzed by intracellular esterases, and indo-1 is trapped within the cells (5-20 μM). Dead cells do not accumulate calcium sensitve fluorochromes and are easily gated out during flow cytometric analysis. The concentrations of indo-1 used for flow cytometric analysis have been shown to be nontoxic to peripheral blood lymphocytes (PBLs) [9].

The requirement of UV excitation for indo-1 is regarded as a limitation for its widespread use in flow cytometry. However. using a long-lived inexpensive HeCd laser for indo-1 excitation gives excellent resolution of analysis of intra- and extracellular Ca^{2+} influx [13]. In addition. the use of dual lasers with indo-1 enables subpopulation-specific analysis in heterogenous cell systems without fluorescence overlap of fluorescein isothiocyanate (FITC) and/or phycoerythrin (PE) used as surface marker labels of monoclonal antibodies (mAbs) [8-10,12].

10.2 Material

- Synchronous or asynchronous suspension cell cultures or freshly isolated cells sensitive to receptor stimulation.
- Flow cytometer with UV excitation capability (indo-1 only). Optional dual laser UV and 488-nm excitation for subpopulation (FITC and/or

PE) specific indo-1/Ca^{2+}analysis. Gating of violet and blue indo-1 fluorescence signals and signal rationing are required for data aquisition. Direct cytogram storage and data transfer capability to PC/AT computers is preferred. Software for data analysis should enable the calculation of both the percentage Ca^{2+} positive cells and the indo-1 ratio of Ca^{2+} positive cells versus resting population as a function of time and display of these data as time histograms.

Filters

- **Optical filters:** UV right angle scatter is selected by a beamsplitter DC 375 longpass (Omega) and UG 11 bandpass (Schott). The UV forward scatter signal (UG 11 bandpass) is used as trigger signal.
- **Emission filters (indo-1 only, single laser):**
  Violet: DF 395/25 bandpass (Omega)
  Blue: DF 510/30 bandpass (Omega)
  Beamsplitter violet/blue: DC 420 longpass (Omega)
- **Emission filters (indo-1 and PE, dual laser):**
  Violet: DF 395/25 bandpass (Omega)
  Blue: DF 510/30 bandpass (Omega)
  Orange (PE): DF 580/20 bandpass (Omega)
  Beamsplitter #1 violet/blue: DC 420 longpass (Omega)
  Beamsplitter #2 orange/blue: DC 560 shortpass (Omega)
- **Emission filters (DNA and FITC/PE, dual laser):**
  Violet: DF 395/25 bandpass (Omega)
  Blue: DF 510/30 bandpass (Omega)
  Green (FITC) DF 530/30 bandpass (Omega)
  Orange (PE): DF 580/20 bandpass (Omega)
  Beamsplitter #1 1st/2nd laser: half mirror
  Beamsplitter #2 green-orange: DR 560 shortpass (Omega)
  Beamsplitter #3 violet/blue: DC 420 longpass (Omega)

Indo-1 staining and cell activation

- Indo-1 AM ester (Boehringer Mannheim)
- Water free dimethylsulfoxide (DMSO; Sigma)
- Thrombin (Sigma) formyl-methionyl-leucyl-phenylalanine (fMLP; Sigma)
- Mouse CD3 (Boehringer Mannheim)
- Goat „mouse“ (Boehringer Mannheim)
- Synperonic F127 (Boehringer Mannheim)
- Ionomycin (Calbiochem)
- EGTA (Merck)

Cell culture

- Cell culture media (Boehringer Mannheim)
- Fetal calf serum (FCS; Boehringer Mannheim)
- 15-ml centrifuge tubes (Falcon)

Miscellaneous

- Minifuge (Heraeus)
- Fluorescence microscope
- MTIME software for data analysis (Phoenix Flow Systems)

10.3 Method

Indo-1 staining

Indo-1 AM stock solution (1 mg/ml) is prepared in water-free DMSO, and small aliquots are stored at -20 °C in the dark. Stock solutions may be used up to several months. EGTA is dissolved in water as 100 m*M* stock adjusted to pH 7.4, synperonic F127 (or pluronic F127) as 20% (wt/vol) in DMSO, and ionomycin as 2 mg/ml in absolute ethanol. Avoid the use of sodium azide in the labeling medium throughout indo-1 AM loading. Use sodium azide free mAbs for labeling of cells.

1. Harvest cells by conventional techniques. Centrifuge at 200 *g* at room temperature for 10 min.
2. Resuspend cell pellet at $5x10^6$ cells/ml in RPMI 1640/10% FCS. Add 3 µg/ml indo-1 AM, and mix gently.
3. Incubate at 37 °C for 45 min in the dark.
4. Centrifuge cells at 200 *g* for 10 min, remove supernatant completely, and resuspend pellet carefully in RPMI 1640/10% FCS at $1x10^6$ cells/ ml.
5. Keep samples at room temperature in the dark and raise to 37 °C prior to analysis. Analyze samples within 2–3 h. Control indo-1 loading of cells by microscopic analysis. Cells should be labeled brightly and uniformly, showing no intracellular bright spots of Indo-1 fluorescence (compartmentation of indo-1)

Subpopulation-specific indo-1 staining

1. Indo-1 loading as described above (steps 1–4) except resuspension of cells at $1x10^6$ cells/100 µl RPMI 1640/10% FCS.
2. Label cells not of interest for Ca^{2+} analysis using a cocktail of FITC- and/or PE-labeled mAbs for 20 min at room temperature in the dark. Avoid labeling of cell population of interest due to possible interference of the receptor binding of mAb with Ca^{2+} signal activation (negative gating procedure; see below).
3. Resuspend cells in 2 ml RPMI 1640/10% FCS.
4. Centrifuge cells at 200 *g* for 10 min. Remove supernatant completely and resuspend pellet carefully in RPMI 1640/10% FCS at $1x10^6$ cells/ ml.
5. Keep samples at room temperature in the dark and raise to 37°C prior analysis. Analyze samples within 2–3 h.

Flow cytometric analysis

1. Tune argon laser to 351/364 nm and 50 mW or use HeCd laser at 325 nm and 10 to 30 mW for excitation. Select viable cells by gating on forward scatter signals. For subpopulation specific indo-1 analysis use a second argon laser tuned at 488 nm and 50 mW for FITC and/or PE excitation. Delay both lasers for 30–60 µs. First/second laser adjustment depends on optical configuration of instrument.
2. Run samples at 200–600 cells/s at 37 °C. Use saline or phoshate-buffered saline as sheath fluid.
3. Record blue and violet fluorescence as linear signals (exclude lowest and highest channels from ratio analysis). Adjust maximum of blue and violet histograms of resting cells in the upper and lower half of the histogram, respectively. Gate on scatter characteristics of cells (e.g.,

lympho-, mono-, or granulocytes; exclude dead cells from analysis) and on non-mAb-labeled cell fraction, performing subpopulation specific Ca^{2+} analysis (negative gating).

4. Analyse nonactivated cells and adjust gaussian distributed violet/blue fluorescence ratio signals in the lower region of the ratio histogram.
5. Stop sample flow, add activating agonist to cells, and restart analysis as quickly as possible.
6. Store indo-1 violet/blue ratio histograms as a function of time (time slices) preferentially as cytograms. In subpopulation-specific analysis obtain several indo-1 ratio/time cytograms using gating procedures.
7. Optimal indo-1 loading of cells and adjustment of instrument should be controlled by induction of a maximal Ca^{2+} response by the Ca^{2+} ionophore ionomycin (2 μg/ml). The increase in the indo-1 ratio of all human PBLs should be at about factor 6–8 over the baseline of the resting population.
8. The release of intracellular Ca^{2+} from endoplasmic reticulum is analyzed by resuspension of the cells either in Ca^{2+}-free medium or the addition of 5 m*M* EGTA 2–5 min prior to cell activation.

Data analysis

- Define region of resting and responding cell population on time axis.
- **„Percentage Ca^{2+} positive cells“:** Calculate either the percentage of Ca^{2+} positive cells above an indo-1 ratio channel threshold defined by the resting population (accept 2%–5 % background of low-level Ca^{2+} positive cells; percentage above threshold) or substract resting population from the distribution of activated cells (percentage of responding cells). Calculation of the percentage of responding cells is less sensitive to deviations in the indo-1 ratio histogram from a normal distribution [14].
- **„Increase in indo-1 ratio“:** Calculate the mean indo-1 ratio of the Ca^{2+} responding cell population versus the resting nonactivated cell fraction. The intracellular concentration of ionized Ca^{2+} is calculated using the formula and calibration procedure described by Grynkiewcz and Rabinovitch [9, 11].
- Calculation of the percentage of Ca^{2+} positive cells and the absolute and relative values of intracellular Ca^{2+} is implemented in the kinetic analysis program MTIME (written by P.S. Rabinovitch).

10.4 Example

Figure 1 illustrates the Ca^{2+} response of human PBLs activated by incubation with CD3 followed by <mouse> cross-linking (panel A) and human thrombocytes stimulated with thrombin (panel B). Human PBLs and thrombocytes were isolated according to standard procedures and cells were identified by their forward/right-angle scatter characteristics. The resting populations of both cell types exhibit a gaussian distributed shape

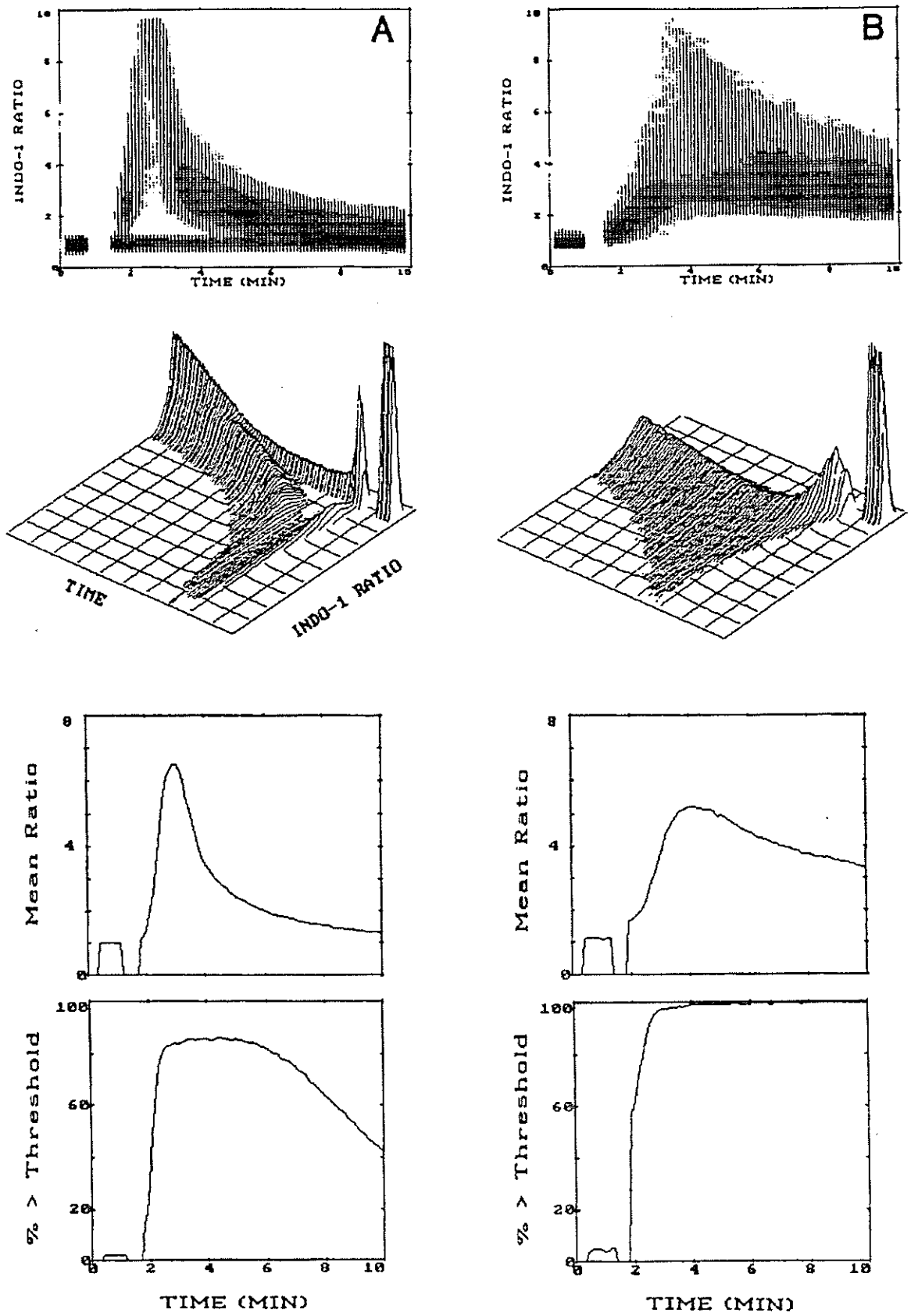

Figure 1. Increase in intracellular Ca^{2+} in human lymphocytes (A) and thrombocytes (B) activated with <CD3>/<mouse> (5 µg/ml each), and thrombin (1 µg/ml), respectively. The agonists were added 1 min after start of the experiment (see gaps). The isometric plots and the calculations of the mean ratio (indo-1 ratio of activated versus resting population), and the percentage of cells above the threshold (percentage of Ca^{2+} positive cells) are shown below to illustrate the quantitative changes in intracellular Ca^{2+}

in the 1st min after the start of flow cytometric analysis (see isometric plots below panels A and B respectively). The gap indicates the stop of the sample flow in order to add the stimulating agonists. The flow cytometric indo-1 ratio analysis was restarted 30 s later.

The human PBLs show a rapid and high Ca^{2+} influx within 1.5 min. However. Ca^{2+} is pumped out of the PBLs rapidly and declines to almost normal values within 5 min after maximum response (panel A). It is evident that a distinct fraction of 17.8% of the PBLs is nonresponsive to <CD3> activation (cell population showing an indo-1 ratio of 1.0). In contrast. the Ca^{2+} response of thrombocytes is slower. and the intracellular Ca^{2+} level reaches its maximum 2.3 min after addition of thrombin (panel B). However all cells exhibit an increase in intracellular Ca^{2+}. The Ca^{2+} efflux from the cytoplasma of thrombocytes is slower. and almost all cells still show significantly increased intracellular Ca^{2+} levels within the observation period. The quantitative data on the kinetics of the increased indo-l ratio and the percentage of positive cells are shown below the cytograms.

The Ca^{2+} response of human mono- and granulocytes is shown in Figure 2 (panels A and B, respectively). These cells were gated from the leukocyte forward/right-angle scatter cytogram (whole blood lysis). Compared to PBLs and thrombocytes the Ca^{2+} influx occurs more rapidly, and the Ca^{2+}-responding cells were almost positive at the restart of flow cytometric analysis. The Ca^{2+} efflux of f-MLP activated monocytes was complete within 4 min after maximum response (panel A) and approached to the baseline level in fMLP-stimulated granulocytes (panel B). However, within the observation period, the latter cells showed greater heterogeneity of intracellular Ca^{2+} levels (higher CV of the indo-1 ratio histogram).

The quantitative data from these two figures are summarized in Table 1. It is obvious that flow cytometric indo-1 Ca^{2+} flux analysis shows several advantages. Small CVs of the resting population, improving the detection limit of the Ca^{2+} response, correct quantitation of the heterogeneity of the Ca^{2+} response (e.g., nonresponding versus responding population), and second laser analysis (FITC and/or PE) enables subpopulation-specific analysis.

Table 1. Calculation of the percentage of calcium-positive cells, increase in intracellular Ca^{2+} (indo-1 ratio), and time delay to maximum Ca^{2+} response (min) from the figures (analysis performed using the MTIME program written by P.S. Rabinovitch).

	CD3: PBLs	Thrombin: thrombocytes	fMLP: monocytes	granulocytes
Indo-1 ratio	7.1	4.6	2.1	3.6
Percentage positivecells	82.2	99.5	81.6	96.0
Delay to maximum response	1.5	2.3	0.9	0.4

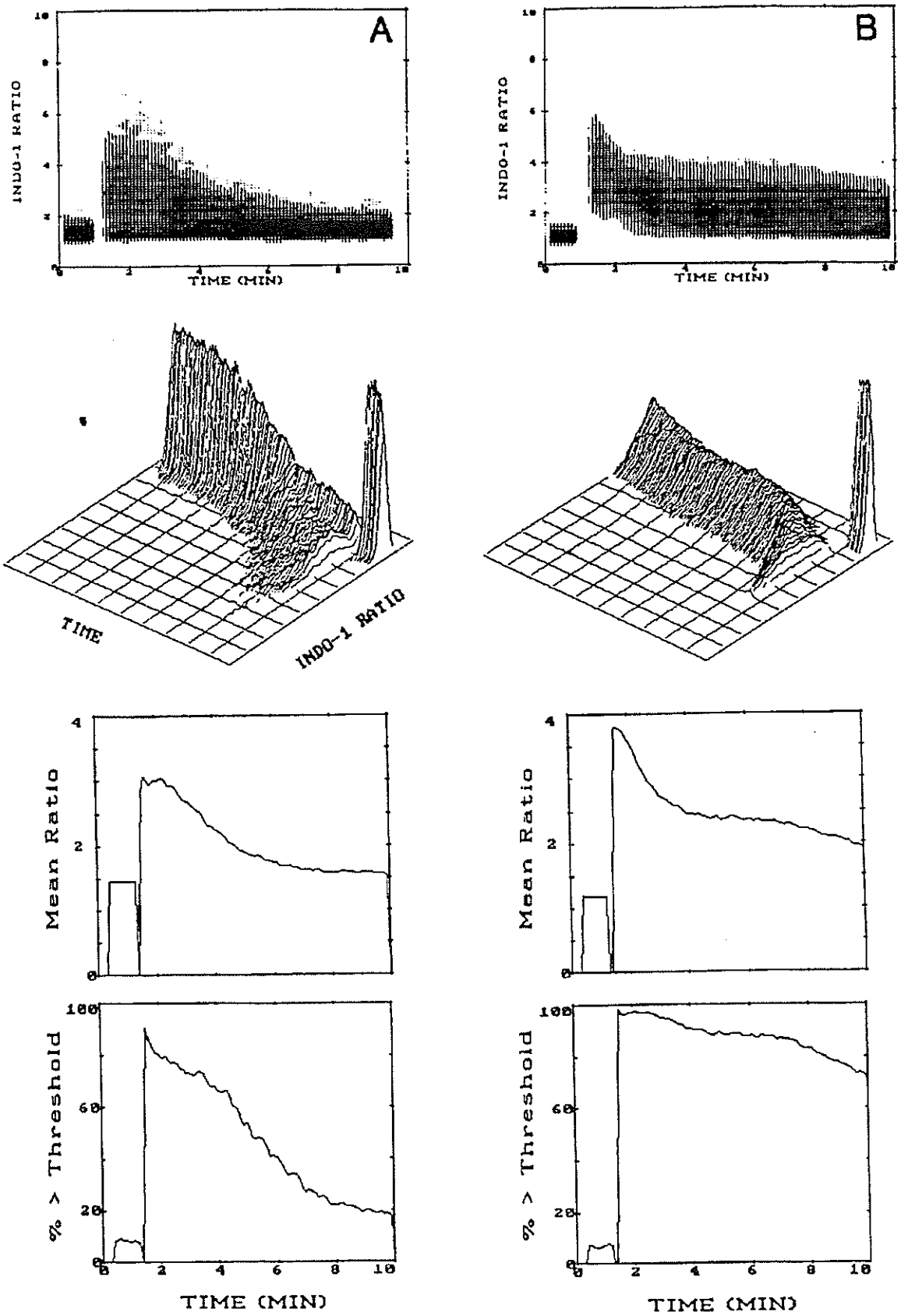

Figure 2. Intracellular release of Ca^{2+} in fMLP ($1x10^{-7}$ *M*) stimulated human monocytes (A) and granulocytes (B). fMLP was added 1 min after start of flow cytometric analysis

10.5 Modifications

The concentration of cells to be loaded with indo-1 AM can vary between 1 and $5x10^6$ cells/ml loading medium. Any culture medium optimal for cell viability and physiology can be used instead of RPMI. The FCS can be omitted or the concentration decreased (e.g. 1% FCS) if cells remain viable throughout the staining procedure.

Optimal loading with indo-1 may depend on cell type under investigation, and the concentration should be in the range of 1–5 µg/ml. Higher CV values of resting population and Ca^{2+} buffering can occur at lower or higher indo-1 AM concentrations respectively. Loading of cells with indo-1 can be performed at lower temperatures of 25°–30°C and incubation time can be decreased to 30 min.

10.6 Tips, Tricks, and Troubleshooting

Compartmentalization

- Enrichment of indo-1 in non-Ca^{2+}-responsive intracellular compartments decreases the maximum Ca^{2+} response detectable by alteration in violet/blue indo-1 fluorescence (control uniform loading of cells). Compartmentation can be minimized by addition of 2 µ*M* synperonic F127 (or pluronic F127; disolve at 20% w/v in DMSO) during indo-1 AM loading of cells, and decrease of incubation temperature to 25°–30°C.

Labeling medium

- Do not use sodium azide in the labeling medium. Use dialyzed mAb preparations (this may not always be required; check control sample). Cells become leaky to Ca^{2+}, and show increased indo-1 ratios. Skewing of the resting, gaussian distributed population toward higher indo-1 ratios occurs.

Controls for antibody activation

- Subpopulation-specific Ca^{2+}analysis requires labeling of cells by mAbs. However, mAb binding may induce alterations in the Ca^{2+} flux. Use negative gating procedure: label all cells not of interest for Ca^{2+} analysis by mAbs (FITC or PE). Gate on the unlabeled cell fraction recording violet and blue indo-1 fluorescence.

Indo-1 problems

- Indo-1 loading of cells can be affected by various cellular and/or cytochemical factors. Some cells show no activity of intracellular esterases (loading of cells must be done by injection of indo-1). Indo-1 AM may be hydrolyzed prior use (disolve indo-1 AM in water-free DMSO and store in sealed caps at -20°C).
- Fluorescent agonists or inhibitors alter indo-1 ratios which might mimic an increase (more violet) or decrease (more blue) of the indo-1 ratio without any physiological relevance.

- Check the number of AMs coupled to indo-1 for cell loading. AMs released intracellularly by unspecific esterases may be toxic to cells. Use Indo-1 with a lower number of AM esters.

Cross-linking antibodies for activation

- Although mAbs used for activation recognize identical receptors. slight differences in receptor epitope specificity or mAb affinity results in altered Ca^{2+} response. Cross-linking of mAbs by <mouse> F(ab)2 fragment may be required.

Consistency control

- Analyze the Ca^{2+} flux of control cells at the end of each series of experiments to control the constancy of Ca^{2+} response.

Filter selection

- Selection of optical filters for analysis of violet and blue fluorescence affects maximal response recorded. For optimal indo-1 ratio analysis use violet bandpass filters with a maximum below 410 nm. The blue fluorescence should be analyzed using longpass or bandpass filters above 490 nm.

Oscillations

- Cells may show Ca^{2+} oscillations after agonist stimulation. Oscillations are not detectable by flow cytometry. Use digital video imaging for analysis of oscillatory Ca^{2+} processes.

References

1. McCormack JG, Cobbold PH (eds.): Cellular calcium: a practical approach. IRL Press, Oxford, 1991.
2. Cheung WY (ed): Calcium and cell function. Vol. VII. Academic Press, New York, 1987.
3. Abdel-Latif AA: Calcium-mobilizing receptors, polyphosphinositides, and the generation of second messengers. Pharm Rev 38: 227,1986.
4. Linch DC, Wallace DL, O'Flynn K: Signal transduction in human T lymphocytes. Immunol Rev 95:137,1987.
5. Gelfand EW, Cheung RK, Grinstein S, Mills GB: Characterization of the role for calcium influx in mitogen-induced triggering of human T cells: identification of calcium-dependent and calcium-independent signal. Eur J Immunol 16:907, 1986.
6. Raspe E, Reuse S, Roger PP Dumont JE: Lack of correlation between the activation of the Ca^{2+} phoshatidylinositol cascade and the regulation of DNA-synthesis on the dog thyrocyte. Exp Cell Res 198:17,1992.
7. Berridge MJ, Galione A: Cytosolic calcium oscillators. FASEB 2:3074,1988.
8. Rabinovitch PS, June CH: Measurement of intracellular ionized calcium and membrane potential. In: Flow cytometry and sorting, Melamed MR, Lindmo T, Mendelsohn ML (eds). Wiley-Liss, New York, p. 651,1990.
9. Rabinovitch PS, June CH, Grossmann A, Ledbetter JA: Heterogeneity of T-cell intracellular free calcium responses after mitogen stimulation with PHA or anti-CD3: use of Indo-1 and simultaneous immunofluorescence with flow cytometry. J Immunol 137: 952,1986.
10. June CH, Rabinovitch PS: Measurement of intracellular ions by flow cytometry. In: Current protocols in Immunology. Coligan JE, et al (eds.), John Wiley & Sons, New York, p. 5.5.1.,1991.
11. Grynkiewcz G, Poenie M, Tsien R: A new generation of Ca^{2+} indicators with greatly improved fluorescence properties. J Biol Chem 260:3440,1985.

12. Kubbies M, Goller B, Russmann E, Stockinger H, Scheuer W: Complex Ca^{2+} flux inhibition as primary mechanism of staurosporine induced impairment of T-cell activation. Europ J Immunol 19:1393,1989.
13. Goller B, Kubbies M: UV-lasers for flow cytometric analysis: HeCd vs argon laser excitation. J Histochem Cytochem, 40:451,1992.
14. Rabinovitch PS: Analysis of percent responding cells in kinetic experiments by application of curve substraction. Cytometry Suppl. 5:138,1991.

Chapter 1

INTRODUCTION

I. OVERVIEW

Hormones and growth factors are important regulatory substances present in metazoan organisms. These substances represent biological signals involved in the regulation of cell growth and differentiation during both pre- and postnatal life. Some hormones and growth factors act in a restricted manner on specific types of responsive cells, whereas others may have a broad, perhaps universal, spectrum of activity for different types of cells and tissues.

Hormones are defined as chemical messengers synthesized in the endocrine glands of multicellular organisms and secreted into the extracellular body fluids. Upon their arrival to the respective target organs, hormones are recognized by and binded to specific cellular receptors. The formation of a hormone-receptor complex determines the cellular responses that are specific for both the hormone and the target cell.[1,2]

Peptide growth factors, commonly called in an abbreviate manner "growth factors", are hormone-related substances with an important role in the control mechanisms of growth and development in a diversity of organs and tissues as well as in cultured cells.[3-10] In contrast to the classical hormones, growth factors are usually not synthesized in specialized endocrine organs but are produced and secreted by cells from different tissues in a steady flow to diffuse to responsive cells, which are frequently located not far from the site of release. Different types of growth factors are produced by a diversity of normal cells as well as by neoplastically transformed cells. Isolation and characterization of growth factors and other tumor-secreted products may be facilitated by culturing cells in appropriate conditions, for example, in a defined protein-free medium.[11]

The biological properties of hormones and growth factors can be studied either in vitro or in vivo. Growth factors are usually defined by their ability to induce stimulation of target cell multiplication and their activity is measured by assays where either the increase of cell populations or the incorporation of labeled thymidine into DNA is determined. The latter can be estimated by autoradiography and counting of labeled cells or by determination of radioactivity in liquid scintillation vials. The most suitable routine test for detection and determination of growth factor activity lies on measuring the incorporation of tritiated thymidine into DNA of target cells with a scintillation counting.[12] A list of the most important hormones, growth factors, and other exogenous agents of cellular origin involved in growth-regulatory phenomena appears in Table 1. Available data corresponding to the chromosomal assignment and location of the genes coding for some of the hormones and growth factors discussed in this volume, as well as those corresponding to the genes coding for their cellular receptors, are indicated in Table 2.

II. THE CELL CYCLE

Serum contains many different hormones and growth factors capable of stimulating the growth of animal cells in vivo and in vitro. Cultured mouse fibroblasts, such as BALB/c 3T3 cells, have been conveniently used as an assay system for evaluating the activity of hormones and growth factors in the stimulation, or inhibition, of cell proliferation. Fibroblasts whose growth has been arrested by serum starvation undergo a synchronous progression through the cell cycle by the addition of serum. A schematic representation of the cell cycle appears in Figure 1.

The cell cycle can be divided into four major phases: G_1, S (DNA synthesis period), G_2,

Table 1
GROWTH FACTORS, HORMONES, AND OTHER GROWTH-REGULATING AGENTS OF EXOGENOUS CELLULAR ORIGIN

Well characterized growth factors
- Insulin-like growth factor I (IGF-I) or somatomedin C
- Insulin-like growth factor II (IGF-II), somatomedin A, or multiplication-stimulating activity (MSA)
- Epidermal growth factor (EGF) or urogastrone (URO)
- Fibroblast growth factor (FGF) or fibroblast-derived growth factor (FDGF)
- Nerve growth factor (NGF)
- Transforming growth factor α (TGF-α)
- Transforming growth factor β (TGF-β)
- Hemopoietin-2, interleukin-3 (IL-3), mast-cell growth factor (MCGF), or erythroid burst-promoting activity (EBPA)
- Interleukin-1 (IL-1)
- Interleukin-2 (IL-2) or T-cell growth factor (TCGF)
- Colony-stimulating factor 1 (CSF-1) or macrophage colony-stimulating factor (MCSF)
- Colony-stimulating factor 2 (CSF-2) or granulocyte-macrophage colony-stimulating factor (GM-CSF)
- Granulocyte colony-stimulating factor (G-CSF)
- Erythropoietin
- Platelet-derived growth factor (PDGF)

Partially characterized growth factors
- EGF-like mitogens
- TGF-like growth factors
- PDGF-like growth factors
- Melanocyte growth factor (MGF)
- Hepatopoietin
- Hepatocyte-stimulating factor (HSF)
- Prostate growth factor
- Cartilage-derived growth factor (CDGF)
- Chondrocyte growth factor (CGF)
- Bone-derived growth factor (BDGF)
- Osteosarcoma-derived growth factor (ODGF)
- Neuronal-derived transforming growth factor (ND-TGF)
- Glial growth-promoting factor (GGPF)
- Colostrum basic growth factor (CBGF)
- Endothelial cell growth factor (ECGF)
- Tumor angiogenesis factor (TAF)
- Hemopoietin-1
- IL-3-like proteins
- Eosinophil differentiation factor (EDF) or interleukin-4 (IL-4)
- B-cell growth factor 1 (BCGF) or B-cell stimulating factor 1 (BSF-1)
- B-cell stimulating factor 2 (BSF-2)
- B-cell differentiation factor (BCDF)
- Leukemia-derived growth factor (LDGF)
- Myelomonocytic growth factor (MMGF)
- Macrophage-derived growth factor (MDGF)
- Macrophage-activating factor (MAF)
- Erythroid-potentiating activity (EPA)

Hormones and other growth-regulating agents
- Insulin
- Growth hormone (GH) or somatotropin
- Thyroid-stimulating hormone (TSH) or thyrotropin
- Adrenocorticotropic hormone (ACTH)
- Gonadotropins
- Prolactin
- Melanocyte-stimulating hormone (MSH)
- Placental lactogen (PL)
- Thyroid hormone

Table 1 (continued)
GROWTH FACTORS, HORMONES, AND OTHER GROWTH-REGULATING AGENTS OF EXOGENOUS CELLULAR ORIGIN

- Parathyroid hormone (PTH)
- Calcitonin
- Steroid hormones
- Transferrin
- Interferon (IFN)
- Tumor necrosis factor α (TNF-α)
- Tumor necrosis factor β (TNF-β) or lymphotoxin

Table 2
CHROMOSOMAL ASSIGNMENT AND LOCATION OF THE HUMAN GENES CODING FOR SOME HORMONES AND GROWTH FACTORS AND FOR SOME CELLULAR RECEPTORS

Chromosome	Location	Agent	Ref.
1	1p22—p22.1	NGF	13
2	2p11—p13	TGF-α	14
2	2q13—q21	IL-1	200
3	3q15—q25	Transferrin	15
3	3q26.2	Transferrin receptor	16
4	4q25—q27	EGF	17
4	4q26—q28	IL-2	18
5	5q21—32	CSF-2	19
5		Glucocorticoid receptor	20
6		IFn-α receptor	201
6		TNFs α and β	21
7	7pter—q22	PDGF-A	202
9		IFNs α and β	22
10	10p14—p15	IL-2 receptor	23
11	11p11.21	PTH	24
11	11p15	IGF-II	17
11	11p14.1	Insulin	24
12	12q22—q24.1	IGF-I	17
12		IFN-γ	25
17		GH	26
19	19p13.2—p13.3	Insulin receptor	27
19	19q13.1—q13.3	TGF-β	203
22	22q13.1	PDGF-β	94

and M (mitosis).[28] G_1 is the gap period between mitosis and the initiation of DNA synthesis, and G_2 is the period between S and M. Cells in G_2 contain double amount of DNA than cells in G_1. For most cells growing exponentially in culture, the interval between cell divisions is 10 to 30 hr. Variation in cell cycle between different cell types, or different environmental conditions, is mainly due to variation in the length of G_1, with the duration of S (6 to 8 hr) + G_2 (2 to 6 hr) + M (1 hr) being relatively constant. In addition, there is much variability in the length of G_1 among individual cells in a single population.[28]

Animal cells, both in vivo and in vitro, can also exist in a nongrowing, quiescent state during which they do not divide for long periods. Most frequently, normal cells that have

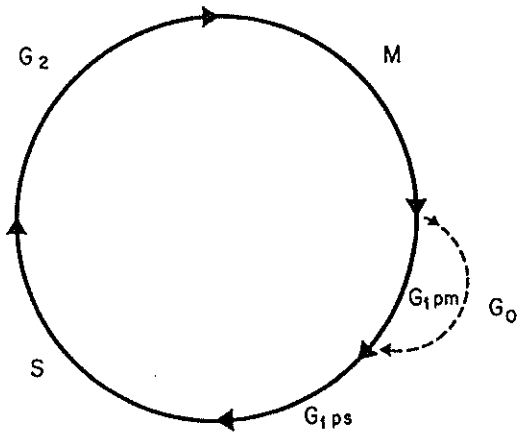

FIGURE 1. Schematic representation of the cell cycle.

ceased to grow have the G_1 content of DNA. Most or all of these quiescent cells are metabolically different from cycling G_1 cells and are considered to be in a qualitatively distinct state, termed G_0.

The crucial control events for the regulation of cell proliferation seem to reside in the G_1 phase of the cycle. Evidence has accumulated for the existence of a restriction or commitment point in mid- to late G_1, at which time a cell "decides" whether to initiate DNA synthesis and undergo division or to cease proliferation.[28] Environmental conditions, including the presence of certain hormones and growth factors, may influence this decision. Suboptimal conditions, like the absence of serum, usually shift normal cells into quiescence. In contrast, neoplastically transformed cells can lose this restriction-point control in whole or in part and may grow even in the absence of serum (or in the absence of specific hormones and growth factors contained in serum).

On the basis of the cell cycle arrest rapidly induced by brief serum starvation or transient inhibition of protein synthesis, the G_1 period of exponentially proliferating 3T3 cells can be subdivided into two physiologically discrete phases: one postmitotic (G_1pm) and one pre-DNA-synthetic (G_1ps).[29] During G_1pm the cells complete the growth factor-dependent processes leading to commitment for proliferation. Thereafter they enter the growth-factor-independent pre-DNA-synthetic part of G_1. The commitment process of G_1pm may be successfully completed in the presence of PDGF as the only supplied growth factor. EGF and insulin are insufficient for the completion of the commitment processes in G_1pm. Under conditions optimal for proliferation, the cells complete the commitment processes of G_1pm within a remarkably constant time period (3 to 4 hr after mitosis). The duration of G_1ps, on the other hand, shows a large intercellular variability, consistent with a transition probability event. In fact, G_1ps accounts for most of the variability in G_1 and cell cycle time.[29]

III. ROLE OF HORMONES AND GROWTH FACTORS IN THE REGULATION OF DNA SYNTHESIS AND CELLULAR PROLIFERATION

Hormones and growth factors are critically involved in the regulation of DNA synthesis and cellular proliferation in the respective target tissues. Hormones and growth factors contained in serum are required for the growth of cells cultured in vitro.[30] Although each

of these factors may have a differential effect on DNA, RNA, protein synthesis, and cell division of particular cell types, the combined action of them is required for the optimal growth of cells.[31-34] Some growth factors, called competence factors, act early in the G_1 phase of the cell cycle, rendering cells competent to DNA replication whereas other growth factors, called progression factors, would allow the progression of cells through the prereplicative phase of the cycle.[35] Competence and progression factors would therefore act sequentially and synergistically in the cell cycle. The similar action of some growth factors in the prereplicative phase of cells suggests the operation of certain common intracellular pathways.[36]

The responsiveness of different types of cells to the mitogenic action of hormones and growth factors may show great variation according to the state of development and differentiation. In general, cells from newborn animals have greater mitogenic responsiveness to growth factors than adult cells. The responsiveness of cultured human fibroblasts to hormones and growth factors contained in fetal calves serum declines with age.[37,38] As a general rule, neoplastic cells are less dependent on the exogenous supply of hormones and growth factors than are normal cells.[39] However, the growth of neoplastic cells is not always characterized by an autonomy from the exogenous supply of hormones and growth factors.[40,41] Moreover, the proliferative response of neoplastic cells to growth factors may show great variation according to factors such as the microenvironment and the presence of chromosome abnormalities.[42] The progression, or regression, of hormone-dependent tumors may depend on nonspecific changes in gene expression.[43]

In addition to their characteristic effects on cell proliferation, growth factors may be involved in the control of physiological processes not associated with cell proliferation. For example, PDGF, EGF, and FGF regulate the production of IFN-γ by lymphocytes through a mechanism unrelated to their known proliferative effects on cells.[44] Other secretory processes may also be regulated by hormones and growth factors by mechanisms independent from DNA synthesis and cell proliferation. In general it can be said that hormones and growth factors are crucially involved in controlling the expression of differentiated functions in many types of cells and tissues.

Cultured growing cells, as well as certain normal and tumor cells growing in vivo, may produce hormone- and growth factor-like substances which are apparently useful and/or required for their proliferation. Murine BALB/c 3T3 cells in culture express a mRNA coding for proliferin, which is a 24,000 dalton protein with clear homology to preprolactin.[45] In the mouse, proliferin is a glycoprotein apparently produced only in the placenta, being especially abundant between days 8 and 10 of pregnancy.[46] A proliferin-related protein (PRP) has also been detected in the mouse placenta but, in contrast to proliferin, PRP is not present in proliferating BALB/c 3T3 cells in culture.[47] Structurally, PRP is closely related to both its peak level at the start of DNA synthesis. The high level of expression of the proliferin gene in certain growing cells in culture suggests that it may also serve as an autocrine growth factor in nonplacental cells in vitro, perhaps related to the immortality of these cell lines.

A. Mechanisms of Regulation of DNA Synthesis and Cell Proliferation by Hormones and Growth Factors

The mechanisms by which hormones and growth factors may influence DNA synthesis and cell proliferation are little understood. The mitogenic action of growth factors and the antiproliferative effects of interferon may be independent cell cycle events, as demonstrated in studies with vascular smooth muscle cells and endothelial cells.[48] Changes in cyclic AMP (cAMP) levels and polyamine synthesis may be involved in the regulation of the complex metabolic pathways leading to DNA synthesis and cell division. An increase in intracellular cAMP and polyamine concentration would depend on the activity of adenylate cyclase and ornithine decarboxylase, respectively. The latter enzyme is rate-limiting in the polyamine

biosynthesis pathway. Insulin and several growth factors with mitogenic properties (EGF, PDGF, NGF) induce the expression of ornithine decarboxylase activity in the presence of amino acids like asparagine, and this activity is closely related to the synthesis of polyamines and the initiation of DNA synthesis.[49] Inhibition of ornithine decarboxylase without the concurrent administration of polyamine leads to cessation of DNA synthesis and cell proliferation. However, an increase in ornithine decarboxylase activity is necessary but is not sufficient for cell division to occur, and an increase in cAMP concentration may be neither necessary nor sufficient for the induction of cell division in particular types of cells.[50] It seems thus clear that polyamines and cAMP must act synergistically with other agents in the regulation of DNA synthesis and cellular proliferation stimulated by hormones and growth factors.

The level of expression of many different genes may show variation in relation to the different phases of the cell cycle in both normal and transformed proliferating cells.[51] Obviously, the fact that certain genes are expressed in a cell cycle-dependent manner does not mean that they are involved in cell cycle regulatory phenomena. It is thus difficult to recognize which of these genes are directly responsive, for example, for the induction of DNA synthesis. Over 3300 proteins can be distinguished in Swiss 3T3 cells by two dimensional electrophoresis on giant gels; 34 of these proteins are consistently induced more than threefold by growth factors (PDGF, CDGF) or fetal bovine serum after stimulation for 3 hr.[52] An additional 30 inductions are variable present and some of these inductions are inhibited by dexamethasone. However, only some of these proteins show a constant linear relationship to DNA synthesis, suggesting that they play an important role in early control of the cell cycle. Nuclear proteins that are differentially expressed in the cell cycle may be good candidates for playing a role in cell cycle control. A human histone H4 gene exhibits cell cycle-dependent changes in chromatin structure that correlate with its expression.[53] Identification of sets of genes that are specifically expressed in transition stages of the cell cycle, for example, in G_0/G_1 transition,[54] may be important for understanding the genetic mechanisms involved in the molecular controls of the cell cycle.

1. Cyclin

Cyclin is an acidic nuclear protein of 36,000 mol wt which may be involved in the control of DNA synthesis and cell proliferation. Cyclin has been identified in various types of normal or transformed cells from different animal species.[55,56] Cyclin is identical to a previously described protein called proliferating cell nuclear antigen (PCNA).[57-59] Isolated human epidermal basal cells synthesize very little cyclin, whereas simian virus 40 (SV40)-transformed keratinocytes synthesize this protein constitutively.[60] Induction of cyclin in serum-stimulated cultured cells is independent of DNA synthesis and cell transformation but it precedes DNA synthesis and correlates with cell proliferation.[61,62] Moreover, the synthesis of cyclin is not triggered by DNA replication, but changes in the nuclear distribution of cyclin are observed in relation to the S phase of the cell cycle.[63] Immunofluorescence analysis of synchronously growing transformed human amnion cells using autoantibodies specific for cyclin reveals remarkable changes in the nuclear distribution of cyclin during the S phase of the cell cycle.[64] Moreover, individual nuclei in polykaryons produced by polyethylene glycol-induced fusion of populations of transformed human amnion cells can control cyclin distribution and DNA synthesis in spite of the fact that they share a common cytoplasm.[60] These results suggest that cyclin may be an important component of the events leading to DNA replication and cell division.

B. Growth-Inhibiting Factors

Most frequently, hormones and growth factors have stimulatory actions on the respective target cells but some of these agents may have inhibitory effects when acting on particular

types of cells. The growth inhibitory properties of glucocorticoids, for example, are profited for the treatment of many different types of inflammatory or neoplastic diseases.

Particular types of growth-inhibiting factors may be produced by either normal or neoplastic cells. An antimitogenic peptide factor with capability for inhibiting growth of cells in several normal and neoplastic cell lines has been detected in acetic acid extracts of the porcine hypothalamus.[66] A growth inhibitory factor is apparently produced by human monocytic leukemia cells and can be detected in the serum-free culture medium.[67] Another inhibitory factor, termed tumor-inhibitory factor (TIF), has been identified in rat ascites fluid and a human colon carcinoma cell line.[68,69] TIF acts in a partially reversible, nontoxic manner and coexists in the same malignant cells with TGF activity, which suggests that control of cell growth, either normal or neoplastic, may involve a balance between positive and negative factors.

Two types of tumor cell growth-inhibiting factors, termed TIF-1 and TIF-2, have been isolated and partially purified from the A673 human rhabdomyosarcoma cell line.[70,71] TIF-1 is a low-molecular-weight polypeptide (10,000 to 16,000 mol wt) that is inactivated by trypsin and dithiothreitol. TIF-1 inhibits the growth of a wide range of human tumor cells and virally transformed human and rat cells in soft agar and monolayer culture but stimulates the growth of normal human fibroblasts and a normal epithelial cell line.[70] TIF-1 blocks the stimulatory effect of both TGF-α and EGF in a soft agar assay with human tumor cells. TIF-2, purified from the same human rhabdomyosarcoma cell line, shares many properties in common with TIF-1 but can be distinguished by its molecular weight, chromatographic properties, and its effects on certain target cells.[71] TIF-1 and TIF-2 have no antiviral activity and their growth-inhibiting effects are reversible when the affected cells are no longer exposed to the factor. TIFs may be a family of related polypeptides which selectively inhibit the growth of tumor cells.

The physiological role of inhibitory growth factors in the regulation of cell proliferation is unknown. Regulation of many physiological phenomena and biological activities is probably governed by processes that activate or inhibit specific pathways. In the immune system, for example, the existence of antigen-specific and antigen-nonspecific regulatory proteins that either promote or inhibit immune functions has been well documented. Soluble immune response suppressor (SIRS) is a protein of 14,000 mol wt produced by mitogen- or interferon-activated suppressor T-cells that inhibits antibody secretion by B-lymphocytes and cell division by neoplastic cell lines.[72] IL-1, IL-2, and EGF each inhibit SIRS-mediated suppression of antibody secretion by cultured mouse spleen cells.[73] These results indicate that growth factors may act in some biological systems by interfering the action of growth-inhibiting factors.

Factors classically considered as stimulators of cell proliferation and/or transformation may act in certain types of cells, or even in the same type of cell under different conditions, as inhibitors of these phenomena. EGF, for example, stimulates growth in a wide variety of cells in vivo and in vitro but inhibits the growth of human A431 cells despite the fact that these cells express a very high number of EGF receptors.[74] TGF-β is capable of inducing anchorage-independent growth in mouse embryo AKR-2B cells as well as in normal rat kidney (NRK) cells, although in the latter case either EGF of TGF-α is required in association with TGF-β. However, TGF-β is a bifunctional factor because it is capable of inhibiting the anchorage-independent growth of many human tumor cell lines at concentrations in the same range as those than enhance the anchorage-independent growth of NRK or AKR-2B cells.[75] Moreover, in Fischer rat 3T3 fibroblasts transfected with a c-*myc* proto-oncogene, TGF-β can function as either an inhibitor or an enhancer of anchorage-independent growth, depending on the particular set of growth factors operant in the cell together with TGF-β.[75] These results suggest that transformation may result not only from the action of some positive, stimulating factors in susceptible cells, but also from the failure of some cells to respond

Table 3
ACUTE TRANSFORMING RETROVIRUSES AND THEIR RESPECTIVE ONCOGENES

Oncogene	Isolate origin	Prototype virus strain
abl	Rodent	Abelson murine leukemia virus (A-MuLV)
erb-A	Avian	Avian erythroblastosis virus (AEV)
erb-B	Avian	Avian erythroblastosis virus (AEV)
ets	Avian	Avian leukemia virus E26 (E26-ALV)
fes	Feline	Snyder-Theilen feline sarcoma virus (ST-FeSV)
fgr	Feline	Gardner-Rasheed feline sarcoma virus (GR-FeSV)
fms	Feline	McDonough feline sarcoma virus (MD-FeSV)
fos	Rodent	FBJ murine osteosarcoma virus (FBJ-MOV)
mht	Avian	Mill Hill 2 avian carcinoma virus (MH2-ACV)
mos	Rodent	Moloney murine sarcoma virus (M-MuSV)
myb	Avian	Avian myeloblastosis virus (AMV)
myc	Avian	MC29 avian myelocytomatosis virus (MC29-AMCV)
raf	Rodent	3611 murine sarcoma virus (3611-MuSV)
H-*ras*	Rodent	Harvey murine sarcoma virus (H-MuSV)
K-*ras*	Rodent	Kirsten murine sarcoma virus (K-MuSV)
rel	Avian	Avian reticuloendotheliosis virus (ARV)
ros	Avian	Rochester URII avian sarcoma virus (URII-ASV)
sis	Primate	Simian sarcoma virus (SSV)
ski	Avian	SKV 770 avian virus (SKV 770 AV)
src	Avian	Rous sarcoma virus (RSV)
yes	Avian	Yamaguchi avian sarcoma virus (Y-ASV)

to specific factors with inhibitory properties. Moreover, the general or local environmental conditions may critically modify the type of response of particular cells to different hormones or growth factors.

IV. ONCOGENES AND PROTO-ONCOGENES

Recent evidence strongly suggests the existence of important relationships between different types of growth-regulating agents, including several hormones and growth factors, proto-oncogene protein products, and the appearance and/or development of neoplastic diseases.[76,77] Oncogenes have been defined as genes with potential properties for the induction of neoplastic transformation in either natural or experimental conditions.[78] Most oncogenes have been isolated from acute transforming retroviruses, which act as oncogene transducers (Table 3). Acute transforming retroviruses are defective, nonreplicating viruses. These viruses are not infectious agents under natural conditions but have been isolated from different types of animal tumors and are originated from recombination events that may occur between cellular sequences and sequences derived from infectious chronic transforming retroviruses (Figure 2). No transforming sequences (oncogenes) are contained in chronic transforming retroviruses. The viral oncogenes (v-*onc* genes) contained in acute transforming retroviruses are responsible for the oncogenic potential exhibited by these viruses under experimental conditions and are derived from sequences of cellular origin, which are termed proto-oncogenes or c-*onc* genes. Some proto-oncogenes are apparently not present in the genomes of acute transforming retroviruses but have been isolated directly from the cellular genome. Proto-oncogenes have been detected in all vertebrate species studied so far and are also present in the genome of invertebrates.

Apparently, proto-oncogenes are normal constituents of the genome of all multicellular organisms, and at least some types of proto-oncogenes are present in unicellular eukaryotes.

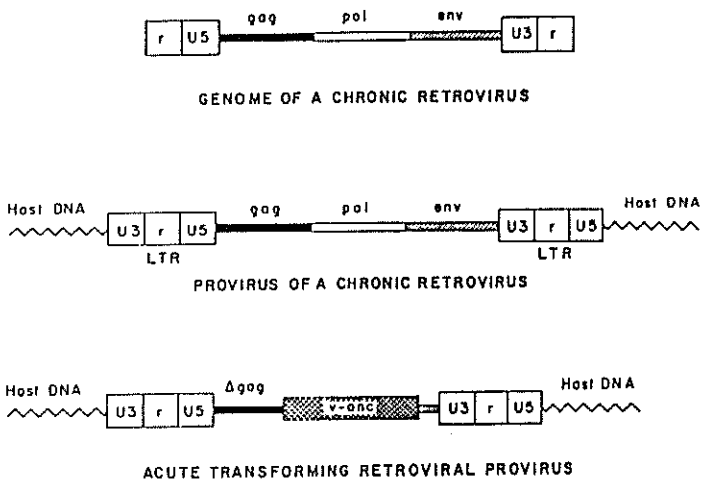

FIGURE 2. Schematic representation of the general structure of chronic and acute transforming retroviruses.

DNA sequences related to several oncogenes (v-*ras*, v-*mos*, and v-*abl*) are present in a variety of fungi and some of them are linked to actin-related sequences.[79] Moreover, DNA sequences related to the oncogene v-*myb* have been detected in primitive living organisms like archaebacteria.[80]

According to the criteria currently used for their definition, the total number of proto-oncogenes is probably limited to about 2 dozens. Most of the known proto-oncogenes have already been assigned to particular chromosomes, and particular regions within chromosomes, of the human karyotype and research work is under way in several laboratories for the chromosomal assignment and chromosomal sublocalization of proto-oncogenes in several nonhuman animal species. A list of the human proto-oncogenes with their respective chromosome assignment and chromosome location appears in Table 4 and is also indicated in the human idiogram represented in Figure 3.

A. Functions of the Proto-Oncogene Protein Products

The normal functions of proto-oncogene protein products are only partially understood but there is evidence that many of these products have important roles in the control mechanisms of metabolic processes as well as in the processes of cell differentiation and cell proliferation, which suggests *a priori* the existence of important interactions between proto-oncogene protein products and the cellular mechanisms of action of hormones and growth factors. The expression of many proto-oncogenes is subjected to developmental and tissue-specific regulation, and different types of hormones and growth factors may participate in these complex regulatory phenomena. Moreover, some proto-oncogene products are structurally and functionally related to either particular types of hormones and growth factors or to their cellular receptors.

B. Proto-Oncogenes and Cancer

Although viral oncogenes are genes with clear oncogenic potential in susceptible hosts, the possible role of proto-oncogenes in neoplastic diseases occurring in humans and other animals is currently a subject of high controversy.[104] Both quantitative and qualitative changes

Table 4
CHROMOSOMAL LOCATION OF HUMAN PROTO-ONCOGENES

Chromosome	Location	Proto-oncogene	Ref.
1	1p11—p13	c-N-*ras*	81, 82
1	1p32	c-B-*lym*-1	83
1	1p34—p36	c-*src*-2	84
1	1p36.1—p36.2	c-*fgr*	85
2	2p23—p24	c-N-*myc*	86
3	3p25	c-*raf*	87
5	5q34	c-*fms*	88
6	6p11—p12	c-K-*ras*-1	82
6	6q22—q24	c-*myb*	89
7	7pter—q22	c-*erb*-B	90
7	7q21—q31	c-*met*	91
8	8q11	c-*mos*	92
8	8q24	c-*myc*	93
9	9q34.1	c-*abl*	94
11	11q23—q24	c-*ets*-1	95
11	11p14.1	c-H-*ras*-1	96
12	12p11.1—p12.1	c-K-*ras*-2	82
12	12pter—q14	c-*int*-1	97
14	14q21—q31	c-*fos*	98
15	15q26.1	c-*fes*	94
17	17q21	c-*neu*	99
17	17q21—q22	c-*erb*-A	100
18	18q21.3	c-*yes*	101
20	20q12—q13	c-*src*-1	84
21	21q22.1—22.3	c-*ets*-2	102
22	22q13.1	c-*sis*	94
X		c-H-*ras*-2	103

of proto-oncogene expression could, in principle, be involved in oncogenic phenomena under either natural or experimental conditions. Four basic types of mechanisms could be responsible for a role of proto-oncogene alterations in carcinogenic processes:

1. Increased transcriptional activity of particular proto-oncogenes at unscheduled sites or times
2. Amplification and overexpression of proto-oncogenes
3. Translocation and/or rearrangement of proto-oncogenes
4. Mutation of proto-oncogenes

From these possible mechanisms, only translocation of particular types of proto-oncogenes is regularly detected in specific hematologic malignant diseases, but such translocations and rearrangements are heterogeneous at the molecular level. Thus, there is no strong evidence in favor of the hypothesis that proto-oncogene alterations constitute a kind of universal, indispensable and critical pathway leading to the origin of cancer, especially to the common forms of human solid tumors.[104] However, proto-oncogenes may be involved, in conjunction with other genes, in the multistage phenomena contributing to the origin and/or development of tumors. A detailed discussion on oncogenes and proto-oncogenes is contained in *Oncogenes*.[78]

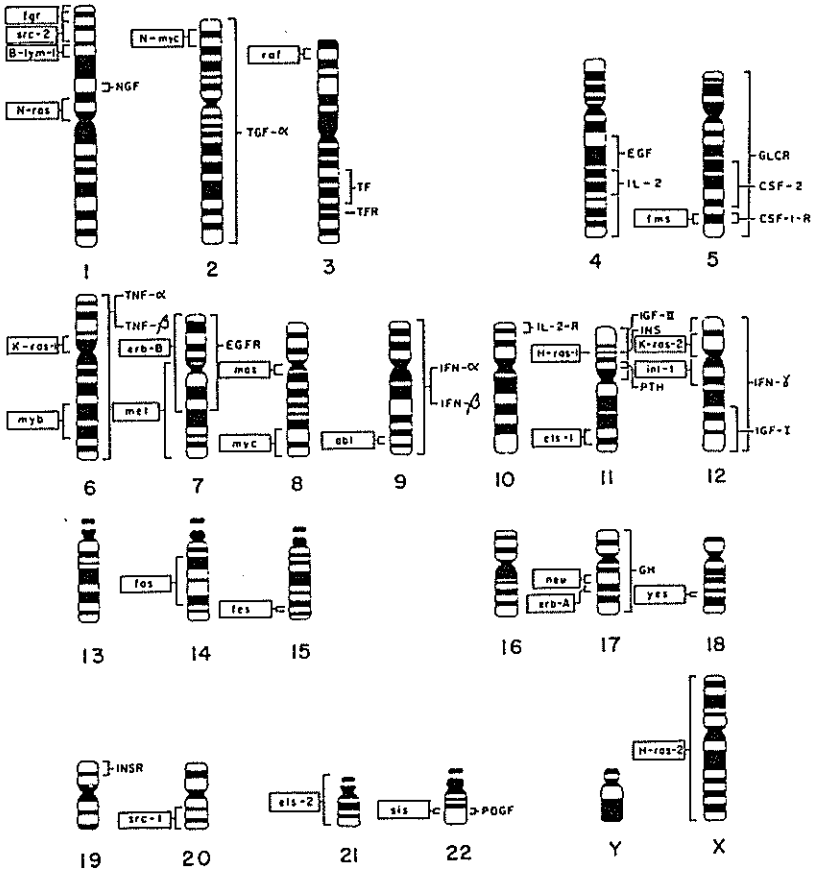

FIGURE 3. Human idiogram with indication of the location of proto-oncogenes (on the left side of each chromosome) and the location of the genes coding for some hormones and growth factors or their cellular receptors (on the right side of each chromosome). TF = transferrin, TFR = transferrin receptor, GLCR = glucocorticoid receptor, EGFR = EGF receptor, INSR = insulin receptor. Other symbols are indicated in the general list of abbreviations.

V. HORMONES AND GROWTH FACTORS IN RELATION TO ONCOGENIC PROCESSES

Hormones and growth factors are the most important environmental factors regulating cellular proliferation and differentiation, two processes that are critically altered in malignant neoplastic diseases. Thus, it is evident by itself that the hormonal environment of the whole organism, as well as the local action of hormones and growth factors, are of great importance for the origin and/or development of neoplastic diseases, not only under experimental conditions,[105-109] but also in human cancer.[110,111] Moreover, hormonal changes occur in specific types of tumors, which may allow the use of hormones, or their respective precursors and/or fragments, as potential tumor markers for the diagnosis and following-up of patients with these tumors.[112,113]

A. Animal Tumors

Animal tumors are constituted by a relatively autonomous population of transformed cells and are characterized, as a general rule, by a reduced dependence on the exogenous supply of hormones and growth factors in comparison with the respective normal tissue. Mouse cells transformed by chemical carcinogens may be less dependent on the exogenous supply of growth factors like EGF.[114] The requirements of mouse 3T3 cells for exogenous insulin and PDGF are diminished or abolished after SV40-induced transformation.[115] Cultured cells infected by acute transforming retroviruses may become independent of the presence of serum. Rat adrenal cells fully transformed by K-MuSV, which transduces the v-K-*ras* oncogene, loss the differential response to growth factors contained in serum.[116] Viral oncogene protein products may act as potent mitogens, inducing a relative autonomy of the transformed cells, which is reflected in their capacity to grow in the absence of exogenous growth factors. For example, the protein product of the v-*src* oncogene of RSV is a potent and complete mitogen which is able to stimulate host cell proliferation without the help of exogenous growth factors.[117,118]

The sensitivity of different tumors to particular types of hormones and growth factors may show great variation according to the type of tumor. Even a given type of tumor may respond in different ways to these agents according to the histological subtype and biological behavior. Human nonHodgkin lymphomas (NHLs), for example, may derive from both T- and B-cell precursors. The neoplastic lymphoid cells from these tumors respond normally (increased thymidine incorporation) to the respective specific interleukin growth factor, TCGF, or BCGF, when the tumors are histologically classified as small T-cell and small B-cell NHLs, respectively. Large-cell NHLs, on the other hand, are quite different tumors both clinically and biologically. Both the T- and B-cell types of large-cell NHLs tend to be rather aggressive tumors and the cells from these tumors do not show a normal response (i.e., do not show increased thymidine incorporation) when they are exposed to the specific interleukin growth factor.[119]

The cellular sensitivity of cells to different types of growth factors (TGF, EGF, PDGF) may show variation even among different subclones of the same cultured cells.[120] Clones from the rat fibroblastoid cell line F2408 that respond most efficiently to one growth factor are also the most sensitive to the other growth factor, and resistant clones are resistant to all of the growth factors examined. Moreover, clones responsive to growth factors are the more susceptible to transformation induced by two acute transforming retroviruses, K-MuSV and the A-MuLV, which transduce the oncogenes v-K-*ras* and v-*abl*, respectively. Complex interactions between different hormones and growth factors may be important for the cloning of human tumor cells.[121]

1. The Autocrine Hypothesis of Oncogenesis

Cells transformed by acute retroviruses transducing different types of oncogenes may become independent from the exogenous supply of growth factors and may produce different types of these factors, especially TGFs.[122-130] Similar factors may be present in human tumor cells.[131,132] The possibility that such factors are involved in the expression of a transformed phenotype is reinforced by the observation that the expression of a growth factor cDNA in a factor-dependent cell line may result in autonomous growth and tumorigenicity.[133] According to the autocrine hypothesis of oncogenesis, transformed cells maintained in culture would produce factors that, upon interaction with the specific receptors on the cell surface, would stimulate their own growth in monolayer or in suspension culture.[134] A similar phenomenon could be responsible for the autonomous growth of malignant tumor cell populations in vivo.

Evidence in favor of the autocrine hypothesis of neoplasia has been obtained, for example, with the study of in vitro growth of human small cell lung cancer (SCLC) cell lines, which

produce and secrete bombesin-like peptides and express high-affinity receptors for these peptides.[135-137] A monoclonal antibody to bombesin binds to the carboxyterminal region of bombesin-like peptides, blocks the binding of the hormone to cellular receptors, and inhibits the clonal growth of SCLC cells in vitro and the growth of SCLC xenografts in vivo.[138] Avian retroviruses containing oncogenes of the v-*src* family render v-*myb*-transformed myeloblasts and, in most cases, v-*myc*-transformed macrophages, independent of exogenous growth factors.[139] In v-*myb*-transformed myeloid cells, this independence is achieved via the induced secretion of a specific growth factor activity.

However, the general validity of the autocrine hypothesis of neoplasia is questionable. There is evidence that transformation induced by viral oncogenes is not necessarily dependent on the endogenous production of growth factors according to an autocrine type of mechanism. For example, A-MuLV is capable of transforming growth factor-dependent, nontumorigenic myeloid cell lines into growth factor-independent, tumorigenic cell lines but the v-*abl*-induced transformation is not associated with an endogenous synthesis of growth factors capable of determining autocrine stimulation.[140-142] A-MuLV-derived transformants of mast cells do not express or secrete detectable levels of the specific growth factor nor is their growth inhibited by an antiserum against the growth factor.[142] Such results, as well as the results obtained in other systems,[143] argue strongly against the general validity of the autocrine hypothesis of neoplastic transformation.

2. Cellular Responses to v-onc Products

Acute transforming retroviruses carrying v-*onc* genes are capable of inducing malignant transformation in a diversity of cells both in vivo and in vitro. However, the production of both a viral oncogene protein and a transforming growth factor may not be sufficient for the maintenance of the transformed phenotype. Flat revertants of K-MuSV-transformed cells, although expressing elevated levels of the v-K-*ras* p21 protein product and producing transforming growth factors, nevertheless express a majority of the properties associated with the nontransformed state.[144] In murine myeloid leukemic myeloblastic cells maintained in suspension cultures, no relationship could be demonstrated between the capacity of a cell line to grow autonomously and its capacity to release autostimulating growth factors.[145] It may be concluded that the expression of a viral oncogene protein product is not necessarily associated with the expression of a transformed phenotype and that transformation induced by viral oncogenes may be independent from the endogenous production of growth factors by an autocrine type of growth stimulation.

The avian acute leukemia retrovirus E26 contains two oncogenes, v-*myb* and v-*ets*, and is capable of inducing malignant transformation of various cell types in vitro (myeloblasts, erythroblasts, fibroblasts) and causes a mixed erythroid/myeloid leukemia in chicks.[146] E26 virus mutants that are temperature-sensitive (ts) for myeloblast transformation have been isolated.[147] At the permissive temperature, ts E26-transformed myeloid cells resemble macrophage precursors and proliferate rapidly, provided the medium contains a specific growth factor (chicken myelomonocytic growth factor). When shifted to the nonpermissive temperature, the cells stop growing, differentiate into macrophage-like cells, and lose the responsiveness to the particular growth factor but secrete the factor or a substance similar to the factor.[147]

Chick heart mesenchymal cells transformed with a c-*myc* proto-oncogene and treated with heparin become proliferative quiescent and assume a normal morphology but are hypersensitive to stimulation with EGF, FGF, and PDGF.[148] These cells, however, do not respond to insulin. On the other hand, the same chicken cells transformed with a v-*ras* oncogene and treated with heparin are refractory to mitogenic stimulation with EGF or FGF but are hypersensitive to insulin or IGFs. It is thus apparent that transformation by different viral oncogenes may result in specific altered responses of the cells to specific types of hormones

and growth factors and that in some cases the v-*onc*-transformed cells become hypersensitive to the stimulation by particular types of hormones and growth factors.

3. Growth Factor Independence and Proto-Oncogene Expression

Progression of tumor cells through stages of increased tumorigenic properties is frequently accompanied by a decreased ability of the cells to differentiate as well as by a change from growth factor dependence to growth factor independence. It may be argued that the growth factor-independent proliferation of malignant cells may be due to the differential expression of proto-oncogenes.[149] In order to test this hypothesis, the differential expression of a series of 18 different proto-oncogenes was examined in a group of cultured murine T-cell lymphomas that were induced following virus inoculation into, or X-irradiation of, C57BL/6 mice.[149] Two classes of T-lymphoma cell lines were studied: growth factor-dependent cells and growth factor-independent cells. Of the 18 proto-oncogenes examined, 5 (c-*myc*, c-*myb*, c-*abl*, c-H-*ras*, and c-K-*ras*) were consistently expressed in all cell lines tested. The results indicated no significant differences in proto-oncogene expression between growth factor-dependent and growth factor-independent cells, which demonstrates that proto-oncogene expression is in itself not sufficient to induce progression of T-lymphoma cells to growth factor independence.[149] The results further suggest that expression of other cellular genes, which may not be proto-oncogenes, is required for the progression of tumors from growth factor dependence to growth factor independence.

B. Plant Tumors

A phenomenon that is something similar to the autonomous, growth-independent proliferation of animal tumor cells is observed in tumors occurring in plants. Dicotyledonous plants may be affected by a neoplastic disease, crown gall, which is induced by the bacterium *Agrobacterium tumefaciens*.[150] The bacteria transfer a specific portion of a large plasmid, Ti, to the plant cell and the transferred DNA may be stably integrated into the plant nuclear DNA, which results in autonomous growth in the absence of the phytohormones, auxin, and cytokinin.[151,152] The tumor morphology locus, *tms*, of the Ti plasmid is transcribed into two mRNA species, and one of these species code for a protein which has significant homology to the adenine binding region of an enzyme (*p*-hydroxybenzoate hydroxylase from *Pseudomonas fluorescens*), suggesting that the protein binds adenine either as substrate or cofactor.[153]

1. Hormones and Oncogene Products in Plant Tumors

The origin of the sequences at the *tms* locus has not been determined but the possibility of an eukaryotic origin exists, and if this origin is confirmed such sequences contributing to the origin of neoplastic diseases in plants and conferring hormone- and growth-factor-independent growth to plant tissues, would be analogous to the oncogenes described in animal cells. At least three genes, or oncogenes, of the Ti plasmid are responsible for the transformed plant cell phenotype: oncogenes 1 and 2, which have roles in auxin independence, and gene 4, which is involved in cytokinin independence. Gene 4 from the T-region of Ti plasmids is responsive for cytokinin effects in crown gall cells and it has been demonstrated that this gene codes for an enzyme of cytokinin biosynthesis.[154] However, there are genetic differences between Ti plasmids from different *A. tumefaciens* strains, and differences in the oncogene complements of the Ti plasmids as well as other Ti oncogenes and undefined host factures may influence their host range characteristics and tumorigenic effects.[155,156] In particular, it is not known if specific plant hormones are involved in the regulation of plant tumor growth and if plant tumors are characterized by hormone independency. Certain plant hormones, like auxin, act very rapidly at the nuclear level in the regulation of transcriptional functions in plant tissues.[157] Phosphotyrosine is more abundant

in normal plant tissues than in normal animal tissues but, in contrast to animal cells where transformation may result in a severalfold increase in phosphotyrosine content, no increase of the modified amino acid is detected in Ti plasmid-transformed crown gall tissue.[158] Further studies are required for a better characterization of the relationships between hormones, growth factors, and putative oncogene products in the tumorigenic processes occurring in plants.

VI. INFLUENCE OF HORMONES AND GROWTH FACTORS ON PROTO-ONCOGENE EXPRESSION

The levels of expression of some proto-oncogenes, proto-oncogene-like sequences, or other cellular genes may show important fluctuation in association with the different stages of the cell cycle and the proliferative stimuli acting on the susceptible cells. In general, proto-oncogenes should be considered, like other cellular genes, as cell cycle-dependent genes.[46,159,160] However, there are exceptions to this general rule and the levels of expression of certain proto-oncogenes, like c-*myc*, are constant throughout the cell cycle.[161,162] However, the level of c-*myc* proteins may show transient variation when resting cells are stimulated by serum.[163] In any case, it is clear that the level of expression of some proto-oncogenes will show variation according to the action of agents that, like hormones and growth factors, are involved in the control of cell proliferation. Moreover, the results of important research work performed during the last few years in several laboratories has demonstrated the existence of close relationships between hormones, growth factors, the cellular receptors for hormones and growth factors, and the protein products of proto-oncogenes. However, it seems obvious that not all the genes (including proto-oncogenes) regulated by hormones and growth factors in a cell cycle-dependent manner are necessarily involved in the control mechanisms of the cell cycle. The biochemical phenomena related to the expression of cell cycle-dependent genes are also not clear. These genes may be fully expressed, or may be even overexpressed, in the presence of cycloheximide,[164] which indicates that protein synthesis is not required for the induction of at least some genes (including proto-oncogenes) regulated during the cell cycle by hormones and growth factors. The molecular mechanisms involved in this induction remain unknown.

The influence of hormones and growth factors on proto-oncogene expression may be conveniently ascertained by measuring the mRNA levels for different types of proto-oncogene protein products after stimulation of quiescent cultured cells with serum (which contains a complex mixture of hormones and growth factors) or known amounts of each one of the purified hormones and growth factors. In general, the agents capable of initiating the first phase of a proliferative response, termed competence, can enhance the expression of specific proto-oncogenes. For example, a strong induction of c-*myc* expression occurs very soon following the activation of T-lymphocytes with concanavalin A, B-lymphocytes with lipopolysaccharide (LPS), and 3T3 fibroblasts in PDGF.[165] A large increase in c-*myc* expression is also induced in human T-lymphocytes stimulated with phytohemagglutinin (PHA).[166] Early increase of c-*myc*-encoded proteins is observed in synchronized mouse 3T3 cells upon stimulation by growth factors contained in serum.[167] Thyrotropic hormone (TSH) and cAMP enhance the expression of c-*myc* and c-*fos* in cultured thyroid cells.[168]

The c-*myc* protein may act as an intracellular competence factor, rendering cells competent to progress into S phase of the cycle. Upon microinjection into nuclei of quiescent mouse fibroblasts (Swiss 3T3 cells), the c-*myc* protein cooperates with platelet-poor plasma in the stimulation of cellular DNA synthesis.[169] Extracellular competence factors include growth factors like PDGF and FGF.

A. Mechanisms of Proto-Oncogene Regulation by Hormones and Growth Factors

The regulation of proto-oncogene expression by hormones or growth factors may involve activation of phosphoinositide turnover and Ca^{2+} mobilization. In Swiss 3T3 cells, PDGF induces Ca^{2+} mobilization and c-*myc* expression, and a similar expression is stimulated by the calcium ionophores, A23187 and ionomycin.[170] These results suggest that Ca^{2+} may serve as a messenger for expression of the c-*myc* proto-oncogene induced by PDGF and other growth factors, which probably involves stimulation of phosphoinositide turnover to activate protein kinase C and to generate inositol trisphosphate, the latter being responsible for Ca^{2+} mobilization from intracellular stores to the cytoplasm.[171]

B. Kinetics of Growth Factor-Regulated Proto-Oncogene Expression

An analysis has been performed with quiescent mouse fibroblasts (NIH/3T3 cells) stimulated after 3 days of serum deprivation with 20% fetal calf serum (FCS), which leads to synchronous cell cycle initiation.[172] The results clearly demonstrated that:

1. The expression of the proto-oncogene c-*fos* increases as early as 5 min after stimulation and reaches at 1 hr levels that are two orders of magnitude higher than those existing before serum stimulation, decreasing to basal levels 1 hr later.
2. Transcripts of the c-*myc* gene are significantly elevated after 30 min of stimulation and are induced more than 20-fold 1 hr after the addition of serum, followed by a slow decrease until reaching the basal level of quiescent cells after about 18 hr.
3. The levels of c-H-*ras* and c-K-*ras* mRNA increase no more than threefold in serum-stimulated cells at any of the time points analyzed.
4. Transcripts of c-*abl* and c-*raf* do not show significant changes in the level of expression.
5. Transcripts of c-*sis* are not detectable in this cell system.

When the action of purified growth factors was studied in the same cellular system the following findings were obtained:[172]

1. Expression of c-*fos* increases markedly 1 hr after stimulation with FGF or PDGF and is then abolished rapidly, whereas in cells treated with EGF the induction of c-*fos* is much less pronounced.
2. The strong initial induction of c-*myc* expression by FCS is reproduced using either FGF, PDGF, or EGF alone but it is much more stable in FCS- or FGF-treated cells than in PDGF- or EGF-stimulated cells, where the concentration of c-*myc* decreases to relatively low levels 2 hr after stimulation.
3. No changes in c-H-*ras* expression are observed after stimulation with FGF, PDGF, or EGF.

C. Mechanisms of Growth Factor-Regulated Proto-Oncogene Expression

The action of the protein synthesis inhibitor cycloheximide in serum-stimulated quiescent NIH/3T3 cells yields interesting results:[172]

1. Cultivation of the quiescent cells in 0.05% FCS for 4 hr in the presence of cycloheximide results in a slightly increased expression of both c-*myc* and c-*fos* mRNA.
2. Cultivation of the quiescent cells for 4 hr with 20% FCS and cycloheximide leads to the accumulation of c-*fos* and c-*myc* mRNA concentrations severalfold higher than the maximum observed in the absence of cycloheximide.

These results suggest that c-*fos* and c-*myc* genes may be modulated through repression by an unstable protein or by autoregulation. The mRNAs of these proto-oncogenes could

become more stable when a protein normally causing their rapid degradation is absent as a consequence of cycloheximide treatment. Results obtained in other studies suggest that c-*myc* expression is regulated mainly at the post-transcriptional level.[173,174] The proto-oncogene is transcribed at a high rate in G_0-arrested hamster lung fibroblasts, although the level of mature c-*myc* mRNA is barely detectable. Stimulation by growth factors is not accompanied by any appreciable change in the transcription rate of c-*myc*, which supports a model of regulation of c-*myc* expression at the level of mRNA degradation.[174]

D. Physiological Significance of Growth Factor-Regulated Proto-Oncogene Expression

The rapid induction of c-*fos* and c-*myc* expression after stimulation by either serum or purified growth factors, in contrast to the slight response or lack of response of other proto-oncogenes, has been detected in an independent study.[175] A transcriptional enhancer element is contained upstream from the c-*fos* proto-oncogene.[176] The results suggest that c-*fos* and c-*myc* may have a primary role in the control of proliferation in at least certain types of cells. In general, expression of c-*fos* and c-*myc* is higher in rapidly proliferating than in quiescent cells.[172] However, persistence of the competent state in cells like mice fibroblasts may be independent from c-*fos* and c-*myc* expression. Cells can remain competent in spite of expressing c-*fos* and c-*myc* genes at very low levels (i.e., at levels similar to those of quiescent cells), which suggests that these proto-oncogene products are not directly involved in maintenance of competence.[177] Apparently, cells rendered competent by growth factors like PDGF do not require high levels of c-*fos* and c-*myc* gene expression to progress through G_1. However, the transient induction of c-*fos* and c-*myc* in quiescent stimulated cells could play an important role in making the cells competent.[177]

The c-*fos* gene would participate, in association with other cellular genes, in the regulatory phenomena related to expression of cellular differentiation.[140] The highest levels of c-*fos* and c-*myc* expression are detected in NIH/3T3 cells transformed by either a long terminal repeat (LTR)-activated c-*raf* proto-oncogene or the McDonough strain of FeSV, which carries the v-*fms* oncogene. However, the levels of both c-*myc* and c-*fos* may be as high or even higher at certain times in serum-stimulated normal cells than in NIH/3T3 transformed cells. Transient accumulation of c-*fos* mRNA following serum stimulation requires a conserved 5′ element and c-*fos* 3′ sequences.[179]

As a general rule, in the NIH/3T3 system there is a correlation between the expression of c-*fos* and c-*myc* proto-oncogenes and cellular proliferative activity.[172] Studies performed in other types of cells or tissues (fetal membranes and placenta, bone marrow, early fetal liver, and differentiated macrophages) suggest a correlation between c-*fos* expression and cell differentiation.[180-182] Rapid increase in c-*fos* expression is observed when PC12 rat pheochromocytoma cells are induced to differentiate by treatment with NGF.[183] This induction is enhanced more than 100-fold in the presence of peripherally active benzodiazepines. Expression of the c-*fos* proto-oncogene and a c-*fos*-related gene is increased in quiescent BALB/c 3T3 mouse fibroblasts upon treatment with purified PDGF.[184] Rapid and early expression of c-*fos* proto-oncogene also occurs when the promyelocytic cell line HL-60 or the monocytic cell line U-937 are induced to differentiation with phorbol ester.[185] Expression of c-*fos* is inducible when quiescent terminally differentiated macrophages are treated with the macrophage-specific growth factor CSF-1, although the kinetics of c-*fos* induction in this system is entirely different from that in growth factor-stimulated fibroblasts, which supports the view that the c-*fos* gene protein product may serve different functions in different cell types.[186] Moreover, rapid induction of c-*fos* is not observed when the HL-60 cell line is induced to differentiation by either calcitriol or retinoic acid,[186] which indicates that c-*fos* induction is not universally related to cell differentiation phenomena.

Growth control may be associated with hormone- and growth factor-dependent cell-cycle-timed proto-oncogene expression. Hypothetically, a relaxed regulation of proto-oncogene expression may contribute to loss of growth control in neoplastic transformation but such

alteration should have some kind of specificity for both the cell type and the proto-oncogene. Although expression of both c-*myc* and c-K-*ras* is dependent upon the cellular growth state, c-*myc*, but not c-K-*ras*, is expressed constitutively in chemically transformed mouse fibroblasts.[187] Expression of c-*myc* is, however, independent of the different phases of the cell cycle in both normal and transformed cells.[161-163]

E. Action of Growth Factors in v-*onc*-Transformed Cells

The growth of oncogene-transformed cells may not be completely autonomous but may depend on the presence of particular growth factors. Fischer rat 3T3 fibroblasts transfected with a c-*myc* gene linked to an SV40 promoter can be induced to grow and form colonies in soft agar by treatment either with EGF alone or with a combination of PDGF and TGF-β.[73] The mechanism involved in this induction, however, may be different, as ascertained by the action of a differentiation-inducing agent like retinoic acid. Colony formation induced by the combined action of PDGF and TGF-β in c-*myc* transformed cells is 100-fold more sensitive to inhibition by retinoic acid than is colony formation induced by treatment of the same cells with EGF.[188]

F. Summary

Expression of certain proto-oncogenes, especially c-*fos* and c-*myc* is closely related to cell proliferation and/or differentiation induced by particular types of growth factors in certain types of cells responsive to these factors. The same or other proto-oncogenes may have a similar role in the responses elicited by different hormones and growth factors in different types of cells and tissues. The possible role of hormones, growth factors and proto-oncogenes in the origin and/or development of malignant diseases is not immediately apparent on the basis of such results. However, it seems likely that hormones, growth factors, and proto-oncogene protein products participate through complex interactions in the multi-stage processes leading to tumorigenesis.

VII. COMMON FUNCTIONS OF HORMONES, GROWTH FACTORS, AND ONCOGENE PROTEIN PRODUCTS

Hormones, growth factors, and oncogene protein products may share some common cellular mechanisms of action, exerting similar or identical functional changes at the cellular level. A particular mRNA species, termed pTR1 RNA, is present in significantly high levels in rat fibroblasts transformed by polyoma virus, RSV, or the EJ mutant human c-H-*ras* oncogene, and the same RNA is rapidly induced by the addition of EGF to the culture medium of rat fibroblasts.[189] Both the growth factor and the oncogene proteins control expression of the corresponding gene at the transcriptional level. pTR1 RNA is not present in serum-stimulated cells and is apparently not a participant of the "normal" or general cellular growth response. The function of the pTR1-derived protein has not been established but the results indicate that both growth factors and oncogene proteins may act by controlling the transciptional activity of similar or identical genes.

Another protein that may be induced by both growth factor(s) and an oncogene protein product is the mammalian heat shock protein 70 (hsp 70). Expression of the hsp 70 gene may be induced by both serum stimulation and the c-*myc* protein.[190,191] Protein hsp 70 could be involved in the control of cell growth, acting during the S phase of the cell cycle. Heat shock proteins usually have a nuclear location, suggesting a role in the regulation of genomic functions. In parasitic protozoa like *Trypanosoma* and *Leishmania*, expression of heat shock genes may be responsible for differentiation processes involving extensive morphological and physiological changes upon transmission of the parasite from the insect vector to the mammalian host, which implicates a marked difference in temperature (from 25°C in the vector to 37°C in the mammalian host).[193]

It is possible that some protein products of proto-oncogenes are involved in the regulation of differentiated functions of the nervous system, including the generation of neurotransmitters. This possibility is suggested by the observation that in neuronal cells (quail embryo neuroretina cultures) the protein product of the v-*src* oncogene, pp60 $^{v\text{-}src}$, can selectively stimulate the activity of the enzyme glutamic acid decarboxylase (GAD), which is responsible for the synthesis of the neurotransmitter gamma-aminobutyric acid (GABA).[193] GAD activity is also stimulated in the same cells by retroviruses carrying the v-*mil* oncogene. The possible physiological significance of these results is suggested by the fact that the c-*src* proto-oncogene is expressed at high levels specifically during organogenesis of neural tissues in humans and other vertebrates.[178,194-197] In both chick neural retina and cerebellum, expression of the c-*src* proto-oncogene occurs in developing neurons at the onset of differentiation, at a stage when cell proliferation ceases.[198,199] In general, expression of the c-*src* gene is associated more with cell differentiation than with cell proliferation.[197] Further studies are required for a better characterization of the respective roles of hormones, growth factors, and proto-oncogene protein products in the regulation of the functional properties of different organs and tissues at different stages of development.

REFERENCES

1. Pimentel, E., Cellular mechanisms of hormone action. I. Transductional events, *Acta Cient. Venez.*, 29, 73, 1978.
2. Pimentel, E., Cellular mechanisms of hormone action. II. Posttransductional events, *Acta Cient. Venez.*, 29, 147, 1978.
3. Gospodarowicz, R. A. and Moran, J. S., Growth factors in mammalian cell culture, *Ann. Rev. Biochem.*, 45, 531, 1976.
4. Golde, D. W., Herschman, H. R., Lusis, A. J., and Groopman, J. E., Growth factors, *Ann. Intern. Med.*, 92, 650, 1980.
5. Gospodarowicz, D., Growth factors and their action in vivo and in vitro, *J. Pathol.*, 141, 201, 1983.
6. Carpenter, G. and Cohen, S., Peptide growth factors, *Trends Biochem. Sci.*, 9, 169, 1984.
7. James, R. and Bradshaw, R. A., Polypeptide growth factors, *Ann. Rev. Biochem.*, 53, 259, 1984.
8. Courty, J., Courtois, Y., and Barritault, D., Propriétés *in vitro* de quelques facteurs de croissance et effets *in vivo*, *Biochimie*, 66, 419, 1984.
9. Heinemann, V. and Jehn, U., Wachstumfaktoren: Eine neue Dimension im Verständnis der Onkogenese, *Klin. Wochenschr.*, 63, 740, 1985.
10. Goustin, A. S., Leof, E. B., Shipley, G. D., and Moses, H. L., Growth factors and cancer, *Cancer Res.*, 46, 1015, 1986.
11. Alderman, E. M., Lobb, R. R., and Fett, J. W., Isolation of tumor-secreted products from human carcinoma cells maintained in a defined protein-free medium, *Proc. Natl. Acad. Sci. U.S.A.*, 82, 5771, 1985.
12. Plouët, J., Courty, J., Olivié, M., Courtois, Y., and Barritault, D., A highly reliable and sensitive assay for the purification of cellular growth factors, *Cell. Mol. Biol.*, 30, 105, 1984.
13. Zabel, B. U., Eddy, R. L., Lalley, P. A., Scott, J., Bell, G. I., and Shows, T. B., Chromosomal locations of the human and mouse genes for precursors of epidermal growth factor and the beta subunit of nerve growth factor, *Proc. Natl. Acad. Sci. U.S.A.*, 82, 469, 1985.
14. Brissenden, J. E., Derynck, R., and Francke, U., Mapping of transforming growth factor alpha gene on human chromosome 2 close to the breakpoint of the Burkitt's lymphoma 7(2;8) variant translocation, *Cancer Res.*, 45, 5593, 1985.
15. Huerre, C., Uzan, G., Grzeschik, K. H., Weil, D., Levin, M., Hors-Cayla, M.-C., Boué, J., Kahn, A., and Junien, C., The structural gene for transferrin (TF) maps to 3q21 → 3qter, *Ann. Genet. (Paris)*, 27, 5, 1984.
16. Rabin, M., McClelland, A., Kühn, L., and Ruddle, F. H., Regional localization of the human transferrin receptor gene to 3q26.2 → ter, *Am. J. Human Genet.*, 37, 1112, 1985.
17. Morton, C. C., Byers, M. G., Naka, H., Bell, G. I., and Shows, T. B., Human genes for insulin-like growth factors I and II and epidermal growth factors are located on 12q 22 → q 24.1, 11p 15, and 4q 25 → q 27, respectively, *Cytogenet. Cell Genet.*, 41, 245, 1986.
18. Seigel, L. J., Harper, M. E., Wong-Staal, F., Gallo, R. C., Nash, W. G., and O'Brien, S. J., Gene for T-cell growth factor: location on human chromosome 4q and feline chromosome B1, *Science*, 223, 175, 1984.

19. Huebner, K., Isobe, M., Croce, C. M., Golde, D. W., Kaufman, S. E., and Gasson, J. C., The human gene encoding GM-CSF is at 5q21-q32, the chromosome region deleted in the 5q- anomaly, *Science*, 230, 1282, 1985.
20. Gehring, U., Segnitz, B., Foellmer, B., and Francke, U., Assignment of the human gene for the glucocorticoid receptor to chromosome 5, *Proc. Natl. Acad. Sci. U.S.A.*, 82, 3751, 1985.
21. Nedwin, G. E., Jarrett-Nedwin, J., Smith, D. H., Naylor, S. L., Sakaguchi, A. Y., Goeddel, D. V., and Gray, P. W., Structure and chromosomal localization of the human lymphotoxin gene, *J. Cell. Biochem.*, 29, 171, 1985.
22. Owerbach, D., Rutter, W. J., Shows, T. B., Gray, P. W., Goeddel, D. V., and Lawn, R. M., Leukocyte and fibroblast interferon genes are located on human chromosome 9, *Proc. Natl. Acad. Sci. U.S.A.*, 78, 3123, 1981.
23. Leonard, W. J., Donlon, T. A., Lebo, R. V., and Greene, W. C., Localization of the gene encoding the human interleukin-2 receptor on chromosome 10, *Science*, 228, 1547, 1985.
24. Chaganti, R. S. K., Germ-line chromosomal localization of genes in chromosome 11p linkage: parathyroid hormone, beta-globin, c-Ha-ras-1, and insulin, *Somat. Cell Mol. Genet.*, 11, 197, 1985.
25. Sagar, A. D., Sehgal, P. B., May, L. T., Inouye, M., Slate, D. L., Shulman, L., and Ruddle, F. H., Interferon-beta-related DNA is dispersed in the human genome, *Science*, 223, 1312, 1984.
26. Owerbach, D., Rutter, W. J., Martial, J. A., Baxter, J. D., and Shows, T. B., Genes for growth hormone, chorionic somatomammotropin, and growth hormone-like gene on chromosome 17 in humans, *Science*, 209, 289, 1980.
27. Yang-Feng, T. L., Francke, U., and Ullrich, A., Gene for human insulin receptor: localization to site on chromosome 19 involved in pre-B-cell leukemia, *Science*, 228, 728, 1985.
28. Pardee, A. B., Dubrow, R., Hamlin, J. L., and Kletzien, R. F., Animal cell cycle, *Ann. Rev. Biochem.*, 47, 715, 1978.
29. Zetterberg, A. and Larsson, O., Kinetic analysis of regulatory events in G_1 leading to proliferation or quiescence of Swiss 3T3 cells, *Proc. Natl. Acad. Sci. U.S.A.*, 82, 5365, 1985.
30. Holley, R. W. and Kiernan, J. A., Control of the initiation of DNA synthesis in 3T3 cells: serum factors, *Proc. Natl. Acad. Sci. U.S.A.*, 71, 2908, 1974.
31. Olashaw, N. E., Harrington, M., and Pledger, W. J., The regulation of the cell cycle by multiple growth factors, *Cell Biol. Int. Rep.*, 7, 489, 1983.
32. Shipley, G. D., Childs, C. B., Volkenant, M. E., and Moses, H. L., Differential effects of epidermal growth factor, transforming growth factor, and insulin on DNA and protein synthesis and morphology in serum-free cultures of AKR-2B cells, *Cancer Res.*, 44, 710, 1984.
33. McKeehan, W. L., Adams, P. S., and Rosser, M. P., Direct mitogenic effects of insulin, epidermal growth factor, glucocorticoid, cholera toxin, unknown pituitary factors and possibly prolactin, but not androgen, on normal rat prostate epithelial cells in serum-free, primary cell culture, *Cancer Res.*, 44, 1998, 1984.
34. Balk, S. D., Morisi, A., Gunther, H. S., Svoboda, M. F., Van Wyk, J. J., Nissley, S. P., and Scanes, C. G., Somatomedins (insulin-like growth factors), but not growth hormone, are mitogenic for chicken heart mesenchymal cells and act synergistically with epidermal growth factor and brain fibroblast growth factor, *Life Sci.*, 35, 335, 1984.
35. O'Keefe, E. J. and Pledger, W. J., A model of cell cycle control: sequential events regulated by growth factors, *Mol. Cell. Endocrinol.*, 31, 167, 1983.
36. Westermark, B. and Heldin, C.-H., Similar action of platelet-derived growth factor and epidermal growth factor in the prereplicative phase of human fibroblasts suggests a common intracellular pathway, *J. Cell. Physiol.*, 124, 43, 1985.
37. Pilsko, A. and Glichrest, B. A., Growth factor responsiveness of cultured human fibroblasts declines with age, *J. Gerontol.*, 38, 513, 1983.
38. Phillips, P. D., Kaji, K., and Cristofalo, V. J., Progressive loss of the proliferative response of senescing WI-38 cells to platelet-derived growth factor, epidermal growth factor, insulin, transferrin, and dexamethasone, *J. Gerontol.*, 39, 11, 1984.
39. Scher, C. D. and Todaro, G. J., Selective growth of human neoplastic cells in medium lacking serum growth factor, *Exp. Cell Res.*, 68, 479, 1972.
40. Metcalf, D., Moore, M. A. S., Sheridan, J. W., and Spitzer, G., Responsiveness of human granulocytic leukemia cell to colony-stimulating factor, *Blood*, 43, 847, 1974.
41. Greenberg, B. R., Hirasuna, J. D., and Woo, L., In vitro response to erythropoietin in erythroblastic transformation of chronic myelogenous leukemia, *Exp. Hematol.*, 8, 52, 1980.
42. Haas, M., Altman, A., Rothenberg, E., Bogart, M. H., and Jones, O. W., Mechanism of T-cell lymphomagenesis: transformation of growth-factor-dependent T-lymphoblastoma cells to growth-factor-independent T-lymphoma cells, *Cancer Res.*, 81, 1742, 1984.
43. Huang, F. L. and Cho-Chung, Y. S., Alteration in gene expression at the onset of hormone-dependent mammary tumor regression, *Cancer Res.*, 43, 2138, 1983.

44. Johnson, H. M. and Torres, B. A., Peptide growth factors PDGF, EGF, and FGF regulate interferon-gamma production, *J. Immunol.*, 134, 2824, 1985.
45. Linzer, D. I. H. and Nathans, D., Growth-related changes in specific mRNAs of cultured mouse cells, *Proc. Natl. Acad. Sci. U.S.A.*, 80, 4271, 1983.
46. Linzer, D. I. H., Lee, S.-J., Ogren, L., Talamantes, F., and Nathans, D., Identification of proliferin mRNA and protein in mouse placenta, *Proc. Natl. Acad. Sci. U.S.A.*, 82, 4356, 1985.
47. Linzer, D. I. H. and Nathans, D., A new member of the prolactin-growth hormone gene family expressed in mouse placenta, *EMBO J.*, 4, 1419, 1985.
48. Heyns, A. du P., Eldor, A., Vlodavsky, I., Kaiser, N., Fridman, R., and Panet, A., The antiproliferative effect of interferon and the mitogenic action of growth factors are independent cell cycle events: studies with vascular smooth muscle cells and endothelial cells, *Exp. Cell Res.*, 161, 297, 1985.
49. Rinehart, C. A., Jr. and Canellakis, E. S., Induction of ornithine decarboxylase activity by insulin and growth factors is mediated by amino acids, *Proc. Natl. Acad. Sci. U.S.A.*, 82, 4365, 1985.
50. Willey, J. C., Laveck, M. A., McClendon, I. A., and Lechner, J. F., Relationship of ornithine decarboxylase activity and cAMP metabolism to proliferation of normal human bronchial epithelial cells, *J. Cell. Physiol.*, 124, 1985.
51. Bravo, R. and Celis, J. E., Gene expression in normal and virally transformed mouse 3T3B and hamster BHK21 cells, *Exp. Cell Res.*, 127, 249, 1980.
52. Levenson, R., Iwata, K., Klagsbrun, M., and Young, D. A., Growth factor- and dexamethasone-induced proteins in Swiss 3T3 cells: relationship to DNA synthesis, *J. Biol. Chem.*, 260, 8056, 1985.
53. Chrysogelos, S., Riley, D. E., Stein, G., and Stein, J., A human histone H4 gene exhibits cell cycle-dependent changes in chromatin structure that correlate with its expression, *Proc. Natl. Acad. Sci. U.S.A.*, 82, 7535, 1985.
54. Lau, L. F. and Nathans, D., Identification of a set of genes expressed during the G_0/G_1 transition of cultured mouse cells, *EMBO J.*, 4, 3145, 1985.
55. Bravo, R., Fey, S. J., Bellatin, J., Larsen, P. M., Arevalo, J., and Celis, J. E., Identification of a nuclear and of a cytoplasmic polypeptide whose relative proportions are sensitive to changes in the rate of cell proliferation, *Exp. Cell Res.*, 136, 311, 1981.
56. Bravo, R. and Celis, J. E., Updated catalogue of HeLa cell proteins: percentages and characteristics of the major cell polypeptides labeled with a mixture of 16 (14C)-labeled amino acids, *Clin. Chem.*, 28, 766, 1982.
57. Miyachi, K., Fritzler, M. J., and Tan, E. M., Autoantibody to a nuclear antigen in proliferating cells, *J. Immunol.*, 121, 2228, 1978.
58. Tan, E. M., Autoantibodies to nuclear antigens: their immunobiology and medicine, *Adv. Immunol.*, 33, 167, 1982.
59. Mathews, M. B., Bernstein, R. M., Franza, B. R., Jr., and Garrels, J. I., Identity of the proliferating cell nuclear antigen and cyclin, *Nature (London)*, 309, 374, 1984.
60. Celis, J. E., Fey, S. J., Larsen, P. M., and Celis, A., Expression of the transformation-sensitive protein "cyclin" in normal human epidermal basal cells and simian virus 40-transformed keratinocytes, *Proc. Natl. Acad. Sci. U.S.A.*, 81, 3128, 1984.
61. Bravo, R. and Graf, T., Synthesis of the nuclear protein cyclin does not correlate directly with transformation in quail embryo fibroblasts, *Exp. Cell Res.*, 156, 450, 1985.
62. Macdonald-Bravo, H. and Bravo, R., Induction of the nuclear protein cyclin in serum-stimulated quiescent 3T3 cells is independent of DNA synthesis, *Exp. Cell Res.*, 156, 455, 1985.
63. Bravo, R. and Macdonald-Bravo, H., Changes in the nuclear distribution of cyclin (PCNA) but not its synthesis depend on DNA replication, *EMBO J.*, 4, 655, 1985.
64. Celis, J. E. and Celis, A., Cell cycle-dependent variations in the distribution of the nuclear protein cyclin (proliferating cell nuclear antigen) in cultured cells: subdivision of S phase, *Proc. Natl. Acad. Sci. U.S.A.*, 82, 3262, 1985.
65. Celis, J. E. and Celis, A., Individual nuclei in polykaryons can control cyclin distribution and DNA synthesis, *EMBO J.*, 4, 1187, 1985.
66. Redding, T. W. and Schally, A. V., Inhibition of cell growth by a hypothalamic peptide, *Proc. Natl. Acad. Sci. U.S.A.*, 79, 7014, 1982.
67. Gaffney, E. V., Tsai, S.-C., Dell'Aquila, M. L., and Lingenfelter, S. E., Production of growth-inhibitory activity in serum-free medium by human monocytic leukemia cells, *Cancer Res.*, 43, 3668, 1983.
68. Levine, A. E., Hamilton, D. A., Yeoman, L. C., Busch, H., and Brattain, M. G., Identification of a tumor inhibitory factor in rat ascites fluid, *Biochem. Biophys. Res. Comm.*, 119, 76, 1984.
69. Levine, A. E., McRae, L. J., Hamilton, D. A., Brattain, D. E., Yeoman, L. C., and Brattain, M. G., Identification of endogenous inhibitory growth factors from a human colon carcinoma cell line, *Cancer Res.*, 45, 2248, 1985.
70. Iwata, K. K., Fryling, C. M., Knott, W. B., and Todaro, G. J., Isolation of tumor cell growth-inhibiting factors from a human rhabdomyosarcoma cell line, *Cancer Res.*, 45, 2689, 1985.

71. Fryling, C. M., Iwata, K. K., Johnson, P. A., Knott, W. B., and Todaro, G. J., Two distinct tumor cell growth-inhibiting factors from a human rhabdomyosarcoma cell line, *Cancer Res.*, 45, 2695, 1985.
72. Aune, T. M., Webb, D. R., and Pierce, C. W., Purification and initial characterization of the lymphokine soluble immune response suppressor, *J. Immunol.*, 131, 2848, 1983.
73. Aune, T. M., Inhibition of soluble immune response suppressor activity by growth factors, *Proc. Natl. Acad. Sci. U.S.A.*, 82, 6240, 1985.
74. Gill, G. N. and Lazar, C. S., Increased phosphotyrosine content and inhibition of proliferation in epidermal growth factor-treated A431 cells, *Nature (London)*, 293, 305, 1981.
75. Roberts, A. B., Anzano, M. A., Wakefield, L. M., Roche, N. S., Stern, D. F., and Sporn, M. B., Type beta transforming growth factor: a bifunctional regulator of cellular growth, *Proc. Natl. Acad. Sci. U.S.A.*, 82, 119, 1985.
76. Heldin, C.-H. and Westermark, B., Growth factors: mechanism of action and relation to oncogenes, *Cell*, 37, 9, 1984.
77. Deuel, T. F. and Huang, J. S., Roles of growth factor activities in oncogenesis, *Blood*, 64, 951, 1984.
78. Pimentel, E., *Oncogenes*, CRC Press, Boca Raton, Fla., 1986.
79. Prakash, K. and Seligy, V. L., Oncogene related sequences in fungi: linkage of some to actin, *Biochem. Biophys. Res. Commun.*, 133, 293, 1985.
80. Perbal, B. and Kohiyama, M., Existence de séquences homologues de l'oncogene V-MYB dans le génome des archaebactéries, *C. R. Acad. Sci. (Paris)*, 300, 177, 1985.
81. Rabin, M., Watson, M., Barker, P. E., Ryan, J., Breg, W. R., and Ruddle, F. H., N-*ras* transforming gene maps to region p11 → p13 on chromosome 1 by in situ hybridization, *Cytogenet. Cell Genet.*, 38, 70, 1984.
82. Popescu, N. C., Amsbaugh, S. C., DiPaolo, J. A., Tronick, S. R., Aaronson, S. A., and Swan, D. C., Chromosomal localization of three human *ras* genes by in situ molecular hybridization, *Somat. Cell Mol. Genet.*, 11, 149, 1985.
83. Morton, C. C., Taub, R., Diamond, A., Lane, M. A., Cooper, G. M., and Leder, P., Mapping of the human *Blym*-1 transforming gene activated in Burkitt lymphomas to chromosome 1, *Science*, 223, 173, 1984.
84. Le Beau, M. M., Westbrook, C. A., Diaz, M. O., and Rowley, J. D., Evidence for two distinct c-*src* loci on human chromosomes 1 and 20, *Nature (London)*, 312, 70, 1984.
85. Tronick, S. R., Popescu, N. C., Cheah, M. S. C., Swan, D. C., Amsbaugh, S. C., Lengel, C. R., DiPaolo, J. A., and Robbins, K. C., Isolation and chromosomal localization of the human *fgr* porotooncogene, a distinct member of the tyrosine kinase gene family, *Proc. Natl. Acad. Sci. U.S.A.*, 82, 6595, 1985.
86. Schwab, M., Varmus, H. E., Bishop, J. M., Grzeschik, K. H., Naylor, S. L., Sakaguchi, A. Y., Brodeur, G., and Trent, J., Chromosome localization in normal cells and neuroblastomas of a gene related to c-*myc*, *Nature (London)*, 308, 288, 1984.
87. Bonner, T., O'Brien, S. J., Nash, W. G., Rapp, U. R., Morton, C. C., and Leder, P., The human homologous of *raf (mil)* oncogene are located on human chromosomes 3 and 4, *Science*, 223, 71, 1984.
88. Groffen, J., Heisterkamp, N., Spurr, N., Dana, S., Wasmuth, J. J., and Stephenson, J. R., Chromosomal localization of the human c-*fms* oncogene, *Nucleic Acids Res.*, 11, 6331, 1983.
89. Harper, M. E., Franchini, G., Love, J., Simon, M. I., Gallo, R. C., and Wong-Staal, F., Chromosomal sublocalization of human c-*myb* and c-*fes* cellular *onc* genes, *Nature (London)*, 304, 169, 1983.
90. Spurr, N. K., Solomon, E., Jansson, M., Sheer, D., Goodfellow, P. N., Bodmer, W. F., and Vennström, B., Chromosomal localisation of the human homologues to the oncogenes *erb* A and B, *EMBO J.*, 3, 159, 1984.
91. Dean, M., Park, M., LeBeau, M. M., Robins, T. S., Diaz, M. O., Rowley, J. D., Blair, D. G., and Vande Woude, G. F., The human *met* oncogene is related to the tyrosine kinase oncogene, *Nature (London)*, 318, 385, 1985.
92. Caubet, J.-F., Mathieu-Mahul, D., Bernheim, A., Larsen, C.-J., and Berger, R., Human proto-oncogene c-*mos* maps to 8q11, *EMBO J.*, 4, 2245, 1985.
93. Neel, B. G., Jhanwar, S. C., Chaganti, R. S. K., and Hayward, W. S., Two human c-*onc* genes are located on the long arm of chromosome 8, *Proc. Natl. Acad. Sci. U.S.A.*, 79, 7842, 1982.
94. Jhanwar, S. C., Neel, B. G., Hayward, W. S., and Chaganti, R. S. K., Localization of the cellular oncogenes ABL, SIS, and FES on human germ line chromosomes, *Cytogenet. Cell Genet.*, 38, 73, 1984.
95. de Taisne, C., Gegonne, A., Stehelin, D., Bernheim, A., and Berger, R., Chromosomal localization of the human protooncogene c-*ets*, *Nature (London)*, 310, 581, 1984.
96. de Martinville, B., Giacalone, J., Shih, C., Weinberg, R. A., and Francke, U., Oncogene from human EJ bladder carcinoma is located on the short arm of chromosome 11, *Science*, 219, 498, 1983.
97. van't Veer, L. J., van Kessel, A. G., van Heerikhuizen, H., van Ooyen, A., and Nusse, R., Molecular cloning and chromosomal assignment of the human homolog of *int*-1, a mouse gene implicated in mammary tumorigenesis, *Mol. Cell. Biol.*, 4, 2532, 1984.

98. Barker, P. E., Rabin, M., Watson, M., Breg, W. R., Ruddle, F. H., and Verma, I. M., Human c-*fos* oncogene mapped within chromosomal region 14q21-q31, *Proc. Natl. Acad. Sci. U.S.A.*, 81, 5826, 1984.
99. Schechter, A. L., Hung, M-C., Vaidyanathan, L., Yang-Feng, T. L., Francke, U., Ullrich, A., and Coussens, L., The *neu* gene: an *erb*B-homologous gene distinct from and unlinked to the gene encoding the EGF receptor, *Science*, 229, 976, 1985.
100. Jhanwar, S. C., Chaganti, R. S. K., and Croce, C. M., Germ-line chromosomal localization of human c-*erb*-A oncogene, *Somat. Cell Mol. Genet.*, 11, 99, 1985.
101. Yoshida, M. C., Sasaki, M., Mise, K., Semba, K., Nishizawa, M., Yamamoto, T., and Toyoshima, K., Regional mapping of the human proto-oncogene c-*yes*-1 to chromosome 18 at band q21.3, *Jpn. J. Cancer Res.*, 76, 559, 1985.
102. Watson, D. K., McWilliams-Smith, M. J., Nunn, M. F., Duesberg, P. H., O'Brien, S. J., and Papas, T. S., The *ets* sequence from the transforming gene of avian erythroblastosis virus, E26, has unique domains on human chromosomes 11 and 21: both loci are transcriptionally active, *Proc. Natl. Acad. Sci. U.S.A.*, 82, 7294, 1985.
103. O'Brien, S. J., Nash, W. G., Goodwin, J. L., Lowy, D. R., and Chang, E. H., Dispersion of the *ras* family of transforming genes to four different chromosomes in man, *Nature (London)*, 302, 839, 1983.
104. Pimentel, E., Oncogenes and human cancer, *Cancer Genet. Cytogenet.*, 14, 347, 1985.
105. Pierpaoli, W., Haran-Ghera, N., Bianchi, E., Mueller, J., Meshorer, A., and Bree, M., Endocrine disorders as contributory factor to neoplasia in SJL/J mice, *J. Natl. Cancer Inst.*, 53, 731, 1974.
106. Pierpaoli, W., Haran-Ghera, N., and Kopp, H. G., Role of host endocrine status in murine leukaemogenesis, *Br. J. Cancer*, 35, 621, 1977.
107. Pierpaoli, W. and Meshorer, A., Host endocrine status mediates onocogenesis: leukemia virus-induced carcinomas and reticulum cell sarcomas in acyclic or normal mice, *Eur. J. Cancer*, 18, 1181, 1982.
108. Mishkin, S. Y., Farber, E., Ho, R. K., Mulay, S., and Mishkin, S., Evidence for the hormone dependency of hepatic hyperplastic nodules: inhibition of malignant transformation after exogenous 17 beta-estradiol and tamoxifen, *Hepatology*, 3, 308, 1983.
109. Lupulescu, A., Glucagon control of carcinogenesis, *Endocrinology*, 113, 527, 1983.
110. Henderson, B. E., Ross, R. K., Pike, M. C., and Casagrande, J. T., Endogenous hormones as a major factor in human cancer, *Cancer Res.*, 42, 3232, 1982.
111. de Waard, F., Hormonal factors in human carcinogenesis, *J. Cancer Res. Clin. Oncol.*, 108, 177, 1984.
112. Pimentel, E., Hormones as tumor markers, *Cancer Detect. Prevent.*, 6, 87, 1983.
113. Pimentel, E., Peptide hormone precursors, subunits and fragments as human tumor markers, *Ann. Clin. Lab. Sci.*, 15, 381, 1985.
114. Moses, H. L. and Robinson, R. A., Growth factors, growth factor receptors, and cell cycle control mechanisms in chemically transformed cells, *Fed. Proc.*, 41, 3008, 1982.
115. Powers, S., Fisher, P. B., and Pollack, R., Analysis of the reduced growth factor dependency of simian virus 40-transformed 3T3 cells, *Mol. Cell. Biol.*, 4, 1572, 1984.
116. Auersperg, N. and Calderwood, G. A., Development of serum independence in Kirsten murine sarcoma virus-infected rat adrenal cells, *Carcinogenesis*, 5, 175, 1984.
117. Durkin, J. P. and Whitfield, J. F., Partial characterization of the mitogenic action of $pp60^{src}$, the oncogenic protein product of the *src* gene of avian sarcoma virus, *J. Cell. Physiol.*, 120, 135, 1984.
118. Durkin, J. P. and Whitfield, J. F., The mitogenic activity of $pp60^{src}$, the oncogenic protein product of the *src* gene of avian sarcoma virus, is independent of external serum growth factors, *Biochem. Biophys. Res. Comm.*, 123, 411, 1984.
119. Ford, R. J., Davis, F., and Ramirez, I., Growth factors for human lymphoid neoplasms, in *Mediators in Cell Growth and Differentiation*, Ford, R. J. and Maizel, A. L., Eds., Raven Press, New York, 1985, 233.
120. Kaplan, P. L. and Ozanne, B., Cellular responsiveness to growth factors correlates with a cell's ability to express the transformed phenotype, *Cell*, 33, 931, 1983.
121. Singletary, S. E., Tomasovic, B., Spitzer, G., Tucker, S. L., Hug, V., and Drewinko, B., Effects and interactions of epidermal growth factor, insulin, hydrocortisone, and estradiol on the cloning of human tumor cells, *Int. J. Cell Cloning*, 3, 407, 1985.
122. De Larco, J. E. and Todaro, G. J., Growth factors from murine sarcoma virus-transformed cells, *Proc. Natl. Acad. Sci. U.S.A.*, 75, 4001, 1978.
123. Kryceve-Martinerie, C., Lawrence, D. A., Crochet, J., Julien, P., and Vigier, P., Cells transformed by Rous sarcoma virus release transforming growth factors, *J. Cell Physiol.*, 113, 365, 1982.
124. Roberts, A. B., Anzano, M. A., Lamb, L. C., Smith, J. M., Frolik, C. A., Marquardt, M., Todaro, G. J., and Sporn, M. B., Isolation from the murine sarcoma cells of novel transforming growth factors potentiated by EGF, *Nature (London)*, 295, 417, 1982.
125. Marquardt, H., Hunkapiller, M. W., Hood, L. E., Twardzik, D. R., De Larco, J. E., Stephenson, J. R., and Todaro, G. J., Transforming growth factors produced by retrovirus-transformed rodent fibroblasts and human melanoma cells: amino acid sequence homology with epidermal growth factor, *Proc. Natl. Acad. Sci. U.S.A.*, 80, 4684, 1983.

126. Anzano, M. A., Roberts, A. B., Smith, J. M., Sporn, M. B., and De Larco, J. E., Sarcoma growth factor from conditioned medium of virally transformed cells is composed of both type alpha and type beta transforming growth factors, *Proc. Natl. Acad. Sci. U.S.A.*, 80, 6264, 1983.
127. Hirai, R., Yamaoka, K., and Mitsui, H., Isolation and purification of a new class of transforming growth factors from an avian sarcoma virus-transformed rat cell line, *Cancer Res.*, 43, 5742, 1983.
128. Yamaoka, K., Hirai, R., Tsugita, A., and Mitsui, H., The purification of an acid- and heat-labile transforming growth factor from an avian sarcoma virus-transformed rat cell line, *J. Cell. Physiol.*, 119, 307, 1984.
129. Massagué, J., Type beta transforming growth factor from feline sarcoma virus-transformed rat cells: isolation and biological properties, *J. Biol. Chem.*, 259, 9756, 1984.
130. Anzano, M. A., Roberts, A. B., De Larco, J. E., Wakefield, L. M., Assoian, R. K., Roche, N. S., Smith, J. M., Lazarus, J. E., and Sporn, M. B., Increased secretion of type beta transforming growth factor accompanies viral transformation of cells, *Mol. Cell. Biol.*, 5, 242, 1985.
131. Hamburger, A. W. and White, C. P., Autocrine growth factors for human tumor clonogenic cells, *Int. J. Cell Cloning*, 3, 399, 1985.
132. Richmond, A., Lawson, D. H., Nixon, D. W., and Chawla, R. K., Characterization of autostimulatory and transforming growth factors from human melanoma cells, *Cancer Res.*, 45, 6390, 1985.
133. Lang, R. A., Metcalf, D., Gough, N. M., Dunn, A. R., and Gonda, T. J., Expression of a hemopoietic growth factor cDNA in a factor-dependent cell line results in autonomous growth and tumorigenicity, *Cell*, 43, 531, 1985.
134. Sporn, M. B. and Todaro, G. J., Autocrine secretion and malignant transformation, *N. Engl. J. Med.*, 303, 878, 1980.
135. Moody, T. W., Russell, E. K., O'Donohue, T. L., Linden, C. D., and Gazdar, A. F., Bombesin-like peptides in small cell lung cancer: biochemical characterization and secretion from a cell line, *Life Sci.*, 32, 487, 1983.
136. Moody, T. W., Carney, D. N., Cuttitta, F., Quattrocchi, K., and Minna, J. D., High affinity receptors for bombesin/GRP-like peptides on human small cell lung cancer, *Life Sci.*, 37, 105, 1985.
137. Miller, Y. E., Growth factors, oncogenes, and lung cancer, *Am. Rev. Respir. Dis.*, 132, 178, 1985.
138. Cuttitta, F., Carney, D. N., Mulshine, J., Moody, T. W., Fedorko, J., Fischler, A., and Minna, J. D., Bombesin-like peptides can function as autocrine growth factors in human small-cell lung cancer, *Nature (London)*, 316, 823, 1985.
139. Adkins, B., Leutz, A., and Graf, T., Autocrine growth induced by *src*-related oncogenes in transformed chicken myeloid cells, *Cell*, 39, 439, 1984.
140. Oliff, A., Agranovsky, O., McKinney, M. D., Murty, V. V. S., and Bauchwitz, R., Friend murine leukemia virus-immortalized myeloid cells are converted into tumorigenic cell lines by Abelson leukemia virus, *Proc. Natl. Acad. Sci. U.S.A.*, 82, 3306, 1985.
141. Cook, W. D., Metcalf, D., Nicola, N. A., Burgess, A. W., and Walker, F., Malignant transformation of a growth factor-dependent myeloid cell line by Abelson virus without evidence of an autocrine mechanism, *Cell*, 41, 677, 1985.
142. Pierce, J. H., Di Fiore, P. P., Aaronson, S. A., Potter, M., Pumphrey, J., Scott, A., and Ihle, J. N., Neoplastic transformation of mast cells by Abelson-MuLV: abrogation of IL-3 dependence by a non-autocrine mechanism, *Cell*, 41, 685, 1985.
143. Rein, A., Keller, J., Schultz, A. M., Holmes, K. L., Medicus, R., and Ihle, J. N., Infection of immune mast cells by Harvey sarcoma virus: immortalization without loss of requirement for interleukin-3, *Mol. Cell. Biol.*, 5, 2257, 1985.
144. Salomon, D. S., Zwiebel, J. A., Noda, M., and Bassin, R. H., Flat revertants derived from Kirsten murine sarcoma virus-transformed cells produce transforming growth factors, *J. Cell. Physiol.*, 121, 22, 1984.
145. Fichelson, S., Heard, J.-M., and Levy, J.-P., The in vitro autocrine secretion of CSFs alone does not account for the longterm growth of murine myeloid leukemic cells in suspension cultures, *J. Cell. Physiol.*, 124, 487, 1985.
146. Moscovici, M. G., Jurdic, P., Samarut, J., Gazzolo, L., Mura, C. V., and Moscovici, C., Characterization of the hemopoietic target cells for the avian leukemia virus E26, *Virology*, 129, 65, 1983.
147. Beug, H., Leutz, A., Kahn, P., and Graf, T., *Ts* mutants of E26 leukemia virus allow transformed myeloblasts, but not erythroblasts or fibroblasts, to differentiate at the nonpermissive temperature, *Cell*, 39, 579, 1984.
148. Balk, S. D., Riley, T. M., Gunther, H. S., and Morisi, A., Heparin-treated, v-*myc*-transformed chicken heart mesenchymal cells assume a normal morphology but are hypersensitive to epidermal growth factor (EGF) and brain fibroblast growth factor (bFGF); cells transformed by the v-Ha-*ras* oncogene are refractory to EGF and bFGF but are hypersensitive to insulin-like growth factors, *Proc. Natl. Acad. Sci. U.S.A.*, 82, 5781, 1985.
149. Mally, M. I., Vogt, M., Swift, S. E., and Haas, M., Oncogene expression in murine splenic T cells and murine T-cell neoplasms, *Virology*, 144, 115, 1985.

150. Smith, E. F. and Townsend, C. O., A plant tumor of bacterial origin, *Science*, 25, 671, 1907.
151. Nester, E. W. and Kosuge, T., Plasmids specifying plant hyperplasias, *Ann. Rev. Microbiol.*, 35: 531, 1981.
152. Bevan, M. W. and Chilton, M.-D., T-DNA of *Agrobacterium* Ti and Ri plasmids, *Ann. Rev. Genet.*, 16, 357, 1982.
153. Klee, H., Montoya, A., Horodyski, F., Lichtenstein, C., Garfinkel, D., Fuller, S., Flores, C., Peschon, J., Nester, E., and Gordon, M., Nucleotide sequence of the *tms* genes of the pTiA6NC octopine Ti plasmid: two gene products involved in plant tumorigenesis, *Proc. Natl. Acad. Sci. U.S.A.*, 81, 1728, 1984.
154. Buchmann, I., Marner, F.-J., Schröder, G., Waffenschmidt, S., and Schröder, J., Tumour genes in plants: T-DNA encoded cytokinin biosynthesis, *EMBO J.*, 4, 853, 1985.
155. Buchholz, W. C. and Thomashow, M. F., Comparison of T-DNA oncogene complements of *Agrobacterium tumefaciens* tumor-inducing plasmids with limited and wide host ranges, *J. Bacteriol.*, 160, 319, 1984.
156. Buchholz, W. C. and Thomashow, M. F., Host range encoded by the *Agrobacterium tumefaciens* tumor-inducing plasmid ptiAg63 can be expanded by modification of its T-DNA oncogene complement, *J. Bacteriol.*, 160, 327, 1984.
157. Hagen, G. and Guilfoyle, T. J., Rapid induction of selective transcription by auxins, *Mol. Cell Biol.*, 5, 1197, 1985.
158. Elliott, D. C. and Geytenbeck, M., Identification of products of protein phosphorylation in T37-transformed cells and comparison with normal cells, *Biochim. Biophys. Acta*, 845, 317, 1985.
159. Calabretta, B., Kaczmarek, L., Mars, W., Ochoa, D., Gibson, C. W., Hirschhorn, R. R., and Baserga, R., Cell-cycle-specific genes differentially expressed in human leukemias, *Proc. Natl. Acad. Sci. U.S.A.*, 82, 4463, 1985.
160. Kaczmarek, L., Calabretta, B., and Baserga, R., Expression of cell-cycle-dependent genes in phytohemagglutinin-stimulated human lymphocytes, *Proc. Natl. Acad. Sci. U.S.A.*, 82, 5375, 1985.
161. Thompson, C. B., Challoner, P. B., Neiman, P. E., and Groudine, M., Levels of c-*myc* oncogene mRNA are invariant throughout the cell cycle, *Nature (London)*, 314, 363, 1985.
162. Hann, S. R., Thompson, C. B., and Eisenman, R. N., c-*myc* oncogene protein synthesis is independent of the cell cycle in human and avian cells, *Nature (London)*, 314, 366, 1985.
163. Eisenman, R. N. and Hann, S. R., Proteins expressed by the c-*myc* oncogene in lymphomas of human and avian origin, *Proc. R. Soc. London Ser. B*, 226, 73, 1985.
164. Rittling, S. R., Gibson, C. W., Ferrari, S., and Baserga, R., The effect of cycloheximide on the expression of cell cycle dependent genes, *Biochem. Biophys. Res. Comm.*, 132, 327, 1985.
165. Kelly, K., Cochran, B. H., Stiles, C. D., and Leder, P., Cell-specific regulation of the c-*myc* gene by lymphocyte mitogens and platelet-derived growth factor, *Cell*, 35, 603, 1983.
166. Persson, H., Hennighausen, L., Taub, R., De Grado, W., and Leder, P., Antibodies to human c-*myc* oncogene product: evidence of an evolutionarily conserved protein induced during cell proliferation, *Science*, 225, 687, 1984.
167. Persson, H., Gray, H. E., and Godeau, F., Growth-dependent synthesis of c-*myc*-encoded proteins: early stimulation by serum factors in synchronized mouse 3T3 cells, *Mol. Cell. Biol.*, 5, 2903, 1985.
168. Tramontano, D., Chin, W. W., Moses, A. C., and Ingbar, S. H., Thyrotropi and dibutyryl cyclic AMP increase levels of c-myc and c-fos MRNAs in cultured rat thyroid cells, *J. Biol. Chem.*, 261, 3919, 1986.
169. Kaczmarek, L., Hyland, J., Watt, R., Rosenberg, M., and Baserga, R., Microinjected c-*myc* as a competence factor, *Science*, 228, 1313, 1985.
170. Tsuda, T., Kaibuchi, K., West, B., and Takai, Y., Involvement of Ca^{2+} in platelet-derived growth factor-induced expression of c-*myc* oncogene in Swiss 3T3 fibroblasts, *FEBS Lett.*, 187, 43, 1985.
171. Kaibuchi, K., Tsuda, T., Kikuchi, A., Tanimoto, T., Yamashita, T., and Takai, Y., Possible involvement of protein kinase C and calcium ion in growth factor-induced expression of c-*myc* oncogene in Swiss 3T3 fibroblasts, *J. Biol. Chem.*, 261, 1187, 1986.
172. Müller, R., Bravo, R., Burckhardt, J., and Curran, T., Induction of c-*fos* gene and protein by growth factors precedes activation of c-*myc*, *Nature (London)*, 312, 716, 1984.
173. Dani, C., Blanchard, J. M., Piechaczyk, M., El Sabouty, S., Marty, L., and Jeanteur, P., Extreme instability of *myc* mRNA in normal and transformed human cells, *Proc. Natl. Acad. Sci. U.S.A.*, 81, 7046, 1984.
174. Blanchard, J.-M., Piechaczyk, M., Dani, C., Chambard, J.-C., Franchi, A., Pouyssegur, J., and Jeanteur, P., c-*myc* gene is transcribed at high rate in G_0-arrested fibroblasts and is post-transcriptionally regulated in response to growth factors, *Nature (London)*, 317, 443, 1985.
175. Greenberg, M. E. and Ziff, E. B., Stimulation of 3T3 cells induces transcription of the c-*fos* proto-oncogene, *Nature (London)*, 311, 433, 1984.
176. Deschamps, J., Meijlink, F., and Verma, I. M., Identification of a transcriptional enhancer element upstream from protooncogene *fos*, *Science*, 230, 1174, 1985.

177. **Bravo, R., Burckhardt, J., and Muller, R.,** Persistence of the competent state in mouse fibroblasts is independent of c-*fos* and c-*myc* expression, *Exp. Cell Res.*, 160, 540, 1985.
178. **Ruther, U., Wagner, E., and Muller, R.,** Analysis of the differentiation-promoting potential of inducible c-*fos* genes introduced into embryonal carcinoma cells, *EMBO J.*, 4, 1775, 1985.
179. **Treisman, R.,** Transient accumulation of c-*fos* RNA following serum stimulation requires a conserved 5′ element and c-*fos* 3′ sequences, *Cell*, 42, 889, 1985.
180. **Muller, R., Tremblay, J. M., Adamson, E. D., and Verma, I. M.,** Tissue and cell type-specific expression of two human c-*onc* genes, *Nature (London)*, 304, 454, 1983.
181. **Muller, R., Muller, D., and Guilbert, L.,** Differential expression of c-*fos* in hematopoietic cells: correlation with differentiation of monomyelocytic cells, *in vitro*, *EMBO J.*, 3, 1887, 1984.
182. **Gonda, T. J. and Metcalf, D.,** Expression of *myb*, *myc* and *fos* proto-oncogenes during the differentiation of a murine myeloid leukaemia, *Nature (London)*, 310, 249, 1984.
183. **Curran, T. and Morgan, J. I.,** Superinduction of c-*fos* by nerve growth factor in the presence of peripherally active benzodiazepines, *Science*, 229, 1265, 1985.
184. **Cochran, B. H., Zullo, J., Verma, I. M., and Stiles, C. D.,** Expression of the c-*fos* gene and of an *fos*-related gene is stimulated by platelet-derived growth factor, *Science*, 226, 1080, 1984.
185. **Mitchell, R. L., Zokas, L., Schreiber, R. D., and Verma, I. M.,** Rapid induction of proto-oncogene *fos* during human monocytic differentiation, *Cell*, 40, 209, 1985.
186. **Muller, R., Curran, T., Müller, D., and Guilbert, L.,** Induction of c-*fos* during myelomonocytic differentiation and macrophage proliferation, *Nature (London)*, 314, 546, 1985.
187. **Todaro, G. J., De Larco, J. E., and Cohen, S.,** Transformation by murine and feline sarcoma viruses specifically blocks binding of epidermal growth factor to cells, *Nature (London)* 264, 26, 1976.
188. **Usui, T., Moriyama, N., Ishibe, T., and Nakatsu, H.,** Loss of epidermal growth factor receptor on the renal neoplasm induced in vivo with xenotropic pseudotype Kirsten murine sarcoma virsus, *Biochem. Biophys. Res. Comm.*, 120, 879, 1984.
189. **Robinson, R. A., Branum, E. L., Volkenant, M. E., and Moses, H. L.,** Cell cycle variation in ^{125}I-labeled epidermal growth factor binding in chemically transformed cells, *Cancer Res.*, 42, 2633, 1982.
190. **Wakshull, E., Kraemer, P. M., and Wharton, W.,** Multistep change in epidermal growth factor receptors during spontaneous neoplastic progression in Chinese hamster embryo fibroblasts, *Cancer Res.*, 45, 2070, 1985.
191. **Chua, C. C., Gelman, D. E., Schreiber, A. B., and Ladda, R. L.,** Nonfunctional epidermal growth factor receptor in cells transformed by Kirsten sarcoma virus, *Biochem. Biophys. Res. Comm.*, 118, 538, 1984.
192. **LaX, I., Kris, R., Sasson, I. Ullrich, A., Hayman, M. J., Beug, H., and Schlessinger, J.,** Activation of c-*erb*-B in avian leukosis virus-induced erythroblastosis leads to the expression of a truncated EGF receptor kinase, *EMBO J.*, 4, 3179, 1985.
193. **Bodine, P. V. and Tupper, J. T.,** Calmodulin antagonists decrease binding of epidermal growth factor to transformed, but not to normal human fibroblasts, *Biochem. J.*, 218, 629, 1984.
194. **Cotton, P. C. and Brugge, J. S.,** Neural tissues express high levels of the cellular *src* gene product pp60$^{c\text{-}src}$, *Mol. Cell. Biol.*, 3, 1157, 1983.
195. **Jacobs, C. and Rübsamen, H.,** Expression of pp60$^{c\text{-}src}$ protein kinase in adult and fetal human tissue: high activities in some sarcomas and mammary carcinomas, *Cancer Res.*, 43, 1696, 1983.
196. **Levy, B. T., Sorge, L. K., Meymandi, A., and Maness, P. F.,** pp60$^{c\text{-}src}$ kinase is in chick and human embryonic tissues, *Dev. Biol.*, 104, 9, 1984.
197. **Schartl, M. and Barnekow, A.,** Differential expression of the cellular *src* gene during vertebrate development, *Dev. Biol.*, 105, 415, 1984.
198. **Sorge, L. K., Levy, B. T., and Maness, P. F.,** pp60$^{c\text{-}src}$ is developmentally regulated in the neural retina, *Cell*, 36, 249, 1984.
199. **Fults, D. W., Towle, A. C., Lauder, J. M., and Maness, P. F.,** pp60$^{c\text{-}src}$ in the developing cerebellum, *Mol. Cell. Biol.*, 5, 27, 1985.
200. **Webb, A. C., Collins, K. L., Auron, P. E., Eddy, R. L., Nakai, H., Byers, M. G., Haley, L. L., Henry, W. M., and Shows, T. B.,** Interleukin-1 gene (IL1) assigned to long arm of human chromosome 2, *Lymphokine Res.*, 5, 77, 1986.
201. **Rashidbaigi, A., Langer, J. A., Jung, V., Jones, C., Morse, H. G., Tischfield, J. A., Trill, J. J., Kung, H., and Pestka, S.,** The gene for the human immune interferon receptor is located on chromosome 6, *Proc. Natl. Acad. Sci. U.S.A.*, 83, 384, 1986.
202. **Betsholtz, C., Johnsson, A., Heldin, C. H., Westermark, B., Lind, P., Urdea, M. S., Eddy, R., Shows, T. B., Philpott, K., Mellor, A. L., Knott, T. J., and Scott, J.,** cDNA sequence and chromosomal localization of human platelet-derived growth factor A-chain and its expression in tumour cell lines, *Nature (London)*, 320, 695, 1986.
203. **Fujii, D., Brissenden, J. E., Derynck, R., and Francke, U.,** Transforming growth factor beta gene maps to human chromosome 19 long arm and to mouse chromosome 7, *Somat. Cell Mol. Genet.*, 12, 281, 1986.

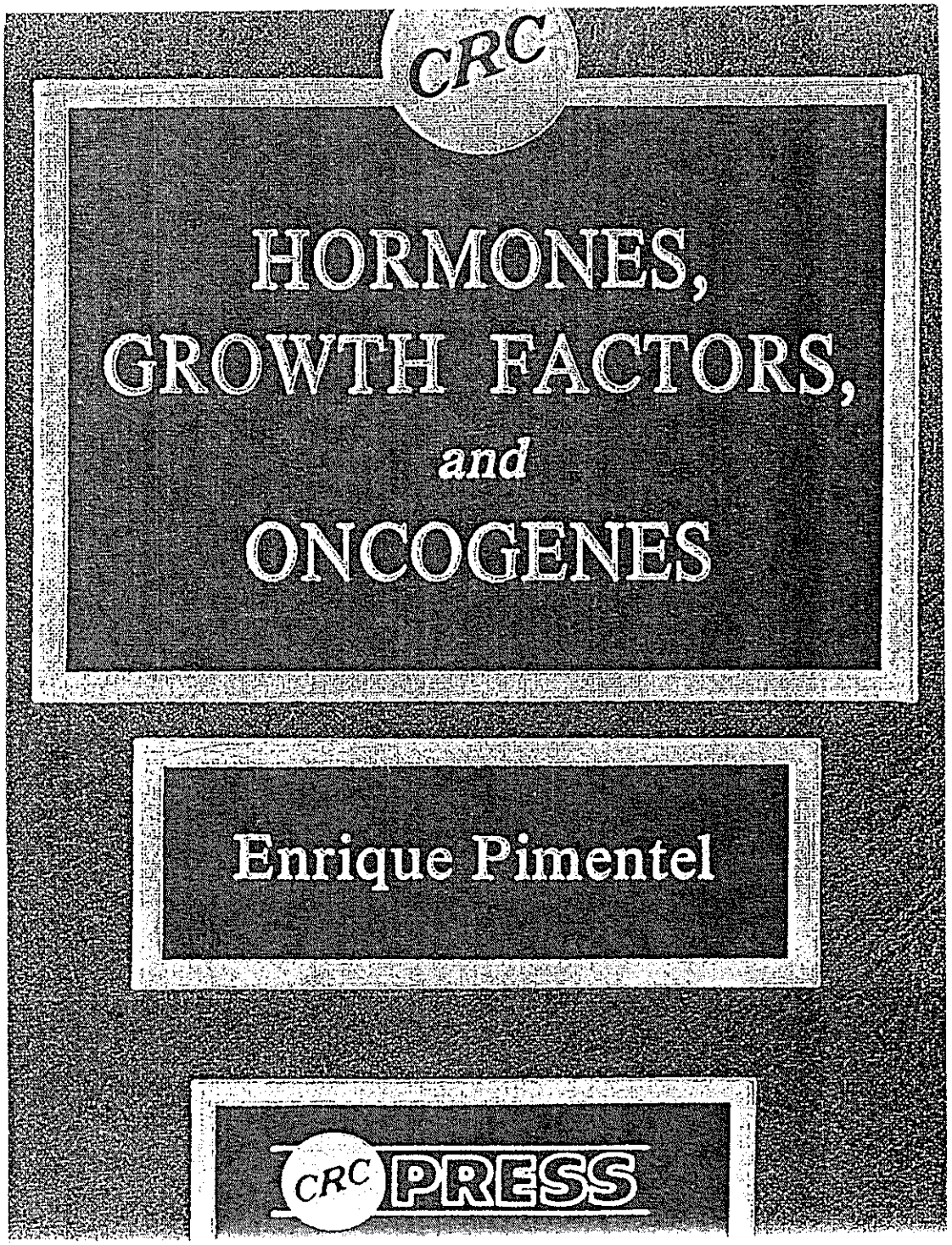

Experimental Cell Biology
Editors: J.R. Rüttner, Zürich; G.V. Sherbet, Newcastle upon Tyne; H. Ramseier, Zürich; L. Helson, New York, N.Y.

Reprint
Publisher: S. Karger AG, Basel
Printed in Switzerland

Expl Cell Biol. *55:* 225–236 (1987)

Differences in Growth Factor Sensitivity between Primary and Transformed Murine Cell Cultures Revealed by BrdU/Hoechst Flow Cytometry

M. Kubbies[a], *H. Hoehn*[a], *P.S. Rabinovitch*[b]

[a] Department of Human Genetics, University of Würzburg, FRG;
[b] Department of Pathology, University of Washington, Seattle, Wash., USA

Key Words. Growth factors · Epidermal growth factor · EGF · Insulin · Cell culture · Spontaneous transformation · Flow cytometry · Bromodeoxyuridine · BrdU

Abstract. Spontaneous cell transformation is a common feature of all murine cell cultures grown in vitro for extended periods of time. During early passages, these cultures show either progressively reduced growth or complete cessation of growth; after such a 'crisis' they display increasing growth rates and unlimited lifespan. Here we use a novel bromodeoxyuridine/Hoechst flow-cytometric technique to examine the growth response of diploid and transformed cells of the murine species *Micromys minutus* under a variety of growth conditions. After spontaneous transformation, growth factor exposure results in increased G0/G1 cell recruitment and higher growth rates than shown by the nontransformed diploid cell fraction. Despite clonal heterogeneity, this difference is seen at all fetal calf serum (FCS) concentrations, although it is most pronounced with low serum. Epidermal growth factor and insulin are shown to act synergistically and promote growth equal to exposures of transformed cultures to 10% FCS. The observed differences in growth factor response between diploid and aneuploid cells could explain the reported lack of a classical growth crisis in growth factor-supplemented media during the spontaneous in vitro transformation of primary murine cell cultures.

Introduction

In contrast to primary cell cultures of human origin, cultures established from murine tissues undergo a growth crisis within less than 10 passages after initiation. Those cells that resume growth after the crisis stage display chromosomal changes, phenotypic alterations and the capacity for unlimited proliferation. This conversion is known as spontaneous in vitro transformation [6, 13, 17, 20]. When murine primary cultures are propagated in the presence of certain growth factors in addition to serum, the conversion

of the primary cell strain to the established cell line has been shown to occur without a recognizable growth crisis [11]. Although such growth factor supplemented cultures lack the characteristic growth crisis, their primary diploid cell component is replaced by aneuploid populations that display phenotypic and growth-kinetic features of established cell lines [11]. The kinetics of the transition from the original diploid to the entirely aneuploid state of these cultures does not speak in favor of a large-scale conversion of diploid to aneuploid cells, as originally postulated by Todardo and Green [20]. Rather, the demise of the diploid population could be due either to gradual senescence or to dilution of the diploid cell fraction by transformed cells. In order to distinguish between these two possibilities, we employed a novel and highly sensitive cytokinetic assay, bromodeoxyuridine (BrdU)-Hoechst flow cytometry [8–11, 15]. The present report confirms that this technique is uniquely suited to monitor cell activation and cell cycle progression in response to mitogenic stimuli using serum-free and hormone-supplemented media [1–3, 21].

Material and Methods

Primary Cell Cultures

Lung and kidney tissue of newborn harvest mice *(Micromys minutus)* was minced and washed three times in minimal essential medium (MEM) and 20 m*M* Hepes, pH 7.3. Lung pieces were explanted into 25-cm² Nunc tissue culture grade plastic flasks. Minced kidney was incubated in a 0.25% trypsin solution (Gibco; 1:250) for 15 min at 37 °C. Seedings of trypsinized cells were used for further subculturing. Parallel cultures were started from lung- and kidney-derived cells in supplemented medium. All cultures were incubated at 37 °C and 5% CO_2 in humidified incubators and fed at 3- to 4-day intervals. A 50:50 mixture of commercial HAM F12 medium and Dulbecco's MEM was used as basic formula (HD medium). Clonal cultures were derived via dilute plating and isolation by plastic cloning cylinders.

BrdU/Hoechst Cell Kinetic Assay

Under low serum conditions [0.01 and 0.1% fetal calf serum (FCS)], 2×10^5 cells were plated into Nunc tissue culture flasks. After 3 days these serum-deprived cultures were washed once with phosphate-buffered saline (PBS). Growth was stimulated by adding various amounts of FCS, the desired growth hormones, 5.0×10^{-5} *M* BrdU and equimolar concentrations of deoxycytidine. Cells were detached in the dark by trypsinisation and pelleted at 400 *g* for 10 min at room temperature. The pellet was resuspended in freezing medium [MEM, 10% FCS, 10% dimethyl sulfoxide (DMSO)] and stored at −20 °C. For flow-cytometric analysis, the frozen samples were thawed in cold water, centrifuged for 10 min at 400 *g* and stained with 1.2 µg/ml Hoechst 33258 in a detergent lysis buffer (see below) for 15 min at 4 °C. Thereafter, ethidium bromide was added at a final concentration of 1.5 µg/ml for 15 min. Stained aliquots of $3–10 \times 10^4$ cells were analyzed. Flow-cytometric analysis was done using an ICP 22 flow cytometer (Ortho Diagnostic Systems, Westwood, Mass., USA) and excitation using UG1 and BG35 glass filters (Schott, Mainz, FRG). The emitted fluorescence was collected using K45 and K65 bandpass filters (Balzers, FRG). Data aquisition and data analysis was by software as previously described [8–10, 15].

Conventional Hoechst Flow Cytometry

Murine cells were stained together with chicken red blood cells as DNA content reference. The staining buffer contained 100 m*M* Tris 7.4, 154 m*M* NaCl, 1 m*M* $CaCl_2$, 0.5 m*M* $MgCl_2$, 0.1% Non-idet P40, 0.2% bovine serum albumin (BSA) and 2 µg/ml Hoechst 33258. Staining was for 1 h at 4 °C. Flow-cytometric analysis and gaussian curve fitting was as described [9].

Results

The BrdU/Hoechst assay distinguishes between cycling and noncycling cells and resolves cell cycle maturity states throughout

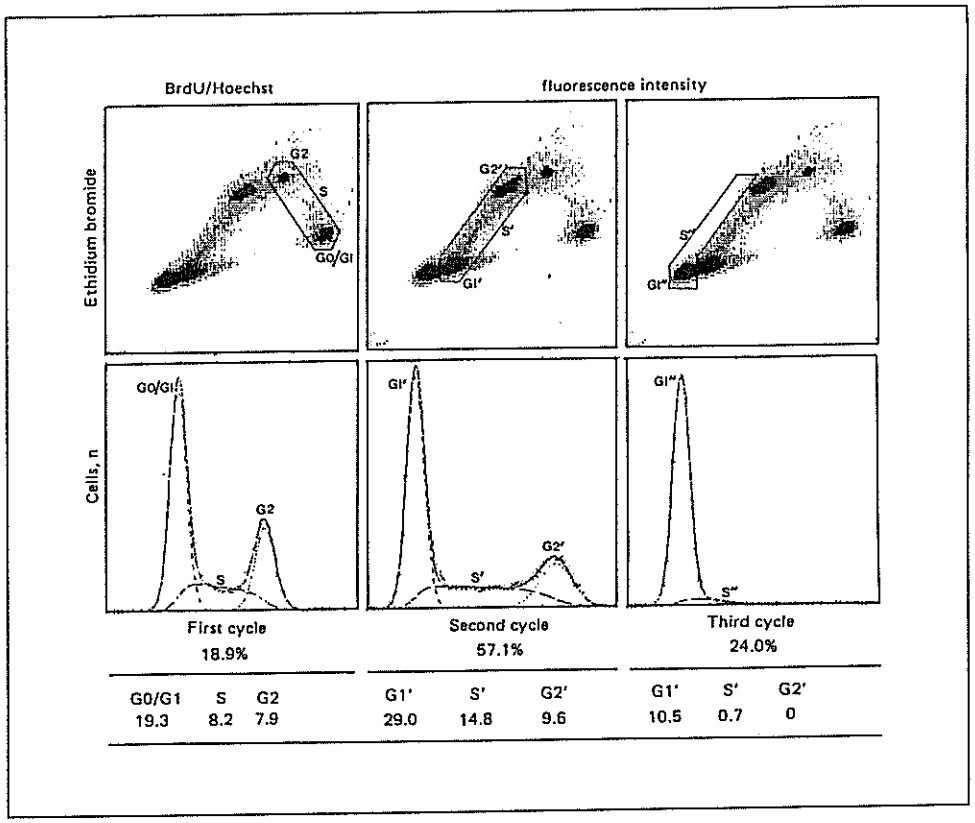

Fig. 1. Cell cycle distribution of spontaneously transformed *M. minutus* cells after a 42-hour exposure to 10 ng/ml epidermal growth factor. The one-parameter histograms (bottom row) represent rotated X axis (first cell cycle G0/G1, S and G2) and rotated Y axis projections (second G1′, S′ and G2′ and third G1″, S″ and G2″ cell cycle) of the bivariate dot plot data. Conventional curve fitting was used to obtain the quantitative cell cycle distribution data which are corrected for the number of divisions (see text).

three successive cycles after cell activation. Figure 1 shows representative ethidium bromide-BrdU/Hoechst bivariate flow-cytometric analyses. The figure depicts the distribution of fluorescence signals of spontaneously transformed murine cells at 42 h after serum stimulation of a previously serum-deprived culture. Each cell fraction belonging to the first, second and third cell cycle is identified by a separate region of the bivariate plot. Replicating cells incorporate BrdU, and the unifilarily substituted chromatin quenches the fluorescence of the Hoechst dye 33258 to 60–70% of the original fluorescence intensity [8, 9]. The quench effect during the second round of replication is less than that of

the first round. This difference in quenching efficiency by uni- and bifilarily substituted chromatin explains the opposite directions of the first versus the second and third cell cycle axes [9]. At the 42-hour timepoint after cell activation, a number of cells have entered the third cycle (G1″ phase; fig. 1, rightmost panel). The culture therefore consists of three kinetically distinct G1-phase populations: cells which have not replicated at all (G0/G1), those which have undergone one (G1′) and those which have undergone two (G1″) rounds of cell division. The bottom row of figure 1 shows the rotated projections of the framed cell cycle regions onto the ethidium bromide axis. These projections illustrate how the proportions of cells in the G1, S and G2 compartments of the respective cycles are analyzed by conventional curve fitting. Of the total of 56,464 cells analyzed in this example, 18.9% are in the first, 57.1 in the second and 24.0% in the third cell cycle. It is most useful to describe the cell cycle fractions as percentages of the behavior of the original cells in culture; there are two daughter cells for each original cell which progressed to the second cycle and 4 for each in the third cycle. Normalization by the factors of 2 and 4 is routinely applied on this account. Most of the S phase cells in the harvest shown in figure 1 are in the second cycle (14.8% of the original cells). The noncycling cell fraction (G0/G1 phase) amounts to 19.3% of the original population.

Figure 2 illustrates the application of this technique to the assessment of the growth response of spontaneously transformed murine cells exposed to specific growth factor supplements. In a different display than in figure 1, the bottom panels of figure 2 show projections of the bivariate fluorescence distributions of the entire population onto the Hoechst axis. This type of projection facilitates the visual recognition of differences in the respective peak amplitudes of each cell cycle fraction. The quantitative assessment of individual cell cycle fractions, however, utilizes the rotated EB axis projections (cf. fig. 1).

The data displayed in figure 2 are derived from cell cultures that were serum-deprived for three days and stimulated by 42-hour continuous exposures to the indicated growth factor supplements. Insulin and epidermal growth factor (EGF) supplementation alone yield rather similar growth responses, although EGF is slightly more effective as shown by the quantitative data: 37.6, 50.7 and 11.7% of the EGF-supplemented cells are in the first, second and third cell cycle, whereas the corresponding distributions of the insulin-supplemented culture are 46.0% in the first, 42.8 in the second and 11.2% in the third cell cycle. The combined application of EGF and insulin, however, clearly is more effective than either factor alone (fig. 2, rightmost panel): only 5% of the total population remain in the noncycling compartment (G0/G1 phase), and the majority of cells has entered the third cycle G1″, S″ and G2″ phases); in addition, 3% of the original population have even reached the G1 phase of the fourth cell cycle (denoted G1‴).

Table I summarizes the results of a series of such 42-hour stimulation experiments carried out with various concentrations and combinations of insulin and EGF. The exposure to both insulin and EGF at optimum concentrations yields a growth pattern that is equivalent to activation by 10% FCS alone. If serum and growth factors are combined, growth is even better; this is evidenced by the nearly complete recruitment of G0/G1

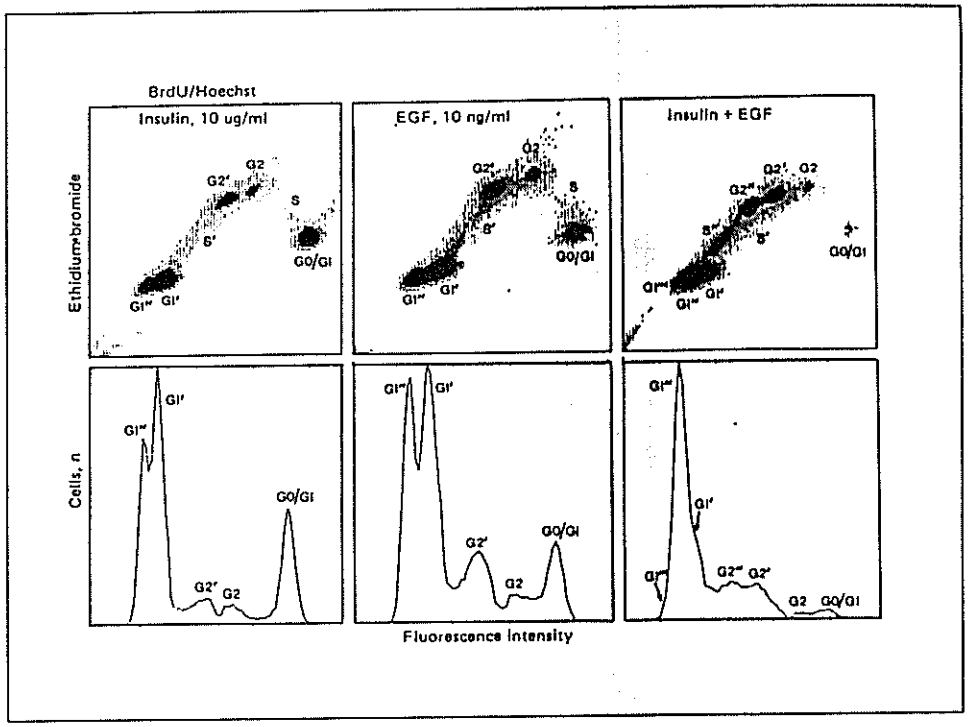

Fig. 2. Cell activation and cell cycle effects of epidermal growth factor (EGF) and insulin visualized by the BrdU/Hoechst assay. The bivariate dot plot panels show the cell cycle distribution recorded at 42 h after stimulation of a spontaneously transformed, aneuploid lung derived culture. Bottom row: X axis projection of the ungated Hoechst fluorescence dot plot pattern showing differences in peak amplitudes as a measure of cell cycle distribution.

phase cells, and by the sizeable fraction of cells that have entered the fourth cell cycle (bottom line of table I).

Analogous titration experiments were carried out using various concentrations and combinations of three additional growth factors, hydrocortisone, transferrin and triiodothyronine (data not shown). By itself, none of these factors was as effective as either insulin or EGF. However, optimal growth was achieved if insulin and EGF were combined with these three factors at the following concentrations: 5×10^{-8} *M* hydrocortisone, 5 µg/ml transferrin and 1×10^{-10} *M* triiodothyronine. A combination of all 5 factors together with 10% FCS was used in our cultures that lacked a classical growth crisis during the transition from the primary culture to the established cell line [11].

Figure 3 shows the comparison of the growth response of the original diploid cell fraction to that of the spontaneously trans-

Table I. Titration of EGF and insulin response and their synergistic effects by the BrdU/Hoechst EB assay at 42 h after stimulation of spontaneously transformed murine cell cultures

Growth factor	Concentration	Percent cells/cycle					Percent increase in cell numbers
		G0/G1	1st	2nd	3rd	4th	
Insulin	0.1 µg/ml	77.6	83.6	15.6	0.8	–	118.0
	1.0 µg/ml	53.5	63.3	33.5	3.2	–	142.9
	10.0 µg/ml	33.6	46.0	42.8	11.2	–	176.4
	50.0 µg/ml	41.0	56.9	38.1	5.0	–	153.0
	100.0 µg/ml	50.3	65.0	32.2	2.8	–	140.5
EGF	0.1 ng/ml	33.7	52.0	40.8	7.2	–	162.3
	1.0 ng/ml	22.4	38.2	49.6	12.2	–	186.2
	10.0 ng/ml	19.3	37.6	50.7	11.7	–	185.7
	50.0 ng/ml	20.4	35.7	52.6	11.6	–	187.5
	100.0 ng/ml	25.0	42.3	47.8	9.9	–	177.7
EGF, Insulin	10.0 ng/ml, plus						
	0.1 µg/ml	10.0	24.0	52.5	23.5	–	223.1
	1.0 µg/ml	8.9	23.8	45.7	30.5	–	237.2
	10.0 µg/ml	5.0	11.2	40.6	48.2	–	285.2
	50.0 µg/ml	14.4	32.2	50.9	16.9	–	201.6
	100.0 µg/ml	18.8	38.9	50.7	10.4	–	181.8
FCS	10.0%	3.9	9.4	46.2	44.4	–	279.4
FCS EGF Insulin	10.0% plus 10.0 ng/ml plus 10.0 µg/ml	0.1	0.1	6.9	77.8	15.2	354.6

formed population. Both types of cultures were grown in HD media but exposed to varying serum concentrations in the constant presence of the 5 growth factors at the concentrations listed above. In analogy to the bottom part of figure 2, the results from this experiment are presented in figure 3 as single-parameter Hoechst fluorescence distributions. In this form of display successive cell cycle compartments are indicated by a series of peaks whose amplitudes reflect the number of cells within a given compartment. The greatest difference in growth response between diploid and transformed cells is seen at the lowest serum concentration (fig. 1a, d): 32 h after growth stimulation at 1% serum, only 9.5% of diploid but 53.5% of the transformed cells exit from their respective G0/G1 compartments. At 10% serum (fig. 1c, f), 42.9% of the primary cells fail to cycle, whereas the transformed culture shows only 16.6% noncycling cells. Moreover, at all serum concentrations, only the transformed cultures display a small but consistent cell fraction that has entered the third cell cycle (G1″ phase). These observations prove that a greater proportion of the transformed cells enter the cell cycle in response

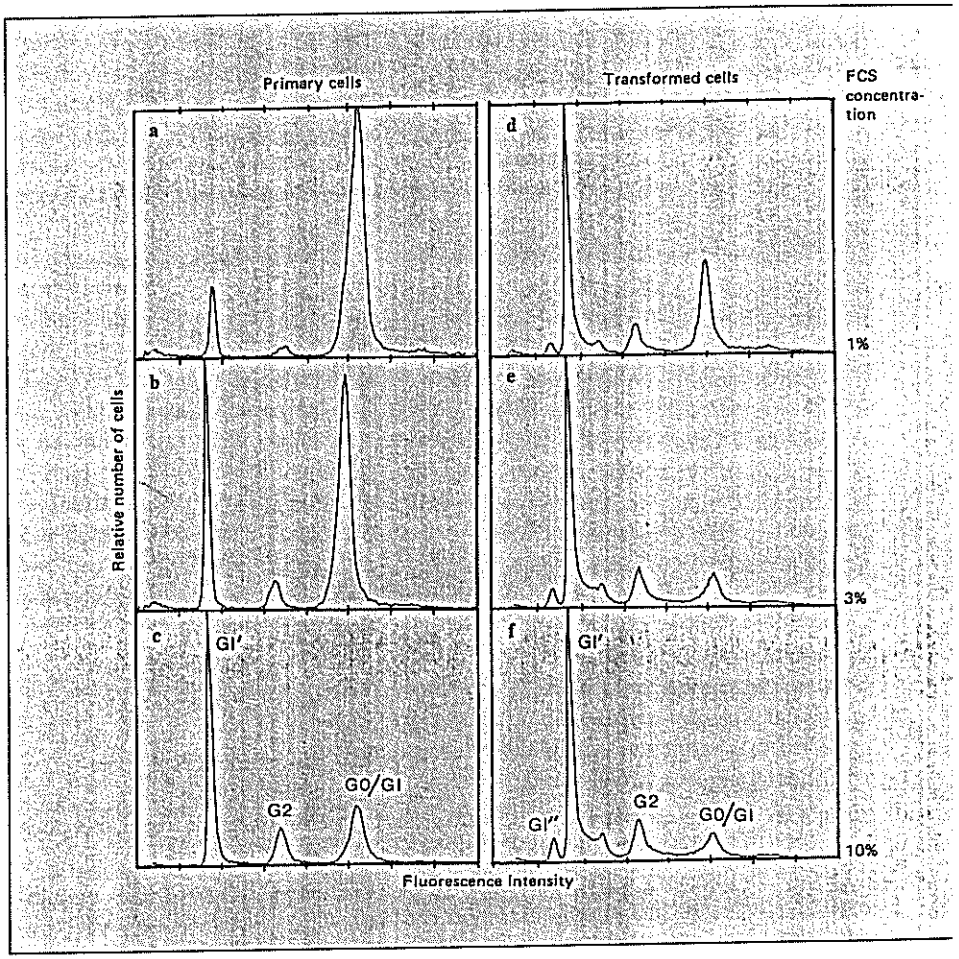

Fig. 3. Different sensitivity of primary (a, c, e) and transformed (b, d, f) *M. minutus* cells to growth fact supplements as a function of FCS concentration. Lung-derived fibroblast-like cells at 32 h after stimulatic with 1, 3 and 10% FCS in the presence of 5 growth factor supplements at concentrations indicated in the te Cumulative Hoechst axis projections as in bottom row of figure 2.

to serum stimulation and, once activated, these cells appear to cycle faster than their diploid counterparts.

The cultures tested in these experiments were aliquots taken from the murine mass cultures before and after conversion to het roploidy. Since at least one of our spont neous transformation experiments had r sulted in a mixture of several aneuploid c lineages [11], it was of interest whether t

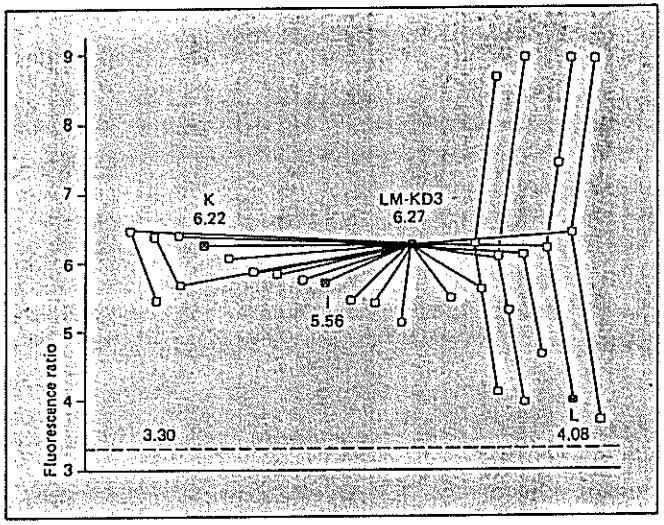

Fig. 4. Subclone DNA content variability of a transformed, hypotetraploid, lung-derived cell clone (LM-KD3; □). Relative DNA content is expressed as fluorescence ratio to chicken red blood cell standard. The dashed horizontal line (3.30) indicates the relative DNA content of primary diploid *Micromys* cells. The variant subclones (⊠) were used for testing of growth factor response (see figure 5).

superior response to serum mitogens of the transformed cells would be seen irrespective of their degree of aneuploidy. Genomically divergent cell lineages were prepared by subcloning and subsequent flow cytometric assessment from a single parental (transformed) cell clone of near-tetraploid DNA content. Figure 4 shows the panel of subclones from which the isolates L (near diploid), I (hypertriploid) and K (near-tetraploid) were selected for further testing.

Figure 5 compares the growth response of the chosen chromosomally divergent clonal isolates to that of a diploid primary culture. In all 4 experiments, culture aliquots were exposed to increasing serum concentrations in the presence (open symbols) or absence (closed symbols) of our standard combination of 5 growth factors. The parameters recorded are the size of the noncycling cell fraction (as a measure of cell recruitment; dashed lines) and the percent cell increase (as a measure of overall growth performance; solid lines). With respect to both parameters, the diploid culture (fig. 5, Primary) is seen to benefit much less from the exposure to the growth factor supplement than each of the (transformed) clonal isolates. In the presence of growth factors, the transformed isolates show a much better response to stimulation and they achieve optimal growth at much lower serum levels. In addition, figure 5 documents a surprising degree of interclonal heterogeneity. For example, the G0/G1 cell fraction of isolate I is much more responsive to low-dose serum stimulation under both growth conditions than either isolates K and L; isolate I clearly is the 'most transformed' of the three isolates in the sense of being closest to growing in FCS-free media and with respect to the complete absence of noncycling cells at 3% serum or 1% serum plus growth factor supplements. In contrast, isolates K and L show a residual portion of non-

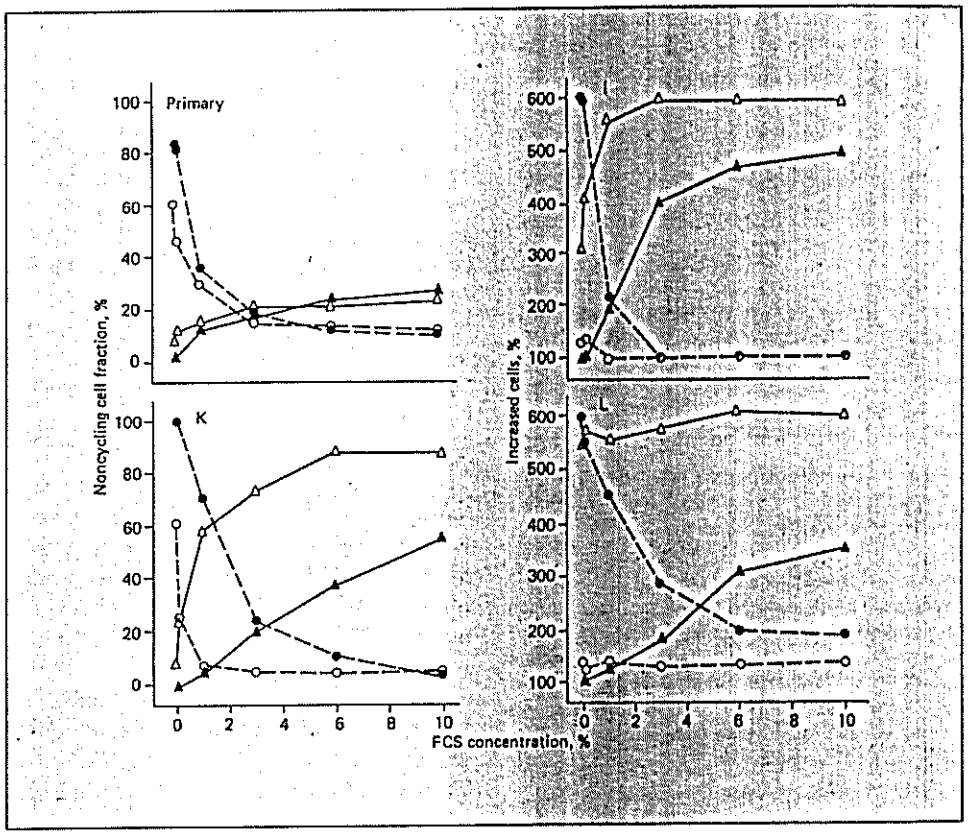

Fig. 5. Increased growth factor sensitivity of spontaneously transformed cells. Changes of the noncycling cell fraction (circles, ----) and percent increase in cell number (triangles, ——) are plotted as a function of FCS concentration and growth factor supplementation. Closed symbols = Without, open symbols = with growth factor supplements. Primary = Diploid, lung-derived cell strain; I, K, L = transformed clones with different DNA contents, as indicated in figure 4.

cycling cells at all serum concentrations. There is no evident correlation between growth performance and genome size.

A summary figure of a larger series of analogous experiments is given in figure 6. This figure shows that transformed cells benefit to a much greater extent from growth factor supplementation than the primary cultures, particularly at low serum concentrations. The figure also confirms that the transformed clones vary greatly in their individual sensitivities to growth factor supplements: this heterogeneity is greatest at low FCS levels and decreases with increasing concentration. The important message of this figure is that the transformed cells re-

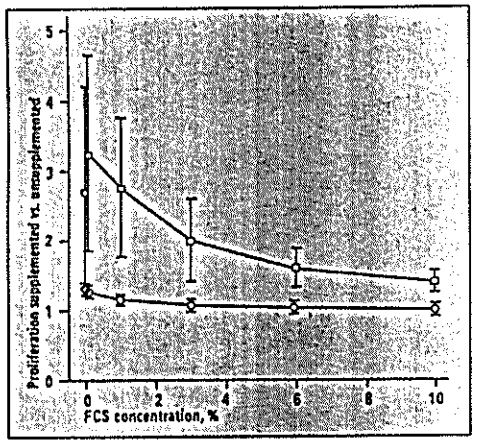

Fig. 6. Improvement of the proliferative capacity of cells exposed to growth factor supplements as a function of various FCS concentrations. Data on the Y axis represent the ratios of the percent increase in cell number (calculated from the BrdU/Hoechst flow histograms) at 48 and 72 h with and without growth factor supplementation. A level of 1 indicates identical growth capacity of cells grown with or without growth factors. The open circles show the mean values of the normal diploid cell strains. The open squares summarize the data from kidney- and lung-derived clonal isolated with 100% aneuploid DNA content.

main more sensitive to the growth factor supplement than diploid cells, even at the 10% serum concentration employed throughout our original study [11].

Discussion

The BrdU/Hoechst flow technique employed in this study demonstrates major differences between primary and spontaneously transformed murine cells in their response to exogenous growth factors. Murine cells which emerge during the process of spontaneous transformation clearly are much more sensitive to these factors than their primary cell counterparts. Their greater sensitivity could result from increased numbers of cell surface receptors and/or amplification of any of the various signal transduction pathways. In this sense, the acquisition of enhanced growth factor sensitivity would correspond to a first step in the direction of an autocrine mechanism of growth control [4, 5, 18, 19]. The transformed cells display their greatest sensitivity at low serum concentrations. However, growth factor supplements were still effective with 10% FCS.

Such were the conditions under which our previous study failed to reveal a classical growth crisis during the long-term growth of primary *M. minutus* cells [11]. The number of the noncycling G0/G1 cell fractions, as monitored by the BrdU/Hoechst flow-cytometric technique, did not change significantly from the initiation of the murine culture system until the rapid disappearance of the diploid cell fraction (data not shown). Therefore, a progressive loss of growth factor responses in senescing cell populations as suggested by Phillips et al. [14] does not explain the early disappearance of the diploid cells in our culture system [11]. An increased responsiveness of the emerging aneuploid culture components, however, could account for the ultimate loss of the primary cell population. A second factor, which would likewise enhance the take-over of the primary culture by the emerging aneuploid components, could be an effect akin to paracrine stimulation. Such effects have been demonstrated in cocultivation experiments between normal and tumor cells [7], and all of our cultures showed rather extended periods of coexistence of diploid and aneuploid

cells [11]. In addition to a combination of factors such as increased growth factor response and, possibly, paracrine mechanism of growth enhancement, our data seem to suggest that the lack of an apparent growth crisis could be the cumulative result of growth conditions which appear to favor 'high-responder' cells. Variable degrees of growth responsiveness were in fact observed in our cloning experiments (fig. 5, 6), although we did not see a correlation between particular degrees of aneuploidy and growth factor responsiveness.

Very recently, Loo et al. [12] succeeded in establishing long-term diploid murine cell cultures. These authors attribute their success to the complete omission of serum during all culture stages. According to their results, the common growth crisis in murine primary cell cultures would be due to some inhibitory effect of one or more FCS components. It remains to be seen whether serum-free culture conditions as a general rule can yield similar long-term diploid strains with cells derived from newborn animals of other murine species as used in the present study.

As an important result of this study we wish to draw attention to the unprecedented potential of the BrdU/Hoechst technique in deciphering individual growth factor responses. The data shown in figures 3 and 5 indicate, for example, that EGF and insulin supplements may also act as partial competence factors in spontaneously transformed, but not in primary rodent cells. Likewise, figure 2 and table I provide definitive evidence for a synergistic effect of EGF and insulin [16]. Detailed growth factor response measurements by means of BrdU/Hoechst flow cytometry (e.g., table I) include both an assessment of cell activation (by determination of the size of the noncycling cell fraction) and of cell cycle progression (by enumeration of cells in up to 4 cell cycles after stimulation). We highly recommend this informative technique for use in cell culture assays of cellular growth responses.

Acknowledgements

We thank Mrs. B. Zierlein and R. Friedl for skilful technical assistance. This work was supported by DFG grants SFB 105 and HO 868-2/1, and NIA grant AG 01751.

References

1 Barnes, D.; Sato, G.: Serum free cell culture: a unifying approach. Cell *22:* 649–655 (1980).
2 Barnes, D.; Sato, G.: Methods for growth of cultured cells in serum free medium. Analyt. Biochem. *102:* 255–270 (1980).
3 Chung, S.D.; Alavi, N.; Livingston, D.; Hiller, S.; Taub, M.: Characterization of primary rabbit kidney cultures that express tubule functions in a hormonally defined medium. J. Cell Biol. *95:* 118–126 (1982).
4 Cuttitta, F.; Carnes, D.N.; Mulshine, J.; Moody, T.W.; Fedorka, J.; Fischler, A.; Minna, J.D.: Bombesin-like peptides can function as autocrine growth factors in human small-cell lung cancer. Nature *316:* 832–836 (1985).
5 Hamburger, A.W.; White, C.P.: Autocrine growth factors for human tumor clonogenic cells. Int. J. Cell Cloning *3:* 399–406 (1985).
6 Handleman, S.L.; Sanford, K.K.; Tarone, R.E.; Parshad, R.: The cytology of spontaneous neoplastic transformation in culture. In Vitro *13:* 526–536 (1977).
7 Holzer, C.; Maier, P.; Zbinden, G.: Comparison of exogenous growth stimuli for chemically transformed cells: growth factors, serum and cocultures. Expl Cell Biol. *54:* 237–244 (1986).
8 Kubbies, M.; Rabinovitch, P.S.: Flow cytometric analysis of factors which influence the Hoechst/BrdU quenching effect in cultivated human fibroblasts and lymphocytes. Cytometry *3:* 276–281 (1983).

9 Kubbies, M.; Friedl, R.: Flow cytometric correlation between BrdU/Hoechst quench effect and base pair composition in mammalian cell nuclei. Histochemistry *83:* 133–137 (1985).
10 Kubbies, M.; Schindler, D.; Hoehn, H.; Rabinovitch, P.S.: BrdU/Hoechst flow cytometry reveals regulation of human lymphocyte growth by donor age related transition probability and growth fraction. J. cell. Physiol. *125:* 229–234 (1985).
11 Kubbies, M.; Friedl, R.; Bettecken, T.; Hoehn, H.: The fate of the primary diploid population during spontaneous transformation of growth factor supplemented murine cell cultures. Cytometry *7:* 551–557 (1986).
12 Loo, D.T.; Fuquay, J.I.; Rawson, C.L.; Barnes, D.W.: Extended culture of mouse embryo cells without senescence: inhibition by serum. Science *236:* 200–201 (1987).
13 Meek, R.L.; Bowmann, P.D.; Daniel, C.W.: Establishment of mouse embryo cells in vitro: relationship of DNA-synthesis, senescence and malignant transformation. Expl Cell Res. *107:* 277–284 (1977).
14 Phillips, P.D.; Kajii, K.; Cristofalo, V.J.: Progressive loss of the proliferative response of senescing WI-38 cells to platelet derived growth factor, epidermal growth factor, insulin, transferrin and dexamethasone, J. Geront. *38:* 513–518 (1984).
15 Rabinovitch, P.S.: Regulation of human fibroblast growth rate by both non-cycling cell fraction and transition probability is shown by growth in BrdU following by Hoechst 33258 flow cytometry. Proc. natn. Acad. Sci. USA *80:* 2951–2955 (1983).
16 Ronning, O.W.; Petterson, E.O.: Effect of different growth factors on cell cycle traverse and protein growth of human cells in culture. Expl Cell Res. *157:* 29–40 (1985).
17 Rothfels, K.H.; Kupelwieser, E.B.; Parker, R.C.: Effects of irradiated feeder layers on mitotic activity and development of aneuploidy in mouse embryo cells in vitro. Can. Cancer Conf. *5:* 191–223 (1963).
18 Sporn, M.B.; Todardo, G.J.: Autocrine secretion and malignant transformation of cells. New Engl. J. Med. *303:* 878–880 (1980).
19 Sporn, M.B.; Roberts, A.B.: Autocrine growth factors and cancer. Nature *313:* 745–747 (1985).
20 Todardo, G.J.; Green, H.: Quantitative studies of the growth of mouse embryo cells in culture and their development into established cell lines. J. Cell Biol. *17:* 299–313 (1963).
21 Wu, R.; Smith, D.: Continuous multiplication of rabbit tracheal epitheloid cells in a defined hormone-supplemented medium. In Vitro *18:* 800–812 (1982).

Received: May 25, 1987
Accepted: August 24, 1987

Dr. Manfred Kubbies
Institut für Humangenetik
Universität Würzburg
Koellikerstrasse 2
D-8700 Würzburg (FRG)

Colony-stimulating factors, cytokines and hematopoiesis

N. Nakayama, K. Hatake, A. Miyajima, K. Arai and T. Yokota

Department of Molecular Biology, DNAX Research Institute of Molecular and Cellular Biology, Palo Alto, California, USA

Current Opinion in Immunology 1989, 2:68–77

Introduction

In response to antigenic stimulation, T helper (T_H) cells secrete a set of lymphokines that regulate proliferation, differentiation and maturation of target cells. Recent work on the molecular cloning and characterization of many T cell lymphokine genes, for example the genes for interleukin (IL)-2, IL-3, IL-4, IL-5, granulocyte/macrophage colony-stimulating factor (GM-CSF), interferon (IFN) γ, tumor necrosis factor (TNF) α and lymphotoxin has suggested that there may be a regulatory network limiting lymphoid cells and hematopoietic cells through the actions of pleiotrophic lymphokines (Fig. 1). This network can be differentially activated by unique combinations of lymphokines, as illustrated by the T_H1 and T_H2 systems of the mouse [1]. IL-3, IL-4 and IL-5 produced by T_H2 cells enhance the immunoglobulin (Ig)E-mediated allergic response, whereas IFNγ produced by T_H1 cells suppresses it. Thus, T cells, in cooperation with macrophages, which also secrete cytokines [IL-1, TNFα, IL-6, granulocyte CSF (G-CSF), IFNγ, GM-CSF], have a vital role in coordinating the immune and inflammatory responses (Fig. 2) [2]. In T cells, the activation of lymphokine genes by antigens is rapid and temporary. Therefore, an inflammatory response that requires target cell proliferation and maturation may be restricted to the site of lymphokine production. This 'inducible' hematopoiesis appears to be regulated differently from the 'constitutive' hematopoiesis taking place in the bone marrow microenvironment (Fig. 1). The latter process is likely to be controlled by a developmental program that proceeds in the absence of immunological stimuli.

Hematopoietic cells are produced continuously in the bone marrow under the control of precise mechanisms which maintain homeostatic conditions. The evidence indicates that all hematopoietic cells are ultimately derived from self-renewing pluripotent hematopoietic stem cells (Dexter *et al.*, *BioEssays* 1984, 2:154). During this normal 'constitutive' hematopoiesis, stem cells are usually in the resting G_0 state but can be mobilized into a proliferative state when required. In the main *in vivo* site of hematopoiesis, the bone marrow and lymphoid organs, the developing hematopoietic cells are found in association with a complex stromal cell network containing diverse cell types. The stromal cells can also support hematopoiesis *in vitro*, indicating that bone marrow stromal cells have a major role in regulation of this 'constitutive' hematopoiesis. Stromal cells may influence the growth and differentiation of pluripotent stem cells and committed progenitor cells in either a positive or restrictive way. This could be achieved by the production of soluble mediators (Table 1) or by complex cell–cell interactions which maintain the microenvironment for stem cells.

Cytokines that affect the growth and differentiation of hematopoietic stem cells

Purification of hematopoietic stem cells

Purification of hematopoietic stem cells is necessary to demonstrate the roles of extracellular signals on the regulation of stem cell differentiation. As the undifferentiated blast cells give rise to multi-lineage colonies in culture, they represent hematopoietic stem cells and multipotential progenitors (Nakahata and Ogawa, *Proc Natl Acad Sci USA* 1982, 79:3843–3847). To date, the most frequently used method for enriching the undifferentiated blast cell population is 5-fluorouracil treatment, as stem cells are thought to exist mainly in the G_0 phase *in vivo*, in which cells are resistant to 5-fluorouracil. However, to isolate pluripotent stem cells from the blast cell population, a biochemically defined probe is needed. The main area of progress made in this line of research was the discovery of stem cell surface markers that allow the virtual purification of the hematolymphoid stem cell population from bone marrow by fluorescence-activated cell sorting [3]. Among the cells that are derived from bone

Abbreviations

cDNA—complementary DNA; **cMGF**—chicken myelomonocytic growth factor; **CSF**—colony-stimulating factor, **CTMC**—connective tissue type mast cells; **DIA**—embryonic stem cell differentiation inhibitory activity; **G-CSF**—granulocyte CSF; **GM-CSF**—granulocyte/macrophage CSF; **HILDA**—human IL for DA; **IFN**—interferon; **Ig**—immunoglobulin; **IGF**—insulin-like growth factor; **IL**—interleukin; **LIF**—leukemia inhibitory factor; **MAF**—macrophage activation factor; **M-CSF**—macrophage CSF; **MFF**—macrophage fusion factor; **MMC**—mucosal mast cells; **TGF**—transforming growth factor; T_H—T helper cell; **TNF**—tumor necrosis factor.

© Current Science Ltd ISSN 0952-7915

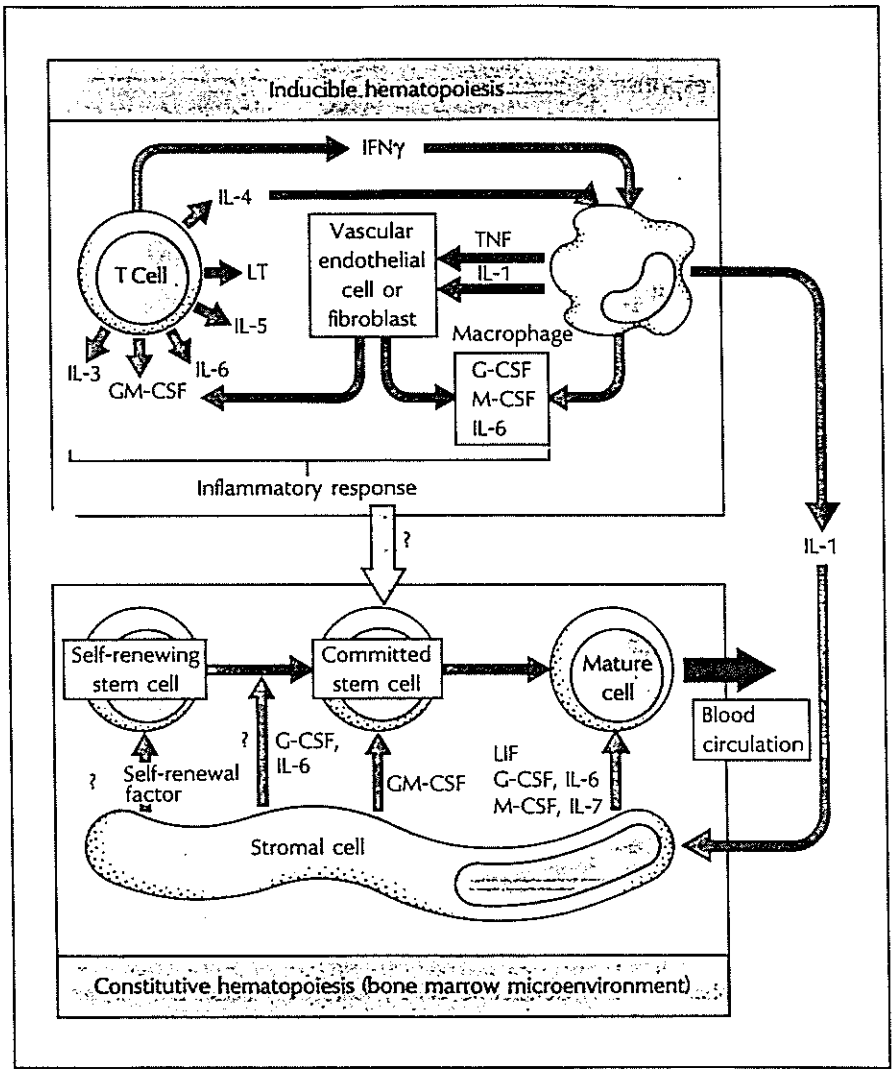

Fig. 1. Two types of hematopoiesis. G-CSF, granulocyte colony-stimulating factor; IFN, interferon; IL, interleukin; LIF, leukemia inhibitory factor; LT, lymphotoxin; M-CSF, macrophage colony-stimulating factor; TNF, tumor necrosis factor.

marrow, those which express low levels of Thy-1 (Thy-1^{lo} and no lineage-specific markers ($Lin^- = T^-B^-G^-M^-$: T for the T cell markers, CD4 and CD8; B for a B cell marker, B220; G for a granulocyte marker, Gr-1; and M for a myelomonocytic cell marker, Mac-1) were found to be enriched in populations of cells that can home to the thymus and differentiate into mature T cells [4], and also in population of hematopoietic stem cells (Müller-Sieburg *et al*, *Cell* 1986, 44:653–662) [5]. In addition, using monoclonal antibodies raised against pre-T cell hybridomas, Sca-1, a new cell surface marker, which can be used for enrichment of the progenitors of the lymphoid lineages, has recently been found [6]. The Thy-1^{lo} Sca-1^+ fraction of bone marrow cells represents the population that includes pluripotent hematopoietic stem cells as well as committed progenitors of the lymphoid lineages. The Sca-1 antibody can also separate Thy-1^{lo} Lin^- cells into two groups: one is the Sca-1^- population that is composed largely of colony-forming units–spleen and granulocyte–macrophage precursors, and the other is the Sca-1^+ population which consists mostly of hematolymphoid stem cells [3]. Cells in the Thy-1^{lo} Lin^- Sca-1^+ population express all the characteristics that the hematopoietic stem cells are thought to have, and quantitative analyses suggested that the Thy-1^{lo} Lin^- Sca-1^+ fraction might be a pure population of pluripotent hematopoietic stem cells [3]. The Sca-1 protein has proved to be antigenically related to the Ly-6 family [7].

IL-3 affects early stages in hematopoietic cell differentiation

IL-3, secreted by activated T cells and previously known as multi-CSF, supports multi-lineage colony formation in serum-containing culture and supports mast cell growth. Therefore, it was proposed that IL-3 acts on all stages in the development of hematopoietic cells. However, the availability of purified recombinant IL-3 and the establishment of serum-free culture systems have revealed that human IL-3 may act on hematopoietic stem cells and/or multipotential progenitors at early stages of development rather than cells in the terminal process of maturation [8]. In the serum-free culture, IL-3 supported only a few cell divisions and could not maintain the variability of future generations of progeny cells. However, when IL-3 was combined with the lineage-restricted fac-

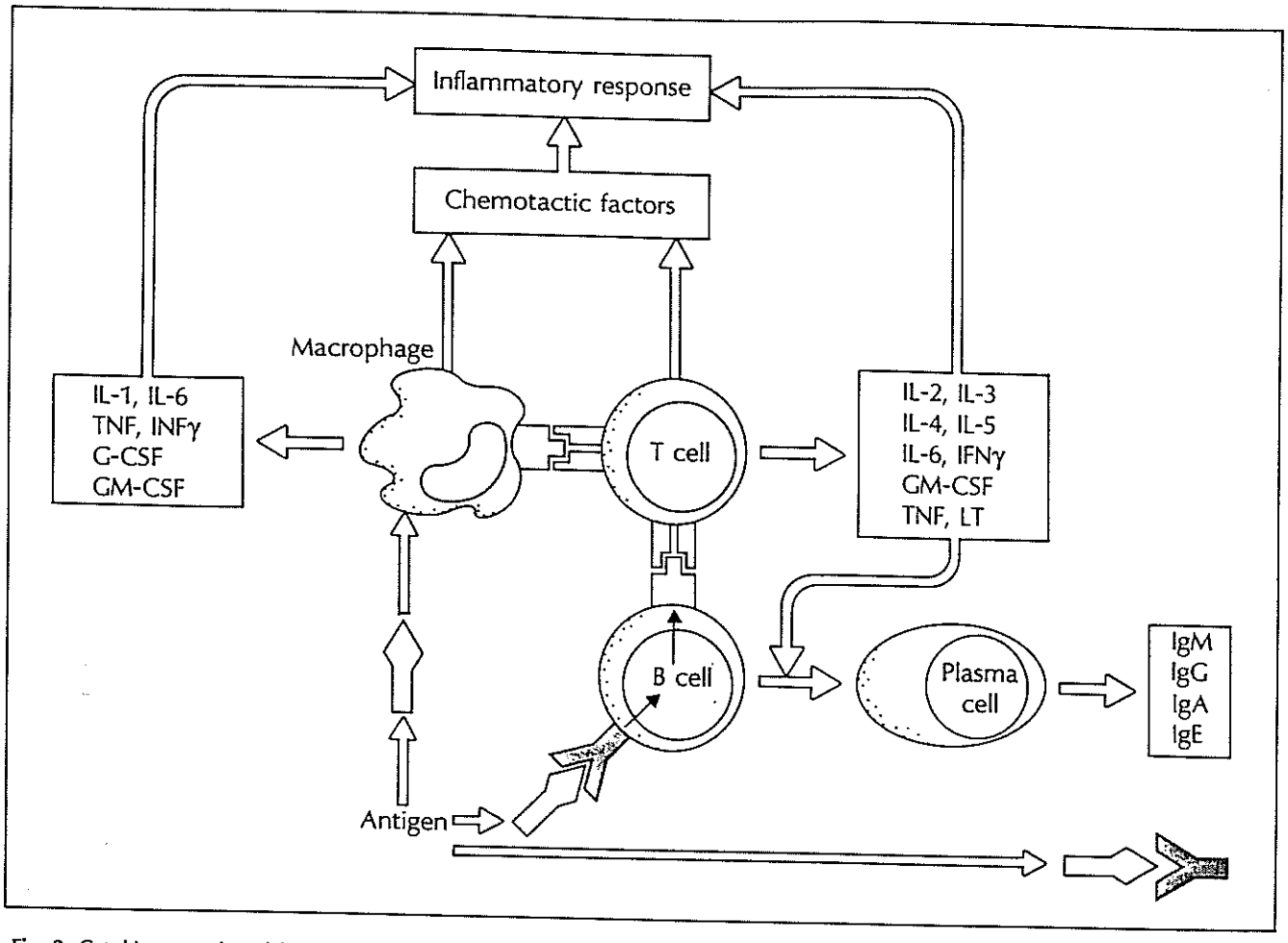

Fig. 2. Cytokines produced by activated T cells and macrophages. G-CSF, granulocyte colony-stimulating factor; GM-CSF, granulocyte/macrophage colony-stimulating factor; IFN, interferon; Ig, immunoglobulin; IL, interleukin; LT, lymphotoxin; TNF, tumor necrosis factor.

tor G-CSF or erythropoietin, it augmented the formation of neutrophil colonies or erythroid bursts, respectively. In mouse systems, it has been proposed that IL-3 supports the proliferation of blast cells which later develop into multi-lineage colonies, and thus maintains the multipotential progenitor population (Spivak *et al.*, *J Clin Invest* 1985, 76:1613–1622; Suda *et al.*, *J Cell Physiol* 1985, 124:182–191). In fact, the Thy-1^{lo} Lin^{-} population of bone marrow cells, > 98% of which is undifferentiated blast cells, is highly enriched in mouse hematopoietic stem cells, and was found to be rich in IL-3-responsive progenitors (one in every seven cells), in support of the model that IL-3 affects stem cell growth and differentiation [5].

G-CSF and IL-6 act synergistically with IL-3

Both G-CSF and IL-6 were found to enhance the activity of IL-3 on colony formation in a synergistic way (Ikebuchi *et al.*, *Proc Natl Acad Sci USA* 1987, 84:9–11). G-CSF is known as a lineage-specific CSF which specifically supports granulocyte colonies in serum-free culture [8], and also stimulates terminal differentiation of some promyelocytic leukemia cell lines (for example, WEHI3B [D^{+}]). IL-6 was previously known as IFNβ_2, B cell stimulatory factor-2 or B cell differentiation factor. Using large quantities of pure G-CSF and IL-6, it has been shown that both factors by themselves also stimulate blast colony and multi-lineage colony formation in spleen cell culture. However, neither factor supports secondary multi-lineage colony formation from pooled blast cells, which IL-3 is able to do, although they do support secondary granulocyte/macrophage colony formation. Thus, G-CSF and IL-6 may act directly on some of the granulocyte/macrophage progenitors, but their effects on the multipotential progenitors seem to be indirect. On the other hand, G-CSF or IL-6 significantly hasten the time at which multipotential progenitors enriched by 5-fluorouracil treatment start proliferation in the presence of IL-3 compared with IL-3 alone. Since the growth rate of individual blast colonies in IL-3 + G-CSF or IL-3 + IL-6 culture does not differ statistically from that in IL-3-containing culture, it has been suggested that G-CSF and IL-6 act synergistically with IL-3 by shortening the average time that multipotential progenitors remain in the G_0 phase.

Although the structural similarity between IL-6 and G-CSF has been pointed out (Hirano *et al.*, *Nature* 1986,

Table 1. Some important activities of cytokines.

Cytokine	Major activities and other names	Cytokine	Major activities and other names
IL-1α	EP, LAF, BAF, LEM, MNCF	Chemotactic factors	
IL-1β	Catabolin, OAF, H-1	NAP-1	MDNCF, TCF, LYNAP, IL-8
IL-2	TCGF, KHF	MCP-1	LDCF, GDCF, MCAF
IL-3	Multi-CSF, MCGF, BPA, CFU–S MF, MEG-CSF, HCGF, PSF	MIP-1α	EP, SISα, TY5
		MIP-1β	EP, SISγ, H400
IL-4	BSF-1, IgE-EF, TCGFII, MCGFII, MFF, MAF, THCGF	MIP-2	
		SISβ	LD78
IL-5	TRF1, BCGF2, Eo-DF, Eo-CSF, IgA-EF, KHF	SISδ	RANTIES
		SISε	TCA3, P500
IL-6	BSF2, BCDF, IFN-β2, HSF, HGF, PCTGF, THCGF, LAK	PF-4	
		PBP	CTAPIII, low-affinity PF-4, β-TG
IL-7	PBGF, THCGF	γIP-10	IFNγ inducible cytokine
GM-CSF	GM-CSF, BPA, Eo-CSF, HCGF, MGI-GM	MGSA	gro
G-CSF	G-CSF, MGI-IG		
M-CSF	M-CSF, CSF-1	Growth factors	
LIF	LIF, HILDA, DIA	EGF	
EPO		TGF-α	ECGF
p40	TCGF, MCGF		Acidic FGF, β-ECGF, α-ECGF,
TNFα	EP, cachectin		AGF, HBGF-1, EDGFII, α-RDGF, prostatropin
TNFβ	Lymphotoxin	bFGF	Basic FGF, cHDGF, HBGF-2, β-RDGF, HDGFII, HSDGF, PGF
IFNα	Leukocyte IFN, EP	PDGF-A	MDGF
IFNβ	Fibroblast IFN	PDGF-B	c-sis, MDGF
IFNγ	Immune IFN, MAF	PD-ECGF	Platelet-derived ECGF
		INS	
TGFβ1	CIF-A	IGF-I	Somatomedin C
TGFβ2	G-TsF, CIF-B	IGF-II	Somatomedin A, MSA
TGFβ3		NGF-β	
Inhibin	Inhibin A ($\alpha\beta_B$ inhibin B (αβ), FSH release inhibitor		
Activin	Activin A $(\beta_A)_2$, activin B (β_A,β_B), FRP, FSH-releasing protein		

A ATL-derived factor, AGF, astroglial growth factor; ATL, adult T cell leukemia; BAF, B cell-activating factor; BCDF, B cell differentiation factor; BCGF, B cell growth factor; BPA, burst-promoting activity; BSF, B cell-stimulating factor; CDGF, cartilage-derived growth factor; CFU, colony-forming unit; CFU–S, CFU–spleen; CFU–S MF, CFU–S maintenance factor; cHDGF, cationic hypothalamus-derived growth factor; CIF, cartilage inducing factor; CSDGF, chondrosarcoma-derived growth factor; CSF, colony-stimulating factor; CTAP, connective tissue activating protein; DIA, differentiation inhibitory activity; ECGF, endothelial cell growth factor; EDF, erythroid differentiation factor (= β_A); EDGF, eye-derived growth factor; EF, enhancing factor; EGF, epidermal growth factor; Eo, eosinophil; Eo-DF, eosinophil differentiation factor; Eo-CSF, eosinophil CSF; EP, endogenous pyrogen; EPO, erythropoietin; ES, embryonic stem; ESCGF, ES cell growth factor; FGF, fibroblast growth factor; FRP, FSH-releasing protein; FSH, follide-stimulating hormone; G-CSF, granulocyte CSF; GDCF, glioma-derived monocyte chemotactic factor; GM-CSF, granulocyte/macrophage CSF; HBGF, heparin-binding growth factor; HCGF, hemopoietic cell growth factor; HDGF, hepatoma-derived growth factor; HGF, hybridoma growth factor; H-1, hematopoietin-1; HILDA, human IL for DA cells; HSF, hepatocyte-stimulating factor; IFN, interferon; Ig, immunoglobulin; IGF, insulin-like growth factor; IL, interleukin; KHF, killer helper factor; LAF, lymphocyte-activating factor; LAK, lymphokine-activated killer; LDCF, lymphocyte-derived chemotactic factor; LEM, leukocyte endogenous mediator; LIF, leukemia inhibitory factor; LT, lymphotoxin; LYNAP, leukocyte-derived neutrophil activating peptide; MAF, macrophage activation factor; MCGF, mast cell growth factor; MCAF, monocyte chemotactic and activating factor; MCP, monocyte chemoattractant protein; M-CSF, macrophage CSF; MDGF, macrophage-derived growth factor; MDNCF, monocyte-derived neutrophil chemotactic factor; MEG, megakaryocyte; MFF, macrophage fusion factor; MSA, multiplication stimulating activity; NAP, neutrophil-activating protein; NGF, nerve growth factor; MNCF, mononuclear cell factor; OAF, osteoclast-activating factor; PBGF, pre-B cell growth factor; PBP, platelet basic protein; PCTGF, plasmacytoma growth factor; PDGF, platelet-derived growth factor; PF, platelet factor; PGF, prostatic growth factor; PMN, polymorphonuclear leukocyte; PSF, P cell-stimulating factor; RDGF, retina-derived growth factor; SIS, small inducible secreted; TCF, T cell chemotactic factor; TCGF, T cell growth factor; TG, thromboglobulin; TGF, transforming growth factor; T_H, T helper; THCGF, thymocyte growth factor; TNF, tumor necrosis factor; TRF, T cell replacing factor.

324:73–76), the similarities in the roles of G-CSF and IL-6 were emphasized by the isolation and characterization of a chicken myelomonocytic growth factor (cMGF) complementary DNA (cDNA) [12]. cMGF stimulates the growth of v-*myb* or v-*myc*-transformed chicken myeloid cells in culture and macrophage and granulocyte colony formation in normal bone marrow cultures (Leutz *et al.*, *EMBO J* 1984, 3:3191–3199). The primary structure of cMGF predicted from its cDNA showed significant homology to both human and mouse G-CSF (56 and 52%, respectively) and human and mouse IL-6 (41 and 39%, respectively). This suggest that cMGF is a distant relative of G-CSF and IL-6.

It is worth noting that G-CSF has recently been shown to act as a survival factor for the mature progeny of the WEHI3B(D^+) cell line instead of as a differentiation inducer [13]. Therefore, it is conceivable that the same mechanism may be used for granulocyte colony formation in culture. However, the mode of action of G-CSF as a synergistic factor for IL-3 remains to be clarified.

Cytokines in inducible hematopoiesis and inflammation

IL-4 as MAF and MFF

Activated T cells are known to produce a diverse array of factors that affect various macrophage activities. Recently, it was shown that the mouse T cell product, IL-4, induces tumoricidal activity in cultured macrophages (Crawford *et al.*, *J Immunol* 1987, 139:135–142) in a way similar to the activity previously described as macrophage activation factor (MAF). IL-4 was also found to stimulate the fusion of bone marrow and alveolar macrophages to form giant multinucleated cells [14]. This effect on IL-4 seems to be the activity that had previously been reported to be macrophage fusion factor (MFF; Galindo *et al.*, *Infect Immun* 1974, 9:212–216). Giant multinucleated cells are associated with granulomatous lesions and have been called Langhan's giant cells, giant foreign body cells, and giant cells of inflammation. In addition, IL-4 diminishes macrophage migration in semi-solid agar and causes macrophages to aggregate, an event which precedes cell fusion [14]. These observations suggest that IL-4 may have a role in the development of the granulomatous response.

Effects of IL-5 on eosinophils

Mouse IL-5 produced by activated mouse T_H2 cells selectively stimulates human eosinophil colony formation and activates mature eosinophils. Other factors known to induce eosinophil differentiation are GM-CSF and IL-3, but their effects, which produce eosinophils along with a number of other cell types, are not specific to the eosinophil lineages. Moreover, the actions of IL-3 and GM-CSF are species specific for mouse and humans. The human eosinophil produced *in vitro* by mouse IL-5 contain both immature myelocytes and mature cells, and both are functionally active in an antibody-dependent, cell-mediated cytotoxicity assay [15]. Mature cells, however, lose their activity after 7 weeks despite being more than 90% viable and having a normal appearance under the light microscope. This may indicate that functional activity is of shorter duration than cell viability or that activation is a separate pathway from differentiation.

Control of mast cell differentiation

Mast cells are derived from multipotential hematopoietic stem cells and have an important role in inflammatory responses as they secrete a variety of mediators. Undifferentiated precursors of mast cells produced in the bone marrow migrate through various tissues in the blood stream. They proliferate and differentiate into two types of mast cells depending on the tissue they reside in [16]. Mucosal mast cells (MMC) found in mucosa are phenotypically distinct from connective tissue type mast cells (CTMC) found in the skin, peritoneal cavity, and muscularis propria of the digestive tract. Although CTMC contain heparin proteoglycan and store relatively large amounts of histamine, MMC contain chondroitin sulphate proteoglycan and relatively small amounts of histamine. Cells with many features of MMC developed in suspension cultures of normal hematopoietic cells in the presence of mast cell growth factor. Cultured mast cells and MMC proliferate in response to the T cell-derived lymphokines, IL-3 and IL-4 [16]. Although proliferation of CTMC was initially proposed to be T cell-independent, combinations of IL-3 and IL-4 greatly enhanced colony formation of peritoneal mast cells (Hamaguchi *et al.*, *J Exp Med* 1987, 165:268–275).

Mature mast cells have high-affinity receptors for IgE (FcεRI), regardless of phenotype. Binding of IgE to the receptor activated mast cells to release histamine and other pharmacological mediators, causing inflammatory reactions. In addition, FcεRI-mediated activation of mast cells results in the production of a set of lymphokines including IL-3, IL-4, IL-5, IL-6 and GM-CSF [17,18], indicating that mast cells have an important role in inflammatory responses by stimulating proliferation and differentiation of inflammatory cells such as neutrophils, eosinophils, and macrophages [17,18]. Activation of FcεRI on CTMC stimulates the proliferation of CTMC, suggesting that there is an autocrine mechanism controlling CTMC growth by IgE stimulation [19].

In contrast to the progeny of multipotential hematopoietic stem cells such as erythrocytes, neutrophils and platelets, which leave the bone marrow after maturation and have limited proliferative capacity, mast cells have extensive proliferative activity even after morphological differentiation. Committed mast cell progenitors are enriched in the mesenteric lymph node of mice infected with *Nipponstrongylus brasiliensis* [20].

Committed mast cell progenitors are able to proliferate and differentiate in the absence of IL-3 or IL-4 when cultured on a monolayer of embryonic skin or 3T3 fibroblasts and can form colonies in the presence of fibroblast-conditioned medium. They acquire a connective tissue phenotype when cultured in a fibroblast monolayer and

a mucosal phenotype when cultured in the presence of IL-3 or IL-4 [20]. Therefore, committed mast cell progenitors are bipotential and grow in response to an unknown soluble factor secreted from fibroblasts (Fig. 3). Similarly, cocultivation of IL-3-dependent mast cell clones derived from bone marrow with 3T3 fibroblasts also induces a phenotypic change from mucosal type to connective tissue type [21]. These data indicate a strong influence of the connective tissue microenvironment on maturation of mast cells; the involvement of soluble factors remains to be clarified.

Mutation at either the W locus or the Sl locus in the mouse causes depletion of mast cells, erythrocytes and melanocytes. Even with these genetic defects, mast cells can develop *in vitro* when bone marrow cells from either W/W^v or Sl/Sl^d mice are cultured in the presence of IL-3. However, although normal fibroblasts support the proliferation of mast cells derived from normal and Sl/Sl^d mice, they do not support the proliferation of the W/W^v mouse-derived mast cells. This indicates that mast cells from the W/W^v mutant mouse are defective in their ability to respond to fibroblasts but that the Sl/Sl^d mouse-derived mast cells still maintain this capability. On the other hand, fibroblasts derived from Sl/Sl^d mice cannot support the development of normal mast cells. Thus, the Sl gene product(s) appears to be essential for the fibroblast to support mast cell maturation, and the W gene product seems important for the interaction of the mast cell with fibroblasts [16]. The proto-oncogene product c-kit, a transmembrane tyrosine kinase receptor for an unknown ligand, has proved to be encoded by the W locus [22,23], and the c-kit-associated tyrosine kinase may be important for the W phenotype [24]. It is conceivable that the W locus (c-kit) encodes a receptor for the Sl gene product expressed in fibroblasts, and that the Sl product may be a new, as yet unknown, cytokine.

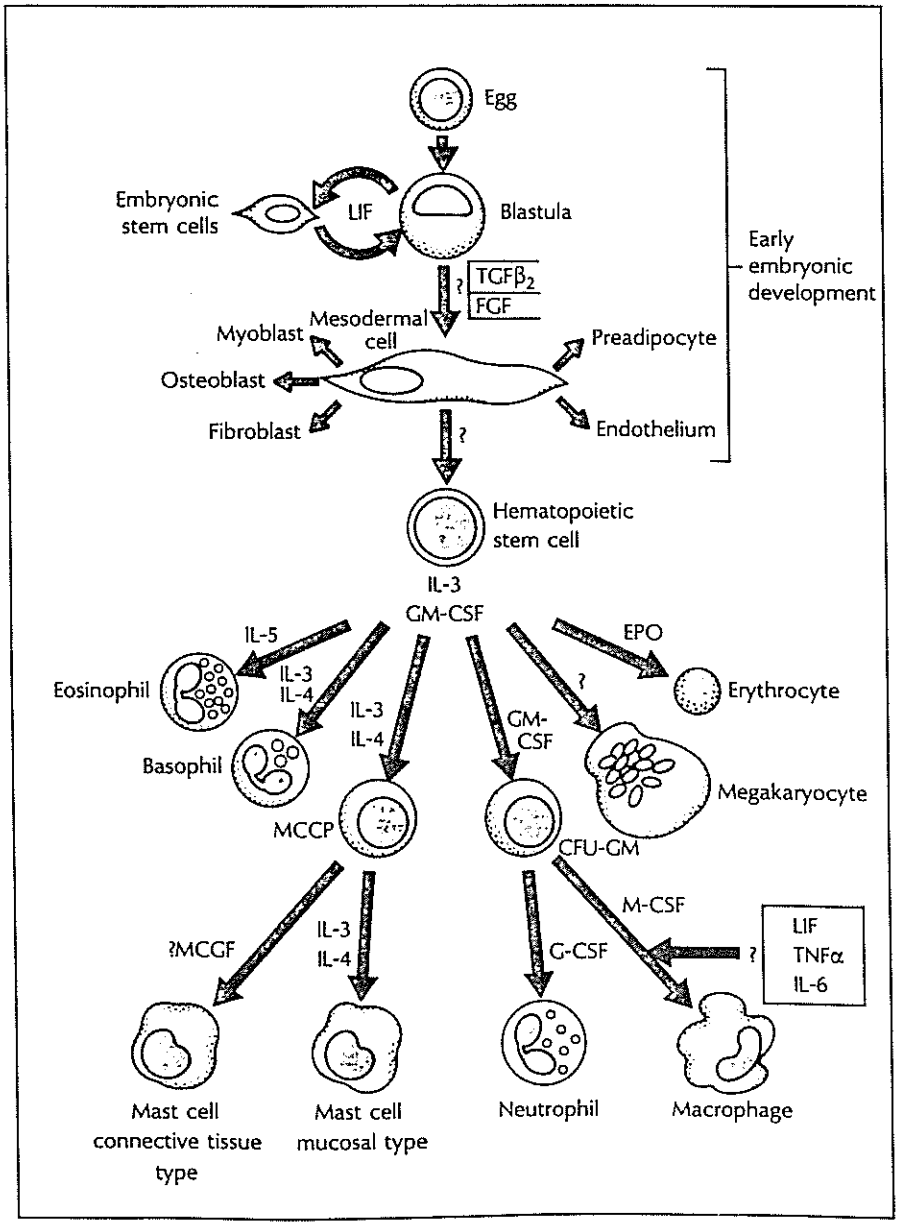

Fig. 3. Role of cytokines in development. CFU-GM, colony-forming unit–granulocyte macrophage; EPO, erythropoietin; FGF, fibroblast growth factor; G-CSF, granulocyte colony-stimulating factor; GM-CSF, granulocyte/macrophage colony-stimulating factor; IL, interleukin; LIF, leukemia inhibitory factor; MCGF, mast cell growth factor; M-CSF, macrophage colony-stimulating factor; TGF, transforming growth factor; TNF, tumor necrosis factor.

Some stromal cell-derived cytokines are constitutive factors in the regulation of hematopoiesis

Much evidence has accumulated suggesting that IL-3 acts on multipotential and/or pluripotential stem cells to support their growth and differentiation. However, the fact that expression of IL-3 has been limited mainly to activated T cells is evidence against it being important in constitutive hematopoiesis. The question of what substitutes for IL-3 function in the bone marrow microenvironment is important for the understanding of the normal regulation of hematopoiesis. Hematopoietic stems cells are in contact with stromal cells (a mixture of macrophages, endothelial cells, fibroblasts and adipocytes) in bone marrow. Cytokines active under these circumstances may be produced by stromal cells. Alternatively, they could be produced by hematopoietic progenitor cells in an autocrine manner under the regulation of stromal cells.

CSF produced by stromal cells

The production of GM-CSF, G-CSF and IL-6 by stromal cells is in most cases induced by other factors, including IL-1 and TNFα, and the constitutive levels of expression are undetectable or very low, suggesting that these cytokines are involved in inductive hematopoiesis. However, GM-CSF has recently been shown to be constitutively expressed in microvascular endothelial cells which are in very close contact with cells in the marrow [25]. Given the possibility that GM-CSF could be compartmentalized on the surface of stromal cells by binding to an extracellular matrix component (Gordon *et al.*, *Nature* 1987, 326:403–405), it could be that GM-CSF serves as a regulatory factor in constitutive hematopoiesis. In serum-containing culture, GM-CSF supports the formation of blast cell colonies, multi-lineage colonies, and erythroid bursts in the presence of erythropoietin; however, the effect is weaker than that of IL-3. In serum-free culture, GM-CSF is inefficient at supporting colony formation by itself and appears to be incapable of supporting the terminal maturation of granulocyte/macrophage progenitors, but it cooperates with the lineage-restricted CSF, G-CSF and erythropoietin, in supporting neutrophil and erythroid colony formation, respectively, again at lower efficiencies than IL-3 [8,26–28]. Thus, GM-CSF, like IL-3, supports the growth of multipotential progenitors, probably at later stages than IL-3, so that GM-CSF could be an IL-3 counterpart in bone marrow. However, it is still possible that another IL-3 like molecule(s) exists or that another mechanism (for example, directed cell-to-cell contact) may fulfil the IL-3-like function.

In contrast, macrophage CSF (M-CSF) and IL-7 are constitutively produced by stromal cells [29]. Interestingly, two forms of M-CSF [30,31] have been identified. The major transcripts of M-CSF (CSF-1) are 4 kb and 1.6 kb in size, and are created by alternative splicing. The 4 kb transcript encodes a 554 amino acid product that is synthesized as an integral membrane glycoprotein but is rapidly proteolyzed to generate mature soluble factors, whereas the 1.6 kb transcript encodes a 256 amino acid product, expressed as a stable membrane-bound glycoprotein that can stimulate the c-*fms* product, the CSF-1 receptor [30,31]. These results suggest that a membrane-bound CSF may contribute to constitutive hematopoiesis. IL-7, which was originally identified as a pre-B cell factor [29], also affects the growth of mature T cells [32] and thymocytes (Murray *et al.*, *Int Immunol*, in press). However, its role in constitutive hematopoiesis remains to be clarified.

Other regulators of hematopoiesis

Hematopoiesis is regulated not only by CSF but also by factors with no colony-forming activities. One group of these includes the terminal differentiation factors that suppress growth of precursors and induce stable differentiated phenotypes (G-CSF and GM-CSF also have this effect on some leukemic cells lines). Another group contains the negative regulators that suppress the actions of CSF. Two interesting factors, leukemia inhibitory factor (LIF), human IL for DA (HILDA), and transforming growth factor (TGF)β, provide examples of each group of factors.

LIF/HILDA: a novel non-CSF type regulator in hematopoiesis?

LIF was independently identified in various cell systems through seemingly contradictory assays (Fig. 3), firstly in terms of its differentiation stimulation/growth inhibition activity on the mouse myeloid leukemic cell line M1 [33–35], secondly as a differentiation inhibition/growth supporting activity for mouse embryonic stem cells (DIA) [36], and thirdly as a human T cell-derived factor, HILDA, that triggers the proliferation of the mouse IL-3-dependent cell line, DA-1 [37]. Recent cloning studies have revealed that human LIF is the same molecule as HILDA, and that LIF has the same activities and molecular characteristics as DIA [35,36,38,39]. HILDA was shown to be a potent chemoattractant and activator of mouse and human eosinophils. It also displayed burst-promoting activity on human marrow, but had no GM-CSF eosinophil-CSF activities (Moreau *et al.*, *J Immunol* 1987, 138:3844–3850). This has been partly confirmed by the characterization of LIF, the mouse version of HILDA, since LIF was originally isolated as a molecule that was distinct from G-CSF and GM-CSF. LIF-binding activity on the membrane appears to be specific for LIF, implying that its receptor is distinct from those of the other cytokines, and is distributed in embryonic stem cells [38], bone marrow cells (especially macrophages, monocytes, and their precursors), spleen, and the peritoneal cavity [40]. As LIF prevents embryonic stem cells from becoming committed to irreversible differentiation processes and, most importantly, allows them to grow (self-renew) while retaining their pluripotent nature, it is tempting to speculate that hematopoietic stems cells may also be under the control of a differentiation inhibitory factor(s),

similar to LIF, which supports their self-renewal in the bone marrow.

TGFβ, a negative factor in hematopoiesis?

It is worth noting that TGFβ1, unlike TGFβ2, inhibits colony formation by mouse factor-dependent hematopoietic progenitor cells in response to IL-3 or G-CSF and also inhibits colony formation by marrow progenitor cells responding to IL-3, GM-CSF and M-CSF (Ohta *et al*, *Nature* 1987, 329:539–541).

Annotated references and recommended re ing

- • Of interest
- •• Of outstanding interest

1. •• MOSMANN TR, COFFMAN RL: TH1 and TH2 cells: different patterns of lymphokine secretion lead to different functional properties. *Annu Rev Immunol* 1989, 7:145–173.

A review by the group that proposed that there are 2 types of helper T cells. Possible differences in their *in vivo* roles are discussed

2. •• MIYAJIMA A, MIYATAKE S, SCHREURS J, DE VRIES J, ARAI N, YOKOTA T, ARAI K: Coordinate regulation of immune and inflammatory responses by T cell-derived lymphokines. *FASEB J* 1988, 2:2462–2473.

An interpretive review on the immuno-regulatory network by lymphokines.

3. •• SPANGRUDE GJ, HEIMFELD S, WEISSMAN IL: Purification and characterization of mouse hematopoietic stem cells. *Science* 1988, 241:58–62.

Using a cell surface marker, Sca-1, together with Thy-1 and lineage-specific markers for T cells, B cells, granulocytes, and monocytes, the authors successfully enriched the hematolymphoid stem cells to produce a nearly pure population. This fractions of cells is represented by Thy-1^{lo} $^{-}$ Sca-1^{+} phenotype.

4. • SPANGRUDE GJ, MÜLLER-SIEBURG CE, HEIMFELD S, WEISSMAN IL: Two rare populations of mouse Thy-1^{lo} bone marrow cells repopulate the thymus. *J Exp Med* 1988, 167:1671–1683.

Quantitative analyses of the thymic colony-forming unit in the Thy-1^{lo} population of bone marrow cells are presented.

5. •• MÜLLER-SIEBURG CE, TOWNSEND K, WEISSMAN IL, RENNICK D: Proliferation and differentiation of highly enriched mouse hematopoietic stem cells and progenitor cells in response to defined growth factors. *J Exp Med* 1988, 167:1825–1840.

The authors demonstrate that the Thy-1^{lo} Lin^{-} population is > 98% blast cells and is highly enriched in hematopoietic stem cells and multipotential progenitors which give rise to multi-lineage colonies in culture in the presence of IL-3 or GM-CSF.

6. •• SPANGRUDE GJ, KLEIN J, HEIMFELD S, AIHARA Y, WEISSMAN IL: Two monoclonal antibodies identify thymic-repopulating cells in mouse bone marrow. *J Immunol* 1989, 142:425–430.

Characterizations of Sca-1 and Sca-2, 2 new cell surface antigens for selecting thymic colony-stimulating units are presented. They concluded that the majority of thymic-repopulating bone marrow cells are Thy-1^{lo} and Sca-1^{+}.

7. • VAN DE RIJN M, HEIMFELD S, SPANGRUDE GJ, WEISSMAN IL: Mouse hematopoietic stem-cell antigen Sca-1 is a member of the Ly-6 antigen family. *Proc Natl Acad Sci USA* 1989, 86:4634–4638.

The anti-Ly-6 antibody and anti-Sca-1 antibody appear to precipitate the same polypeptide of 18 kD. Thy-1^{lo} Lin^{-} Sca-1^{-} do not express Ly-6 messenger RNA but Thy-1^{lo} Lin^{-} Sca-1^{+} cells do. Therefore it is likely that the Sca-1 antigen is a member of the Ly-6 family.

8. •• SONODA Y, YANG Y-C, WONG GG, CLARK SC, OGAWA M: Analysis in serum-free culture of the targets of recombinant human hemopoietic growth factors: interleukin 3 and granulocyte/macrophage-colony-stimulating factor are specific for early developmental stages. *Proc Natl Acad Sci USA* 1988, 85:4360–4364.

This is the first attempt to reconstitute human bone marrow cell differentiation *in vitro* using enriched human hemopoietic progenitors, recombinant CSF and a serum-free culture system.

9. •• WONG GG, WITEK-GIANNOTTI JS, TEMPLE PA, KRIZ R, FERENZ C, HEWICK M, CLARK C, IKEBUCHI K, OGAWA M: Stimulation of murine hemopoietic colony formation by human IL-6. *J Immunol* 1988, 140:3040–3044.

The authors cloned a human lymphokine that supports mouse granulocyte/macrophage colony formation; it turned out to be IL-6. It also supports the secondary granulocyte/macrophage colony formation in the pooled blast cell culture as effectively as IL-3.

10. • LEARY AG, IKEBUCHI K, HIRAI Y, WONG GG, YANG YC, CLARK SC, OGAWA M: Synergism between interleukin-6 and interleukin-3 in supporting proliferation of human hematopoietic stem cells — comparison with interleukin-1-alpha. *Blood* 1988, 71:1759–1763.

The synergistic effect of IL-6 on IL-3 dependent blast cell colony formation is demonstrated with the My-10^{+} human bone marrow cells.

11. •• IKEBUCHI K, CLARK SC, IHLE JN, SOUZA LM, OGAWA M: Granulocyte colony-stimulating factor enhances interleukin 3-dependent proliferation of multipotential hemopoietic progenitors. *Proc Natl Acad Sci USA* 1988, 85:3445–3449.

The synergistic effect of G-CSF on the IL-3-dependent blast cell proliferation and multi-lineage colony formation is described.

12. • LEUTZ A, DAMM K, STERNECK E, KOWENZ E, NESS S, FRANK R, GAUSEPOHL H, PAN Y-CE, SMART J, HAYMAN M, GRAF T: Molecular cloning of the chicken myelomonocytic growth factor (cMGF) reveals relationship to interleukin 6 and granulocyte colony stimulating factor. *EMBO J* 1989, 8:175–182.

The cDNA encoding cMGF, which stimulates the growth of v-*myb*- or v-*myc*-transformed chicken myeloid cells *in vivo*, and macrophage and granulocyte colony formation in normal bond marrow cultures, is cloned. The structural similarity to G-CSF and IL-6 is discussed.

13. • BOHMER RM, BURGESS AW: Granulocytic colony-stimulating factor (G-CSF) does not induce differentiation of WEHI3B(D^{+}) cells but is required for the survival of the mature progeny. *Int J Cancer* 1988, 42:53–58.

The mouse myelomonocytic leukemia cell line WEHI3B(D^{+}) differentiates into mature monocyte in the presence of G-CSF in soft agar, but in suspension culture G-CSF appears to support the viability of the differentiated WEHI3B(D^{+}) cells induced by actinomycin D and does not by itself induce the differentiation.

14. • MCINNES A, RENNICK DM: Interleukin 4 induces cultured monocytes/macrophages to form giant multinucleated cells. *J Exp Med* 1988, 167:598–611.

This report suggests that the direct action of IL-4 on monocytes leads to giant multi-nucleated cell formation by promoting cell fusion.

15. • CLUTTERBUCK EJ, SANDERSON CJ: Human eosinophil hematopoiesis studied in vitro by means of murine eosinophil differentiation factor (IL5) — production of functionally active eosinophils from normal human bone marrow. *Blood* 1988, 71:646–651.

A liquid culture system for human bone marrow cells, in which eosinophil becomes the predominant cell type (41–89%) in the presence of IL-5, is described.

16. •• KITAMURA Y: Heterogeneity of mast cells and phenotypic change between subpopulations. *Annu Rev Immunol* 1989, 7:59–76.

A review on the mast cell differentiation in normal and mutant mice.

17. • PLAUT M, PIERCE JH, WATSON CJ, HANLEY-HYDE J, NORDAN RP, PAUL WE: (Letter to the Editor) Mast cell lines produce lymphokines in response to cross-linkage of FcεRI or to calcium ionophores. *Nature* 1989, 339:64–67.
This report shows that cross-linkage of the high-affinity Fcε receptors on mouse mast cell lines increases both the messenger RNA levels and the secretion of lymphokines, including IL-3, IL-4, IL-5, and IL-6, from T_H2 cells.

18. • WODNAR-FILIPOWICZ A, HEUSSER CH, MORONI C: (Letter to the Editor) Production of the haemopoietic growth factors GM-CSF and interleukin-3 by mast cells in response to IgE receptor-mediated activation. *Nature* 1989, 339:150–152.
The authors have demonstrated that mouse mast cells from mouse bone marrow induced gene expression and secretion of IL-3 and GM-CSF through the high-affinity Fcε receptor-mediated signal.

19. • TAKAGI M, NAKAHATA T, KOBAYASHI T, TSUJI K, KOIKE K, KOJIMA S, HIRANO T, MIYAJIMA A, ARAI K, AKABANE T: Stimulation of connective tissue-type mast cell proliferation by crosslinking of cell-bound IgE. *J Exp Med* 1989, 170:233–244.
This report shows that crosslinking of cell-bound IgE on mouse CTMC by a multivalent antigen or anti-IgE antibody induces clonal growth of CTMC in the presence of IL-3.

20. •• JARBOE DL, MARSHALL JS, RANDOLPH TR, KUKOLJA A, HUFF TF: The mast cell-committed progenitor. I. Description of a cell capable of IL-3 independent proliferation and differentiation without contact with fibroblasts. *J Immunol* 1989, 142:2405–2417.
The authors have developed a method to enrich committed mast cell progenitor cells whose differentiation is later than that of mast cell progenitors in bone marrow and earlier than the granulation stage. The cells are bipotential, so they acquire a connective tissue phenotype on embryonic skin or 3T3 fibroblasts (without IL-3 and IL-4) and also a mucosal phenotype in the presence of the conditioned medium from pokeweed mitogen-stimulated spleen cells. These cells can also form colonies in 3T3 fibroblast-conditioned medium which does not contain IL-3.

21. •• DAYTON ET, PHARR P, OGAWA M, SERAFIN WE, AUSTEN KF, LEVI-SCHAFFER F, STEVENS RL: 3T3 fibroblasts induce cloned interleukin 3-dependent mouse mast cells to resemble connective tissue mast cells in granular constituency. *Proc Natl Acad Sci USA* 1988, 85:569–572.
Using cloned IL-3-dependent mast cells, mouse skin-derived 3T3 fibroblasts are shown to induce the mast cells to change their phenotype from mucosal-like to connective tissue-like in the presence of WEHI-3 conditioned medium.

22. •• CHABOT B, STEPHENSON DA, CHAPMAN VM, BESMER P, BERNSTEIN A: The proto-oncogene c-*kit* encoding a transmembrane tyrosine kinase receptor maps to the mouse *W* locus. *Nature* 1988, 335:88–89.
The mouse W^{19H} mutant was a deletion of the c-*kit* proto-oncogene. The W locus is also tightly linked to c-*kit* and the 2 loci cannot be segregated by the interspecific backcross analysis. This suggests that the W locus encodes c-kit.

23. •• GEISSLER EN, RYAN MA, HOUSMAN DE: The dominant-white spotting (W) locus of the mouse encodes the c-kit proto-oncogene. *Cell* 1988, 55:185–192.
2 spontaneously isolated mutant W alleles have genomic rearrangements in the c-*kit* structural gene, and W^{44} homozygotes show a marked reduction in levels of c-*kit* messenger RNA. This suggests that the W locus encodes c-kit.

24. • NOCKA K, MAJUMDER S, CHABOT B, RAY P, CERVONE M, BERNSTEIN A, BESMER P: Expression of c-kit gene products in known cellular targets of W mutations in normal and W mutant mice: evidence for an impaired c-kit kinase in mutant mice. *Gene Devel* 1989, 3:816–826.
Expression of c-*kit* is found in tissues known to be affected by W mutations. The c-kit product in W/W^v mutant mast cells shows an impaired tyrosine kinase activity.

25. •• MALONE DG, PIERCE JH, FALKO JP, METCALFE DD: Production of granulocyte-macrophage colony-stimulating factor by primary cultures of unstimulated rat microvascular endothelial cells. *Blood* 1988, 71:684–689.
First report on constitutive and high level expression of GM-CSF from unstimulated microvascular endothelial cells in serum-free culture. Microvascular endothelial cells are most closely adjacent anatomically to hematopoietic progenitor cells.

26. • SONODA Y, YANG Y-C, WONG GG, CLARK SC, OGAWA M: Erythroid burst-promoting activity of purified recombinant human GM-CSF and interleukin-3 — studies with anti-GM-CSF and anti-IL-3 sera and studies in serum-free cultures. *Blood* 1988, 72:1381–1386.
Both IL-3 and GM-CSF support erythroid burst formation in the presence of erythropoietin in a serum-free culture containing insulin-like growth factor (IGF)-1. IGF-1 is found to raise the efficiency of burst formation to the levels found in serum-containing culture. IL-3 + GM-CSF is not more effective than IL-3 in the presence of IGF-1 and erythropoietin, suggesting that the burst forming units–erythroid that are targets of GM-CSF are subsets of those which are responsive to IL-3.

27. • MIGLIACCIO G, MIGLIACCIO AR, ADAMSON JW: In vitro differentiation of human granulocyte/macrophage and erythroid progenitors — comparative analysis of the influence of recombinant human erythropoietin, G-CSF, GM-CSF, and IL-3 in serum-supplemented and serum-deprived cultures. *Blood* 1988, 72:248–256.
This report is concerned with reconstitution of granulocyte/macrophage and erythroid differentiation systems in serum-free culture. Although there are some discrepancies with the other serum-free system [26], the authors show that GM-CSF and IL-3 can support erythroid burst formation in the presence of erythropoietin.

28. • MIGLIACCIO AR, MIGLIACCIO G, ADAMSON JW: Effect of recombinant hematopoietic growth factors on proliferation of human marrow progenitor cells in serum-deprived liquid culture. *Blood* 1988, 72:1387–1392.
The authors demonstrate that IL-3 increases the number of burst-forming units–erythroid, and that GM-CSF only maintains their viability.

29. • NAMEN AE, LUPTON S, HJERRILD K, WIGNALL J, MOCHIZUKI DY, SCHMIERER A, MOSLEY B, MARCH CJ, URDAL D, GILLIS S, COSMAN D, GOODWIN RG: (Letter to the Editor) Stimulation of B-cell progenitors by cloned murine interleukin-7. *Nature* 1988, 333:571–573.
IL-7, previously known as a pre-B cell factor, produced from bone marrow stromal cells is cloned. Multiple species of the IL-7 messenger RNA are detected in spleen and thymus.

30. •• RETTENMIER CW, ROUSSEL MF: Differential processing of colony-stimulating factor 1 precursors encoded by two human cDNAs. *Mol Cell Biol* 1988, 8:5026–5034.
The 1.6 kb CSF-1 cDNA and 4 kb CSF-1 cDNA are stably transfected into NIH3T3 cells. Both give rise to focus formation when cotransfected with c-*fms* cDNA, indicating that both cDNA encode active CSF-1 which acts in an autocrine fashion. The 4 kb cDNA product is expressed on the plasma membrane, dimerized, then rapidly proteolyzed to generate a mature soluble CSF-1. On the other hand, the 1.6 kb cDNA product is stable as a precursor at the cell surface and is slowly cleaved to a soluble form.

31. • MANOS MM: Expression and processing of a recombinant human macrophage colony-stimulating factor in mouse cells. *Mol Cell Biol* 1988, 8:5035–5039.
Rapid secretion of the expressed 4 kb CSF-1 cDNA product is demonstrated.

32. • MORRISSEY PJ, GOODWIN RG, NORDAN RP, ANDERSON D, GRABSTEIN KH, COSMAN D, SIMS J, LUPTON S, ACRES B, REED SG, MOCHIZUKI D, EISENMAN J, CONLON PJ, NAMEN AE: Recombinant interleukin-7, pre-B cell growth factor, has costimulatory activity on purified mature T cells. *J Exp Med* 1989, 169:707–716.
This report demonstrates that IL-7, in the presence of concanavalin A, induces IL-2 and IL-2 receptor production from purified peripheral T

cells, leading to their proliferation. This resembles the activity of IL-6, but IL-7 is shown to act independently of IL-6.

33. • HILTON DJ, NICOLA NA, METCALF D: Purification of a murine leukemia inhibitory factor from Krebs ascites cells. *Analyt Biochem* 1988, 173:359–367.

See [34].

34. • HILTON DJ, NICOLA NA, GOUGH NM, METCALF D: Resolution and purification of three distinct factors produced by Krebs ascites cells which have differentiation-inducing activity on murine myeloid leukemic cell lines. *J Biol Chem* 1988, 263:9238–9243.

2 forms of LIF, LIF-A and LIF-B, are identified, and LIF-A is purified to homogeneity. LIF-A and LIF-B have identical biological activities and share the same receptor, suggesting that they are probably identical polypeptides but differ in their modification.

35. • GOUGH NM, GEARING DP, KING JA, WILSON TA, HILTON DJ, NICOLA NA, METCALF D: Molecular cloning and expression of the human homologue of the murine gene encoding myeloid leukemia-inhibitory factor. *Proc Natl Acad Sci USA* 1988, 85:2623–2627.

Tl man LIF cDNA is cloned and expressed in yeast. The human LIF protein appears to recognize the same receptor as mouse LIF and can induce differentiation of M1 cells.

36. •• SMITH AG, HEATH JK, DONALDSON DD, WONG GG, MOREAU J, STAHL M, ROGERS D: Inhibition of pluripotential embryonic stem cell differentiation by purified polypeptides. *Nature* 1988, 336:688–690.

Highly purified DIA from Buffalo rat liver cell-conditioned media is capable of supporting continued *in vitro* growth of DA-1a, murine Moloney leukemia virus induced leukemia cells, on which HILDA/LIF has similar actions. Purified recombinant HILDA/LIF has exactly the same molecular weight and has the same activity on embryonic stem cell lines as DIA.

37. •• GODARD A, GASCAN H, NAULET J, PEYRAT M-A, JACQUES Y, SOULILLOU J-P, MOREAU J-F: Biochemical characterization and purification of HILDA, a human lymphokine active on eosinophils and bone marrow cells. *Blood* 1988, 71:1618–1623.

Highly purified HILDA is shown to be a potent chemoattractant for mouse eosinophils and an activator for human eosinophils. Although it does not have an eosinophil-CSF activity, it displays burst-promoting activity on human marrow.

38. •• WILLIAMS RL, HILTON DJ, PEASE S, WILSON TA, STEWART CL, GEARING DP, WAGNER EF, METCALF D, NICOLA NA, GOUGH NM: (Letter to the Editor). Myeloid leukaemia inhibitory factor maintains the developmental potential of embryonic stem cells. *Nature* 1988, 336:684–687.

Purified recombinant LIF can substitute for DIA in the maintenance of totipotent embryonic stem cell lines that retain the potential to form chimeric mice. High-affinity binding sites for LIF are present on embryonic stem cell and embryonal carcinoma cell lines.

39. •• MOREAU J-F, DONALDSON DD, BENNETT F, WITEK-GIANNOTTI J, CLARK SC, WONG GG: (Letter to the Editor). Leukaemia inhibitory factor is identical to the myeloid growth factor human interleukin for DA cells. *Nature* 1988, 336:690–691.

Cloning and characterization of HILDA cDNA have revealed that the encoded protein is structurally identical to human LIF.

40. •• HILTON DJ, NICOLA NA, METCALF D: Specific binding of murine leukemia inhibitory factor to normal and leukemia monocytic cells. *Proc Natl Acad Sci USA* 1988, 85:5971–5975.

This report demonstrates that LIF has a specific receptor on M1 cells that allow LIF, but not other cytokines, to bind. The interaction of LIF with its receptor is of high affinity. LIF binding sites are found in the bone marrow, the spleen and the peritoneal cavity.

Cytokines

A Practical Approach

Edited by

F. R. BALKWILL

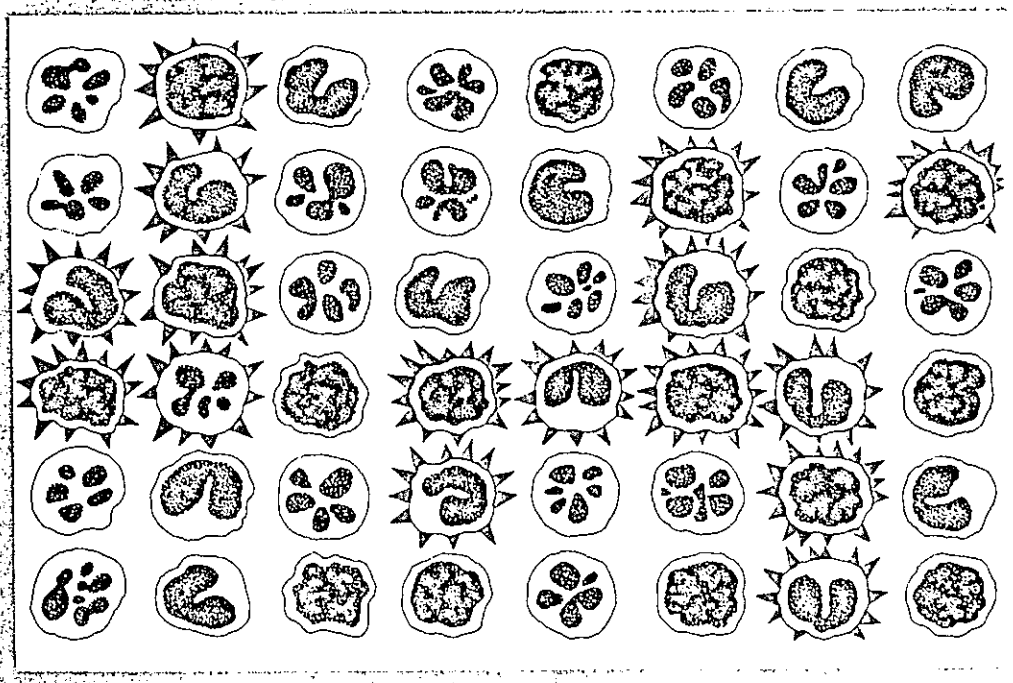

The Practical Approach Series

A2

Alternative and historical names of cytokines

Cytokine	Other names
IL-1α IL-1β	Haemopoetin-1, lymphocyte activating factor, B cell activating factor, leukocyte endogenous mediator, activating factor, endogenous pyrogen, catabolin mononuclear cell factor, osteoclast activating factor, epidermal derived thymocyte activating factor
IL-2	T cell growth factor
IL-3	Multi-CSF, multi-lineage haemopoeitic cell growth factor, mast cell growth factor, eosinophilic CSF, megakaryocytic CSF, burst promoting activity, erythroid CSF, neutrophil granulocyte CSF, persisting cell stimulating factor, histamine producing cell stimulating factor, Thy-1 inducing factor, CFU-s stimulating factor, haemopoetin-1
IL-4	B cell stimulatory factor-1, BCGF1, BCGF-γ
IL-5	Eosinophil differentiation factor, Eosinophil-csf, TRF (in mice), IgA enhancing factor, killer helper factor
IL-6	26 kDa protein, hepatocyte stimulatory factor, IFN-β2, plasmacytoma growth BCDF2/BCGF2, BSF-2, myeloma cell growth factor, monocyte granulocyte inducer II
IL-7	Pre-B cell growth factor, lymphopoietin-1 factor
IL-8	Family of cytokines incl monocyte chemo-factor attractant protein-1, IP1, CGP, lymphocyte derived NAP, monocyte derived neutrophil chemoattractant factor, MCP-1, MGSA, NAP-1, gro, γIP10
IL-9	p40, mast cell growth factor, mast cell enhancing activity, T cell growth factor
IL-10	Cytokine synthesis inhibitory factor
IL-11	Plasmacytoma stimulator activity
TNF	Cachectin, TNF-α
LT	TNF-β
IFN-α	Leukocyte interferon, Type I interferon
IFN-β	Fibroblast interferon, Type I interferon
IFN-γ	Immune interferon, Type II interferon
TGF-β	At least 3 forms—TGF-β1, TGF-β2, TGF-β3
GM-CSF	CSF-2, CSF-α

Appendix 2

G-CSF	
M-CSF	CSF-1
EGF	Urogastrone
TGF-α	
PDGF	
Acidic FGF	Endothelial cell growth factor. Eye derived growth factor, heparin binding growth factor, chondrosarcoma derived growth factor, prostatropin
Basic FGF	b heparin binding growth factor, endoethelial cell growth factor, cartilage derived growth factor, tumour angiogenesis factor
IGF-I	Somatomedin-C, sulphation factor
IGF-II	Multiplication stimulating activity
NGF	

Zusätzliche Literatur

1. Arai K.I., F.Lee, A.Miyajima, S.Miyatake, N.Arai, T.Yokota: (1990) Cytokines: Coordinators of immune and inflammatory responses. Ann.Rev.Biochem. **59**, 783-836

2. Sporn M.B., .B.Roberts: (1988) Peptide growth factors are multifactorial. Nature **332**, 217-219

3. Sporn M.B., .B.Roberts: (1985) Autocrine growth factors and cancer. Nature **313**, 745-747

4. Heidin C.H., Westermark B.: (1984) Growth factors: Mechanisms of action and relation to oncogenes. Cell **37**, 9-20

MIKRONUKLEI-BILDUNG UND ZYTOTOXIZITÄT

Dr.M.Nüsse

GSF-Forschungszentrum für Umwelt und Gesundheit
Neuherberg

Measurement of Micronuclei by Flow Cytometry

MICHAEL NÜSSE, WOLFGANG BEISKER, JOHANNES KRAMER, BEATE M. MILLER, GEORG A. SCHREIBER, SILVIA VIAGGI, EVA MARIA WELLER, JURINA WESSELS

GSF-Institut für Biophysikalische Strahlenforschung
D-8042 Neuherberg

Author's adress:

Dr. Michael Nüsse
GSF-Forschungszentrum für Umwelt und Gesundheit
Institut für Biophysikalische Strahlenforschung
AG Durchflußzytometrie
Ingolstädter Landstr. 1
D-8042 Neuherberg
Germany
Tel: 089-31873426
FAX: 089-31873349

I. Introduction

The induction of micronuclei in cell cultures or human lymphocytes exposed to ionizing radiation or chemicals can be used as a measure of both structural and numerical chromosome aberrations. Micronuclei represent genetic material that is lost from the genome of the cell during mitosis. They may contain one or several acentric chromosome fragments (clastogenic action) or one or several whole chromosomes (by interfering of the inducing agent with the mitotic spindle apparatus), or even combinations of both. Usually, the frequency of micronuclei in cells is measured by microscopic scoring of micronuclei in several hundred or thousand cells. Some attempts have therefore been made to automate micronucleus scoring by image analysis (Pincu et al., 1985, Fenech et al., 1988, Romagna and Staniforth, 1989, Tates et al., 1990) or by flow cytometry (Hutter and Stöhr, 1982, Hayashi et al., 1992, Grawe et al., 1992 for micronucleus scoring in mouse erythrocytes, Nüsse and Kramer, 1984, Nüsse et al., 1992, 1993, Schreiber et al., 1992, Schreiber et al., 1993, Nüsse and Miller, 1993 for micronucleus scoring in cell cultures or human lymphocytes).

We describe here a technique to obtain a suspension of micronuclei and nuclei for flow cytometric measurement of the frequency of micronuclei per main nuclei in cell cultures or human lymphocytes exposed to ionizing radiation or chemicals. With this technique it is additionally possible to measure the DNA content of micronuclei and main nuclei for a simultaneous analysis of the cell cycle distribution (main nuclei) and the DNA distribution of micronuclei. Analysis of the DNA distribution of micronuclei can give additional information on the mechanisms of action of the inducing agent (Nüsse et al., 1993, Miller and Nüsse, 1993). The two-step method includes a treatment of the cells with a salt solution I that contains a detergent followed by an additional treatment with solution II containing citric acid and sucrose. Both solutions contain ethidium bromide (EB) as DNA specific fluorescent dye, in some cases Hoechst 33258 (HO) is used additionally. By this two-step treatment the cellular membrane and the cytoplasm is destroyed completely and nuclei and micronuclei are released in suspension. No mechanical treatment or centrifugation steps are necessary to obtain a solution of main nuclei and micronuclei, because mechanical treatment would induce cellular or nuclear debris that could overlap the small micronuclei during flow cytometric measurement. The nuclear membrane is maintained and mitotic cells that could release chromosomes in the suspesnion are usually not destroyed (Nüsse et al., 1990).

Flow cytometric measurements of DNA content of micronuclei and nuclei are performed simultaneously using log-mode, because the differences in DNA content between micronuclei and

nuclei can be a factor of 100. Light scatter signals (forward light scatter and side scatter) are measured simultaneously for a discrimination of unspecific debris from micronuclei.

II. Application

The primary applications of the technique are measurement of the frequency of micronuclei in cell cultures exposed to ionizing radiation or chemicals (Nüsse and Kramer, 1984, Nüsse et al., 1992, Miller and Nüsse, 1993), measurement of the DNA distribution of micronuclei (Nüsse et al., 1993, Miller and Nüsse, 1993, Weller et al., in preparation) and also sorting of micronuclei with the same DNA content for further analysis of the chromosomal content of micronuclei with fluorescence in situ hybridization using for example centromeric DNA probes (Miller and Nüsse, 1993). The technique was also used to analyse micronuclei in primary cultures of rat hepatocytes exposed to chemicals in vitro (Cao et al., 1993). With a modification of the technique we have studied micronucleus induction in human lymphocytes exposed to ionizing radiation (Schreiber et al., 1993). We are currently studying the applicability of the technique for a biological dosimetry in humans exposed to ionizing radiation. The method can probably not be used with in vivo material as for example tumor cells (with the exception of rat hepatocytes and human lymphocytes), because in vivo cells usually show a high amount of debris that will overlap the micronuclei during flow cytometric measurement and will therefore not allow an anambiguous identification of micronuclei.

III. Materials

Two solutions are used for the preparation of a suspension of nuclei and micronuclei:

Solution I (prepare 500 ml stock):

584 mg/ml NaCl
1000 mg/l Nacitrate
10 mg/l RNase from bovine pancreas (Serva)
0.3 ml/l Nonidet P40

Solution II (prepare 500 ml stock):

15 mg/l citric acid
0.25 M sucrose

These solutions are made up using distilled water and should be filter-sterilized. They can be stored at $4^{o}C$ for at least several months. Ethidium bromide is added before use from a stock solution of 1 mg/ml in distilled water. Both solutions are used at room temperature.

Cells: Micronucleus induction in several cell lines has been studied with this technique including Chinese hamster embryo cells, various strains of V79 cells, mouse Ehrlich ascites tumor cells growing in suspension, mouse NIH-3T3 cells, human lymphoma K37 cells, rat hepatocytes and human lymphocytes. The cells are usually treated with radiation or chemicals and analysed during exponential growth.

IV. Cell Preparation and Staining

For flow cytometric analysis of micronuclei, an exponentially growing cell culture should be used, because the cells have to progress through the cell cycle for the induction of micronuclei after (ionizing radiation, chemicals) or during (chemicals) treatment. $0.5\text{-}1 \times 10^6$ cells are centrifuged at about 100 g (around 800-1000 rpm) for 5 min. The supernatant medium should be removed completely by aspirating or carefully pouring off. The small cell pellet should be shaken slightly (no vortexer) to resuspend the cells in the remaining medium (less than 50 μl).

1 ml of solution I containing 10 μg/ml EB (prepared before use and filtered again) is added to the cell pellet, the cell suspension can be vortexed for a short time interval (2 sec).

After about 1 h at room temperature, 1 ml of solution II containing also 10 μg/ml EB (prepared before use and filtered again) is added to the the cell suspension, the suspension is vortexed again (2 sec) and stored at $4^{o}C$ before flow cytometric measurement. The suspension of nuclei and micronuclei can be measured directly after preparation or can be stored at $4^{o}C$ for at least 2-3 days before measurement.

If the DNA distribution of nuclei has to be measured additionally it is recommended to use 25 μg/ml EB in solution I and 40 μg/ml EB in solution II. A better coefficient of variation CV of the G_1-peak is obtained with these concentrations. The CV of the G_1-peak in several different cell cultures was usually found to be between 2% and 3%.

For a better discrimination of debris from micronuclei, especially in human lymphocytes, 1.5 μg/ml Hoechst 33258 can be added to solution II. With this double staining technique two lasers are necessary to excite EB and HO simultaneously (see below).

V. Critical Aspects of the Procedure

Several aspects have been found to influence the preparation of a suspension of nuclei and micronuclei containing a low frequency of unspecific debris:

1. Cell number: If cell numbers higher than $1.5x10^6$ cells are treated with solution I and II (1 ml each), a fraction of the cells was found to have cytoplasm and cellular membranes. These cells could contain micronuclei that were not released in suspension thus influencing the results of micronucleus frequency. In this case a high amount of debris was usually observed. It is therefore recommended not to use too many cells.

2. Before measurement, the suspension of nuclei and micronuclei should be checked in a fluorescence microscope using additionally phase contrast optics. All nuclei should be free of cytoplasm and membranes, micronuclei should be separated from nuclei. If this is not the case, three reasons should be considered:
A) The cell number was too high (see 1).
B) Solution I should be prepared again. Because of the high viscosity of Nonidet P40 it could be that solution I did not contain the proper concentration of the detergent.
C) The cell pellet contained too much medium. In this case try to remove the medium completely or use 2 or 3 ml of solution I and II instead of 1 ml each.

3. A large amount of unspecific debris always hampers the simultaneous measurement of micronuclei and nuclei. Usually, most of the debris can be gated out using forward or side scatter measurements if the debris is produced by fragments of cytoplasm or membranes (see below). However, dying cells in the cell culture as for example necrotic or apoptotic cells could lead to DNA fragments that show similar fluorescence intensities and light scatter signals as micronuclei but are clearly no micronuclei as verified by sorting of the respective particles. If plateau phase cultures are studied or if chemicals are used for the induction of micronuclei, this effect has to be taken into consideration. It is therefore recommended to sort the particles considered to be micronuclei for visual examination before using the technique extensively.

4. Some chemicals (i.e. colcemid or the tear gas CS) induce polyploid cells containing several nuclear fragments. Because the cellular membrane is destroyed, these nuclear fragments are released in suspension and will overlap the micronuclei during flow cytometric measurement. It can therefore not always be expected that the frequency of micronuclei measured by flow cytometry agrees with results obtained by microscopic scoring. The criteria for the definition of

micronuclei are not the same for microscopic scoring and for flow cytometry (see Nüsse et al., 1992 and below).

VI. Standards

It is recommended to use a good preparation of a suspension of micronuclei and nuclei as a standard before starting the flow cytometric measurements of freshly prepared samples. Because the suspensions of nuclei and micronuclei can usually be stored for several weeks, such a sample could be helpful for adjusting the flow cytometer.

VII. Instruments

1. Flow cytometry:

EB fluorescence (pulse height and pulse area) and side scatter as well as forward scatter of micronuclei and nuclei were measured simultaneously in list-mode using a FACSstar$^+$ cell sorter (Becton Dickinson). Excitation of EB was provided by the 488 nm line (500 mW) of an argon laser, EB fluorescence was collected with a longpass filter (combination of KV 550 and OG 590). All parameters were registered in log mode (4 decades). This is usually necessary, because micronuclei can have relative DNA contents between 0.5% and 50% of the DNA content of G_1-phase nuclei. The trigger was set between 0.5% and 1% of the mean EB fluorescence of the G_1-peak.

It is also possible to measure both types of particles in linear mode (as done earlier with a CYTOFLUOROGRAF, Ortho Instruments). In this case usually not all micronuclei are registered together with the nuclei, because due to the electronic threshold particles with DNA content lower than about 2% of G1-nuclei will be cut off.

If nuclei and micronuclei were double stained with EB and HO, dual laser flow cytometry has to be performed (FACStar$^+$). In this case the first laser was adjusted to 488 nm (500 mW), the second laser to the UV-multilines (351.1-363.8 nm, 200-500 mW). Pulse height of forward light scatter and side scatter were recorded from the first laser as well as direct EB fluorescence (long pass filter as above). EB fluorescence was used as main trigger parameter. The second laser was used for excitation of HO. Direct fluorescence emission of HO was registered at wavelengths around 424 nm (bandpass filter 424DF20, Becton Dickinson). Fluorescence emission of EB excited by energy transfer from HO was measured at wavelengths around 630 nm (bandpath filter 630DF20, Becton Dickinson). Both fluorescences were split by a dichroic mirror with transmission between 340 nm and 490 nm and reflection between 590 nm and 640 nm.

2. Data analysis:

For analysis of the frequency and DNA distribution of micronuclei stained with EB alone (single laser flow cytometry), a first gate has to be set to exclude unspecific debris according to side scatter and forward scatter (see Fig. 1). The frequency of micronuclei (number of micronuclei: N_{mn}) per nuclei (number of nuclei: N_n), N_{mn}/N_n, is calculated using additional gates for

micronuclei (usually between 1% and 50% of the mean DNA content of G1-phase nuclei) and nuclei (all nuclei are included).

For analysis of micronuclei that were double stained with EB and HO, quotients of two of the three fluorescences measured have to be calculated for all particles included in the first gate. Only particles with the same quotients as the main nuclei are considered to be DNA containing particles (micronuclei). Details of this more complicated technique are published elsewhere (Schreiber et al., 1992, 1993).

VIII. Results and Discussion

Fig. 1 a-f show typical measurements of a suspension of nuclei and micronuclei prepared as described above and stained with EB. In this example, human lymphoma cells (K37 cells growing in vitro) were irradiated with ionizing radiation and analysed 36 h after exposure, when all cells have divided. Fig. 1 a-c show the unirradiated control, Fig. 1 d-f the irradiated sample (1 Gy). In the first two dot plots (a and d) forward scatter (FSC) is plotted against EB fluorescence, in the second two dot plots (b and e) side scatter (SSC) is plotted against EB fluorescence. All parameters were measured in log mode. The large windows include nuclei and micronuclei and exclude unspecific debris, the two smaller windows (in Fig. 1 b and e) are used for the calculation of N_{mn}/N_n. Micronuclei were counted in the region between 1% and 10% of the mean DNA content of G_1-phase nuclei. Fig. 1 c and f show the DNA distributions of micronuclei and nuclei.

Fig. 1 shows that with both light scatter signals micronuclei can be separated from unspecific debris as verified by sorting of the respective particles. We usually measure both light scatter signals simultaneously with EB fluorescence and use the two gates (Fig. 1a,b or d,e) to exclude debris.

After treatment of cell cultures with ionizing radiation, the results (frequency of micronuclei: N_{mn}/N_n) obtained with this flow cytometric technique agree well with results from microscopic scoring. This is caused by the fact that radiation-induced micronuclei are mainly formed by acentric chromosome fragments that have a well defined size distribution (see for details Nüsse et al., 1993). This is not always the case, especially when certain chemicals are used to induce micronuclei. In this case micronuclei can sometimes be formed by whole single chromosomes or even by several chromosomes due to spindle damage (see for details Nüsse et al., 1992, Miller et al., 1992, Miller and Nüsse, 1993). In this case micronuclei can be found that have DNA contents between 1% and more than 50% of the mean DNA content of G_1-phase nuclei. Therefore, depending on the size of the window used to count the number of micronuclei N_{mn}, different values of N_{mn}/N_n can be obtained that not necessarily agree with results obtained by microscopic scoring.

Besides measurements of the frequency of micronuclei, the DNA distribution of micronuclei can be measured and analysed. We have shown recently that several factors can influence the DNA content of micronuclei (Nüsse et al., 1993): The size distribution of the chromosomes, DNA synthesis in micronuclei (see also Kramer et al., 1990) and the presence of chromosome fragments or whole chromosomes in micronuclei. Flow cytometric measurement of the DNA distribution of micronuclei alone can not be used to completely understand the mechanisms that

lead to the formation of micronuclei. Other techniques, as for example the use of DNA probes (chromosome specific probes or a combination of telomeric and centromeric DNA probes) and fluorescence in situ hybridization are necessary as shown recently by us (Miller et al., 1992, Nüsse et al., 1993, Miller and Nüsse, 1993).

Fig. 2 show two examples to illustrate this point. The left DNA distribution of micronuclei and nuclei (Fig. 2b) was obtained after treating Chinese hamster embryo cells (CCHE) with the tear gas 2-chlorobenzylidene malonitrile (CS). The peaks in the micronucleus distribution show that the majority of micronuclei induced by CS was formed by whole single chromosomes as verified by anti-kinetochore staining of micronuclei with the CREST serum (see for details Nüsse et al., 1992). Similar results were obtained in mouse NIH-3T3 cells. Here the presence of whole single chromosomes in micronuclei was independently verified using fluorescence in situ hybridization with centromeric and telomeric DNA probes (Miller and Nüsse, 1993). Fig. 2 d shows in contrast to these results the DNA distribution of micronuclei induced in CCHE cells by bromodeoxyuridine (BrdUrd). In this case most BrdUrd-induced micronuclei (more than 95%) were formed by acentric chromosome fragments as verified by anti-kinetochore staining of micronuclei (Weller et al., in preparation). The peaks in this micronucleus distribution were caused by a non-random breakage of specific chromosomes (see for details Weller et al., in preparation).

In conclusion, flow cytometry can be used to analyse frequency and DNA distribution of micronuclei induced in cell cultures by ionizing radiation or chemicals. For this measurement, a suspension of micronuclei and nuclei has to be prepared. Light scatter signals in combination with fluorescence intensity measurements are used to discriminate micronuclei from unspecific debris. With the same preparation the DNA distribution of nuclei can additionally be measured showing the effects of the treatments on the cell cycle progression.

References

Cao, J., Leibold, E., Beisker, W., Schranner, T., Nüsse, M., and Schwarz, L.R. (1993). Toxicology in Vitro, in press.
Fenech, M., Jarvis, L.R., and Morley, A.A. (1988). Mutat. Res. 203, 33-38.
Grawe, J., Zetterberg, G., and Anneus, H. (1992). Cytometry 13, 750-758.
Hayashi, M., Norppa, H., Sofuni, T., and Ishidate, M. (1992). Mutagenesis 7, 251-256.
Hutter, K.-H., and Stöhr, M. (1982). Histochemistry 75, 353-362.
Kramer, J., Schaich-Walch, G. and Nüsse, M. (1990). Mutagenesis 5, 491-495.
Miller, B.M., and Nüsse, M. (1993). Mutagenesis, in press.
Miller, B.M., Werner, T., Weier, H.-U., and Nüsse, M. (1992). Radiat. Res. 130, 177-185.
Nüsse, M., Beisker, W., Hoffmann, C., and Tarnok, A. (1990). Cytometry 11, 813-821.
Nüsse, M., and Kramer, J. (1984). Cytometry 5, 20-25.
Nüsse, M., Kramer, J., and Miller, B.M. (1993). Int. J. Radiat. Biol. in press.
Nüsse, M., Recknagel, S., and Beisker, W. (1992). Mutagenesis 7, 57-67.
Pincu, M., Callisen, H., and Norman, A. (1985). Int. J. Radiat. Biol. 47, 423-432.
Romagna, F., and Staniforth, C.D. (1989). Mutat. Res. 213, 91-104.
Schreiber, G.A., Beisker, W., Bauchinger, M., and Nüsse, M. (1992). Cytometry 13, 90-102.
Schreiber, G.A., Beisker, W., Braselmann, H., Bauchinger, M., Bögl, K.W., and Nüsse, M. (1993). Int. J. Radiat. Biol., in press.
Tates, A.D., van Welie, M.T., and Ploem, J.S. (1990). Int. J. Radiat. Biol. 58, 813-825.

Figure legends

Fig. 1:

Flow cytometric measurement of a suspension of micronuclei and nuclei. Human lymphoma cells K37 were irradiated with gamma radiation (D = 1 Gy).

a-c: control, d-f: irradiated sample.

The dot plots (10.000 events measured) show:
a and d: Forward scatter (FSC) against EB fluorescence (relative DNA content). The window shows the discrimination between micronuclei and debris according to forward scatter.
b and e: Side scatter (SSC) against EB fluorescence (relative DNA content). The window shows the discrimination between micronuclei and debris according to side scatter. The windows for micronuclei (N_{mn}) and nuclei (N_n) are indicated additionally.
c and f: DNA distribution of the suspension of nuclei and micronuclei. All particles found in both large windows are displayed.

Fig. 2:

Flow cytometric measurement of a suspension of micronuclei and nuclei.
Left panel (a,b): Micronuclei induced by the tear gas CS (16 h, 60 μM).
Right panel (c,d): Micronuclei induced by bromodeoxyuridine (16 h, 100 μM).
a,c: Forward scatter against EB fluorescence.
b,d: DNA distribution of micronuclei and nuclei from the particles defined by the gate in Fig. 2 a and c.

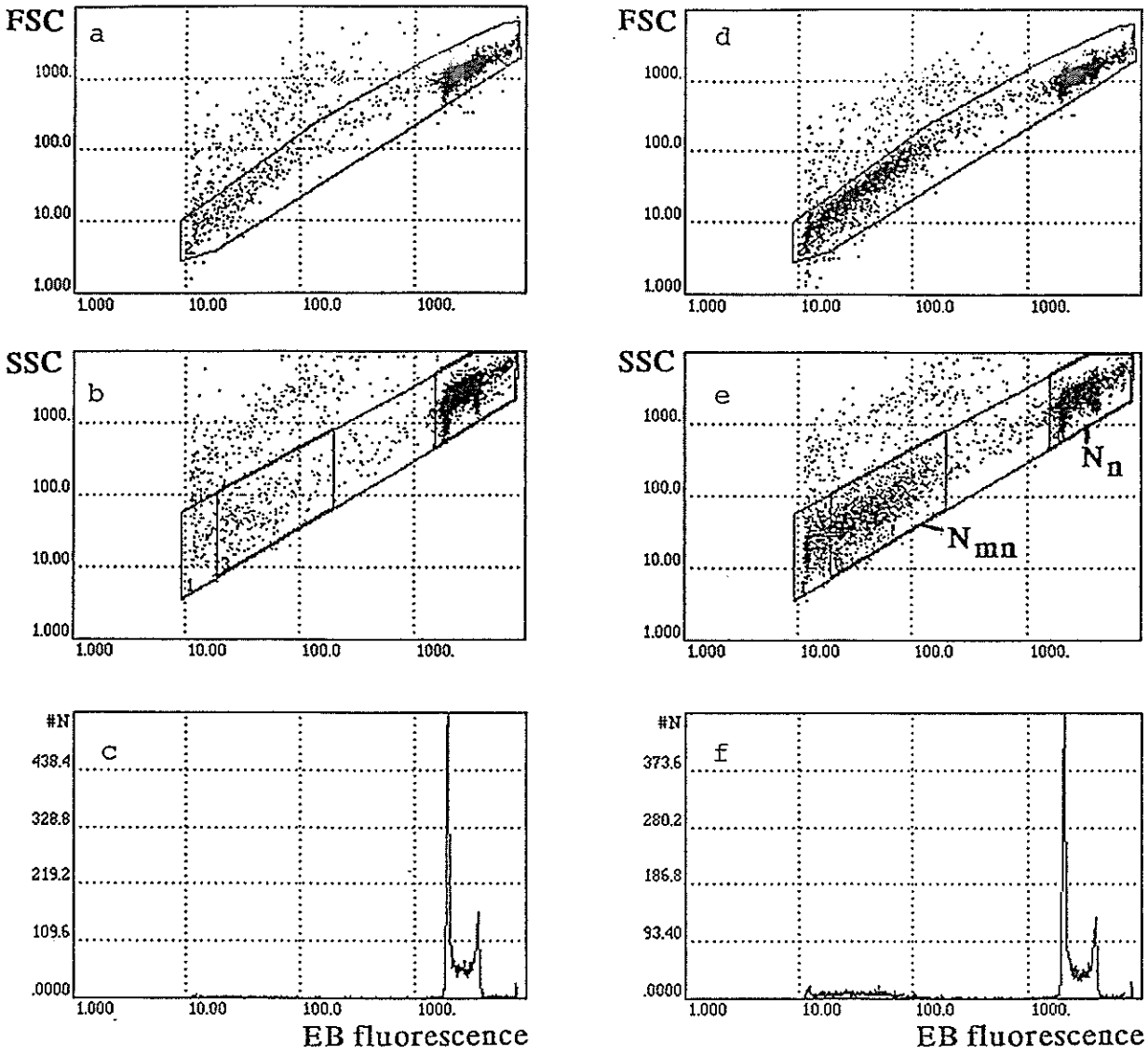
FSC
a
1000.
100.0
10.00
1.000
1.000
10.00
100.0
1000.
FSC
d
SSC
b
SSC
e
N_n
N_{mn}
#N
c
438.4
328.8
219.2
109.6
.0000
#N
f
373.6
280.2
186.8
93.40
.0000
EB fluorescence
EB fluorescence

Fig. 1

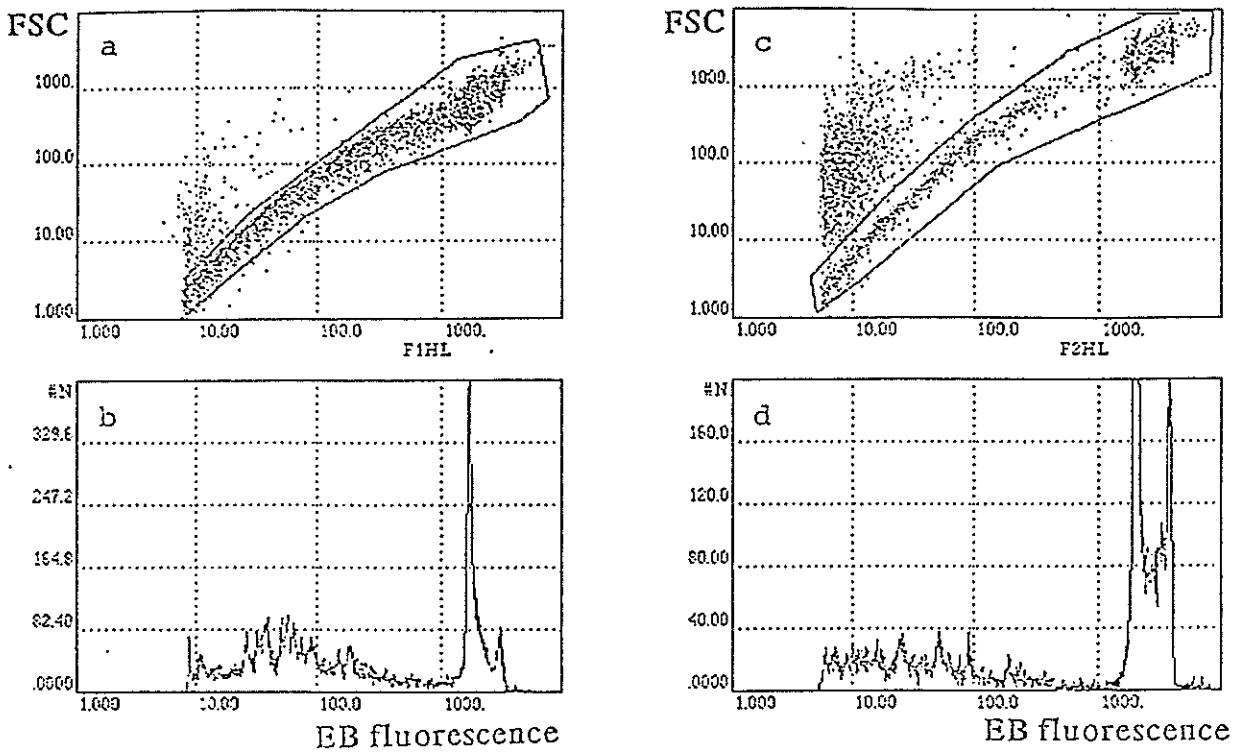
FSC
a
1000.
100.0
10.00
1.000
1.000
10.00
100.0
1000.
F1HL
FSC
c
1000.
100.0
10.00
1.000
1.000
10.00
100.0
1000.
F2HL
#N
b
329.6
247.2
164.8
82.40
.0000
1.000
10.00
100.0
1000.
EB fluorescence
#N
d
160.0
120.0
80.00
40.00
.0000
1.000
10.00
100.0
1000.
EB fluorescence

Fig. 2

© 1992 Wiley-Liss, Inc.

Cytometry 13:90–102 (1992)

Multiparametric Flow Cytometric Analysis of Radiation-Induced Micronuclei in Mammalian Cell Cultures

Georg A. Schreiber, Wolfgang Beisker, Manfred Bauchinger, and Michael Nüsse
Institut für Sozialmedizin und Epidemiologie des Bundesgesundheitsamtes 1000 Berlin (G.A.S.), and GSF-Institut für Biophysikalische Strahlenforschung (W.B., M.N.) and GSF-Institut für Strahlenbiologie (M.B.), 8042 Neuherberg, Germany

Received for publication March 11, 1991; accepted July 30, 1991

A new flow cytometric method is presented that quantifies the frequency of radiation-induced micronuclei in mammalian cell cultures with high precision. After preparing a suspension of main nuclei and micronuclei stained with ethidium bromide and Hoechst 33258, both types of particles are measured simultaneously in a flow cytometer using forward light scatter and three fluorescence emission intensities excited by UV, 488 nm, and by energy transfer from Hoechst 33258 to ethidium bromide. Nonspecific debris overlapping the micronucleus distribution especially in the low fluorescence intensity region was discriminated from micronuclei by calculating ratios of the different fluorescences. The frequencies of radiation-induced micronuclei measured with this new technique agreed well with results obtained by conventional microscopy. The lower limit of the DNA content of micronuclei identified by this technique was found to be about 0.5%–0.75% of the DNA content of G_1-phase nuclei. Dose effect curves and the time-dependent induction of micronuclei were measured for two different mouse cell lines.

Key terms: Ionizing radiation, automated micronucleus test, micronucleus size, sorting of micronuclei, energy transfer, dose and time dependence of micronucleus induction

The induction of micronuclei in cell cultures exposed to ionizing radiation or chemicals can be used as a measure of both structural and numerical chromosome aberrations (10). Micronuclei represent genetic material that is lost from the genome during mitosis. They may either contain acentric chromosome or chromatid fragments, as for example after irradiation (11,22), or whole chromosomes, as for example after treatment of cells with chemicals interfering with the mitotic spindle apparatus (22). It has been shown recently that a discrimination between these two types of micronuclei can be achieved by using anti-kinetochore antibodies (4,5,12,22,23). Even DNA synthesis in radiation-induced micronuclei has been demonstrated using incorporation of bromodeoxyuridine (BrdUrd) and anti-BrdUrd antibodies (15,18).

Usually, microscopic scoring of micronuclei in some hundreds of cells is a time-consuming procedure. Therefore several attempts have been made to automate micronucleus scoring by image analysis (3, 8,24,25,27) or by flow cytometric techniques (9,17, 21,28). Flow cytometry seems to be an especially powerful technique to analyse rapidly large numbers of cells. A disadvantage of this technique, however, is that each particle present in the suspension produces a signal that will be registered separately. It is therefore difficult or sometimes impossible to discriminate between micronuclei and nonspecific background.

Some years ago we developed a technique enabling one to obtain a suspension of nuclei and micronuclei for flow cytometric measurements of these particles according to their DNA content. Using this technique it was not only possible to measure the number of micro-

Address reprint requests to Dr. Michael Nüsse, GSF-Forschungszentrum für Umwelt und Gesundheit, Institut für Biophysikalische Strahlenforschung, Arbeitsgruppe Durchflußzytometrie, Ingolstädter Landstr. 1, 8042 Neuherberg, Federal Republic of Germany.

nuclei per cell nucleus but also to measure the size distribution of micronuclei. A fast and precise measurement of the size distribution of micronuclei seems to be of interest because it was shown to be related to the inducing agent (13,29). However, with this technique, micronuclei with a DNA content lower than 2% of the DNA content of the G_1-phase cells could not be discriminated from debris particles of various origin which overlapped the DNA distribution of micronuclei especially in the low DNA content region.

Because various amount of debris were found in suspensions of micronuclei and nuclei prepared from several mammalian cell lines and human lymphocytes, we tried to modify the preparation of the suspensions as well as the flow cytometric measurements using various parameters in addition to DNA content measurements alone. With this modified technique it is now possible to separate most of the debris from the micronuclei according to their different physical properties. Therefore, sensitivity and reproducibility of this flow cytometric technique to measure number and size distribution of micronuclei are greatly improved. It appears to be possible to detect rather low dose exposures to ionizing radiation for a biological dosimetry in humans. The determination of DNA distribution of micronuclei can be used for an analysis of mechanisms underlying the formation of micronuclei by various chemicals and ionizing radiations.

MATERIALS AND METHODS

Cells

Cells of an Ehrlich ascites tumor (EAT) cell line (DI = 1.2) were cultured as described earlier (19,21). Briefly, the cells growing in suspension were passaged by daily dilution to 2×10^5 cells/ml in A_2-medium especially designed for these cells (14) to ensure continuous exponential growth. For experiments measuring the number of micronuclei (N_{mn}) per main nuclei (N_n), N_{mn}/N_n, after irradiation as function of dose, cells were diluted to 5×10^4 cells/ml, irradiated after 24 h (at about 2×10^5 cells/ml), and harvested 13 h after irradiation. To measure the time dependence of micronucleus formation after irradiation, cells were irradiated 12 h after dilution. At indicated times, 1–2 ml aliquots were taken from cultures set up with 35 ml medium in 75 cm^2 culture flasks.

3T3-cells (attached growing cells) were cultured under the same conditions described for EAT cells, except that cells grew in RPMI 1640 medium supplemented with 15% FCS, 1% L-glutamine and 1% penicillin/streptomycin. Cells were passaged by dilution to 5×10^6 cells per 75 cm^2 flask every third day. For measurements of dose dependence, cells were diluted to 1×10^6 cells per 25 cm^2 flask, irradiated after 24 h, and harvested by trypsinization after an additional 25 h. For measurements of time dependence, cells were diluted to 5×10^5 cells per 25 cm^2 flask.

Irradiation

Cells were irradiated with ^{137}Cs γ-rays of a HWM-2000 machine (Siemens, Erlangen). The dose rate was 0.9 Gy/min. The total irradiation time had to be chosen in 0.1 min periods which resulted in a lowest applicable dose of 0.09 Gy. For measurements of dose response curves in the range between 0 and 1 Gy, three tissue culture flasks per dose were irradiated together and analysed in parallel.

Preparation of a Suspension of Micronuclei and Nuclei for Flow Cytometry

A slightly modified two-step precedure described by Nüsse and Kramer (21) was used for the preparation of a suspension of micronuclei and main nuclei. Briefly, 5×10^5 cells were centrifuged at 140*g* for 5 min. The supernatant was removed completely, the cell pellet was vortexed, and 0.5 ml of solution 1 (584 mg/l NaCl, 1 g/l Nacitrate, 10 mg/l RNAse from bovine pancreas, Serva, 0.3 ml/l Nonidet P40, 10 μg/ml ethidium bromide (EB)) was added and vortexed again. Samples were kept for 15 min at room temperature. An equal amount of solution 2 (1.5% citric acid, 250 mM sucrose, 10 μg/ml ethidium bromide, 1.5 μg/ml Hoechst 33258) was added and vortexed. After 30 min at room temperature either the flow cytometric measurements were performed or the samples were stored at 4°C until analysis which was always within 2 d.

Preparation and Microscopic Scoring of Micronuclei

Cells were centrifuged at 140*g* for 5 min. After adding 2 ml of a weak hypotonic solution (8.1 g/l NaCl, 0.056 g/l KCl) for 15 min cells were fixed with a methanol/acetic acid (1:3) solution for at least 20 min and centrifuged on slides for 5 min at 140*g* in a cytocentrifuge. After air drying, the DNA in main nuclei and micronuclei was stained with 5 μg/ml propidium iodide. Scoring of main nuclei and micronuclei was done by fluorescence microscopy in cells with preserved cytoplasm only.

Flow Cytometry

Dual laser flow cytometry and sorting were performed using a FACSTAR$^+$ flow cytometer (Becton Dickinson, BD). Data recording was done with a HP 9000 Series 300 computer (Hewlett Packard) in list mode using the FACSTAR$^+$ RESEARCH software. The first laser (Innova 90, Coherent Radiation) was adjusted to the 488 nm line (1,000 mW) and the second laser (Innova 100) to the UV multilines (351.1 nm–363.8 nm, 500 mW). Pulse height of forward light scatter (FSC) as well as of EB-emission excited at 488 nm (EB^{48}) was recorded using a 488 nm bandpass filter (BD, 488BP10) and a combination of KV 550 and OG 590 filters (Schott), respectively. Pulse area of Hoechst 33258 emission (HO^{360}) was recorded using a 424 nm bandpass filter (BD, 424DF44), and additionally pulse

area of EB-emission excited by the emission of the Hoechst 33258 dye and to a lower extent by the UV multiline laser (EB^{HO}) was recorded using a 630 nm bandpass filter (BD, 630DF22). Fluorescence from HO^{360} and EB^{HO} was split by a dichroic mirror with transmission between 340 nm and 490 nm and reflection between 590 and 640 nm. EB emission excited by the 488 nm line of the first laser (EB^{488}) was used as trigger. All parameters were recorded in log-scale (4 decades). The trigger was set to 0.5% of the mean fluorescence of the G_1-peak of the main nuclei. For each sample 40,000 events were recorded.

Data Analysis

Besides discriminating micronuclei and main nuclei from nonspecific debris particles in the dot plot of FSC vs. EB^{HO} fluorescence using a first gating procedure, the following two quotients of recorded fluorescence were calculated to specify DNA-containing particles: EB^{488}/HO^{360} and EB^{488}/EB^{HO}. Only particles with the same quotients as the main nuclei were considered to be DNA-containing particles. Particles that were defined by the first FSC vs. EB^{HO} gate and EB^{488}/HO^{360} and EB^{488}/EB^{HO} quotients (second and third gate) and with EB^{HO} intensities between 0.5% and 10% were assumed to be micronuclei.

For these calculations, data were transferred to an MS-DOS IBM-compatible computer system by FAST-file-software (BD). All multidimensional numerical calculations, interactive data manipulation, and automatic data analysis as well as color graphic display of data were performed with the *D*ata *A*nalysis *S*oftware (DAS V3.21) developed by us (Beisker, in preparation). In the following, a short description of this software package is given:

The DAS package is an interactive program system as well as an interpretative language with elements from FORTRAN 77, BASIC, C, and other special implementations. It is entirely written in FORTRAN 77 (MICROSOFT FORTRAN 77 VERSION 5.0). Graphic support of all graphic adapters (CGA, Hercules, EGA, VGA) for IBM-compatible computers is included as well as arithmetical coprocessor support.

DAS allows handling of one- and two-dimensional correlated histograms as well as list mode data of up to 15 parameters. The length of the list mode files that the package can handle is only restricted by the available disk space and not by computer memory. All commands which can be entered by command string or via a menu system can be stored as programs to be run by DAS. Up to a depth of ten, programs can call each other to allow efficient programming for automatic and routine work.

Mathematical commands such as numerical integration, differentiation, and Fourier transformations have been implemented in DAS. Graphic input of up to eight gates for selecting certain areas in the up to 15 dimensional data space can be done numerically, by a mouse or cursor, or as a result of numerical calculations. Each of the mathematical operations can be applied to all or to a subset of events in list mode data files. Therefore ratios, logarithms, square roots, and all other functions can be applied to list mode data after data recording. List mode data from nearly all commercially available flow cytometers can be transferred to the DAS system. A more detailed description of this software is far beyond the scope of this paper and will be given in further publications.

Using the list mode data operations, the ratioing and gating of data for the micronucleus determination can automatically be done to separate main nuclei and micronuclei from cellular debris.

RESULTS

Analysis of Micronuclei Using EB-Fluorescence and Forward Scatter Measurements

The suspension of EB-stained main nuclei and micronuclei always contains debris of unknown origin and unknown amount. It is therefore expected that the debris could overlap the DNA-distribution of the micronuclei especially in the low fluorescence area, thus influencing the EB-fluorescence distribution and number of micronuclei measured in the flow cytometer. Because it is expected that these particular debris particles will usually be irregularly shaped and thus have different light scatter properties compared to the round micronuclei, forward light scatter (FSC) and EB-fluorescence (EB^{488}) were measured simultaneously. Figure 1a shows a dot plot (log FSC against log EB^{488}) of a suspension of micronuclei and main nuclei. This dot plot allows discrimination between micronuclei and debris with higher FSC. Figure 1b shows the DNA distribution of micronuclei and main nuclei from the window in Figure 1a. The DNA distribution of the main nuclei shows, additional to the hyperdiploid cell nuclei, a small fraction of hypertetraploid cell nuclei demonstrated by sorting of these nuclei. About 3–5% of the cells in this cell culture were hypertetraploid cells (no clumping of cell nuclei was observed by the preparation procedure).

Sorting of the area indicated as MN in Figure 1a revealed that most particles with EB^{488} larger than 2% of the G_1-nuclei were in fact micronuclei. Micronuclei sorted from an area below 2% of the G_1-nuclei, however, showed an increased contamination with small debris. Therefore, only micronuclei larger than 2% of G_1-nuclei can be detected easily. This is demonstrated in Figure 2, showing, as an example, the number of micronuclei per main nuclei, N_{mn}/N_n, as a function of dose in 3T3-cells. For this analysis the number of micronuclei N_{mn} was calculated using different lower thresholds in the distributions (EB^{488} between 0.65% and 3% of G_1-nuclei). Figure 2 shows that with decreasing threshold (0.65%), a well-defined dose dependence was not obtained; the points are more scattered due to the different amount of debris with low fluorescence signals in the various samples. Especially for doses below 0.72 Gy a dose dependence was not found. Using

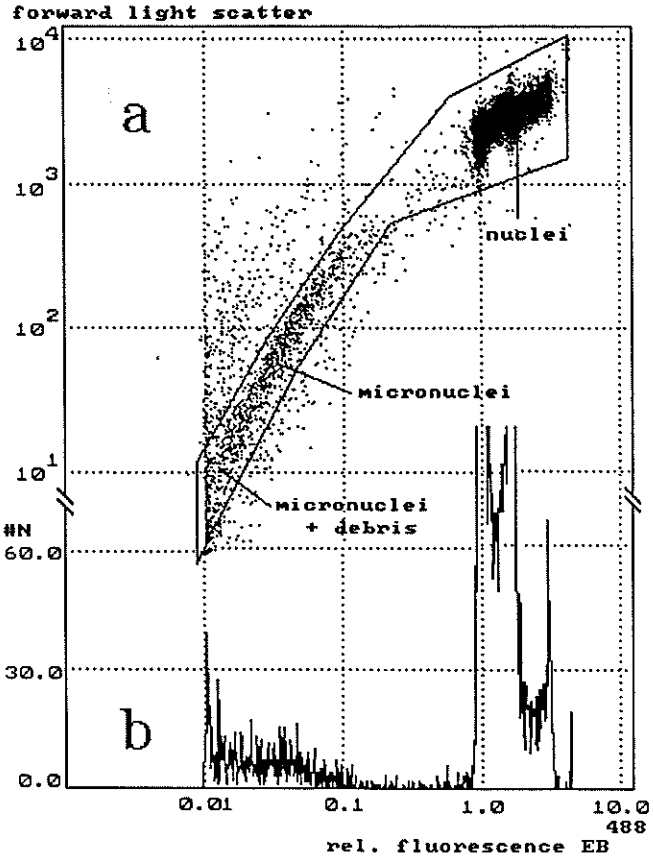

FIG. 1. a: Dot plot (forward light scatter vs. EB-fluorescence excited with 488 nm EB^{488}) of micronuclei and main nuclei in suspension. The suspension of micronuclei and main nuclei was prepared from EAT cells 13 h after irradiation with 1 Gy γ-radiation. The gate (window) used for the calculations of N_{mn}/N_n (N_{mn}: number of micronuclei, N_n: number of main nuclei) is indicated. b: DNA distribution of micronuclei (including some debris) and main nuclei defined by the window in a. Number of particles (#N) as a function of relative EB^{488}-fluorescence intensity (logarithmic scale). The G_1-phase nuclei are positioned at EB^{488} = 1.0. The hypertetraploid main nuclei have EB^{488}-fluorescence intensities larger than 2.0.

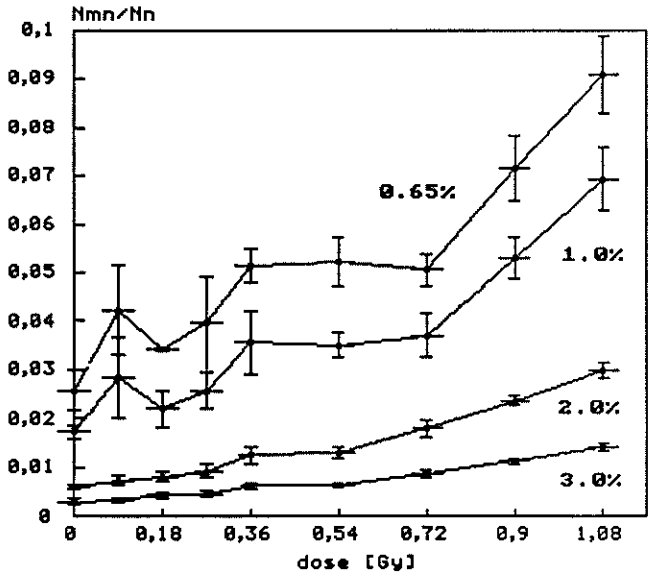

FIG. 2. Fraction of micronuclei (N_{mn}) per main nuclei (N_n), N_{mn}/N_n, as a function of dose in 3T3-cells prepared 20 h after irradiation. In these measurements, the trigger of the EB^{488}-fluorescence of micronuclei was set at 0.65% of the EB^{488}-fluorescence of the G_1-phase nuclei. The number of micronuclei N_{mn} was calculated by setting the thresholds to 0.65%, 1%, 2%, and 3% of the G_1-peak fluorescence respectively. Three culture flasks were irradiated and analysed for each point.

the higher thresholds (2% or 3%), an improved dose dependence was observed. The number of micronuclei per main nuclei was, however, smaller compared to results obtained by microscopic scoring (see also Fig. 9) because a fraction of the micronuclei with lower DNA content was cut off by this analysis.

Analysis of Micronuclei Using EB/Hoechst-Fluorescence and Forward Scatter Measurements

To improve the discrimination of micronuclei from nonspecific debris especially in the lower fluorescence region, a double staining technique of the DNA in nuclei and micronuclei was developed using a dye combination of EB and Hoechst 33258 (HO) that allows energy transfer from HO to EB. EB was excited by 488 nm from the first laser and additionally by the HO-fluorescence. HO was excited by the UV multilines from the second laser. Therefore, three fluorescence signals were measured simultaneously: 1) EB-fluorescence (EB^{488}) excited by 488 nm, 2) HO-fluorescence (HO^{360}) excited by 360 nm (UV-laser), 3) EB-fluorescence (EB^{HO}) excited by energy transfer from HO. Figure 3a shows these three fluorescences, EB^{488}, EB^{HO}, and HO^{360} (mean channel number of G_1-peak); Figure 3b shows the coefficient of variation CV of the G_1-peak as a function of the Hoechst dye concentration in solution 2. The optimal Hoechst dye concentration (maximal EB^{HO}- and HO^{360}-fluorescence, minimal CV) was found to be about 1.5 μg/ml.

Figure 4 shows a dot plot of EB^{HO} against FSC for the data in Figure 1. In this plot the critical area of low EB^{488} fluorescence is split into two distinct separated subpopulations corresponding to specific EB-binding (micronuclei) and unspecific EB-binding (debris). Sorting of the subpopulations indicated in Figure 4 showed that the purity of the sorted micronuclei is increased considerably (Fig. 5, sorts 2–4), although a few debris particles were still found in the very low EB^{HO} region (sort 4). Only debris particles were found in sorts 5 and 6 (Fig. 5).

Analysis of Micronuclei Using Additional Gating Procedures for a Better Discrimination of Debris

Assuming that the DNA binding properties of the two dyes EB and HO are similar in micronuclei and main nuclei, two ratios of the fluorescence signals mea-

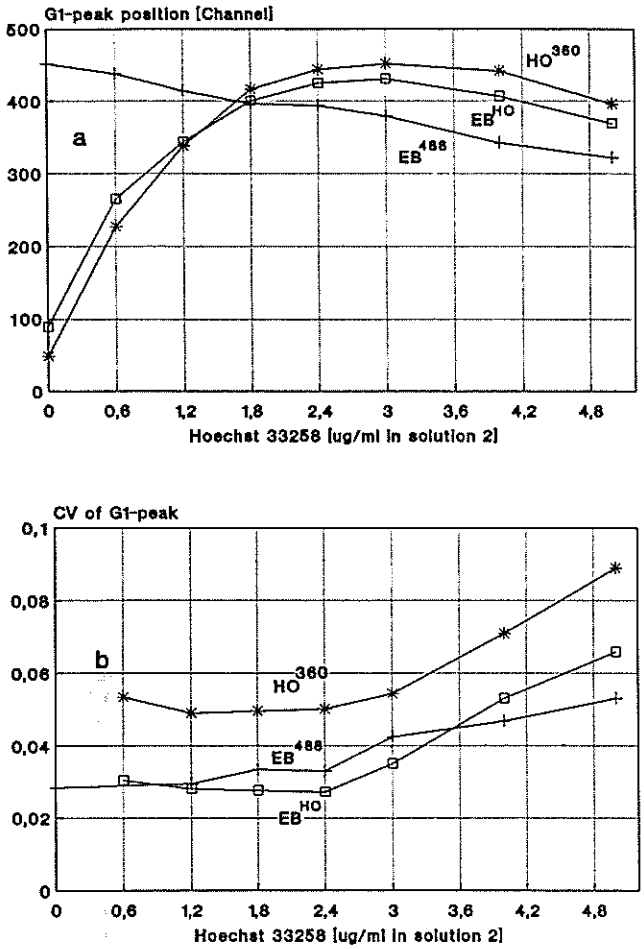

FIG. 3. (a) Mean channel number and (b) coefficient of variation of EB^{488}-, EB^{HO}- and HO^{360}-fluorescences of G_1-phase cells as a function of the concentration of Hoechst 33258 in solution 2. 3T3 cells were treated by adding same volumes of solutions 1 and 2. Both solutions contained 10 μg/ml ethidium bromide.

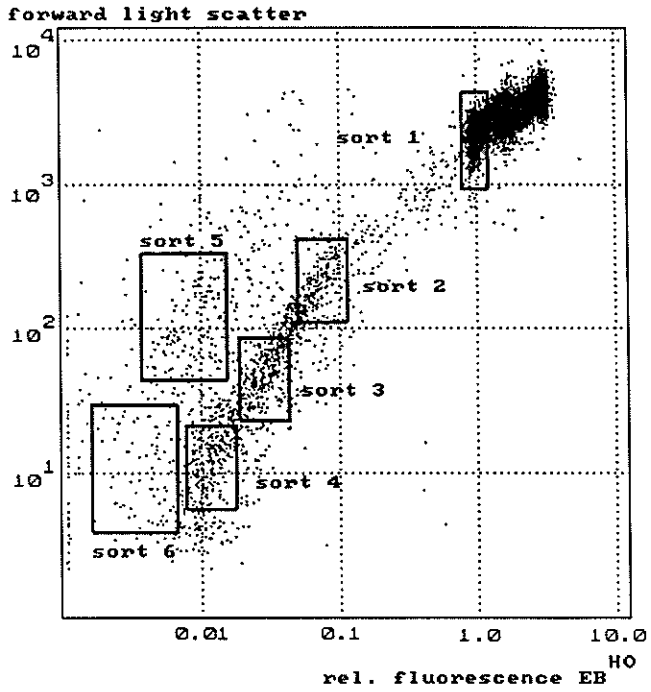

FIG. 4. Dot plot (forward light scatter vs. EB^{HO}-fluorescence) of the same suspension of micronuclei and nuclei shown in Figure 1. The DNA in these particles was stained with EB and Hoechst 33258 simultaneously. Several sort windows (1–6) are indicated.

sured simultaneously were calculated for an even better discrimination between micronuclei and debris (EB^{488}/HO^{360} and EB^{488}/EB^{HO}). Figure 6 (micronuclei and nuclei of irradiated 3T3-cells, D = 2 Gy) shows dot plots of EB^{488} against FSC (I) and EB^{HO} against FSC (II), as well as dot plots of the ratio EB^{488}/HO^{360} against EB^{HO} (III) and the ratio EB^{488}/EB^{HO} against HO^{360} (IV). By the first gating procedure (window in Fig. 6II) nonspecific debris with high FSC intensities is excluded. A second gate (window in Fig. 6III) is used that includes only those particles having the same ratio EB^{488}/HO^{360} as the main nuclei. Finally, a third gate (window in Fig. 6IV) is used that includes only those particles having the same ratio EB^{488}/EB^{HO} as the main nuclei. Only those particles that are found in all three gates were assumed to be micronuclei. Particles with EB^{HO}-fluorescence between 0.5% and 10% of the G_1-peak fluorescence were counted as micronuclei and used for the quantitative analysis.

By these three gating procedures most nonspecific debris could be separated from the micronuclei. The result of the gating procedures is shown in Figure 7 (a: unirradiated control, b: irradiated samples). The EB^{488}-fluorescence for main nuclei and micronuclei is shown for the ungated particles in (I). The EB^{HO}-fluorescence after activating the 1. gate, the 1. and the 2. gate as well as the 1., 2., and 3. gate is shown in Figure 7II, III, and IV respectively. The EB^{HO}-distribution (II) shows two populations in the low fluorescence range. The left population is strongly reduced by the second gate (III) and nearly totally reduced by the third gate (IV). The right population is however reduced only slightly.

Figure 8 shows an analysis of the same data presented in Figure 2 after using the three additional gating procedures. An improved dose dependence was obtained for a trigger setting of 0.65% compared to the same trigger setting in Figure 2. Differences in the relative amount of debris between various samples can therefore be minimized. Figure 9 shows a comparison between this new flow cytometric technique and results from microscopic observations for 3T3 cells. A very good agreement between both methods is observed.

Lower Limits of the Micronucleus Distribution

A comparison of Figure 7b (II) and (IV) shows that particles with EB^{HO} fluorescences smaller than about

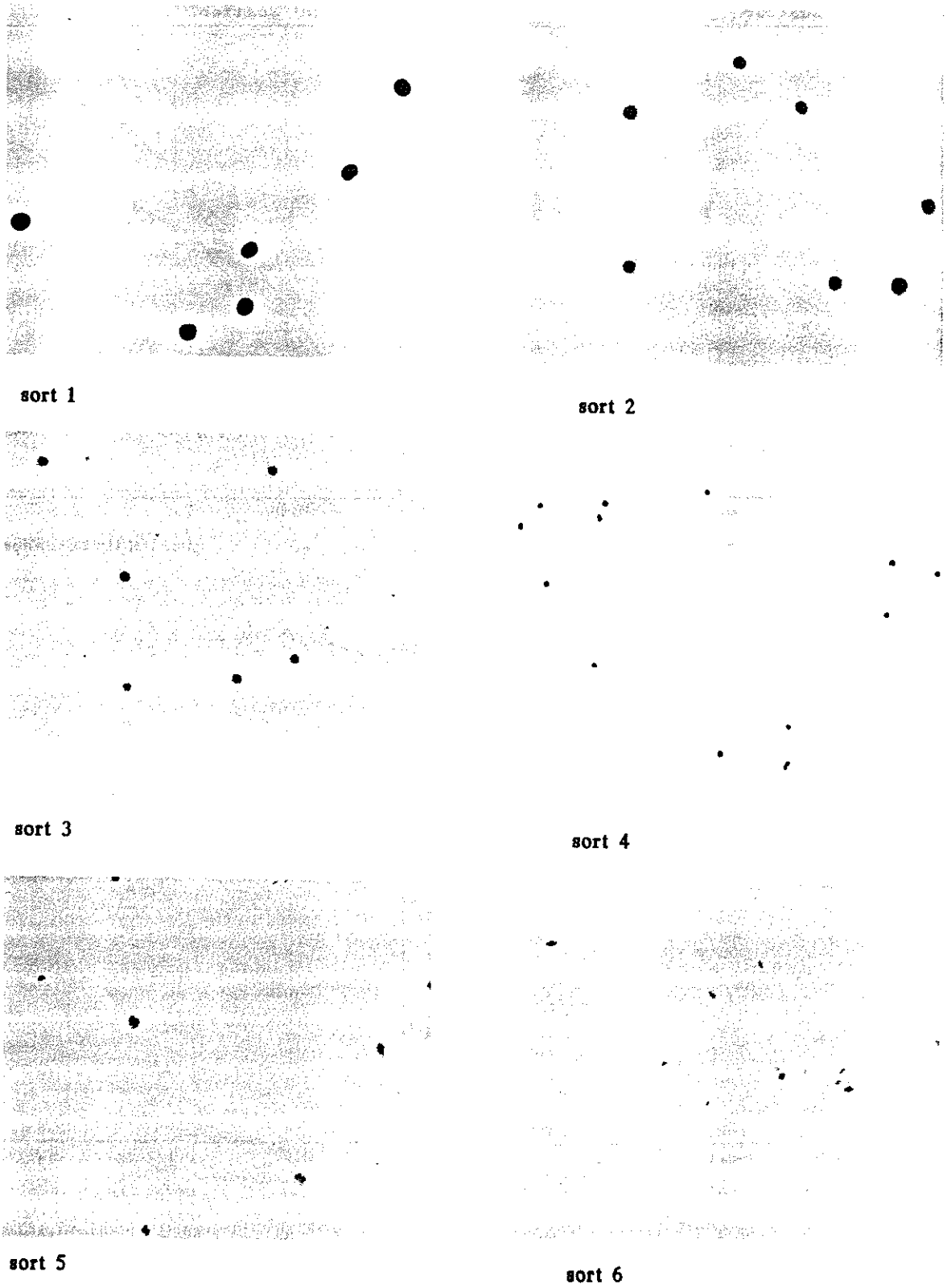

FIG. 5. Photographs of particles sorted from the windows 1–6 indicated in Figure 4. Sort 1: G_1-phase nuclei. Sort 2: Large micronuclei. Sort 3: Intermediate micronuclei. Sort 4: Small micronuclei and debris. Sorts 5 and 6: Debris. Magnification of all photographs is the same. Ca. ×800.

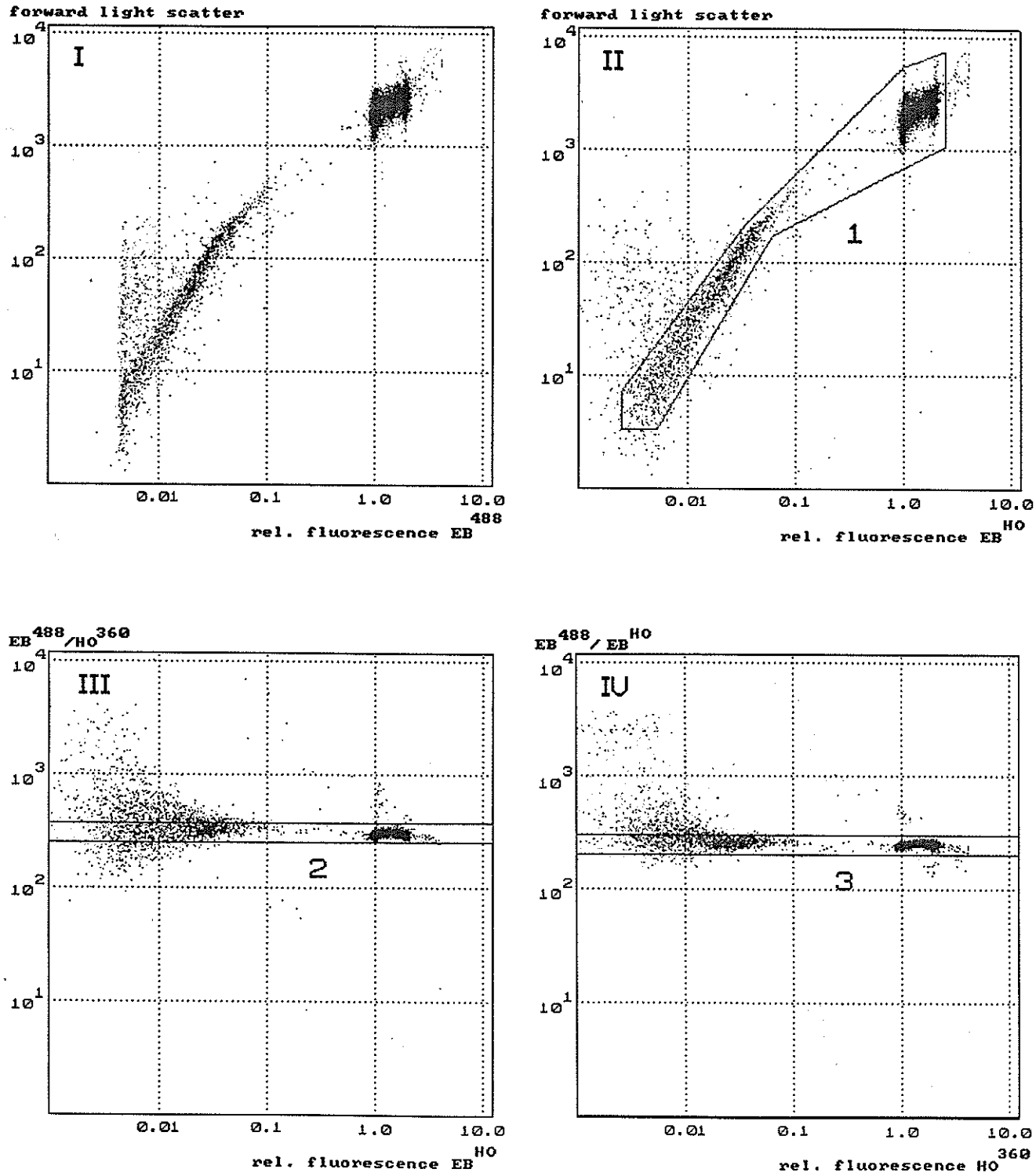

FIG. 6. Micronucleus analysis using ratios of various DNA fluorescence signals in addition to analysis of forward light scatter and EB^{HO}-fluorescences as shown in Figure 4. Data were obtained with 3T3 cells (D = 2 Gy). I: Dot plot of forward scatter vs. EB^{488}. Trigger at 0.5% of the mean channel number of the G_1-phase nuclei. All measured particles are plotted blue. II: Dot plot of forward scatter vs. EB^{HO}. The green window indicates the first gate for the calculations of N_{mn}/N_n. III: Dot plot of the quotient of the EB^{488}- and HO^{360}-fluorescence, EB^{488}/HO^{360}, vs. EB^{HO}-fluorescence. The second gate (red) is defined by the quotient range of the nuclei. All particles inside the green window in histogram II are plotted green. Particles outside the green window in histogram II are plotted blue. IV: Dot plot of the quotient of the EB^{488}- and EB^{HO}-fluorescence, EB^{488}/EB^{HO}, vs. HO^{360}-fluorescence. Again, the third gate (dark blue) is defined by the quotient range of the nuclei. Particles inside the red gate in histogram III are plotted red. After activating gates 1 (green) and 2 (red), only those dots that have the same color as the nuclei (red) and that are within the third gate (dark blue) are considered for the calculation of N_{mn}/N_n.

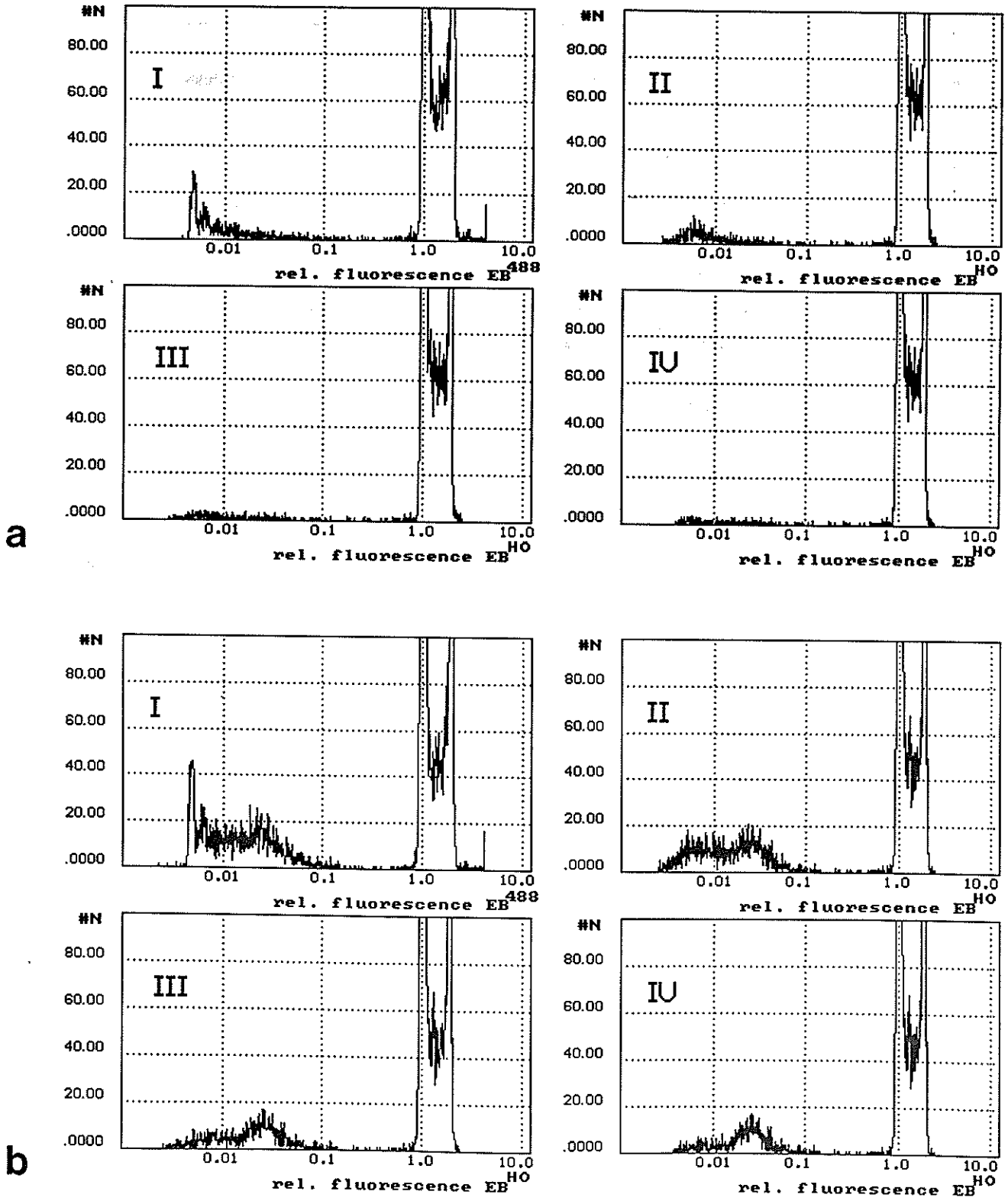

FIG. 7. DNA distributions corresponding to the dot plots of Figure 6 for unirradiated (a) and irradiated (2 Gy) 3T3 cell preparations (b). I: EB^{488}-fluorescence distributions of ungated data. II: EB^{HO}-fluorescence distributions after activating gate 1. II: EB^{HO}-fluorescence distributions after activating gates 1 and 2. III: EB^{HO}-fluorescence distributions after activating gates 1, 2, and 3.

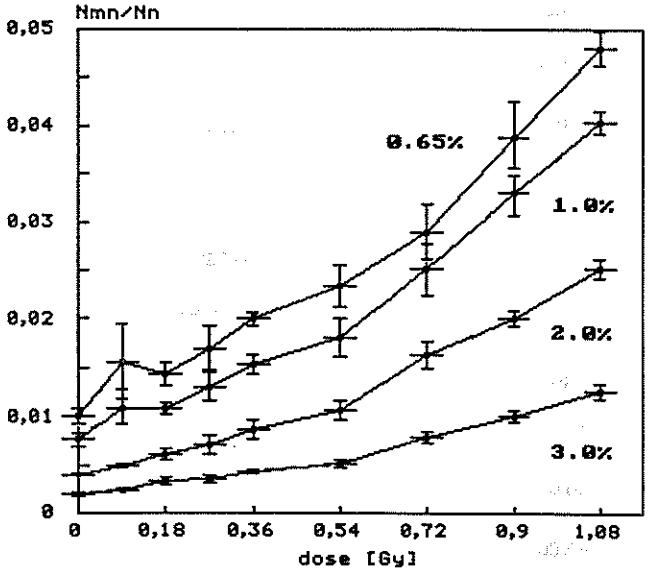

FIG. 8. Fraction of micronuclei per main nuclei, N_{mn}/N_n, as a function of dose in 3T3-cells prepared 20 h after irradiation (same data as in Fig. 2). For this analysis the three gates were activated as indicated in Figures 6 and 7. The number of micronuclei N_{mn} was again calculated for different thresholds (EB^{488}-fluorescence between 0.65% and 3% of G_1-phase nuclei). Three culture flasks were irradiated and analysed for each point.

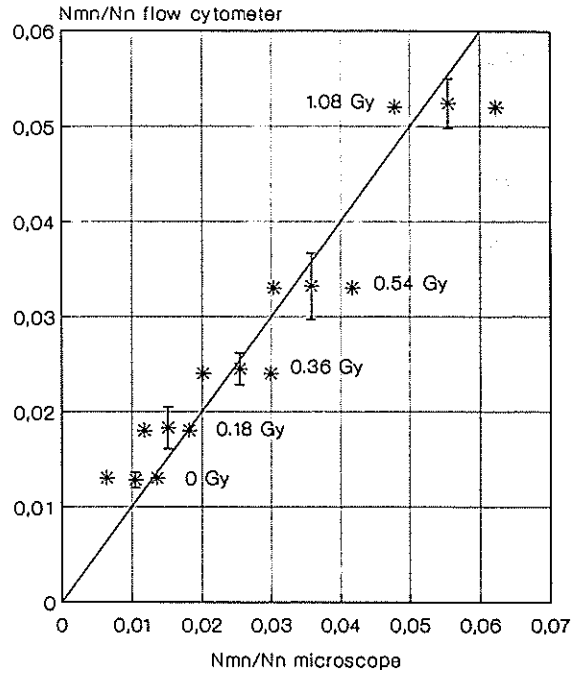

FIG. 9. Comparison between the micronucleus frequencies N_{mn}/N_n of 3T3 cells measured by microscopic observation and by the flow cytometric analysis. For each data point three culture flasks were irradiated simultaneously. From each flask a micronucleus preparation was done by flow cytometry; 40,000 events were measured for each preparation. Data analysis was performed with the three gates according to Figures 6 and 7. SD are indicated. For microscopic analysis cells were fixed with methanol/acetic acid and centrifuged on slides. After staining with 5 μg/ml propidium iodide, micronuclei and nuclei were scored in cells with preserved cytoplasm. For each data point 1,000 nuclei were scored. The calculated range of standard deviations is indicated by asterisks.

1% of the G_1-peak fluorescences do not contribute to a large extent to the frequency of micronuclei. Most micronuclei observed and defined by this technique have a DNA content larger than about 1% of the G_1-phase nuclei. This result is shown in more detail in Figure 10. Samples of a suspension of main nuclei and micronuclei induced by radiation with 1 Gy and 2 Gy were repeatedly measured with a constant trigger channel (channel No. 15) by moving the G_1-peak fluorescence from channel No. 500 (trigger is positioned at 3% of G_1-peak) to channel No. 4000 (trigger is positioned at 0.37% of G_1-peak). The data were analysed according to the method described in Figure 7 except that all particles with EB^{HO}-fluorescence below 10% of the G_1-peak fluorescence were registered as micronuclei. Figure 10 shows the frequency of micronuclei N_{mn}/N_n as a function of the position of the G_1-peak during measurement. The frequency of micronuclei N_{mn}/N_n increased as long as the G_1-peak was moved from channel No. 500 to 2000 and reached a plateau when the G_1-peak was positioned between channel No. 2000 and 4000. Although the relative number of particles with low fluorescence intensities increased with increasing position of the G_1-peak during measurement, the frequency of micronuclei defined by the repeated gating procedures remained constant at relative trigger settings between about 0.37% and 0.75% of the G_1-peak (Fig. 10, lower abscissa). This result indicates 1) that nearly all of the particles with EB^{488} fluorescences lower than 0.75% of the G_1-peak fluorescence are assumed to be debris and are therefore not considered to be micronuclei and 2) that the smallest micronuclei identified by this method have DNA contents between about 0.75% and 1% of the G_1-phase nuclei.

Applications

Figure 11 shows the dose response relationships for the induction of micronuclei in 3T3-cells and EAT-cells. As compared to EAT-cells, background and induced micronucleus frequencies were always lower in 3T3-cells. This probably reflects a differential radiosensitivity of both cell lines. Figure 12 shows the time dependence of the micronucleus induction in these two cell lines (a: exponentially growing 3T3-cells, b: exponentially growing EAT-cells) after irradiation with various doses. Due to the shorter cell cycle time of EAT-cells (t_c = 12 h) the maximum of N_{mn}/N_n is reached earlier compared to 3T3-cells (t_c = 24 h).

DISCUSSION

The primary objective of the investigations described here was the development and application of a new flow cytometric technique to measure the frequency of radiation-induced micronuclei in cell cultures. We

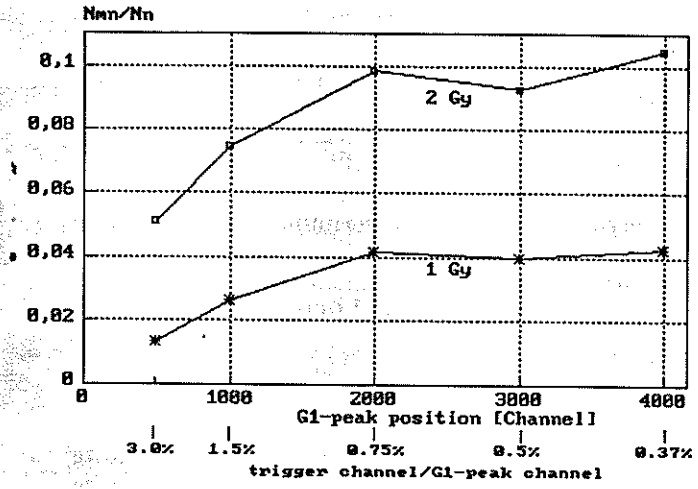

FIG. 10. Micronucleus frequency, N_{mn}/N_n, as a function of the position of the G_1-peak during measurement. For the measurements, the threshold of the EB^{488}-fluorescence was constantly set to channel No. 15 of the log scale. The G_1-peak was registered at different channel numbers ranging from channel No. 500 to 4000. Data analysis was performed by activating the two quotient gates EB^{488}/HO^{360} and EB^{488}/EB^{HO} only. Particles with an EB^{HO}-fluorescence below 10% of the G_1-peak fluorescence were considered to be micronuclei.

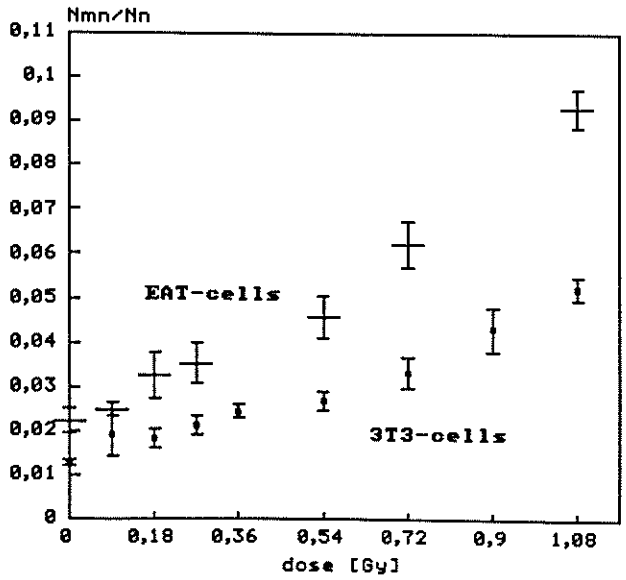

FIG. 11. N_{mn}/N_n as a function of dose in irradiated EAT and 3T3 cells in 13 h and 24 h after irradiation, respectively. For each data point three culture flasks were irradiated simultaneously. At harvest time, micronuclei were prepared from each flask; 40,000 events were measured from each preparation. Data analysis was performed with three gates according to Figures 6 and 7. SD are indicated.

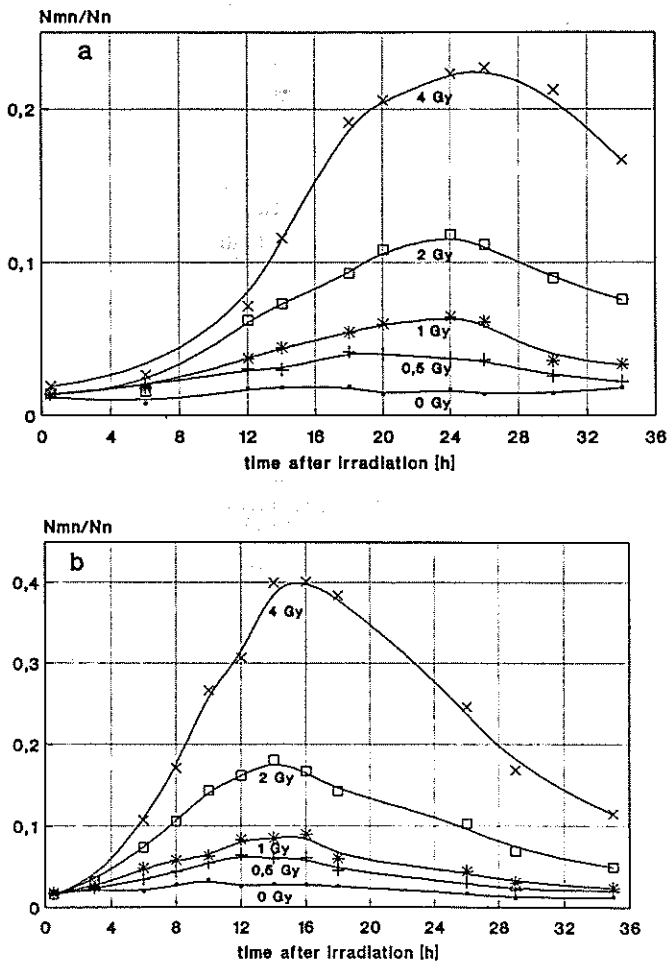

FIG. 12. Time dependence of micronucleus formation in irradiated 3T3 (a) and EAT cells (b). For each data point 25,000 events were measured per sample. Data analysis was performed with three gates according to Figures 6 and 7. For each data point one culture flask of 3T3 cells was irradiated. At harvest time, cells were trypsinized and a suspension of micronuclei and main nuclei was prepared. EAT cells were irradiated in one culture flask at a cell concentration of 1×10^5 cells/ml. At harvest time an aliquot of cells was taken for preparation.

have previously published a method to obtain a suspension of micronuclei and nuclei for measurements of the DNA content and the frequency of radiation-induced micronuclei in a mouse tumor cell line using flow cytometry (21). The advantages of this technique were that rapid scoring of micronuclei and main nuclei from irradiated cells could be achieved, and additionally that DNA distributions of micronuclei could be measured. A disadvantage of this technique is that it cannot always be applied to other cell lines, for example attached growing cells or human lymphocytes due to nonspecific debris present in the suspension of micronuclei and main nuclei. This debris was found to overlap with micronuclei in the low DNA content region so that only those micronuclei with a DNA content larger than about 2% of the G_1-nuclei could be registered. Because of the different amount of debris in various samples, the precision of dose effect curves of micronucleus induction can be hampered by this effect.

The modified technique presented here deals especially with the discrimination of debris from micronuclei so that the frequency and DNA distribution of micronuclei could be measured precisely by flow cytometry.

Several flow cytometric parameters were measured, and additionally, numerical calculations of the measured data were performed to obtain a better discrimination of micronuclei and debris. At first, forward light scatter signals in combination with EB-fluorescence alone were used for a rough discrimination of debris showing different light scattering properties compared to micronuclei. This was demonstrated by sorting the respective particles. With this technique, however, a well defined dose dependence could not be obtained because of different amount of debris in various samples still overlapping the micronuclei in the low fluorescence region. Discrimination of micronuclei and debris using forward light scattering in addition to EB-fluorescence measurements was also performed by Ludwikow and coworkers (17) using the same preparation technique. They showed that dose effect curves established by this flow cytometric technique did not quite agree with results obtained by microscopic observations, probably due to unspecific debris still overlapping the micronucleus distribution that could not be discriminated from micronuclei using the forward scatter signal alone.

In our experiments, even after gating according to forward scatter, the sorted particles in the low EB-fluorescence region were found to contain both debris and micronuclei. Therefore, the assay was further developed to discriminate the small unspecific debris from micronuclei. For an optimal micronuclei vs. debris detection a highly specific staining technique had to be worked out to stain only double stranded DNA (ds-DNA). The topologic properties of ds-DNA in main nuclei or micronuclei can be used to discriminate between DNA binding and nonspecific binding. Energy transfer between two dyes depends on the topologic properties. Binding sites of both donor and acceptor molecules as well as their mutual orientation and distance influence to a high degree the amount of energy transfer. One major prerequisite of energy transfer is the overlap between the fluorescence emission spectrum of the donor and the absorption spectrum of the acceptor (26). We have used the two DNA binding dyes Hoechst 33258 (HO) and ethidium bromide (EB) as donor and acceptor (1,2). EB has even more the advantage of being excitable by the 488 nm emission of the first laser which allows precise determination of the total amount of EB in main nuclei and micronuclei not influenced by energy transfer from HO. Cellular debris, which may bind one or even both of the dyes a certain amount, may not fulfill the necessary spatial conditions to fully conform to the rules for energy transfer.

Micronuclei show a similar structure compared to main nuclei; they have a nuclear membrane and perform DNA synthesis in phase with the cell nucleus (15). Therefore, the ratio of the different fluorescence signals measured by flow cytometry should be the same in micronuclei and main nuclei. This assumption was used here to discriminate micronuclei from debris measured simultaneously in the same fluorescence intensity region. Two ratios of fluorescences, EB^{488}/HO^{360} and EB^{488}/EB^{HO}, were calculated for all data and plotted as function of EB^{HO} and HO^{360}, respectively. After a first gating procedure according to the forward scatter for a rough discrimination of debris and micronuclei, only those particles were considered to be micronuclei that showed the same two ratios of these fluorescence signals compared to the ratios of the nuclei.

Using this new technique the dose effect relationship for radiation-induced micronuclei were analysed for Ehrlich ascites mouse tumor cells growing in suspension and attached growing 3T3 cells. Both agree quite well with independent measurements by fluorescence microscopy. The courses of these dose responses were cell-line specific but independent of the different amount of debris in various samples.

Furthermore, the time-dependence of the micronucleus induction by ionizing radiation could be measured for these two cell lines with high precision. Since micronuclei are expressed only in cells that have divided at least once in culture, cell cycle progression after irradiation plays an important role in the analysis of radiation-induced micronuclei. In cell cultures most cells will divide at least once after irradiation with doses up to about 4 Gy (19). However, the radiation-induced dose dependent G_2-block has to be considered additionally, if the time dependence of the micronucleus induction is measured (19,21). In the cell lines studied here, the frequency of micronuclei has reached a plateau when nearly all cells have divided once (21). It was therefore unnecessary to correct our data for the presence of undivided cells. This correction is, however, especially necessary, if micronuclei in irradiated human or mouse lymphocytes have to be analysed. Using the cytochalasin B-technique (5–8) the cell kinetic problems can be solved easily, if micronuclei are analysed by microscopic observation. Cytochalasin B inhibits cytokinesis without inhibiting nuclear division. In the resulting binucleated cells micronuclei can be scored easily. With the flow cytometric BrdUrd/Hoechst quenching technique (16) this problem can, however, also be solved for the analysis of radiation-induced micronuclei in human lymphocytes as shown in another publication (manuscript in preparation).

With the new flow cytometric technique presented here, the frequencies of radiation-induced micronuclei can easily be measured. The results agree with microscopic measurements if the number of micronuclei per main nuclei is calculated and if only those micronuclei are measured that have a DNA content between about 0.5% and about 10% of the G_1 nucleus. The analysis of the DNA distribution of micronuclei obtained by flow cytometry shows that most of the debris is found in the low fluorescence region (< 1% of the DNA content of

nuclei). Therefore, most radiation-induced micronuclei have a relative DNA content that is larger than 0.5% of the DNA content of main G_1-nuclei. The lower limit for the detection of micronuclei by flow cytometry is therefore caused by the infrequency of very small micronuclei and the increasing frequency of debris with very low fluorescence intensities. This lower limit agrees well with microscopic observations of the size distribution of micronuclei in mouse bone marrow cells (11) or in human lymphocytes (3,24). By image analysis of the size distribution of micronuclei, the smallest micronuclei that can be detected also have relative DNA contents of about 0.5–1% of the main nucleus (8). It can only be speculated whether small micronuclei exist that cannot be detected by microscopic observation or by flow cytometry. The smallest chromosome of a mouse Ehrlich ascites tumor cell has a DNA content of about 1% of the G_1-nucleus as demonstrated by flow karyotyping (20). Breakage could occur in this or other chromosomes producing a micronucleus with DNA content even less than 0.5% of the G_1-phase nucleus. However, the fact that the frequency of micronuclei measured by flow cytometry agrees well with results obtained by microscopic scoring shows that the presence of very small micronuclei (smaller than 0.5% of the DNA content of G_1-phase nuclei) does not play a significant role in measurement of the frequency of radiation-induced micronuclei.

Larger micronuclei are usually not found after irradiation; they can, however, be induced by chemicals that interfere with the spindle apparatus (22). In this case, the flow cytometric technique will give results that do not always agree with microscopic observation.

If only the fraction of cells containing micronuclei is measured by microscopic observation, the flow cytometric results do not agree due to the dose-dependent fraction of those cells that contain more than one micronucleus per cell (21). It should therefore be emphasized that in some circumstances, useful information concerning the number of micronuclei per cell is lost using the flow cytometric technique.

The new automated flow cytometric method presented here allows a rapid and precise analysis of the frequency and the DNA distribution of radiation-induced micronuclei; 20,000 to 40,000 particles including nuclei and micronuclei can be registered in 2–4 min. The preparation of the samples from irradiated tissue cultures is performed during 30 min. For automated computer aided analysis of the data less than 1 min per sample is necessary. The strength of the method is its potential high degree of automation and the objectiveness of the results. For conventional microscopic counting of micronuclei usually 15 min–1 h per sample is needed depending on the frequency of micronuclei in the sample. Therefore, flow cytometric analysis of micronucleus induction seems to be a fast and precise method especially if large numbers of samples have to be analysed. It could even be used to study effects of chemicals on cell cultures for toxicological studies or possibly also for routine toxicology testing. The minimum dose of ionizing radiation that can be observed using this technique is in the range of 0.05–0.1 Gy γ-rays. This is similar to the sensitivity of microscopic scoring. However, we do not expect that it is possible to further increase this sensitivity using the flow cytometric method.

ACKNOWLEDGMENTS

This work was financially supported in part by the Commission of the European Communities, Radiation Protection Programme, contract B17-0038-C (TT).

LITERATURE CITED

1. Böhmer RM, Ellwart J: Cell cycle analysis by combining the 5-bromodeoxyuridine/33258 Hoechst technique with DNA-specific ethidium bromide staining. Cytometry 2(1):31, 1981.
2. Brodie S, Giron J, Latt SA: Estimation of accessibility of DNA in chromatin from fluorescence measurements of electronic excitation energy transfer. Nature 253:470–471, 1975.
3. Callisen H, Norman A, Pincu M: Computer scoring of micronuclei in human lymphocytes. In: Biological Dosimetry. Cytometric Approaches to Mammalian Systems, Eisert WG, Mendelsohn ML (eds). Springer-Verlag, Berlin, 1984, pp 171–179.
4. Degrassi F, Tanzarella C: Immunofluorescent staining of kinetochores in micronuclei: a new assay for the detection of aneuploidy. Mutat Res 203:339–345, 1988.
5. Eastmond DA, Tucker JD: Kinetochore localization in micronucleated cytokinesis-blocked Chinese hamster ovary cells: a new and rapid assay for identifying aneuploidy-inducing agents. Mutat Res 224:517–525, 1989.
6. Fenech M, Morley A: Solutions to the kinetic problem in the micronucleus assay. Cytobios 43:233–246, 1985.
7. Fenech M, Morley A: Measurement of micronuclei in human lymphocytes. Mutat Res 148:29–36, 1985.
8. Fenech M, Jarvis LR, Morley AA: Preliminary studies on scoring micronuclei by computerized image analysis. Mutat Res 203:33–38, 1988.
9. Hayashi M, Norppa H, Sofuni T, Ishidate M: Automation of mouse micronucleus test by flow cytometry and image analysis. Cytometry [Suppl] 4:35, 1990.
10. Heddle JA, Benz RD, Countryman PI: Measurement of chromosomal breakage in cultured cells by the micronucleus technique. In: Mutagene-Induced Chromosome Damage in Man, Evans HJ, Lloyd DC (eds). Edinburgh University Press, Edinburgh, 1978, pp 191–200.
11. Heddle JA, Carrano AV: The DNA content of micronuclei induced in mouse bone marrow cells by γ-irradiation: evidence that micronuclei arise from acentric chromosomal fragments. Mutat Res 44:63–69, 1977.
12. Hennig UGG, Rudd NL, Hoar DI: Kinetochore immunofluorescence in micronuclei: a rapid method for the in situ detection of aneuploidy and chromosome breakage in human fibroblasts. Mutat Res 203:405–414, 1988.
13. Hogstedt B, Karlsson A: The size of micronuclei in human lymphocytes varies according to inducing agent used. Mutat Res 156: 229–232, 1985.
14. Iliakis G, Pohlit W: Quantitative aspects of repair of potentially lethal damage in mammalian cells. Int J Radiat Biol 36:649–658, 1979.
15. Kramer J, Schaich-Walch G, Nüsse M: DNA synthesis in radiation induced micronuclei studied by bromodeoxyuridine (BrdUrd) labelling and anti-BrdUrd antibodies. Mutagenesis 5:491–495, 1990.
16. Kubbies M, Friedl R, Köhler J, Rabinovitch PS, Hoehn H: Improvement of human lymphocyte proliferation and alteration of IL-2 secretion kinetics by alpha-thioglycerol. Lymphokine Res 9:95–106, 1990.
17. Ludwikow G, Stalnacke CG, Johanson KJ, Sundell-Bergman S,

Richter S: Microscopic and flow cytometric study of micronuclei in iododeoxyuridine labelled cells irradiated with soft X-rays. Acta Oncol 29:761–767, 1990.
18. Masunaga S, Ono K, Wandl EO, Fushiki M, Abe M: Use of the micronucleus assay for the selective detection of radiosensitivity in BUdr-unincorporated cells after pulse-labelling of exponentially growing tumor cells. Int J Radiat Biol 58:303–311, 1990.
19. Nüsse M: Cell cycle kinetics of irradiated synchronous and asynchronous tumor cells with DNA distribution analysis and Brd-Urd-Hoechst 33258-technique. Cytometry 2:70–79, 1981.
20. Nüsse M, Egner HJ, Krämer M: Flow karyotyping of mouse tumor cell lines. Cytometry [Suppl] 1:91, 1987.
21. Nüsse M, Kramer J: Flow cytometric analysis of micronuclei found in cells after irradiation. Cytometry 5:20–25, 1984.
22. Nüsse M, Krämer M, Viaggi S, Bartsch A, Bonatti S: Antikinetochore antibodies and flow karyotyping: new techniques to detect aneuploidy in mammalian cells induced by ionizing radiation and chemicals. Mol Toxicol 1:393–405, 1987.
23. Nüsse M, Viaggi S, Bonatti S: Induction of kinetochore positive and negative micronuclei in V79 cells by the alkylating agent diethylsulphate. Mutagenesis 4:174–178, 1989.
24. Pincu M, Callisen H, Norman A: DNA content of micronuclei in human lymphocytes. Int J Radiat Biol 47:423–432, 1985.
25. Romagna F, Staniforth CD: The automated bone marrow micronucleus test. Mutat Res 213:91–104, 1989.
26. Stryer L: Fluorescence energy transfer as a spectroscopic ruler. Annu Rev Biochem 47:819, 1978.
27. Tates AD, van Welie MT, Ploem JS: The present state of the automated micronucleus test for lymphocytes. Int J Radiat Biol 58:813–825, 1990.
28. Tometsko AM, Leary JF: A peripheral blood micronucleus assay based on flow cytometry. Cytometry [Suppl] 4:35, 1990.
29. Yamamoto KI, Kikuchi Y: A comparison of diameter of micronuclei induced by clastogens and by spindle poisons. Mutat Res 71:127–131, 1980.

Mutagenesis vol.7 no.1 pp.57–67, 1992

Micronuclei induced by 2-chlorobenzylidene malonitrile contain single chromosomes as demonstrated by the combined use of flow cytometry and immunofluorescent staining with anti-kinetochore antibodies

Michael Nüsse, Stefan Recknagel[1] and Wolfgang Beisker

GSF-Forschungszentrum für Umwelt und Gesundheit, Institut für Biophysikalische Strahlenforschung, AG Durchflußzytometrie, Ingolstädter Landstr. 1, D-W-8042 Neuherberg, and [1]Institut für Biophysik, Universität Frankfurt, Frankfurt, FRG

The effects of the tear gas 2-chlorobenzylidene malonitrile (CS) on micronucleus induction and cell cycle kinetics were studied in Chinese hamster and Ehrlich ascites tumour cells using flow cytometric analysis of micronuclei and nuclei in suspension, and indirect immunofluorescent staining of kinetochores in micronuclei. In both cell lines CS induced a concentration-dependent inhibition of the fraction of cells in mitosis as observed by simultaneous flow cytometric measurements of DNA content and side scatter intensities of cell nuclei. Micronucleus frequency increased during the delayed division of cells accumulated by CS in mitosis and reached a plateau when most of these cells have divided. The height of this plateau depended on the CS concentration. Results obtained by flow cytometric analysis of the frequency of CS-induced micronuclei did not agree quantitatively with results obtained by microscopic analysis due to cells showing CS-induced fragmented nuclei. Nearly all CS-induced micronuclei exhibited kinetochores, the majority of which (60–70%) showed one kinetochore per micronucleus implying the presence of a single metaphase chromosome in these micronuclei. DNA distributions of micronuclei measured by flow cytometry showed pronounced peaks corresponding to the DNA distribution of chromosomes measured by flow karyotyping. Even micronuclei containing two of the large chromosomes could be observed as distinct peaks in the distributions. The combined results of flow cytometric analysis of micronucleus distributions and immunofluorescence staining of kinetochores in micronuclei suggest that CS induces micronuclei mainly by damaging the spindle fibres of single chromosomes during mitosis, thus possibly leading to aneuploidy and polyploidy.

Introduction

2-Chlorobenzylidene malonitrile (CS) is a strong sensory irritant currently used in several countries as a tear gas. The biological activity of CS has been shown to be attributed to covalent interactions with thiol (Cucinell *et al.*, 1971; Önfeld, 1987) or amino groups (Jones, 1972) in proteins. A covalent binding of CS to nuclear proteins but not to DNA has also been demonstrated by von Däniken *et al.* (1981). No significant mutagenic effects were induced by CS in different strains of *Salmonella typhimurium* (von Däniken *et al.*, 1981; Rietveld *et al.*, 1983) or in growing yeast cells (Nestman and Lee, 1983). It was therefore concluded that CS 'will not create a risk for the induction of point mutations or of carcinogenic processes mediated by DNA binding' (von Däniken *et al.*, 1981). Recently, however, it has been shown that CS interacts with the mitotic spindle apparatus, thus inducing a mitotic delay and mitotic anomalies (Schmid *et al.*, 1989; Salassidis *et al.*, 1991) as well as micronuclei. It has also been shown that mutants resistant to 6-thioguanine in Chinese hamster cells were induced by CS (Ziegler-Skylakakis *et al.*, 1989). It has therefore been suggested that the ability of CS to cause spindle disturbances may result in aneuploid mammalian cells and therefore CS should be considered as a potentially hazardous agent (Schmid *et al.*, 1989; Schmid and Bauchinger, 1991).

It was shown recently that the analysis of micronuclei induced by chemicals or ionizing radiation can be improved using anti-kinetochore antibodies in combination with immunofluorescence techniques (Vig and Swearngin, 1986; Nüsse *et al.*, 1987; Degrassi and Tanzarella, 1988; Hennig *et al.*, 1988; Nüsse *et al.*, 1989; Eastmond and Tucker, 1989a,b; Miller and Adler, 1990; Miller *et al.*, 1991). Micronuclei containing fragments arising as a consequence of chromosome breakage and those containing whole chromosomes caused by spindle disturbances can be discriminated by visualizing kinetochores within micronuclei. Additional information about mechanisms of action of different drugs could possibly be obtained if the DNA distribution of micronuclei is measured either microscopically (Heddle and Carrano, 1977; Yamamoto and Kikuchi, 1980; Hogstedt and Karlson, 1985; Pincu *et al.*, 1985; Bonatti *et al.*, 1986; Vanderkerken *et al.*, 1989) or by flow cytometry (Nüsse and Kramer, 1984; Hernandez-Verdun *et al.*, 1986; Labidi *et al.*, 1987). Flow cytometry seems to be especially suited to the analysis of micronuclei DNA distributions, because a large number of micronuclei can be measured easily and with high precision. In addition, several parameters can be measured simultaneously. For example, light scatter signals and different fluorescence intensities of micronuclei enable discrimination of micronuclei from debris particles which are also present in the suspension of nuclei and micronuclei (Schreiber *et al.*, 1992). We have also shown that the frequency of micronuclei, their DNA distribution and the cell cycle distributions of main nuclei including a discrimination of M-phase from G_2-phase cells can be measured easily in a flow cytometer using the same preparative technique (Nüsse and Kramer, 1984; Nüsse *et al.*, 1990).

It has been shown by Hernandez-Verdun *et al.* (1986) and Labidi *et al.* (1987) that a fraction of the colchicine-induced micronuclei in rat kangaroo PtK_1 cells seem to contain one whole chromosome. This was demonstrated by measuring DNA distributions of micronuclei in a flow cytometer that showed distinct peaks overlapping a broad background distribution. Sorting of the particles in these peaks revealed that most of them were in fact micronuclei containing exclusively one chromosome.

We have used a similar technique to measure DNA distributions of micronuclei induced in Chinese hamster and mouse tumour cell lines by CS. These DNA distributions showed pronounced peaks corresponding to the chromosome distribution of the cells. The reason for the occurrence of these peaks was that the majority (>60%) of the CS-induced micronuclei contained exclusively one chromosome as demonstrated by immunofluorescent staining of the kinetochores in micronuclei. Mitotic delay and perturbation of the cell cycle kinetics induced

© Oxford University Press

by CS was additionally studied using a flow cytometric technique to measure the fraction of mitotic cells (Nüsse *et al.*, 1990). By combining the results from cell kinetic studies, micronucleus induction measured either by flow cytometry or microscopic scoring, analysis of DNA distributions of micronuclei and kinetochore staining in micronuclei, a more detailed understanding of the mechanism of action of CS seems to be possible.

Materials and methods

Cells

A subclone CHE-0 of the Chinese hamster embryo cell line CCHE/27 (obtained from Scott Cram, Los Alamos National Laboratory, Los Alamos, NM) was used in these investigations. The cells were grown in α-MEM (Gibco) supplemented with 15% fetal calf serum (Gibco) at 37°C in an atmosphere of 6% CO_2.

A strain of hyperdiploid *E*hrlich *a*scites *t*umour cells (EAT, clone F5, DNA-index DI = 1.2) growing in suspension was also studied. The cells were maintained at 37°C under 6% CO_2 in a special medium (A_2) supplemented with 20% horse serum developed for optimal growth of these cells (Iliakis and Pohlit, 1979).

Treatment with CS

CS was kindly supplied by Klever, Aham. It was purified by recrystallization (three times) from hot ethanol before use. A stock solution of CS was prepared in DMSO (100 mM) a day before use and stored at 4°C. For treatment of CHE-0 cells with CS, 10^6 exponentially growing cells were seeded in 80 cm^2 flasks. The medium was replaced 24 h later with 10 ml prewarmed medium containing CS at different concentrations (10−60 μM) diluted from the stock solution immediately before the medium change. At various time intervals after the initiation of CS treatment the cells were trypsinized to prepare nuclei and micronuclei for flow cytometric analysis. For treatment of EAT cells with CS, 10^6 exponentially growing cells were incubated in 10 ml A_2 medium in 60 mm culture dishes. CS was added to the medium 24 h later by appropriate dilution. After various time intervals the cells were centrifuged, the supernatant discarded, and nuclei and micronuclei prepared for flow cytometric analysis.

For immunofluorescent staining of kinetochores in micronuclei, 10^5 CHE-0 cells were seeded in 100 mm plastic dishes containing three coverslips (15 × 15 mm). The cells were treated with CS 24 h later as described above. At appropriate time intervals, the coverslips were removed, the cells were washed three times with phosphate-buffered saline (PBS), fixed in cold methanol and stored at −20°C in methanol.

Anti-kinetochore staining with CREST antibodies

Immunofluorescent staining of kinetochores in micronuclei and nuclei was performed as described previously (Nüsse *et al.*, 1989). Coverslips were washed twice and treated with antibodies to kinetochores from the serum of a scleroderma patient (CREST syndrome, the serum was kindly provided by Dr Solberg, University Hospital, Frankfurt/M, FRG). A 20 μl aliquot of the diluted serum (1:30−1:100 in PBS) was dropped onto a microscope slide, covered with the inverted coverslip and incubated at 37°C in a wet atmosphere. After 1−3 h the coverslip was removed and washed three times with PBS to remove unbound antibodies. Then 20 μl of fluoresceine (FITC)-conjugated goat antihuman antibodies (Sigma), diluted 1:50−1:100, was dropped onto another slide, covered again with the inverted coverslip and incubated at 37°C in a wet atmosphere. After 60 min the coverslip was rinsed three times with PBS, and the DNA of nuclei and micronuclei was counterstained with propidium iodide (PI, 0.2−0.5 μg/ml in PBS). To avoid fading of the green FITC fluorescence the coverslips were embedded with DABCO (9 parts glycerol containing 2.3% (w/v) 1,4-diazabicyclo-(2,2,2)-octane, Sigma, and 1 part 0.2 M Tris−HCl, 0.02% NaN_3, pH 8.0).

The fraction of micronuclei (number of micronuclei: N_{mn}) per cell nuclei (number of nuclei: N_n), N_{mn}/N_n, was measured by counting only those CHE-0 cells that contained one main nucleus and one to four micronuclei per cell. Cells containing more than four micronuclei per cells and/or several fragmented nuclei of different sizes were scored separately. In addition, the fraction of micronuclei containing kinetochores ('kinetochore-positive micronuclei', N_{mn+}) and the distribution of the number of kinetochores per micronucleus were measured by microscopic observation. Approximately 1000 cells were scored per time point. The experiments were repeated twice and the data pooled.

Preparation and staining of nuclei and micronuclei for flow cytometry

A suspension of micronuclei and nuclei was prepared according to the procedure described by Nüsse and Kramer (1984). Cells (2−3 × 10^6) were centrifuged, and 1 ml of solution I (584 mg/l NaCl, 1000 mg/l sodium-citrate, 25 mg/l ethidium bromide (EB), 10 mg/l RNase and 0.3 ml/l Nonidet P-40) was added to the cell pellet. After at least 30 min, 1 ml of solution II (1.5% citric acid, 0.25 M sucrose and 40 mg/l EB) was added and the suspension agitated. After this second step the cell membranes and the cytoplasm were disintegrated, and the suspension contained only cell nuclei and micronuclei. Even the nuclei from mitotic cells were found to be well preserved. A certain amount of irregularly shaped debris particles of unknown origin was sometimes also observed (Schreiber *et al.*, 1992). The samples could be stored at 4°C for at least 2 weeks.

Preparation of chromosomes for flow karyotyping

Chromosome suspensions were prepared according to a modification of the method proposed by van den Engh *et al.* (1984). Mitotic cells were accumulated by the treatment of exponentially growing cells with colcemid (0.2 μg/ml in medium for 3 h), isolated by mitotic shake off in the case of CHE-0 cells (mitotic cells of EAT cells could not be separated from interphase cells, therefore all cells were treated in the same manner) and centrifuged for 15 min at 500 *g*. The sedimented cells were treated at room temperature with 1 ml of hypotonic buffer containing 50 mM KCl, 10 mM $MgSO_4$, 5 mM K_2HPO_4, 0.25 mg/ml RNase, 3 mM β-mercaptoethanol and 20 μg/ml PI. After 10 min, 25 μl of 10% Triton X-100 was added; 10 min later the cells were forcefully syringed six times through a thin needle to release the chromosomes and incubated at 37°C for 30 min. The chromosome suspensions were stored at 4°C and measured 1−2 days after preparation.

Flow cytometry and data analysis

Cell cycle distributions. Bivariate DNA and side scatter (SSC) distributions of cell nuclei (Nüsse *et al.*, 1990) were measured with a Cytofluorograf 30L (Ortho Diagnostics) equipped with the PC-AT based data acquisition system developed by Kachel *et al.* (1990). Excitation of EB was provided by the 488 nm line (500 mW) of an argon ion laser (model 2025-05, Spectra-Physics). The emitted EB fluorescence was collected with a longpass filter (OG 570), side scatter signals were measured simultaneously with EB-fluorescence using an additional dichroic mirror that reflects blue scattered light. Bivariate DNA-SSC distributions were displayed as contour plots or dot plots using the newly developed Data Analysis Software DAS (W.Beisker, in preparation). The fraction of cells in the G_1-, S-, G_2- and M-phase cell cycle compartments were calculated using various windows as shown previously (Nüsse *et al.*, 1990).

Chromosome analysis (flow karyotype). PI fluorescence of the chromosomes was collected with a 610 nm long pass filter and displayed as PI fluorescence distributions. The mean numbers of chromosomes per cell per chromosome peak in the flow karyotypes were calculated according to Nüsse *et al.* (1987).

Analysis of micronuclei. EB fluorescence and small angle forward light scatter signals (FSC) of micronuclei were measured simultaneously to discriminate micronuclei from unspecific debris. As shown by sorting of the respective particles (Schreiber *et al.*, 1992), particles with higher FSC signals were unspecific debris whereas particles with lower FSC signals were found to be micronuclei. Both could be separated according to their different forward light scatter intensities. G_1-phase nuclei were stored around channel no. 900, micronuclei were counted in the region between 1 and 50% of the DNA content of G_1-phase nuclei. The fraction of micronuclei (N_{mn}) per main nuclei (N_n) was calculated using different windows as indicated in Figure 2. Analysis of the DNA distributions of micronuclei was performed using the DAS software (W.Beisker, in preparation).

Sorting of micronuclei. Sorting of micronuclei was performed using a FACStar-PLUS cell sorter equipped with an argon ion laser (model INNOVA 90-5, Coherent Radiation) operating at 488 nm. Measurements of EB fluorescence and FSC were similar to those measured with the Cytofluorograf. About 1000 or more micronuclei were sorted on glass slides for visual examination of their shape and morphology with a fluorescence microscope.

Results

CS-induced perturbation of the cell cycle

To study the perturbation of the cell cycle induced by treatment of CHE-0 cells and EAT cells with various concentrations of CS, DNA-SSC histograms were measured as a function of time during treatment with CS. With this technique the fractions of cells in the G_1-, S-, G_2- and M-phases could be calculated. Figure 1a shows as an example the DNA-SSC histogram of CHE-0 cells at 4 h after treatment with 40 μM CS. This histogram shows clearly a CS-induced accumulation of cells in the M-phase compartment. The fraction of cells in mitosis (MI) as function of time is shown in Figure 1b for unexposed cells, and for cells treated with 20, 40 and 60 μM CS. MI increased due to a CS-induced mitotic block and decreased again shortly thereafter.

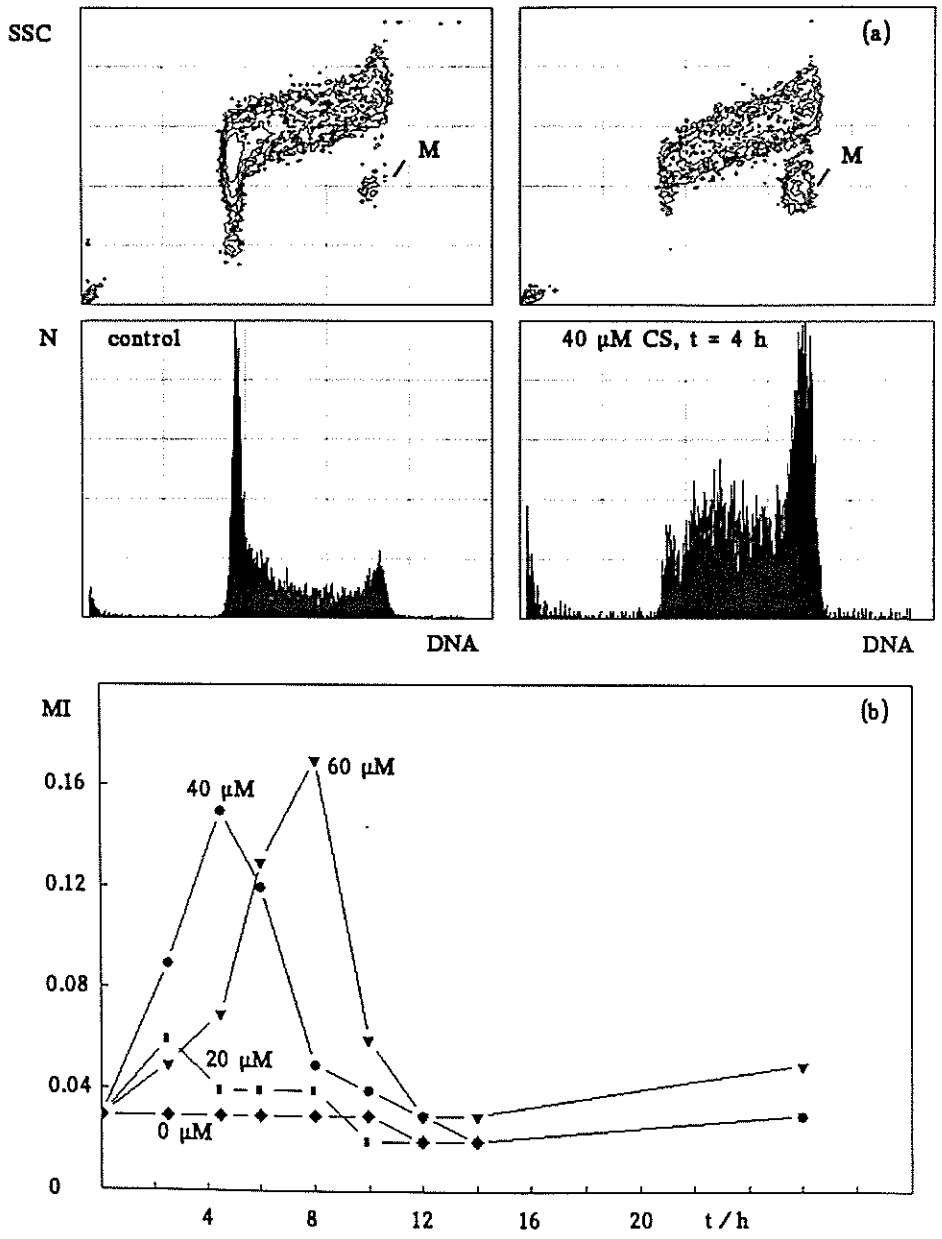

Fig. 1. (a) DNA-SSC histograms (upper figures) and DNA distributions (lower figures) of untreated CHE-0 cells (left) and CHE-0 cells treated for 4 h with 40 μM CS (right). The cells in mitosis are represented by the population with low side scatter intensity. (b) Fraction of cells in mitosis, MI, as function of time for cells treated with 0, 20, 40 and 60 μM CS.

Therefore, a maximum of MI was obtained that was dependent upon the concentration of CS: with 20 μM CS this maximum was rather small and found at t = 2 h, with 40 μM CS the maximum was found at t = 4 h and with 60 μM the maximum was found at t = 8 h. With 10 μM no accumulation of M-phase cells was observed compared to the control values (data not shown). The height of the maximum depended on the concentration of CS.

The decrease of MI after a concentration dependent time interval was probably due to hydrolysis of CS in aqueous medium to malonitrile and *o*-chlorobenzaldehyde. Both compounds were shown to be inefficient at inducing either a mitotic delay or micronuclei (Ziegler-Skylakakis *et al.*, 1989). Therefore, exposure of cells to CS in medium occurs as a pulse treatment, the duration of which depends on the concentration of CS at t = 0. Treatment of cells with CS induced a wave of partial synchronization in CHE-0 and EAT cells due to this temporary mitotic block.

Micronucleus induction by CS

Flow cytometric analysis of CS-induced micronuclei. The fraction of micronuclei per main nuclei, N_{mn}/N_n, was measured as a function of time and concentration of CS using flow cytometric simultaneous measurements of DNA content and FSC intensities of micronuclei and nuclei in suspension. FSC measurements in addition to DNA content measurements were used to discriminate micronuclei from unspecific debris (Schreiber *et al.*, 1992). Figure 2a shows a DNA-FSC histogram of a suspension of micronuclei and nuclei of CHE-0 cells treated with 40 μM CS (t = 8 h) indicating the position of micronuclei (debris and micronuclei were both identified by sorting of the respective particles) and nuclei. Figure 2b shows the fraction of micronuclei

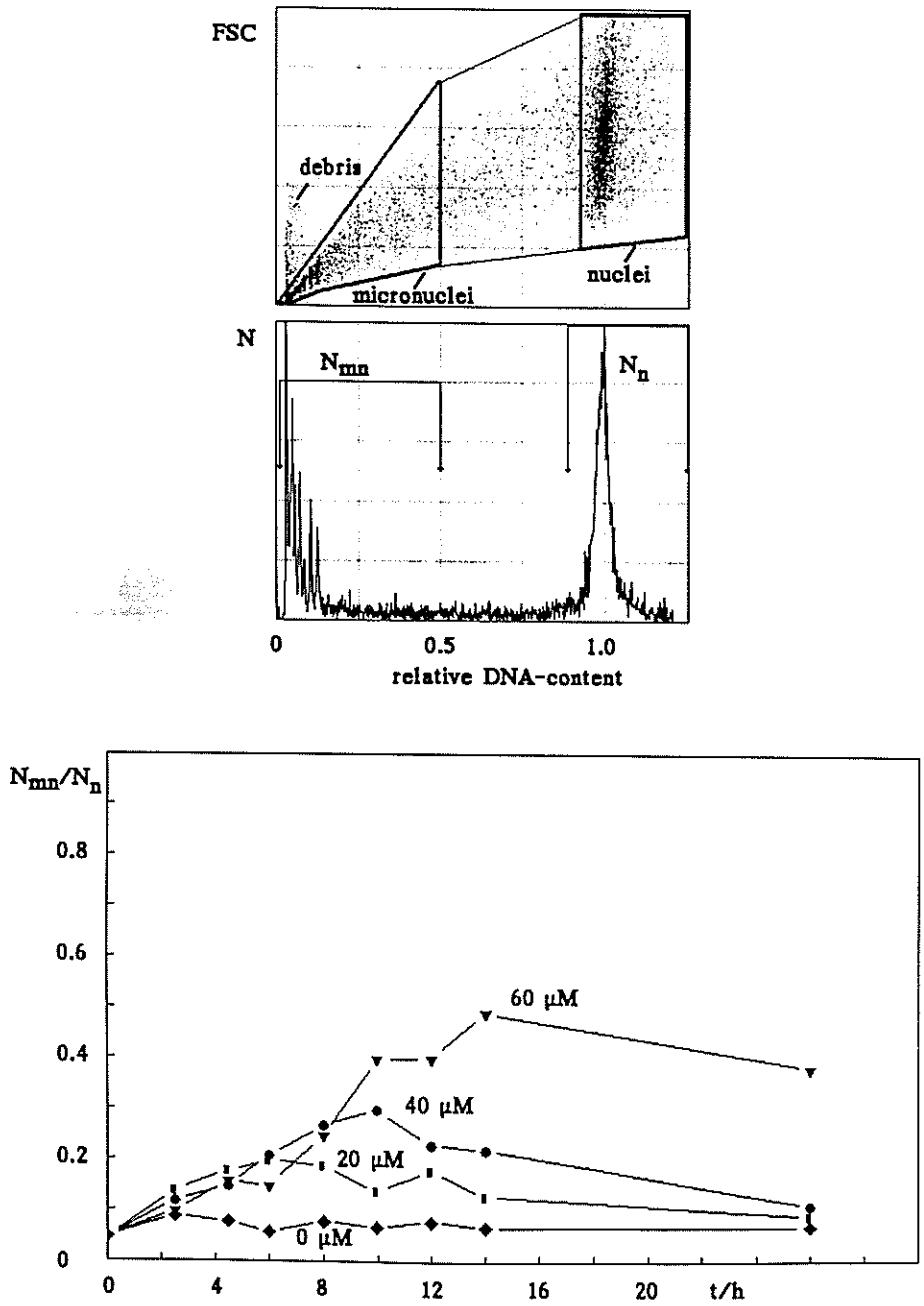

Fig. 2. (a) Upper histogram: DNA-FSC histogram of a suspension of nuclei and micronuclei stained with ethidium bromide. CHE-0 cells were incubated in medium containing 40 μM CS and analysed at t = 8 h.The positions of nuclei, micronuclei and debris are indicated. Lower histogram: DNA distribution of micronuclei and nuclei as defined by the window in the DNA-FSC histogram. Particles (micronuclei and fragmented nuclei) with a DNA content between 1 and 50% of the DNA content of G_1-phase cells are counted as N_{mn}. Nuclei with relative DNA content between 1 (G_1-phase) and 2 (G_2/M-phase) are counted as N_n. (b) Fraction of micronuclei per nuclei, N_{mn}/N_n, as function of time in medium containing different concentrations of CS (0, 20, 40 and 60 μM).

per main nuclei, N_{mn}/N_n, as a function of time for different concentrations of CS. Beginning with the division of the first cells after mitotic block, N_{mn}/N_n increased until it reached a plateau, when all the cells, previously accumulated in mitosis, had divided. The height of the plateau therefore depended again upon the concentration of CS. Figure 3 shows N_{mn}/N_n as a function of the CS-concentration (curve a) measured in the plateau of Figure 2b. A linear increase with CS-concentration was observed.

Analysis of CS-induced micronuclei with anti-kinetochore antibodies. N_{mn}/N_n was also measured by microscopic scoring of micronuclei in CS-treated CHE-0 cells stained with anti-kinetochore antibodies. Micronuclei exhibiting and those not exhibiting kinetochores were scored separately. Figure 4a shows as an example a photograph of micronucleated cells with four micronuclei each containing one kinetochore. Figure 4b shows a typical cell with a fragmented nucleus. Each of these fragments exhibit one, two or three kinetochores. The results of the microscopic analysis are presented in Table I and Figure 5a–c: N_{mn}/N_n (Figure 5a), N_{mn+}/N_{mn} (Figure 5b) and N_{mn1+}/N_{mn} (Figure 5c) are shown as a function of time during treatment with 20 and 40 μM CS, and for unexposed control cells. Starting with division of the first cells accumulated by CS in mitosis (see Figure 1b), N_{mn}/N_n increased and reached a plateau, when all

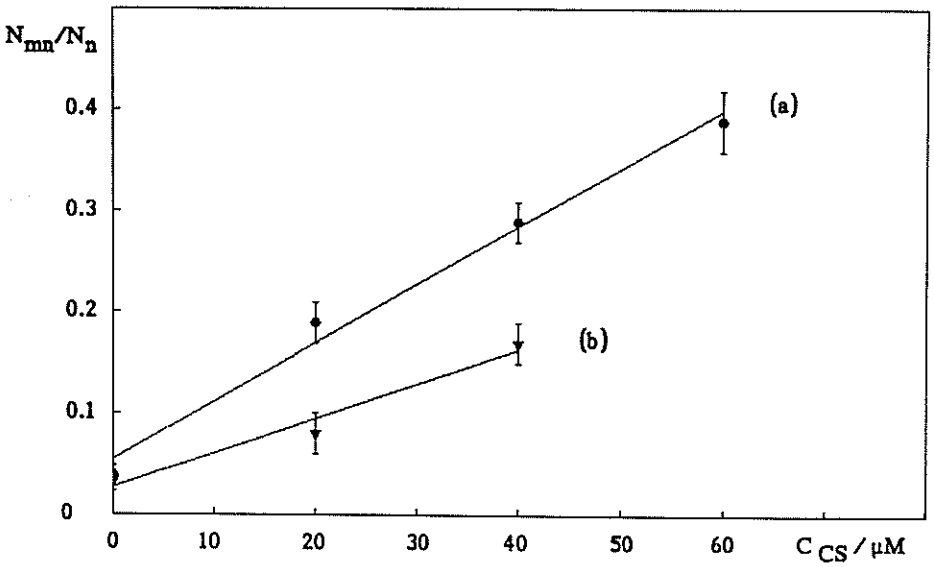

Fig. 3. (a) N_{mn}/N_n as a function of the CS concentration in medium (CHE-0 cells) measured by flow cytometry in the plateau of the curves shown in Figure 2b. Mean values of the data measured at t = 10, 12 and 14 h (60 μM), at t = 8, 10 and 12 h (40 μM) or at t = 6, 8 and 10 h (20 μM). (b) N_{mn}/N_n as a function of the CS concentration in medium (CHE-0 cells) measured by microscopic observation (Table I). Mean values of the data measured at t = 8, 10, 12 and 14 h.

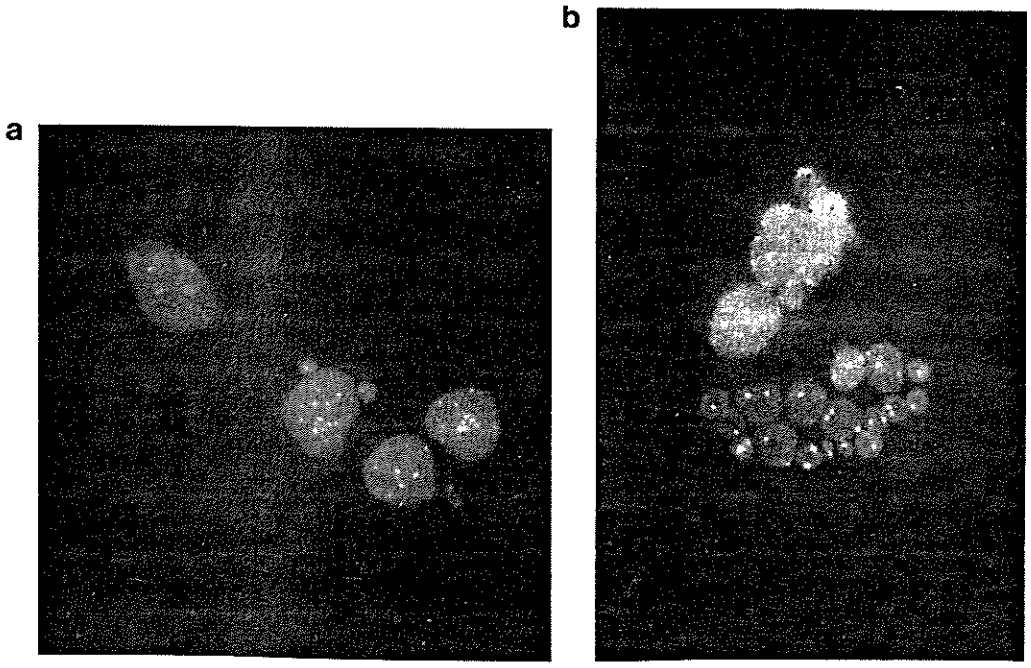

Fig. 4. (a) CHE-0 cells with four CS-induced micronuclei, each containing one kinetochore. (b) CHE-0 cells with fragmented nuclei. The lower cell contains 17 fragments (micronuclei), nine with one kinetochore each, six with two kinetochores each and two with three kinetochores.

cells accumulated in mitosis have divided. At this time ~70–80% of the micronuclei at a concentration of 40 μM CS and ~50–60% of the micronuclei at 20 μM CS showed kinetochores compared to ~30% in unexposed control cells. This difference between the results obtained with 20 and 40 μM CS was due to the higher fraction of kinetochore-negative micronuclei in unexposed cells (~70%). By subtracting the frequency of micronuclei found in unexposed cells it was calculated that nearly all CS-induced micronuclei (>90%) contained kinetochores.

Most of the kinetochore-positive micronuclei exhibited only one kinetochore. This is demonstrated in Figure 4a, where all four micronuclei contained one kinetochore. Table I shows that between 60 and 70% of all micronuclei had one kinetochore in cells treated with 40 μM CS and ~40–50% had one kinetochore in cells treated with 20 μM CS. This difference was mainly due to the fraction of kinetochore-negative micronuclei found in these cells without CS-treatment.

The distribution of the number of kinetochores per micronucleus is shown in Table II and Figure 5d. With increasing concentration of CS the fraction of micronuclei exhibiting exactly one kinetochore (N_{mn1+}/N_{mn} in Table II) increased. Most of these CS-induced micronuclei contained one kinetochore, but with increasing concentration of CS micronuclei with multiple kinetochores were observed.

Table I. Microscopic analysis of CS-induced micronuclei in Chinese hamster cells

	N_n	N_{mn}	N_{mn}/N_n	N_{mn+}	N_{mn+}/N_{mn}	N_{mn1+}	N_{mn1+}/N_{mn}
Control	5130	182	0.035	60	0.33	41	0.23
20 μM							
4 h	1009	64	0.063	33	0.52	25	0.39
6 h	1498	115	0.077	73	0.63	53	0.46
8 h	961	82	0.085	42	0.51	40	0.49
10 h	952	77	0.081	49	0.64	40	0.52
12 h	867	68	0.078	35	0.51	30	0.44
14 h	952	75	0.079	43	0.57	35	0.47
40 μM							
4 h	1500	136	0.091	65	0.48	64	0.47
6 h	2767	203	0.073	159	0.78	125	0.62
8 h	2006	320	0.16	231	0.72	194	0.61
10 h	2332	413	0.18	340	0.82	274	0.66
12 h	2190	365	0.17	279	0.76	233	0.64
14 h	2325	393	0.17	311	0.79	219	0.56

Figure 3 shows, additionally, N_{mn}/N_n measured by microscopic scoring of micronuclei as a function of the CS-concentration in the medium (curve b). Compared to the flow cytometric analysis of CS-induced micronuclei (curve a) the results of the microscopic scoring showed a smaller slope. This was due to the fact that with the flow cytometric analysis all particles with DNA content between 1 and 50% of the DNA content of G_1-phase nuclei were registered as micronuclei. Therefore, smaller nuclei from cells with fragmented nuclei (Figure 4b) were also included in this analysis. It was not possible to discriminate between micronuclei and fragmented nuclei, because both types of particles were found in the suspension. By microscopic scoring, however, only those micronuclei were registered that were found in cells containing one main nucleus and up to four micronuclei per cell. In our experiments, the fraction of fragmented nuclei was found to be $N_{fr}/N_n = 0.014$ in cells treated with 40 μM CS compared to $N_{fr}/N_n = 0.002$ for untreated cells. It must therefore be emphasized that with both techniques, flow cytometric analysis of micronuclei and microscopic scoring of micronuclei, different results are obtained. Usually, with flow cytometry more micronuclei are found

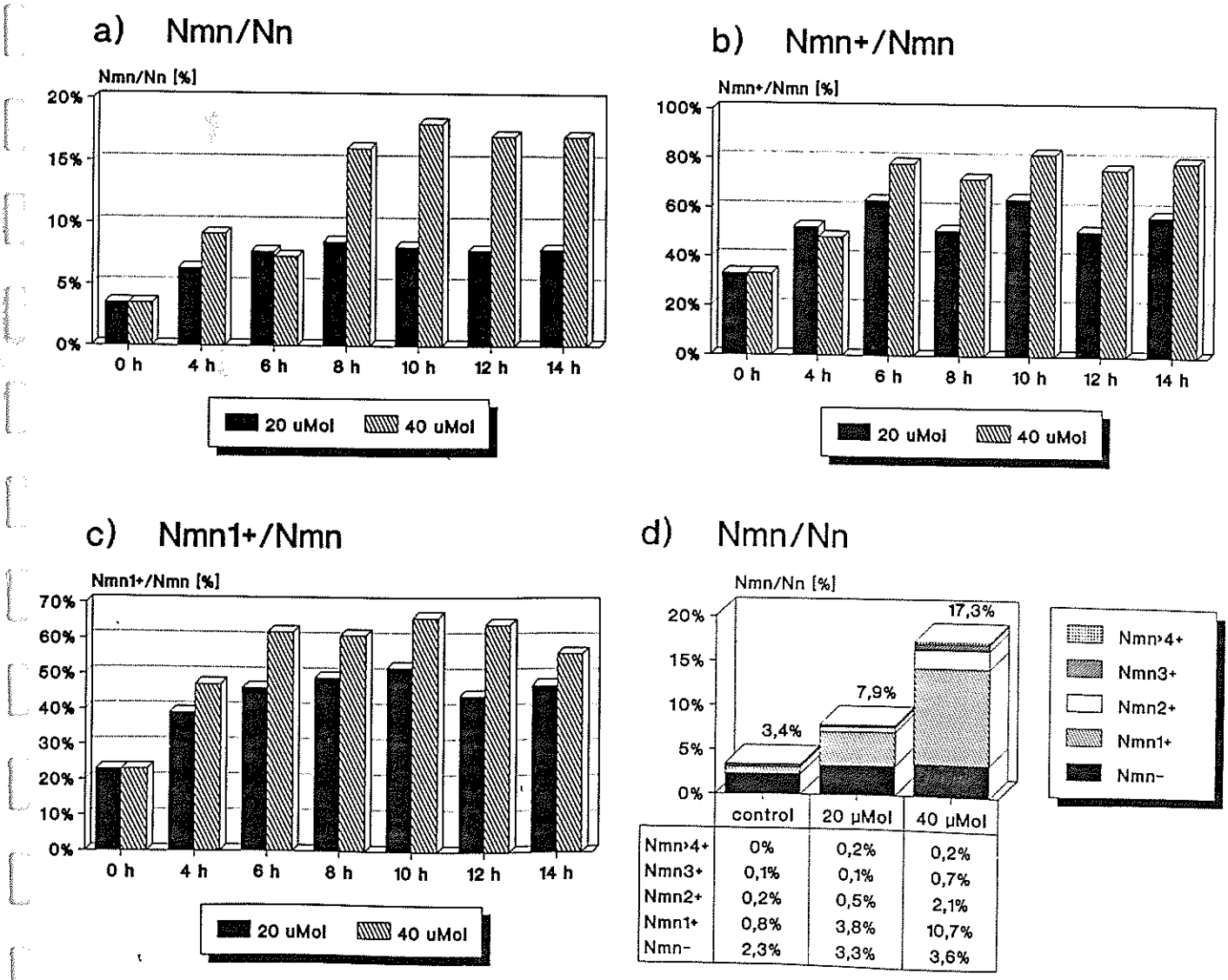

	control	20 µMol	40 µMol
Nmn>4+	0%	0,2%	0,2%
Nmn3+	0,1%	0,1%	0,7%
Nmn2+	0,2%	0,5%	2,1%
Nmn1+	0,8%	3,8%	10,7%
Nmn-	2,3%	3,3%	3,6%

Fig. 5. (a) Frequency of micronuclei, N_{mn}/N_n. (b) Fraction of kinetochore-positive micronuclei, N_{mn+}/N_{mn}. (c) Fraction of kinetochore-positive micronuclei, N_{mn1+}/N_{mn}, showing exactly one kinetochore as function of time for 20 and 40 μM CS (results from microscope scoring, see Table I). (d) Frequency of micronuclei showing no (N_{mn-}/N_n), one (N_{mn1+}/N_n), two (N_{mn2+}/N_n), three (N_{mn3+}/N_n) and more than four ($N_{mn>4+}/N_n$) kinetochores per micronucleus (see Tables I and II).

compared to results from microscopic scoring. The difference between both results depends on the size of the window in the DNA-FSC histogram used for the counting of micronuclei (Figure 2a). This window was chosen arbitrarily to include CS-induced fragmented nuclei in these flow cytometric measurements. It is possible to decrease the size of the window for a better agreement with results from microscopic scoring of micronuclei, this was, however, not the aim of the studies presented here.

Analysis of the DNA distribution of CS-induced micronuclei

Careful examination of Figure 2a revealed that in the flow cytometric DNA-FSC histograms clusters of micronuclei with similar DNA contents were found. To show this effect more clearly, the same sample was measured again after increasing the gain of the amplifier measuring EB-fluorescence (Figure 6a). Several clusters can be observed that correspond to micronuclei with the same DNA content. The DNA distribution of these micronuclei is also displayed. Figure 6b shows similar distributions of CS-induced micronuclei in mouse EAT cells. These distributions of micronuclei are quite similar to the distributions of chromosomes in Chinese hamster cells or EAT cells measured by flow karyotyping. Flow karyotypes of the Chinese hamster cells and EAT cells used for these experiments are shown in Figure 7 for comparison. Nearly all peaks of the chromosome distributions were also found in the distribution of micronuclei. The distributions of micronuclei were, however, still overlapped by an additional background. Only some of the peaks in the micronucleus distributions representing the smallest chromosomes could not always be resolved due to an overlap with unspecific debris in the very low fluorescence region. Sorting of particles found in various peaks of the micronucleus distributions revealed that they had the typical round shape of micronuclei. Almost no chromosome shaped particles (<3%) were found (Figure 8).

An analysis of the relative peak areas in the micronucleus distribution in CS-treated CHE-0 cells (Figure 6a) revealed that the relative number of micronuclei in each peak containing one chromosome was the same as calculated from the respective chromosome distribution (Figure 7a). This result shows that CS did not selectively damage the spindle of certain chromosomes, all chromosomes have the same probability of forming a micronucleus.

By careful examination of the micronucleus distributions of CHE-0 cells, additional peaks of higher DNA content could be observed (Figure 9). These peaks were found at a DNA content

Table II. Distribution of CS-induced micronuclei containing multiple kinetochores[a]

	N_{mn}	N_{mn-}	N_{mn1+}	N_{mn2+}	N_{mn3+}	$N_{mn>4+}$
Control	182	122	41	11	5	3
		(0.67	0.23	0.06	0.03	0.01)
20 μM	220	93	105	13	3	6
		(0.42	0.48	0.06	0.01	0.03)
40 μM	1171	241	726	138	49	17
		(0.21	0.62	0.12	0.04	0.01)

[a]Micronuclei containing no (N_{mn-}), one (N_{mn1+}), two (N_{mn2+}), three (N_{mn3+}) and more than four ($N_{mn>4+}$) kinetochore per micronucleus. N_{mn}: number of micronuclei scored. Micronuclei scored between 10 h and 14 h of treatment (see Table I) are pooled for this analysis. (The numbers in brackets are fractions of the respective micronuclei.)

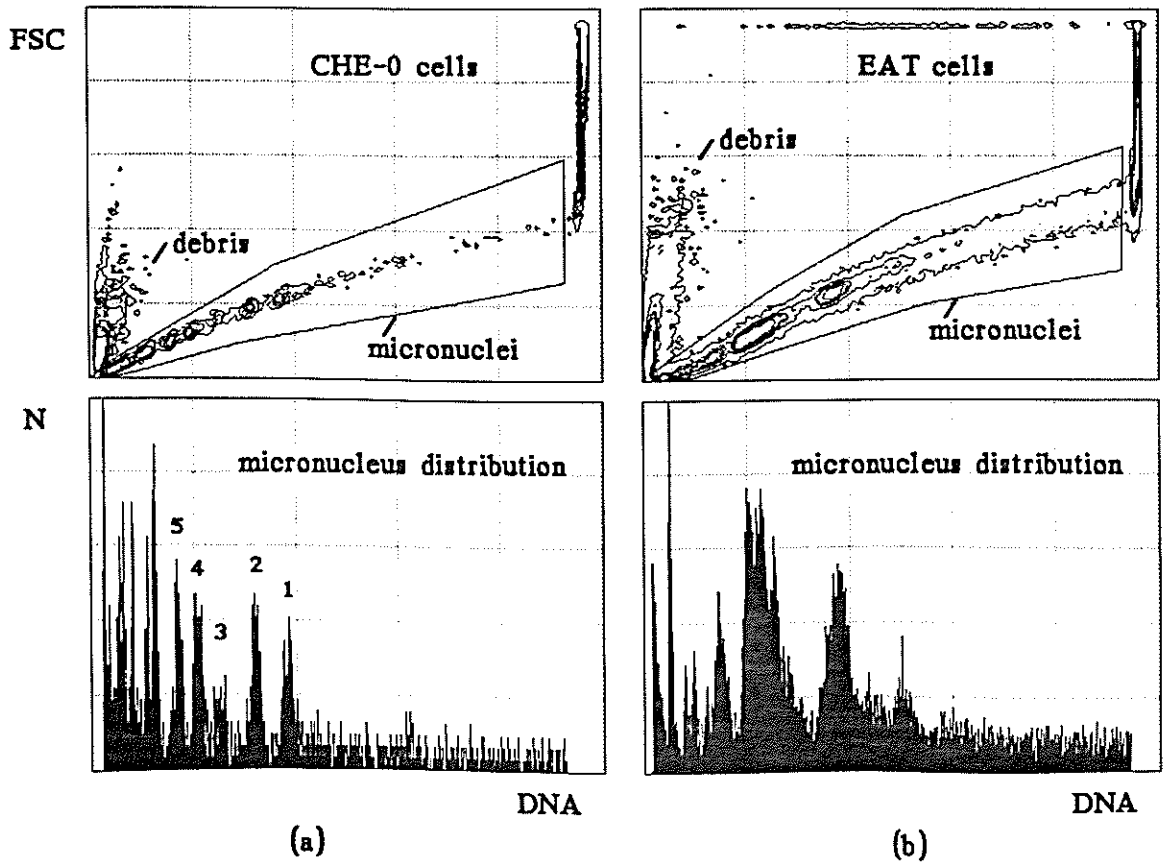

Fig. 6. DNA-FSC distributions of micronuclei induced in CHE-0 cells (a) and EAT cells (b) by CS (40 μM, t = 8 h). DNA distributions of micronuclei indicated by the window in the DNA−FSC distributions.

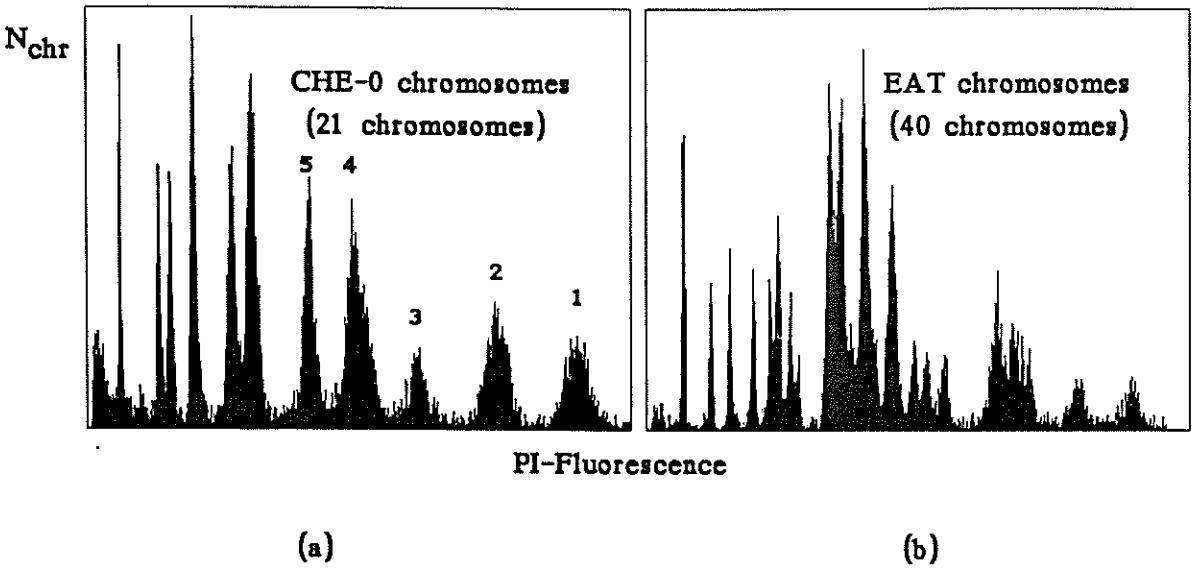

Fig. 7. Flow karyotypes of CHE-0 cells (a) and EAT cells (b). The five peaks containing the large chromosomes in CHE-0 cells are indicated by numbers 1–5. Peaks 1, 2 and 5 contains two, peak 3 contains one and peak 4 contains three chromosomes per cell.

Fig. 8. Micronuclei sorted from peak 1 of the micronucleus distribution shown in Figure 6a (CHE-0 cells).

representing the micronuclei containing various combinations of the largest chromosomes 1, 2 or 3 indicated in the flow karyotype of Figure 7a. Table III shows the relative DNA content of five additional peaks (a–e) identified in the micronucleus distribution and the combinations of two of the largest chromosomes that could have produced these peaks. Sorting of the micronuclei in peaks (a)–(e) and microscopic examination of the sorted particles revealed that nearly all particles (>95%) were single micronuclei. Only ~5% of the sorted micronuclei were found to be doublets of two micronuclei. This result shows indeed that a fraction of micronuclei found in the peaks (a)–(e) (~10%) represents micronuclei containing two distinct chromosomes.

By subtracting the background of the micronucleus distribution (Figure 9) from the distribution of the peaks it was calculated that ~60% of the particles registered in this distribution could be attributed to the distinct peaks representing micronuclei containing one kinetochore. This result agrees very well with the results from microscopic scoring of kinetochore-positive micronuclei presented in Tables I and II. About 60% of the micronuclei were found to contain one kinetochore per micronucleus in cells treated with 40 μM CS.

Discussion

It has been shown previously that the sensory irritant tear gas CS induces micronuclei in V79 cells (Ziegler-Skylakakis *et al.*, 1989). Schmid *et al.* (1989) have also demonstrated that CS caused spindle disturbances, c-mitoses and a metaphase block. Later, Schmid and Bauchinger (1991) showed that CS could induce chromosomal aneuploidy in V79 cells and polyploidy at higher concentrations. These effects of CS were attributed in part

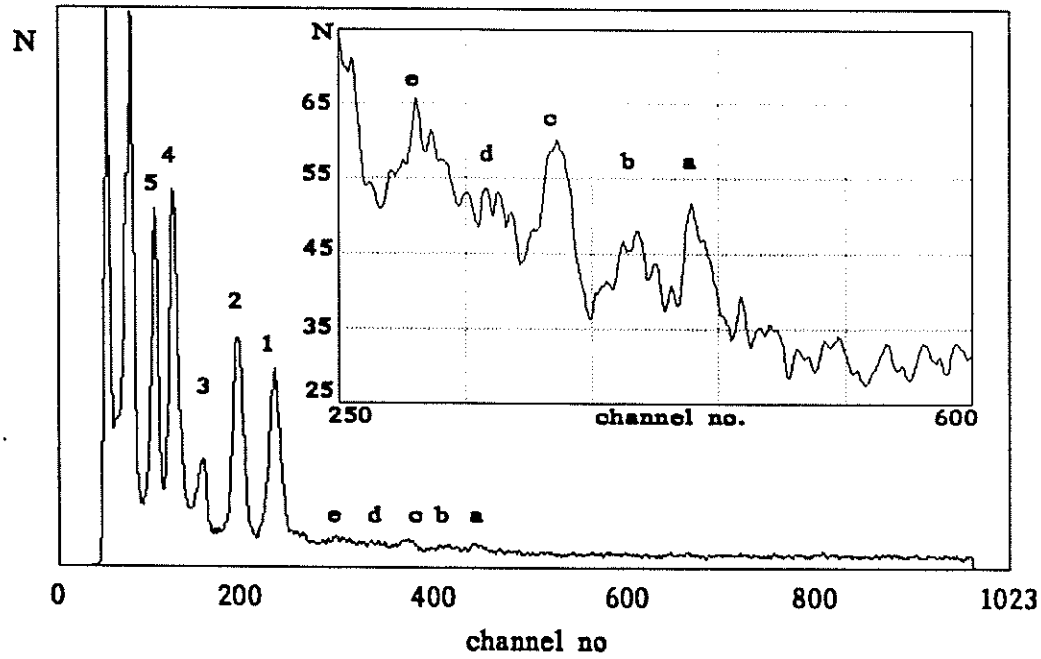

Fig. 9. DNA distribution of CS-induced micronuclei in CHE-0 cells. The peaks (a)–(e) represent micronuclei containing two of the large chromosomes found in peaks 1, 2 or 3 of the chromosome distribution (Figure 7). For clarity, the insert shows the distribution of these peaks between channel 255 and 600 only (see also Table III).

to one of its metabolites: *o*-chlorobenzaldehyde. Salassidis and Bauchinger (1990) and Salassidis *et al.* (1991) demonstrated by differential staining of the spindle apparatus and the chromosomes in c-mitoses that CS induced mitotic spindle damage that was similar to the damage induced by colcemid. They suggested, however, different mechanisms of action of both chemicals: whereas colcemid inhibits microtubule assembly, CS may direct attack the preformed spindle microtubules.

We have studied the ability of CS to induce micronuclei in Chinese hamster cells using a combination of flow cytometric techniques (Nüsse and Kramer, 1984; Schreiber *et al.*, 1992) and anti-kinetochore antibodies to detect single chromosomes in micronuclei. With a new flow cytometric technique to detect metaphase cells (Nüsse *et al.*, 1990) it was additionally possible to study the cell cycle progression of CS-treated Chinese hamster and mouse tumour cells and, in particular, the CS-induced mitotic block.

CS treatment resulted in an accumulation of mitotic cells; the timing and duration of the mitotic block depended on the CS concentration in the medium. After the mitotic block most cells were able to progress into the next interphase presumably due to degradation of the compound. After division, CS-induced micronuclei were found as a function of time after treatment both by microscopic observation and by flow cytometry. Microscopic observation of the cells after division showed additionally that a concentration dependent fraction of the cells were found to contain several fragmented nuclei. This is in agreement with the results of Schmid and Bauchinger (1991) who demonstrated that CS (37.5 μM) induced aneuploidy and also polyploid mitoses when analysed 20 h after treatment. Mitotic cells (including polyploids) which were unable to divide probably progressed into the next interphase producing cells with fragmented nuclei containing several chromosomes (Frackowiak *et al.*, 1986).

Using kinetochore staining, it was found that nearly all CS-induced micronuclei contained kinetochores and that 62% of the micronuclei found after 40 μM CS treatment contained exactly one kinetochore per micronucleus, 12% contained two kinetochores and 5% contained three and more kinetochores. The fraction of micronuclei without kinetochores (21%) was attributed to the micronuclei found in the untreated cells. Salassidis *et al.* (1991) observed that ~94% of the metaphases analysed after a 3 h treatment of V79 cells with 18.8 μM CS were c-metaphases. About 38% of these metaphases contained residual unarranged spindle fibres, 54% contained only microtubule material and 8% did not contain any spindle material. This was in contrast to the results obtained with colcemid treatment where 99% of the c-metaphases were of the latter type. Taking these results into consideration we conclude that the high fraction of CS-induced kinetochore-positive micronuclei containing one kinetochore

Table III. Micronuclei containing two large chromosomes measured by flow cytometry[a]

	Peak number									
	Single chromosomes					two chromosomes				
	1	2	3	4	5	a	b	c	d	e
Mean channel no.[b]	231	191	154	122	103	450	419	373	338	302
Combination of two chromosomes:[c]						1+1	1+2	2+2	2+3	3+3
Calculated channel number[d]						462	422	382	345	308

[a]Mean relative DNA contents (mean channel no.) of various peaks found in the distribution of micronuclei induced in CHE-0 cells by CS (analysis of the data presented in Figure 9).
[b]Mean channel number of the various peaks containing single chromosomes (1–5, left; see also flow karyotype in Figure 7a) and combinations of two chromosomes (a–e, right). Peak (a) represents micronuclei containing two chromosomes 1, peak (b) represents micronuclei containing the chromosomes 1 and 2, peak (c) represents micronuclei containing two chromosomes 2, peak (d) represents micronuclei containing the chromosome 2 and 3 and peak (e) represents micronuclei containing two chromosomes 3.
[c]Possible combinations of two chromosomes that could have formed peaks (a)–(e).
[d]Calculated mean channel number of the respective combinations of chromosomes. The mean channel number of the peaks was calculated using a least square fit of Gaussian distributions to the respective peaks.

observed in our experiments were created from single chromosomes lacking spindle fibers during mitosis.

Flow cytometric analysis of the micronucleus distributions showed several peaks representing micronuclei containing one chromosome. At higher DNA content even peaks representing micronuclei containing two chromosomes could be resolved. The distribution of these peaks was exactly the same as that of single chromosomes measured by flow karyotyping. Also the relative peak area of each identified peak representing the number of respective chromosomes per cell was quite similar in the micronucleus distribution compared to the chromosome distribution. The result that no chromosome was over- or under-represented in the micronucleus distribution demonstrates that CS acted similarly upon the spindles of all chromosomes.

Micronucleus distributions with peaks representing micronuclei containing one specific chromosome were also found after treatment of rat kangaroo PtK_1 cells with colchicine (Frackowiak *et al.*, 1986; Hernandez-Verdun *et al.*, 1986; Labidi *et al.*, 1987). Because these cells contained only 12 chromosomes it was easy to detect peaks in micronucleus distributions of the colchicine treated PtK_1 cells. It is, however, surprising that also in CS-treated cells containing 22 chromosomes (Chinese hamster cells) and even in cells containing ~40 chromosomes (mouse Ehrlich ascites tumour cells) micronucleus distributions with pronounced peaks could be observed. After treatment of these cells with colchicine or chloral hydrate we have also found peaks in the micronucleus distributions. In these cases the distributions were, however, overlapped by a broad background. With kinetochore-staining of micronuclei we observed that only ~20–30% of the micronuclei after colchicine treatment and 10–20% after chloral hydrate treatment contained one kinetochore, the remainder containing multiple kinetochores per micronucleus.

It can therefore be concluded that an analysis of the occurrence of peaks and the proportion between peaks and underlying background in the DNA distributions of micronuclei may give information about possible mechanisms of actions of various chemicals. The background of the micronucleus distributions is produced by micronuclei containing more than one chromosome, when the chemical under study induces mainly kinetochore-positive micronuclei. This was verified here by an analysis of the relative fraction of particles in the background continuum and the peaks found in the micronucleus distributions of CS-treated cells. About 60% of the micronuclei were found in the various peaks, a result that corresponded very well with the 62% of micronuclei showing exactly one kinetochore spot after kinetochore staining. Even micronuclei containing several combinations of two of the large chromosomes could be identified as peaks with corresponding DNA contents in the DNA distribution of CS-induced micronuclei.

However, if the physical or chemical agent under study induces a majority of micronuclei containing no kinetochores (as in the case of ionizing radiation; see Nüsse and Kramer, 1984; Nüsse *et al.*, 1987), the micronucleus distribution is composed of chromosome fragments of different sizes and no peaks can be observed. For an understanding of the DNA distributions of micronuclei induced by various agents measured by flow cytometry or by image analysis it is therefore necessary to know the fraction of micronuclei containing nil, one, two or more kinetochores and also the DNA distributions of chromosomes (flow karyotype). This is at present possible using anti-kinetochore antibodies, but only if the chemical under study does not damage the kinetochores themselves (Miller *et al.*, 1991). An alternative would be the use of *in situ* hybridization of centromere-specific DNA probes as shown by Miller *et al.* (1991). An analysis of the size distribution of micronuclei alone gives only a rough estimate of clastogenic effects (small micronuclei formed from chromosome fragments) and spindle damaging effects (large micronuclei formed from whole chromosomes) of various agents as shown by Yamamoto and Kikuchi (1980), Hogstedt and Karlson (1985) and Vanderkerken *et al.* (1989).

The shape of the DNA distributions of micronuclei can, in addition to the described factors, also be influenced by DNA synthesis in micronuclei. We have recently shown that radiation-induced micronuclei perform DNA synthesis in phase with the cell nucleus (Kramer *et al.*, 1990). This is also the case for micronuclei induced by various chemicals (not shown here, to be presented elsewhere). It is therefore to be expected that the shape of the micronucleus distribution depends on the time of measurement after treatment. In fact, after CS treatment, the pronounced peaks in the micronucleus distribution observed during the first hours slowly decreased at later time intervals after treatment due to DNA synthesis in micronuclei.

Another question regarding kinetochores in micronuclei can be answered by the results of the experiments presented here: do micronuclei that show a single kinetochore spot contain a whole metaphase chromosome or only a chromatid (or G1-phase chromosome)? If such a micronucleus contains a whole metaphase chromosome, two kinetochore spots would be expected as observed on metaphase chromosomes. It could be argued that only one chromatid containing a single kinetochore has formed a micronucleus (Schiffmann and de Boni, 1991). This is, however, not the case, because the relative DNA contents of the peaks in the micronucleus distribution induced by CS show that the micronuclei in each peak have exactly the DNA content of the corresponding metaphase chromosome. It may therefore be concluded that a micronucleus having only one kinetochore spot probably contains one whole metaphase chromosome since the two kinetochore spots usually found in a metaphase chromosome cannot be resolved in the corresponding micronucleus. This may be due to fusion of the two kinetochore spots in the micronucleus after entry into G_1-phase following division. However, it cannot be excluded that one of the kinetochore spots is inactivated in a G_1-phase micronucleus.

References

Bonatti,S., De Ferrari,M., Pisano,V. and Abbondandolo,A. (1986) Cytogenetic effects induced by alkylated guanine in mammalian cells. *Mutagenesis*, **1**, 99–105.

Cucinell,S.A., Hornfeldt,H., Vogl,L., Lichtmanegger,J. and Summer,K.H. (1971) Biochemical interactions and metabolic fate of riot control agents. *Fedn. Proc.*, **30**, 86–91.

von Däniken,A., Friedrich,U., Lutz,W.K. and Schlatter,C. (1981) Tests for mutagenicity in Salmonella and covalent binding to DNA and proteins in the rat of the riot control agent *o*-chlorobenzylidene malonitrile (CS). *Arch. Toxicol.*, **49**, 15–27.

Degrassi,F. and Tanzarella,C. (1988) Immunofluorescent staining of kinetochores in micronuclei: a new assay for the detection of aneuploidy. *Mutat. Res.*, **203**, 339–345.

Eastmond,D.A. and Tucker,J.D. (1989a) Kinetochore localization in micronucleated cytokinesis-blocked Chinese hamster ovary cells: a new and rapid assay for identifying aneuploidy-inducing agents. *Mutat. Res.*, **224**, 517–525.

Eastmond,D.A. and Tucker,J.D. (1989b) Identification of aneuploidy-inducing agents using cytokinesis-blocked human lymphocytes and an antikinetochore antibody. *Environ. Mol. Mutagenesis*, **13**, 44–43.

van den Engh,G., Trask,B., Cram,L.S. and Bartholdi,M.F. (1984) Preparation of chromosome suspensions for flow cytometry. *Cytometry*, **5**, 105–117.

Frackowiak,S., Labidi,D., Hernandez-Verdun,D. and Bouteille,M. (1986)

Preservation of chromosome integrity during micronucleation induced by colchicine in PtK_1 cells. *Chromosoma*, **94**, 468–472.

Heddle,J.A. and Carrano,A.V. (1977) The DNA content of micronuclei induced in mouse bone marrow by γ-irradiation: evidence that micronuclei arise from acentric chromosomal fragments. *Mutat. Res.*, **44**, 63–69.

Hennig,U.G.G., Rudd,N.L. and Hoar,D.I. (1988) Kinetochore immunofluorescence in micronuclei: a rapid method for the *in situ* detection of aneuploidy and chromosome breakage in human fibroblasts. *Mutat. Res.*, **203**, 405–515.

Hernandez-Verdun,D., Gregoire,M., Labidi,B. and Bouteille,M. (1986) Sorting of micronuclei from PtK_1 cells. *Exp. Cell Res.*, **164**, 243–250.

Hogstedt,B. and Karlsson,A. (1985) The size of micronuclei in human lymphocytes varies according to inducing agent used. *Mutat. Res.*, **156**, 229–232.

Jones,G.R.N. (1972) CS and its chemicals relatives. *Nature*, **235**, 257–261.

Iliakis,G. and Pohlit,W. (1979) Quantitative aspects of repair of potentially lethal damage in mammalian cells. *Int. J. Radiat. Biol.*, **36**, 649–658.

Kachel,V., Messerschmidt,R. and Hummel,P. (1990) Eight-parameter PC-AT based flow cytometric data system. *Cytometry*, **8**, 805–812.

Kramer,J., Schaich-Walch, G. and Nüsse,U. (1990) DNA synthesis in radiation-induced micronuclei studied by bromodeoxyuridine (BrdUrd) and anti-BrdUrd antibodies. *Mutagenesis*, **5**, 491–495.

Labidi,B., Frackowiak,S. and Hernandez-Verdun,D. (1987) Identification and sorting of micronuclei containing individual chromosomes. *Exp. Cell Res.*, **173**, 617–627.

Miller,B.M. and Adler,I.D. (1990) Application of antikinetochore antibody staining (CREST staining) to micronuclei in erythrocytes induced *in vitro*. *Mutagenesis*, **5**, 411–415.

Miller,B.M., Zitzelsberger,H.F., Weier,H.U.G. and Adler,I.D. (1991) Classification of micronuclei in murine erythrocytes: immunofluorescent staining using CREST antibodies compared to *in situ* hybridization with biotinylated gamma satellilte DNA. *Mutagenesis*, **6**, 297–302.

Nestman,E.R. and Lee,E.G.H. (1983) Mutagenicity of constituents of pulp and paper mill effluent in growing cells of *Saccharomyces cerevisiae*. *Mutat. Res.*, **119**, 273–280.

Nüsse,M. and Kramer,J. (1984) Flow cytometric analysis of micronuclei found in cells after irradiation. *Cytometry*, **5**, 20–25.

Nüsse,M., Krämer,M., Viaggi,S., Bartsch,A. and Bonatti,S. (1987) Anti-kinetochore antibodies and flow karyotyping: new techniques to detect aneuploidy in mammalian cells induced by ionizing radiation and chemicals. *Mol. Toxicol.*, **1**, 393–405.

Nüsse,M., Viaggi,S. and Bonatti,S. (1989) Induction of kinetochore positive and negative micronuclei in V79 cells by the alkylating agent diethylsulphate. *Mutagenesis*, **4**, 174–178.

Nüsse,M., Beisker,W., Hoffmann,C. and Tarnok,A. (1990) Flow cytometric analysis of G_1- and G_2/M-phase subpopulations in mammalian cell nuclei using side scatter and DNA content measurements. *Cytometry*, **11**, 813–821.

Önfeld,A. (1987) Spindle disturbances in mammalian cells. III. Toxicity, c-mitosis and aneuploidy with 22 different compounds. Specific and unspecific mechanisms. *Mutat. Res.*, **182**, 135–154.

Pincu,M., Callisen,H. and Norman,A. (1985) DNA content of micronuclei in human lymphocytes. *Int. J. Radiat. Biol.*, **47**, 423–432.

Rietveld,E.C., Delbressine,L.P.C., Waegemaekers,T.H.J.M. and Seutter-Berlage,F. (1983) 2-chlorobenzylmercapturic acid, a metabolite of the riot control agent 2-chlorobenzylidene malonitrile (CS) in the rat. *Arch. Toxicol.*, **54**, 139–144.

Salassidis,K. and Bauchinger,M. (1990) Mitotic spindle damage induced by 3,4-dichloroaniline in V79 Chinese hamster cells examined by differential staining of the spindle apparatus and chromosomes. *Mutagenesis*, **5**, 367–370.

Salassidis,K., Schmid,E. and Bauchinger,M. (1991) Mitotic spindle damage induced by 2-chlorobenzylidene malonitrile (CS) in V79 Chinese hamster cells examined by differential staining of the spindle apparatus and chromosomes. *Mutat. Res.*, **262**, 263–266.

Schiffmann,D. and De Boni,U. (1991) Dislocation of chromatin elements in prophase induced by diethylstilbestrol: a novel mechanism by which micronuclei can arise. *Mutat. Res.*, **246**, 113–122.

Schmid,E., Bauchinger,M., Ziegler-Skylakakis,K. and Andrae,U. (1989) 2-chlorobenzylidene malonitrile (CS) causes spindle disturbances in V79 Chinese hamster cells. *Mutat. Res.*, **226**, 133–136.

Schmid,E. and Bauchinger,M. (1991) Analysis of the aneuploidy inducing capacity of 2-chlorobenzylidene malonitrile (CS) and its metabolites in V79 Chinese hamster cells. *Mutagenesis*, **6**, 303–305.

Schreiber,G.A., Beisker,W., Bauchinger,M. and Nüsse,M. (1992) Multiparametric flow cytometric analysis of radiation induced micronuclei in mammalian cell cultures. *Cytometry*, **13**, in press.

Vanderkerken,K., Vanparys,P., Verschaeve,L. and Kirsch-Volders,M. (1989) The mouse bone marrow micronucleus assay can be used to distinguished aneugens from clastogens. *Mutagenesis*, **4**, 6–11.

Vig,B.K. and Swearngin,S.E. (1986) Sequence of centromere separation: kinetochore formation in induced laggards and micronuclei. *Mutagenesis*, **1**, 461–465.

Yamamoto,K.I. and Kikuchi,Y. (1980) A comparison of diameter of micronuclei induced by clastogens and by spindle poisons. *Mutat. Res.*, **71**, 127–131.

Ziegler-Skylakakis,K., Summer,K.H. and Andrae,U. (1989) Mutagenicity and cytotoxicity of 2-chlorobenzylidene malonitrile (CS) and metabolites in V79 Chinese hamster cells. *Arch. Toxicol.*, **63**, 314–319.

Received on July 1, 1991; accepted on September 9, 1991

INT. J. RADIAT. BIOL., 1992, VOL. 62, NO. 5, 587–602

Factors influencing the DNA content of radiation-induced micronuclei

M. NÜSSE†, J. KRAMER‡ and B. M. MILLER†

(Received 7 February 1992; revised 18 May 1992; accepted 8 June 1992)

Abstract. The distribution of the DNA content of radiation-induced micronuclei was analysed in several cell lines (Chinese hamster, Syrian hamster and mouse NIH-3T3 cells) by flow cytometry. Frequency and DNA content of micronuclei were measured simultaneously using fluorescence and forward scatter signals of micronuclei and nuclei in suspension stained with ethidium bromide. Computerized random breakage of chromosomes and random combination of fragments was performed to compare the measured micronucleus distributions in synchronized cells irradiated during G_1-phase with calculated distributions. The measured DNA distribution of radiation-induced micronuclei was found to be influenced by several factors: (1) the DNA distribution and the centromeric index of the chromosomes in the various cell lines; (2) the cell cycle phase at time of micronucleus measurement due to DNA synthesis in micronuclei; (3) the presence of chromosome fragments in micronuclei; and (4) the presence of whole chromosomes in micronuclei. These factors were shown to be responsible for the previously found large radiation-induced micronuclei which could not be explained by the classic assumption only that radiation-induced micronuclei are mainly produced by single acentric fragments.

1. Introduction

The frequency of micronuclei in cell cultures, human lymphocytes or in polychromatic erythrocytes of mouse bone marrow cells can be used as a quantitative measure of both structural and numerical chromosome aberrations induced by ionizing radiation or chemicals (Heddle *et al.* 1978). It is generally assumed that micronuclei found in interphase cells can arise from acentric chromosome or chromatid fragments or from whole chromosomes that lag behind at anaphase and are not incorporated into the daughter nuclei during division. Countryman and Heddle (1976) proposed that radiation-induced micronuclei arise primarily from acentric chromosome fragments that are either terminal deletions, interstitial deletions or produced during exchange aberrations. This hypothesis was further supported by an analysis of the distribution of DNA content of radiation-induced micronuclei in mouse bone marrow cells (Heddle and Carrano 1977). It was proposed by these authors that micronuclei arise from acentric chromosomal fragments induced by random breakage of the chromosomes. Several authors, however, found that a significant fraction of radiation-induced micronuclei in human lymphocytes (Pincu *et al.* 1985) or mouse Ehrlich ascites tumour cells (Nüsse and Kramer 1984) appeared to be too large to be due to this mechanism alone. Pincu *et al.* (1985) already proposed that these large micronuclei could probably be the result both of spindle defects and of DNA synthesis in micronuclei. In addition it has been mentioned (Heddle and Carrano 1977, Pincu *et al.* 1985) that a fraction of micronuclei could contain more than one acentric fragment leading to micronuclei that are larger than expected.

On the other hand, the DNA content of micronuclei was found to be influenced by the agent used to induce micronuclei (Yamamoto and Kikuchi 1980, Valadaud-Barrieu 1983, Hogstedt and Karlsson 1985, Gustavino *et al.* 1987, Wakata and Sasaki 1987, Vanderkerken *et al.* 1989). Chemicals interfering with the spindle mechanisms during mitosis usually induce larger micronuclei that contain one or several single chromosomes. It was therefore proposed to use the analysis of the distribution of DNA content of micronuclei to discriminate between clastogenic or spindle damaging effects of chemicals.

Recently, several new techniques were developed to study in detail the chromosomal composition of micronuclei. The presence of whole chromosomes in micronuclei can be detected using anti-kinetochore antibodies (Frackowiak *et al.* 1986, Vig and Swearngin 1986, Nüsse *et al.* 1987, 1989, 1992, Degrassi and Tanzarella 1988, Hennig *et al.* 1988, Thomson and Perry 1988, Eastmond and Tucker 1989a, b, Fenech and Morley 1989, Miller and Adler 1990, Cornforth and Goodwin 1991) or *in situ* hybridization (Ford *et al.* 1988, Becker *et al.* 1990, Miller *et*

†GSF-Institut für Biophysikalische Strahlenforschung. Neuherberg, Germany

‡GSF-Institut für Biophysikalische Strahlenforschung, Frankfurt/M, Germany

Address correspondence to: Dr Michael Nüsse, GSF-Institut für Biophysikalische Strahlenforschung, AG Durchflußzytometrie, Ingolstädter Landstr. 1, 8042 Neuherberg, Germany

0020-7616/92 $3.00 © 1992 Taylor & Francis Ltd

al. 1991, 1992, Salassidis *et al.* 1992). In some of these studies, the fraction of radiation-induced micronuclei containing one or more whole chromosomes was found to be in the range of only 3–20% depending on the cells investigated and on the experimental conditions. For example, we have found in Chinese hamster cells that only about 4–5% of radiation-induced micronuclei showed kinetochores (Nüsse *et al.* 1987). This small fraction of micronuclei containing whole chromosomes alone could therefore not be responsible for the fraction of large micronuclei (about 20% of the micronuclei have a DNA content that is larger than the largest chromosome arm) found in these cells after irradiation.

Using incorporation of bromodeoxyuridine (BrdUrd) in nuclei and micronuclei during S-phase and monoclonal antibodies to BrdUrd we have recently shown that radiation-induced micronuclei in Chinese hamster cells perform DNA synthesis in phase with the cell nucleus (Kramer *et al.* 1990). DNA synthesis could increase the DNA content of micronuclei by at least a factor of two depending on the time of measurement after irradiation and could be responsible at least in part for some of the large micronuclei found after irradiation.

A third factor assumed to be responsible to a certain degree for the DNA content of radiation-induced micronuclei is the fact that several single acentric chromosome fragments can be incorporated into a common micronucleus. With fluorescence *in situ* hybridization (FISH) using simultaneously a telomeric DNA probe of the hexameric repeat (TTAGGG) and a centromeric mouse gamma-satellite DNA probe we have recently shown in mouse NIH-3T3 cells (Miller *et al.* 1992) that about 19% of radiation-induced micronuclei exhibit centromere-positive hybridization signals and about 2–4 telomeric signals suggesting their origin from whole chromosomes. This fraction was higher than that observed in Chinese hamster cells using anti-kinetochore antibodies. Sixty-percent of the micronuclei showed 1–6 telomeric signals only revealing their origin from either single acentric fragments or several fused fragments. Therefore, several acentric fragments per micronucleus, probably caused by exchange aberrations mainly due to the formation of dicentric chromosomes, could also be responsible at least in part for the presence of larger micronuclei found in cells after ionizing radiation.

Although most of the factors described that influence the DNA content of radiation-induced micronuclei are quite well known, quantitative data demonstrating the relative contribution of each of these factors are rare. We have therefore performed experiments to study in detail several of these factors that influence the DNA content of radiation-induced micronuclei. The DNA content of micronuclei was measured using a technique to obtain a suspension of nuclei and micronuclei for flow cytometric measurement of micronuclei induced by irradiation (Nüsse and Kramer 1984, Schreiber *et al.* 1992) or chemicals (Nüsse *et al.* 1992). With this flow cytometric technique distributions of the DNA content of micronuclei were measured in various cell lines analysed at different time intervals after irradiation to study the influence of the cell cycle after the formation of micronuclei. The measured distributions of DNA content were compared with theoretical distributions of acentric chromosome fragments obtained by calculations based on the assumption of random breakage of chromosomes and random combination of fragments similar to Pincu *et al* (1985). For these calculations the DNA distribution of the chromosomes measured by flow karyotyping (see for example Gray and Langlois 1986, Nüsse *et al.* 1987) and the centromeric index of the chromosomes measured microscopically was used. It was additionally assumed that acentric chromosome fragments consisted of terminal deletions, interstitial deletions and random combinations of these deletions to include fragments produced as a result of exchange aberrations. In addition to the factors mentioned above it was shown that the karyotype can also influence the DNA content of micronuclei induced in various cell lines by ionizing irradiation.

2. Materials and methods

2.1. *Cell culture*

A subclone 10G2 (Nüsse *et al.* 1987) of the Chinese hamster embryo cells CCHE/27 (Ray *et al.* 1986) obtained from Scott Cram (Los Alamos National Laboratory, Los Alamos, USA) was used for the experiments. Cells were grown in α-MEM (Gibco) supplemented with 15% fetal calf serum at 37°C in an atmosphere of 6% CO_2. Cell cycle data of Chinese hamster cells were $t_{G1}=5$ h, $t_S=7$ h, $t_{G2M}=2$ h and $t_c=14$ h (Kramer *et al.* 1990).

A primary culture of Syrian hamster embryo cells (SHE, obtained from L. Hieber, GSF-Institut für Strahlenbiologie, Neuherburg, Germany) was grown for 2 weeks under the same conditions as described for Chinese hamster cells. The relative DNA content of SHE cells, measured by flow cytometry, was 15% higher than the DNA content of the Chinese hamster cells.

NIH-3T3 cells (permanent mouse fibroblastic line) with a cell cycle time of about 22 h were grown

(37°C, 6% CO_2) in D-MEM/F12 medium (Gibco) supplemented with 1% glutamine and 10% fetal calf serum (Gibco). This cell line was hypertriploid with a mean number of 68 chromosomes per cell. About 3% of the cells were diploid and contained 40 chromosomes. The relative DNA content of NIH-3T3 cells was 70% higher compared with the DNA content of Chinese hamster cells.

2.2. *Cell synchronization*

For some experiments, Chinese hamster cells were synchronized by selection of G_1-phase cells using velocity sedimentation (Nüsse 1982) in a Percoll gradient (5–25% Percoll in growth medium). Tubes were filled (50 ml) with the Percoll gradient using a gradient former, 2 ml of a cell suspension containing exponentially growing cells (1×10^7 cells/ml) were overlayed and the tubes were centrifuged at 550 rpm for 2–3 min. G_1-phase cells were found in the upper layers (8 ml) of the gradient. They were washed once and incubated in fresh medium for the experiments. About 1×10^6 G_1-phase cells were obtained per tube.

2.3. *Irradiation*

Cells were irradiated in medium with ^{60}Co γ-rays at a dose rate of 1 Gy/min.

2.4. *Preparation and staining of micronuclei and nuclei for flow cytometry*

Micronuclei and nuclei in suspension were prepared according to a modification of the two-step method published earlier (Nüsse and Kramer 1984, Nüsse *et al.* 1992). About 2×10^6 cells were centrifuged and 1 ml of solution I was added to the cell pellet after agitation. Solution I contained 584 mg/l NaCl, 1000 mg/l Na-citrate, 25 mg/l ethidium bromide (EB), 10 mg/l RNase, and 0·3 mg/l Nonidet P40. After about 1 h, 1 ml of solution II was added containing 1·5% citric acid, 0·25 M sucrose and 40 mg/l EB. The cell suspension was only slightly agitated. After this second step the cell membranes and the cytoplasm were disintegrated and the suspension usually contained only micronuclei and cell nuclei. Even the nuclei from mitotic cells were found to be well preserved (Nüsse *et al.* 1990). It was found that the samples could be stored at 4°C for at least 1 week.

2.5. *Chromosome preparation for flow karyotyping*

Chromosome suspensions for flow karyotyping were prepared according to a modification of the method proposed by van den Engh *et al.* (1984). Mitotic cells were enriched in exponentially growing cells by treatment with colcemid (0·2 μg/ml) in medium for 4 h, isolated by mitotic shake off and centrifuged for 10 min at 600*g*. The sedimented cells were treated at room temperature with 1 ml of hypotonic buffer containing 50 mM KCl, 10 mM $MgSO_4$, 5 mM K_2HOP_4, 0·25 mg/ml RNase, 3 mM β-mercaptoethanol, and 20 μg/ml propidium iodide (PI). After 10 min, 25 μl of 10% Triton X-100 was added; 10 min later the cells were forcefully syringed 4–6 times through a thin needle to release the chromosomes and incubated at 37°C for 30 min. The chromosome suspensions were stored at 4°C and measured 1–2 days after preparation.

2.6. *Flow cytometry and data analysis*

To measure micronuclei: EB fluorescence (DNA) and forward scatter (FSC) distributions of nuclei and micronuclei were measured simultaneously with a Cytofluorograf 30L (Ortho Diagnostics) equipped with the PC-AT-based data aquisition system developed by Kachel *et al.* (1990). Excitation of EB was provided by the 488 nm line (500 mW) of an argon ion laser model 2025-05 (Spectra-Physics). The emitted EB fluorescence was collected with a long-pass filter (OG 570). Bivariate DNA-FSC distributions were displayed as contour plots or dot plots using the newly developed Data Analysis Software DAS (Beisker, in preparation). G_1-phase nuclei were registered at around channel no. 900, S- and G_2/M-phase nuclei were stored in the last channel no 1023. Micronuclei were registered in the region between 1 and 40% of the relative DNA content of G_1-phase nuclei. Simultaneous measurement of FSC was performed to discriminate micronuclei from unspecific debris still present in the suspension of nuclei and micronuclei. As shown by sorting of the respective particles (Schreiber *et al.* 1992), particles with higher FSC were found to be unspecific debris whereas particles with lower FSC were found to be micronuclei. Micronuclei with relative DNA contents higher than about 1% of the G_1-phase cells could be separated well from debris according to their different FSC intensities. Micronuclei with lower relative DNA contents were still mixed with some debris and were therefore excluded from the measurement and the following analysis. We have shown recently that the majority of micronuclei have

DNA contents higher than this value (Schreiber *et al.* 1992). The fraction of micronuclei (N_{mn}) per nuclei (N_n), N_{mn}/N_n, was calculated using the window indicated in Figure 1.

Chromosome fluorescence distributions (flow karyotypes) were measured by collecting PI-fluorescence with a longpass filter (OG610). Analysis of chromosome flow karyotypes of the three cell lines studied were performed according to Nüsse *et al.* (1987).

2.7. *Distributions of radiation-induced acentric fragments caused by random breakage of chromosomes*

To calculate theoretical distributions of DNA content of radiation-induced micronuclei it was assumed that all micronuclei arose from acentric chromosome fragments (irradiation during G_1-phase) that are mainly terminal and interstitial deletions and combinations of these fragments due to exchange aberrations. Chromatid aberrations were not taken into consideration in these calculations. Random breakage of chromosomes was assumed for a calculation of the distribution of DNA content of radiation-induced acentric fragments (see also Pincu *et al.* 1985). For this calculation, the relative DNA content of each chromosome (measured for various cell lines by flow karyotyping) and the position of the centromere of each chromosome (centromeric index, measured by microscopic observation) had to be taken into consideration. The centromeric index CI ($CI = p/(p+q)$, where p is length of the short arm and q is length of the long arm) was calculated by measuring the arm lengths of metaphase chromosomes in the microscope. It was assumed that each acentric fragment consisted of two chromatids duplicated between the time of irradiation during G_1-phase and the time of observation during the following G_1-phase after division. It was further asumed that only one break could occur on one of the two chromosome arms (for metacentric chromosomes) and that the probability of this break depended on the length of the chromosome arm and was independent from the position on the chromosome arm (no 'hot spots'). Two breaks on one chromosome arm, neglected in our calculations, could lead to interstitial chromosome fragments. The DNA content distribution of such interstitial fragments should, however, be similar to the distribution of chromosome fragments caused by terminal deletions alone. The relative frequency of an acentric fragment caused by a terminal or interstitial deletion with DNA content d was therefore assumed to be proportional to the relative frequency of chromosome arms that have at least the DNA content d. To include chromosome fragments caused by exchange aberrations random combinations of two and three fragments was assumed.

3. Results

3.1. *Measurement of frequency and DNA distributions of micronuclei*

Figure 1a shows a typical flow cytometric measurement of DNA (EB-fluorescence) and FSC (forward scatter) of micronuclei and nuclei in suspension induced in Chinese hamster cells by irradiation (3 Gy). In this bivariate distribution G_1-phase nuclei with high DNA content were measured at around channel no. 900 and micronuclei between channel no. 10 and about 400. Unspecific debris with higher FSC signals compared with those of micronuclei could be easily separated using the window indicated in Figure 1a. The distribution of DNA content of micronuclei and nuclei measured in the window of Figure 1a is shown in Figure 1b. In such a measurement, the number of micronuclei N_{mn} is counted between channel number 10 and 400, the number of nuclei N_n between channel number 800 and 1023. Figure 1c shows a dose effect curve of micronucleus induction measured in asynchronous Chinese hamster cells 16 h after irradiation with ^{60}Co γ-radiation, when most cells have divided. This dose effect curve agrees well (within 10%) with curves measured by microscopic observation (not shown). Doses as low as about 0·1 Gy can be detected easily and with high precision.

3.2. *Influence of karyotype on DNA content of radiation-induced micronuclei*

As a first parameter influencing the DNA content of micronuclei the effect of chromosome size was studied. The shape of the distribution of DNA content of radiation-induced micronuclei should depend on the DNA content of the various chromosomes. The mean DNA content of micronuclei induced in cells with large chromosomes should be larger compared with the mean DNA content of micronuclei induced in cells with smaller chromosomes. Also the position of the centromere of each chromosome (centromeric index) should influence the DNA content of micronuclei. To study this effect in detail, micronuclei were induced in various cell lines having different karyotypes. Figure 2 shows flow karyotypes (DNA distributions of chromo-

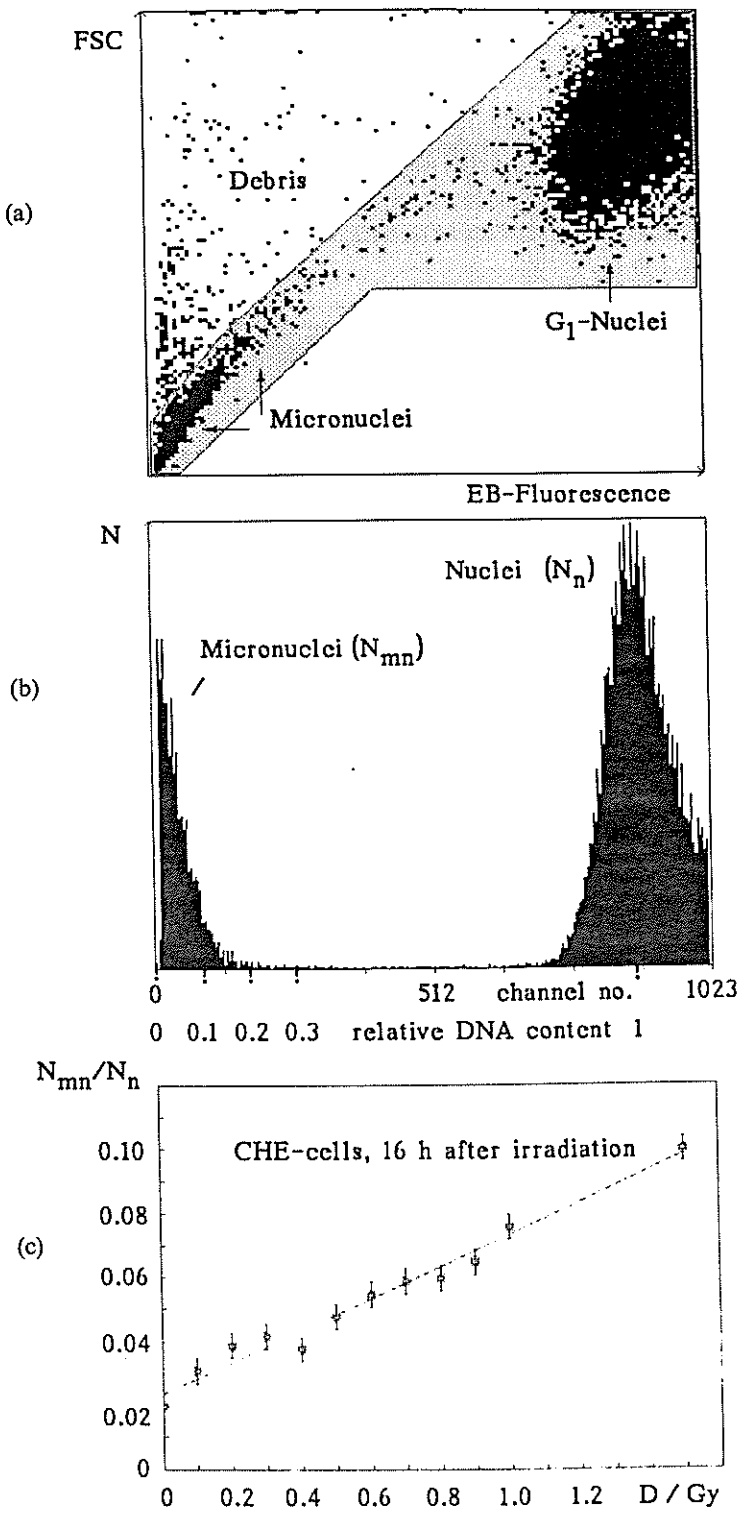

Figure 1a. Flow cytometric simultaneous measurement of DNA (EB-fluorescence) and forward scatter (FSC) of a suspension of micronuclei and nuclei from irradiated Chinese hamster cells. Discrimination of debris and micronuclei as indicated by the window. b, Distribution of DNA content of micronuclei and nuclei (particles inside the window of Figure 1a are displayed only). N_{mn}, number of micronuclei measured between relative DNA content 0·01 and 0·4; N_n, number of nuclei. c, frequency of micronuclei N_{mn}/N_n as a function of dose in irradiated asynchronous Chinese hamster cells measured at 16 h after irradiation.

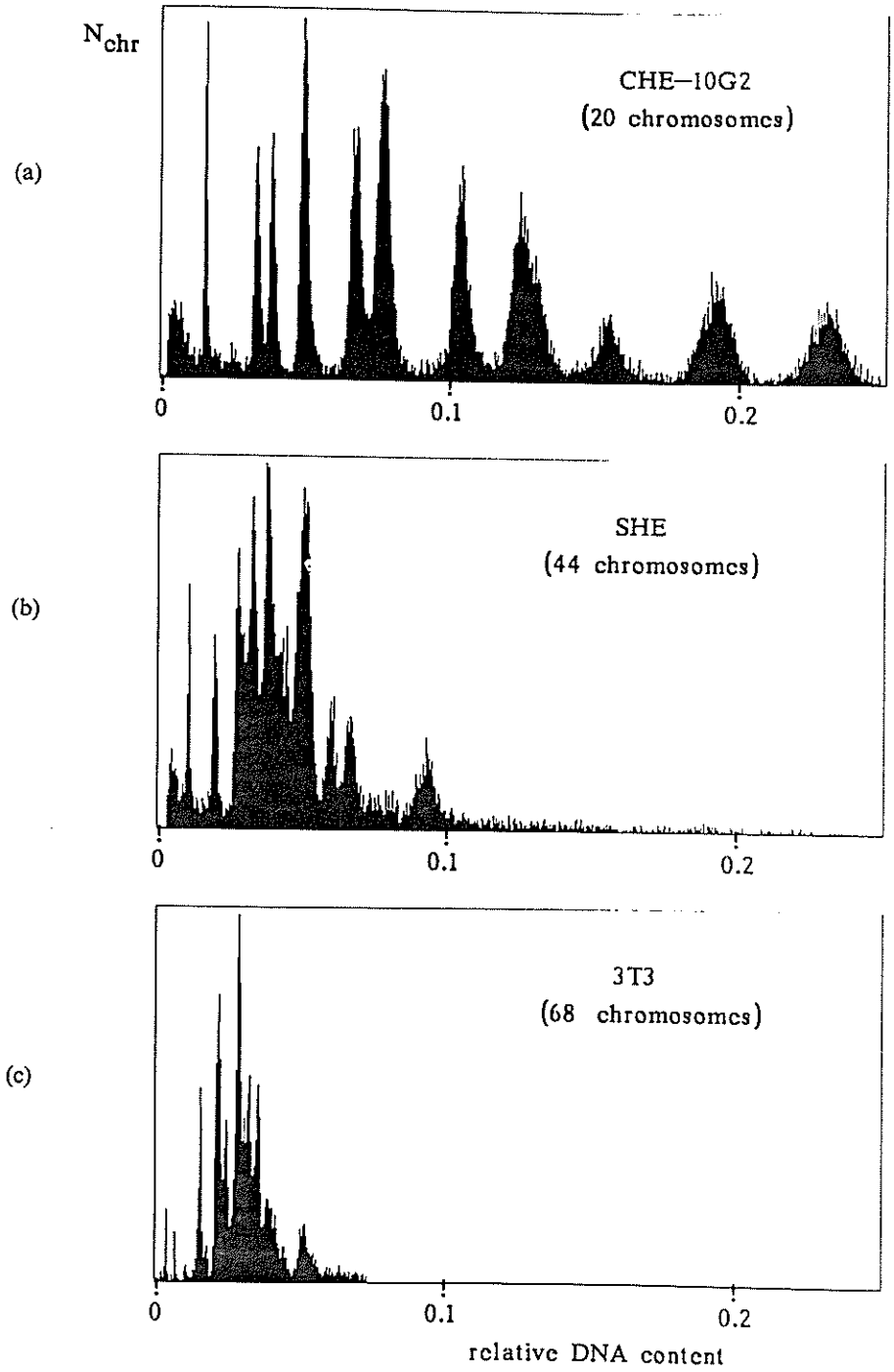

Figure 2. Chromosome fluorescence distributions (flow karyotypes) of (a) Chinese hamster cells (clone 10G2), (b) Syrian hamster cells and (c) mouse 3T3 cells. The relative DNA content of the chromosomes was normalized so that the G_1-phase nuclei of all three cell types had a relative DNA content 1.

somes) of three cell lines: (a) Chinese hamster cells clone 10G2 (mean no. of chromosomes per cell: 20); (b) Syrian hamster cells (44 chromosomes per cell; and (c) NIH-3T3 cells (mean no. of chromosomes per cell: 68). The relative DNA content plotted on the abscissa of these karyotypes is normalized so that G_1-phase cells of all cell lines have the relative DNA content 1. The differences of the relative DNA contents between Chinese hamster and Syrian hamster cells were small. Syrian hamster cells were found

to have a relative DNA content that was about 15% higher than the DNA content of Chinese hamster cells (flow cytometric analysis of DNA content, not shown). The DNA content of NIH-3T3 was about 70% higher compared with the Chinese hamster cell line. Figure 2 demonstrates clearly the differences in the mean relative DNA content of the chromosomes in Chinese hamster and Syrian hamster cells: Chinese hamster cells have larger chromosomes compared with Syrian hamster cells. The mouse NIH-3T3 chromosomes seem to be smaller, this was, however, caused artificially by the normalization of the G_1-phase cells on the same relative DNA content 1·0 in all three cell lines (Table 1).

Table 1 shows the centromeric index CI of the chromosomes of these three cell lines measured in several metaphases. Most of the chromosomes in Chinese hamster cells and in Syrian hamster cells were metacentric, some were submetacentric or acrocentric. On the other hand, all chromosomes in the mouse 3T3 cells were acrocentric chromosomes. It is therefore to be expected that the distribution of radiation-induced acentric fragments and micronuclei in these three cell lines should have different shapes.

Figure 3a shows calculated distributions of micronuclei from acentric fragments (terminal and interstitial deletions were considered only) in Chinese hamster and Syrian hamster cells (comparable DNA content) using random breakage of chromosomes and the data presented in Table 1 (irradiation during G_1-phase). As expected, the mean DNA content of acentric fragments induced in Syrian hamster cells is smaller compared with the mean DNA content of acentric fragments in Chinese hamster cells. This is due to the smaller, mainly metacentric chromosomes in these cells.

Figure 3b shows measured distributions of DNA content of micronuclei induced by irradiation in these two cell lines. For these experiments asynchronous cells were irradiated with 3 Gy and micronucleus distributions measured when all cells have divided. As expected, different micronucleus distributions were observed. The smallest micronuclei

Table 1. Relative DNA content and centromeric index CI of the chromosomes in Chinese hamster CHE-10G2 (own measurements), Syrian hamster SHE (Suzuki *et al.* 1989) and mouse NIH-3T3 cells. The relative DNA content of G_1-phase cells in all three cell lines was defined as 1·0. Compared with Chinese hamster 10G2 cells (relative DNA content 1·0) SHE-cells have a relative DNA content 1·15 and NIH-3T3 cells have a relative DNA content 1·7.

Relative DNA content per G_1-phase nucleus of each chromosome and the number of chromosomes per cell per chromosome peak was calculated using the flow karyotypes of Figure 2. The centromeric index was measured microscopically from chromosomes in metaphase cells.

CHE-10G2		SHE		3T3	
Relative DNA content	Centromeric-index	Relative DNA content	Centromeric-index	Relative DNA content	Centromeric-Index
0·223	0·42	0·093	0·5	0·053 (5x)	0
0·223	0·42	0·093	0·4	0·045 (2x)	0
0·174	0·47	0·093	0·3	0·042 (3x)	0
0·174	0·49	0·081 (2x)	0·4	0·039 (3x)	0
0·146	0·47	0·067	0·4	0·036 (8x)	0
0·115	0·48	0·067 (2x)	0·35	0·033 (7x)	0
0·115	0·46	0·059 (2x)	0·2	0·031 (3x)	0
0·115	0·44	0·049 (3x)	0·4	0·029 (14x)	0
0·097	0·46	0·049 (3x)	0·3	0·025 (6x)	0
0·097	0·43	0·049 (3x)	0·1	0·022 (10x)	0
0·069	0·44	0·043 (2x)	0·5	0·018 (1x)	0
0·069	0·41	0·043	0·25	0·016 (4x)	0
0·069	0·39	0·038 (2x)	0·0	0·007 (1x)	0
0·063	0·41	0·038 (6x)	0·3	0·004 (1x)	0
0·063	0·46	0·033 (2x)	0·5		
0·044	0·18	0·033	0·4		
0·044	0·29	0·033 (2x)	0·0		
0·036	0·40	0·029 (2x)	0·4		
0·030	0·45	0·027 (3x)	0·0		
0·012	0·0	0·019 (2x)	0·5		
		0·010 (2x)	0·2		
Sum	20 chromosomes/cell	44 chromosomes/cell		68 chromosomes/cell	

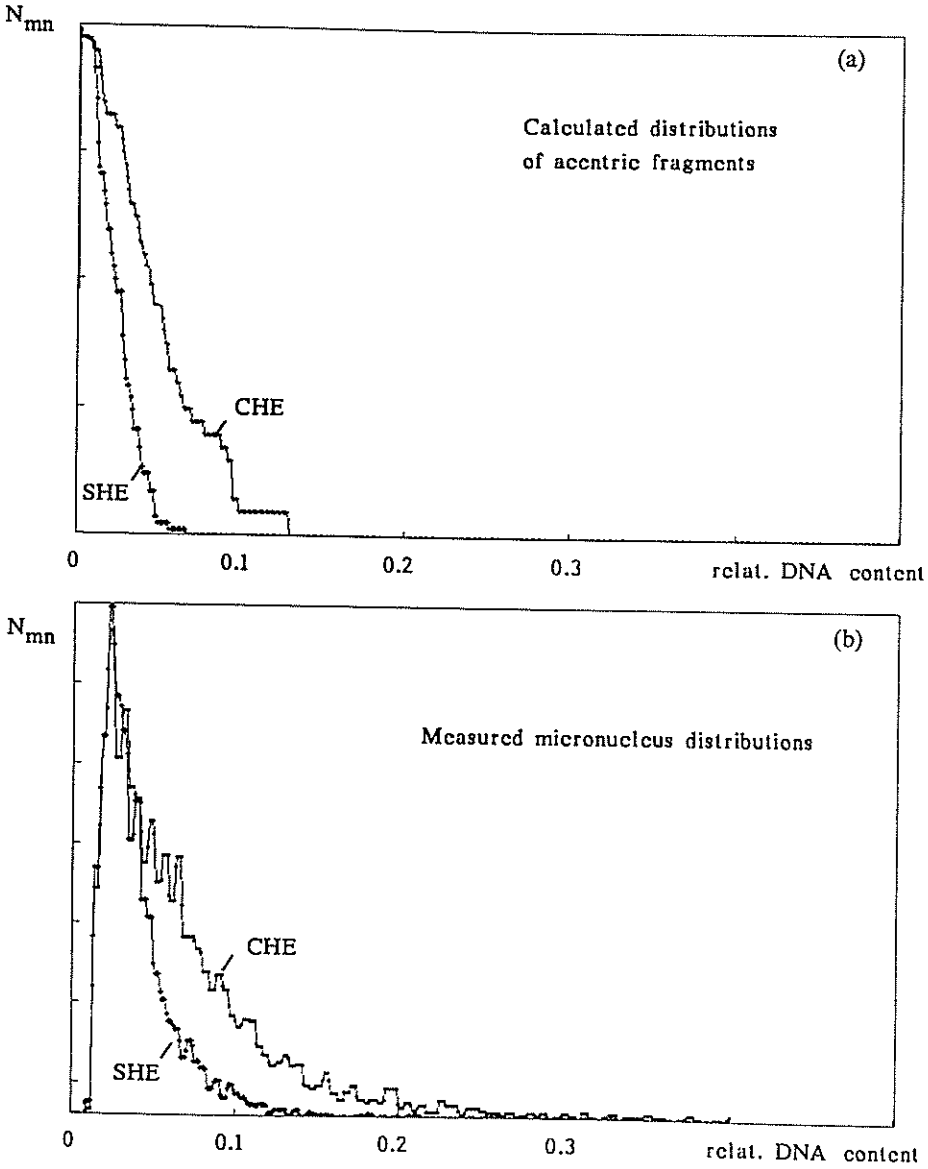

Figure 3a. Calculated distributions of acentric fragments (terminal deletions only) in Chinese hamster 10G2 cells and Syrian hamster cells. b, Measured micronucleus distributions in irradiated asynchronous Chinese hamster cells (clone 10G2) and asynchronous Syrian hamster cells at about 16 h after irradiation.

were obtained in Syrian hamster cells, larger micronuclei were found in Chinese hamster cells. A more detailed analysis of the different factors influencing the DNA content of micronuclei is shown in the following sections.

3.3. *DNA content of micronuclei in synchronized Chinese hamster cells irradiated during G_1-phase*

Figure 3b shows that micronuclei induced by ionizing radiation in asynchronous Chinese hamster cells and analysed, when all cells have divided, have relative DNA contents between 1% (lower limit of detection in these experiments) and about 20% of the DNA content of G_1-phase nuclei. The largest whole chromosome (two chromatids) in this cell line has a relative DNA content of about 22% of the G_1-phase nucleus and a centromeric index of about CI = 0·42 (see Table 1, Figure 2). If it is assumed that radiation-induced micronuclei arise from single acentric fragments caused by terminal or interstitial deletions only that have doubled their DNA content during S-phase directly after irradiation and before the formation of micronuclei, the largest micronucleus induced by irradiation in G_1-phase should

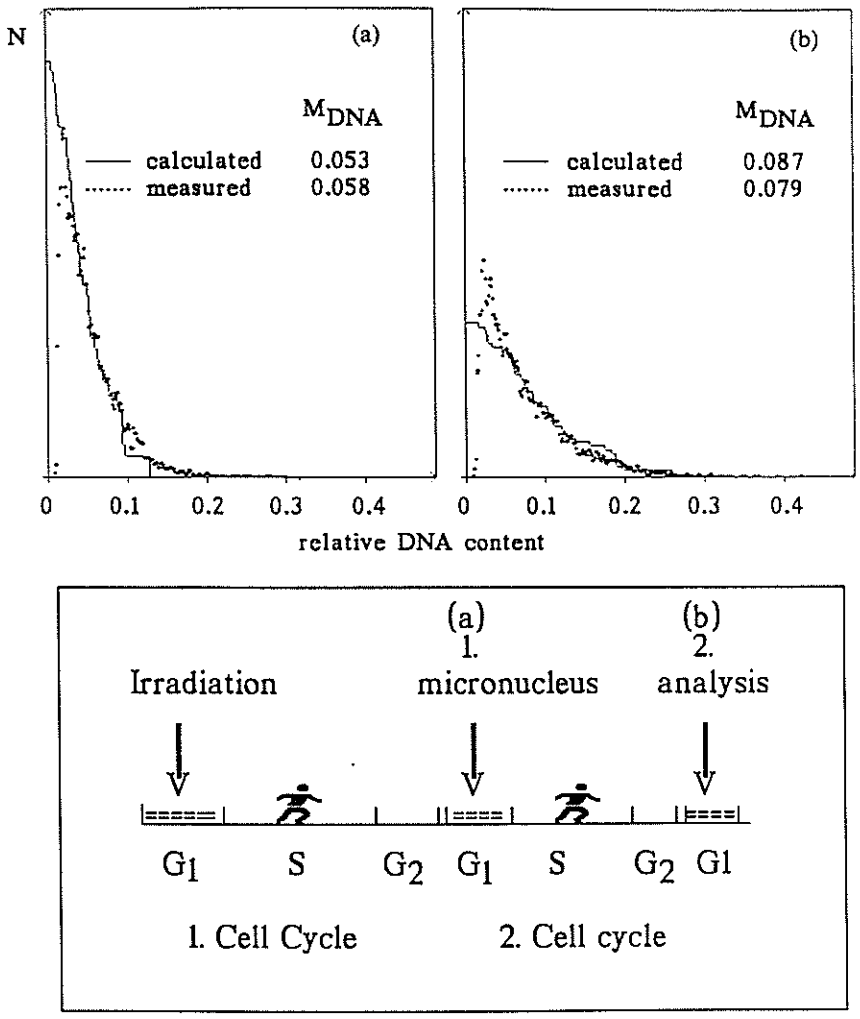

Figure 4. Upper figures. Micronucleus distributions of synchronized 10G2 Chinese hamster cells irradiated during G_1-phase (3 Gy). Comparison with calculated distributions of acentric fragments from terminal and interstitial deletions (random breakage) in Chinese hamster chromosomes. a, Micronucleus distribution in cells analysed during the 1. G_1-phase after division (no DNA synthesis in micronuclei). b, Micronucleus distribution in cells analysed during the 2. G_1-phase after division (DNA synthesis in micronuclei included). M_{DNA}, median of the distributions. Lower figure. Schematic diagram of irradiation and analysis during the cell cycle.

therefore have a maximal DNA content of 13% of the G_1-phase nucleus. One factor to explain the presence of micronuclei larger than 13% could be DNA synthesis in micronuclei (Kramer *et al.* 1990). The second reason for the presence of larger micronuclei could be that they were caused by acentric fragments from exchange aberrations (see § 4).

To investigate the influence of DNA synthesis on the DNA content of radiation-induced micronuclei, experiments were performed with synchronized cells irradiated during G_1-phase (3 Gy) and analysed during the following G_1-phase after the first division and again during the G_1-phase after the second division. Figure 4 shows design and results of these experiments together with results of theoretical distributions of acentric fragments from terminal or interstitial deletions only induced by irradiation in G_1-phase. The curves (a) in Figure 4 show a comparison of the distribution of DNA content of micronuclei in cells irradiated with 3 Gy during G_1-phase and measured during the first G_1-phase after division with the calculated distribution of acentric fragments according to random breakage of chromosomes in this cell line (Figure 3a). Both distributions agree quite well, only a small fraction of micronuclei have DNA contents that are higher than the DNA content of the largest possible fragment (13%). At very low DNA content ($<0{\cdot}02$) the curves do not agree, because micronuclei with relative DNA contents $<0{\cdot}01$ were cut off during measurement. The

median of these two distributions, calculated between a relative DNA content of 0·02 and 0·2, was 0·058 (experiment) and 0·053 (random breakage model). It can therefore be concluded that the general shape of the distribution of DNA content of micronuclei irradiated during G_1-phase and analysed at a time interval, when DNA synthesis in micronuclei is excluded, can be explained mainly by the assumption that acentric fragments (terminal and interstitial deletions) have formed these micronuclei. But still some micronuclei were found to be larger than the largest single acentric fragment from a terminal or interstitial deletion (see § 4).

The curves in Figure 4(b) show a comparison of the distribution of DNA content of micronuclei in cells irradiated with 3 Gy during G_1-phase and measured during the second G_1-phase after division with a theoretical distribution of acentric fragments that have twice the DNA content as those shown in the curves of Figure 4(a). In this experiment micronuclei were able to perform DNA synthesis. Again, both distributions agree quite well, especially in the DNA content region between 0·05 and 0·25. They disagree however at low DNA contents ($<0{\cdot}05$) probably caused by an increasing amount of small unspecific debris that could not be gated out. The median of these two distributions, calculated between a relative DNA content of 0·02 and 0·3 was 0·079 (experiment) and 0·087 (random breakage). The results of these experiments show clearly that micronuclei increase their DNA content during S-phase by a factor of nearly two.

3.4. *Influence of the presence of several acentric fragments and of whole chromosomes on the DNA content of radiation-induced micronuclei*

Radiation-induced micronuclei can also contain several acentric fragments caused by fusion of the two fragments during exchange aberrations (i.e. dicentrics). Little is known about the fraction of micronuclei including one, two or more acentric fragments. Recently, using *in situ* hybridization with telomeric and centromeric DNA probes, we have shown in mouse NIH-3T3 cells that about 35% of radiation-induced micronuclei contain at least one acentric fragment, about 21% contain at least two acentric fragments and about 5% at least three or more acentric fragments. Twenty-two per cent of the micronuclei showed neither telomeric nor centromeric signal probably due to the low sensitivity of the telomeric DNA probe to recognize the telomers of all chromosomes or to the fact that they were formed from interstitial deletions (Miller *et al.* 1992). Additionally, about 19% of the micronuclei showed centromeric signals accompanied with 2–4 telomeric signals revealing their origin from whole chromosomes.

To estimate how these effects could influence the DNA content of radiation-induced micronuclei calculations based on random breakage of the chromosomes and random combination of the fragments in mouse NIH-3T3 cells were performed. The mean number of chromosomes per cell, $N_{chr}=68$, was assumed to be the chromosome number in all cells. In these calculations the relative DNA content and the DNA distribution of the chromosomes as shown in Table 1 were used. The 22% of micronuclei showing neither telomeric nor centromeric signals were attributed to the fraction of micronuclei containing one, two or three fragments according to their relative ratios. Figure 5a shows calculated distributions of micronuclei containing one fragment and random combinations of two or three fragments. Figure 5b shows the calculated distribution of micronuclei assuming that 47% of the micronuclei contained one fragment, 28% two fragments, 6% three fragments per micronucleus and 19% whole chromosomes. Figure 5c shows a comparison of this calculated distribution with a measured micronucleus distribution in cells irradiated during G_1-phase and analysed during the following G_1-phase (no DNA synthesis in micronuclei, see also Figures 3a and 4a for Chinese hamster cells). Although peaks in the distribution caused by single chromosomes in micronuclei could not clearly be observed in the measured distribution, the comparison shows that the general shape of the micronucleus distribution in these cells can quantitatively be explained by the presence of several fragments and the presence of whole chromosomes in micronuclei.

Similar calculations were performed for a better understanding of the micronucleus distribution in Chinese hamster cells. Unfortunately, no data exist about the presence of several fragments in micronuclei due to the lack of DNA probes. Figure 5d shows a calculated distribution of micronuclei induced in Chinese hamster cells assuming that 60% of the micronuclei contained one single fragment, 30% two fragments and 10% three fragments and for comparison the measured distribution shown already in Figure 4a. Comparison of both curves in Figure 5d demonstrates that those micronuclei of the distribution shown in Figure 4a that has DNA content larger than that of the largest single acentric fragment ($\geqslant 13\%$) could have been formed by micronuclei containing more than one single acentric fragment (i.e. by fusion of the fragments produced during the formation of dicentric chromosomes). The presence

of whole chromosomes does not play a significant role in the analysis of the micronucleus distribution in Chinese hamster cells because only about 4% of radiation-induced micronuclei were found to contain whole chromosomes (Nüsse *et al.* 1987).

4. Discussion

The aim of these studies was to analyse in detail the different factors influencing the distribution of DNA content of radiation-induced micronuclei. Flow cytometry was used to measure the DNA content of micronuclei in a suspension of nuclei and micronuclei prepared carefully after radiation exposure and stained with fluorescent dyes (Nüsse and Kramer 1984, Ludwikowa *et al.* 1990, Schreiber *et al.* 1992). We have already shown that it is possible to measure the frequency of radiation-induced micronuclei with this flow cytometric technique using several flow cytometric parameters as for example light scattering intensities in addition to fluorescence signals for a discrimination of unspecific debris still present in this suspension. The results obtained with this technique agree well with results obtained by microscopic scoring of micronuclei (Schreiber *et al.* 1992).

Recently, we have even shown that an analysis of the distribution of DNA content of micronuclei induced by the tear gas 2-chlorobenzylidene malonitrile (CS) reveals that this chemical induces micronuclei containing predominantly single chromosomes. Micronuclei containing single chromosomes were found as peaks in the micronucleus distribution, the shape of this distribution was quite similar to the flow karyotype of chromosomes (Nüsse *et al.* 1992). Other chemicals that interfere with the spindle formation during mitosis (i.e. colchicine, chloralhydrate) were also found to induce micronucleus distributions with peaks representing micronuclei containing single chromosomes. These flow cytometric results were quantitatively supported by the analysis of micronuclei stained with anti-kinetochore antibodies.

Because radiation-induced micronuclei are known to be formed mainly from acentric chromosome or chromatid fragments (Heddle and Carrano 1977), peaks in the micronucleus distributions representing micronuclei containing single chromosomes are not to be expected. In fact, analysis of radiation-induced micronuclei with anti-kinetochore antibodies revealed that only a small fraction of micronuclei may have been formed from whole chromosomes, probably by radiation-induced spindle defects. Published values for the fraction of radiation-induced kinetochore-positive micronuclei range from 3 to 14% in human lymphocytes or fibroblasts (Thomson and Perry 1988, Cornforth and Goodwin 1991, Fenech and Morley 1989) or in Chinese hamster cells (Nüsse *et al.* 1987, Degrassi and Tanzarella 1988). Slightly higher results (10–20%) were obtained for radiation-induced micronuclei in mouse cells using *in situ* hybridization with centromeric DNA probes (Salassidis *et al.* 1992) or simultaneous use of centromeric and telomeric DNA probes (Miller *et al.* 1992). Therefore, the influence of whole chromosomes in micronuclei on the DNA distribution of radiation-induced micronuclei has to be considered additionally, especially in mouse cell lines. This effect is even more important, if the DNA content of micronuclei induced by certain chemicals has to be analysed (Nüsse *et al.* 1992).

The distribution of DNA content of radiation-induced micronuclei in the three cell lines studied here (Chinese hamster cells, Syrian hamster cells, mouse NIH-3T3 cells) showed different shapes. For example, micronuclei in Chinese hamster cells were larger compared with micronuclei induced in Syrian hamster cells. These differences were due to the radiation-induced random breakage of chromosomes as shown already by Heddle and Carrano (1977), Pincu *et al.* (1985) and also by our model calculations using computer-aided random breakage of chromosomes. If a random breakage of chromosomes and, additionally, random combination of fragments is assumed to be responsible for the size distribution of acentric chromosome fragments, the relative sizes of the chromosomes and the position of the centromeres of the chromosomes should influence the distribution of fragments and, because micronuclei are formed mainly from these acentric fragments, also the shape of the micronucleus distribution. This assumption was verified here by studying the DNA content of micronuclei induced in various cell lines that showed different chromosome karyotypes. Micronuclei induced in Syrian hamster cells with small, mainly metacentric chromosomes were smaller than micronuclei induced in Chinese hamster cells having larger and also mainly metacentric chromosomes. The influence of the position of the centromeres in the chromosomes was additionally shown in mouse 3T3 cells. These cells contain also small chromosomes comparable with the Syrian hamster chromosomes, but all chromosomes were acrocentric. The differences in the shape of the micronucleus distributions in these three cell lines were therefore caused by their different karyotypes, verified by model calculations and by our experiments.

Using microscopic analysis, different size distributions of micronuclei in three different cell lines (mouse fibroblasts, human pharynx carcinoma cells and rhesus monkey kidney cells) were also found by Kaffenberger *et al.* (1990). The authors interpreted their results, however, by assuming different particularly radiosensitive regions in the chromosomes, so called 'hot spots', that might be responsible for regular occurence of certain classes of micronuclei and therefore also for the different size distributions of micronuclei found in these three cell lines. Such an interpretation can at present not be excluded, but our results show quite clearly that the different distributions of DNA content of micronuclei in various cell lines can easily be explained by their different karyotypes without assuming 'hot spots' on the chromosomes.

Comparison of the calculated distribution of acentric chromosome fragments from terminal or interstitial deletions in Chinese hamster cells with distributions of DNA content of micronuclei induced in synchronized G_1-phase cells and measured directly after division (no DNA synthesis in micronuclei, no chromatid aberrations) shows that the general shape of the micronucleus distribution can be explained by the assumption that radiation-induced micronuclei are formed mainly by single acentric chromosome fragments as already suggested by Heddle and Carrano (1977). In our calculations we assumed probabilities for breaks on the chromosomes that were independent from the position on the chromosomes. It is, however, known that breakpoints have a tendency to accumulate at certain positions on the chromosomes ('hot spots', the majority is found near the end of the chromosomes, see Bauchinger and Götz 1979). In our calculations

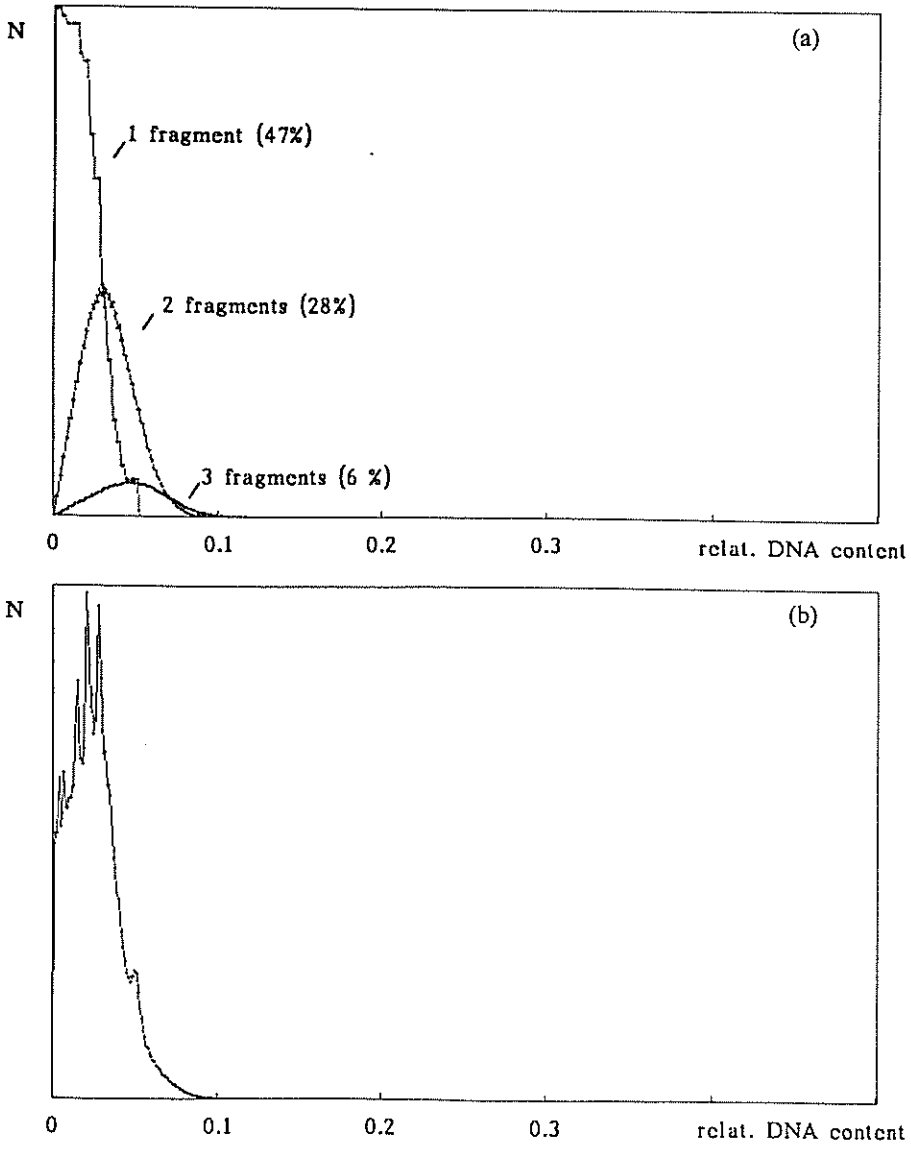

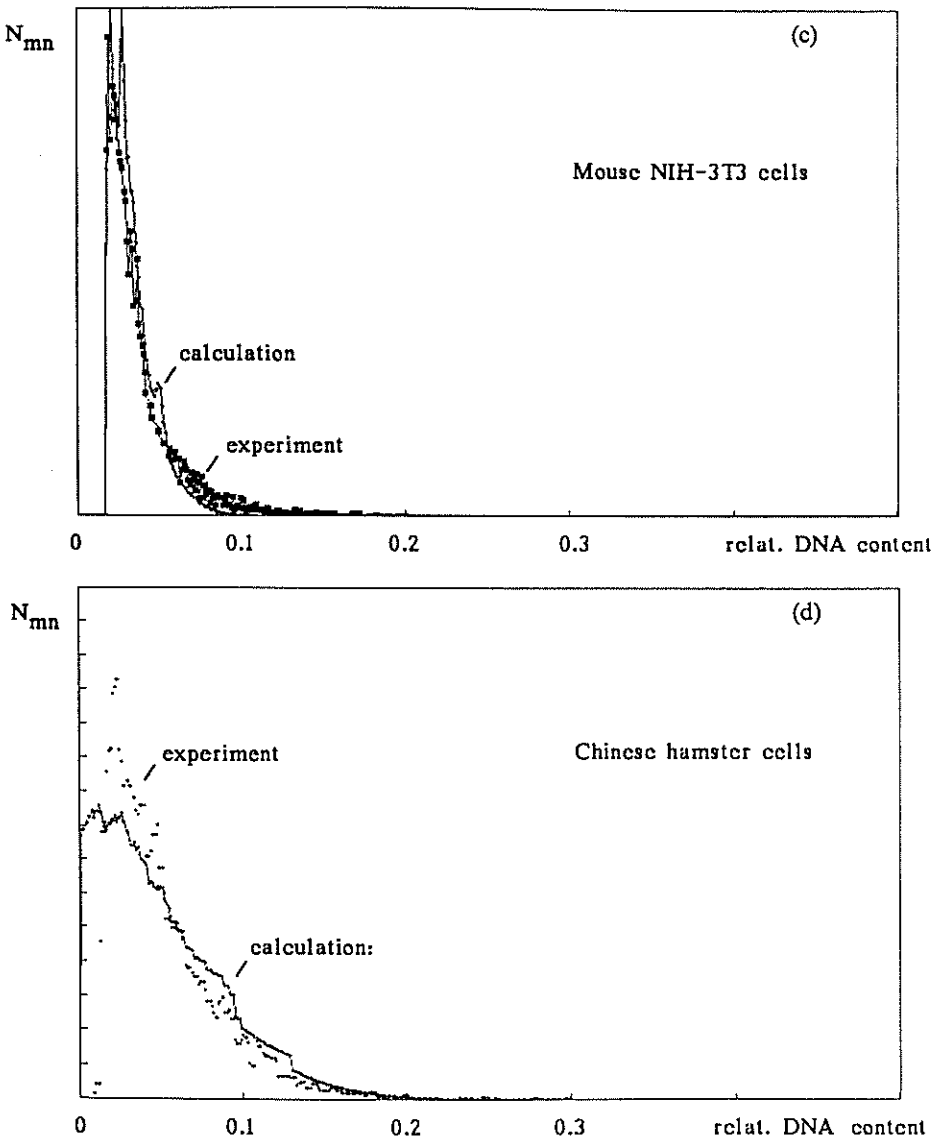

Figure 5a. Calculated distributions of single acentric fragments (terminal and interstitial deletions) and random combinations of two and three acentric fragments (from exchange aberrations) in mouse NIH-3T3 cells. b, Calculated distribution of radiation-induced micronuclei in NIH-3T3 cells assuming 47% micronuclei containing one fragment, 28% containing two fragments, 6% containing three fragments and 19% containing single chromosomes (data from Miller *et al.* 1992). c, Comparison of the measured micronucleus distribution (closed squares) in NIH-3T3 cells irradiated during G_1-phase (4 Gy) and analysed during the 1. G_1-phase after division with the calculated distribution (small points) shown in b. The curves were normalized on the same number of micronuclei with relative DNA content between 0·016 and 0·2. Micronuclei with a relative DNA content lower than 0·016 were cut off. d, Comparison of the measured micronucleus distribution in Chinese hamster 10G2 cells irradiated during G_1-phase (3 Gy) and analysed during the 1. G_1-phase after division (Figure 4a) with a calculated distribution of micronuclei assumed to contain one fragment (60%), two fragments (30%) and three fragments (10%). The curves were normalized on the same number of micronuclei.

this effect was not taken into consideration, because little is known about preferential break points in the cell lines studied here. This effect should, however, lead to an underestimation of small micronuclei in the calculated distributions of single acentric fragments as compared with the distributions of micronuclei observed in the experiments. In fact, this was observed in our experiments. The smallest micronuclei were, however, cut off before analysis, because it was sometimes difficult to discriminate very small micronuclei (smaller than 1% of the G_1-phase nuclei) from unspecific debris (see also Schreiber *et al.* 1992).

The comparison between calculation and experi-

ments in irradiated Chinese hamster cells shows that some of the micronuclei observed experimentally are still larger than the largest single acentric fragment from a terminal or interstitial deletion having about 13% of the DNA content of G_1-phase cells according to the length and the centromeric index of the largest chromosome in these cells. Because DNA synthesis in micronuclei was excluded in these experiments, the only explanation for this deviation between theoretical calculations and experimental results could be that several single acentric fragments are included in a single micronucleus. It is well known that after ionizing radiation dicentric chromosomes are the most frequent chromosome aberrations (i.e. Bloom 1972, Bauchinger and Götz 1979, Cornforth and Goodwin 1991). In the analysis of dicentric chromosomes the associated acentric fragment is usually included. Most of the two fragments produced by complete exchange during the formation of dicentric chromosomes can fuse (about 90% in human lymphocytes, see Bauchinger and Götz 1979) and can therefore form a single micronucleus which should therefore show four telomeric signals. In fact, we have recently shown using *in situ* hybridization simultaneously with centromeric and telomeric DNA probes that a considerable fraction of radiation-induced micronuclei in mouse 3T3 cells contained two or more single acentric fragments (Miller *et al.* 1992). If this effect is quantitatively taken into account in our calculations, the measured micronucleus distribution in these cells agrees well with the calculated distribution. If similar effects are assumed to occur also in Chinese hamster cells, theoretical calculations of micronucleus distributions including micronuclei containing one (60%), two (30%) and three (10%) fragments per micronucleus show also a good agreement with the distributions measured experimentally, especially in the larger DNA content region. No data exist at present about the distribution of fused fragments in micronuclei of Chinese hamster cells. The reason is that telomeric DNA probes show a telomere-only pattern on mouse chromosomes, whereas on Chinese hamster chromosomes three or more sites of hybridization signals usually as large as centromeric blocks can be observed additionally.

A third, important factor that can influence the DNA content of radiation-induced micronuclei (and also of chemically-induced micronuclei) is DNA synthesis in micronuclei. We have recently shown that most radiation-induced micronuclei in Chinese hamster cells perform DNA synthesis in phase with the cell nucleus during S-phase (Kramer *et al.* 1990). Similar results were obtained by Gosh and Paweletz (1984) in multinucleated cells induced by colcemid. Micronuclei should therefore increase their DNA content during S-phase following the first cell division after irradiation. In fact, our experiments with synchronized Chinese hamster cells irradiated during G_1-phase show that micronuclei increase their DNA content during S-phase by a factor of nearly two. It can therefore be expected that the shape of the distribution of DNA content of micronuclei induced in asynchronous cells should depend on the time of measurement after irradiation. A fraction of the larger micronuclei observed in various cells by other authors (Heddle and Carrano 1977, Pincu *et al* 1985, Kaffenberger *et al.* 1990) could therefore also be produced by DNA synthesis during S-phase and not necessarily by whole chromosomes in micronuclei as proposed by these authors.

Finally, it should be mentioned that usually only a fraction of the radiation-induced chromosome fragments are excluded at the first division after irradiation to give rise to micronuclei (Savage 1988, 1989). For example, Littlefield *et al.* (1989) and Cornforth and Goodwin (1991) have shown that only about 50% of the fragments found in metaphases of human lymphocytes or human fibroblasts gave rise to micronuclei. The factors that control that exclusion are not known. If the exclusion is not a random process and fragment size has an influence, a biased distribution of DNA contents of micronuclei should be expected. Because little is known about this effect it could not be included into our calculations of the DNA content of micronuclei and their comparison with measured distributions.

In conclusion, several factors were found and analysed that could influence the DNA content of radiation-induced micronuclei. These factors are: (1) the size distribution and the centromeric index of the chromosomes; (2) the presence of one (e.g. from terminal or interstitial deletions) or several acentric fragments (e.g. from exchange aberrations) in micronuclei; (3) DNA synthesis in micronuclei during S-phase; and (4) the presence of whole chromosomes in micronuclei. The latter can play a significant role in understanding the micronucleus size distribution in mouse NIH-3T3 cells. In Chinese hamster cells only a small fraction of micronuclei was found to be formed by whole chromosomes measured by anti-kinetochore staining. Anti-kinetochore staining, however, seems not to be the ideal technique to analyse the fraction of micronuclei containing whole chromosomes because the kinetochore itself could be damaged by ionizing radiation. All of these four factors should also influence the DNA content of micronuclei induced by chemicals, the relative importance of these factors should, however, depend on the chemical under study.

Acknowledgements

This work was financially supported in part by the Commission of the European Communities, Radiation Protection Programme, contract B17-0038-C (TT).

References

BAUCHINGER, M. and GÖTZ, G., 1979 Distribution of radiation-induced lesions in human chromosomes and dose-effect relation analysed with G-banding. *Radiation and Environmental Biophysics*, **16**, 355–366.

BECKER, P., SCHERTHAN, H. and ZANKL, H., 1990, Use of a centromere-specific DNA probe (p82H) in nonisotopic *in situ* hybrization for classification of micronuclei. *Genes Chromosomes and Cancer*, **2**, 59–62.

BLOOM, A. B., 1972, Induced chromosome aberrations in man. *Advances in Human Genetics*, **3**, 99–172.

CORNFORTH, M. N. and GOODWIN, E. H., 1991, Transmission of radiation-induced acentric chromosomal fragments to micronuclei in normal human fibroblasts. *Radiation Research*, **126**, 33–36.

COUNTRYMAN, P. I. and HEDDLE, J., 1976, The production of micronuclei from chromosome-aberrations in irradiated cultures of normal human fibroblasts, *Radiation Research*, **126**, 210–217.

DEGRASSI, F. and TANZARELLA, C., 1988, Immunofluorescent staining of kinetochores in micronuclei: a new assay for the detection of aneuploidy. *Mutation Research*, **203**, 339–345.

EASTMOND, D. A. and TUCKER, J. D., 1989a, Kinetochore localization in micronucleated cytokinesis-blocked Chinese hamster ovary cells: a new and rapid assay for identifying aneuploidy-inducing agents. *Mutation Research*, **224**, 517–525.

EASTMOND, D. A . and TUCKER, J. D., 1989b, Identification of aneuploidy-inducing agents using cytokinesis-blocked human lymphocytes and an antikinetochore antibody. *Environmental Molecular Mutagenesis*, **13**, 34–43.

VAN DEN ENGH, G., TRASK, B., CRAM, L. S. and BARTHOLDI, M. F., 1984, Preparation of chromosome suspensions for flow cytometry. *Cytometry*, **5**, 105–117.

FENECH, M. and MORLEY, A. A., 1989, Kinetochore detection in micronuclei: an alternative method for measuring chromosome loss. *Mutagenesis*, **4**, 98–104.

FORD, J. H., SCHULTZ, C. J. and CORELL, A. T., 1988, Chromosome elimination in micronuclei: a common cause of hypoploidy. *American Journal of Human Genetics*, **43**, 733–740.

FRACKOWIAK, S., LABIDI, D., HERNANDEZ-VERDUN, D. and BOUTEILLE, M., 1986, Preservation of chromosome integrity during micronucleation induced by colchicine in PtK1 cells. *Chromosoma*, **94**, 468–472.

GHOSH, S. and PAWELETZ, N., 1984, Synchronous DNA synthesis and mitosis in multinucleate cells with one chromosome in each nucleus. *Chromosoma*, **89**, 304–311.

GRAY, J. W. and LANGLOIS, R. G., 1986, Chromosome classification and purification using flow cytometry and sorting. *Annual Review of Biophysics and Chemistry*, **15**, 195–235.

GUSTAVINO, B., VITAGLIANO, E., SCOTTILI, E. and RIZZONI, M., 1987, A comparison between short-term evolution of micronuclei induced by X-rays and colchicine in root tips of *Vicia faba*. *Mutation Research*, **192**, 109–119.

HEDDLE, J. A. and CARRANO, A. A., 1977, The DNA content of micronuclei induced in mouse bone marrow by gamma-irradiation: evidence that micronuclei arise from acentric chromosomal fragments. *Mutation Research*, **44**, 63–69.

HEDDLE, J. A., BENZ, R. D. and COUNTRYMAN, P. I., 1978, Measurement of chromosomal breakage in cultured cells by the micronucleus technique. In: *Mutagene-Induced Chromosome Damage* (Edinburgh University Press, Edinburgh), pp. 191–200.

HENNIG, U. G. G., RUDD, N. L. and HOAR, D. I., 1988, Kinetochore immuno-fluorescence in micronuclei: a rapid method for the *in situ* detection of aneuploidy and chromosome breakage in human fibroblasts. *Mutation Research*, **203**, 405–414.

HOGSTEDT, B. and KARLSSON, A., 1985, The size of micronuclei in human lymphocytes varies according to inducing agent used. *Mutation Research*, **156**, 229–232.

KACHEL, V., MESSERSCHMIDT, R. and HUMMEL, P., 1990, Eight-parameter PC-AT based flow cytometric data system. *Cytometry*, **8**, 805–812.

KAFFENBERGER, W., BECKER, K. and VAN BUENINGEN, D., 1990, Comparison of micronucleus frequencies and proliferation kinetics in three X-irradiated cell lines. *Strahlentherapie und Onkologie*, **166**, 617–625.

KRAMER, J., SCHAICH-WALCH, G. and NÜSSE, M., 1990, DNA synthesis in radiation-induced micronuclei studied by bromodeoxyuridine (BrdUrd) labelling and anti-BrdUrd antibodies. *Mutagenesis*, **5**, 491-495.

LITTLEFIELD, L. G., SAYER, A. M. and FROME, E. L., 1989, Comparison of dose-response parameters for radiation-induced acentric fragments and micronuclei observed in cytokinesis-arrested lymphocytes. *Mutagenesis*, **4**, 265–280.

LUDWIKOWA, G., STALNAKE, C. G., JOHANSON, K. J., SUNDELL-BERGMAN, S. and RICHTER, S., 1990, Microscopic and flow cytometric study of micronuclei in iododeoxyuridine labelled cells irradiated with soft X-rays. *Acta Oncologica*, **29**, 761–767.

MILLER, B. M. and ADLER, I.-D., 1990, Application of antikinetochore antibody staining (CREST staining) to micronuclei in erythrocytes induced *in vivo*. *Mutagenesis*, **5**, 411–415.

MILLER, B. M., ZITZELSBERGER, H. F., WEIER, H.-U. G. and ADLER, I.-D., 1991, Classification of micronuclei in murine erythrocytes: immunofluorescent staining using CREST-antibodies compared to *in situ* hybridization with biotinylated gamma satellite DNA. *Mutagenesis*, **6**, 297–302.

MILLER, B. M., WERNER, T, WEIER, H.-U. and NÜSSE, M., 1992, Analysis of radiation-induced micronuclei by fluorescence *in situ* hybridization using telomeric and centromeric DNA probes. *Radiation Research*, **130**, 177–185.

NÜSSE, M., 1982, Synchronization of mammalian cells by selection and additional chemical block studied by DNA distribution analysis and BrdUrd-Hoechst 33258-technique. *Cell and Tissue Kinetics*, **15**, 529–543.

NÜSSE, M. and KRAMER, J., 1984, Flow cytometric analysis of micronuclei found in cells after irradiation. *Cytometry*, **5**, 20–25.

NÜSSE, M., KRÄMER, M., VIAGGI, S., BARTSCH, A. and BONATTI, S., 1987, Anti-kinetochore antibodies and flow karyo-

typing: new techniques to detect aneuploidy in mammalian cells induced by ionizing radiation and chemicals. *Molecular Toxicology*, **1**, 393–405.

NÜSSE, M., VIAGGI, S. and BONATTI, S., 1989, Induction of kinetochore positive and negative micronuclei in V79 cells by the alkylating agent diethylsulphate. *Mutagenesis*, **4**, 174–178.

NÜSSE, M., BEISKER, W., HOFFMANN, C. and TARNOK, A., 1990, Flow cytometric analysis of G1- and G2/M-phase subpopulations in mammalian cell nuclei using side scatter and DNA content measurements. *Cytometry*, **11**, 813–821.

NÜSSE, M., RECKNAGEL, S. and BEISKER, W., 1992, Micronuclei induced by 2-chlorobenzylidene malonitrile contain single chromosomes as demonstrated by the combined use of flow cytometry and immunofluorescent staining with anti-kinetochore antibodies. *Mutagenesis*, **7**, 57-67.

PINCU, M., CALLISEN, H. and NORMAN, A., 1985, DNA content of micronuclei in human lymphocytes. *International Journal of Radiation Biology*, **74**, 423-432.

RAY, F. A., BARTHOLDI, M. F., KRAEMER, P. M. and CRAM, S. L., 1986, Spontaneous *in vitro* neoplastic evolution: recurrent chromosome changes of newly immortalized Chinese hamster cells. *Cancer Genetics and Cytogenetics*, **21**, 35–51.

SALASSIDIS, K., HUBER, R., ZITZELSBERGER, H. and BAUCHINGER, M., 1992, Centromere detection in vinblastine- and radiation-induced micronuclei of cytokinesis-blocked mouse cells using *in situ* hybridization with a mouse gamma (major) satellite DNA probe. *Environmental Molecular Mutagenesis*, **19**, 1–6.

SAVAGE, J. R., 1988, A comment on the quantitative relationship between micronuclei and chromosome aberrations. *Mutation Research*, **207**, 210–217.

SAVAGE, J. R., 1989, Acentric chromosomal fragments and micronuclei: the time-displacement factor. *Mutation Research*, **225**, 171–173.

SCHREIBER, G. A., BEISKER, W., BAUCHINGER, M. and NÜSSE, M., 1992, Multiparametric flow cytometric analysis of radiation-induced micronuclei in mammalian cell cultures. *Cytometry*, **13**, 90–102.

SUZUKI, K., SUZUKI, F., WATANABE, M. and NIKAIDO, O., 1989, Multistep nature of X-ray-induced neoplastic transformation in golden hamster embryo cells: expression of transformed phenotypes and stepwise changes in karyotypes. *Cancer Research*, **49**, 2134–2140.

THOMSON, E. P. and PERRY, P. E., 1988, The identification of micronucleated chromosomes: a possible assay for aneuploidy. *Mutagenesis*, **3**, 415–418.

WAKATA, A. and SASAKI, M. S., 1987, Measurement of micronuclei by cytokinesis-block method in cultured Chinese hamster cells: comparison with types and rates of chromosome aberrations. *Mutation Research*, **190**, 51–57.

VALADAUD-BARRIEU, D., 1983, Un 'test d'induction de micronoyau' sur Allium sativum; différentiation de substances clastogènes et mitoclasiques. *Mutation Research*, **119**, 55–58.

VANDERKERKEN, K., VANPARYS, P., VERSCHAEVE, L. and KIRSCH-VOLDERS, M., 1989, The mouse bone marrow micronucleus assay can be used to distinguish aneugens from clastogens. *Mutagenesis*, **4**, 6–11.

VIG, B. K. and SWEARNGIN, S. E., 1986, Sequence of centromere separation: kinetochore formation in induced laggards and micronuclei. *Mutagenesis*, **1**, 461–465.

YAMAMOTO, K. I. and KIKUCHI, Y., 1980, A comparison of diameter of micronuclei induced by clastogens and by spindle poisons. *Mutation Research*, **71**, 127–131.

METHODIK UND ANWENDUNG DER DURCHFLUSSZYTOMETRISCHEN CHROMOSOMENANALYSE

Dr.F.Otto

Fachklinik Hornheide
Experimentelle Tumorforschung
Münster

Friedrich J.Otto
Fachklinik Hornheide, Experimentelle Tumorforschung
W-4400 Münster-Handorf

CHROMOSOMEN

- Präparation Färbung Messung -

1. Einführung

Schon bald nach der Etablierung der Durchflußzytometrie als Meßverfahren für den zellulären DNA-Gehalt wurden Versuche unternommen, diese Methode auch für die Chromosomenanalyse einzusetzen. Es zeigte sich, daß die neue Technik ausreichend empfindlich und genau ist, die im Vergleich zu ganzen Zellkernen geringe DNA-Menge der Chromosomen zu erfassen und die oft kleinen Unterschiede zwischen den Chromosomentypen aufzulösen. Durch vielfache Verbesserungen der Präparation, Färbung und Meßtechnik ist inzwischen ein hoher Standard an Genauigkeit und Reproduzierbarkeit erreicht worden. Die durchflußzytometrische Chromosomenanalyse stellt jetzt ein Verfahren dar, das ohne besondere Fertigkeiten und spezielle Ausrüstungen durchgeführt werden kann.

Das vorliegende Protokoll beschreibt eine Präparationsmethode für die Einparametermessung, bei der 4',6-Diamidino-2-phenylindol (DAPI) als Fluoreszenzfarbstoff benutzt wird. DAPI hat nach seiner Einführung in die Durchflußzytometrie (Göhde et al., 1978) als spezifischer, intensiv fluoreszierender DNA-Farbstoff weite Verbreitung gefunden. DAPI eignet sich auch für präzise Messungen der chromosomalen DNA (Otto and Tsou,1985; Otto, 1988) und liefert Einparameterhistogramme von hoher Auflösung und Aussagefähikeit.

Dem Protokoll ist eine Übersicht über die bei durchflußzytometrischen Chromosomenanalysen am häufigsten benutzten Reagenzien und Methoden mit einem Verzeichnis ausgewählter Publikationen beigefügt.

2. Reagenzien und Methoden:

2.1 Reagenzien:

Colcemid-Lösung: 100 ml entionisiertes Wasser
1 mg Demecolcin (SERVA 18238)
sterilfiltrieren, dunkel und kühl aufbewahren

Hypotone Lösung: 100 ml Tris-HCl-Puffer 10 mmol/l, pH 7,5
220 mg KCl
100 mg $MgCl_2 \cdot 6H_2O$
46 mg Dithioerythritol (DTE) (SERVA 20697)

Triton X-100 10 %: 9,0 ml entionisiertes Wasser
1,0 ml Triton X-100
kühl aufbewahren, wöchentlich frisch bereiten

Stammlösung DAPI: 10 ml entionisiertes Wasser
3,5 mg 4',6-Diamidino-2-phenylindol (Partec 7202)
dunkel und kühl aufbewahren

Hypertone Lösung: 100 ml entionisiertes Wasser
2,0 g NaCl
1,2 g tri-Natriumcitrat$\cdot 2H_2O$
0,5 ml Stammlösung DAPI

2.2 Präparation und Färbung:

- Exponentiell wachsende Monolayer-Kulturen in Plastik-Flaschen (250 ml) mit 10 ml Wachstumsmedium
- 0,25-0,50 ml Colcemid-Lösung zugeben und 2-6 Stunden bei 37 °C inkubieren
- Metaphasezellen durch Schütteln ablösen (im Mikroskop prüfen)
- Suspension der Metaphasezellen in Zentrifugenröhrchen übertragen und 45 Minuten auf Eis halten
- 10 Minuten bei 150·g zentrifugieren, Überstand entfernen
- Zellpellet in 1 ml hypotoner Lösung resuspendieren und 10 Minuten bei Raumtemperatur inkubieren, leicht schütteln
- 50 μl 10 %ige Lösung von Triton X-100 zugeben und 10 Minuten auf Eis inkubieren, leicht schütteln
- Zellsuspension mehrere Male durch eine Kanüle Nr. 20 spritzen
- 5 μl Stammlösung DAPI zugeben
- Vereinzelung und Morphologie der Chromosomen im Fluoreszenzmikroskop überprüfen
- 1 ml hypertone Lösung zugeben
- vor der Messung einige Stunden bis über Nacht bei Raumtemperatur inkubieren

2.3 Durchflußzytometrie:

Für die Messung der DAPI-gefärbten Chromosomen mit dem Durchflußzytometer PAS II werden folgende Filter (Abb. 1) verwendet:

KG 1 + BG 38	als Hitzeschutzfilter
UG 1	als Anregungsfilter
TK 420	als erster dichroitischer Spiegel
TK 560	als zweiter dichroitischer Spiegel
GG 435	als Sperrfilter.

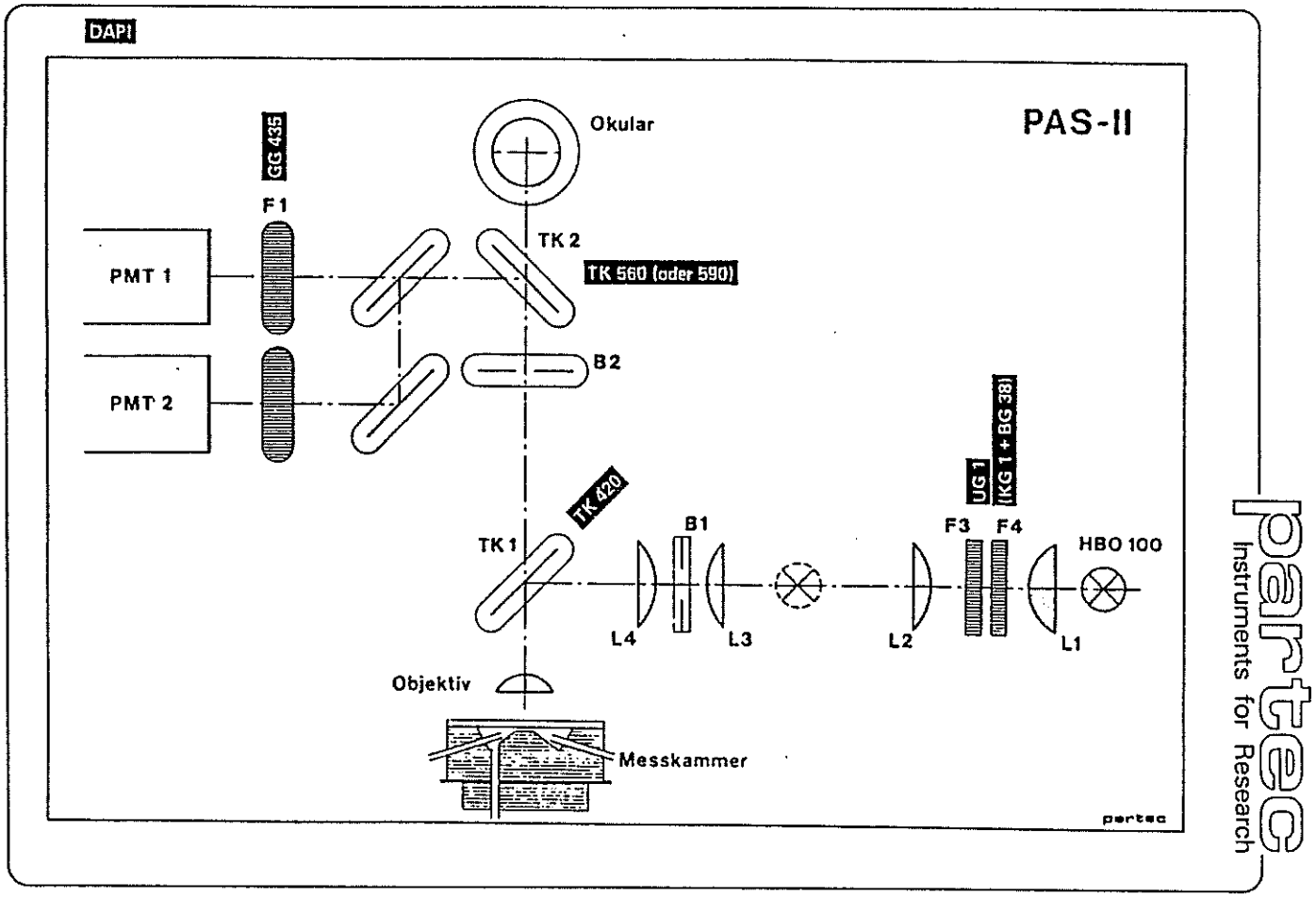

Abb. 1: Empfohlene Filterkombination für die Messung DAPI-gefärbter Chromosomen

3. Ergebnisse

Die durchflußzytometrischen Messungen der DAPI-gefärbten Chromosomen ergeben Histogrammme von hoher Auflösung, so daß bei Zellklonen des Chinesischen Hamsters beispielsweise alle Chromosomentypen dargestellt werden (Abb. 2).
Mit diesem Protokoll lassen sich bei den Peaks der großen Chromosomen Variationskoeffizienten von 1 % oder kleiner erreichen.
Durch Berechnung der Peakflächen lassen sich die relativen Häufigkeiten der Chromosomentypen bestimmen. In Kulturen geklonter Zellen findet man distinkte Häufigkeitsgruppen, die Paare von Chromosomen oder einzelne Homologe repräsentieren (3).
Diese Vorschrift ist bei verschiedenen Zellinien und Zellklonen des Chinesischen Hamsters getestet worden. Bei anderen Zelltypen ist es möglicherweise notwendig, die Colcemidkonzentration, die Inkubationszeit, Konzentration des Detergenz oder die Technik der Chromosomenvereinzelung zu modifizieren.

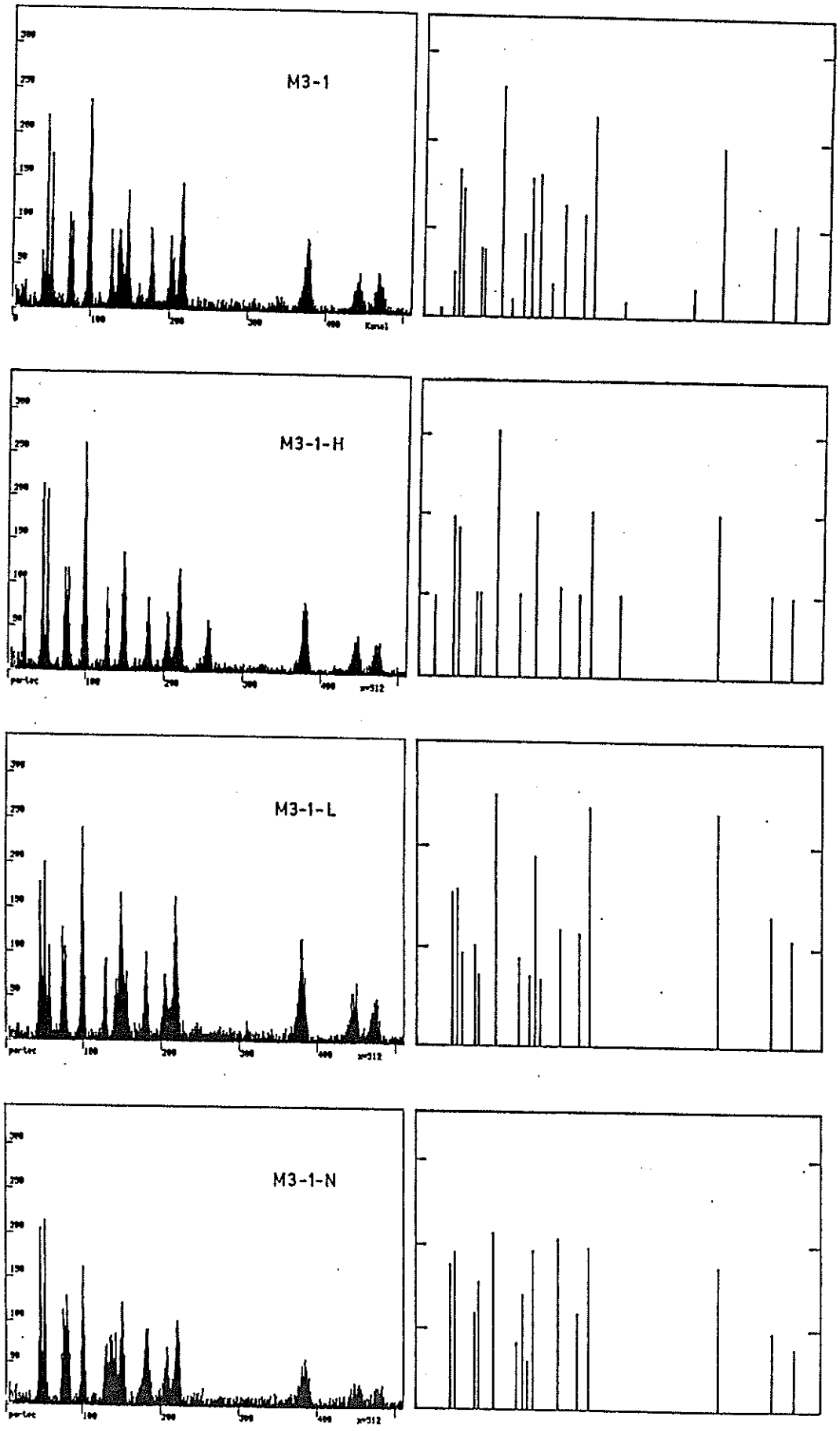

Abb. 2: Durchflußzytometrische Histogramme der Zellinie M3-1 des Chinesischen Hamsters und von 3 Klonen aus dieser Linie

4. Referenzen

Göhde, W., Schumann, J., Zante, J.: The use of DAPI in pulse cytophotometry.
In: Lutz, D. ed.: Pulse Cytophotometry: 229-232, 1978.

Otto, F., Tsou, K.C.: A comparative study of DAPI, DIPI, and Hoechst 33258 and 33342 as chromosomal stains.
Stain Technology 60: 7-11, 1985.

Otto, F.J.: Assessment of persisting chromosome aberrations by flow karyotyping of cloned Chinese hamster cells.
Zeitschrift für Naturforschung 43c: 948-954, 1988.

5. Überblick über Reagenzien und Methoden der Chromosomenpräparation und -färbung für die Durchflußzytometrie (nach Literaturdaten und eigenen Erfahrungen): Mit einem Sternchen sind Reagenzien und Methoden gekennzeichnet, die sich als besonders geeignet erwiesen haben.

Spindelgifte für die Akkumulation der Zellen in der Metaphase:

	Colchicin	MW: 399	0,1 µmol/l
*	Colcemid	MW: 371	0,1-1,6 µmol/l
	Vinblastinsulfat	MW: 911	0,02-0,5 µmol/l
	Vincristinsulfat	MW: 923	

Hypotone Lösungen für das Schwellen der Zellen:

*	KCl	75 mmol/l
*	Tris-HCl-Puffer	5-20 mmol/l
	Natriumcitrat	3,4 mmol/l
	Zellkulturmedium, 1:4 verdünnt	
		mit oder ohne Fluoreszenzfarbstoff

Reagenzien für die Auflösung der Zellmembran:

*	Triton X-100	0,1-1,0 %
	Saponin	0,1-0,25 %
*	Digitonin	0,1 %
	Brij-58	0,2 %
	Citronensäure	2,0 %
	Essigsäure	50 %
	Ethanol	20 %

Methoden der Membranzerstörung und Chromosomenvereinzelung:

- Vortexmischer
- * Spritzen durch enge Kanüle (Nr. 18-20)
- Homogenisieren (verschiedene Homogenisatortypen)
- Zellzerreißbombe
- Ultraschall

Fluoreszenzfarbstoffe für die Färbung der chromosomalen DNA:

*	4',6-Diamidino-2-phenylindol (DAPI)	MW: 350	5-100 µmol/l
	4',6-Bis(2'-imidazolinyl-4H,5H)-2-phenylindol (DIPI)	MW: 403	5 µmol/l
*	Bisbenzimid (Hoechst 33258)	MW: 588	3,4-9,0 µmol/l
	Bisbenzimid (Hoechst 33342)	MW: 616	5-10 µmol/l
	Chromomycin A3 (CA3)	MW: 1183	3-70 µmol/l
	Mithramycin (M)	MW: 1085	11-25 µmol/l
*	Ethidiumbromid (EB)	MW: 394	6-250 µmol/l
*	Propidiumjodid (PI)	MW: 668	15-75 µmol/l
	Kombination EB + M		25 + 25 µmol/l

Für Zweiparameter-Messungen:

*	Hoechst 33258 + Chromomycin A3	1,3-7 µmol/l + 3-20 µmol/l
	DAPI + Chromomycin A3	1,6 µmol/l +20 µmol/l

Ausgewählte Literatur:

Arkesteijn, G.J.A., Martens, A.C.M., Jonker, R.R., Hagemeijer, A., Hagenbeek, A.: Bivariate flow karyotyping of acute myelocytic leukemia in the BNML rat model. Cytometry 8: 618-624, 1987.

Arkesteijn, G.J.A., Dekken, H. van, Martens, A.C.M., Hagenbeek, A.: Clinical application of flow karyotyping in myelocytic leukemia by stimulation of different subpopulations of cells in blood or bone marrow samples. Cytometry 11: 196-201, 1990.

Aten, J.A., Buys, C.H.C.M., Veen, A.Y. van der, Mesa, J.R., Yu, L.C., Gray, J.W., Osinga, J. Stap, J.: Stabilization of chromosomes by DNA intercalators for flow karyotyping and identification by banding of isolated chromosomes. Histochemistry 87: 359-366, 1987.

Bartholdi, M.F., Sinclair, D.C., Cram, L.S.: Chromosome analysis by high illumination flow cytometry. Cytometry 3: 395-401, 1983.

Bartholdi, M.F., Ray, F.A., Cram, L.S., Kraemer, P.M.: Flow karyology of serially cultured Chinese hamster cell lineages. Cytometry 5: 534-538, 1984.

Bartholdi, M.F.: DNA content and base composition of of human chromosomes. Journal of Colloid and Interface Science 105: 426-434, 1985.

Bartholdi, M.F., Ray, F.A., Cram, L.S., Kraemer, P.M.: Karyotype instability of Chinese hamster cells during in vivo tumor progression. Somatic Cell and Molecular Genetics 13: 1-10, 1987.

Bartholdi, M.F., Meyne, J., Johnston, R.G., Cram, L.S.: Chromosome banding analysis by slit-scan flow cytometry. Cytometry 10: 124-133, 1989.

Bartholdi, M.F.: Flow cytogenetics. Pathobiology 58: 118-128, 1990.

Bartholdi, M.F., Parson, J.D., Albright, K.A., Cram, L.S.: System for flow sorting chromosomes on the basis of pulse shape. Cytometry 11: 165-172, 1990.

Bernheim, A., Miglierina, R.: Flow cytogenetics. Biology of the Cell 58: 179-182, 1986.

Bijman, J.Th.: Optimization of mammalian chromosome suspension preparation employed in a flow cytometric analysis. Cytometry 3: 354-358, 1983.

Boschmann, G.A., Manders, E.M.M., Rens, W., Slater, R., Aten, J.A.: Semi-automated detection of aberrant chromosomes in bivariate flow karyotypes. Cytometry 13: 469-477, 1992.

Buys, C.H.C.M., Aten, J.A., Koerts, T., Osinga, J., Veen, A.Y. van der: Isolated metaphase chromosomes stabilized by DNA-intercalation or polyamine addition: a comparison. Cell Biology International Reports 8: 273, 1984.

Carrano, A.V., Gray, J.W., Moore, D.H., Minkler, J.L., Mayall, B.H., VanDilla, M.A., Mendelsohn, M.L.: Purification of the chromosomes of the Indian muntjac by flow sorting. Journal of Histochemistry and Cytochemistry 24: 348-354, 1976.

Carrano, A.V., Gray, J.W., Langlois, R.G., Burkhart-Schultz, K.J., VanDilla, M.A.: Measurement and purification of human chromosomes by flow cytometry and sorting. Proceedings of the National Academy of Sciences USA 76: 1382-1384, 1979.

Carter, N.P., Ferguson-Smith, M.E., Affara, N.A., Briggs, H., Ferguson-Smith, M.A.: Study of X chromosome abnormality in XX males using bivariate flow karyotype analysis and flow sorted dot blots. Cytometry 11: 202-207, 1990.

Collard, J.G., Philippus, E., Tulp, A., Lebo, R.V., Gray, J.W.: Separation and analysis of human chromosomes by combined velocity sedimentation and flow sorting applying single- and dual-laser flow cytometry. Cytometry 5: 9-19, 1984.

Conia, J., Bergounioux, C., Perennes, C., Muller, P., Brown, S., Gadal, P.: Flow cytometric analysis and sorting of plant chromosomes from Petunia hybrida protoplasts. Cytometry 8: 500-508, 1987.

Cram, L.S., Bartholdi, M.F., Ray, F.A., Meyne, J., Moyzis, R.K., Schwarzacher-Robinson, T., Kraemer, P.M.: Overview of flow cytogenetics for clinical applications. Cytometry Supplement 3: 94-100, 1988.

Dean, P.N., Kolla, S., VanDilla, M.A.: Analysis of bivariate flow karyotypes. Cytometry 10: 109-123, 1989.

Dietzel, A.H., Hain, J., Virsik-Peuckert, R.P., Harder, D.: Algorithms for the evaluation of radiation induced chromosome aberration yields per cell from flow karyotypes. Cytometry 11: 708-715, 1990.

Engh, G. van den, Trask, B., Cram, S., Bartholdi, M.: Preparation of chromosome suspensions for flow cytometry. Cytometry 5: 108-117, 1984

Engh, G.J. van den, Trask, B.J., Gray, J.W.: The binding kinetics and interaction of DNA fluorochromes used in the analysis of nuclei and chromosomes by flow cytometry. Histochemistry 84: 501-508, 1986.

Engh, G. van den, Trask, B., Lansdorp, P., Gray, J.W.: Improved resolution of flow cytometric measurements of Hoechst- and chromomycin-A3-stained human chromosomes after addition of citrate and sulfite. Cytometry 9: 266-270, 1988.

Engh, G. van den, Hanson, D., Trask, B.: A computer program for analyzing bivariate flow karyotypes. Cytometry 11: 173-183, 1990.

Fantes, J.A., Green, D.K., Elder, J.K., Malloy, P., Evans, H.J.: Detecting radiation damage to human chromosomes by flow cytometry. Mutation Research 119: 161-168, 1983.

Fantes, J.A., Green, D.K., Malloy, P., Sumner, A.T.: Flow cytometry measurements of human chromosome kinetochore labeling. Cytometry 10: 134-142, 1989.

Gray, J.W., Carrano, A.V., Moore, D.H., Steinmetz, L.L., Minkler, J., Mayall, B.H., Mendelsohn, M.L., VanDilla, M.A.: High-speed quantitative karyotyping by flow microfluorometry. Clinical Chemistry 21: 1258-1262, 1975.

Gray, J.W., Carrano, A.V., Steinmetz, L.L., VanDilla, M.A., Moore, D.H., Mayall, B.H., Mendelsohn, M.L.: Chromosome measurement and sorting by flow systems. Proceedings of the National Academy of Sciences USA 72: 1231-1234, 1975.

Gray, J.W., Langlois, R,G.: Chromosome classification and purification using flow cytometry and sorting. Annual Review of Biophysics and Biophysical Chemistry 15: 195-235, 1986.

Gray, J.W., Dean, P.N., Fuscoe, J.C., Peters, D.C., Trask, B.J., Engh, G.J. van den, VanDilla, M.A.: High-speed chromosome sorting. Science 238: 323-329, 1987.

Gray, J.W., Trask, B., Engh, G. van den, Silva, A., Lozes, C., Grell, S., Schonberg, S., Yu, L.-C., Golbus, M.S.: Application of flow karyotyping in prenatal detection of chromosome aberrations. American Journal of Human Genetics 42: 49-59, 1988.

Harris, P., Boyd, E., Ferguson-Smith, M.A.: Optimizing human chromosome separation for the production of chromosome-specific DNA libraries by flow sorting. Human Genetics 70: 59-65, 1985.

Harris, P., Boyd, E., Young, B.D., Ferguson-Smith, M.A.: Determination of the DNA content of human chromosomes by flow cytometry. Cytogenetics and Cell Genetics 41: 14-21, 1986.

Harris, P., Cooke, A., Boyd, E., Young, B.D., Ferguson-Smith, M.A.: The potential of family flow karyotyping for the detection of chromosome abnormalities. Human Genetics 76: 129-133, 1987.

Hutter, K.-J., Stoehr, M.: Detection and separation of the submetacentric marker chromosome of the WALKER (W-256) carcinoma using flow cytometry and sorting. Histochemistry 82: 469-475, 1985.

Jensen, R.H., Langlois, R.G., Mayall, B.H.: Strategies for choosing a deoxyribonucleic acid stain for flow cytometry of mataphase chromosomes. Journal of Histochemistry and Cytochemistry 25: 954-964, 1977.

Kooi, M.W., Aten, J.A., Stap, J., Kipp, J.B.A., Barendsen, G.W.: Preparation of chromosome suspensions from cells of a solid experimental tumour for measurement by flow cytometry. Cytometry 5: 547-549, 1984.

Langlois, R.G., Yu, L.-C., Gray, J.W., Carrano, A.V.: Quantitative karyotyping of human chromosomes by dual beam flow cytometry. Proceedings of the National Academy of Sciences USA 79: 7876-7880, 1982.

Lebo, R.V., Golbus, M.S., Cheung, M.-C.: Detecting abnormal human chromosome constitutions by dual laser flow cytogenetics. American Journal of Medical Genetics 25: 519-529, 1986.

Matsson, P., Rydberg, B.: Analysis of chromosomes from human peripheral lymphocytes by flow cytometry. Cytometry 1: 369-372, 1981.

Meyne, J., Bartholdi, M.F., Travis, G., Cram, L.S.: Counterstaining human chromosomes for flow karyology. Cytometry 5: 580-583, 1984.

Nüsse, M., Krämer, M.: Antikinetochore antibodies and flow karyotyping: new techniques to detect aneuploidy in mammalian cells induced by ionizing radiation and chemicals. Molecular Toxicology 1: 393-405, 1987.

Otto, F.J, Oldiges, H.: Requirements and procedures for chromosomal DNA measurement for rapid karyotype analysis in mammalian cells. Pulse Cytophotometry Vol. III: 393-400, 1978.

Otto, F.J., Oldiges, H., Göhde, W., Barlogie, B., Schumann, J.: Flow cytogenetics of uncloned and cloned Chinese hamster cells. Cytogenetics and Cell Genetics 27: 52-56, 1980.

Otto, F.J., Oldiges, H.: Flow cytogenetic studies in chromosomes and whole cells for the detection of clastogenic effects. Cytometry 1: 13-17, 1980.

Otto, F., Oldiges, H., Göhde, W., Dertinger, H.: Flow cytometric analysis of mutagen induced chromosomal damage. Acta Pathologica et Microbiologica Scandinavica, Section A, Supplement 274: 284-286, 1981.

Otto, F., Tsou, K.C.: A comparative study of DAPI, DIPI, and Hoechst 33258 and 33342 as chromosomal DNA stains. Stain Technology 60: 7-11, 1985.

Otto, F.J.: Assessment of persisting chromosome aberrations by flow karyotyping of cloned Chinese hamster cells. Zeitschrift für Naturforschung 43c: 948-954, 1988.

Schmitz, A., Chaput, B., Fouchet, P., Guilly, M.N., Frelat, G., Vaiman, M.: Swine chromosomal DNA quantification by bivariate flow karyotyping and karyotype interpretation. Cytometry 13: 703-710, 1992.

Severin, E., Ohnemus, B.: Flow cytometric analysis of chromosomes and cells using a modified BrdU-Hoechst method. Histochemistry 76: 113-121, 1982.

Sillar, R., Young, B.D.: A new method for the preparation of metaphase chromosomes for flow analysis. Journal of Histochemistry and Cytochemistry 29: 74-78, 1981.

Stöhr, M., Hutter, K.-J., Frank, M., Futterman, G., Goerttler, K.: A flow cytometric study of chromosomes from rat kangaroo and Chinese hamster cells. Histochemistry 67: 179-190, 1980.

Stoehr, M., Hutter, K.-J., Frank, M., Goerttler, K.: A reliable preparation of mono-dispersed chromosome suspensions for flow cytometry Histochemistry 74: 57-61, 1982.

Stubblefield, E., Cram, S., Deaven, L.: Flow microfluorometric analysis of isolated Chinese hamster chromosomes. Experimental Cell Research 94: 464-468, 1975.

Trask, B., Engh, G. van den, Nussbaum, R., Schwartz, C., Gray, J.: Quantification of the DNA content of structurally abnormal X chromosomes and X chromosome aneuploidy using high resolution bivariate flow karyotyping. Cytometry 11: 184-195, 1990.

Young, B.D., Ferguson-Smith, M.A., Sillar, R., Boyd, E.: High resolution analysis of human peripheral lymphocytic chromosomes by flow cytometry. Proceedings of the National Academy of Sciences USA 78: 7727-7731, 1981.

Yu, L.-C., Aten, J., Gray, J., Carrano, A.V.: Human chromosome isolation from short-term lymphocyte culture for flow cytometry. Nature 293: 254-155, 1981.

Assessment of Persisting Chromosome Aberrations by Flow Karyotyping of Cloned Chinese Hamster Cells

Friedrich J. Otto

Abteilung für experimentelle Tumorforschung Fachklinik Hornheide, Dorbaumstraße 300, D-4400 Münster, Bundesrepublik Deutschland

Z. Naturforsch. 43c, 948–954 (1988); received May 2/July 18, 1988

Chinese Hamster Cells, Chromosomal Aberrations, Karyotyping, Flow Cytometry, Cytogenetics

A preparation, staining and measuring protocol for high resolution flow cytometry of chromosomes was developed. This method allows us to identify all chromosome types and is suited for characterization of permanent cell lines and cell clones by establishing their flow karyotypes. In cell clones this procedure can be used for the detection of chromosomal aberrations which appear spontaneously or are induced by mutagen treatment and persist in the cell population.

Introduction

In 1980 we studied the flow karyotypes of uncloned and cloned Chinese hamster cell cultures [1]. Though the resolution of the chromosome histograms was unsatisfactory at that time, it became evident, that the quality of the histograms obtained for cloned cell lines surpassed that for uncloned cells. Thus, we recommended the use of cell clones for flow cytometric investigations in experimental genetics and mutagenicity testing. Using advanced preparation and measuring techniques, these conclusions were now confirmed. Suitable clones yield an excellent resolution which allows the identification of all chromosome types and opens a way for the detection of persisting aberrations. In earlier approaches to utilize flow cytometric chromosome histograms for mutagenicity studies, the authors analyzed the first mitoses after treatment and used the broadening of the peaks and/or the increasing background for the quantitation of the mutagenic effect [2–7]. These approaches remained unsatisfactory, because the sensitivity was low and the specificity was impaired by cytotoxic effects.

Materials and Methods

The Chinese hamster cell line M3-1 and clones derived from this line were used for the methodological development and mutagenicity experiments. The cells were grown as monolayer cultures in Eagle's minimum essential medium supplemented with 5% fetal calf serum and gentamycin.

For the preparation of chromosomes, exponentially growing cultures were treated with 0.7 µmol of colcemid/l for 5 h. Metaphase cells were harvested by shaking, kept on ice for 45 min, pelleted by centrifugation for 10 min at $100 \times g$, and resuspended in a hypotonic solution consisting of tris-HCl buffer (10 mmol/l, pH 7.4), KCl (30 mmol/l), MgCl (5 mmol/l), and dithioerythritol (DTE; 3 mmol/l). The cells were incubated for 10 min at room temperature. Triton X-100 was then added to a final concentration of 0.5%. The cell membranes were disrupted and the chromosomes dispersed by syringing through a 27 gauge cannula. The chromosomes were stained by adding the same volume of hypertonic solution consisting of NaCl (350 mmol/l), Na citrate (40 mmol/l) and containing 4′,6-diamidino-2-phenylindole (DAPI; 5 µmol/l) which was introduced to flow cytometry by Göhde *et al.* [8]. Measurements were performed using a PAS II flow cytometer (Partec AG, Arlesheim, Switzerland) equipped with a UG 1 excitation filter, a TK 420 dichroic mirror and a GG 435 barrier filter.

For quantitative evaluation of the histograms, a computer program (Partec AG) was used to calculate the median of each peak (= mean relative DNA content of the chromosome), the integral (relative frequency of the chromosome) and the coefficient of variation (CV) of each peak.

Results and Discussion

1. Flow karyotyping of Chinese hamster cell lines and cell clones

The flow karyotypes of established Chinese hamster cell lines exhibit considerable differences [1].

Reprint requests to Dr. Friedrich J. Otto.

Verlag der Zeitschrift für Naturforschung, D-7400 Tübingen
0341–0382/88/1100–0948 $ 01.30/0

The 3 examples shown in Fig. 1 demonstrate the variability in the region of the small chromosomes and the tendency towards polymorphism of chromosome 1. The two homologues of chromosome 1 differ in DNA content by more than 5% in line M3-1 and by 2% in line V79. In B14F28 cells there is also a small difference as can be seen from the width of the peak. Chromosome 2 proved to be very stable. The established cell lines contain mixtures of different karyotypes and therefore produce complex chromosomal histograms, particularly in the region of the small chromosomes.

Clones originate from single karyotypes and therefore exhibit relatively simple chromosome histograms. Fig. 2 shows the histograms of the parental cell line M3-1 and of 3 clones selected from a series of clones obtained by a subcloning experiment.

The histograms of the clones allow us to identify all chromosome types. Particularly, clone H exhibits a karyotype favorable for flow cytometry with 22 chromosomes represented in the form of 15 well separated peaks. The chromosome number can be determined easily from the histogram on the basis of clear-cut groups of frequencies: There is one peak representing 3 chromosomes, five peaks containing pairs of chromosomes with homologues exhibiting the same DNA content, and nine peaks containing single chromosomes depicting homologues with different DNA content.

This homogeneity of the karyotype remains for some time before new chromosomal changes develop in the cell population. During this period the cell clone can be used to study spontaneous and induced chromosome mutations.

2. *Detection of persisting chromosome aberrations*

In order to check the stability of the flow karyotype and prove the feasibility of a new mutagenicity assay based on the detection of persisting chromosomal aberrations, the following experiment was performed:

One flask of the cell clone M3-1-H was taken as the control. From this flask a series of subcultures were grown, each starting with a very low number of cells (4 cells on average). The subcultures were propagated for at least 22 cell generations. Then chromosomes were prepared for flow cytometry. Evaluation of the histograms (4 examples are given in Fig. 3) showed that 11 out of 12 subcultures exhibited an unchanged flow karyotype, one subculture exhibited a deviation in the region of the smallest chromosomes. The peak of the smallest chromosome was reduced and a new peak had appeared at a position of higher DNA content. It is assumed that these two changes are produced by one chromosomal aberration, probably a translocation. Taking into account that the originating cell number in the 12 subcultures was 48, the spontaneous aberration rate observed in this experiment is about 2%.

Another flask of the same cell clone was treated with the mutagen N-methyl-N′-nitro-N-nitrosoguadinine (MNNG; 10 μmol/l for 24 h). Thereafter subcultures were established, propagated for 22 cell generations, and the chromosomes were prepared for flow cytometry. Evaluation of the histograms (4 examples are given in Fig. 4) showed that 6 out of 9 subcultures exhibited paired or multiple alterations in the flow cytometric pattern. These alterations are considered as induced aberrations. Considering the initial cell numbers of the 9 subcultures in this experiment, the number of events underlying the observed deviations can be estimated to be at least 8 alterations induced in 36 cells, thus corresponding to an aberration rate of about 22%.

From theoretical considerations it becomes obvious that in this type of experiment each chromosome mutation event (*e.g.* deletion or translocation) produces a pair of changes in the histogram, namely a reduction or disappearance of a peak plus an appearance of a new peak (or less frequently an increase of an existing peak). From the position of a new peak the type of aberration can be concluded. The reduction or disappearance of a peak in connection with a new peak at a position of higher DNA content must be assigned to a translocation, in connection with a new peak at a position of lower DNA content to a chromosomal deletion. The results of the present experiments have to be confirmed by microscopical analyses and the morphological characterization of the aberrations remains to be done. However, the first observations already demonstrate that persisting chromosome aberrations may be analyzed by this type of assay.

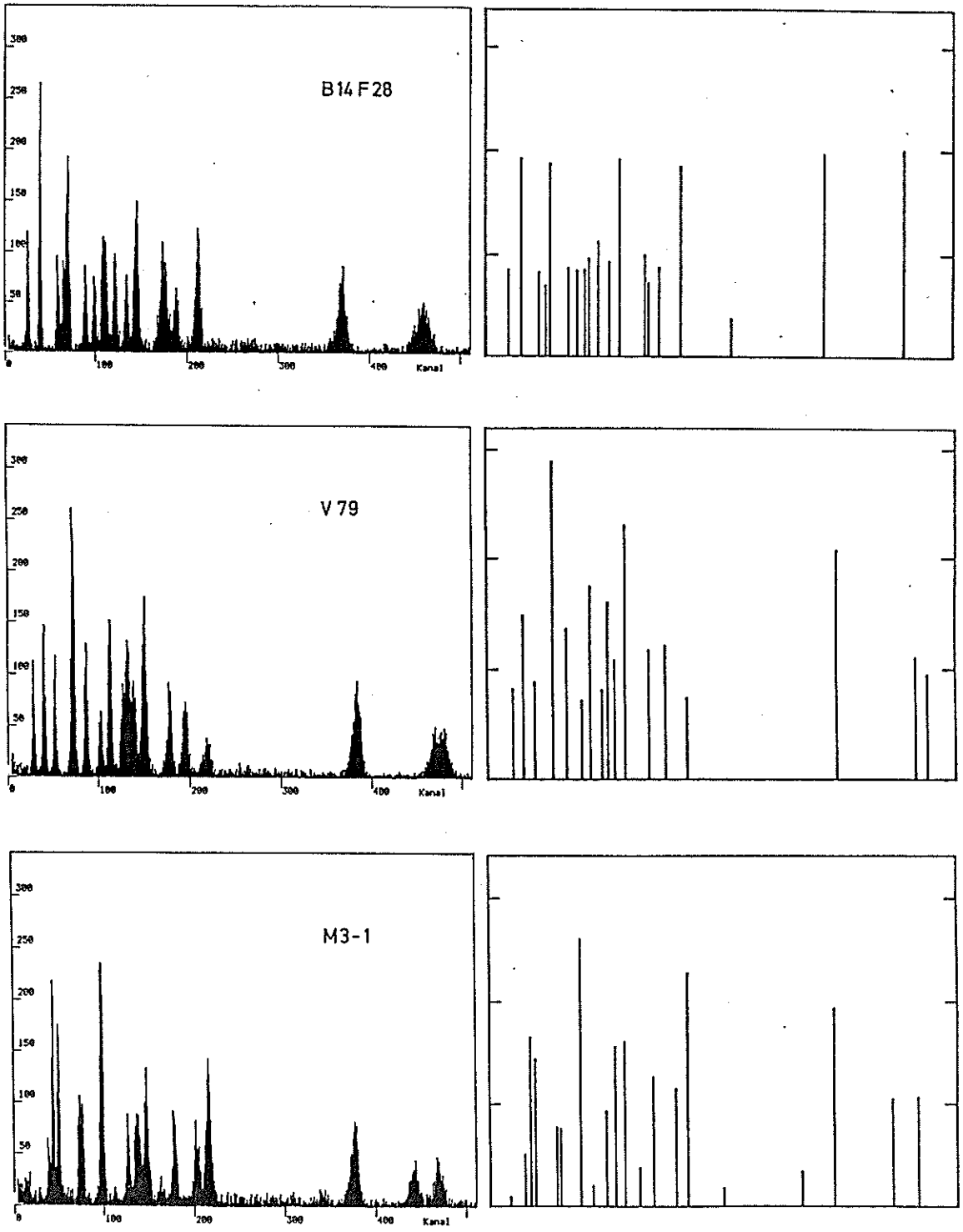

Fig. 1. Flow cytometric chromosome histograms of 3 permanent Chinese hamster cell lines. In the histogram evaluations (right) the position of each line depicts the mean relative DNA content and the height of each line represents the relative frequency of the chromosome type.

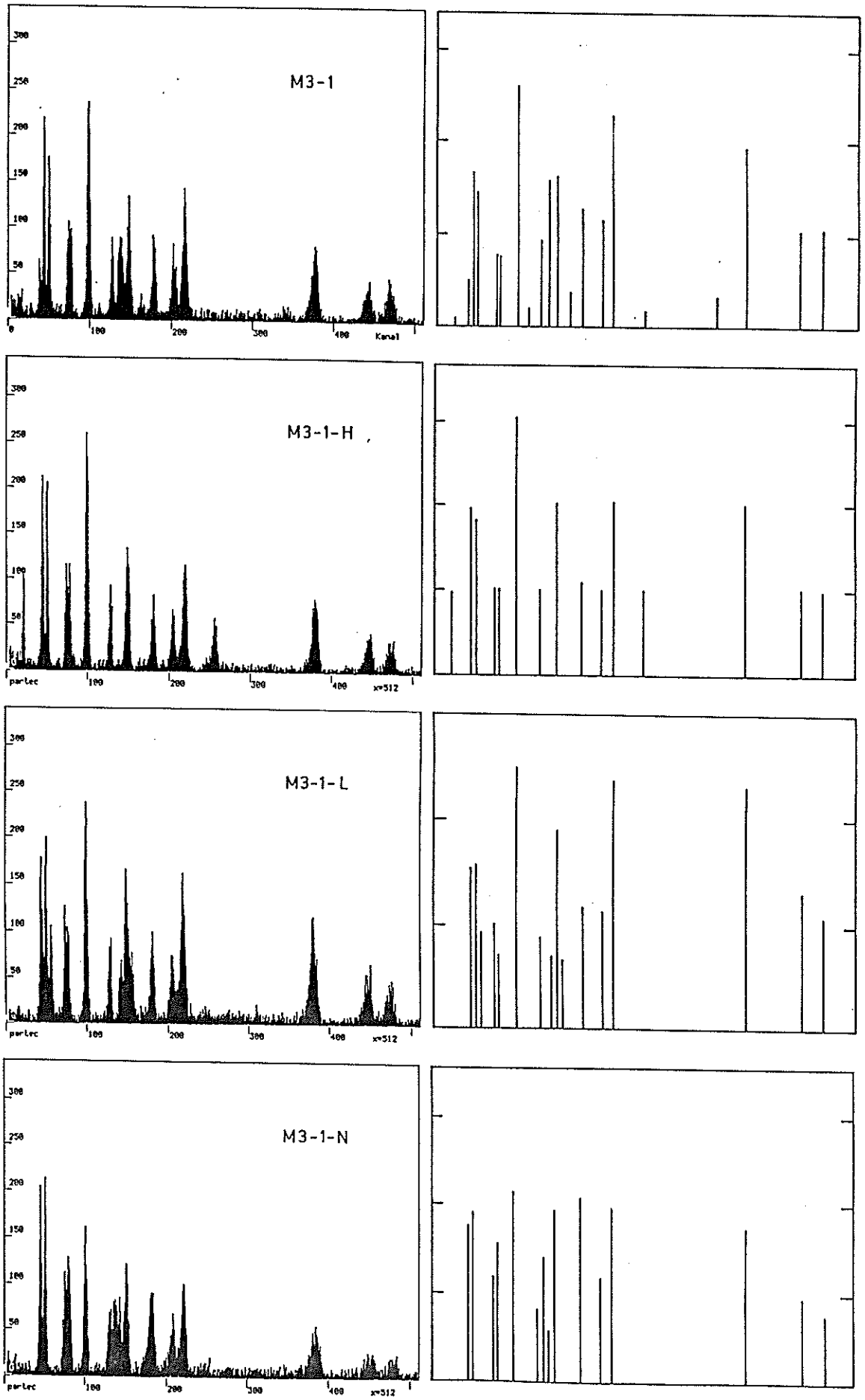

Fig. 2. Flow cytometric chromosome histograms of the parental cell line M3-1 and 3 clones derived from this line.

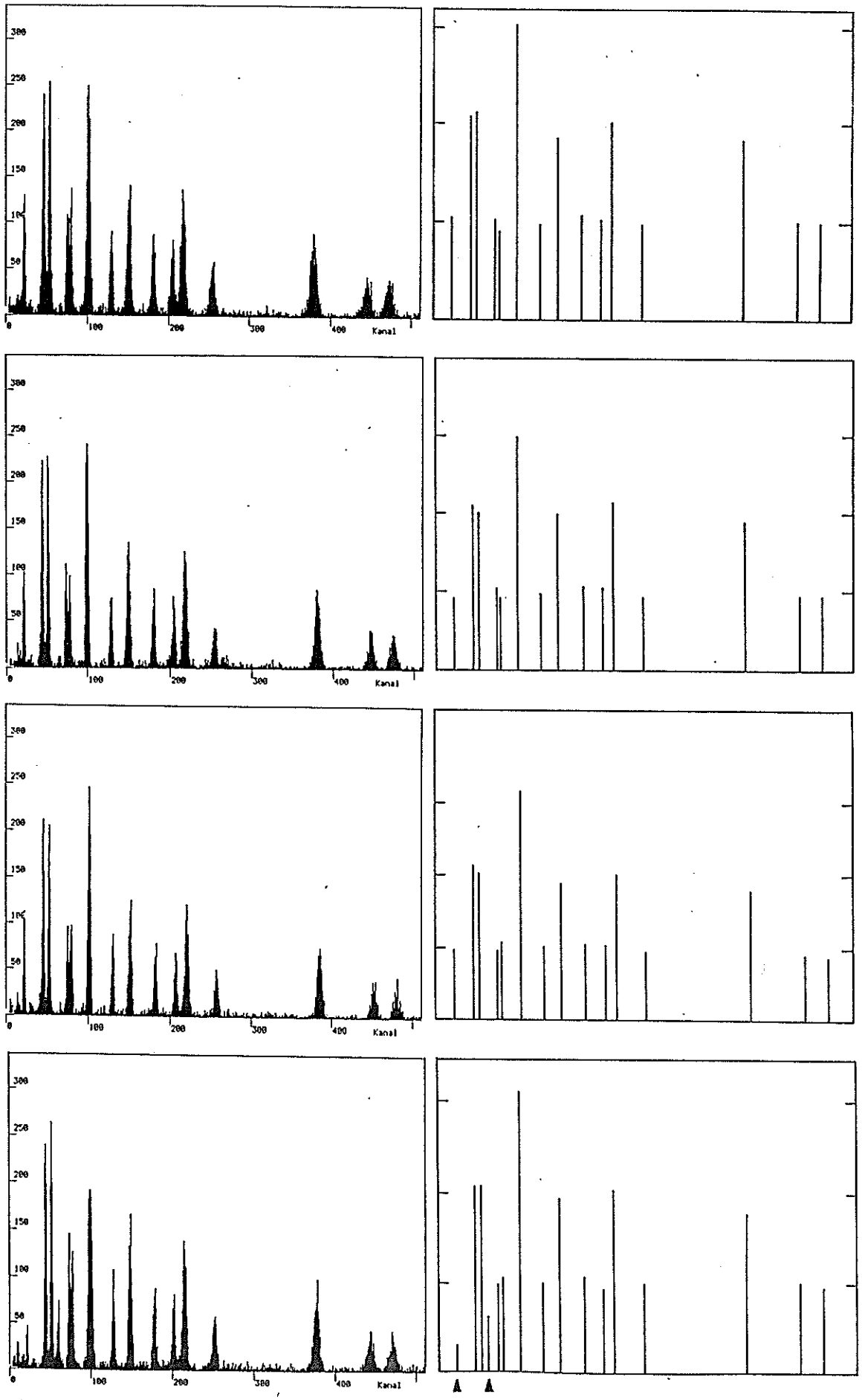

Fig. 3. 4 chromosome histograms out of 12 subcultures grown from a control culture of M3-1 clone H.

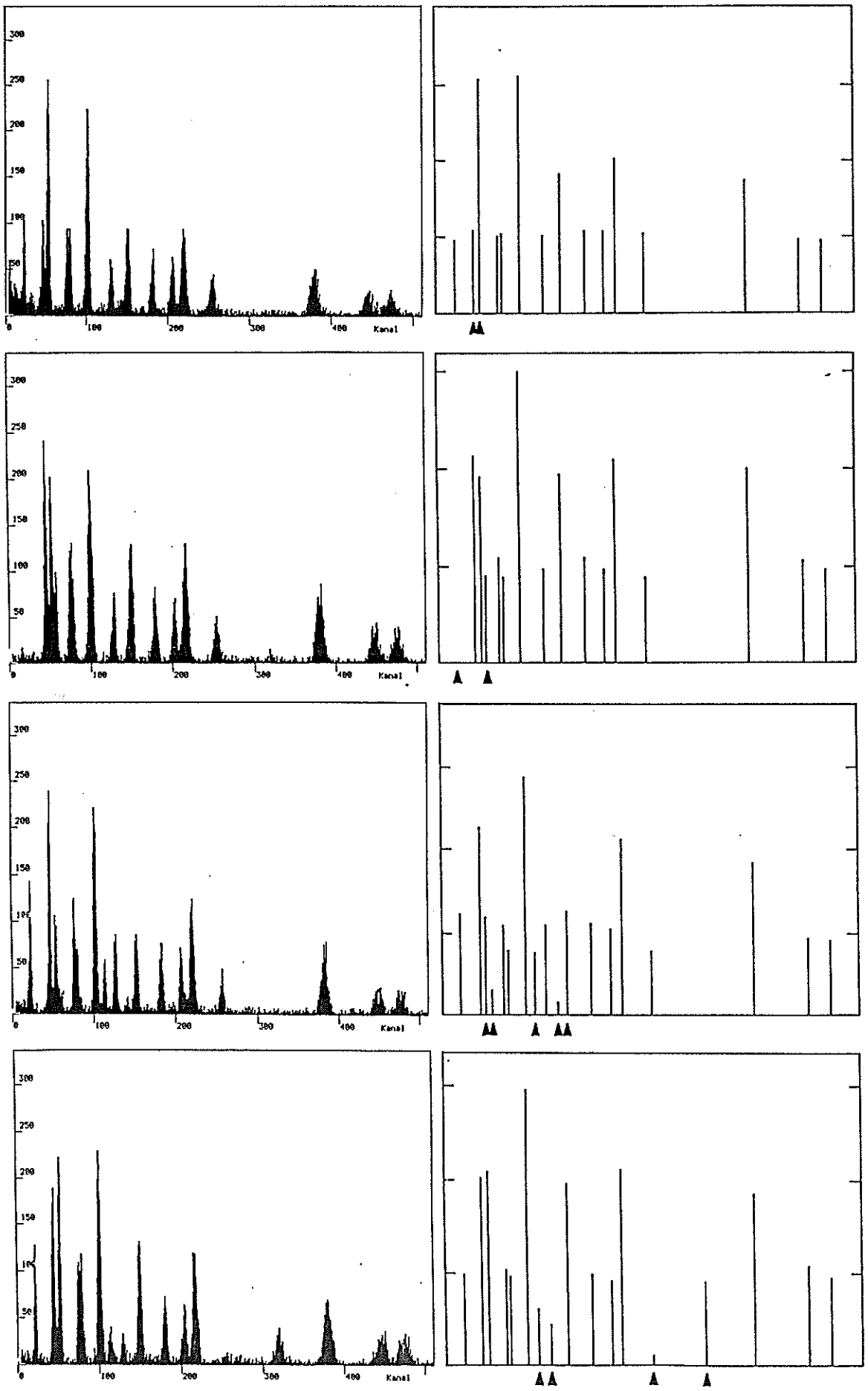

Fig. 4. 4 chromosome histograms out of 9 subcultures grown from a culture of M3-1 clone H treated with MNNG (10 μmol/l).

[1] F. J. Otto, H. Oldiges, W. Göhde, B. Barlogie, and J. Schumann, Cytogenet. Cell Genetics **27**, 52–56 (1980).
[2] F. J. Otto and H. Oldiges, Cytometry **1**, 13–17 (1980).
[3] F. J. Otto, H. Oldiges, W. Göhde, and H. Dertinger, Acta Pathol. Microbiol. Scand. Sect. A, Suppl. **274**, 284–286 (1981).
[4] J. A. Aten, J. B. A. Kipp, and G. W. Barendsen, Acta Pathol. Microbiol. Scand. Sect. A, Suppl. **274**, 287–292 (1981).
[5] J. A. Fantes, D. K. Green, J. K. Elder, P. Malloy, and H. J. Evans, Detecting radiation damage to human chromosomes by flow cytometry. Mutat. Res. **119**, 161–168 (1983).
[6] P. Matsson, G. Anneren, and I. Gustavsson, Hereditas **104**, 49–54 (1986).
[7] V. K. Jain, F. J. Otto, and P. M. Gopinath, in: (K. M. Marimuthu, P. M. Gopinath, eds.), Recent Trends in Medical Genetics, 273–289, Oxford (1986).
[8] W. Göhde, J. Schumann, and J. Zante, The use of DAPI in pulse cytophotometry, in: (D. Lutz, ed.), Pulse Cytophotometry III, 229–232, Ghent (1978).

ZELLPROLIFERATION

Dr.M.Poot

Institut für Humangenetik
der Universität
Würzburg

© 1992 Wiley-Liss, Inc.

Cytometry 13:678–685 (1992)

Cell Cycle Analysis of Asynchronous Cell Populations by Flow Cytometry Using Bromodeoxyuridine Label and Hoechst-Propidium Iodide Stain[1]

Michael G. Ormerod[2] and Manfred Kubbies

The Institute of Cancer Research, The Haddow Laboratories, Cotswold Road, Sutton, SM2 5NG, England (M.G.O.); Department of Cell Biology, Boehringer Mannheim Research Centre, Nonnenwald 2, 8122 Penzberg, Germany (M.K.)

Received for publication October 23, 1991; accepted April 21, 1992

Continuous labelling of cells with deoxybromouridine (BrdUrd) followed by staining with a bis-benzimidazole (Hoechst 33258) and a phenanthridinium (propidium iodide or ethidium bromide) allows the cells to be separated by flow cytometry according to the extent of their DNA replication. This BrdUrd-Hoechst/PI method has been used mainly to observe perturbations of the cell cycle in synchronously growing cells. In this paper we demonstrate that, when the method is applied to asynchronously dividing cells, more extensive information can be derived about the effects of cytotoxic and other treatments on the kinetics of the cell cycle. The interpretation of the data is explained, the effects of different types of cytotoxic agent are described, and the method is compared briefly to other methods for following cell cycle kinetics. © 1992 Wiley-Liss, Inc.

Key terms: Cell cycle kinetics, DNA, counterstaining

Knowledge of the proliferative characteristics of cells is important in many areas of biology and oncology and, over the years, many flow cytometric methods have been developed for the study of cell cycle kinetics. The more powerful of these methods have employed 5-bromodeoxyuridine (BrdUrd), which is incorporated into DNA in place of thymidine. Detection of BrdUrd in the cellular DNA enables the fraction of cells in the S phase of their cycle to be enumerated and, using multiparametric flow cytometry, also gives detailed information about the kinetics of the cell cycle.

There are three approaches to these measurements. Monoclonal antibodies which react specifically with BrdUrd have been used to provide an analysis of the kinetics of cells pulse-labelled with BrdUrd both in vitro (9,12) and in vivo (1,27,42). Counterstaining with propidium iodide (PI) is used to display cell cycle dependent anti-BrdUrd labelling. The second approach makes use of the observation by Latt (26) that the fluorescence of bis-benzimidazoles (Hoechst 33258 and 33342) bound to DNA is quenched by BrdUrd, the degree of quenching depending on the amount of BrdUrd incorporated (2,21). By staining cells with a combination of Hoechst 33258 and an intercalating dye such as PI or ethidium bromide (EB) whose fluorescence is unaffected by BrdUrd, the resolution of the different compartments of the cell cycle in cells continuously labelled with BrdUrd is greatly improved (3,4,13,20,21, 31,32,37). The third technique, which detects BrdUrd in pulse-labelled cells, takes advantage of the decrease of Hoechst and increase of mithramycin fluorescence in the presence of BrdUrd (7). This technique requires more complex data recording due to the subtraction of fluorescence signals in real time.

The continuous BrdUrd labelling technique applying the BrdUrd/Hoechst quenching effect has been used to examine the cell cycle kinetics of quiescent cells which have been stimulated into cycle (6,14,16,19,21,23–25,31,32,36,37). The method can also be applied to asynchronously dividing cells (10,11,13,29,30); this has the advantage that it does not require artificial cell synchronisation with possible interference in the process of cell activation and cell cycle progression. How-

[1]This work was presented as a poster at the XVth Congress of ISAC, Bergen, Norway, August 25–30, 1991. M.G.O. was supported by a programme grant from the Cancer Research Campaign.

[2]Address reprint requests to Dr. M.G. Ormerod, 34 Wray Park Road, Reigate, Surrey, RH2 ODE, England.

ever, to date, this has been used less extensively, possibly due to the more complex nature of the data generated. Despite this apparent drawback, we have found that the Hoechst-BrdUrd/PI method yields a wealth of information which permits one to study the effects of cytotoxic agents on cells in different stages of their cycle within an asynchronous culture.

The purpose of this paper is to demonstrate the use of this method in studying asynchronous cultures. We describe its application to different types of cell, explain how the data can be interpreted, and briefly compare the results with the complementary method using antibodies against BrdUrd.

THE BASIC METHOD

The basic method has been described in detail elsewhere (13,20,21,31,32). Briefly, cells are grown in medium containing between 10 and 100 μM BrdUrd. An equimolar concentration of deoxycytidine may be added. The cells are harvested at the required time intervals and suspended in an ice-cold staining buffer consisting of 100 mM Tris, 154 mM NaCl, 1 mM $CaCl_2$, 0.5 mM $MgCl_2$, 0.1% (v/v) Nonidet-P40, 0.2% (w/v) bovine serum albumen, 1.2 μg/ml Hoechst 33258, pH 7.4. After 15 min on ice, PI, EB, or 7-actinomycin-D (7-AAD) is added from a stock solution to give a final concentration of 2 μg/ml (EB or PI) or 10 μg/ml (7-AAD). The latter dye may be preferred if the measurement of cell kinetic parameters is being combined with the detection of a fluorescein- or phycoerythrin-labelled antibody in a two laser system (37).

Once BrdUrd has been added to the cultures, all subsequent operations must be carried out in subdued light and cells should always be incubated and stored in the dark. BrdUrd is a powerful photo- and radiosensitiser (8).

For flow cytometry, the cells are excited with ultraviolet (UV) light and a bivariate cytogram of red (>600 nm, PI, EB, or 7-AAD) vs. blue (460 nm, Hoechst) fluorescence is recorded. If the instrument permits it, an investigation of the signal shape of the red fluorescence can be used to exclude any clumps and debris from the analysis (28).

DATA ANALYSIS

Synchronised Cells

The majority of studies using the BrdUrd-Hoechst/PI method have used synchronised cells. Many such investigations have used human peripheral blood lymphocytes (PBLs), normally in G0 phase of the cell cycle, which were stimulated into cycle by the addition of a mitogen such as phytohaemagglutinin (PHA) (14,16–18,21–25,36–40). Another approach has been to render fibroblasts quiescent by the removal of serum and then to stimulate them by the re-addition of serum (5,6,19, 21,35,37,41). Melanoma cells (42), mouse CTLL-cells (17), and rat keratinocytes (34) have also been studied by this method.

A guide to the interpretation of the data obtained

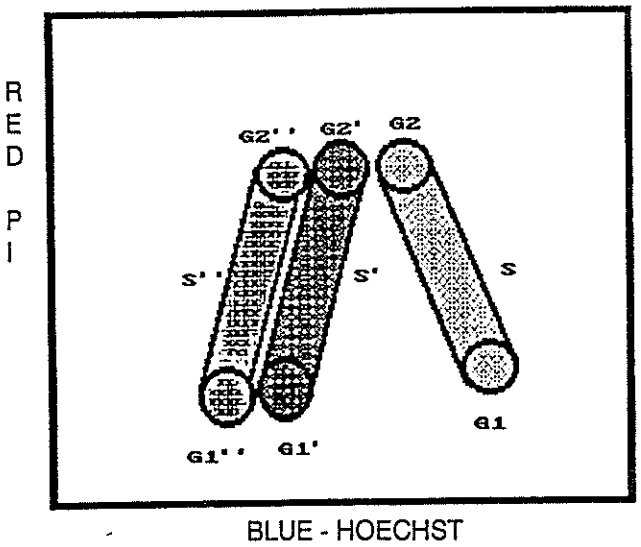

FIG. 1. Drawing illustrating the BrdUrd-Hoechst/PI pattern from a synchronous cell culture. Cells initially in G0 of their cycle have been stimulated into cycle in the presence of BrdUrd. G0/G1-S-G2/M: first cell cycle; G1′-S′-G2/M′: second cell cycle; G1″-S″-G2/M″: third cell cycle.

from synchronised cells stimulated into cycle in the presence of BrdUrd is illustrated in Figure 1. As the cells move into S phase, the red fluorescence increases with increasing DNA content while the blue fluorescence decreases due to quenching by the BrdUrd. As time progresses, the cells which have completed their cycle and returned to G1 (G1′) can be distinguished from those which have not entered the cycle. If the resolution of the cytogram and the concentration of BrdUrd is sufficient, three rounds of replication can be observed. The entry and exit kinetics of the cells into successive S, G2/M, and G1 phases can be measured and the effect of various growth factors (6,14,16, 19,20,39), cytotoxic agents (14,17,18,22,33,35,41,42) or endogenous cell cycle disturbances (22,25,38,39) can be observed.

Figure 2 shows typical data from initially synchronous G0/G1 phase PBLs stimulated with PHA. BrdUrd was added at the onset of PBL culture. This 72 h harvest displays three cell cycle lanes representing subsequent first (G0/G1, S, G2/M), second (G1′, S′, G2/M′), and third (G1″, S″, G2/M″) cell cycles. Due to asynchronous cell activation in G0/G1, a 72 h harvest consists of cells with different replicative histories. Therefore the non- or slowly cycling cells are diluted by the faster proliferating cells and the numbers of cells at the start of the experiment are under- and overestimated, respectively. Quantitative cell cycle analysis via the BrdUrd/Hoechst technique enables the calculation of the actual numbers of cells in the initial population activated or inhibited during cultivation.

Asynchronous Cells

The picture generated with asynchronous cells is more complicated but, potentially, more informative.

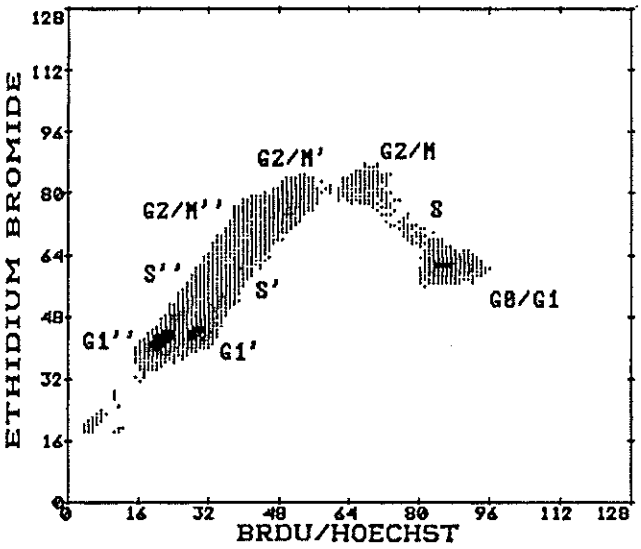

FIG. 2. BrdUrd-Hoechst/PI cytograms from a synchronous human lymphocyte culture. Cells activated with PHA were harvested 72 h later. Compare the figure to the lanes illustrated in the Figure 1 drawing.

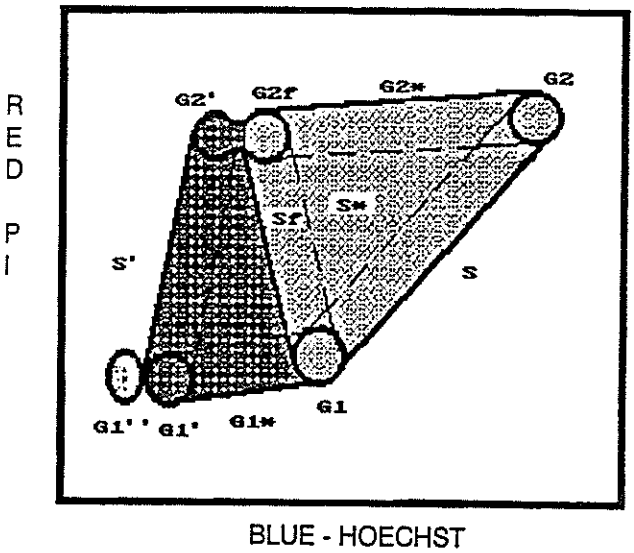

FIG. 3. Drawing illustrating the BrdUrd-Hoechst/PI pattern from asynchronous cells. G1-S-G2: initial cell cycle; S^*-S_f-$G2_f$-$G2^*$: first cycle cells originating from G1 (S_f, $G2_f$) and S phase (S^*, $G2^*$), respectively; G1′-G1*-S′-G2′: second cycle cells originating from G1 (G1′, S′, G2′) and S phase (G1*, G2′), respectively.

An interpretative guide is shown in Figure 3 and typical data are illustrated in Figure 4. Initially the normal cell cycle can be observed with cells in G1, S, and G2/M. When BrdUrd is added to the culture, cells moving out of G1 into S (S_f) phase and then into G2/M ($G2_f$) can be identified. On division, the new G1 (G1′) can be observed as in synchronous cultures. On continuing to cycle, these cells give rise to new S (S′) and G2/M (G2′) phases. This represents the BrdUrd/Hoechst cell cycle pattern of initially synchronous populations (see above).

Cells starting in G1 can be distinguished from those starting in S phase which, when they reach G2/M, lie on a line on the cytogram between $G2_f$ and G2 (G2*). The position on this line will depend on their position within S phase at the time of addition of BrdUrd. When these cells divide, their G1 will lie between the original G1 and G1′ (G1*) and, as they cycle, the new S phase lies between Sf and S. Beyond this point, the distinction between cells starting in G1 and those starting in S is lost.

Referring to Figure 4, without BrdUrd (Fig. 4A), both blue (Hoechst) and red (PI) fluorescence give a normal DNA histogram. Shortly after the addition of BrdUrd, the S phase appears curved due to the uptake of BrdUrd by these cells and the consequent quenching of blue fluorescence. There is a reduction in the number of cells in G2/M as they divide and move into G1 without, of course, taking up any label (Fig. 4B, 3 h). At the next time point, the movement of cells out of G1 into S_f can be also observed (Fig. 4C, 6 h). At this time, the cells which started in S have now reached G2*; many have divided and have started to appear in G1* to the left of the G1 peak. At 9 h, all the cells starting from S have divided and G1* is at its maximum; S_f has fully developed, cells have reached $G2_f$, and a few have divided (G1′) (Fig. 4D). The growth of G1′ continues and cells start to move into a new S phase (S′) (Fig. 4E, 12 h). Cells are also moving from G1* into S. At the last time shown (Fig. 4F, 15 h), the movement of cells out of G1′ into S (S′) is clear and another G2 (G2′) is starting to form.

ANALYSIS OF THE CYTOGRAMS

Analysis of the data from asynchronous cultures is carried out by drawing regions around the different cell cycle compartments. Data derived from Figure 4 are shown in Table 1. The percentages were recalculated to take into account that, as the cycling cells divide, they dilute any undivided cells in the culture. The numbers are therefore expressed in terms of the number of cells at the start of the experiment.

Using this simple method, because of the overlaps between G1 and early S phase and G2M and late S, the G phases will therefore be overestimated and S underestimated. It is difficult to resolve this without recourse to a fairly complex computer program.

Figure 5 shows a graphic representation of some of the data; note the apparent lag in the movement of cells out of G1. This is because, in the first few hours, unlabelled cells in G2 divide and move into G1. The time taken for G1′ to reach half its maximum value gives a measure of the average cell cycle time (in this case, about 13 h).

EFFECT OF CYTOTOXIC TREATMENTS

BrdUrd-Hoechst/PI flow cytometry can give a wealth of information about the effects of cytotoxic

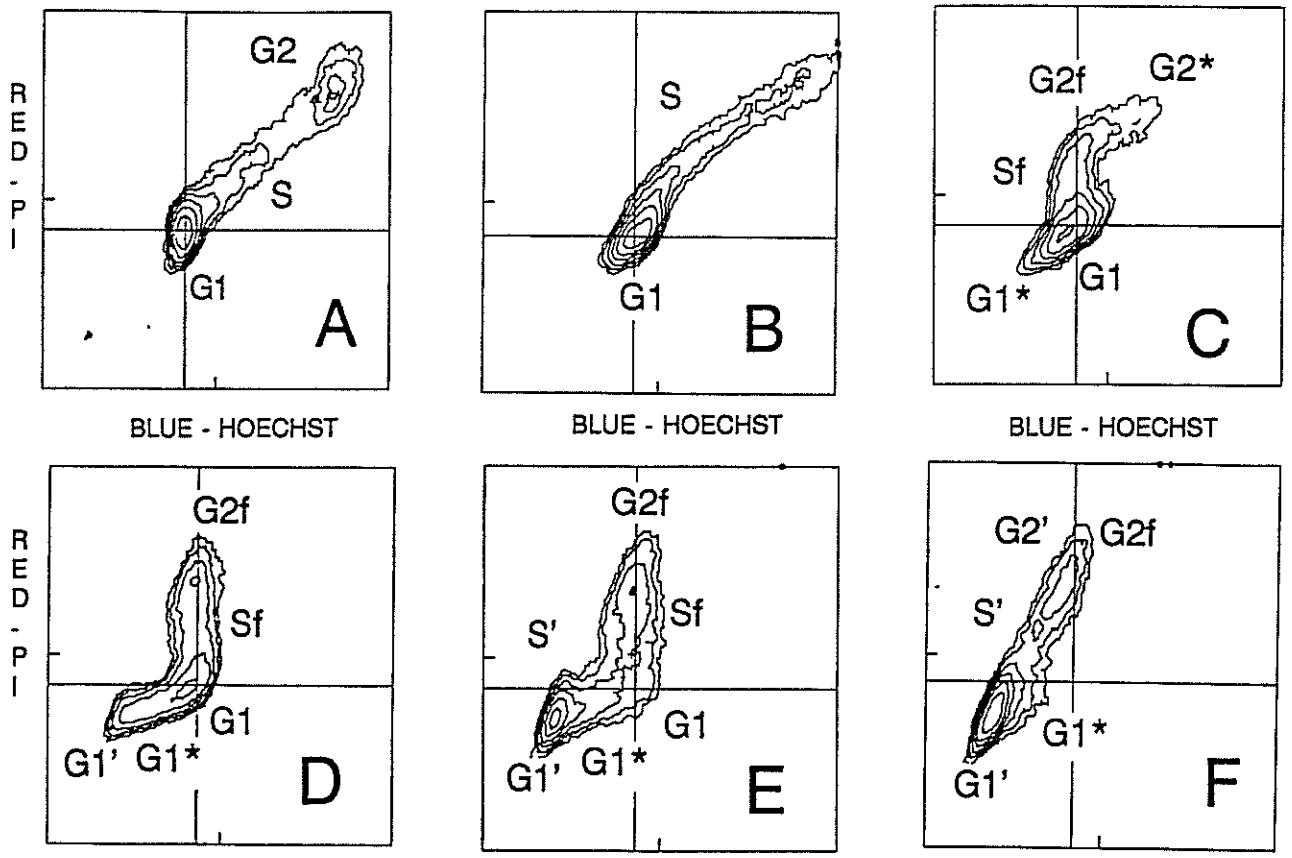

FIG. 4. BrdUrd-Hoechst/PI cytograms from an exponentially growing culture of a cell line derived from rat fibroblasts. (A) 0 h; (B) 3 h after the addition of 20 μM BrdUrd; (C) 6 h; (D) 9 h; (E) 12 h; (F) 15 h. (Cells prepared by Dr. Trevor Littlewood.)

Table 1
Numerical Data Relating to Phases of the Cell Cycle Derived From Figure 4 Together With Three Additional Time Points[a]

	Percentage of cells in cell cycle phase									
Time (h)	G1	S	G2	G2*	S_f	G1*	$G2_f$	G1′	S′	G2′
0	63	24	12	0	0	0	0	0	0	0
3	67	10	5	9	7	1	0	0	0	0
6	52	0	1	11	26	4	6	0	0	0
9	34	0	0	2	26	14	18	6	0	0
12	17	0	0	1	25	12	19	24	1	0
15	2	0	0	2	6	4	11	58	14	2
18	2	0	0	0	3	2	8	60	17	8
21	2	0	0	0	0	0	6	62	20	10
24	0	0	0	0	0	0	0	66	21	12

[a]The significance of the different phases described in the text.

treatments on the cell cycle. Broadly, three types of effect are observed and these are illustrated below.

G1 Arrest

This effect is shown in a line derived from murine haemopoietic cells after the withdrawal of a growth factor (interleukin 3) (Fig. 6). The cytogram in Figure 6B shows that, in the absence of the growth factor, some of the cells have not left G1, while others have progressed round the cycle before arresting in G1 (G1′).

S Slowdown

A general slowing of DNA synthesis has the effect of producing a bow-shaped curve in the S phase on the Hoechst-PI cytogram (Fig. 7B). Unlike a synchronous cell population, in asynchronous cultures, S phase

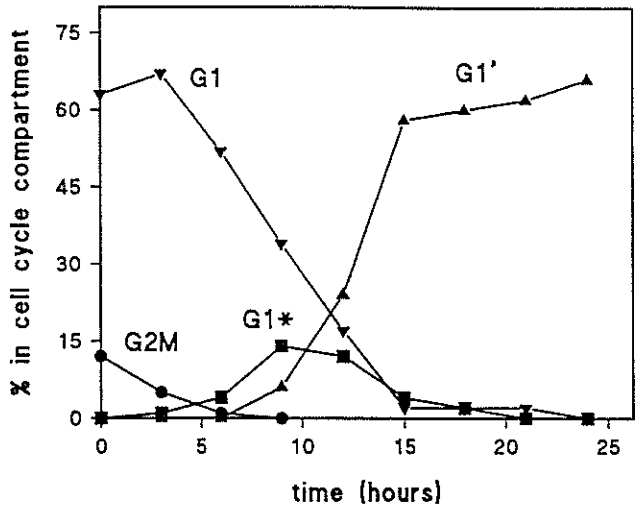

FIG. 5. Graphical data derived from the cytograms in Figure 4 (together with three further time points: 18, 21, and 24 h) showing changes in the percentage of cells in G1, G2/M, G1*, and G1'.

slowdown and possible subsequent S phase arrest are directly visualised.

G2/M Arrest

Arrest in the G2/M phase is shown by Chinese hamster V79 cells which were heated to 43°C for 1 h (Fig. 7C). Cells which were in S at time 0 have arrested in G2/M (G2*); many of the cells in G1 at the time of treatment have moved through a complete cycle into G1' and have started to cycle again. This probably reflects the greater sensitivity to heat of cells in S (29) and is an example of how this method can reveal differences in cytotoxicity in different phases of the cycle. This would be difficult to achieve using other methods.

PROBLEMS

Cytotoxicity of BrdUrd

Cells may be adversely affected by the incorporation of BrdUrd into their DNA. Apart from direct effects on the cell cycle, cells become sensitised both to light (8) and to oxygen (5,35). Many normal diploid cells and permanent cell lines show no cell cycle disturbances in the conventional short-term cultures (5,15,24,36). However, the effect of BrdUrd should always be tested using a conventional DNA histogram obtained by staining with PI alone.

A comparison of the conventional DNA histogram with the results of the BrdUrd-Hoechst/PI experiment is an important control. For example, any treatment which changes the size of the thymidine pool (e.g., via fluorodeoxyuridine or methotrexate) or metabolic conversion of exogenously supplied BrdUrd may affect the BrdUrd-Hoechst/PI cytogram.

Resolution of the Cell Cycle Phases

The quality of the preparation of nuclei and of the flow cytometry is clearly important in determining the resolution of the different phases of the cell cycle. The resolution also depends on the amount of BrdUrd incorporated. This will vary with cell type and AT/GC ratio of cells (15,21); the optimum concentration needs to be determined for each series of experiments, bearing in mind the possible cytotoxicity of high concentrations of BrdUrd.

Dying Cells

Many cytotoxic treatments induce cell necrosis which produces nuclear debris. Signals from debris can be excluded by pulse shape analysis but they can provide additional information on cell cycle or cell compartment specific death (14).

ADVANTAGES AND DISADVANTAGES OF THE METHOD

The major advantage to the BrdUrd-Hoechst/PI method is its simplicity and the wealth of information which can be derived from the basic bivariate cytogram. The resolution of cells which have passed through different stages of their cycle and, in particular, the distinction between cells which have traversed the cycle to return to G1 from those which have never left G1/G0 are difficult to obtain by other methods.

In addition, the preparative procedures are comparatively gentle and can easily be combined with an antibody label of cellular antigens for, e.g., analysis of cell cycle dependent gene expression (13).

The limitations to the method are: 1) cells cannot be labelled in vivo because of the need for continuous labelling with BrdUrd, 2) continuous BrdUrd labelling could affect the cell cycle progression in some cell systems, and 3) the need for a source of UV light.

Comparison With the Anti-BrdUrd Antibody Method

In this method, cells are generally pulse-labelled with BrdUrd, which is subsequently detected in fixed cells by an anti-BrdUrd antibody labelled with fluorescein. The DNA is counterstained with PI and a cytogram of green (anti-BrdUrd) vs. red (DNA) fluorescence is recorded. The cells initially in S phase are visualised and, by taking sequential samples, the movement of these cells through the cycle can be followed. From such an experiment, cell cycle parameters, such as the transit times through the different phases, can be calculated and the effect of cytotoxic treatments on these parameters can be observed.

The important advantage of this method is its high sensitivity. Only a small amount of BrdUrd is incorporated into the DNA and problems with cytotoxicity of BrdUrd are unlikely to be encountered. The application of a pulse label is especially useful in the study of cell kinetics in vivo and can give unique information about the proliferative behaviour of tumours (1,27,43). With cultured cells, since the method picks out cells in S phase, small perturbations in S are easier to detect.

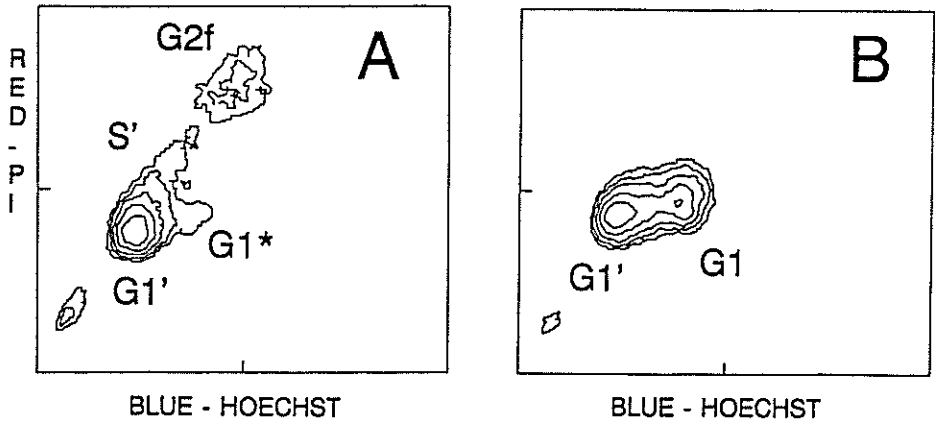

FIG. 6. Cytograms from an interleukin 3 (IL-3) dependent cell line derived from murine haemopoietic cells grown for 18 h plus 20 μM BrdUrd. (A) In the presence of IL-3; (B) without IL-3. (Cells prepared by Gordon Perkins.)

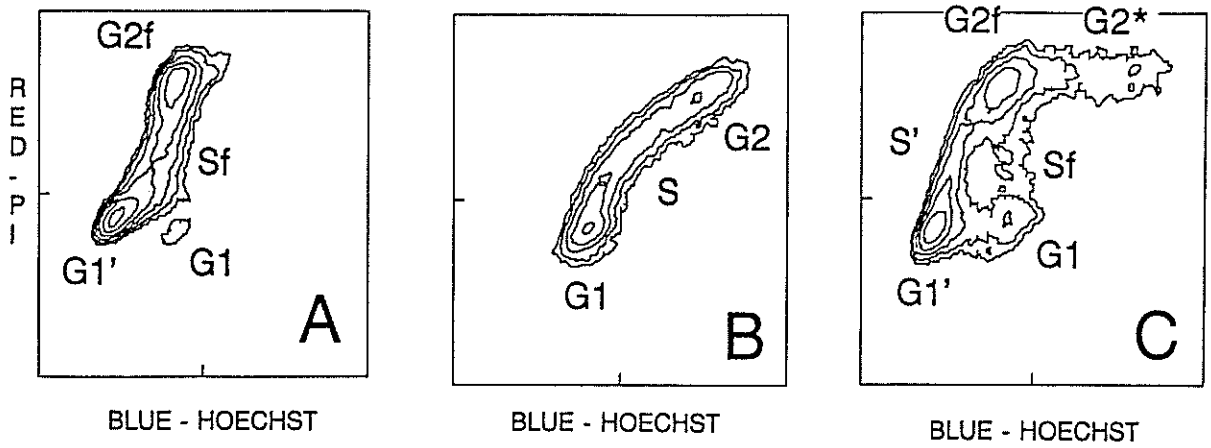

FIG. 7. BrdUrd-Hoechst/PI cytograms from Chinese hamster V79 cells incubated with BrdUrd. (A) Untreated, 8 h after the addition of BrdUrd. (B,C) Heated to 43°C for 1 h and then BrdUrd added: (B) 8 h later; (C) 24 h later. The unheated cells (not shown) had undergone two rounds of division at 24 h. (Cells prepared by Pam Loverock.)

It also has the advantage that it uses blue light, available on all flow cytometers.

The main disadvantages of the antibody method are: 1) the cytochemical procedure is complex, and 2) there is a requirement for DNA denaturation which often leads to a significant loss of cells and which makes the simultaneous detection of a cellular antigen difficult. The method does not yield the same wealth of information obtained from BrdUrd-Hoechst/PI, particularly in regard to the different cell cycles which can be resolved.

CONCLUSIONS

Although the quenching of Hoechst fluorescence by BrdUrd was first applied to the study of cell cycle kinetics nearly 20 years ago, the BrdUrd-Hoechst/PI method has not found widespread use, particularly in asynchronous cultures. In this paper we have attempted to demonstrate the undoubted value of the method in the hope that other workers will be persuaded to exploit its potential.

ACKNOWLEDGMENTS

The authors thank their colleagues for permission to use results from collaborative work, in particular, Dr. Trevor Littlewood, Imperial Cancer Research Fund Laboratories at St. Bartholomew's Hospital, London, and Pam Loverock, Section of Physics, and Gordon Perkins, Section of Cell and Molecular Biology.

LITERATURE CITED

1. Begg AC, McNally NJ, Shrieve DC, Karcher H: A method to measure the duration of DNA synthesis and the potential doubling time from a single sample. Cytometry 6:620–626, 1985.
2. Boehmer RM: Flow cytometric cell cycle analysis using the quenching of 33258 Hoechst fluorescence by bromodeoxyuridine incorporation. Cell Tissue Kinet 12:101–110, 1979.

3. Boehmer RM, Ellwart J: Combination of BUdR-quenched Hoechst fluorescence with DNA-specific ethidium bromide fluorescence for cell cycle analysis with a two parameter flow cytometer. Cell Tissue Kinet 14:653–658, 1981.
4. Boehmer RM, Ellwart J: Cell cycle analysis by combining the 5-bromodeoxyuridine/33258 Hoechst technique with DNA-specific ethidium bromide staining. Cytometry 2:31–34, 1981.
5. Brachertz M, Kubbies M, Feige A, Salk D: Decreased oxygen supply enhances growth in culture of human mid-trimester amniotic fluid cell. Hum Genet 64:334–338, 1983.
6. Chen Y, Rabinovitch PS: Platelet-derived growth factor, epidermal growth factor and insulin-like growth factor I regulate specific cell-cycle parameters of human diploid fibroblasts in serum-free culture. J Cell Physiol 140:59–67, 1989.
7. Crissman HA, Steinkamp JA: A new method for rapid and sensitive detection of bromodeoxyuridine in DNA replicating cells. Exp Cell Res 173:256–261, 1987.
8. Djordjevic B, Szybalski W: Genetics of human cell lines. III. Incorporation of 5-bromo- and 5-iododeoxyuridine into deoxyribonucleic acid of human cells and its effect on radiation sensitivity. J Exp Med 112:509–531, 1960.
9. Dolbeare FA, Gratzner HG, Pallavicini MG, Gray JW: Flow cytometric measurement of total DNA content and incorporated bromodeoxyuridine. Proc Natl Acad Sci USA 80:5573–5577, 1983.
10. Fertig G, Miltenburger HG: Flow-cytometric cell-cycle analysis of Chinese hamster cells following exposure to cytotoxicants. Mutat Res 215:61–68, 1989.
11. Giarretti W, Moro G, Quarto R, Bruno S, Di Vinci A, Geido E, Cancedda R: Flow cytometric evaluation of cell cycle characteristics during in vitro differentiation of chick embryo chondrocytes. Cytometry 9:281–290, 1988.
12. Gray JW, Mayall BH (eds): Monoclonal Antibodies Against Bromodeoxyuridine. Alan R. Liss, New York, 1985.
13. Kubbies M: High resolution cell cycle analysis by BrdU/Hoechst flow cytometry. In: Progress in Cytometry: Flow and Image; Reports From the Cytometry Users Conference, Ghent, 1989. Becton-Dickinson Immunocytometry Systems Europe, Erembodegem-Aalst, Belgium 1990, pp 30–42.
14. Kubbies M: Flow cytometric recognition of clastogen induced chromatin damage in G0/G1 lymphocytes by non-stoichiometric Hoechst fluorochrome binding. Cytometry 11:386–394, 1990.
15. Kubbies M, Friedl R: Flow cytometric correlation between BrdU/Hoechst quench effect and base pair composition in mammalian cell nuclei. Histochemistry 83:133–137, 1985.
16. Kubbies M, Friedl R, Koehler J, Rabinovitch PS, Hoehn H: Improvement of human lymphocyte proliferation and alteration of IL-2 secretion kinetics by alpha-thioglycerol. Lymphokine Res 9:95–106, 1990.
17. Kubbies M, Goller B, Schetters B, Albert W: Undisturbed cell proliferation in cis-platinum toxified human PBLs after treatment with reduced glutathione. In: Advances in Analytical Cellular Pathology, Burger G, Oberholzer M, Vooijs GP (eds). Excerpta Medica, Amsterdam, 1990, pp. 305–306.
18. Kubbies M, Goller B, Schetters B, Bartosek I, Albert W: Glutathione restores normal cell activation and cell cycle progression in cis-platinum treated human lymphocytes. Br J Cancer 64:843–849, 1991.
19. Kubbies M, Hoehn H, Rabinovitch PS: Differences in growth factor sensitivity between primary and transformed murine cell cultures revealed by BrdU/Hoechst flow cytometry. Exp Cell Biol 55:225–236, 1987.
20. Kubbies M, Hoehn H, Schindler D, Chen Y, Rabinovitch PS: Cell cycle analysis via BrdU/Hoechst flow cytometry: Principles and applications. In: Flow Cytometry: Advanced Research and Clinical Applications, Vol. 2, Yen A (ed). CRC Press, Boca Raton, FL, 1989, pp. 5–28.
21. Kubbies M, Rabinovitch PS: Flow cytometric analysis of factors which influence the BrdU-Hoechst quenching effect in cultured human fibroblasts and lymphocytes. Cytometry 3:126–281, 1983.
22. Kubbies M, Schindler D, Hoehn H, Friedl R, Rabinovitch PS: BrdU/Hoechst cell cycle analysis applied to Fanconi anemia and inhibitory agents. In: Clinical Cytometry and Histometry, Burger G, Ploem JS, Goerttler K (eds). Academic Press, London, 1987, pp 243–245.
23. Kubbies M, Schindler D, Hoehn H, Rabinovitch PS: Cell cycle kinetics by BrdU-Hoechst flow cytometry: An alternative to the differential metaphase technique. Cell Tissue Kinet 18:551–559, 1985.
24. Kubbies M, Schindler D, Hoehn H, Rabinovitch PS: BrdU-Hoechst flow cytometry reveals regulation of human lymphocyte growth by donor-age-related growth fraction and transition rate. J Cell Physiol 125:229–234, 1985.
25. Kubbies M, Schindler D, Hoehn H, Schinzel A, Rabinovitch PS: Endogenous blockage and delay of the chromosome cycle despite normal recruitment and growth phase explain poor proliferation and frequent endomitosis in Fanconi anemia cells. Am J Hum Genet 37:1022–1030, 1985.
26. Latt SA: Microfluorometric detection of deoxyribonucleic acid replication in human metaphase chromosomes. Proc Natl Acad Sci USA 70:3395–3399, 1973.
27. McNally NJ, Wilson GD: Measurement of tumour cell kinetics by the bromodeoxyuridine method. In: Flow Cytometry. A Practical Approach, Ormerod MG (ed). IRL Press at Oxford University Press, Oxford, 1990.
28. Ormerod MG: Analysis of DNA. General methods. In: Flow Cytometry. A Practical Approach, Ormerod MG (ed). IRL Press at Oxford University Press, Oxford, 1990.
29. Ormerod MG, Imrie PR, Loverock P, Ter Haar G: A flow cytometric study of the effect of heat on kinetics of cell proliferation of Chinese hamster V79 cells. Cell Prolif 25:41–51, 1991.
30. Ormerod MG, Loverock P, Ter Haar G, Imrie PR: Ultrasound enhances the effect of hyperthermia on the cell cycle of Chinese hamster V79 cells. Inst Phys Conf Ser No 98. 1990, pp 817–820.
31. Poot M: Cell kinetic analysis using continuous BrdU labelling and bivariate Hoechst 33258/ethidium bromide flow cytometry. In: Flow Cytometry. A Practical Approach, Ormerod MG (ed). IRL Press at Oxford University Press, Oxford, 1990.
32. Poot M, Kubbies M, Hoehn H, Grossmann A, Chen Y, Rabinovitch PS: Cell cycle analysis using continuous bromodeoxyuridine labelling and Hoechst 33258-ethidium bromide bivariate flow cytometry. In: Methods in Cell Biology: Flow Cytometry, Vol. 33, Darzynkiewcz Z, Crissman H (eds). Academic Press, San Diego, 1990, pp 185–198.
33. Poot M, Rabinovitch PS, Hoehn H: Bromodeoxyuridine amplifies free-radical-mediated DNA-damage. Biochem J 261:269–271, 1990.
34. Poot M, Rizk-Rabin M, Hoehn J, Pavlovitch JH: Cell size and RNA content correlate with cell differentiation and proliferative capacity of rat keratinocytes. J Cell Physiol 143:279–286, 1990.
35. Poot M, Schindler D, Kubbies M, Hoehn H, Rabinovitch PS: Bromodeoxyuridine amplifies the inhibitory effect of oxygen on cell proliferation. Cytometry 9:332–338, 1988.
36. Poot M, Schmitt H, Seyschab H, Koehler J, Chen U, Kaempf U, Kubbies M, Schindler D, Rabinovitch PS, Hoehn H: Continuous bromodeoxyuridine labelling and bivariate ethidium bromide/Hoechst flow cytometry in cell kinetics. Cytometry 10:222–226, 1989.
37. Rabinovitch PS, Kubbies M, Chen YC, Schindler D, Hoehn H: BrdU-Hoechst flow cytometry. A unique tool for quantitative cell cycle analysis. Exp Cell Res 174:309–318, 1988.
38. Schindler D, Kubbies M, Hoehn H, Schinzel A, Rabinovitch PS: Presymptomatic diagnosis of Fanconi's anemia. Lancet 2:937, 1987.
39. Schindler D, Seyschab H, Poot M, Hoehn H, Schinzel A, Fryns JP, Tommerup N, Rabinovitch PS: Screening test for ataxia telangiectasia. Lancet 2:1398–1399, 1987.
40. Seyschab H, Friedl R, Schindler D, Hoehn H, Rabinovitch PS, Chen U: The effects of bacterial lipopolysaccaride, anti-receptor antibodies and recombinant interferon on mouse B cell cycle progression using 5-bromo-2-deoxyuridine/Hoechst 33258 dye flow cytometry. Eur J Immunol 19:1605–1612, 1989.
41. Vogel DC, Rabinovitch PS, Mattet MK: Methyl mercury effects on cell cycle kinetics. Cell Tissue Kinet 19:227–238, 1986.

42. Weilbach FX, Bogdahn U, Poot M, Apfel R, Behl C, Drenkard D, Martin R, Hoehn H: Melanoma-inhibiting activity inhibits cell proliferation by prolongation of the S-phase and arrest of cells in the G2 compartment. Cancer Res 50:6981–6986, 1990.

43. Wilson G, McNally NJ, Dunphy E, Kaercher H, Pranger R: The labelling index of human and mouse tumours assessed by bromodeoxyuridine staining in vitro and in vivo and flow cytometry. Cytometry 6:641–647, 1985.

In: FLOW CYTOMETRY, A PRACTICAL APPROACH
(1990), Ed. M.G.Ormerod,
Oxford University Press, oot

4C. CELL KINETIC ANALYSIS USING CONTINUOUS BrdU LABELLING AND BIVARIATE HOECHST 33358/ETHIDIUM BROMIDE FLOW CYTOMETRY

MARTIN POOT

14. Introduction

Continuous labelling with BrdU and subsequent staining of DNA with the AT specific dye Hoechst 33258 allows the discrimination of chromatids according to the number of replications they underwent during the period of observation (26, 27). The potential of this technique for cell kinetic analysis was subsequently established in several laboratories (28–33). This section describes the analysis of cell kinetics using continuous BrdU labelling and bivariate Hoechst 33258/ethidium bromide flow cytometry. Because BrdU quenches the fluorescence from the Hoechst dye, cells are separated according to how many phases of DNA replication they traversed, whereas the fluorescence of the unquenched ethidium bromide resolves the cell cycle into the G1, S, and G2 compartments.

15. Cell culture and BrdU labelling

The method has been applied to a variety of types of cell, each requiring specific, optimal cell culture conditions which have been described previously (34). Anchorage-dependent cells are rendered quiescent by allowing them to reach contact inhibition of growth and subsequent exposure to a low serum concentration. Diploid human fibroblasts reach quiescence after 48 h at 0.1% FCS but NIH-3T3 cells tolerate only 24 h at 0.5% FCS. Epstein–Barr virus transformed B-lymphoblastoid cells (EBL) reach quiescence if they are left without replenishment of culture medium during four days or longer.

Naturally quiescent, mononuclear cells from peripheral blood, spleen, or thymus cells need only isolation by Ficoll-Hypaque. Adherent cells are trypsinized and replated at a density of $1–25 \times 10^3$ cells per cm^2 of culture flask in culture medium supplemented with 10% FCS and 65 μM of each BrdU and deoxycytidine (human diploid skin fibroblasts), or 100 μM of both base analogue (NIH-3T3 cells, keratinocytes). Mononuclear cells from peripheral blood, spleen, or thymus are stimulated with 16% FCS and appropriate mitogens, but EBL cells need only 10% FCS for optimal growth. These cell types are all grown at an initial density of 50 000 cells/ml in culture media supplemented with 100 μM of BrdU and deoxycytidine and kept as suspension cultures in culture flasks standing upright. The latter condition allows for optimal cell to cell contact, which improves cell proliferation. Exceeding the plating densities described here,

might lead to rapid depletion of BrdU from the culture medium, and thus jeopardize BrdU incorporation into DNA.

As BrdU is a strong photo- and radiosensitizer all cell cultures should be fully protected from any light of short wavelengths. This is achieved by wrapping all culture flasks with aluminium foil and by performing all steps of the experiment after exposure of cells to BrdU in dimmed light or in the dark using red light only. Failure to prevent exposure of cells to DNA damaging light will lead to cell killing and spurious arrest of cells in the S and G2 phase.

After an appropriate period of culture, cells are harvested, resuspended in culture medium supplemented with 10% FCS and 10% dimethylsulphoxide and stored at −20 °C in the dark.

16. Cell staining and flow cytometry

After thawing, cells are centrifuged at 500 *g* for 5 min, and the supernatant is carefully aspirated with a pipette. The cell pellet is resuspended in staining buffer at a density of 4×10^5–10^6 cells/ml. The staining buffer consists of (final concentration): 100 mM Tris pH 7.4, 154 mM NaCl, 1 mM $CaCl_2$, 0.5 mM $MgCl_2$, 0.1% (v/v) Nonidet-P40, 0.2% (w/v) BSA, 1.2 μg/ml Hoechst 33258.

This staining buffer should be ice-cold and cells are incubated for 15 min at 4 °C in the dark. Thereafter, ethidium bromide is added from an ice-cold 100 × concentrated stock solution to a final concentration of 2.0 μg/ml. After a further 15 min in the dark at 4 °C, samples are ready for analysis by flow cytometry. Stained cells do not show significant deterioration during 8 h if kept at 4 °C in the dark.

Batches of staining buffer are prepared weekly from 10 × concentrated stock solutions in deionized water. All staining solutions are stored in dark glass bottles at 4 °C and can be filtered immediately prior to use if necessary.

Flow cytometry can be performed on an arc-lamp-based epi-illumination system (e.g. PHYWE ICP-22, Partec PAS II) or on any type of flow cytometer equipped with a laser emitting in the UV (360 nm). On the arc-lamp-based instruments appropriate excitation light is selected with an UG 1 and an BG 38 filter (Schott) and an FT 450 dichroic mirror. Hoechst fluorescence is obtained with an K45 filter and an FT 510 dichroic mirror, and ethidium bromide fluorescence is collected with an K65 LP filter. Under UV light, Hoechst fluroescence excites the DNA-bound ethidium bromide via resonance energy transfer (see Chapter 2, Section 2); in laser-powered instruments a two-laser excitation can also be used. An optimal CV is obtained at flow rates of 200 to 500 cells/sec, which is equivalent to 0.5 μl of cell suspension per second.

17. Quantitative analysis of data

Figure 17 displays a typical series of bivariate cytograms obtained with the method. At 12 h after serum stimulation cells appeared in a single cluster, which

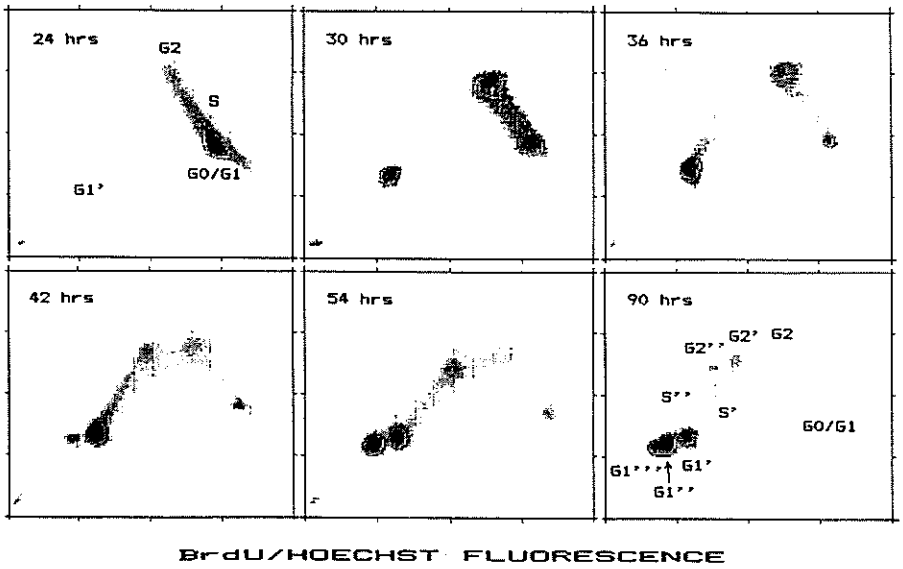

Figure 17. Bivariate cytograms of human diploid fibroblasts after continuous BrdU-labelling for up to 90 h. Abscissa is BrdU-quenched Hoechst fluorescence and ordinate is unquenched ethidium bromide fluorescence. From right to left the arrays of clusters represent the first, second, and third cycle after serum stimulation of quiescent cells. The lowermost clusters are the G1 phases and the uppermost are the G2 phases of each cell cycle.

represents quiescent or G0/G1 cells (not shown). The signal track moving from the G0/G1 cluster to the left represents cells in the first S-phase 24 h after serum stimulation. The G1′ cluster are cells, which traversed a full cell cycle and underwent mitosis; this caused halving of the fluorescence intensity from both the Hoechst and ethidium bromide. The signal track of cells in the second S-phase moves to the right because of bifiliary substitution of the DNA with BrdU (e.g. panels showing 36 h and later).

The bivariate cytogram resolves cells into three successive cell cycles and additionally separates the G1, S, and G2 compartments of each cell cycle. Each component cell cycle can be isolated from the cytogram by electronic framing. Subsequent rotation of the *x*- or *y*-axis in parallel to the framed region of interest and deconvolution of the signals on to the axis yields a conventional cell cycle distribution, which can be analysed with an algorithm of the kind discussed above. Thus, the distribution of cells among cell cycle compartments at a given time point can be calculated.

A full picture of the kinetic pattern of a certain cell culture is obtained by analysing samples taken at different time intervals after serum stimulation. *Figure 18* shows the kinetic pattern thus derived. On the ordinate the times of sampling, and on the logarithmic scale of the abscissa the respective cell cycle distributions are plotted. The curves connect the fraction of cells in a particular cell cycle

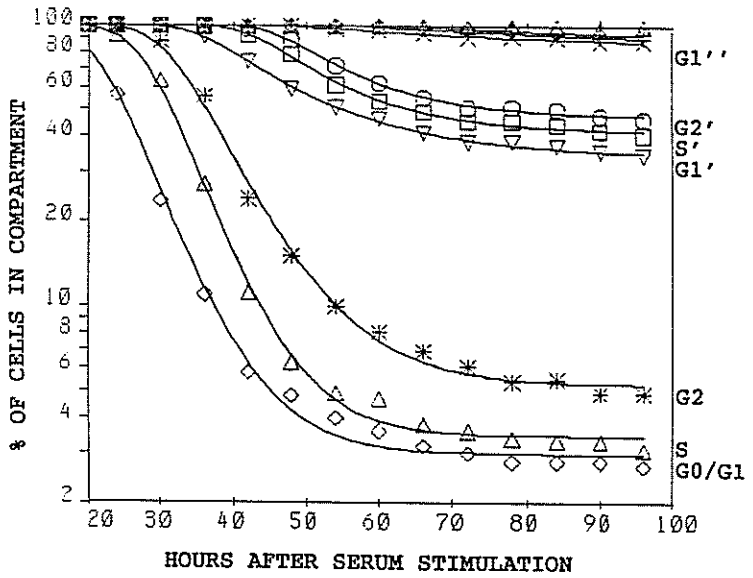

Figure 18. Exit kinetic curves derived from the data shown in *Figure 17*. The subsequent curves denote, from the bottom, the G0/G1, S, and G2 phases of the first cycle, the G1, S, and G2 phases of the second cycle, and so on.

compartment through time, and thus display the exit of cells from the successive cell cycle compartments. In this way, exit kinetics can be derived. Extrapolation of two successive exit curves to 100% cell gives the minimal duration of the compartment between the two curves. The inverse of the slope of the exponential part of the exit added to the minimal duration of the compartment gives the mean duration (35). The plateau level to which each curve asymptotically approaches at the right-hand side of the figure gives the fraction of cells permanently arrested in a given cell cycle compartment. These three parameters fully characterize the growth pattern of cultured cells (32, 36).

18. Application

The method was initially applied to cultures of human diploid fibroblasts and lymphocytes from human peripheral blood (31) and the mitogen response of human lymphocytes as a function of donor age was studied (32). More recently, the cell kinetic pattern of cells from patients displaying chromosomal instability, including Fanconi's anaemia (37, 38), Ataxia telangiectasia (39), and Bloom's syndrome (40, 41) have been elucidated. Perturbation of cell growth by oxygen (36), model compounds of lipid peroxidation (42), AT specific DNA ligands (Poot, Kausch, Koehler, Rabinovitch, and Hoehn, submitted for publication), 5-azacytidine (43), and cytotoxic agents (42, 44) have been assessed. Also less

common types of cell, including chick embryo chondrocytes (33) and rat keratinocytes (45) were amenable to cell kinetic analysis by this method.

19. Trouble-shooting

A typical result as shown in *Figure 17* might not be obtained because of several types of pitfalls.

19.1 Cytoxicity of BrdU

Continuous exposure to a halogenated nucleoside may entail a plethora of adverse effects on cellular functions, including metabolic changes due to alterations in the balance of nucleotide pools, direct DNA damage, alterations in DNA–protein interaction. Directly or indirectly, these effects could impair proliferation. In most cell types tested thus far, proliferation is not detectably affected at BrdU concentrations in the order of 65–100 μM. NIH 3T3 cells were found to tolerate concentrations of BrdU up to 300 μM without any growth inhibition (34). On the other hand, human lymphoblastoid cells lines and human diploid fibroblasts are sensitive to BrdU. Fibroblasts experience a 10–15% growth reduction after 72 h of culture when exposed to 10 μM BrdU, but no further growth reduction occurs in the interval between 10 and 200 μM. A cell line derived from a malignant melanoma showed a strong arrest in the G2 phase of the cell cycle at 50 μM BrdU and ambient oxygen concentration. Lowering BrdU concentrations to 25 μM BrdU and ambient oxygen concentration to 5% (v/v) significantly ameliorated the growth of these cells (Weilbach and Poot, unpublished observation).

The growth of the cells to be analysed should be tested with a series of concentrations of BrdU. As very low BrdU concentrations, which will not allow sufficient quenching of Hoechst fluorescence, bivariate cytograms might not be obtained. Conventional, univariate cell cycle distributions, which clearly reveal BrdU toxicity (36), can best be obtained using DAPI as DNA stain. Concomitantly, cell counting should be performed to assess the overall rate of growth. If accumulation of cells in the G2 phase of the cell cycle or a severe BrdU dependent reduction in cell growth is encountered, lowering the BrdU concentration and/or the addition of an equimolar amount of deoxycytidine can be considred.

19.2 Distorted cytograms

If focusing of G0/G1 cells to a narrow and perfectly round cluster is difficult, the sample delivery channel of the flow cytometer might be dirty. This occurs in particular after many samples stained with ethidium bromide have been analysed, as ethidium bromide tends to lyse some nuclei which subsequently stick

to the tubing. Regular cleaning of the tubing with a detergent, a piece of thin wire, and pressurized air is recommended. Adjustment of the instrument is best performed with unstimulated lymphocytes from human origin or with quiescent cells from the same cell culture to be analysed later.

If cell clumping is excessive, satisfactory cytograms might not be obtained. Passing samples through gauze before or after staining might help. Treatment of samples with nucleases or proteases is not recommended, as these enzymes will continue to act, and thus degrade the nuclei, in the staining buffer. On some instruments, clumps of cells can be excluded from analysis by analysing the shape of the pulse of DNA fluorescence (see Section 3.2.2).

19.3 Poor quenching of Hoechst fluorescence

This might either be due to insufficient BrdU incorporation into DNA or to inappropriate staining. The first phenomenon might occur if the serum batch in use contains significant amounts of thymidine, which will compete with BrdU for the nucleotide salvage pathway and thus jeopardize BrdU labelling. This can be remedied by increasing the BrdU concentration in the culture medium, while controlling for possible cytotoxicity of excess of BrdU (see above). If increasing the BrdU level does not improve the cytogram, a very low AT content of the DNA might be the cause of the trouble. To control this factor, use cells with known AT content (e.g. human lymphocytes or mouse 3T3 cells), which should give the kind of quenched fluorescence from Hoechst shown in *Figure 17*. If with human or mouse cells, poor quenching of Hoechst fluorescence is observed, the staining procedure might be inappropriate. Particularly a long line between the sample holder and the flow cell might perturb staining with ethidium bromide as this dye undergoes equillibrium binding to DNA. Increasing the concentration of ethidium bromide and/or lowering the Hoechst concentration might improve the cytogram.

Acknowledgements

The help of Miss J. Koehler with the preparation of the figures is kindly acknowledged. The author is supported Deutsche Forschungsgemeinschaft grant nr. DFG 849/2-2.

References

1. Sharpless, T. K. and Melamed, M. (1976), *J. Histochem. Cytochem.* 4, 257.
2. Vindelov, L. L., Christensen, I. J., and Nissen, N. I. (1983) *Cytometry* 3, 328.
3. Pallavicini, M. G. (1987). In *Techniques in Cell Cycle Analysis* (eds. J. W. Gray and Z. Darzynkiewicz). Humana Press, Clifton, NJ.
4. Petersen, S. E. (1985). *Cytometry* 6, 452.

5. Hedley, D. W., Friedlander, M. L., Taylor, I. W., Rugg, C. A., and Musgrove, C. A. (1983). *J. Histochem. Cytochem.* **31**, 1333.
6. Schutte, B., Reynders, M. M. J., Bosman, F. T., and Blijham, G. H. (1985). *Cytometry* **6**, 26.
7. Hedley, D. W. (1989). *Cytometry* **10**, 229.
8. Dean, P. N. (1985). In *Progress in Flow Cytometry* (eds. M. Van Dilla, P. N. Dean, O. Laerum, and M. Melamed). Academic Press, San Francisco.
9. Dean, P. N. (1987). In *Techniques in Cell Cycle Analysis* (eds. J. W. Gray and Z. Darzynkiewicz). Humana Press, Clifton, NJ.
10. Watson, J. V., Chambers, S. H., and Smith, P. J. (1987). *Cytometry* **8**, 1.
11. Ormerod, M. G., Payne, A. W. R., and Watson, J. V. (1987). *Cytometry* **8**, 837.
12. Steel, G. G. (1977). *Growth Kinetics of Tumours*. Clarendon Press, Oxford.
13. Dolbeare, F. A., Gratzner, H. G., Pallavicini, M. G., and Gray, J. W. (1983). *Proc. Natl. Acad. Sci. (USA)* **80**, 5573.
14. Gray, J. W. (Guest Editor) (1985). *Cytometry* **6**, 499.
15. Fowler, J. F. (1985). *Int. J. Radiat. Oncol. Biol. Phys.* **12**, 641.
16. Gratzner, H. G. (1982). *Science* **218**, 474.
17. Meyer, J. S. (1982). *Human Path.* **13**, 874.
18. Molinari, R., Costa, A., Silvestrini, R., Mattavelli, F., Cantu, G., Chiesa, F., and Volterrani, F. (1984). In *Head and Neck Oncology* (ed. G. T. Wolf), p. 229. Marinus Nijhoff, Boston.
19. Steel, G. G. and Bensted, J. P. M. (1965). *Eur. J. Cancer* **1**, 275.
20. Begg, A. C., Moonen, L., Hofland, I., Dessing, M., and Bartelink, H. (1988). *Radiother. Oncol.* **11**, 337.
21. Pallavicini, M. G. (1987). In *Techniques in Cell Cycle Analysis* (eds. J. W. Gray and Z. Darzynkiewicz), p. 139. Humana Press, Clifton, NJ.
22. Schutte, B., Reynders, M. M. J., van Assche, C., Hupperets, P. S. G., Bosman, F. T., and Blijham, G. H. (1987). *Cytometry* **8**, 372.
23. Beisker, W., Dolbeare, F., and Gray, J. W. (1987). *Cytometry* **8**, 235.
24. Begg, A. C., McNally, N. J., Shrieve, D. C., and Karcher, H. (1985). *Cytometry* **6**, 6220.
25. Begg, A. C. (1989). *Proc. Int. Symp. on the Scientific Basis of Modern Radiotherapy* (ed. N. J. McNally). British Institute of Radiology, London (in press).
26. Latt, S. A. (1973). *Proc. Natl. Acad. Sci (USA)* **70**, 3395.
27. Latt, S. A. (1977). *J. Histochem. Cytochem.* **25**, 913.
28. Boehmer, R. M. (1979). *J. Cell Tissue Kinet.* **12**, 101.
29. Beck, H. P. (1981). *Cytometry* **2**, 146.
30. Nuesse, M. (1981). *Cytometry* **2**, 70.
31. Rabinovitch, P. S. (1983). *Proc. Natl. Acad. Sci (USA)* **80**, 2951.
32. Rabinovitch, P. S., Kubbies, M., Chen, Y. C., Schindler, D., and Hoehn, H. (1988). *Exp. Cell Res.* **174**, 309.
33. Giaretti, W., Moro, G., Quarto, R., Bruno, S., Di Vinci, A., Geido, E., and Cancedda, R. (1988). *Cytometry* **9**, 281.
34. Poot, M., Schmitt, H., Seyschab, H., Koehler, J., Chen, U., Kaempf, U., Kubbies, M., Schindler, D., Rabinovitch, P. S., and Hoehn, H. (1989). *Cytometry* **10**, 222.
35. Smith, J. A. and Martin, L. (1973). *Proc. Natl. Acad. Sci (USA)* **70**, 1263.
36. Poot, M., Schindler, D., Kubbies, M., Hoehn, H., and Rabinovitch, P. S. (1988). *Cytometry* **9**, 332.

37. Kubbies, M., Schindler, D., Hoehn, H., and Rabinovitch, P. S. (1985). *J. Cell. Physiol.* **125**, 229.
38. Schindler, D., Kubbies, M., Hoehn, H., Schinzel, A., and Rabinovitch, P. S. (1985). *Lancet* ii, 937.
39. Schindler, D., Seyschab, H., Poot, M., Hoehn, H., Schinzel, A., Fryns, I. P., Tommerup, N., and Rabinovitch, P. S. (1987). *Lancet* ii, 1398.
40. Poot, M. (1988). In *Focus on Membrane Lipid Oxidation* (ed. C. Vigo-Pelfrey). CRC Press, Boca Raton, Florida.
41. Poot, M., Nicoterl, T., Rüdiger, H. W., and Hoehn, H. (1990). *Free Rad. Res. Comm.* (in press).
42. Poot, M., Esterbauer, H., Rabinovitch, P. S., and Hoehn, H. (1988). *J. Cell. Physiol.* **137**, 421.
43. Poot, M. Köhler, J., Rabinovitch, P. S., Hoehn, H., and Priest, J. H. (1990). *Hum. Genet.* (in press).
44. Vogel, D. C., Rabinovitch, P. S., and Mattet, M. K. (1986). *J. Cell Tissue Kinet.* **19**, 227.
45. Poot, M., Pavlovitch, J. H., Rizk-Rabin, M., and Hoehn, J. (1990). *J. Cell. Physiol.* (in press).

Experimental Cell Research 174 (1988) 309–318

SPECIAL ARTICLE

BrdU–Hoechst Flow Cytometry: A Unique Tool for Quantitative Cell Cycle Analysis

P. S. RABINOVITCH*,[1] M. KUBBIES,† Y. C. CHEN,* D. SCHINDLER,† and H. HOEHN†

*Department of Pathology, University of Washington, Seattle, Washington 98105, and †Department of Human Genetics, University of Würzburg, Federal Republic of Germany

Unlike other techniques, flow cytometric analysis of BrdU-quenched 33258 Hoechst fluorescence may be used to measure cell activation and the G_1, S, and G_2/M compartment distributions in each of three successive cell cycles after growth stimulation of human peripheral blood lymphocytes. Cell cycle kinetic curves can be constructed from the BrdU–Hoechst flow data which allow the simultaneous assessment of growth fraction, lag-time, compartment exit rate, compartment duration, and compartment arrest. Applications of this new versatile technique include the evaluation of drug and growth factor effets, cell aging, and diagnosis in medicine and immunology. © 1988 Academic Press, Inc.

During the past decade, two different methods of cell cycle analysis have been developed which are based on the fluorometric assessment of nuclear 5-bromodeoxyuridine (BrdU) incorporated during semiconservative DNA replication. Both methods have certain advantages over the traditional methods of assessment of cellular proliferation. One technique utilizes a monoclonal antibody as a probe for detection of BrdU incorporated into DNA [1]. Using flow cytometry, this method has been successfully combined with simultaneous measurement of total DNA content [2] and yields, after pulse labeling with BrdU, excellent estimates of S-phase cell fractions, replication rates, and even cell cycle traverse rates both in synchronous and in asynchronously growing mammalian cell cultures [3, 4]. The other method, applied first to cell proliferation by S. Latt, involves the detection of BrdU incorporation into DNA by virtue of the "quenching" of the fluorescence of bisbenzimidazole dyes such as 33258 Hoechst when bound to BrdU-substituted DNA [5, 6]. Although the latter technique has been applied to flow cytometry in a number of laboratories to differentiate between cycling and noncycling cells [7–16], the resolution previously achieved was insufficient for the demonstration of multiple cell cycles after mitogen stimulation. As illustrated in the present report, recent optimizations of the BrdU–Hoechst technique [15–17] enable a comprehensive analysis of cell activation and cycle progression that may have a variety of applications in cell biology, immunology, and medicine.

[1] To whom reprint requests should be addressed at: Pathology SM-30, University of Washington, Seattle, WA 98195.

Copyright © 1988 by Academic Press, Inc.
All rights of reproduction in any form reserved
0014-4827/88 $03.00

MATERIALS AND METHODS

Cell culture. The BrdU–Hoechst analysis was performed as previously described [15, 16]. In brief, peripheral blood lymphocytes (PBL) were obtained by Ficoll–Hypaque gradient separation of whole blood and washed in RPMI 1640 medium and aliquots of 1×10^5 lymphocytes/ml were incubated in RPMI 1640 medium with 16% fetal bovine serum (FBS), 180 μg/ml phytohemagglutinin (PHA; Wellcome) and 1.0×10^{-4} *M* BrdU. Addition of deoxycytidine (50 μ*M*) does not appear to be necessary for lymphocyte culture [17], but may be useful during culture of adherent cells [15]. At the indicated times cells were harvested, pelleted, resuspended in DMEM with 10% FBS and 10% DMSO, and stored at −20°C. For experiments with immunofluorescence, PBL were harvested, stained with phycoerythrin-conjugated monoclonal antibody (Becton–Dickinson) following the manufacturer's directions, washed, fixed in PBS with 30% (v/v) ETOH, and stored at 4°C.

Flow cytometry. For flow analysis, cells were thawed, pelleted, and resuspended at 5×10^5/ml in a solution of 0.154 *M* NaCl, 0.1 *M* Tris (pH 7.4), 0.5 m*M* $MgCl_2$ 0.2% BSA, 0.1% Nonidet-P40 and 1.2 μg/ml 33258 Hoechst. For two-parameter measurements [18], 1.5 μg/ml ethidium bromide (EB) was added 30 min after prestaining with Hoechst dye, and 15 min later the doubly stained cells were analyzed by an ICP-22 (Ortho Diagnostic Systems) interfaced to a PDP 11/23 microcomputer (Digital Equipment Corp.). Ultraviolet excitation (UG1 filter) was used with analysis of 33258 Hoechst fluorescence at 450–500 nm and EB fluorescence above 600 nm. The relative proportions of cells in successive cell compartments were calculated as described subsequently. For immunofluorescence/BrdU–Hoechst analysis, fixed cells were resuspended in the same buffer as above; after 30 min incubation, 5 μg/ml 7-amino actinomycin D (Calbiochem) was added. Cells were analyzed on a Model 50H cytofluorograf (Ortho Diagnostic Systems) using 100 mW uv excitation (351–364 nm) from an argon ion laser, with detection of 33258 Hoechst fluorescence at 420–500 nm. The spatially separated beam of a krypton ion laser, 150 mW at 531 nm, was used to excite PE and 7AAD, with fluorescence emission detected at 566–586 nm and above 620 nm, respectively. Data were collected and processed in list-mode on the Model 2150 computer (Ortho Diagnostic Systems).

THE BrdU–HOECHST CELL CYCLE HISTOGRAM

Figure 1 illustrates a temporal sequence of activation of human peripheral blood lymphocytes assayed by the BrdU–Hoechst fluorescence technique. Replication of DNA in the presence of BrdU results in BrdU substitution of thymidine; quenching of the 33258 Hoechst fluorescence of BrdU-substituted S- and G_2-phase cells (labeled BS and BG_2) results in reduced fluorescence of these cells. In contrast, the dye ethidium bromide (EB) does not exhibit BrdU-dependent quenching, and simultaneous staining with EB demonstrates increased fluorescence of S and G_2 phases on the EB axis simultaneously with the reduced fluorescence on the Hoechst dye axis [16, 18]. Following division of the BG_2 cells, the 33258 Hoechst fluorescence of the BrdU-substituted G_1 cells (Fig. 1*A*, labeled BG_1) is as little as 30% of that of the original G_1 cells. The magnitude of this quenching is dependent upon the degree of BrdU substitution, which in turn depends on the concentration of BrdU during cell culture, the AT/GC ratio of the target cell type [19], and the concentration of Hoechst dye [8, 16]. Although the relative intensities of 33258 Hoechst and EB fluorescence are altered by energy transfer and quenching, the separation of successive cell cycles and their interpretation is not affected. Figures 1*B* and 1*C* show that a second cell cycle in the presence of BrdU results in increased fluorescence of BBS- and BBG_2-phase cells, the increase being greater in EB than in 33258 Hoechst fluorescence emission (*B*). Division of BBG_2 cells results in a separate peak of BBG_1 cells closer to the origin (*C*); replication of these cells results in increased Hoechst and

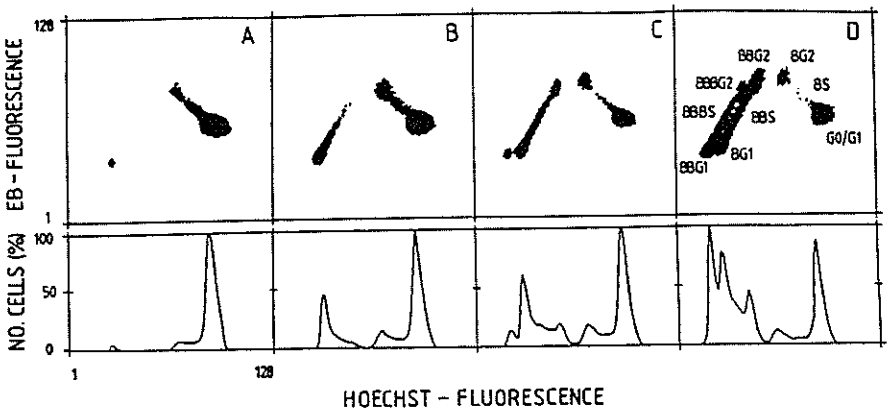

Fig. 1. 33258 Hoechst fluorescence (abscissa, top and bottom panels) and EB fluorescence (ordinate, top panels) of peripheral blood lymphocytes analyzed at (*A*) 36 h, (*B*) 46 h, (*C*) 60 h, and (*D*) 72 h after growth in the presence of PHA and BrdU. The bottom panels show histograms of the X-axis (Hoechst dye) projection of the bivariate displays shown above. Nomenclature of the three cell cycles displayed is indicated in (*D*), where the "B" prefix(es) indicate the number of rounds of replication in the presence of BrdU.

EB fluorescence, distinguishable from the second cycle by the lower Hoechst dye fluorescence of these cells in the third cycle (*D*).

DATA EXTRACTION

G_1, S, and G_2/M compartments of each of these three successive cell cycles can be quantitated by analysis of the respective regions of the one- or two-parameter data; Fig. 2 shows that analysis of the two-parameter data is facilitated by collapse of the two-dimensional region corresponding to a single cell cycle onto an axis parallel to that cell cycle distribution, followed by one-parameter cell cycle fitting by conventional methods [20] (the G_2/G_1 ratio is allowed to deviate from 2.0 but this does not affect the method of quantitation). Treated in this fashion, the sequence of panels displayed in Fig. 2 shows that this particular 72-h aliquot of a human peripheral blood lymphocyte culture has, respectively, 21.4, 24.2, and 54.4% of cells in the first, second, and third cycles. Within each cycle, the distribution of cells inthe G_1, S, and G_2/M compartments is derived by the conventional fittings, as shown in the panels of the bottom row. Furthermore, the cell cycle statistics obtained from the actual cells analyzed ("real data") can be readily converted to numbers which reflect the proliferative history of the cells originally placed in culture ("original data") by including a correction for division of cells which have divided once, twice, or more times [the number of cells in the second cycle (BG_1, BBS, BBG_2) is divided by two, the number in the third cycle (BBG_1, BBBS, $BBBG_2$) is divided by four, and the number in the fourth cycle, if any, is divided by eight. The proportions of "original" cells in each compartment are then normalized to the new total "original" cell number.] The time

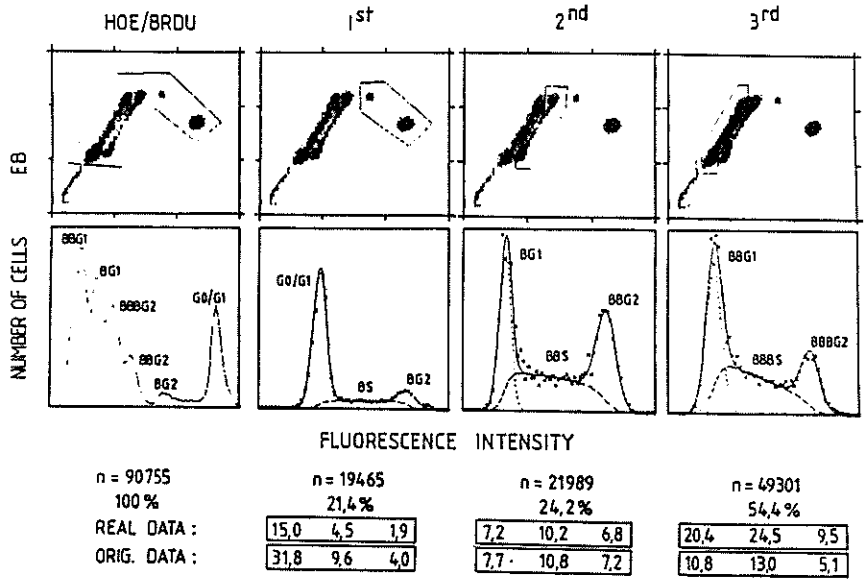

Fig. 2. Derivation of quantitative cell cycle and cell cycle compartment data from bivariate (Hoechst/ethidium bromide) dot plot displays. The top sequence shows data from the same 72-h lymphocyte culture partitioned into (from left to right) total, first, second, and third cycle cell fractions by indicating the respective regions of the bivariate plot using an interactive computer program. The data within the region were collapsed onto a single axis, after first rotating the axis to be parallel to the axis of the bivariate cell cycle within the region. The resulting one-dimensional histogram is deconvoluted into G_1, S, and G_2 compartments by conventional curve-fitting (bottom panels). At the bottom of the figure number-triplets within boxes give the percentages of cells in G_1, S, and G_2/M for cells in the first, second, and third cell cycle (from left to right), respectively. The data are expressed both as proportions of the cells present at the time of analysis ("real data") and as "original data" obtained by correction to reflect the proportions of cells originally placed in culture by accounting for the number of cell divisions undergone by cells in each of the enumerated cycles (see text). The latter figure is more easily interpretable in studies of cell cycle kinetics. n=number of cells analyzed.

required for the extraction of all of this information from a single 72-h lymphocyte culture sample is approximately 15 min distributed evenly between flow measurement and computer analysis.

BrdU-EFFECTS

It is, of course, essential that the method of analysis does not perturb the cell cycle progression. The effects of BrdU incorporation have been examined in human peripheral blood lymphocytes and no cell cycle perturbation is seen when cells are grown (in the dark) in medium containing up to 6.5×10^{-4} M BrdU [17]. In contrast, in human skin fibroblasts, concentrations above 10^{-5} M lead to cell cycle retardation and partial arrest in BG_1 and subsequent phases; concentrations below this level with the addition of deoxycytidine can, however, be used for cell cycle kinetic analyses up to the BG_1 phase, and thus, unlike most techniques, the G_2 to BG_1 transition can still be analyzed [21]. Immortal transformed lines which

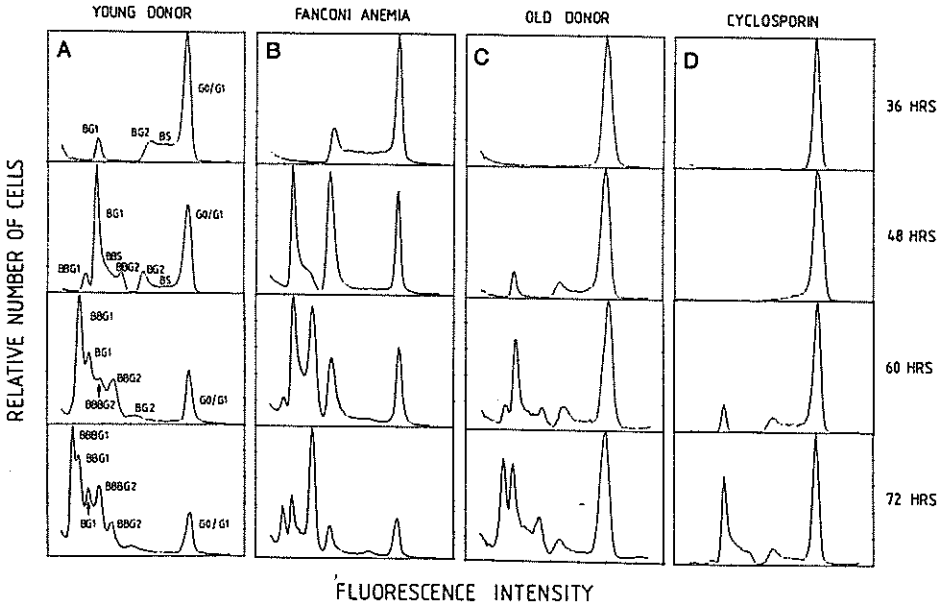

Fig. 3. Univariate 33258 Hoechst fluorescence histograms of peripheral blood lymphocytes from (left to right) a 3-month-old healthy donor, a 17-year-old patient with Fanconi anemia, and a 80-year-old donor, and cells from a 30-year-old donor treated with 0.1 μg/ml cyclosporin. Cells were analyzed at 36, 48, 60 and 72 h after growth in PHA and BrdU.

have been examined (e.g., Chinese Hamster ovary cells, murine spontaneously transformed cell lines, and human tumor lines) are more similar to lymphocytes in tolerating high BrdU concentrations with minimal effects on cell cycle progression (unpublished data).

THE KINETICS OF CELL CYCLE PROGRESSION

Discrimination of three sequential cell cycles over a serial time course provides a unique view of cell cycle kinetics. Figure 3 shows a comparison of the cell cycle progression of PBL cultured from a young donor (*A*), cells from a patient with Fanconi anemia (*B*), an elderly donor (*C*) and cells from a young donor treated with cyclosporin (*D*). Comparison of (*A*) and (*C*) readily demonstrates the qualitative differences between these representative donors of different ages: the lag-time before cells begin to enter S phase is longer in cells from donors of an older age, the rate of cell cycle progression of these cells is slower, and at later times a greater fraction of cells remains noncycling in G_0/G_1 [17]. Figure 3 *B* demonstrates that cells from patients with Fanconi anemia show a substantial arrest in both first and second cycle G_2 phases; thus the presumptive abnormality in DNA repair of these cells yields an observable cell cycle aberration even in the absence of DNA damaging agents [22]. In young cells treated with cyclosporin the principal feature is an extended delay before cell proliferation begins.

CELL CYCLE PHASE TRANSITION CURVES

The kinetic features of serial cell cycle studies are best visualized by quantitation of the cell cycle compartment distributions and graphic analysis of these data. Choice of a suitable model of cell cycle behavior together with computer fitting then permits extraction of the fundamental cell cycle parameters. We have previously demonstrated that the BrdU–Hoechst data can be analyzed in a manner analogous to the data derived by the BrdU-labeled mitosis method; plots of the proportion of cells in the first, second, and third cell cycle versus time are virtually identical by the two techniques [23]. Analysis of these curves can be used to derive interdivisional times [24, 25]. In contrast to the labeled-mitoses method, however, BrdU–Hoechst flow cytometry yields a greater quantity of information: this technique identifies not just the numerical order of the cell cycle of metaphase cells, but instead quantitates the G_1, S, and G_2 compartment distributions of each of three successive cycles of all interphase cells. Direct measurement of cell cycle compartment specific parameters and of information pertaining to progression-arrested cells is thus possible.

We have chosen to analyze the BrdU–Hoechst kinetic data in a fashion which recognizes the heterogeneity of cell cycle times within the population; such heterogeneity implies that estimates of only average cycle times can be incomplete or even misleading. Several models have been proposed to describe this heterogeneity, many of which functionally yield very similar distributions. One of the most widely referenced is that of Smith and Martin [26] who showed that the heterogeneity in time of onset of S phase and of interdivisional times can be explained as a consequence of a first order or exponential process in G_1. This model can be applied to BrdU–Hoechst kinetic data by making several modifications: addition of a normally distributed heterogeneity in the lag-time before the onset of the G_1 to S transition [26], provision for noncycling cells [15], and allowing for cell cycle compartment arrest [17]. Figure 4 shows data derived from experiments such as those shown in Fig. 3 plotted according to the above model. The percentage of cells remaining within a particular cell cycle phase or earlier is plotted semilogarithmically versus the time after stimulation with mitogen. These percentages were obtained by curve-fitting of the BrdU–Hoechst histograms as described earlier, and are corrected for cells having divided once, twice, or more times in order to obtain growth-independent values for each compartment. As shown by the computer fitted solid lines in Fig. 4, the above model provides an excellent correspondence to the data. Each such line is a distribution curve for the times of transition from one compartment (as labeled) to the next. The similarity in transition rates (slopes) of the sequential exit curves in these panels may be explained if a single first order process which occurs in G_0/G_1 is the major source of intercellular variability in cell cycle times. Alternative models which also fit these data have been discussed [17]. Analysis of these data provide the following information: (1) G_0/G_1 lag phase and minimum compartment durations (determined by the time between intercepts with the time axis of successive compartment exit curves); (2) the mean duration of the cell cycle phase, given by the sum of the fixed minimum compartment length and the mean duration of the

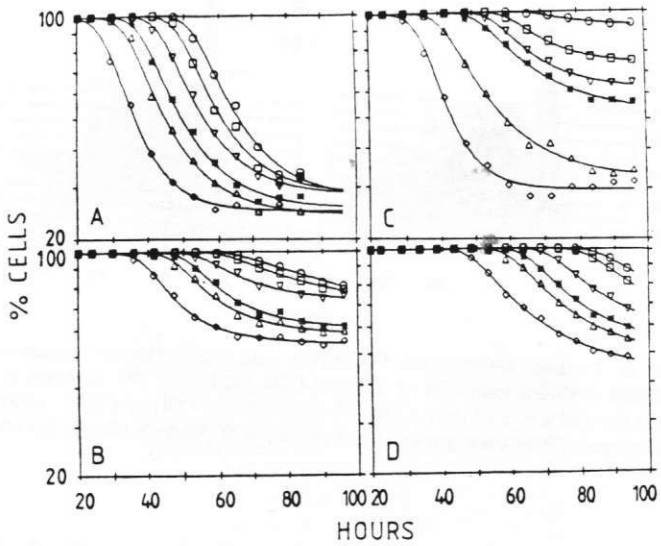

Fig. 4. Cell cycle compartment exit curves derived from BrdU–Hoechst analysis of (*A*) young (3-month-old donor); (*B*) old (80-year-old donor); (*C*) Fanconi anemia (17-year-old); and (*D*) cyclosporin-treated (0.1 μg/ml) cells. In each panel, the exit from G_0/G_1 (◊), BS (△), BG_2 (*), BG_1 (▽), BBS (□) and BBG_2 (○) phases are shown. The solid lines indicate the least-squares fit according to the modified Smith and Martin model.

additional variable component (given by the reciprocal of the transition rate); (3) transition rates from one compartment to the next for cells which are not arrested in the compartment (slope of the exit curve); and (4) compartment-specific cell cycle arrest (determined by the difference of the plateau phase levels between successive exit curves, as extrapolated by the computed fit).

CELL CYCLE PARAMETERS

The cell cycle parameters derived from the data shown in Fig. 4 are listed in Table 1. Comparison of these parameters of PBL from representative young and old donors shows several of the features recently described [17]; cells from older donors have a substantial delay in the onset of G_1 phase exit, and the rate of the G_1- to S-phase transition is lower. In addition, while PBL from the young donors show little or no arrest in subsequent cell cycle phases (the transition curves have plateaus which differ by at most several percent), cells from elderly donors show S and G_2 and subsequent G_1 (BG_1) phase arrests. The mechanism(s) of such arrest may relate to increased sensitivity of PBL from older donors to DNA damage, or defective DNA repair, as previously postulated on the basis of sensitivity to effects of [^{3}H]thymidine [27]. A representative result of analysis of PHA-stimulated PBL from a patient with Fanconi anemia is shown in Fig. 4*C* and compared with the results from the other donors in Table 1. The distinctive feature of the cell cycle in this genetic disease, even in these cells not treated with DNA

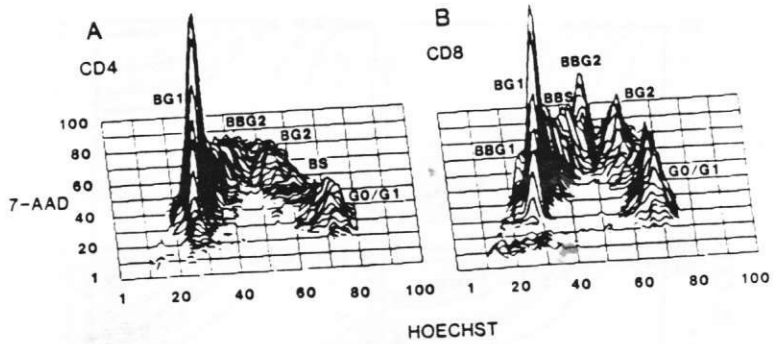

Fig. 5. Analysis of 7-amino actinomycin D (7AAD) and 33258 Hoechst fluorescence of cells simultaneously labeled with PE-anti-CD4 or PE-anti-CD8 antibody. The analysis is gated on PE fluorescence so that the cell cycle of only $CD4^+$ "helper/inducer" (*A*) or $CD8^-$ "cytotoxic/suppressor" cells (*B*) is displayed. Cells were grown in the presence of PHA and BrdU for 60 h.

damaging agents, is a large arrest of cells in the G_2 phase of the first cell cycle, and to some degree in the second cycle as well [22]. There is, in addition, a lengthening of the minimum length of the G_2 phase and a lower transition rate out of S and G_2 phases (compared to the G_0/G_1 exit rate), and thus, a lengthening of the mean S and G_2 compartment durations. This provides an example of how this technique distinguishes, and quantitates separately, cell cycle prolonging and arresting effects; information which is not derived by alternative techniques. Fig. 4*D* and the corresponding section of Table 1 demonstrate that the principal effects of cyclosporin upon PBL cell kinetics are a delay of G_0/G_1 exit (16 h longer than the young control and 5 h longer even than PBL from the elderly donor). Other effects noted are an increased proportion of noncycling (G_0/G_1 blocked) cells, reduced G_0/G_1 transition rates, and an increase in the minimum S-phase compartment length. It is evident from this single example that studies of drug-related cell cycle perturbations could benefit from the use of the BrdU–Hoechst technique.

APPLICATIONS TO IMMUNOLOGY

The BrdU–Hoechst technique is amenable to an analysis which combines identification of immunophenotypes (by use of immunofluorescent monoclonal antibodies) with the measurement of cell activation. Growth of lymphocytes in BrdU, followed by immunofluorescent labeling, then cell permeabilization by ethanol fixation allows the simultaneous detection of the immunofluorescent label and BrdU–Hoechst-quenched cell cycle analysis. Figure 5 shows the analysis of cells labeled with phycoerythrin (PE)-labeled anti-CD4 antibody or PE anti-CD8 antibody simultaneously with 33258 Hoechst fluorescence (BrdU-quenched) and 7-amino actinomycin D (7AAD) fluorescence (non-BrdU-quenched DNA fluorescence). As with the use of ethidium bromide, the 7AAD fluorescence aids in separation of G_1, S, and G_2 phases of each cell cycle. This dye has fluorescence

TABLE 1

Compartment durations, transition rates, and compartment arrest computed from x-axis intercepts, slopes, and extrapolated plateau regions of Fig. 4

Condition / Age	Young 3 months	Elderly 80 years	Fanconi 17 years	Cyclosporin 30 years
Minimum compartment duration (h)				
G_0/G_1	27.5±0.8	38.5±0.9	34.1±1.0	42.2±1.5
S	6.4±0.4	8.8±0.5	6.2±0.4	10.3±0.6
G_2	4.5±0.4	3.7±0.2	10.7±0.5	3.8±0.1
BG_1	6.4±0.6	3.7±0.2	4.4±0.2	7.5±0.2
Transition rates (percent/h)				
G_0/G_1	5.8±0.7	4.2±0.6	6.5±1.0	2.1±0.37
S	4.3±0.5	3.7±0.8	3.3±0.3	1.6±0.32
G_2	4.4±1.0	4.2±1.3	2.8±0.4	1.1±0.25
BG_1	5.0±1.2	1.9±0.3	3.7±0.6	0.5±0.02
Compartment arrest (%)				
G_0/G_1	22.5±0.6	55.4±0.8	29.1±0.6	43.8±2.8
S	0.0	2.5±0.3	2.7±0.1	1.0±0.1
G_2	1.3±0.1	3.9±0.5	19.5±1.0	7.0±1.6
BG_1	3.4±0.2	5.6±0.8	9.6±0.6	0.0

emission characteristics which allow simultaneous quantitation of 7AAD and PE fluorescence when excited by a single laser [28]. The immunofluorescence intensity was used for a gated analysis of the cell cycle: the cell cycle distribution of only $CD4^+$ cells is shown in Fig. 5*A*, and the cell cycle distribution of $CD8^+$ cells is shown in Fig. 5*B*. This example demonstrates that a greater proportion of $CD4^+$ cells leave the G_0/G_1 phase when stimulated with PHA. This is consistent with results obtained previously with sorted populations of $CD4^+$ and $CD4^-$ cells [29]. The figure also demonstrates, however, that of those $CD8^+$ which do cycle, some have progressed through the cycle (to BBS, BBG_2, and BBG_1 phases) more rapidly than $CD4^+$ cells. Use of simultaneous immunofluorescence analysis with the BrdU–Hoechst technique should open a fruitful area of investigation by allowing the sophistication of this cell cycle approach to be applied to analysis of antibody-defined functional subsets.

CONCLUSION

The above descriptions demonstrate that BrdU–Hoechst flow cytometry offers a unique view of the quantitation of cell proliferation. This analysis is rapidly performed and provides considerably greater information than radioactive thymidine uptake or even conventional flow cytometry. Since these studies can be performed on any flow cytometer having uv excitation capabilities, it is hoped

that this presentation will stimulate the more widespread use of this new approach to the studies of mitogen response and the cell cycle.

Supported by NIH Grant AG01751 and DFG Grant 849/2-1.

REFERENCES

1. Gratzner, H. G. (1982) *Science* **218**, 474.
2. Dolbeare, F., Gratzner, H., Pallavicini, M., and Gray, J. W. (1983) *Proc. Natl. Acad. Sci. USA* **80**, 5573.
3. Dean, P. N., Dolbeare, F., Gratzner, H., Rice, G., and Gray, J. W. (1984) *Cell Tissue Kinet.* **17**, 427.
4. Gray, J. W., and Mayall, B. H. (Eds.) (1985) Monoclonal Antibodies against Bromodeoxyuridine. A. R. Liss, New York.
5. Latt, S. A. (1973) *Proc. Natl. Acad. Sci. USA* **70**, 3395.
6. Latt, S. A., Stetten, G., Juergens, L. A., Willard, H. F., and Scher, C. D. (1975) *J. Histochem. Cytochem.* **23**, 493.
7. Latt, S. A. (1977) *J. Histochem. Cytochem.* **25**, 927.
8. Latt, S. A., George, Y. S., and Gray, J. W. (1977) *J. Histochem. Cytochem.* **25**, 927.
9. Bohmer, R. M. (1977) *Cell Tissue Kinet.* **12**, 101.
10. Nusse, M. (1981) *Cytometry* **2**, 70.
11. Beck, H. P. (1981) *Cytometry* **2**, 170.
12. Noguchi, P. D., Johnson, J. B., and Brown, W. (1980) *Cytometry* **1**, 390.
13. Sekaly, R. P., Ceredig, R., and MacDonald, H. R. (1983) *J. Immunol.* **131**, 1085.
14. Sekaly, R. P., MacDonald, H. R., Nabholz, M., Smith, K. A., and Cerottini, J. C. (1984) *J. Cell Physiol.* **121**, 159.
15. Rabinovitch, P. S. (1983) *Proc. Natl. Acad. Sci. USA* **80**, 2951.
16. Kubbies, M., and Rabinovitch, P. S. (1983) *Cytometry* **3**, 276.
17. Kubbies, M., Schindler, D., Hoehn, H., and Rabinovitch, P. S. (1985) *J. Cell Physiol.* **125**, 229.
18. Bohmer, R. M., and Ellwart, J. (1981) *Cytometry* **2**, 31.
19. Kubbies, M., and Friedl, R. (1985) *Histochemistry* **83**, 133.
20. Dean, P. N., and Jett, J. H. (1974) *J. Cell Biol.* **60**, 523.
21. Vogel, D. G., Rabinovitch, P. S., and Mottet, N. K. (1986) *Cell Tissue Kinet.* **19**, 227.
22. Kubbies, M., Schindler, D., Hoehn, H., Schinzel, A., and Rabinovitch, P. S. (1985) *Amer. J. Hum. Genet.* **37**, 1022.
23. Kubbies, M., Schindler, D., Hoehn, H., and Rabinovitch, P. S. (1985) *Cell Tissue Kinet.* **18**, 551.
24. Tice, R. R., Schneider, E. L., Kram, D., and Thorne, P. (1979) *J. Exp. Med.* **149**, 1029.
25. Morimoto, K., and Wolff, S. (1980) *Nature (London)* **228**, 604.
26. Smith, J. A., and Martin, L. (1973) *Proc. Natl. Acad. Sci. USA* **70**, 1263.
27. Staiano-Coico, L., Darzynkiewicz, Z., Hefton, J. M., Dutkowski, R., Darlington, G. J., and Weksler, M. E. (1983) *Science* **219**, 1335.
28. Rabinovitch, P. S., Torres, R. M., and Engel, D. (1986) *Immunology* **136**, 2769.
29. Reinherz, E. L., Kung, P. C., Goldstein, G., and Schlossman, S. F. (1979) *Proc. Natl. Acad. Sci. USA* **76**, 4061.

Received February 13, 1987
Revised version received August 6, 1987

Printed in Sweden

Zusätzliche Literatur

1. Poot M., A.Schuster, H.Hoehn: (1991) Cytostatic synergism between bromodeoxyuridine, bleomycin and chlorambucil, demonstrated by a sensitive cell kinetic assay. Biochemical Pharmcology **41**, 1903-1909

2. Poot M., K.Kausch, J.Köhler, Th.Haaf, H.Hoehn: (1990) The minor-groove binding DNA-ligands Netropsin, Distamycin A and Berenil cause polyploidisation via impairment of the G2 phase of the cell cycle. Cell Struct.Funct. **15**, 151-157

IMMUNZYTOMETRIE UND

ZELLSORTIERUNG

Prof.Dr.A.Radbruch, B.Mechtold

Institut für Genetik
der Universität
Köln

3 Immunofluorescence: Basic Considerations

A. RADBRUCH

3.1 Background

Immunofluorescence involves the staining of cells with antibodies and other specific ligands directly or indirectly labeled with fluorescent dyes. This offers fascinating possibilities for the characterization of cells according to the expression of protein or polysaccharide markers specific for differentiation or activation stages. A few basic considerations will help one to understand the important parameters and to optimize the specificity and sensitivity of immunofluorescence staining. Of the three steps in immunofluorescence analysis–staining, measurement, and data evaluation–the first, preparation of cells and staining, is probably most important and therefore receives the most attention.

3.2 Staining

3.2.1 Preparation of Cells

As a matter of principle, the manipulation of cells should be kept to a minimum because of the risk of introducing artifacts. However, since flow cytometry requires single-cell suspensions, and cells are analyzed one by one, it is obvious that attached or connected cells must be individualized either mechanically or enzymatically. Care must be taken that the enzymes used for separating the cells do not attack the antigens to be analyzed later. Other manipulations frequently used are preenrichment of rare cells and fixation of stained cells prior to analysis to avoid phenotypic changes and to minimize the risk of infection.

Natural single cell suspensions, such as blood or bone marrow, can be stained without any further manipulation of the sample. Most present protocols, however, include preenrichment steps, for example, the depletion of erythrocytes for analysis of leukocytes from blood. This saves reagents due to the smaller staining volume and improves discrimination of rare cells and may also remove dead cells and other cells that could be stained unspecifically. Preenrichment procedures such as density gradient centrifugation, lysis, and magnetic cell sorting are discussed in detail in Chaps. 14 and 15. In choosing a method for preenrichment, however, one

should keep in mind that this is a manipulation which may also affect the cells to be analyzed, especially if the cells are from pathological rather than normal conditions.

3.2.2 Direct Versus Indirect Staining

Direct staining with fluorochrome-conjugated antibodies against specific cellular determinants is preferable, if possible, at least for routine use. Manipulation of cells is minimized, the staining is easy to control, and it allows the combination of several markers for multiparameter analysis, mixing the various staining reagents in one staining step. Conjugation of even small amounts of purified antibodies with fluorochromes is fast and easy to perform in any laboratory (see Chap. 2).

For „negative" control–usually antibodies of the same class, conjugated to the same fluorochrome as the specific antibody but binding to an irrelevant antigen–are used to stain another aliquot of the cells (isotype control). Although „state of the art", this is not a very good control because it is dependent on the quality of the conjugation. A „cellular control" is preferable, using the specific antibody to stain cells not expressing the antigen. In heterogeneous cell populations, such as blood cells, negative cells are usually present and can be compared to unstained cells to evaluate background staining. Cells expressing the antigen in question should be used as „positive" control.

Indirect staining with unconjugated antibodies against specific cellular determinants, detecting the antibodies with second, fluorochrome-conjugated, generally polyclonal anti-antibodies, must be used if the first antibody cannot be purified. Control of indirect staining is not trivial, and multiparameter analysis is even less so. Combination of several parameters requires highly purified isotype-specific second antibodies or complete blocking of the free binding sites of the second antibody before staining of the next parameter, i.e., increasing the number of staining steps from one to four or more. Every reagent used for staining or blocking must be controlled independently in the way indicated above, and in case of cross-reactions of the polyclonal second antibodies may require extensive absorptions on cells or immobilized proteins.

An advantage of indirect over indirect staining is that it can be used to improve the sensitivity of detection since several second antibodies may bind to one first antibody, thus increasing the number of fluorochromes per specific antigenic determinant. A further increase in sensitivity can be obtained if the first antibody is conjugated to the same fluorochrome as the second. High-specificity and sensitive, easy-to-control indirect staining is obtained with first antibodies conjugated to haptens such as nitro-iodophenylacetyl, digoxigenin, or biotin, detected with fluorochrome-conjugated hapten-specific second antibodies or avidin. The biotin/streptavidin system has the advantage of readily commercially available streptavidin conjugates, not only for immunofluorescence but also for

histochemistry or serology. Also, it is easy to conjugate even small amounts of purified antibodies (>100 μg) quantitatively to biotin (Chapter 2).

3.2.3 Staining Parameters: General Considerations

Standardization of concentrations of cells and antibodies is required to obtain reproducible results. Concentrations should be low to support specific high-affinity antigen-antibody interactions over low-affinity cross-reactions but high enough to obtain staining as bright as possible. Manipulation of cells should be kept to a minimum, i.e., the number of staining and washing steps should be as low as possible to avoid loss and damage of cells.

3.2.4 Concentration of Cells

Cell number and concentration should always be chosen to allow staining at the optimal concentration of cells and antibodies, determined by titration beforehand. The lower limit is approximately 10^5 cells in 10 μl since about 10^5 cells are required for flow cytometric analysis, recording 10^4 cells. The lower limit of volume for staining is 10 μl since after washing of the cells a few microliters of washing fluid always remains in the tube, changing the concentration of the staining antibody in an unpredictable way. We use staining volumes not of 10 but of 20–100 μl with 0.2–1x10^7 cells, i.e., cell concentrations of 10^8 per milliliter. For staining of larger numbers of cells the volume and not the concentration of cells or stain should be increased. In principle, all cell concentrations refer to the number of positive cells, and changes in volume due to additional negative, nonstainable cells can be neglected. For the staining of rare cells, however, the volume of negative cells must be taken into consideration in determining the optimal concentration of cells and stain.

3.2.5 Concentration of Staining Reagents

Staining reagents should always be titrated. Titration helps to save reagents and to optimize the staining itself. Concentrations that are too low will result in poor discrimination between positive and negative cell populations, i.e., overlapping populations (see below), making statistical evaluation difficult or impossible. Concentrations that are too high lead to unspecific staining of negative cells or subpopulations on the basis of low affinity cross-reactions.

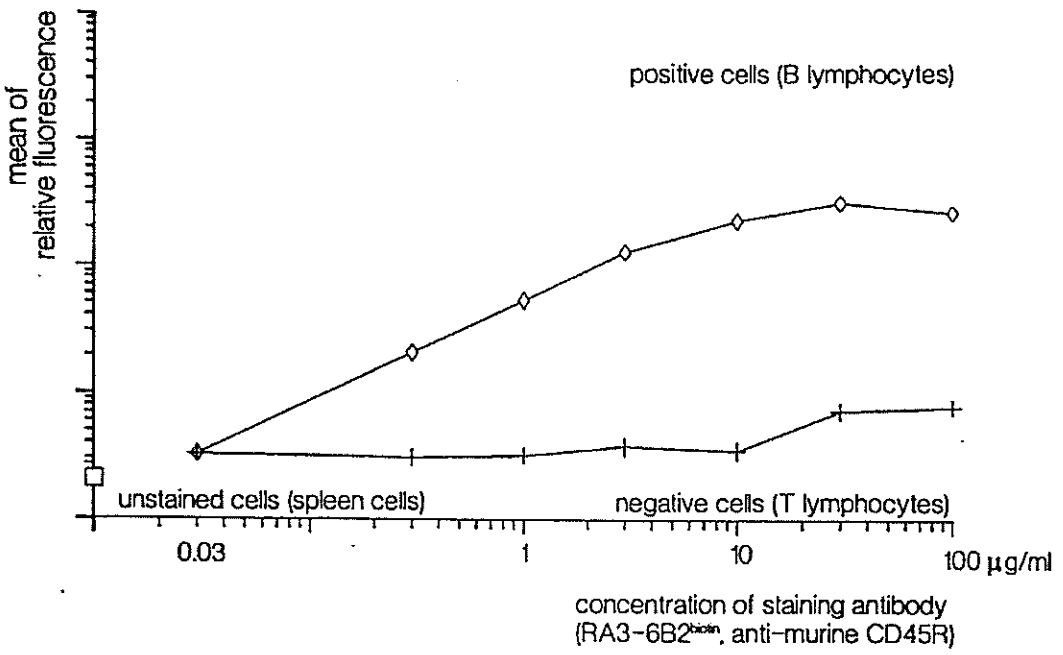

Figure 1. Titration of staining reagents for flow cytometry. RA3-6B2^{biotin} (anti-murine CD45R) was titrated on murine spleen cells, staining 2x10^6 cells in 20 µl staining reagent at concentrations as indicated for 10 min, washing once, then staining with streptavidin-fluorescein at 3 µg/µl, 20 µl for 2x10^6 cells for 10 min on ice, washing once, and analyzing in a FACScan flow cytometer. Murine B lymphocytes, about 50% of the lymphocytes in spleen, are positive for CD45R; T lymphocytes, the other 50% of lymphocytes, are not. For statistical evaluation, gates were set between positive and negative populations, and the mean of relative green fluorescence was determined for the gated populations by FACScan research software (Becton-Dickinson) and plotted versus the concentration of staining reagent. At 0.1 µg/ml positive and negative populations were overlapping and thus not evaluated. The optimal concentration of RA3-6B2^{biotin} is 10 µg/ml for 10^6 cells (50% of 2x10^6 cells, i.e. positive B lymphocytes) stained in 20 µl. For staining of higher cell numbers, the volume must be scaled up linearly, not the concentration. (Data from G. von Hesberg and A. Radbruch, Cologne)

Titration can be performed by flow cytometry (Fig. 1), staining a mixture of positive and negative cells under standardized conditions at given concentration of cells, volume, time, and number of washing steps, with varying concentrations of the staining reagent to be titrated. The mean fluorescence of positive and negative populations is then plotted against the concentration of the staining reagent. The optimal concentration of the staining reagent is usually the concentration at beginning of the plateau of saturation. It is sometimes useful to employ lower concentrations, for example, in case of problems with cross-reactions, or higher concentrations, such as in case of low antigen density.

3.2.6 Staining Time

High-affinity antigen-antibody reactions occur fast, while longer staining times favor low-affinity cross-reactions or adsorptions. Thus, staining times should be as short as possible. Most staining reagents reach about

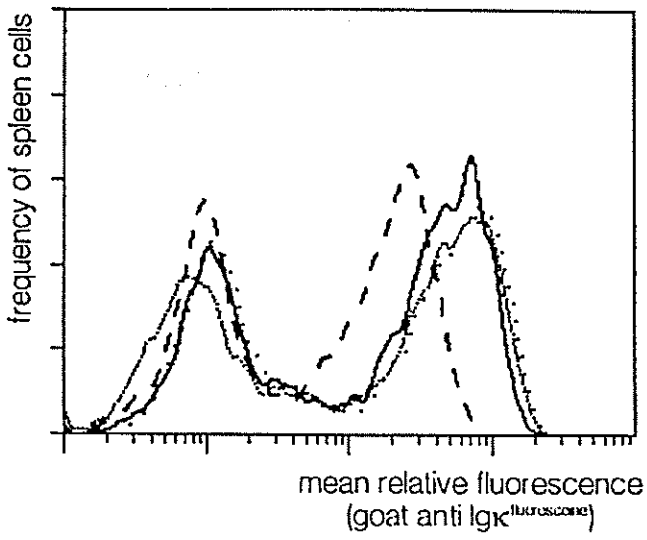

Figure 2. Determination of staining time. Murine spleen cells were stained with fluorescein-conjugated goat anti-murine immunoglobulin κ light chains, labeling most of the B lymphocytes, i.e., about 50% of the spleen cells. At defined time intervalls, aliquots were removed, diluted (see following figure), and immediately analyzed at log amplification in a FACScan flow cytometer. The smoothed fluorescence histograms (number of cells versus fluorescence intensity) of various time points are overlaid to illustrate the differences in staining intensity. After only 1 min positive and negative populations are separated. Maximum staining intensity is reached at about 5 min. Thus, for polyclonal antibodies a staining time of 10 min is generally sufficient. Longer staining times do not improve the staining intensity but support low-affinity cross-reactions. For monoclonal antibodies, in the case of low affinity, the optimal staining time may have to be prolonged, as should be determined in a test staining such as that shown here. For cytoplasmic staining with antibodies or other proteins, the staining (and washing) times must be much longer, 1 h or more, depending on the fixation and the size of the cells, since the staining reagents must penetrate the fixed cytoplasm (see Chap. 5). – –, 1 min; ——, 5 min; - - -, 15 min; · · · ·, 30 min

90% maximum logarithmic staining after 1–5 min (Fig. 2). Doubling the time for safety reasons gives a standard staining time of 10 min. Staining of cytoplasmic parameters of fixed cells (Chap. 5) requires longer times because the staining reagents must diffuse through the cytoplasm. Staining and washing times of about 1 h are adequate for intracellular immunofluorescence. Staining times must also be prolonged if antibodies are not used but rather antibodies conjugated to large particles, such as liposomes or Dynabeads.

3.2.7 Staining Temperature

Staining of live cells at 4°–12°C („on ice") minimizes physiological influences. At room temperature or 37°C most cells are able to modulate expression of the antigenic receptors, especially if these are cross-linked by (staining) antibody. Lymphocytes can „cap" their receptors with the staining antibodies, throw off the cap into the medium, and appear „negative" then. Capping can be inhibited by sodium azide (0.03% in the staining medium), which reversibly blocks cell physiology.

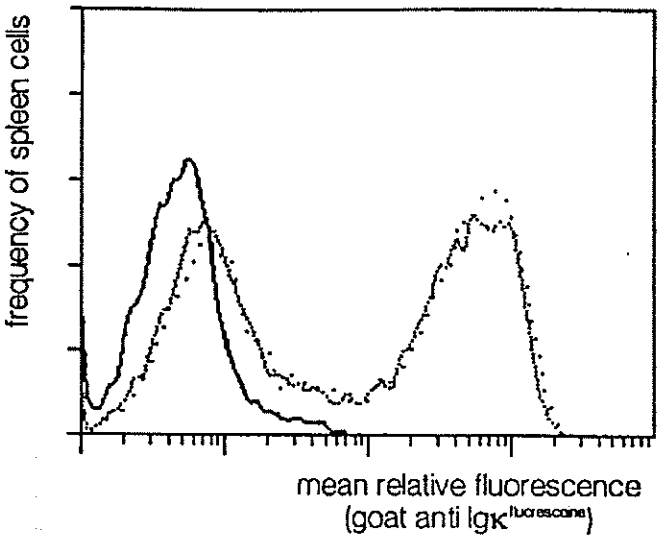

Figure 3. Minimizing washing steps. Murine spleen cells were stained with fluorescein-conjugated goat anti murine immunoglobulin κ light chains, as described for the preceding figure. Cells were either not washed at all, diluted only 1:50 for analysis, or washed once, i.e., diluted 1:50, spun down, the supernatant removed completely, and the cell pellet resuspended in fresh buffer. The cells were then analyzed at log amplification in a FACScan flow cytometer. The smoothed fluorescence histograms (number of cells versus fluorescence intensity) are overlaid to illustrate the differences in staining intensity. Since diluted and washed samples show similar fluorescence distributions, washing is actually not required in this particular system. In most staining systems, washing once is sufficient. Further washing steps do not improve the quality of the staining but result in loss of cells. As many as 10% of cells can become lost per washing step.
——, Cells not stained; - - -, stained cells, diluted; · · · ·, stained cells, washed once

3.2.8 Washing

Like all other manipulations, washing should be restricted to the minimum. Washing–removal of unbound antibodies by centrifugation of the cells, removal of the supernatant, and resuspension of the cells in fresh medium–always leads to a loss in cell numbers, frequently those of selective subpopulations of small or less dense cells. Even under optimal conditions, 10% of cells can be lost per washing step. When the staining is performed with titrated, i.e. low concentrations of antibodies, one washing step is usually sufficient (Fig. 3). For indirect staining, washing twice efficiently prevents reaction of the first reagent with the second one in solution, which would result in suboptimal staining.

3.2.9 Fixation

Like all other manipulations, fixation may have unpleasant side effects. One such side effect is that it becomes difficult to distinguish cells that were dead before staining and therefore stain unspecifically. Such cells are easy to display in live material by propidium iodide staining. After fixation they can be identified only according to scatter and staining with LDS 751, which is not very easy (Chap. 4). For analysis of rare cells, the distinction between rare positive cells and unspecifically stained dead cells is crucial. Such samples are best analyzed unfixed, in the presence of propidium iodide, gating out dead cells according to scatter and propidium iodide fluorescence (Chap. 17).

Nevertheless, for routine analysis of subpopulations cells are usually fixed to limit the risk of infection and to standardize conditions of analysis. For staining of cytoplasmic and nucleic antigens, fixation is obligatory because otherwise the staining antibodies cannot penetrate the cell membrane.

Standard fixation for immunofluorescence is fixation with 0.5%–2% formaldehyde. Since this fixation does not preserve nucleic acids very well, for analysis of RNA or DNA (e.g., of sorted cells) fixation with 70% methanol or ethanol/acetic acid (95/5) should be preferred. For staining of cytoplasmic or nucleic antigens in formaldehyde fixed cells, permeabilization of the membranes is required, for example by 0.1% NP40 or 0.5% saponin (Chap. 5).

3.3 Measurements

From its beginning, flow cytometry has required a certain technological effort; however, the days of self-made machines are now a thing of the past. Today, several manufacturers offer state-of-the-art equipment at prices comparable to those of good microscopes. Analysis of forward and orthogonal scatter and three fluorescence light parameters per cell is now standard. At first sight, five parameters may seem too many for most applications; however, every additional parameter opens new possibilities, for example, increasing the resolution of „gating," i.e., the preselection of cells for analysis according to staining with vital dyes or immunofluorescence. This is extremely important for the analysis of rare cells, enabling, for instance, the direct analysis of leukocytes stained in blood without any further manipulation if the leukocytes are preselected electronically (gated) not only by scatter but also by immunofluorescence (e.g., according to CD45 staining).

Most modern flow cytometers are stably aligned, which had been a problem in the early days and remains so for the flow-in-air cell sorters. They are also easy to operate. Calibration (optimization of sensitivity) and compensation (correction of fluorescence overspill; Chap. 1) are performed semiautomatically with the help of standard particles. Measurement and data storage constitute no problem. Preselection of cells during measurement (live gating) is a dangerous option and should be used only with caution. Live gating always results in loss of information because not all cells of the sample are analyzed. In basic research and clinical routine this may lead to misinterpretation of unexpected and pathological situations.

While the intensity of the light scatter of cells is analyzed on the basis of linear amplification, the intensity of immunofluorescence is analyzed upon logaithmic amplification (Fig. 4). The reason is that logarithmic amplification over four decades which is state-of-the-art technology, allows one to use a single gain, i.e., the same machine settings for up to 10 000-fold differences in fluorescence, which is about that which can be observed with present-day staining technology. Thus, relative fluorescence of various

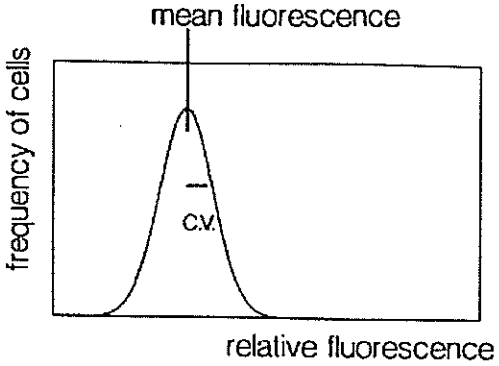

Figure 4. Mean fluorescence and CV. In flow cytometric analysis of immunofluorescence, the cells (usually 10 000) are classified according to relative, logarithmically amplified fluorescence intensity in 256, 512, or 1024 channels, depending on the setup of the machine. Due to variation in the cells and in the measurement a population of homogeneously stained cells is distributed symmetrically around a mean value of relative fluorescence (arithmetic mean for linear amplification, geometric mean for logarithmic amplification), with a dispersion described as coefficient of variation (CV, standard deviation divided by the mean and multiplied x 100). (Histogram produced by computer simulation by K.L. Meyer)

cells can be compared directly. Also, the variation in staining upon logarithmic amplification resembles that of a gaussian normal distribution, which makes it easier to analyze the fluorescence distributions (see below). Finally, logarithmic amplification emphazises the biologically usually more important differences between cells expressing little antigen, while differences between cells expressing a great amount are neglected.

3.4 Data Evaluation

3.4.1 Gating

In flow cytometric analysis all available optical parameters of a particle are recorded if the forward scatter light of this particle exceeds a preset threshold value (trigger). In principle, every other parameter can be used as well to trigger the analysis. For data evaluation, further constraints can be put on the particles to be analyzed, setting lower and upper thresholds for other parameters. This electronic preselection (gating) is used to exclude unspecifically stained particles from analysis (e.g., dead cells or debris) or to enrich rare cells electronically to obtain better statistics.

Gating can be risky if the cells behave abnormally, for example, in pathological situations. Thus, gating requires substantial expertise and can result in unfortunate mistakes. Since gating parameters and gates are frequently not documented, these mistakes are hard to identify. In any case, establishing gates should be controlled by staining of independent parameters, a further advantage of the additional parameters available on modern machines. This control should be obligatory for the definition of „standard" gates, such as the lymphocyte scatter gate, which can easily be controlled by CD45 staining as all $CD45^+$ cells and only these should fall into the scatter gate. If no „independent" parameters are available, gates could be verified by cell sorting, sorting out gated cells and analyzing them by microscope or any other suitable method.

3.4.2 Plotting of Data

From the multitude of data plots available, only a few are relevant for immunofluorescence (Fig. 4). One-dimensional histograms are best suited for illustrating the logarithmically amplified intensity of staining (mean fluorescence and coefficient of variation, CV), i.e., for emphazising the quantitative aspects of flow cytometry. Two-dimensional plots (Fig. 5),

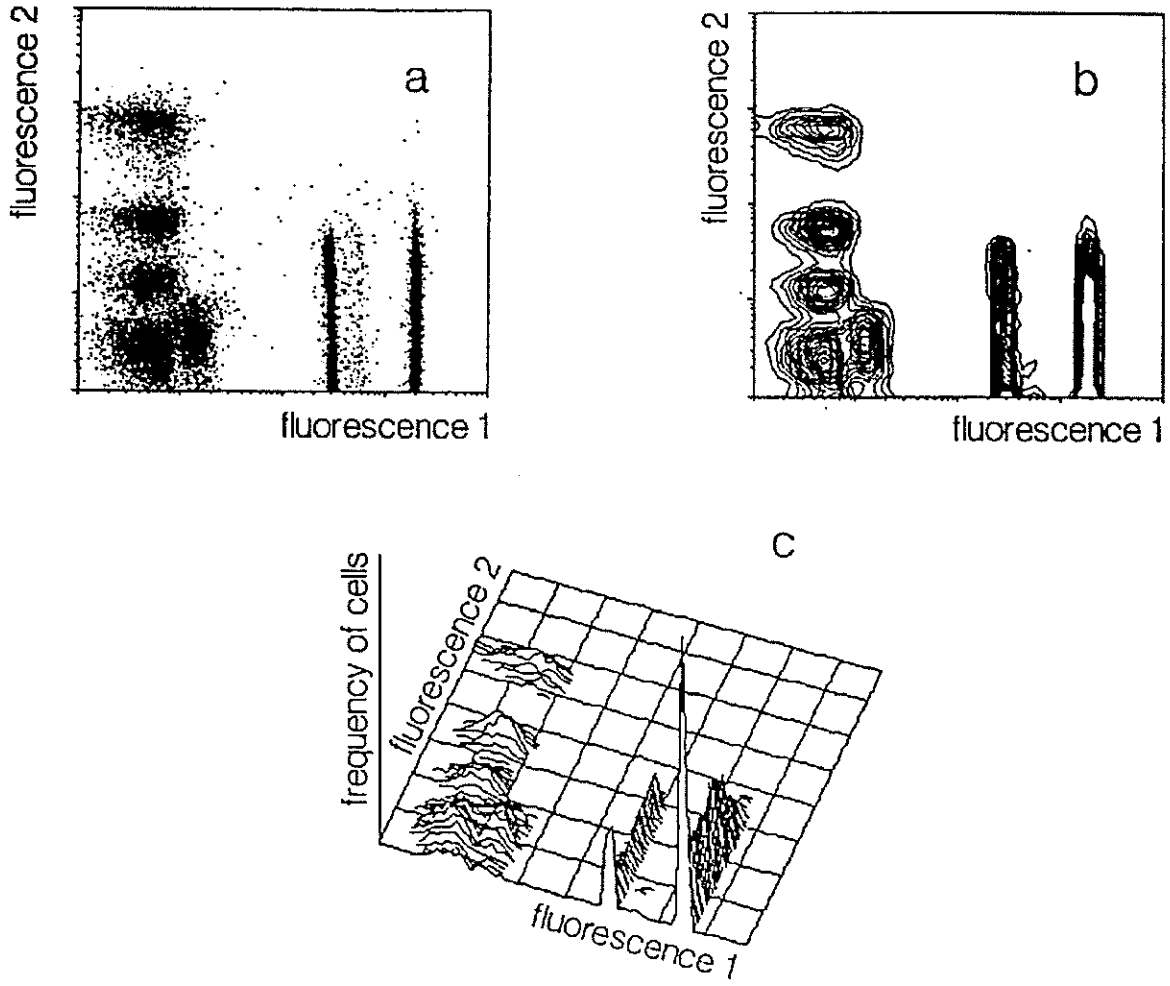

Figure 5. Multiparameter displays in immunofluorescence. For correlated display of two immunofluorescence parameters either dot plot (a) or contour plot (b) are most commonly used. In the dot plot (a) every cell is displayed as a dot according to its classification for intensity of fluorescence 1 and 2 in the coordinates of fluorescence 1 (x-axis) and 2 (y-axis). Cells with the same intensities are superimposed. This makes the dot plot the display of choice for analysis of rare cells, while large cell populations are not well resolved. Contour plots are derived from dot plots by delineating areas of equal density, either linearly, as shown here (1% linear) or logarithmically, or according to probability ([1] Chap. 30). Contour plots are the display of choice for analysis of populations of frequent cells, giving high resolution even if the populations are not well separated by staining. The three-dimensional histogram (c) tends to confuse more than to clarify. It is useless for illustration. The data shown here were obtained from analysis of a mixture of beads from Flow Cytometry Standards Corporation on a FACStar$^+$, evaluated with Lysis II software. Seven beads were used, containing no fluorochrome, 1.1×10^4 fluorescein equivalents (fe), 5.1×10^4 fe, 4.6×10^5 fe, 5.6×10^4 phycoerythrin equivalents (pe), 10^5 pe and 10^6 pe. Such mixtures of beads should be routinely used to check and align sensitivity and compensation of flow cytometers (see Chap. 1)

either as dot or as contour plots, give a better impression of the interrelated expression of two parameters per cell. In a dot plot, every cell is plotted as a dot according to the intensity of its staining between the coordinates of the two parameters. Rare cells are emphasized and frequent cells are not, because areas with many cells appear merely black, and subpopulations are not resolved. Delineating areas that contain classified frequencies or numbers of cells between the coordinates of the two parameters results in contour plots, which tend to give a detailed and graphic picture of densely populated areas while rare cells can become lost. Three-dimensional plots, like three-dimensional histograms or three-parameter dot plots (clouds) are seldom used in immunofluorescence, as they may overtax our visual imagination, at least in two-dimensional display such as on paper or screen.

Sometimes the data are no longer shown, and only the frequency of subpopulations is given in numbers and tables. This can be dangerous, especially in the case of overlapping or shifted populations, as discussed below.

3.4.3 Statistical Evaluation

Statistical evaluation of immunofluorescence analysis is not very demanding. Cell populations, as defined by scatter and fluorescence staining, are described by the relative mean and CV of a particular fluorescence parameter (Fig. 4) and the number of cells in that population. This evaluation is possible, however, only if (a) the distribution of fluorescence intensities for the population analyzed varies symmetrically around the mean value, and (b) the whole population is visible „on scale," i.e., not summed in the first (for negative cells) or last channel, which would make it impossible to determine values for the mean or CV of fluorescence or for the autofluorescence of negative cells. For determining the relative fluorescence of positive cells the relative fluorescence of autofluorescent negative cells should be the reference.

The mean is defined as the arithmetic mean for linear scale and geometric mean for logarithmic scale. The CV (in percent) can be calculated independently of the mean fluorescence, as half the width of the distribution at 0.6 times maximum height:

$$CV = 100 \times (10^{(a-b)/2\,S}-1) = 100 \times (10^{2\,SD/2\,S}-1),\ SD = \log\,[(CV/100 + 1) \times S]$$

with S = channels per decade (usually 256), a = upper channel with 0.6 maximum height, and b = lower channel with 0.6 maximum height [4]. The variation observed and described as CV is the result of both biological variation (e.g., size of cells, density of target antigen, and staining antibody) and variation of measurement (e.g., focusing, orientation), and should describe a logarithmically symmetrical distribution around the mean of relative fluorescence (Fig. 4).

Determination of the absolute number of antigen molecules per cell is difficult today and requires a reference method for calibration of the relative immunofluorescence. The frequency of positive or negative cells

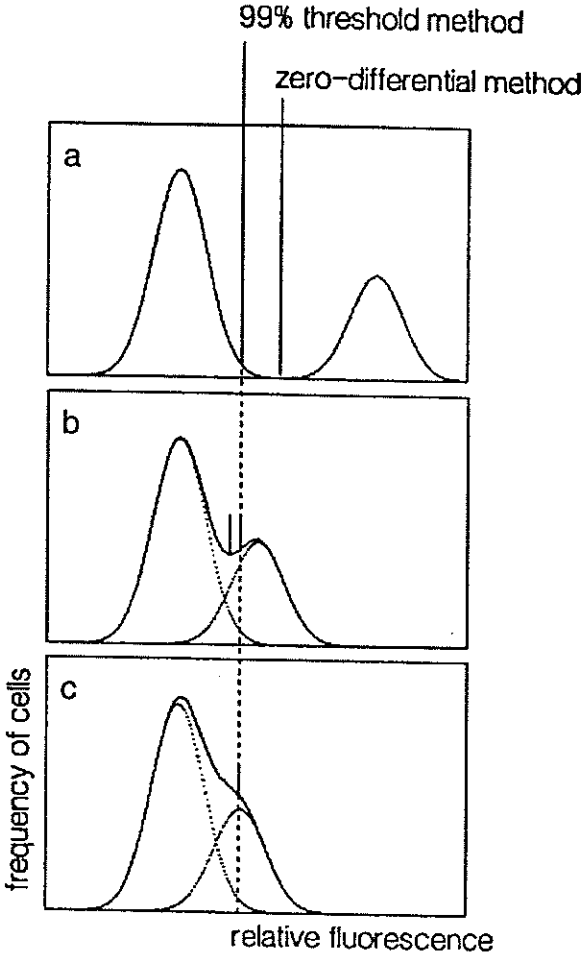

Figure 6. Evaluation of separate and overlapping populations. A mixture of cells, the normal sample for immunofluorescence, is easy to analyze, if the populations of positive and negative cells on the histogram are separate (a; see also figures on determination of staining time and on minimizing washing steps). An analysis gate, either including all cells „not negative" (99% threshold method) or set at middle distance between positive and negative populations, defines areas of the fluorescence scale, for which the mean of fluorescence and CV are determined (see figure on mean fluorescence and CV). Thus the frequency of positive and negative cells and their respective mean fluorescence and CV describe the sample with respect to the parameter of immunofluorescence. Staining should be optimized to achieve this clear and easy-to-analyze situation. (Histogram produced by computer simulation by K.L. Meyer) Bivariate or asymmetrical histograms (b and c) are not that easy to analyse. such histograms could represent kinetic transitions (e.g. activation markers) or a defined number of distinct populations, overlapping in immunofluorescence due to weak expression of antigen or suboptimal staining. The method of choice for evaluation of such histograms would be curve fitting. Curve fitting programs are available from Partec or Verity Software. For daily routine, the „zero- differential"-method can be used, as long as the histograms are bivariate and contain about equal numbers of positive and negative cells. Setting the analysis gate between „positive" and „negative" parts of the histogram, at the point of „zero increment", will allow an estimation of the frequencies of positive and negative cells, because „false positive" and „false negative" cells will level out, as long as the populations occur in about equal frequency. Bivariate histograms with one population being rare and asymmetrical histograms (c) have to be evaluated by curve fitting. In terms of experimental strategy, however, additional parameters, optimizing the staining and, in case of rare cells, preenrichment (see Chap. 14) could improve the resolution of the analysis, allowing evaluation without or controlling curve fitting

can be turned in absolute numbers only if the number of cells is known from which the sample has been taken.

Under optimal conditions, i.e., with perfectly separated populations (Fig. 6), the statistical values for mean and CV of relative fluorescence and the frequency of cells of the various populations are easy to obtain. The distinct populations are defined by analysis gates (lower and upper thresholds of intensity of fluorescence), and the statistical values are determined for the cells within the windows. Frequently the threshold is set to include 99% of the cells of the negative control, with 1% showing higher fluorescence. With separate populations, and even less so with nonseparate populations, there

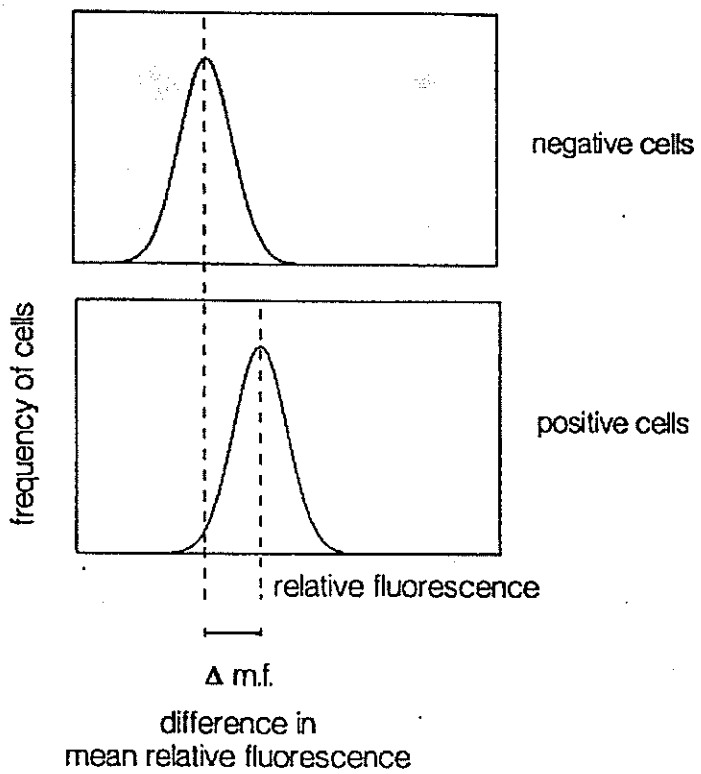

Figure 7. Evaluation of shifted populations. All the cells of a population that stain homogeneously, resulting in a symmetrical fluorescence distribution, defined by mean of fluorescence and CV, are positive, including those classified as dim as the negative control. This classification is due to lack of resolution of the flow cytometric analysis and variation in staining and measurement. The increase in fluorescence staining relative to the negative control is described by the difference in mean fluorescence and CV between negative control and positive, shifted population. The 99% threshold method of data evaluation (see preceding figure) cannot be applied to shifted populations. (Histogram produced by computer simulation by K.L. Meyer)

is no reason to use this method. Setting the threshold anywhere between the populations always gives more accurate frequencies.

It is not very easy to evaluate overlapping and shifted populations (Figs 6 and 7). Frequently, also for these nonseparate populations, threshold gates are used for evaluation, setting the thresholds to include 99% of the „negative" control, a sample of cells stained with an irrelevant antibody, and considering only those cells with higher fluorescence as „positive." For nonseparate populations, this procedure simply gives wrong statistics. This frequent mistake is one of the reasons that it should be made clear in publications, that statistical immunofluorescence data, when presented in tables, refer to histograms with separate populations.

How does one evaluate nonseparate populations? Of the nonseparate fluorescence histograms, shifted populations (Fig. 7) are easy to evaluate because they differ from the negative control only by the mean fluorescence, and the difference in mean fluorescence is sufficient for characterizing the shifted population. Even with small differences and many cells still in the area that would be defined as „negative" by 99% threshold gating, all cells of a shifted symmetrical population are positive. The problem is to recognize a shifted population as such and to refrain from setting analysis gates which always give wrong results.

The nonsymmetrical fluorescence distribution (Fig. 6) is most difficult to evaluate because a correct description would require curve fitting, which is not an option of most state-of-the-art software. Exceptions are the flow cytometry softwares Modfit (Verity) and Multicycle (Partec). A simplified

version of curve fitting is subtraction of the histogram of the negative control, but this can be grossly misleading if the two histograms are not normed for the peak of the negative cells. In any case, interpretation of nonsymmetrical distributions must consider the possibilities of distinct but overlapping populations versus kinetic transitions.

In daily routine, for nonsymmetrical histograms with two peaks, it is assumed that these histograms result from two overlapping populations. As long as these subpopulations have about the same size, an approximation of frequency and mean fluorescence can be obtained, setting a threshold between the two peaks, where the differential of the curve reaches zero, and assuming that as many positive cells fall into the negative fraction as vice versa (valley method). This method is not suitable if one of the populations is very small, i.e., for rare cells, but it is the best that can be used with most present software.

In any case, nonsymmetrical histograms reflect a lack of resolution of immunofluorescence. In practical terms, it is worth devoting some attention to improving the resolution of staining rather than statistics.

3.4.4 From Overlapping to Separate Populations

The difficulties in evaluation of overlapping fluorescence distributions should be one of the major reasons for improving the staining reagents and protocols, as discussed above, for example, absorbing cross-reactive antibodies out of staining reagents, titrate reagents, and using indirect rather than direct staining. Higher resolution can also be obtained by changing the fluorochrome conjugated to the staining antibody, for example, from fluorescein to phycoerythrin, which has a higher quantum yield of fluorescence. Thus, the use of biotinylated antibody and fluorochrome-conjugated streptavidin is a most versatile staining system for weak cellular parameters since it combines amplification due to indirect staining with the option of exchanging fluorochromes easily.

Finally, if available, additional parameters that discriminate even weakly between the two overlapping populations should be used to improve resolution. Populations that overlap in each of two parameters may be separated in two dimensions, such as lymphocytes and monocytes from peripheral blood in forward and side scatter.

References

1. Handbook of experimental immunology, 4th edition eds. Weir, D.M., Herzenberg, L.A., Blackwell,C. and Herzenberg, L.A. Blackwell Sci. Publ., Oxford 1986
2. Clinical applications of flow cytometry: quality assurance and immunophenotyping of peripheral blood lymphocytes eds. A. Landay et al. Natl. Comm. Clin. Lab. Stand. Vol. 9, No. 13 1989
3. Methods in cell biology, Vol. 33: Flow cytometry. eds. Darzynkiewicz, Z. and Crissman, H.A. Academic Press, New York 1990
4. Logarithmic amplifiers. Gandler, W. and Shapiro, H. Cytometry 11:447-450 (1990)

16 Setup of a Flow Sorter

C. GÖTTLINGER, B. MECHTOLD, K.L. MEYER, and A. RADBRUCH

16.1 Background

The option of sorting out cells according to microscopic parameters has made flow cytometry one of the most valuable tools for cell biology. Sorting makes use of either of two different technical principles. One is based on changing the direction of flow of individual cells electromechanically [4]. The cells are pushed in distinct flow channels of a closed flow chamber. The rate of sorting is limited to about 1000 particles per second. Because the particles do not have to pass a narrow nozzle, fragile and large cells or aggregates can be sorted with ease. Since the entire setup is closed, no aerosols are formed, and the risk of infection is minimal. This sorting principle is used in Partec machines and the FACSort of Beckton-Dickinson. Since we have no experience with these instruments we do not discuss them further. The second sorting principle is based on packing the cells into tiny droplets after analysis, charging those droplets that contain cells to be sorted out, and deflecting the charged droplets in an electrical field. This technology is used in free flow-in-air cytometers and allows sorting rates of up to 10^4 particles per second. The arrangement of droplet sorting is shown schematically in Figure 1.

To stabilize the droplet formation and ensure a constant distance between breakoff point and point of laser intersection, a vibration (drop drive) defined by frequency (drop-drive frequency), amplitude, and phase is coupled to the liquid jet via a piezoelectric transducer. A typical value of the drop-drive frequency for a nozzle with an orifice diameter of 70 μm, the jet running at 10 m/s, is 27 kHz, breaking the jet into 27 000 uniform droplets per second at a defined distance from the nozzle tip.

After leaving the nozzle, the cells first pass the laser intersection point, where they are analyzed. The electronic sorting device determines electronically whether the cell fulfils the preset requirements for deflection. The cells travel to the breakoff point in a constant time, the so called "drop delay" time. At the breakoff point, the cells are packed into single droplets. If a droplet is to be deflected, the whole jet is charged for the time of drop formation, then decharged again, leaving the newly formed droplet charged. All droplets then fly through a static electrical field between two metal plates (deflection plates). Charged droplets are deflected from the vertical main stream into a separate collecting tube.

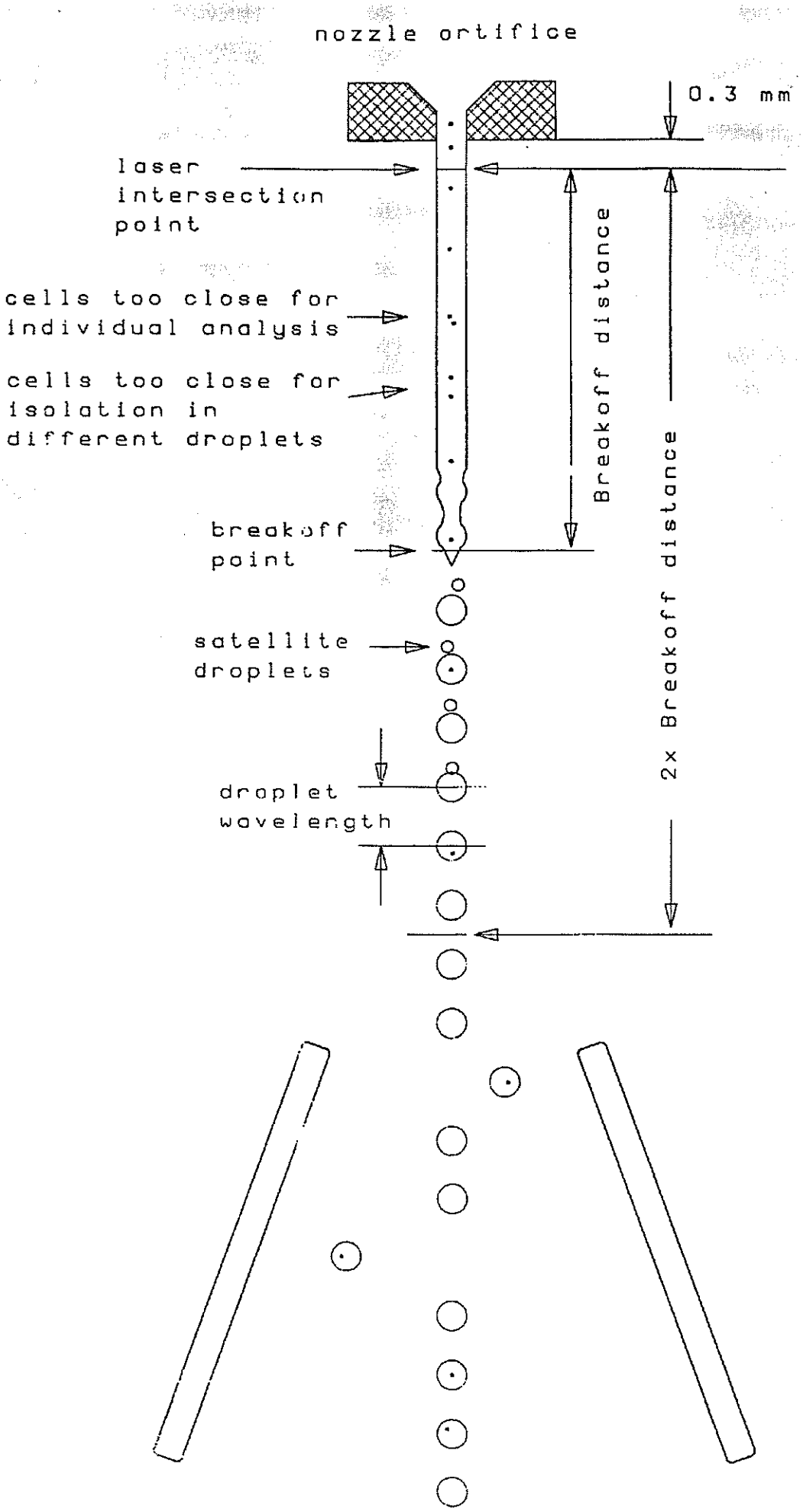

Figure 1. Liquid jet of a sense in air flow cytometer with droplet breakoff

The critical parameter for good sortings is the drop delay, i.e., the time between analysis and droplet formation, which must be constant to allow defined charging of droplets. To account for small irregularities in drop delay and for cell velocity, for good recovery of sorted cells not only the droplet containing the cell but also the droplets before and after can be deflected by merely increasing the time of charging. For the same reasons, better sorting results are obtained with short drop delays, i.e., breakoff points close to the nozzle. For a given diameter of the nozzle ortifice and given viscosity of sheath fluid, the distance between analysis and breakoff points depends on sheath pressure, drop-drive amplitude, and drop-drive frequency. Setting the breakoff point requires optimization of all three parameters. The lowest sheath pressure that still gives a continuous jet and constant drop formation yields the shortest breakoff distance. For the drop-drive frequency, certain frequencies give resonance with nozzle and nozzle holder, self-enforcing the amplitude and stabilizing the position of the breakoff point. Such resonance frequencies can be found easily by observing the breakoff point with the alignment microscope while constantly increasing the frequency from 20 kHz. Resonance frequencies show up because they cause the breakoff distance to shorten. Observing the breakoff point during change of drop-drive frequency, resonances are found with minimum breakoff. Such resonance frequencies should be selected for sorting. Theoretically, the shortest breakoff distance is achieved when the wavelength (droplet spacing) is 4.5 stream diameters [1].

For flow-in-air sorters, sorting speed is limited principally by three factors:

- Cycle time or dead time of the electronics, i.e., time needed for processing data of one cell (typical value: 15–20 μs).
- Time for generating one droplet (reciprocal of drop-drive frequency).
- Statistical distribution of cells. Some cells are always too close together for individual analysis or droplet formation. Such cells are prevented from being sorted by "abort" electronics, lowering the yield of sorting. For a detailed discussion of optimal flow rate at given electronic dead times, drop-drive frequency, and percentage of positive cells see [2]. For high recovery the abort electronics is switched off (ENRICH), lowering the purity of sorted cells. For high purity, abort electronics is switched on, lowering the recovery.

As a basic rule, every sort should be accompanied by a sort protocol containing information on the instrument settings and the purity and recovery of sorted cells (see Table 1).

16.2 Method

Setting up a flow-in-air sorter for sorting

1. Alignment and calibration of the instrument for analysis of cells is described in Chap.1. (Use a nozzle with 70-μm orifice for sorting of lymphocytes.)

Table 1. Protocol of a cell separation

Separation technique	Start population	Fraction	Cell number[a] times 10^6			Purity[c] (%positive)	Recovery[d]
			Living	Dead	Positive[b]		
Centrifugation	Whole blood	Before After				—	—
Lyse and filtration	Peripheral blood mononuclear cells	After				—	—
MACS	Peripheral blood lymphocytes	Positive Negative					
FACS	MACS positive	Deflected					

MACS: Magnetic cell sorting
[a] Haemocytometer or Coulter counter
[b] Frequency of positive cells (Flow cytometer/ Fluorescence microscope)x cell number
[c] Frequency of positive cells
[d] Ratio of number of positive cells recieved from sorting and number of positiv cells in the unsorted sample.

2. Switch fluidics control to SHEATH position; switch on drop-drive frequency and stroboscope for observation of droplets.
3. Set drop-drive frequency to 20 kHz and amplitude to two thirds of maximum.
4. Lower the sheath pressure, observing the breakoff point using the alignment microscope until drop formation is no longer stable; then increase the sheath pressure about 1 psi.
5. Slowly increase the drop drive frequency, while observing droplet breakoff distance. Find a resonance frequency which shortens and stabilizes the breakoff distance (usually around 27 and 33 kHz).
6. Use the drop-drive amplitude to set the breakoff distance somewhere between 2.5 and 4 mm. Avoid setting the amplitude to minimum or maximum since you may have to change it during the sort to adjust the breakoff point.
7. Determine the drop delay: Set horizontal cross-wire of the alignment microscope to the height of the breakoff point. Set the cross-wire to a position twice the distance of breakoff.
8. Move microscope upward, counting the drops (drop plus interim space = 1) until the breakoff point is reached. Use drop number minus 2 for setup of drop delay. Select 1 drop to be deflected.
9. Run sample of chicken red blood cells (CRBCs) and set sorting windows to deflect single CRBCs.
10. Switch on deflection plates and stream charging pulses.
11. Determine the optimal drop delay: Deflect 1000 cells on a slide, increase drop delay for one-half droplet, move slide, and sort again 1000 cells. Repeat until the initial value plus 2 is reached.

12. Determine the deflection spot containing most cells by microscope. Use the corresponding drop delay for sorting.
13. Set the number of deflected droplets to 2 for regular sorts or 1 for sorting of rare cells.
14. Remove CRBC sample and allow backflushing for approximately 1 min. Install sample filter. To sterilize, dip the sample filter and tubing into alcohol, washing off the alcohol with sterile PBS afterwards.
15. Install sample tube with 10^7 cells/ml of the cells to be sorted.
16. During the sort check breakoff distance regularly and correct if necessary by changing the drop drive amplitude or phase, but never the frequency as this would also change the drop delay.
17. Keep cells cool and in suspension during sorting.
18. After sorting determine recovery and purity of sorted cells by microscopy or flow cytometry and do not forget the sort protocol (table). For determination of recovery rate, the absolute cell numbers immediately before and after sorting and the frequencies of sorted cells must be determined.

16.3 Tips, Tricks, and Troubleshooting

Sterile sorting

There are many ways to sterilize a cell sorter–but most contaminations come with the sample! To keep sterile cell suspensions sterile through sorting it is sufficient to sterilize the compressed air and sheath fluid by fresh anti bacterial filters (0.2 µm pore size). Sample line and nozzle can be sterilized by flushing with 0.1% 7X (Flow laboratories) or any other detergent that is tissue-culture "compatible." In any case the sample line should be backflushed extensively with sterile sheath fluid before running cells. Alcohol, if used for sterilizing the sample line, may agglutinate debris from the wall of the sample line and thus cause clogging.

Long-term sorting

With sorting for longer than 30 min sedimentation of the cells in the sample tube may become a problem. To prevent sedimentation a "sample medium" of equal density to the cells can be used [3] or the sample tube agitated from time to time.

Unstable breakoff point

- Check for air bubbles in the nozzle tip or nozzle holder. Remove sample, switch off deflection plates, and switch fluidics control between OFF, FILL, and SHEATH positions to remove air bubbles. Control for success. If this did not help, the nozzle holder must be removed, to clean the nozzle, with a syringe or ultrasonics.
- Check for leakage in the tubings.
- Check for aggregates in the sample; if positive, filter the sample through nylon gaze of 50 µm pore size (e.g., Erbslöh, Düsseldorf, or Schweizerische Seidengazefabrik, Zürich).

- Check for salt crystals at the nozzle tip; remove by gently touching the nozzle tip with a piece of filter paper (e.g. Whatman, Maidstone) while the laser is blocked.

Dispersed side streams

- Control side streams with cold, focused bright light source.
- Use phase control to align the end of liquid stream. The tip of the jet should look like that illustrated in the figure (see above).

Unstable flow rate

- Check for air or liquid leaks of sample tube and tubings, especially the O ring seal between sample tube and sample holder.
- Check sample for aggregates and filter, if necessary, through nylon gaze.
- Check the sample line for clumps and aggregates, especially the connections of tubings and the tubing at the pinch-off valve. Exchange sample line if necessary.

Decharging of collection tubes

Deflected droplets deliver their charge to the collection tube, sometimes causing high local charges of the same polarity as the deflected droplets, causing rejection of later deflected droplets. This can be prevented by grounding the collection vessel. A bent sterile injection needle connected to ground and pinched into the side wall of the collection tube is sufficient for this. Also, it is useful to fill the collection tube with some medium, not only for the comfort of the cells but also for distribution of the charge of deflected drops.

Bad recovery

Determine cell numbers immediately before and after sorting, otherwise the losses due to centrifugation of the cells are added the losses from sorting.

References

1. Kachel V., Fellner-Feldegg H., Menke E. (1990), Hydrodynamic properties of flow cytometry instruments. In: Melamed M.R., Lindmo T., Mendelsohn M.L. (eds) Flow cytometry and sorting. New York: John Wiley & Sons, Inc. pp 27-44.
2. Lindmo et al. (1990), Flow sorters for biological cells. In: Melamed M.R., Lindmo T., Mendelsohn M.L. (eds) Flow cytometry and sorting. New York: John Wiley and Sons, Inc. pp 145-169
3. Mechtold B., Miltenyi S., Irlenbusch S., Göttlinger C., Radbruch A., (1990), Sorting of rare cells. In: Proceedings of the 3rd European Cytometry Users Meeting 1989, Ghent Becton-Dickinson Press, pp74-81
4. Göhde, W. and Dittrich, W. (1971), Impulsefluorometrie – ein neuartiges Durchflussverfahren zur ultraschnellen Mengenbestimmung von Zellinhaltsstoffen. In: Acta Histchem., Suppl. X,p.42–51, 1971.

17 Sorting of Rare Cells

W. WEICHEL, S. IRLENBUSCH, K. KATO, and A. RADBRUCH

17.1 Background

For sorting of cells occurring at frequencies of below 1%, positive selection, i.e., isolation of rare cells on the basis of a molecule that they express, is much more efficient than depletion of the majority of cells, which usually show heterogeneity with respect to any marker that can be used for depletion, making isolation of the rare cells impossible. As one of the most powerful methods for positive selection, fluorescence-activated cell sorting (FACS) has been used for the enrichment and isolation of rare cells ever since its introduction. Examples include immunoglobulin switch variants [1,2], MHC mutants [3,4], and transfectants [5,6]. Such cells occur at frequencies of less than 10^{-2} down to 10^{-8} in a given population. Formerly, rare cells were isolated in several rounds of cell sorting, expanding the enriched cells between the sorts in vitro, thus gradually increasing the frequency of variants until isolation of rare cells and cloning became possible. Under optimal conditions, enrichment rates of up to 10^3 per sort could be achieved, but the number of sorted cells was too low, for reasons indicated below, to allow immediate resorting for purification of the rare cells. Naturally, such experiments could then only be performed with transformed cells, adapted to continuous growth in culture.

Today additional parameters are available in flow cytometry, and new methods for fast and efficient enrichment of cells prior to FACS sorting have been introduced, substantially facilitating the isolation of rare cells.

Basically, the problem with the isolation of rare cells is twofold:

1. Discrimination between rare cells and cells of the major population is difficult because of the variation in immunofluorescence (coefficient of variation) which may lead to a population overlap (Fig. 1), even in otherwise acceptable staining. This and the low absolute number of rare cells makes it difficult to analyze enough cells to identify the population of rare cells with some statistical reliability. This problem is diminished by optimizing the immunofluorescence staining, introducing additional parameters (Chap. 3) and enriching rare cells by fast, parallel magnetic cell sorting (*MACS*) sorting (Figs. 1, 2; Chaps. 14, 15) before FACS analysis and sorting.
2. Large cell numbers must be processed for the sorting of rare cells to obtain enough cells for subsequent analysis. For FACS, cells are

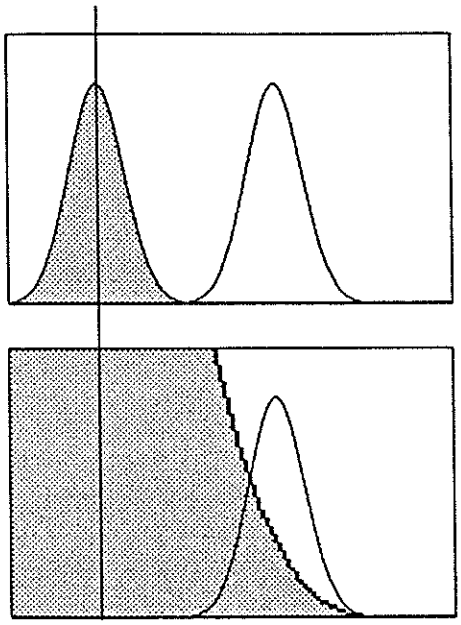

Figure 1. Population overlap. This is one reason why rare cells are difficult to isolate. With regard to any parameter, discrimination between rare and the other cells depends not only on the difference in mean fluorescence but also on the % CV of the major cell population, i.e., the shape of the fluorescence distribution (see Chap. 3), as illustrated here. An overlap of the population of rare cells and the infrequent, diverging cells from the major population is the result, making it impossible to define discriminatory gates for sorting. Population overlap is minimized (a) by optimizing the staining conditions, i.e., maximizing the difference in mean fluorescence, (b) by first enriching the rare cells to equalize population sizes and minimize the effect of variation (e.g., see subsequent figures), and (c) by using as many discriminative parameters as possible, even if they discriminate only between some of the cells of the major population and the rare cells (see Fig. 3)

analyzed one by one (serially) at flow rates of up to 5000 cells per second, i.e., 1.8×10^8 cells in 10 h. This long sorting time means stress for the cells (and the experimenter), and for some applications sorting rare cells out of 2×10^8 cells does not yield sufficient numbers. This problem is solved by use of powerful new parallel enrichment methods which can handle large cell numbers, analyzing and sorting all cells simultaneously. Combination of enrichment of the rare cells by fast, parallel *MACS* (Chap. 15), limited by the use of only one parameter for discrimination, followed by further enrichment with slow, serial FACS, offering several parameters for optimal discrimination, can yield enrichment rates of up to 10^8 fold in one experiment (Fig. 2). Few biological problems require higher enrichment rates.

17.2 Material

The experimental strategy outlined in the figure must be tailored for the individual problem with respect to the frequency of rare cells, markers available for discrimination, and the use of sorted cells. The cell sorting methods to be combined for rare cell sorting are described in detail in Chaps. 14–16. Here we emphazise peculiarities of the sorting of rare cells:

- Single cell suspension of good viability (Ficoll-Hypaque centrifugation removes dead cells and debris. Chap. 14)
- Phosphate buffered saline (PBS) with 1% fetal calf serum (FCS) or bovine serum albumin (BSA) (PBS/FCS or PBS/BSA)
- Propidium iodide (PI), 1 mg/ml in water
- Immunofluorescent and magnetic staining reagents in PBS/FCS with 0.03% sodium azide. For sterile sorting, reagents must either be steri-

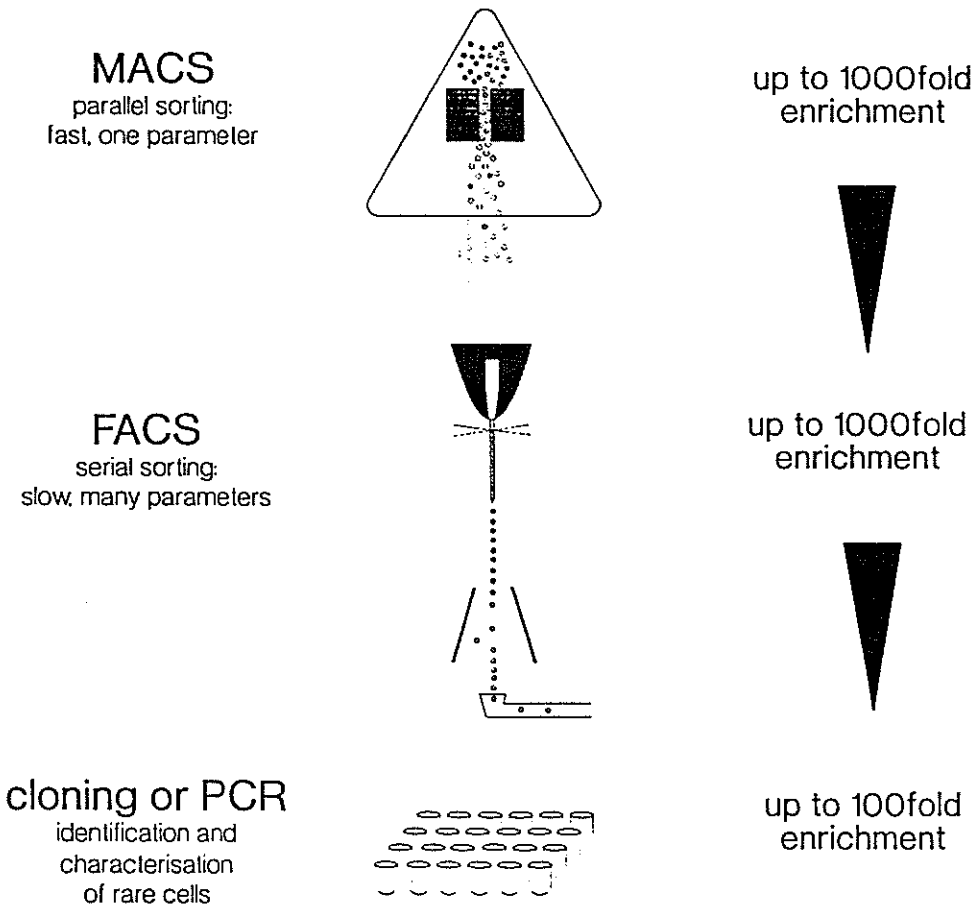

Figure 2. Efficient selection of rare cells by combining cell sorting methods. This general scheme illustrates how enrichment rates of up to 10^8 fold can be achieved for immunofluorescently labeled rare cells by combination of various cell sorting methods. First, an efficient and fast enrichment of stained cells is obtained by *MACS* which can handle very large cell numbers, as required initially, but is restricted to one parameter. Very good enrichment is obtained with *MACS* because the labeled cells can be sorted out (positive sorting) and directly processed further in a fluorescence-activated cell sorter. The FACS sort is based on serial analysis of several parameters per cell and thus offers very good discrimination but is time consuming which is no longer a problem since the cell number has been reduced in the *MACS* sort. Since FACS can deflect single cells, individual cells can be cloned for further studies or analyzed directly, for example, by polymerase chain reaction, spot enzyme-linked immunosorbent assay, or other single cell based assays.

lized by filtration, or staining reagents can be centrifuged to remove aggregates and microorganisms (5 min in Eppendorf centrifuge)
- Standard cell culture plasticware, such as Eppendorf tubes, sample tubes for sorter, pipettes and tips, syringes, needles
- Nylon meshes with 30–60 µm pore size, cut to pieces of about 2 cm^2, autoclaved for sterility
- Tissue-culture safe detergent in water
- Ethanol
- Shandon cytocentrifuge or the like
- Fluorescence microscope, slides, coverslips, Fluoromount-G (SBA)
- *MACS* equipment: *MACS* separator and small columns (A1/A2; see Chap. 15)

- FACS equipment: fluorescence-activated cell sorter with sterile sheath fluid (in-line filter), sample filter, and cooling option (see Chap. 16).
- Cell counting device: Neubauer counting chamber or Coulter counter

17.3 Method

Staining the rare cells

Staining must be carefully optimized (see Chap. 3) to maximize discrimination between rare cells and the majority of cells. For *MACS* any background staining can be deleterious.

1. Spin down all cells (usually 10^8–10^{10})
2. Remove supernatant carefully and loosen pellet by flicking.
3. Add titrated staining reagent, for example, biotinylated antibody to the rare cell marker molecule, to a final volume corresponding to the number of rare cells but exceeding the total cell volume at least twofold. Actually, the "negative" majority of cells provides an "exclusion volume" and does not dilute the staining solution. Increasing the staining volume is not critical, but increased concentrations of stain causes background.
4. Stain for 10 min on ice.
5. Dilute the cells with PBS/FCS; spin down (10 min, 300 *g*)
6. Wash once: remove supernatant, loosen the pellet by flicking, fill up with PBS/FCS, and spin down again.
7. For indirect staining, repeat from step 2 with second reagent, for example, stain the biotinylated first antibody with streptavidin-conjugated superparamagnetic *MACS* microbeads (diluted 1:100 from stock) for 5 min at room temperature; then add titrated amount of phycoerythrin-conjugated streptavidin.

Screening for rare cells:

Depending on their frequency, the detection and analysis of rare cells may be difficult by flow cytometry and require extensive live and multiparameter gating to remove unspecifically stained cells, especially dead cells (Fig. 3). An alternative method is detection by fluorescence microscopy, spinning down a defined number of cells on a defined area of a slide, and screening the area for positive cells. This method allows scanning of about 10^6 cells for single positive cells in about 2 h, providing visual information in addition to verify the phenotype.

1. Stain cells as described above
2. Spin 1.2 x 10^5 cells on each of 10 slides (20% are lost upon centrifugation).
3. Add one drop of Fluoromount-G and coverslip.
4. Analyze by fluorescence microscopy by scanning the slides' areas, counting only positive cells. The number of positive cells on all slides reflects the frequency per 10^6 cells.

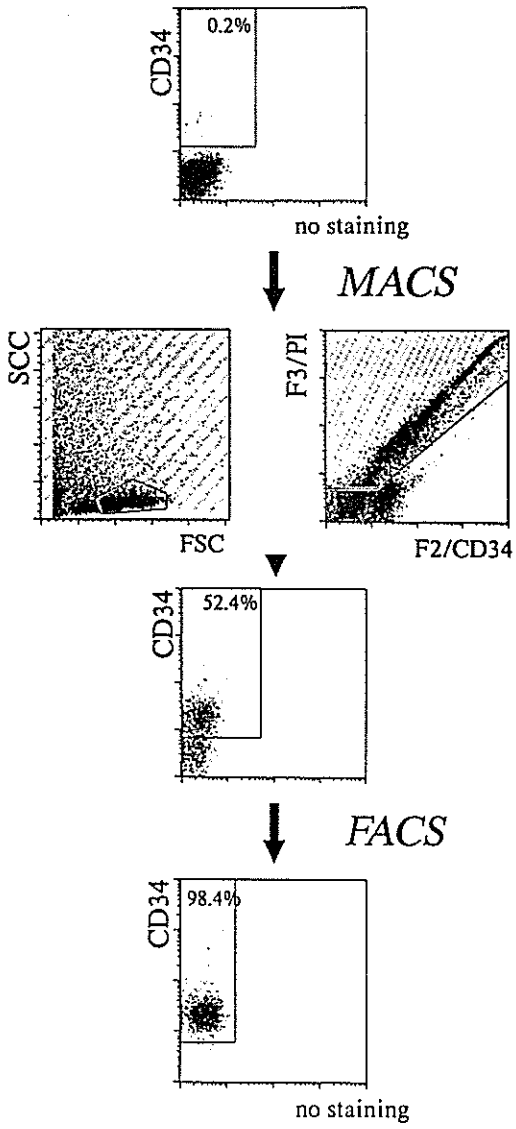

Figure 3. Isolation of CD34+ cells from peripheral blood using *MACS* and FACS. Peripheral blood cells were preenriched by Ficoll-Hypaque gradient centrifugation (Chap. 14) and monocytes and NK cells depleted by leucine methyl ester lysis (Chap. 14). The cells were then stained with a biotinylated, titrated CD34 antibody, washed once, stained with streptavidin-conjugated *MACS* beads (diluted 1:100 from stock; Chap. 15) adding 3 µg/ml streptavidin phycoerythrin after 5 min for another 5 minutes, washed and enriched on an A1 *MACS* column (see Chap. 15 for details). The positive cells were eluted from the column outside of the *MACS*, and an aliquot was analyzed and sorted further by flow cytometry (FACStar+) in the presence of propidium iodide. For the *MACS*-sorted cells, large cells and debris were gated out by forward (180°) and side (90°) scatter, dead cells were gated out according to propidium iodide fluorescence in a fluorescence 2 versus fluorescence 3 plot (F2/F3 gating). This gating is crucial for evaluation of the sorting efficiency since unspecifically stained dead cells are enriched together with the rare specific cells. Due to the different fluorescence spectra of phycoerythrin and propidium iodide, the F2/F3 ratio (570/630 nm) is specific for each dye, irrespective of the intensity of staining. Stained cells appear on two parallel diagonals, which are clearly distinct. It should be noted that this approach also allows use of more than three dyes on a flow cytometer with three fluorescence channels. FACS-sorted cells were reanalyzed on a FACScan using FSC/F3 and F1/SSC to gate on live cells with low side scatter. (The experiment is described in detail in [10].)

The efficiency in terms of recovery of rare cells must be taken into consideration when calculating the number of cells required for sorting. The number of cells prepared for sorting should exceed the number of cells theoretically required at least twofold to compensate for losses during separation, mainly in the FACS.

Magnetic enrichment

For *MACS* of rare cells it is important to reduce background staining, to use small columns with just enough capacity for labeled cells, and to use slow flow rates for efficient positive enrichment.

1. An A1, A2, or B1 *MACS* column is filled and sterilized from the bottom with ethanol. The ethanol is replaced from the top first with PBS and then PBS/BSA or PBS/FCS, and the column inserted in the *MACS*. The whole procedure can be performed in a sterile workbench.
2. Cells, stained as described above, are filtered through the *MACS* column at low flow rates (0.5–2 ml/min) in two cycles, i.e., cells passing the column are collected and filtered through the column for a second

time. The frequency of cells can be monitored, for example, by checking drops under the microscope from time to time. When the majority of cells have passed the column, the column is washed at higher flow rates, depending on the intensity of staining (high relative fluorescence = high flow rate) until only few cells come with the effluent.

3. The column is then closed at the bottom and carefully removed from the *MACS*. A syringe with 2 ml of PBS/FCS is applied to the side of the stopcock, and the adherent cells are pushed off the wires.
4. The column is inserted back into the *MACS*. The cells are again filtered through the column, first at slow flow rates, then washing at higher rates.
5. When no further cells are washed off the column, the column is eluted outside the MACS by flushing with PBS/FCS from the top. If the elution volume is not too high, the cells can be processed further directly; otherwise it is necessary to spin them down (10 min for 300 *g*). An aliquot is used for analysis of enrichment, either by microscope or by flow cytometry (see Fig. 3).

Fluorescence-activated cell sorting

1. The cell sorter should be set up for optimal performance with respect to optical alignment and calibration. The breakoff point should be stable (resonance frequency) and the deflection streams well focused. Sort recovery and purity should have been checked. Collection tubes should be cooled and a decharging device installed. (All this is described in detail in Chap. 16)
2. The cell path in the sorter is cleaned and sterilized using a tissue-culture compatible detergent (7X, Flow), washing it out again before use with sterile PBS/FCS. The sheath fluid is sterilized by in-line filtration. A sample filter of 30–60 μm pore size should be inserted at the bottom of the sample line as described in Chap. 15.
3. If a substantial number of cells are to be processed, it is advisable to filter the cell suspension beforehand, by aspirating 3 ml cell suspension into a 5 ml-syringe, then fixing a piece of 30- to 60-μm pore size nylon mesh between needle and syringe and slowly passing the cells through the filter into a sample tube. Alternatively, the cell suspension can be filtered directly through nylon gauze into the sorter's sample tube. Large numbers of cells should be sorted in sample medium of similar density as the cells (Chap. 15).
4. Add 3 μl PI stock solution per milliliter of cell suspension, mix, and apply to cell sorter.
5. Analyze negative cells to define sort windows. Gate out dead cells and debris by scatter and PI fluorescence as described in the figure. With *MACS*-enriched cells, i.e., low absolute cell numbers, use low flow rates (under 2000/s), deflect two or three drops per cell and use no sort abort. Processing large cell numbers requires high flow rates (5000–7000) and single-droplet deflection. Whether or not to use sort abort depends on whether the rare cells should be enriched or purified.
6. Check deflection streams, which for rare cells may consist of only occasional droplets instead of a consistent, focused stream, by using a

strong cold light source (see Chap. 15). Switch off the "warm" stream illumination because it may dry out the deflected droplets.

7. Relax and check from time to time the stability of flow rate, breakoff point, and deflection streams. If the number of dead cells and clumps increases, they can be removed by Ficoll-Hypaque (Chap. 14).
8. Sorted cells can be analyzed for purity by flow cytometry. A few thousand deflected cells are sufficient if the PBS/FCS or medium in the collection vessel was filtrated to remove debris particles. Still, gating for cells and against debris is required to evaluate the purity of cells (Fig. 3). Purity and recovery should be protocolled through the sort.

17.4 Tips, Tricks, and Troubleshooting

FACS flow rate

During long-term sorting from one sample tube, the sedimentation of cells may cause severe problems [8, 9]. The flow rate first increases, then decrease, and cells die in the sediment, resulting in substantial overall cell loss. This problem can be solved either by resuspending the cells from time to time or by suspending the cells in medium that is made isopygnic by the addition of Percoll (Pharmacia), to minimize sedimentation [9]. The cells are resuspended in the isopygnic sample medium after the last wash–before filtration through the nylon gauze.

Sterility

Sterility may become a problem if the cells are sorted for cellular analysis or expansion in tissue culture. Potential ontamination of sorted cells by bacteria can be avoided by adding an antibiotic which is not normally used, such as gentamycin, immediately after sorting. Frequent contaminations of independent sorts may be due to contamination of the sample tubing, the sheath fluid, or common staining reagents. These problems can be eliminated by exchanging the complete tubing system: sample lines, sheath lines, and in-line 0.22-μm sheath filter, as well as replacing the sheath fluid. Autoclavable parts and sample filters should be steam-sterilized. The most frequent source of contamination are staining reagents, especially if they are used by several persons over some time and stored in a refrigerator. Yeast can be eliminated by fungicides such as Nystatin, but it is advisable to separate yeast from cells by Ficoll-Hypaque gradient centrifugation (Chap. 14).

Flushing the sample line with tissue culture compatible detergent (e.g., 0.1% 7X) for a few hours prior to the experiment sterilizes and cleans the sample line, thus preventing adsorbance of cells to the wall of the tubing i.e., bad recovery due to cell loss.

The various aliquots of deflected cells should not be pooled but expanded separately to minimize the risk of contamination.

Droplet repulsion

A general problem with flow-in-air sorters is the introduction of local charge on the plastic of the collection vessel by droplets that do not fall into

the collection fluid. This static charge can lead to repulsion of further droplets because it is of the same polarity as the deflected droplets. For rare cells, the deflection streams cannot be focused well, making the problem even worse. To prevent charging, a sterile injection needle is bent, hung onto the inner wall of the collection vessel, and grounded.

Viability No problems with viability have been observed with *MACS*. For enrichment of rare cells, however, one should keep in mind that unspecifically stained dead cells, even if they are rare, are also enriched. Such cells can be removed from the positive fraction by Ficoll-Hypaque gradient centrifugation. For flow analysis and sorting, dead cells must be efficiently gated out, for example by FSC/SSC and F2/F3 gating (Fig. 3).

In FACS the fraction of dead cells rises slowly during a long term sort because cells are dying. This is yet another advantage of *MACS* presorting, which reduces the total sorting time considerably. Nevertheless, in a good buffer more than 80% of most cell types should be alive in the morning if kept on ice overnight. If problems with viability arise, the survival rate should be tested this way, and, if necessary, fresh medium purchased or set up from new stock solutions.

Another problem of FACS is that large and fragile cells may not survive the acceleration at the tip of the nozzle, resulting in bad recovery when comparing numbers of deflected cell and collected cells. A nozzle with larger diameter may improve the situation. Another possible cause of a discrepancy between deflected cell number as indicated by the FACS and the number of collected cells is misalignment of breakoff point or drop delay. This should be aligned and tested carefully before or during the procedure, using standard particles or negative cells. The recovery of deflected cells should be monitored from time to time by counting and/or inspection using the fluorescence microscope. Even a small drift of breakoff point and drop drive frequency can reduce the recovery. Phase setting and small flow impairments may change the direction of the deflection stream or its width. All these parameters should be checked frequently during the sort.

References

(1) - Radbruch, A., Liesegang, B. and Rajewsky, K. (1980) Isolation of variants of mouse myeloma X63 that express changed immunoglobulin class. PNAS USA 77 (5), 2909

(2) - Dangl, J.L., Parks, D.R., Oi, V.T. and Herzenberg, L.A. (1982) Rapid isolation of immunoglobulin isotype switch variants using fluorescence activated cell sorting. Cytometry 2 (6), 395

(3) - Holtkamp, B., Cramer, M., Lemke, H. and Rajewsky, K. (1981) Isolation of a cloned cell line expressing variant H-2K^k using fluorescence-activated cell sorting. Nature 289, 66

(4) - Weichel, W., Liesegang, B., Gehrke, K., Goettlinger, C., Holtkamp, B., Radbruch, A., Stackhouse, T.K. and Rajewsky, K. (1985) Inexpensive upgrading of a FACS I and isolation of rare somatic variants by double-fluorescence sorting. Cytometry 6 (2), 116
(5) - Kavathas, P., Sukhatme, V.P., Herzenberg, L.A. and Parnes, J.R. (1984) Isolation of the gene encoding the human T-lymphocyte differentiation antigen Leu-2/T8 by gene transfer and cDNA subtraction. PNAS USA 81 (24), 7688
(6) - Hombach, J., Leclercq, L., Radbruch, A., Rajewsky, K. and Reth, M. (1988) A novel 34 kD protein co-isolated with the IgM molecule in surface-IgM expressing cells. EMBO J 7 (11), 3451
(7) - Göttlinger, C., Meyer, K.L., Weichel, W., Müller, W., Raftery, B. and Radbruch, A. (1986) Cell-cooling in flow cytometry by peltier elements. Cytometry 7 (3), 295
(8) - Göttlinger, C., Lill, F., Miltenyi, S., Mechtold, B. and Radbruch, A. (1989) Improved flow sorting technology: MACS sorting, cell cooling, flow rate stabilization and computer controlled sorting. Anal. Cell. Pathol. 1 (5-6), 319
(9) - Mechtold, B., Miltenyi, S., Irlenbusch, S.,Göttlinger, C. and Radbruch, A. (1990) Sorting of rare cells, Proc. of 3rd European Cytometry Users meeting, Ghent, Becton-Dickinson Press, pp. 74-81

A. Radbruch, Institute for Genetics, Cologne (Ed.)

Flow Cytometry and Cell Sorting

1992. Approx. 223 pp. 58 figs. Hardcover DM 98,-
ISBN 3-540-55594-3

The practical aspects of flow cytometry and sorting are emphasized in this book which introduces the beginner to the technology but also provides tips and tricks for the advanced user. The clear structure makes it easy to address specific problems fast.

The chapters cover the modern applications of these procedures, with emphasis on immunofluorescence (antibody-fluorochrome conjugation, staining principles and data evaluation), the isolation of specific chromosomes, cells and fragile, large particles by magnetic and fluorescence-activated sorting, cellular biochemistry and the dynamics of proliferation. The methods have been field-tested in recent EMBO courses on flow cytometry.

SPRINGER LABORATORY

Please send me

Order Form

☐ Please bill me
☐ Please charge my credit card
☐ Eurocard/Access/MasterCard ☐ American Express
☐ Visa/Barclaycard/BankAmericard ☐ Diners Club

Number: _____ Exp. Date _____

Please order through your bookseller or from

Springer-Verlag
Heidelberger Platz 3
W-1000 Berlin 33

A. Radbruch (Ed.)
Flow Cytometry and Cell Sorting
1992. DM 98,- ISBN 3-540-55594-3

Name/Address .....

.....

.....

.....

.....

Date/Signature .....

Prices are subject to change without notice

IMMUNPHÄNOTYPISIERUNG UND DATENVERARBEITUNG

Dr.A.Raffael

Becton Dickinson GmbH
Immunzytometriesysteme
Heidelberg

FACScan INSTRUMENT

Initial Instrument Checkout

Before turning on the Sensor Module and Computer Power:

1. Check that all instrument components are connected and power plugs are installed.

2. Check Fluid containers: Sheath reservoir is full and waste reservoir is empty but for 100 ml of bleach.

Startup

1. Turn FACScan Sensor Module power to ON. This activates the built-in laser which has a warmup time of five minutes.

2. Turn Computer power on.

   When power to the computer is turned on, the software program is automatically loaded from the hard disk into memory.

Instrument Calibration

To setup instrument parameters for cell surface immunofluorescence work use one of the following: Calibrite beads with AUTOCOMP software in automatic or manual mode; or adjust PMT settings using gluteraldehyde fixed chicken red blood cells (CRBC).

FACScan Shut-down:

1. Flush the system with 1% bleach, ultrapurge of disinfecting solution for five minutes.

2. Install sample tube with 1-3 ml of distilled water to prevent drying of the sample capillary tube and clogging with salt crystals. Allow to run for one to three minutes.

3. Set the Fluidics switch to STANDBY.

4. Turn FACScan Sensor Module and computer power switches to OFF.

5. Remove sheath reservoir and fill with saline.
   Remove waste reservoir and empty contents.

FACSCAN APPLICATIONS

The detailed applications information presented is organized as follows:

1. LEUKOCYTE SUBSET ANALYSIS

1.1 Sample Preparation

Ficol
FACS™ Lysing Solution
Ammonium Chloride Lysis
Viability
Fixation

1.2 Direct Immunofluorescence Stain

Simultest IMK Plus™
Simultest™ Reagents
SimulSET™ Software

1,3 Indirect Immunofluorescence Stain

2. THREE PART DIFFERENTIAL

2.1. Three-part Differential Using Light Scatter

2.2. Three-part Differential Usint Leucogate

3. METHODS OF CONJUGATING FLUOROCHROMES TO ANTIBODIES

Succinimide Chemistry
Maleimide Chemistry
Isothiocyanate Chemistry

3.1 Procedure: FITC Labelling/Biotinylation of Antibodies

4. WET LAB

4.1. Calibration with Chicken Red Blood Cells

4.2. Whole Blood, Two or Three Color Immunofluorescence

Granulocytes and red blood cells collect in a pellet at the bottom of the separation tube. The viable mononuclear cells can then be used for immunophenotyping analysis or cell function studies.

FACS Lysing Solution (Catalog No. 92-0002)

The FACS Lysing Solution is a premixed concentrate which lyses red blood cells and leaves the leukocyte population intact. In this method, a small volume of whole blood is first stained with monoclonal reagents, then treated with the Lysing Solution. Subsequent washes and centrifugations remove debris and platelets to prepare the leukocyte population for subset analysis.

For detailed information on the FACS Lysing Solution, see "Wet Lab, Whole Blood, Two or Three Color Immunofluorescence (4.2.)" or instructions attached or the FACS Lysing Solution package insert.

Ammonium Chloride Lysis

The Ammonium Chloride Lysis method utilizes a salt solution to remove red blood cells from a whole blood specimen while leaving the white blood cell population intact. In this method a small volume of the blood sample is first lysed with the Ammonium Chloride solution. The cells are washed and centrifuged before staining with the monoclonal antibody. The leukocytes are now ready for subset analysis.

For detailed information on the Ammonium Chloride Lysis method, see Becton Dickinson Source Book, Section 2.11.

Viability Staining

Viability Staining is used to check the viability of the leukocyte population after blood processing by Ficoll, or Ammonium Chloride Separation. A solution of two fluorescent dyes, Ethidium Bromide and Acridine Orange, are used with a fluorescence microscope to assess the viability of the leukocyte population prior to staining with the monoclonal reagents. Viable cells fluoresce green, and non-viable cells fluoresce orange when viewed under the microscope.

For detailed information on Viability Staining Using Ethidium Bromide and Acridine Orange, see Becton Dickinson source Book. Section 2.3.

Fixation

Fixation is employed to preserve cellular integrity and fluorescence. Fixation is performed by treating stained cells with a formaldehyde or paraformaldehyde based solution and incubating the cells in the cold, protected from light until analysis.

1. LEUKOCYTE SUBSET ANALYSIS

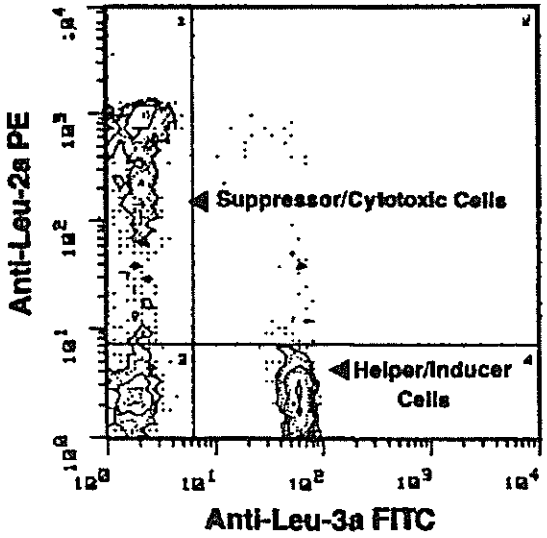

Lymphocyte subset analysis
Normal human lysed whole blood labeled with Becton Dickinson Simultest™ reagents. Lymphocyte gating was based on forward and side scatter.

Quatitation of leukocyte subpopulations is an application easily performed on the FACScan. Leukocyte subset analysis is achieved by measuring size (light scatter) and fluorescence intensity of the cells as they pass through the interrogation point of the laser beam.

1.1 Sample Preparation

Proper sample preparation is essential to achieving good results when performing leukocyte analysis. Specimens for leukocyte subset analysis are prepared from blood collected by venipuncture into an EDTA (k3) blood collection tube. The white blood cell population is separated from other blood components by either density gradient or lytic methodologies. Distinct leukocyte subsets are identified by means of a fluorescent tag bound to an antibody on the cell surface. Once stained, cells are fixed and analyzed with the FACScan within two or three days.

Ficoll

Ficoll gradients can also be used in the isolation of mononuclear cells from human whole blood. The technique is based upon density gradient separation and involves careful layering of diluted blood specimen over a Ficoll and sodium diatrizoate solution. After spinning the gradient in a centrifuge, the mononuclear cells are removed at the resulting interface.

For detailed information on Paraformaldehyde fixation of Stained Cells, see Becton Dickinson Source Book, Section 2.10.

1.2 Direct Immunofluorescence Staining of Cell Surface Markers

Direct Immunofluorescence assays are used to identify leukocyte subpopulations for immunophenotypic analysis. In a direct immunofluorescence assay, a fluorochrome-labelled antibody is incubated with the cells, the unbound antibody is washed away, and the stained cell population is then analyzed. Analysis on the FACScan measures cellular size by forward and right angle light scatter as well as the immunofluorescence properties of the cell. Combinations of fluorochromes, e.g. FITC and PE, allow the simultaneous measurement of additional markers on the cell surface.

For detailed information regarding Single-Color Direct Immunofluorescence, see Becton Dickinson Source Book, Section 2.4.

For detailed information regarding Two-Color Direct Immunofluorescence, see Becton Dickinson Source Book. Secton 2.13.

Simultest IMK Plus™(Catalog No. 92-0017)

The Simultest IMK Plus Kit is based upon a two-color direct immunofluorescence staining procedure. Peripheral blood mononuclear cells or whole blood specimens are incubated with the monoclonal reagent mixtures from the kit, lysed (whole blood), washed, fixed, and then analyzed on the FACScan. Cells are analyzed by forward and right angle light scatter properties correlated with two-color immunofluorescence (FITC and PE). Optional Simultest IMK Plus software is available to provide the operator with automatic gating and analysis or the cellular subsets.

For detailed information on the Simultest IMK Plus Kit, see the Simultest IMK Plus Kit package insert.

Simultest Reagents

The Simultest Reagents are based upon a two-color direct immunofluorescence staining assay. Peripheral blood mononuclear cells or whole blood specimens are incubated with the monoclonal reagent mixtures, lysed (whole blood), washed, fixed, and then analyzed on the FACScan. Cells are analyzed by forward and right angle light scatter correlated with two-color immunofluorescence (FITC and PE). Optional Simultest software is available for use with the Simultest reagents and provides the operator with automatic gating and analysis of the lymphocyte subsets.

1. LEUKOCYTE SUBSET ANALYSIS

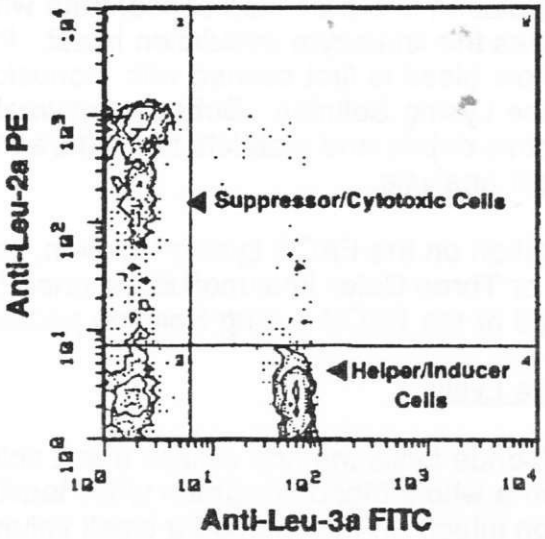

Lymphocyte subset analysis
Normal human lysed whole blood labeled with Becton Dickinson Simultest™ reagents. Lymphocyte gating was based on forward and side scatter.

Quatitation of leukocyte subpopulations is an application easily performed on the FACScan. Leukocyte subset analysis is achieved by measuring size (light scatter) and fluorescence intensity of the cells as they pass through the interrogation point of the laser beam.

1.1 Sample Preparation

Proper sample preparation is essential to achieving good results when performing leukocyte analysis. Specimens for leukocyte subset analysis are prepared from blood collected by venipuncture into an EDTA (k3) blood collection tube. The white blood cell population is separated from other blood components by either density gradient or lytic methodologies. Distinct leukocyte subsets are identified by means of a fluorescent tag bound to an antibody on the cell surface. Once stained, cells are fixed and analyzed with the FACScan within two or three days.

Ficoll

Ficoll gradients can also be used in the isolation of mononuclear cells from human whole blood. The technique is based upon density gradient separation and involves careful layering of diluted blood specimen over a Ficoll and sodium diatrizoate solution. After spinning the gradient in a centrifuge, the mononuclear cells are removed at the resulting interface.

For detailed information on Paraformaldehyde fixation of Stained Cells, see Becton Dickinson Source Book, Section 2.10.

1.2 Direct Immunofluorescence Staining of Cell Surface Markers

Direct Immunofluorescence assays are used to identify leukocyte subpopulations for immunophenotypic analysis. In a direct immunofluorescence assay, a fluorochrome-labelled antibody is incubated with the cells, the unbound antibody is washed away, and the stained cell population is then analyzed. Analysis on the FACScan measures cellular size by forward and right angle light scatter as well as the immunofluorescence properties of the cell. Combinations of fluorochromes, e.g. FITC and PE, allow the simultaneous measurement of additional markers on the cell surface.

For detailed information regarding Single-Color Direct Immunofluorescence, see Becton Dickinson Source Book, Section 2.4.

For detailed information regarding Two-Color Direct Immunofluorescence, see Becton Dickinson Source Book. Secton 2.13.

Simultest IMK Plus™(Catalog No. 92-0017)

The Simultest IMK Plus Kit is based upon a two-color direct immunofluorescence staining procedure. Peripheral blood mononuclear cells or whole blood specimens are incubated with the monoclonal reagent mixtures from the kit, lysed (whole blood), washed, fixed, and then analyzed on the FACScan. Cells are analyzed by forward and right angle light scatter properties correlated with two-color immunofluorescence (FITC and PE). Optional Simultest IMK Plus software is available to provide the operator with automatic gating and analysis or the cellular subsets.

For detailed information on the Simultest IMK Plus Kit, see the Simultest IMK Plus Kit package insert.

Simultest Reagents

The Simultest Reagents are based upon a two-color direct immunofluorescence staining assay. Peripheral blood mononuclear cells or whole blood specimens are incubated with the monoclonal reagent mixtures, lysed (whole blood), washed, fixed, and then analyzed on the FACScan. Cells are analyzed by forward and right angle light scatter correlated with two-color immunofluorescence (FITC and PE). Optional Simultest software is available for use with the Simultest reagents and provides the operator with automatic gating and analysis of the lymphocyte subsets.

For detailed information on the Simultest Reagents, refer to the Becton Dickinson Source Book Data Sheets on the individual Simultest Reagents.

1.3 Indirect Immunofluorescence Staining of Cell Surface Markers

Indirect Immunofluorescence assays are used to identify leukocyte subpopulations for immunophenotypic analysis. In an indirect immunofluorescence assay, cells are incubated with a primary unlabeled antibody, washed, incubated with a secondary antibody which is conjugated to a fluorochrome, washed, then analyzed. Analysis on the FACScan measures cellular size by forward and right angle light scatter as well as the fluorescence properties of the cell.

For detailed information on Indirect Immunofluorescence Staining, See Becton Dickinson Source Book, Section 2.5.

2. THREE PART DIFFERENTIAL

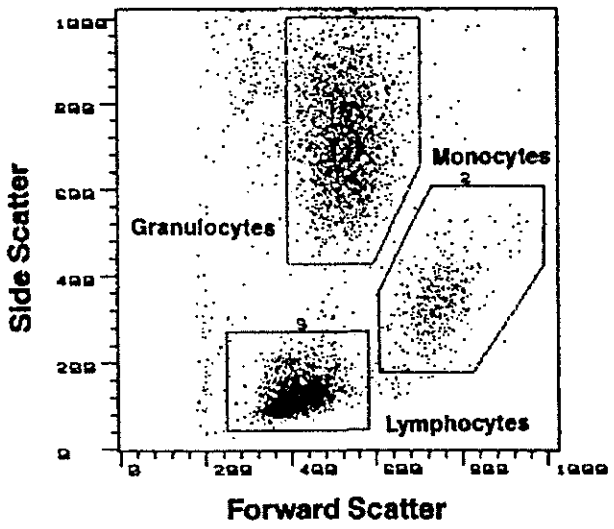

Three-part differential
Dual-parameter correlated dot plot display of forward and side scatter with non-rectangular windows

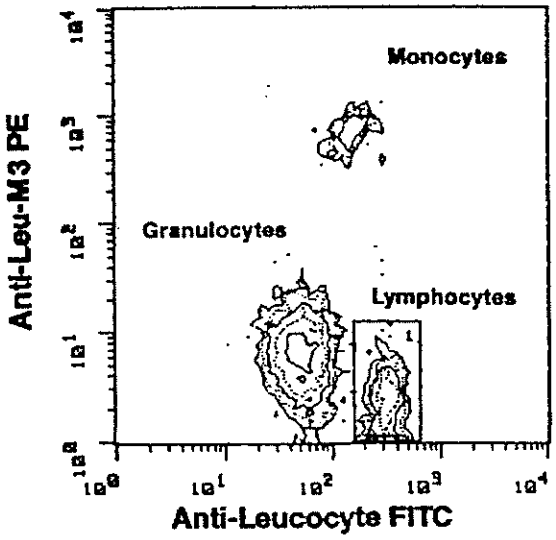

Lysed whole blood analysis
Contour plot of lysed whole blood labeled with Anti-Leucocyte (HLe-1) FITC and Anti-Leu-M3 PE. Window is set on lymphocytes.

The FACScan is capable of performing a three-part differential by examining the percentages of lymphocytes, monocytes, and granulocytes in a lysed whole blood preparation.

2.1 Three-Part Differential Using Light Scatter

A Three-Part Differential is obtained by lysing a small volume of whole blood with either the FACS Lysing Solution or the Ammonium Chloride Lysing Solution. After lysis the cells are washed then taken to the FACScan for analysis. Analysis is performed by examination of the forward and right angle light scatter properties of the cells.

The FACScan is capable of performing a three-part differential by examining the percentages of lymphocytes, monocytes, and granulocytes in a lysed whole blood preparation.

PAINT-A-GATE allows the simultaneous analysis of light scatter and fluorescence for LeucoGATE samples.

2.2 Three-Part Differential Using Leucogate

A Three-Part Differential is obtained by staining a small volume of whole blood with the leucogate monoclonal mixture (anti-HLe-I FITC/anti-Leu-Me PE). The blood is then lysed using the FACS lysing Solution, washed, fixed, and taken to the FACScan for analysis. Analysis is performed by examination of the fluorescence parameters (FITC and PE) of the cells.

WET LAB

4.1. Calibration with CRBC

Note that CRBC will only adjust PMT settings and compensation must be set with a stained cell sample. However they provide a means to quickly calibrate the instrument the same way from day to day. Briefly CRBC are used as follows: with compensation set at zero for all fluorescence parameters an unstained PBMC or lysed whole blood specimen is run. The PMT settings are adjusted so that unstained lymphocytes (mean log fluorescence) are located in approximately channel 120 (1024 full scale) for FL1, FL2 and FL3. Then a CRBC or Fluoresbrite sample in run and the mean log fluorescence determined for the CRBC in each parameter. Subsequently one needs only to run the CRBC sample and set mean log fluorescence to these predetermined values. Our experience is that the predetermined values are also very similar from instrument to instrument.

4.2. Whole Blood, Two or Three Color Immunofluorescence

Stain:
- Add 100 µL whole blood to 20 µL MAb reagent(s).
- Incubate 15 min. at room temperature in the dark.

Lyse:
- Add 2 mL 1x FACS Lysing Solution.
- Vortex immediately and incubate 7-10 minutes at room temperature in the dark. Do not exceed 12 min. for any one tube.
- Spin at 300xg for 5 min.
- Aspirate the supernatant.
- Leave ~50 µL to avoid disturbing the pellet.

Wash:
- Add 2 mL PBS with 0.1% sodium azide.
- Vortex
- Spin at 300xg for 5 min.
- Aspirate supernatent.
- Leave ~50 µL.

Fix:
- Vortex pellet.
- Add 0.5 mL of fixative (0.5% paraformaldehyde in PBS).
- Vortex immediately.
- Allow fixation to proceed for 30 min. at 4°.

Samples may be analyzed immediately or stored in the dark two to three days at 4°.

Biological pigments as fluorescent labels for cytometry

Diether Recktenwald, Barbara Prezelin+, Chia Huei Chen, John Kimura

Becton Dickinson Immunocytometry Systems
2350 Qume Drive, San Jose, CA 95131
+Department of Biology, UCSB, Santa Barbara, CA 93106

ABSTRACT

The use of protein-based biological pigments in combination with low molecular weight organic dye molecules allows the simultaneous detection of up to six independent components of a cell surface by antibody dependent fluorescence (immunofluorescence) excited with a single 488nm laser line. This paper describes the state of the art in multi-color immunofluorescence with 488nm Ar-ion laser excitation. It provides the data to design systems for specialized applications.

1. BIOLOGICAL PIGMENTS

The biological pigments used for immunofluorescence are associated with the photosynthetic system of plants or bacteria. In vivo these pigments act as efficient light collectors and energy transfer donors and acceptors for a wide range of the visible sun spectrum. For photosynthesis in low light environments, these pigments are optimized by nature for efficient light absorption and energy transfer. Most photosynthetic pigments are associated with water-

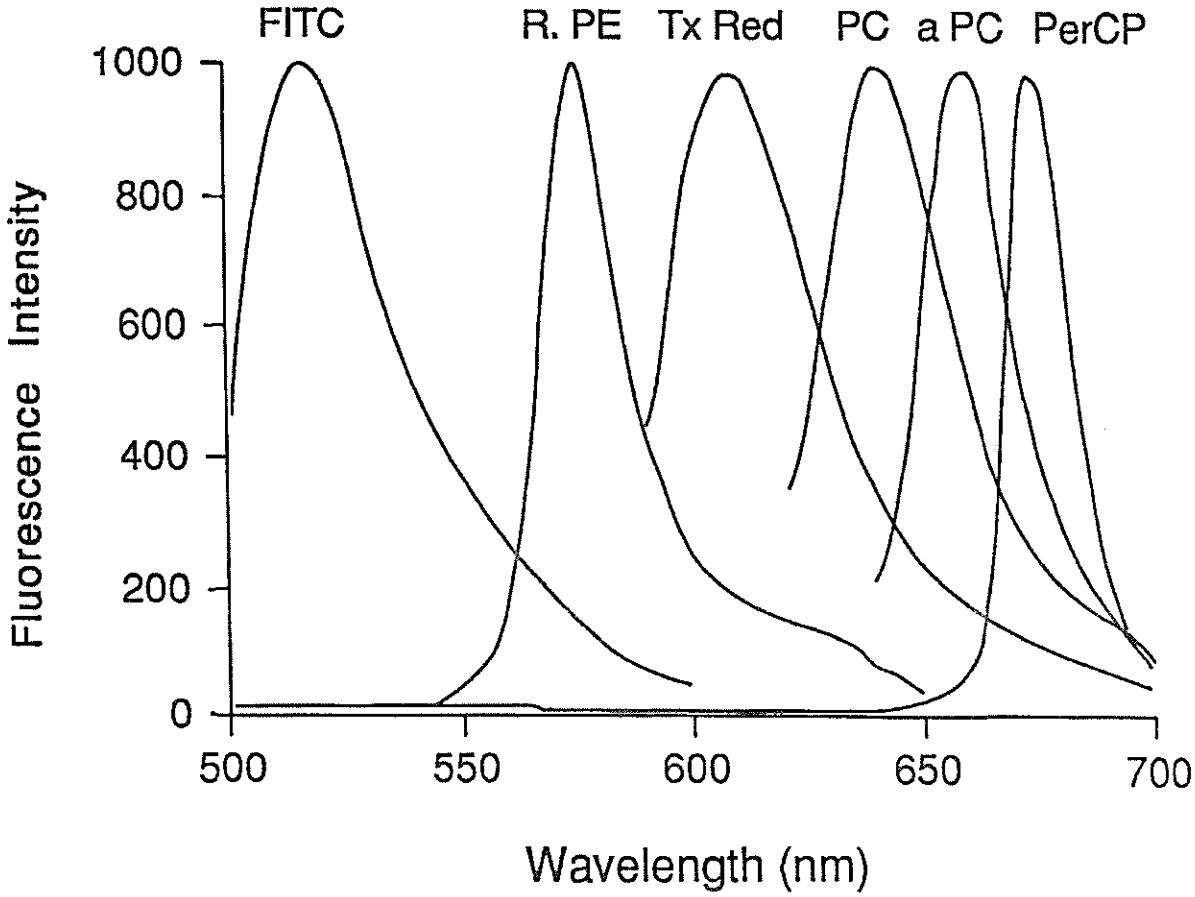

Fig. 1: Fluorescence emission spectra of fluorescein (FITC), R.-phycoerythrin (R.PE), Texas-red (TxRed), c-phycocyanin (PC), allo-phycocyanin (aPC) and peridinin-chlorophyll-a-protein (PerCP). Ecitation at 490nm for FITC, R.PE, PerCP, and at 545nm for TxRed, PC, aPC. Spectra are without correction from a Perkin Elmer MPF-2a spectrofluorimeter interfaced to a Hewlett Packard-200 desktop computer.

insoluble proteins and cannot be used easily as labels for immunofluorescent assays.[1] Two groups of water-soluble pigment protein complexes associated with photosynthetic systems are known:[1]

a. Phycobiliproteins
b. Peridinin - chlorophyll-a protein complexes (PerCP).

a. Phycobiliproteins

Phycobiliproteins are found as part of the photosynthetic systems of red algae and cyanobacteria. Three major pigment proteins are found, namely phycoerythrins, phycocyanins, and allophycocyanin.[2]

	Molecular weight	Abs max	Log E	Em max	Q.Y.
B-phycoerythrin	240,000	545	6.3	575	0.98
R-phycoerythrin	240,000	488,565	6.0	578	0.80
C-phycocyanine	224,000	620	6.2	650	0.50
allo-phycocyanine	104,000	650	5.8	660	0.70
R-phycocyanine	103,000	620	5.9	635	0.70
PerCP	35,000	470	5.5	680	1.00
Fluorescein	390	495	4.9	525	0.50
Texas red	624	595	4.9	620	?

Table 1: Properties of fluorescent dyes used as labels for immunofluorescence analysis. (Abs max = wavelength of the absorbance maximum in nm, Log E = decadic logarithm of the molar extinction coefficient, Em max = wavelength of the technical fluorescence emission maximum in nm, Q.Y. = fluorescence quantum yield data[2,3,4])

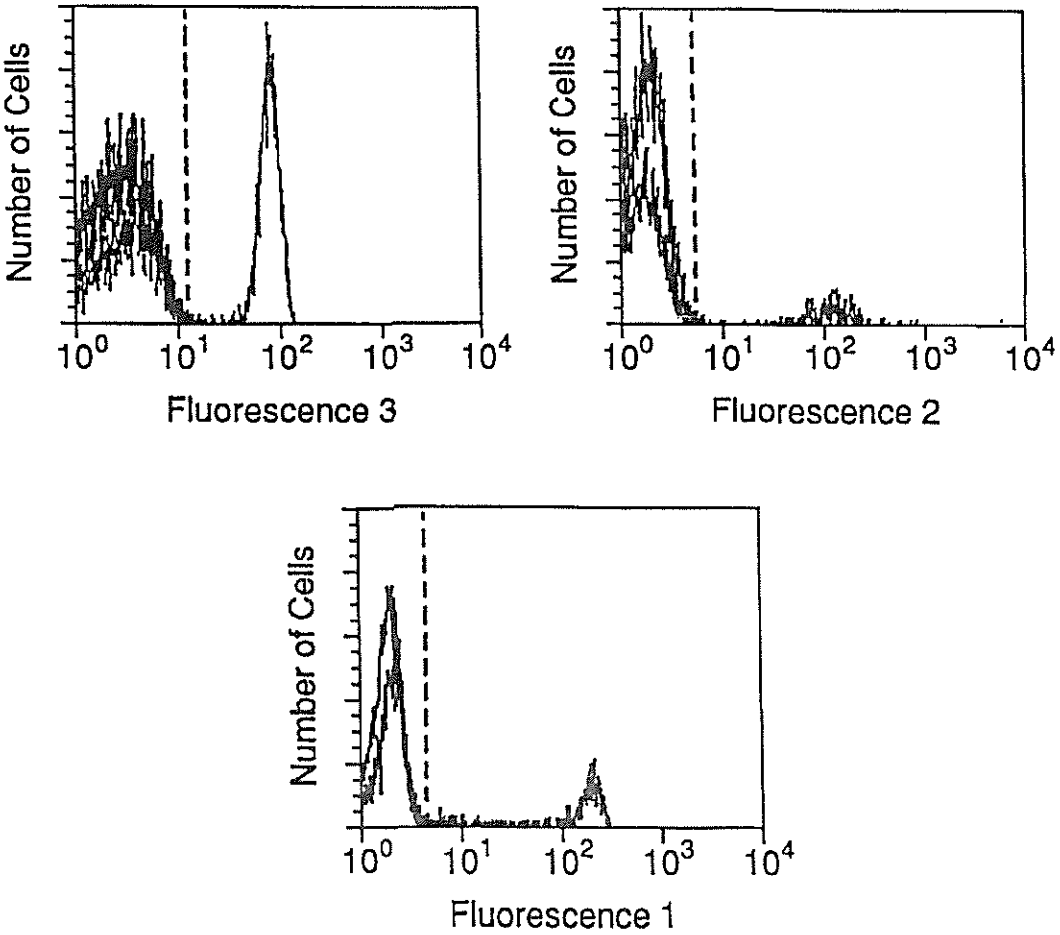

Fig. 2: Fluorescence histograms of lymphocytes stained with leu-2a-FITC (Fluorescence 1), leu-2a-R.PE (Fluorescence 2), and leu-3a-biotin avidin-PerCP (Fluorescence 3) overlaid with histograms of unstained controls. The measurements were performed with a FACScan flow cytometer with 488nm excitation.

b. Peridinin-chlorophyll a-protein complexes

Peridinin-chlorophyll a-protein complexes are found as part of the photosynthetic systems of dinoflagellates. The pigment, a water-soluble protein with a molecular weight of 35,000, contains the chromophors peridinin, a carotene, and chlorophyll-a as light absorbers.

Table1 lists the optical properties of some of these pigments together with two commonly used fluorescent dyes of low molecular weight.

Three of the dyes, fluorescein, R-phycoerythrin, and the peridinin chlorophyll protein can be excited with the 488nm line of an Ar-ion laser. The fluorescence emission spectra are sufficiently different (Fig. 1) to allow the simultaneous determination in a mixture.[5,6] It has been shown that all of these dyes can be conjugated to immunoglobulins (antibodies) without interfering substantially with antigen binding properties[6,7,8,9]. The dyes also do not introduce non-specific cell binding properties into the dye-antibody complex as shown in the histogram of Fig. 2, where the non-reactive cell population is indistinguishable from non-reacted cells.

Therefore, a combination of antibody conjugates of fluorescein, R-phycoerythrin, and the peridinin chlorophyll protein can be used for simultaneous determination of three different antigens in solution or on biological cells.

2. TANDEM PIGMENTS

The dyes of Table 1, which do not absorb significantly at 488nm, can be excited at 488nm by forming a "tandem" molecule with an energy donor, which absorbs 488nm light. A good such donor is R-phycoerythrin[10,11]. Covalently coupled conjugates of Texas red, c-phycocyanin, and allo-phycocyanin with R-phycoerythrin show a relatively small level of R-phycoerythrin emission when excited at 488nm (data not shown). Most of the fluorescence of the conjugates arises from the acceptor molecules. Immunoglobulin conjugates of these fluorescent tandem molecules are reactive with their respective antigens as will be shown later (Fig.4). The spectra in Figure 1 indicate that simultaneous six-color immunofluorescence measurements are possible with fluorescein, phycoerythrin, the peridinin-chlorophyll protein, and the phycoerythrin tandem conjugates of Texas red, c-phycocyanin, and allo-phycocyanin. Experiments showing the feasibility of such measurements are described in Section 4 (Fig.4).

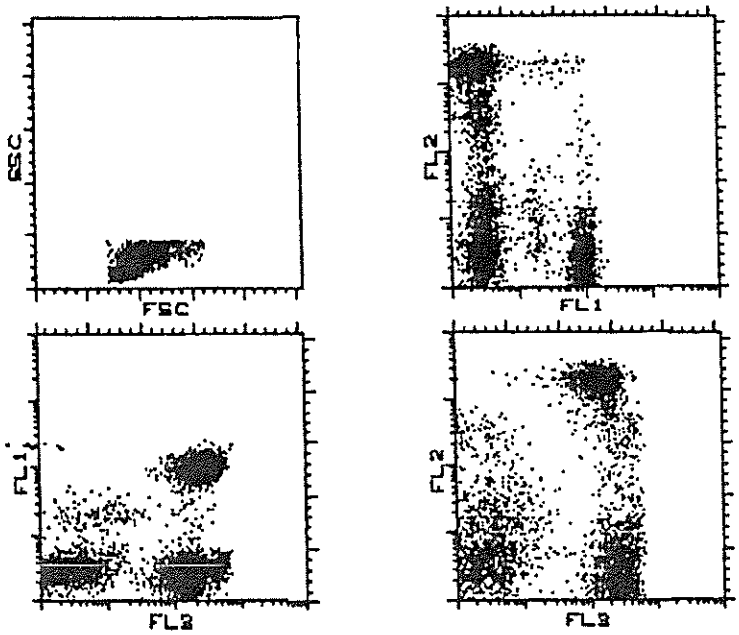

Fig. 3: Dotplots of a three-color immunofluorescence measurement with FITC, R.PE, and PerCP.Human mononuclear cells stained with anti-leu-3a-FITC, anti-leu-2a-PE, and anti-leu-4-PerCP were analyzed with a FACScan flow cytometer. Laser power at 488nm 16.9mW, spectral overlap compensation: Fl1-%Fl2=0.3% Fl2-%Fl1=44.0%,Fl2-%Fl3=0.0%,Fl3-%Fl2=17.5% (data coutesy of Rick Kerndt and Andy Blidy, BDMC)

3. THREE-COLOR IMMUNOFLUORESCENCE WITH SINGLE-LINE 488nm EXCITATION

Several of the dyes discussed above can be used in combination with fluorescein and phycoerythrin for three color fluorescence analysis. The trade off in the selection of the third dye is between sensitivity and spectral overlap. Table 2 lists approximate sensitivities and spectral overlap for most of the dyes measured with a Becton Dickinson FACScan instrument. The sensitivity is expressed as the ratio of the fluorescence intensity of stained and unstained lymphocytes. The data shows that PerCP is the best choice for the third dye since it minimizes spectral overlap. Fig. 3 shows the results of a three-color immunfluorescence experiment with fluorescein, phycoerythrin and PerCP.

		Relative spectral overlap			
	Sensit.	FITC	R.PE	R.PE - Tx. r.	PerCP
FITC	1	1.0	0.20	0.02	0.003
R.PE.	10	0.015	1.0	0.80	0.08
R.PE. - Tx.r.	5	0.01	0.80	1.0	0.10
PerCP	1	0.000	0.000	0.00	1.0

Table 2: Relative sensitivities and spectral overlap for four fluorophors useful for multi-color immunofluorescence measurements. (The sensitivity numbers were determined with cell samples for cell surface immunofluorescence measurements run on a FACScan flow cytometer. The sensitivity for FITC was set to 1. Spectral overlap was estimated from fluorescence emission spectra and agrees well with data from multicolor cell surface immunofluorescence measurements.)

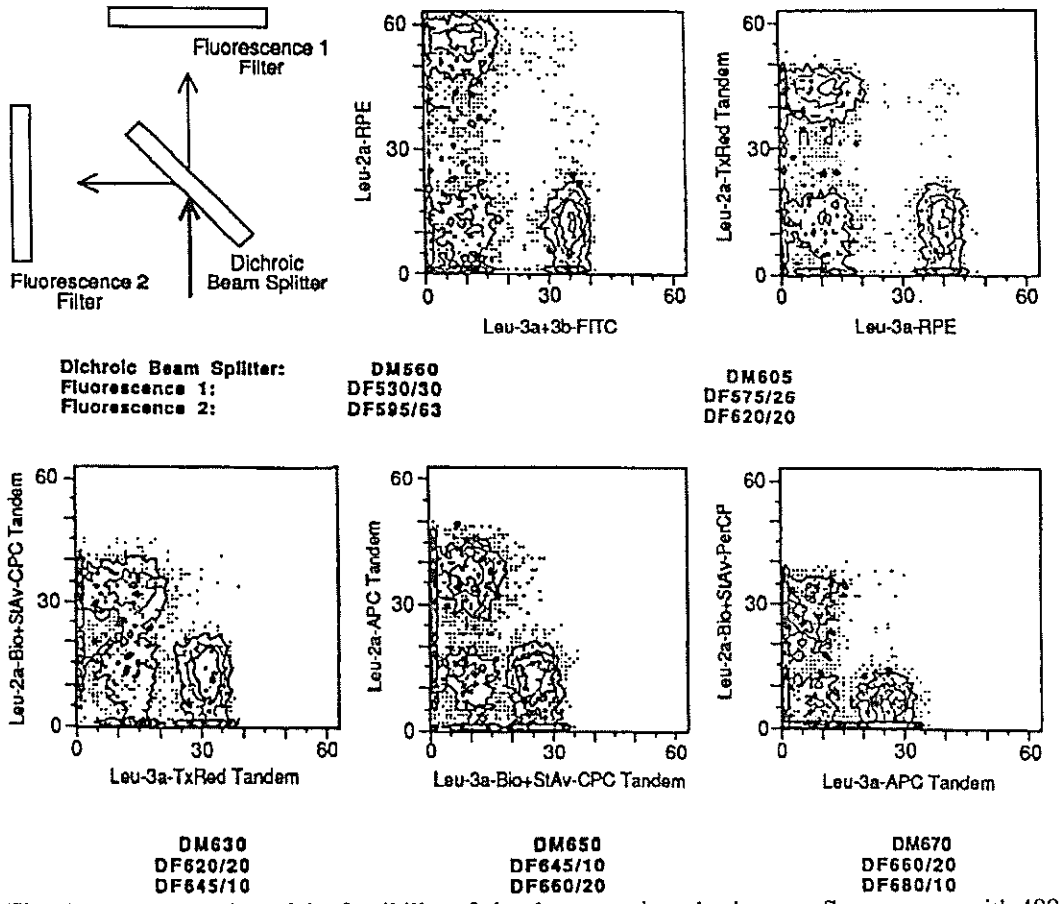

Fig. 4: Demonstration of the feasibility of simultaneous six-color immunofluorescence with 488nm excitation.

4. FEASIBILITY OF SIX-COLOR IMMUNFLUORESCENCE WITH 488nm EXCITATION

Because of instrumental limitations, the feasibilility of the simultaneous detection of six colors (wave length bands) of fluorescence was not performed directly. Instead, it was shown that filters can be selected to allow the independent detection of the cell surface immunfluorescence from all of the five critical pairs i.e. the pairs with most similar emission spectra. Lymphocyte cells from human blood were reacted with an anti-CD4 antibody with one fluorescent label and an anti-CD8 antibody with the other fluroescent label. About 50% of the lymphocytes carry the CD4 antigen, 20% the CD8 antigen, and 30% are not reactive with either of the labels. Fig. 4 shows the filters used for the experiments with the results of the critical two-color measurements. Two lines parallel to the axes can be used to separate the three populations in all the cases, proving that the different dyes can be measured independently. Therefore, this data shows that six-color immunfluorescence with single line 488nm excitation is feasible.

5. APPLICATIONS

The possiblity of performing three or more color immunofluorescence measurements extends the range of applications in cell biology and clinical research substantially. More measurements can be performed on the same sample. Cell subpopulations defined by two-color immunofluorescence techniques can be further subdivided by using three or more color analysis[12].

By using three color immunofluorescence analysis in combination with a measurement of axial light loss, all of the major leukocyte subpopulations including lymphocyte subpopulations can be counted in a single sample.[13]

Helper and suppressor cell ratios can be measured with greater precision in a single sample by adding a third reagent to help eliminate interference from cells other than T cells. In general the measurement of more specific parameters improves the probability for the correct classification of a cell in cell analysis. This is one of the reasons digital imaging microscopy with its many measurement parameters is preferred over flow-cytometry for rare event analysis, even though flow cytometry provides the higher analysis rates desired for rare cell detection. Three or more color immunofluorescence techniques will make it possible to perform rare cell analysis by flow cytometry.

In another application sample preparation for leukocyte subset analysis can be simplified by allowing the analysis of leukocyte cell surface immunofluorescence in the presence of erythrocytes (red cells), thus eliminating the need for a red cell lysis step[14]. In this application reagents are selected to only render leukocytes or a desired subset of leukocytes fluorescent in one color. This fluorescence is then used to trigger the data acquisition electronics of a flow cytometer. Red cells and platelets appear dark and are not analyzed by the system. This approach requires one fluorescent color to identify leukocytes, therefore a three-color system permits two-color subset analysis.

Once three color immunofluorescence techniques become available for routine cell analysis, more applications will be found. This paper has described the state of the art in multi-color immunofluorescence with 488nm Ar-ion laser excitation. It provides the data to design systems for specialized applications.

6. REFERENCES

1. D. Sieferman-Harms, "Carotenoids in photosynthesis," Biochem.Biophys.Acta 811, pp. 325-55. 1985.
2. A.N. Glazer, "Photosynthetic Accessory Proteins with Bilin Prosthetic Groups," The Biochemistry of Plants, Vol. 8, 51 ff, 1981.
3. Richard P. Hangland, "Handbook of Fluorescent Probes and Research Chemicals," Molecular Probes, 1985.
4. B.B. Prezelin, et.al, "Purification and Characterization of Peridinin-Chlorophyll a-Proteins from the Marine Dinoflagellates Glenodinium sp. and Gonyaulax polyedra," Planta (Berlin), 128, pp133-44 , 1976.
5. D.J. Recktenwald, et al., "Multicolor fluorescence analysis with single wavelength excitation," US Patent No. 4,745,285. May 17 1988.
6. D.J. Recktenwald, "Peridinin-chlorophyll complex as fluorescent label," US Patent No. 4,876,190. Oct.24 1989.
7. V.T. Oi, et al., "Fluorescent phycobiliprotein conjugates for analyses of cells and molecules," J. Cell Biol. 93, pp.981-6. 1982.
8. L. Stryer, et al. "Fluorescent conjugates for analyses of molecules and cells," US Patent No. 4,859,582. Aug.22 1989.
9. M.N. Kronick, "The use of phycobiliproteins as fluorescent labels in immunoassay," J. Immunol. Methods 92, pp.1-13. 1986.
10. A.N. Glazer, et al., "Fluorescent Tandem Phycobiliprotein Conjugates," Biophys.J. 43, pp. 383-6. 1983.

11. L. Stryer, et al., "Phycobiliprotein Fluorescent Conjugates," US Patent No. 4,542,104. Sep.17 1985.
12. L. L. Lanier, et al., "Correlation of cell surface antigen expression on human thymocytes by multi-color flow cytometric analysis: implications for differentiation," J. Immunol. 137, pp 2501-7. 1986.
13. C. C. Stewart, et al., "Resolving leukocytes using axial light loss," Cytometry 10, pp.426-32. 1989
14. D.J. Recktenwald, "Method for analysis of subpopulations of blood cells," US Patent No. 4,727,020. Feb.23 1988.

PerCP

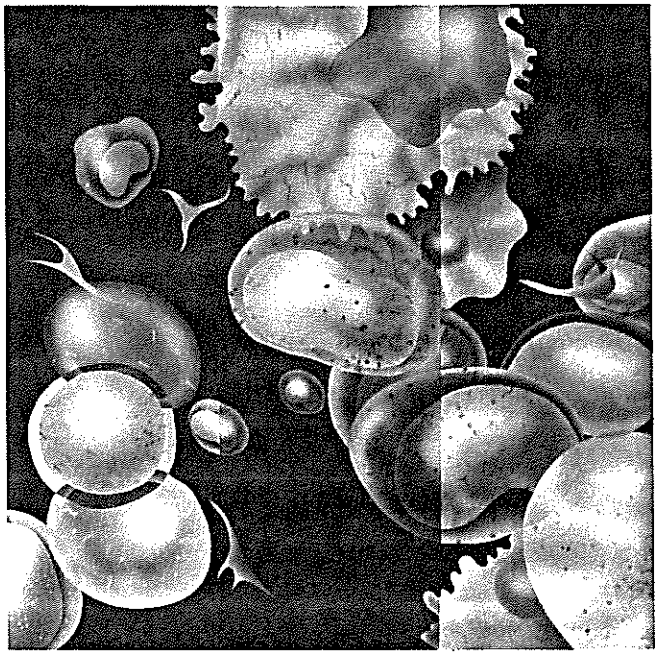

Introducing The First Multidimensional, Three-Color Analysis On A Single Laser System*

For nearly a decade, Becton Dickinson has been helping scientists on the threshold of advanced research and clinical technology with its superior flow cytometric reagents and instrumentation for cell analysis and immune monitoring. In 1983, we were the first to introduce phycoerythrin (PE*) conjugates. And in 1986, we pioneered fluorochrome technology with the introduction of the unique two-color Simultest™ reagents that allow research scientists and clinicians to gather more information quickly and easily.

Now Becton Dickinson Immunocytometry Systems brings you the next generation conjugate. Introducing the world's first directly conjugated peridinin chlorophyll protein reagent (PerCP**) to perform multidimensional, three-color analysis on a single-laser flow cytometer. Another first that provides you with the kind of innovation, quality, and performance that you have come to expect from Becton Dickinson.

*FOR RESEARCH USE ONLY

The research pioneer.
The clinical leader.

BECTON DICKINSON

Multiple Answers In One Experiment

New PerCP single dye conjugate reagents work in conjunction with Becton Dickinson's proven Simultest reagents — FITC and PE — and the world's most widely-used single-laser flow cytometer, the FACScan,™ to perform three-color, five-dimensional cellular analysis. PerCP reagents have a peak emission spectrum (677nm), which minimizes spectral overlap with FITC and PE dyes. Its high fluorescence intensity significantly simplifies multicolor analysis and assists in the evaluation of more lymphocyte subsets based on fluorescence. You can now study activation, differentiation, and proliferation of T-lymphocytes, which is of particular value in studies of AIDS and autoimmune disease and in characterizing T-cell lymphomas and leukemias.

Increase Your Productivity and Efficiency

PerCP conjugates are easy to use and save time in multicolor analysis compared with indirect staining methods. With the direct PerCP conjugates Anti-Leu™-4 (CD3), Anti-Leu-2a (CD8), and Mouse IgG_1 Control, in combination with other FITC and PE reagents, simultaneous detection of single-, double-, and triple-stained cells becomes an easy, one-step staining process — providing more subset information from a single tube. In addition, with PerCP reagents, instrument setup is fast and easy, and compensation is readily achieved. Specimen economy and increased information — all from a single tube.

Put Your Experiments on the Research Edge

Becton Dickinson strives to provide you with the best possible tools to enhance the overall results of your experiments — the kind that put you on the cutting edge of research technology. PerCP, the single dye conjugate reagent, is a dramatic leap in fluorochrome technology that will improve your productivity, significantly increase your subsetting ability, and give you more results from a single experiment. Another product on the forefront of technology from Becton Dickinson.

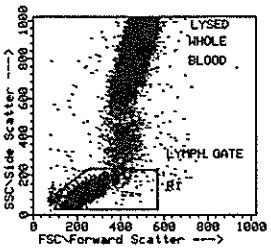

1. Whole blood stained with Simultest™ Leu-4 (CD3) FITC/11+19 (CD16+56) PE, and Anti-Leu-2a(CD8) PerCP. Blood was lysed with FACS® Lysing Solution and analyzed on a FACScan. LYMPH GATE set using forward scatter (FSC) vs. side scatter (SSC) to perform multicolor analysis.

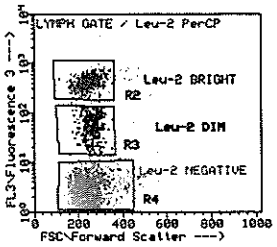

2. Display of FSC vs. Leu-2a PerCP (FL3). Three populations of lymphocytes gated as follows: a) Leu-2a BRIGHT b) Leu-2a DIM and c) Leu-2a NEGATIVE.

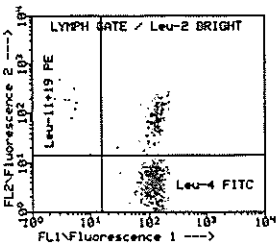

3. Display of Leu-4 FITC (FL1) vs. Leu-11 + 19 PE (FL2) cells that are Leu-2a BRIGHT, and also present in LYMPH GATE.

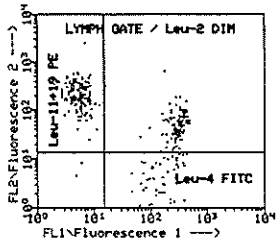

4. Display of Leu-4 FITC (FL1) vs. Leu-11 + 19 PE (FL2) cells that are Leu-2a DIM, and also present in LYMPH GATE.

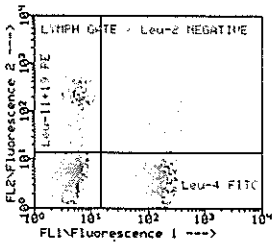

5. Display of Leu-4 FITC (FL1) vs. Leu-11 + 19 PE (FL2) cells that are Leu-2a NEGATIVE, and also present in LYMPH GATE.

Whole blood stained with Leu-4 (CD3) PerCP, Leu-3a (CD4) PE and Leu-2a (CD8) FITC. Blood was lysed with FACS Lysing Solution and analyzed on a FACScan. LYMPH GATE set using FSC vs. SSC to perform multicolor analysis.

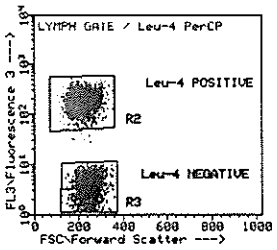

6. Display of FSC vs. Leu-4 PerCP(FL3). Leu-4 POSITIVE, and Leu-4 NEGATIVE lymphocyte populations gated.

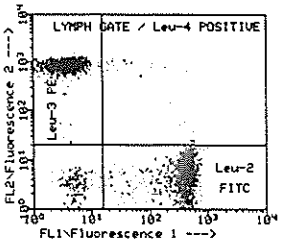

7. Display of Leu-2a FITC (FL1) vs. Leu-3a PE (FL2) cells that are Leu-4 POSITIVE, and are present in LYMPH GATE.

Product	Catalog #	Tests
Mouse IgG_1, PerCP	90-9044	100
Anti-Leu-4 (CD3) PerCP	90-7344	100
Anti-Leu-2a (CD8) PerCP	90-7314	100

NOTE: PerCP conjugates are recommended for use only on the FACScan flow cytometer. For Research use only. Not for use in diagnostic or therapeutic procedures.

FACScan,™ Simultest,™ and Leu™ are registered trademarks of Becton Dickinson Immunocytometry Systems. *U.S. Patent 4,520,110; European Patent 76,695; Canadian Patent 1,179,942. **U.S. Patent 4,876,190; others pending. ©1991 Becton Dickinson

BECTON DICKINSON

Becton Dickinson
Immunocytometry Systems
2350 Qume Drive
San Jose, CA 95131-1807
Ordering Information
(800) 223-8226
Customer Support Center
(800) 448-BDIS
Fax (408) 954-BDIS

Becton Dickinson
Canada, Inc.
2464 South Sheridan Way
Mississauga, Ontario L5J 2M8
Canada
Tel (416) 822-4820
Fax (416) 822-2644

Becton Dickinson
European HQ
Denderstraat 24
B-9320 Erembodegem-Aalst
Belgium
Tel (32) 53-787830
Fax (32) 53-789348

Nippon Becton Dickinson
Company, Ltd
Shimato Bldg
5-34, Akasaka 8-chome
Minato-ku, Tokyo 107
Japan
Tel (81) 3-3403-9991
Fax (81) 3-3403-5008

Becton Dickinson
Worldwide Inc
30 Tuas Avenue #2
Singapore 2263
Tel (65) 860-0633
Fax (65) 860-1590

23-2113-00

Becton Dickinson Procedures

Setting up the FACScan™ for Three-Color Flow Cytometric Analysis with PerCP* Conjugates

This Source Book Section describes a procedure for setting up a FACScan flow cytometer for three-color analysis of human peripheral blood leucocytes that have been stained with fluorescein (FITC)-, phycoerythrin** (PE)-, and peridinin chlorophyll protein (PerCP)-conjugated monoclonal antibodies. NOTE: PerCP conjugates are recommended for use only on the FACScan flow cytometer.

Cells

Human peripheral blood cell suspension. Whole blood or separated mononuclear cells may be used. (For preparation of separated mononuclear cells, see Becton Dickinson Procedure for Preparation of Single-Cell Suspensions from Human Peripheral Blood, Source Book Section 2.2.)

Reagents

1. FITC, PE, and PerCP-conjugated monoclonal antibodies to human leucocyte antigens. NOTE: Care must be taken to match relative antigen density to fluorochrome intensity when performing three-color analysis. Generally, the antigen which is present in the lowest density should be stained with the brightest fluorochrome (PE).

2. 1X phosphate-buffered saline (PBS) containing 0.1% sodium azide. (Dulbecco's PBS without calcium, magnesium or phenol red, pH 7.2 ± 0.2).[1] The PBS should be filtered through a 0.2 µm filter prior to use. Store at 2° to 8°C. WARNING: Sodium azide under aqueous acidic conditions yields hydrazoic acid, an extremely toxic compound. Azide compounds should be diluted with large volumes of water during disposal to avoid deposits in lead or copper plumbing where explosive conditions may develop.

3. 1.0 % paraformaldehyde. Use appropriate laboratory safety precautions. Dissolve 1g of paraformaldehyde in 100 mL of PBS with 0.1% sodium azide by carefully heating at temperatures up to 56°C in a chemical fume hood. Adjust to pH 7.4 ± 0.2, and filter through a 0.45 µm filter. Store in a glass container at 2° to 8°C. WARNING: Formaldehyde is toxic, allergenic, and considered a probable human carcinogen. Exercise precautions in storage and handling. Avoid contact with skin, eyes, and clothing. If skin or eye contact occurs, wash with copious amounts of water. Inhalation or ingestion is harmful and may be fatal. If swallowed, induce vomiting and contact a physician immediately. Dispose of according to federal, state, and local regulations.

4. CaliBRITE™ Beads, Becton Dickinson # 95-0002. Refer to the CaliBRITE Beads package insert for instructions for use.

Equipment

1. Low-speed centrifuge (300 x g) with swinging-bucket rotor and 12 x 75 mm tube carriers

2. 12 x 75 mm polystyrene test tubes (Becton Dickinson Falcon® #2058 or equivalent)

3. Micropipettor with tips (Pipetman™ or equivalent)

4. Ice bath

5. FACScan flow cytometer equipped for three-color fluorescence detection and two-parameter light scatter detection. For detailed information on the use of the FACScan see the FACScan User's Guide.

6. AutoCOMP™ Software. Refer to the FACScan AutoCOMP Software User's Guide.

7. FACScan Research Software or LYSYS™ II Software. Refer to the appropriate Software User's Guide.

Method For Direct Immunofluorescence

1. Peripheral Blood Mononuclear Cells:
   Add 10^6 cells in 50 µL of medium containing 0.1% azide to a mixture containing 20 µL of each monoclonal antibody. Mix gently and incubate in the dark for 15-30 minutes at 2° to 8°C. Wash twice, add 0.5 mL of 1.0 % paraformaldehyde, and analyze. See Becton Dickinson Procedure for Direct Immunofluorescence Staining of Cell Surfaces, Source Book Section 2.4.

*U.S. Patent 4,876,190; others pending.
** U.S. Patent 4,520,110; European Patent 76,695; and Canadian Patent 1,179,942

For research use only. Not for use in diagnostic or therapeutic procedures.

BECTON DICKINSON

Becton Dickinson Immunocytometry Systems
2350 Qume Drive
San Jose, CA 95131-1807
Ordering Information (800) 223-8226; Customer Support Center (800) 448-BDIS

2. Lysed Whole Blood:
   Add 100 µL of blood to a tube containing a mixture of 20 µL of each monoclonal antibody. Mix gently and incubate for 15-30 minutes at room temperature (20° to 25°C) in the dark. Vortex tube gently, then add 2 mL of FACS® Lysing Solution (Catalog No. 92-0002) at room temperature. (Dilute FACS Lysing Solution to 1X prior to use.) Vortex tube gently, then incubate for 10 minutes at room temperature in the dark. Wash cells, add 0.5 mL of 1.0 % paraformaldehyde, and analyze. Refer to the FACS Lysing Solution package insert for details.

Flow Cytometric Analysis

Proper electronic compensation and filter selections are necessary for three-color analysis. To properly set up and compensate the flow cytometer, these additional samples must be run: unstained cells; cells stained with the FITC reagent only; cells stained with the PE reagent only; and cells stained with the PerCP reagent only.

Instrument Setup

1. Run FACScan AutoCOMP software with CaliBRITE Beads. (Refer to the CaliBRITE Beads package insert and AutoCOMP User's Guide.) Print status page and save all PMT settings, gains, and compensation values for FL1 and FL2.

2. Execute acquisition software (FACScan Research Software or LYSYS II). If using FACScan Research Software, proceed to step 3 below. If using LYSYS II, set PMTs, gains, and compensation values for FL1 and FL2 to those obtained with AutoCOMP.

3. While running unlabeled CaliBRITE Beads, adjust the forward scatter (FSC) threshold to eliminate most debris. Set a FSC versus side scatter (SSC) gate around the bead singlet population. Set the FL3 PMT to log mode. Increase the FL3 PMT voltage from a starting value of 150 V until the unlabeled beads appear in channel 140 ± 10 (1024 channel scale) on the fluorescence display of the FL3 histogram (this usually occurs between 500 and 700 V). The unlabeled beads will appear in the lower left-hand corner of the three fluorescence dot displays. If a record of this data is desired, acquire 5,000 events and print a copy of the FL3 histogram analysis display.

4. Remove the beads from the FACScan.

Compensation Techniques

When excited by laser light at 488 nm, FITC, PE, and PerCP emit light at distinct wavelengths. However, there is a slight overlap of their emission spectra. Because the FL1, FL2, and FL3 detectors do not detect FITC, PE, or PerCP emissions exclusively, the amount of spectral overlap observed in these channels must be corrected by using an electronic compensation network. To confirm that compensation has been optimized, cells which have been singly-stained with each fluorochrome-labeled antibody should be run. See Figure 1 for examples of optimal compensation.

1. Set compensation levels for FL3. Set FL2-%FL3 to 0, and FL3-%FL2 to approximately 25.

2. Run the unstained cells. Set a light scatter gate around the lymphocyte population. If necessary, adjust the FL1, FL2, and FL3 PMTs so that the unstained cell population appears in the lower left-hand corner of the fluorescence display.

3. Run the singly-stained FITC cells. While monitoring the FL1 (green) versus FL2 (red-orange) dot display, optimize the FL2-%FL1 compensation level so that the FL1-positive population is horizontally aligned with the FL1-negative population.

4. Run the singly-stained PE cells. While monitoring the FL1 versus FL2 dot display, optimize the FL1-%FL2 compensation level so that the FL2-positive population is vertically aligned with the FL2-negative population. Then while monitoring the FL3 (red) versus FL2 (red-orange) dot display, optimize the FL3-%FL2 compensation level so that the FL2-positive population is vertically aligned with the FL2-negative population. **NOTE: Do not overcompensate FL3-%FL2.**

NOTE: Cells stained with a Simultest™ reagent such as Anti-Human Leu-3a (CD4) FITC/Anti-Human Leu-2a (CD8) PE (Catalog No. 95-0008) may be used in place of singly-stained cells to optimize FL2-%FL1 and FL1-%FL2 compensation. The reagent used should provide a preparation that will produce a sample with distinct FITC-positive and PE-positive populations, and few double-positive cells.

5. Run the singly-stained PerCP cells. The FL2-%FL3 compensation level should be set at 0. While monitoring the FL3 versus FL2 dot display, check to ensure that PerCP fluorescence is not detected in the FL2 channel. If it is detected, prepare a new singly-stained PerCP cell sample.

6. Save the final instrument settings as a file. These settings can be recalled each time a three-color experiment is run. Gains, PMT settings, and compensation levels can then be optimized as necessary. Any significant alterations in the PMT settings or compensation level for any channel should be noted. Refer to troubleshooting procedures listed in the FACScan Operator's Manual or the CaliBRITE Bead package insert.

7. Once compensation has been set, samples are ready for acquisition.

Figure 1: Two-Parameter Displays of Peripheral Blood Lymphocytes Analyzed with a FACScan Flow Cytometer

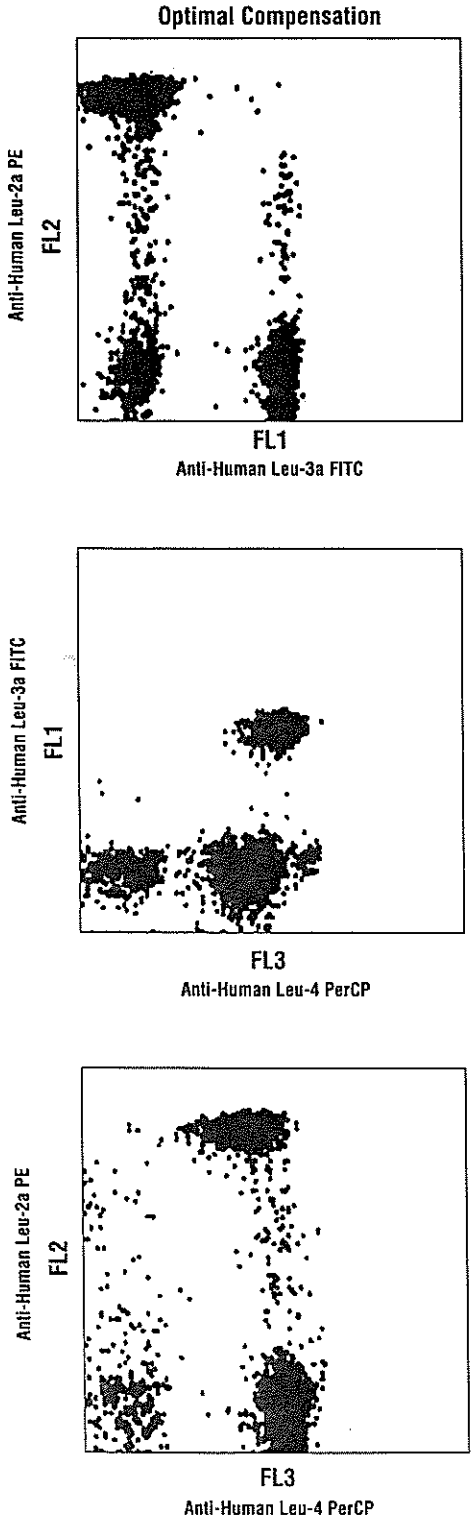

Limitations

1. PerCP conjugates are recommended for use **only** on the FACScan flow cytometer.

2. PMTs and compensation levels should be optimized for each experiment. Care must be taken when optimizing instrument conditions for three-color analysis and when selecting reagent combinations. The validity of data obtained with PerCP reagents is dependent on optimal instrument setup and proper cell handling techniques.

References

1. Rose NR, Friedman H, and Fahey JL. *Manual of Clinical Laboratory Immunology*, 3rd ed. Washington, DC: American Society for Microbiology; 1986:234.

Zusätzliche Literatur

1. Parks D.R., L.A.Herzenberg, L.A.Herzenberg: (1989) Flow cytometry and fluorescence activated cell sorting. In: Fundamental Immunology, Ed: W.E.Paul, Raven Press, New York, S.781-802

2. Normal Values: Definition of a reference range for lymphocyte subsets of healthy adults. Clinical Monographs No.I, Becton Dickinson Immunocytometry Systems, San Jose, USA

3. Loken M.R., J.M.Brosnan, K.A.Ault, B.A.Bach: Establishing optimal lymphocyte gates for immunophenotyping using LeucoGate. Clinical Monographs No.II, Becton Dickinson Immunocytometry Systems, San Jose, USA

FUNKTIONSZYTOMETRIE UND DATENVERARBEITUNG

Prof.Dr.G.Valet, H.Kahle

Max-Planck-Institut für Biochemie
Arb.Gruppe Zellbiochemie
Martinsried

MAX-PLANCK-INSTITUT
FÜR BIOCHEMIE
Arbeitsgruppe Zellbiochemie
Prof.Dr.G.Valet

8033 MARTINSRIED BEI MÜNCHEN
TELEFON: (089) 8578-1
DURCHWAHL: 8578-2518, -2525
TELEX: 52 17 40 mpib d
TELEFAX: (089) 8578-2563, -3777

Munich, Feb.27, 1993

FUNCTIONAL STAINS

INTRODUCTION:

Traditional flow cytometry:

The flow cytometric determination of **cellular constituents** (Tab.1) is in use for many years e.g. for DNA distributions, cellular antigen contents or natural pigment analysis like chlorophyll or phycobiliproteins. Biophysical measurements of electrical or optical (FSC) cell volume and optical granularity (SSC) are used in addition for cell characterization.

Functional flow cytometry:

Although very useful in many cases such measurements do not permit to follow **functional changes** like e.g. changes of intracellular pH, of cellular excitation or energy production.

It is important to realize that cells in many cases react by the alteration of **functions** and **not** by alterations of **constituents**. The knowledge of constituents does, therefore **not exhaustively describe cells.**

This becomes clearer when one compares a cell for a moment with a house. When somebody in the house puts up his coat, the number of persons and coats does not change but a functional change has undoubtedly occurred. Recognizing this functional change will permit the **prognosis** that somebody will soon leave the house. The extraction of prognostic features from cell function measurements is of high interest not only for medicine but also for cell biological research in general.

Microscopical methods:

The determination of cell function has been difficult and limited in the past because **microelectrodes** had to be introduced in single cells e.g. for transmembrane potential or pH-measurements. More recently **patch clamping** techniques have enlarged the potential for functional investigations on cells or membrane fragments but only the development of **laser scanning microscopes** and **digital imaging** techniques has opened the potential for cell function determination with fluorescent dyes. These dyes are similar to the fluorescent dyes in flow cytometry.

The **advantage** of the microscope is the detailed morphological single cell observation, **disadvantages** are difficulty of **quantitation, low speed** of analysis, sample exposure to high light intensities resulting in fluorescence **bleaching** and observation of cells in the small fluid volume under the cover slip which may **influence** their **biochemical behaviour.**

Flow cytometric methods:

Cell functions (Tab.1) can be determined at **high speed** by **flow cytometry** with a multitude of biochemically specific, non toxic and fluorescent indicator molecules at conditions close to the in-vivo state without prolonged exposure to unusual light levels. Heterogeneous cell suspension from the body but probably to a much larger extent than anticipated also from free sweet and salt water microorganism suspensions can be investigated with a minimum of preparation.

The acceleration time in the flow cytometer and the transition of a cell through the sensing light beam last only fractions of a second i.e. the **influence** of the **measurement** process on the cells is **minimal**. Furthermore flow cytometry offers an ideal statistical sampling. This outweighs by far the usual **impossibility** to investigate the same cell **several times** which, in contrast, is very easy under the microscope.

Functional assays are **easily** performed. The addition of dye or dye cocktail is followed by an incubation time between 1 and 15 min. In most instances the stained cell sample can then be measured **immediately**. In some instances there is one **centrifugation** step followed by resuspension in buffer to lower the extracellular dye concentration (e.g. rhodamine123). The centrifugation step can, however, be substituted by a **dilution step** if the primary assay is performed in a small buffer volume.

Tab.1

CELL BIOCHEMISTRY BY FLOW CYTOMETRY

CONSTITUENTS	FUNCTIONS	
- DNA/RNA	- metabolism:	intracellular pH
- proteins	- excitation:	calcium
- carbohydrates	- energy:	transmembrane and mitochondrial potentials
- lipids		
- antigens	- oxidation:	O_2^-,H_2O_2, free radicals
- hormon receptors	- reduction:	glutathione, free protein SH-groups
- fluorescent in-situ hybridization	- enzymes:	esterases, peroxidases proteases (cathepsins) glucosidases phosphatases etc.

Flow cytometer setup for functional stains in marine organisms:

Unicellular marine organisms frequently exhibit a strong natural fluorescence from chlorophyll or other pigments e.g. phycobiliproteins. The concept for the flow cytometric determination of functional parameters in marine organisms is to determine chlorophyll fluorescence above 600nm simultaneously with the fluorescences of functional stains below 600nm.

In case of **UV-excitation** between 350 and 370nm, fluorescence **emission** will be collected in fluorescence channels F1 and F2 between 390-440nm and 400-500nm while natural chlorophyll fluorescence will be determined in fluorescence channel F3 in addition to forward (FSC) and sidward (SSC) light scatter signals.

In case of **FITC-excitation** conditions at 488nm, functional dye fluorescence will be collected between 510-540nm and 540-580nm in fluorescence channels F1 and F2. Chlorophyll fluorescence will again be collected in fluorescence channel F3.

Natural fluorescence may occur in fluorescence channels **F1** or **F2**. In this case, the functional dye due to its brightness should still give valuable information. The natural fluorescence determined for each cell cluster in an unstained control sample has then to be **subtracted** from the observed fluorescence of this cell cluster in the stained sample.

Data evaluation:

Usually several stains are performed on aliquots of the same cell sample. The measurements are recorded as **list mode files** (FSC, SSC, F1, F2, F3, time) and automatically evaluated by the CLASSIF1 program system. The results of this multi window evaluation in several dimensions are stored in databases. Given a learning set of well known cell samples, the software **learns** the most significant differences from the different databases, **merges** the data columns of interest into a new database and **automatically** establishes a self optimizing **classifier**. This classifier can prospectively classify **unknown cell samples**, stained according to the same rules as the training set samples. Provided that the measurements are properly long term standardized with fluorescent calibration particles, **standardized classifiers** can be elaborated which are flow cytometer and laboratory **independent** and suitable for **international standardization.**

EXPERIMENTAL PART:

DYES:

ADB	=	1,4-diacetoxy-2.3-dicyano-benzene (MW: 244.2) Nr.50-010-002, Nr.1383 205 Boehringer, D-6800 Mannheim, Nr.266707 Calbiochem, D-6232 Bad Soden, FRG
INDO1/AM	=	INDO1 pentaacetoxymethyl-ester (MW: 1009.9), Nr. 402096, Calbiochem, D-6232 Bad Soden, Nr.1081 217 Boehringer, D-6800 Mannheim, FRG
OPT	=	ortho-phthaldialdehyde (MW: 134.1), Nr. P-1378, Sigma, St.Louis, USA
HOECHST 33258	=	Bisbenzimide H33258 (MW: 623.97), Serva Nr.15090, D-6900 Heidelberg, FRG, Nr.B-2883 Sigma, St.Louis, USA
HOECHST 33342	=	Bisbenzimide H33342 (MW: 615.99), Serva Nr.15091, D-6900 Heidelberg, FRG, Nr.B-2261 Sigma, St.Louis, USA
DIOC6	=	3,3-dihexyl-oxacarbocyanin (MW: 572.53), Nr. 14414, Eastman Kodak, Rochester, New York, USA
R123	=	rhodamine 123 (MW: 380.8), Nr. R-8004, Sigma, St.Louis, USA

DCFH-DA	=	2',7'-dichlorofluorescin-diacetate, (MW: 487.3), Nr. 19353, Serva, D-6900 Heidelberg, FRG,
DCF	=	2',7'-dichlorofluorescein (MW: 401.2), Nr. 19524, Serva, D-6900 Heidelberg, FRG
DHR123	=	dihydrorhodamine 123 (MW: 346), Nr. D-632, Molecular Probes, Eugene, Oregon, USA
HE	=	hydroethidine (MW: 315) , Nr. 17084, Polysciences, Warrington, PA, USA
R110	=	rhodamine 110 (MW: 366.8), Nr. 136 1468, Eastman Kodak, Rochester, New York, USA
$(Z\text{-}Ala_2)_2$-R110	=	cathepsin G serine protease substrate (MW: 882.94), laboratory synthesis
$(Z\text{-}Arg_2)_2$-R110	=	cathepsin B,L cysteine proteinase substrate (MW: 1369.22), laboratory synthesis
$(Z\text{-}PheArg)_2$-R110	=	cathepsin B,(L) cysteine proteinase substrate (MW: 1351.18), laboratory synthesis
AO	=	acridine orange (MW: 301.83), Nr. 4539, Polysciences, Warrington, PA, USA
PI	=	propidium iodide (MW: 668.4), Nr. P-4170, Sigma, St.Louis, Miss., USA
fluoresceine	=	(MW: 376.3), Serva, Nr.21572 D-6900 Heidelberg, FRG

<u>REAGENTS</u>:

PMA	=	phorbol-myristate-acetate (MW: 662.0), Nr. P8139, Sigma, St.Louis, Miss., USA
H_2O_2	=	perhydrol 30% (MW: 34.01), Nr. 7210, Merck, D-6100 Darmstadt, FRG
A23187BR	=	calcium ionophore (MW: 602), Nr. 100107 Calbiochem
Z-Phe-Ala-CHN_2	=	cathepsine B,H,L cysteine proteinase inhibitor (diazo-methyl-ketone, MW 394.4), Nr. N-1040 Bachem, D-6900 Heidelberg, 10mM stock solution in DMSO, store at -20°C, dilute 1+4 with HBS prior to use
DFP	=	di-isopropylfluorophosphate, cathepsin G serine proteinase inhibitor, (MW181,15), Nr. D12,600-4 Aldrich-Chemie, D-7924 Steinheim, 1M stock solution in DMSO, store at -20°C, dilute 1+4 with HBS prior to use, observe manufacturers safety instruction and handle DFP with extreme care because it is a potent neurotoxin (**volatile cholinesterase inhibitor**, antidot: atropine, detoxification in 5M NaOH, prepare DFP stock solution and 1+4 dilution under ventilated hood, DFP is stable for several days in protein free physiological solutions !)
EDTA	=	0.2 M pH 7.2 (di-Na EDTA, (MW: 372.25), Nr. 8418 Merck, D-6100 Darmstadt, FRG
$CaCl_2$		0.3 M $CaCl_2$.2H2O solution aqua dest. (MW: 110.99), Nr. 2382, Merck, D-6100 Darmstadt, FRG
$HgCl_2$	=	mercury-II-chloride (MW: 200.59), Nr. 4404 Merck, D-6100 Darmstadt, FRG
particles	=	PolybeadTM Carboxylate Microspheres(2.5% Solids-Latex),

365nm UV-excitable Nr. 18340 4.29µm, BB,
488nm FITC-excitable Nr. 16592 4.30µm, YG
Polysciences Ltd., Warrington, PA, USA

NaCl = Natriumchlorid (MW: 58.44), Nr. 6404 Merck, D-6100 Darmstadt, FRG

HEPES = N-(2-Hydroxyethyl)-piperazine-N'-2-ethane-sulfonic acid (MW: 238.3), Nr. 25245 Serva, D-6900 Heidelberg, FRG

DMF = di-methylformamide, (MW: 73.10) Nr.7156 J.T.Baker Chemicals, Deventer, Holland

ASSAYS UV-EXCITATION (365nm):

ADB: **intracellular pH/esterase activity**

assay:
250µl cell suspension
+5µl ADB/PI cocktail 1mg/ml ADB, 2mg/ml PI DMF
5min RT
measure (ADB 20µg/ml (82µM), PI 40µg/ml (60µM))

INDO1: **calcium**

- freeze A23187Br ionophore at -85° C or -180° C to prevent decay

assay1: intracellular calcium
250µl cell suspension
+5µl INDO1/AM (ester) 1mg/ml, PI 2mg/ml cocktail in DMF
15min RT
measure (INDO1 20µg/ml (20µM), PI 40µg/ml (60µM))

assay2: ionophore + EDTA
250µl cell suspension
+5µl INDO1/AM (ester) 1mg/ml, PI 2mg/ml cocktail in DMF
15min. RT
+5µl 0.2M EDTA
+5µl A23187Br ionophore 1mg/ml DMF
15min RT
measure (INDO1 20µg/ml (20µM), PI 40µg/ml (60µM),
EDTA 4mM, A23187Br 20µg/ml (33µM)

assay3: ionophore + calcium
250µl cell suspension
+5µl INDO1/AM (ester) 1mg/ml, PI 2mg/ml cocktail in DMF
15min. RT
+5µl 0.3M CaCl2
+5µl A23187BR ionophore 1mg/ml DMF
5min. RT
measure (**INDO1** 20µg/ml (20µM), **PI** 40µg/ml (60µM), **$CaCl_2$** 6mM, **A23187Br** 20µg/ml (33µM))

OPT: **free Glutathion/free protein-SH-groups**

assay1: glutathione/protein-SH
250µl cell suspension
+5µl OPT 6.70mg/ml in DMF
+5µl PI 2mg/ml
10min. 0°C
measure (**OPT** 134µg/ml, (1mM), **PI** 40µg/ml (60µM))

assay2: Hg^{2+} blocking of free SH-groups
250µl cell suspension
+5µl $HgCl_2$ 27.15mg/ml in HBS
5min. 0°C
+5µl OPT 6.70mg/ml DMF
+5µl PI 2mg/ml
10min. 0°C
measure (**OPT** 134µg/ml, (1mM), **$HgCl_2$** 0.54mg/ml (2.7mM) PI 40µg/ml (60µM))

Hoechst H33258 **vital DNA stain**

assay:
250µl cell suspension
+5µl H33258 0.312mg/ml in HBS
30min 37°C
+5µl PI 2mg/ml in HBS
5min RT
measure (**H33258** 6.24µg/ml, (10µM), **PI** 40µg/ml (60µM))

Hoechst H33342 vital DNA stain assay:

250µl cell suspension
+5µl H33342 0.308mg/ml in HBS
30min 37°C
+5µl PI 2mg/ml in HBS
5min RT
measure (**H33258** 6.16µg/ml, (10µM), **PI** 40µg/ml (60µM))

ASSAYS FITC-EXCITATION (488nm):

DIOC6: transmembrane potential
assay1: 37°C
250µl cell suspension
+5µl DIOC6 10µg/ml (diluted 1/100 in DMF from stock solution 1mg/ml in ethanol)
30 min. 37°C
+1000µl HBS, centrifuge 30 seconds,1000 x g
Sed. + 250µl HBS
+5µl PI 2mg/ml in HBS
+5µl fluoresceine 20µg/ml in HBS to visualize the sample beam
(diluted 1/50 in HBS from 1mg/ml stock fluorescein in HBS)
5min RT
measure (**DiOC6** 0.2µg/ml (0.35µM), **fluoresceine** 0.4µg/ml (1.1µM), **PI** 40µg/ml (60µM))

assay2: 0°C
250µl cell suspension
+5µl DIOC6 10µg/ml DMF
30min. 0°C
+1000µl HBS, centrifuge 30 seconds,1000 x g
Sed. + 250µl HBS
+5µl PI 2mg/ml in HBS
+5µl fluoresceine 20µg/ml in HBS to visualize the sample beam
5min RT
measure (**DiOC6** 0.2µg/ml (0.35µM), **fluoresceine** 0.4µg/ml (1.1µM), **PI** 40µg/ml (60µM))

R123: mitochondrial membrane potential

assay1: 37°C
250µl cell suspension
+5µl R123 0.5mg/ml in DMF

30min 37°C
+1000µl HBS, centrifuge 30 seconds, 1000 x g
Sed. + 250µl HBS
+5µl PI 2 mg/ml in HBS
15 min RT
measure (**R123** 10µg/ml (26µM), **PI** 40µg/ml (60µM))

assay2: 0°C
250µl cell suspension
+5µl R123 0.5mg/ml, PI 2mg/ml in DMF
30min. 0°C
+1000ml HBS, centrifuge 30 seconds, 1000 x g
Sed. + 250µl HBS
+5µl PI 2mg/ml in HBS
5min RT
measure (**R123** 10µg/ml (26µM), **PI** 40µg/ml (60µM))

DCFH-DA: H_2O_2 and peroxidase activity

- DCFH-DA stock solution 4.87mg/ml (10mM) in DMF 1+9 predilution (1mM) in HBS every day

assay1: spontaneous oxidation
250µl cell suspension
+5µl DCFH-DA 0.487µg/ml in HBS
15min RT
+5µl PI 2mg/ml
+5µl fluoresceine (20µg/ml HBS) to visualize the sample beam
5min RT
measure (**DCFH-DA** 9.74µg/ml (20µM), **fluoresceine** 0.4µg/ml (1.1µM), PI 40µg/ml (60µM))

assay2: peroxidase activity
250ml cell suspension
+5ml DCFH-DA 1Nr. in HBS
15min. RT
+5ml H_2O_2 (50mM) diluted 1:200 from Perhydrol (Merck) in HBS
10min RT
+5µl PI 2mg/ml
+5µl fluorescein 20ug/ml to visualize the sample beam
5min RT
measure (**DCFH-DA** 9.74µg/ml (20µM), **H_2O_2 1mM, fluoresceine** 0.4µg/ml (1.1µM), **PI** 40µg/ml (60µM))

DHR: **sensitive H_2O_2 indicator system (8 x DCF)**

- stock solution: 1.5mg/ml (4.0mM) in DMF, freeze at: -180°C
- predilution: 5µl DHR 1.5mg/ml in DMF + 500µl HBS(1/100), freeze at: -180°C

assay:
250µl cells
+5µl DHR 1/100
15min RT
+5µl PI 2mg/ml in HBS
5min RT
measure (**DHR** 0.3µg/ml (.86µM), **PI** 40µg/ml (60µM), **DMF** .02%)

HE: **$O_2^{\bullet}$ radical formation/general oxidation**

- stock-solution: 3.15mg/ml in DMF, freeze at: -180°C, working solution refreeze at: -85°C
- predilution: 5µl HE + 150µl HBS 1/30

assay:
+250µl cell suspension
+5µl HE 1/30 0.105mg/ml
15min 37°C
+5µl PI 2mg/ml in HBS
measure (**HE** 2.1µg/ml (340µM), **PI** 40µg/ml (60µM), **DMF** .07%)

R110 **protease substrates**

- stock solutions (4mM):
  $(Z\text{-}Arg_2)_2$-R110, cath.B: 6.85mg/ml in DMF, dilute 1/20 with DMF 0.274mg/ml (0.2mM)
  $(Z\text{-}PheArg)_2$-R110, cath.B: 5.40mg/ml in DMF, dilute 1/20 with DMF 0.270mg/ml (0.2mM)
  $(Z\text{-}Ala_2)_2$-R110, cath G: 3.53mg/ml in DMF, dilute 1/20 with DMF 0.177mg/ml (0.2mM)

normal assay:
250µl cell suspension
+5µl substrate 1/20
45min 37°C
+5µl PI 0.2mM in HBS
5min RT
measure (**R110** substrate 4µM, **PI** 40µg/ml (60µM))

cathepsin B,H,L inhibitory assay (cystein proteinases):
250µl cell suspension
+5µl Z-Phe-Ala-CHN_2 2mM in HBS
15min 37°C

+5µl substrate 1/20
45min 37°C
+5µl PI 2mg/ml in HBS
5min RT
measure (**R110** substrate 4µM, **Z-Phe-Ala-CHN$_2$** 40µM, **PI** 40µg/ml (60µM))

cathepsin G inhibitory assay (serin proteinases):
250µl cell suspension
+5µl DFP 0.2M in HBS
15min 37°C
+5µl substrate 1/20
45min 37°C
+5µl PI 2mg/ml in HBS
5min RT
measure (**R110** substrate 4µM, **DFP** 40mM, **PI** 40µg/ml (60µM))

R110: pure substance assay:

250µl cells suspension
+5µl R110 0.4mg/ml in DMF
30min 37°C
+1000µl HBS, centrifuge 30 seconds,1000 x g
Sed + 250µl HBS
+5µl PI 2 mg/ml in HBS
15 min RT
measure (**R110** 10µg/ml (27µM), **PI** 40µg/ml (60µM))

AO: vital DNA/RNA

assay:
250µl cell suspension
+5µl AO/PI cocktail 0.4mg/ml AO, 2mg/ml PI in DMF
30min. 0°C
measure (**AO** 8µg/ml (26µM), **PI** 40µg/ml (60µM))

White Cell and Thrombocyte Disorders

Standardized, Self-learning Flow Cytometric List Mode Data Classification with the CLASSIF1 Program System

G. VALET,[a] M. VALET,[b] D. TSCHÖPE,[c] H. GABRIEL,[d] G. ROTHE,[a] W. KELLERMANN,[e] AND H. KAHLE[a]

[a]*Max-Planck-Institut für Biochemie*
D-8033 Martinsried, Germany

[b]*Max-Planck-Institut für Biochemie*
D-8000 München, Germany

[c]*Diabetes Forschungsinstitut der Heinrich-Heine-Universität*
D-4000 Düsseldorf, Germany

[d]*Institut für Sport- und Leistungsmedizin der Universität*
D-6600 Saarbrücken, Germany

[e]*Institut für Anästhesiologie*
Klinikum Großhadern der Universität
D-8000 München, Germany

INTRODUCTION

White blood cells are mediators of systemic cellular functions like immune defense for lymphocytes and monocytes, phagocytosis and digestion of microorganisms for granulocytes, and primary hemostasis for trombonists. The immunological and biochemical features of these cells can be flow-cytometrically determined by (i) immunophenotyping for lymphocytes and monocytes, (ii) the measurement of functional reactions like phagocytosis, killing of bacteria, intracellular calcium levels, and respiratory burst or protease activities, or (iii) the expression of activation antigens for granulocytes, monocytes, and trombonists.

Although one or several multiparametric flow cytometric measurements on any one of these cell types provide a high degree of information, the computer-assisted extraction of the characteristic values of two-dimensional or multidimensional cell clusters such as means, coefficients of variation, modes, or medians as the most widespread method of analysis does not sufficiently extract this information.

Cluster analysis,[1–6] fitting of multidimensional Gaussians,[7,8] principal component/biplot analysis,[9,10] use of neural networks[11–13] or expert systems,[14–17] and multiwindow content evaluation[18,19] have been proposed for automated result extraction. However, progress in view of a generally and routinely applicable automated flow cytometric list mode classification program system has remained quite limited.

The newly developed multiwindow evaluation program system CLASSIF1 presents a practical way for a standardized, generally applicable, self-learning and simultaneous classification of multiple multiparameter measurements. The classifica-

tions are based on observed data. No assumptions with regard to parameter distribution functions are made and unsupervised self-learning is performed.

The following examples of antigenic and functional cell characterization demonstrate the utility of this general list mode data evaluation concept for (i) the recognition of abnormal trombonists in patients with risk for myocardial infarction and manifest diabetes,[20–24] (ii) the evaluation of lymphocyte phenotypes from normal and endurance-trained competition cyclists suffering from an overtraining syndrome,[25–30] and (iii) the recognition of infection and sepsis in intensive-care-unit (ICU) patients.[31]

MATERIALS AND METHODS

Thrombocyte Immunophenotyping (Düsseldorf III Activation Marker Test)

Patients with diabetes type I insulin-dependent diabetes mellitus (IDDM) or type II noninsulin-dependent diabetes mellitus (NIDDM) and patients with clinically manifest, angiographically proven high-grade coronary heart disease (CHD) as high-risk patients for myocardial infarction were investigated,[22,23] whereas healthy volunteers without any drug medication and with negative smoking status served as normal controls.

Fresh venous blood (4.5 mL) was anticoagulated either with 0.5 mL citrate solution containing 0.13 M Na-citrate (Merck 9361, Darmstadt, Germany), 0.05 M $Na/K/HPO_4^{3-}$, 0.034 M NaCl, 55.5 μM Aspisol (Bayer, Germany), and 30 μM prostaglandin E1 (Sigma, St. Louis, Missouri) or with 0.134 M EDTA solution containing 7 mg/mL hydroxychloroquin-sulfate and 20 IU/mL heparin. This was subsequently mixed in a proportion of 1:1 (v/v) with a 1.0% formaldehyde solution in PBS of pH 7.2 and incubated for 15 min at room temperature (RT), followed by centrifugation at 100*g* for 10 min at RT. The supernatant was removed as platelet-rich plasma (PRP) and centrifuged at 700*g* for 5 min at RT, followed by resuspension of the pellet in 1 mL of a 0.13 M Na-tricitrate (Merck 6448) solution. This PRP suspension was diluted to a thrombocyte concentration of 5×10^4/mL and 200 μL of thrombocyte suspension was incubated at RT for 1 h at 90% antibody saturation with 50 μL of plateau-titered monoclonal antithrombospondin P10 (Dianova, Hamburg, Germany) and CD62 [2.17] or CD63 [2.28] antibodies [kindly provided by Nieuwenhuis *et al.* (Utrecht, the Netherlands) or obtained from Dianova]. The unspecific isotype-matched IgG was from Coulter (Hialeah, Florida). The assays were developed for 30 min at RT in the dark by addition of 100 μL of titered anti-mouse $F(ab)_2$-FITC antibodies (Sigma), followed by addition of 1 mL of washing solution and centrifugation at 700*g* for 5 min at RT. The supernatant was diluted 1:1 (v/v) with sheath fluid [Becton Dickinson (BD), Heidelberg, Germany] and was measured in a FACS 440 cell sorter (BD).

Four-decade logarithmically amplified forward (FSC) and sideward (SSC) scatter signals and FITC fluorescence signals of individual thrombocytes were collected and stored as FCS1.0 list mode files. Fluorescence signal intensity and discrimination were calibrated daily with standard fluorescent microbeads conjugated with definite numbers of FITC molecules (Flow Cytometry Standards Corporation, Research Triangle Park, North Carolina).[32]

Lymphocyte Immunophenotyping

Three to six blood samples of endurance-trained cyclists of the regional and national class were taken according to a standardized procedure at physical rest[28] during normal training and regenerative phases over a period of about 20 months. In addition, each athlete was examined when complaining of typical overload-induced overtraining symptoms such as decrease of performance, soreness of muscles, unusual constant fatigue, disturbances during sleep, and gastrointestinal or other symptoms.[27] Leukocytes in fresh EDTA (ethylenediaminetetraacetic acid)–anticoagulated full blood (20 μL) were incubated at room temperature (RT) for 25 min with directly FITC (fluorescein isothiocyanate)– or PE (phycoerythrin)–labeled antibodies (20 μL) against lymphocyte membrane antigens in combinations of CD45RO/CD4, CD45RO/CD8, CD3/HLA-DR, CD3/CD16, and CD19 and with appropriate IgG1/IgG2 controls (BD and DAKO, Hamburg, Germany). The antibodies were used in 1/2 to 1/5 dilution after appropriate titration experiments in the FACSCAN flow cytometer. Following the antibody incubation, erythrocytes were lysed by FACS lysing solution (BD) for 7 min and centrifuged for 5 min at 250*g* at RT. The cell pellet was shortly vortexed with 2 mL of cell wash (BD), followed by 5 min of 250*g* centrifugation at RT and resuspension of the cell pellet in 0.5 mL Ultracount (BD).

Linear FSC and SSC scatter signals in combination with four-decade logarithmic FITC and PE fluorescence signals of lymphocytes, monocytes, and granulocytes were collected with a FACSCAN (BD) flow cytometer and were stored as FCS1.0 list mode files.[25,26,29,30]

The day-to-day reproducibility for both flow cytometers was assured by a mixture of monosized, fluorescent CaliBRITE (BD) beads of various fluorescence intensity.

Granulocyte and Monocyte Functions

Heparinized fresh venous blood was overlaid onto a cushion of Histopaque-1077 separation medium (Sigma) for 30 min at room temperature to deplete erythrocytes by aggregation at the Histopaque/blood interface and 1*g* sedimentation. The upper two-thirds of the supernatant containing between 0.4×10^7 and 1.2×10^7 leukocytes/mL was carefully removed to avoid any contact of leukocytes with the separating medium and was subsequently stored on ice.[33]

The oxidative activity of granulocytes and monocytes was determined by incubation for 15 min at 37 °C of 1/50 HBS-buffer (0.15 M NaCl, 5 mM HEPES, pH 7.35)–diluted leukocyte supernatant in the presence of 43 μM dihydrorhodamine123 (DHR) (Molecular Probes, Eugene, Oregon)[34] and 60 μmoles of the DNA dye propidium iodide (PI, Sigma) to counterstain the dead cells. DHR-loaded cells were incubated for 15 min at 37 °C either with 10 ng/mL of recombinant tumor necrosis factor–α (TNF-α) (Sigma, produced in yeast, specific activity of 2×10^7 U/mg protein) or with 10^{-7} moles of the bacterial peptide *N*-formyl-Meth-Leu-Phe [FMLP, Sigma, stock of 1 mM in dimethylformamide (DMF)] or they were first primed with FMLP for 15 min followed by TNF-α for another 15 min at 37 °C or were incubated in buffer alone to record the spontaneous cellular oxidative activity. Another leukocyte aliquot was incubated with 10^{-7} M phorbol 12-myristate 13-acetate (PMA, Sigma, stock of 1 mM in DMF) as a positive control.

Intracellular calcium levels were determined following 15 min of 22 °C incubation of leukocytes in HBS-buffer as described earlier in the presence of 20 μM INDO1/AM calcium indicator dye[35] and 60 μM PI. Fifty μL of heparinized (20 U/mL) blood was incubated for 30 min at 37 °C with 5 μL of a suspension of *E. coli* K12 strain (Sigma) at a concentration of 7×10^9 bacteria/mL[36] or with buffer as a control prior to staining with INDO1/AM.

Protease activity measurements were performed with the rhodamine110 (R110) cysteine protease substrates, $(Z\text{-Phe-Arg})_2$-R110 and $(Z\text{-Arg-Arg})_2$-R110, and the serine protease substrate, $(Z\text{-Ala-Ala})_2$-R110, at final concentrations of 4 μM in the absence or presence of 10 μM cysteine proteinase inhibitor Z-Phe-Ala-CHN_2 or 1 mM serine proteinase inhibitor diisopropyl-fluorophosphate (DFP).[33,37]

The flow cytometric measurements for DHR and the protease substrates were performed on a FACSCAN flow cytometer (BD) and the INDO1 measurements were performed on either a PASIII (PARTEC, Münster, Germany) or a FLUVOMETRICELL flow cytometer.[38]

Data Processing

F1

The CLASSIF1 program system (FIGURE 1) operates in personal computers under MS-DOS 3.0 to 5.0 or WINDOWS3.1. The FCS1.0 or FCS2.0 list mode files of up to eight parameters from the Becton Dickinson, Coulter, or PARTEC instruments are processed by the DATLYS procedure, which generates three-, two-, and one-parameter histograms. The two-parameter histograms are obtained through gated or ungated projection of the multidimensional list mode on any wanted coordinate plane and are evaluated by the multiwindow calculation procedure CALC.

Procedure CALC determines for each window the cell or particle content, the mean abscissa and ordinate values, and the ratio and standard deviation of these values supplemented by the respective coefficients of variation. The list mode collected from logarithmic amplifiers is relinearized during the calculation either by a software lookup table for each amplifier generated via standardized internal electronic pulse calibration with a deviation of <1% (PARTEC) or according to the logarithmic decade information of the manufacturer (Becton Dickinson/Coulter).

Calculated results are introduced by task-specific procedures into binary data bases. A data base decompression (DECOMP) and compression (COMPRESS) function assures either the export of CLASSIF1 data bases in ASCII format for further treatment in external evaluation procedures, for example, dBase or EXCEL program systems, or the import of externally generated ASCII data bases.

Procedure LEARN, in a first step, determines for each data base column the 0, 1, 2, 5, 10, 15, 20, 25, 30, 70, 75, 80, 85, 90, 95, 98, 99, and 100 percentiles of the value distributions of the normal samples. The learning set contains, in the initial phase, data from approximately 50 normal samples and 10 to 30 samples of each disease state from different patients. Procedure LEARN classifies samples by percentile analysis using the three most significantly different columns of each data base for the distinction between normal and abnormal samples. A sample is called abnormal if one of the three classifiers is outside of the 90, 95, 98, 99, or 100 percentile of the distributions for the normal samples of the learning set. In addition, the means, the

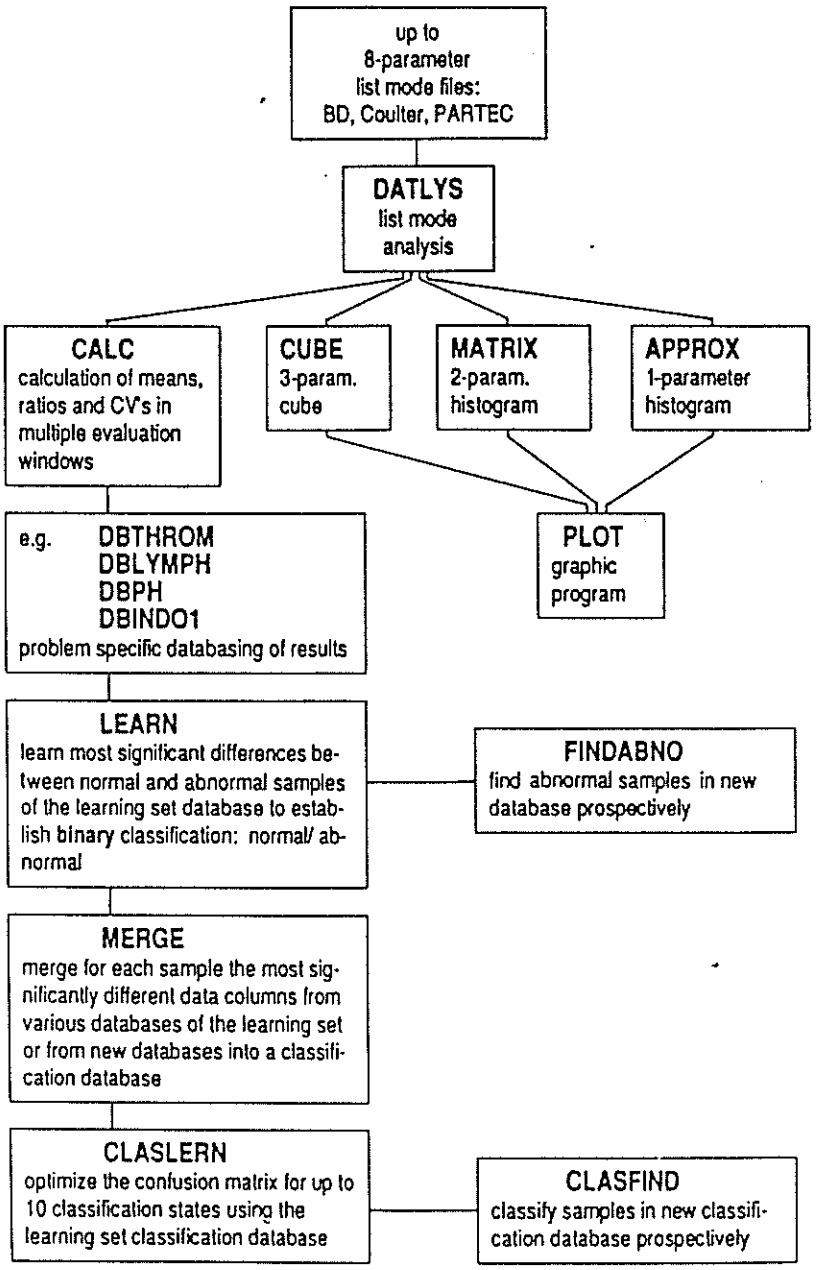

FIGURE 1. Schematic block diagram of the CLASSIF1 program system.

standard deviations (SD), and the standard errors (SE) of each data base column for

the normal and abnormal samples of the learning set are determined by procedure LEARN.

Procedure LEARN, in a second step, introduces the 5 data base columns with the most distinctive percentiles into a multifactorial data base after standardization of the values of each data base column onto the respective mean of the normal samples. Multifactors are calculated by multiplying or dividing the imported data base column values of each sample in all possible permutations. Multiplication is performed if the mean of the abnormal samples is higher than the mean of the normal samples and division is used if it is lower. This provides multifactors with maximum discrimination potency. The percentiles of the 27 newly generated data base columns are calculated and the 3 data base columns with the most discriminant percentiles of all data columns are selected for the final distinction between normal and abnormal samples. The percentile values of the selected columns are stored and used by procedure FINDABNO for the prospective classification of unknown samples.

The multifactorial classification in practically all instances is significantly more sensitive than the classification by the original data base columns because several small, but individually nonsignificant differences of single data base columns are concentrated and amplified in appropriate multifactors.

The multifactorial classification is useful for binary decisions, for example, for the automated recognition of cancer cells,[39,40] but it is insufficient for the distinction between several classification states, for example, danger of sepsis, danger of shock, and transitional and stable state in intensive-care patients using functional granulocyte parameters.[31]

Multiple classifications are obtained with the CLASSIF1 program system in the following way: Between 1 and 5 of the percentilewise most distinctive data base columns for each disease state from procedure LEARN from up to 10 different data bases with a maximum of 50 columns per data base are merged by procedure MERGE into a classification data base. Procedure CLASLERN uses a symmetric pair of percentiles, for example, the 10 and 90 or the 15 and 85 percentiles, of the value distribution of the normal samples of each transferred data base column and this generates a triple-state replica matrix of the classification data base where "+" is assigned to column values above the upper percentile, "0" is assigned to values between both percentiles, and "−" is assigned to values below the lower percentile. By repeated iterations, a triple-matrix classification mask for each disease state is optimized from the learning set in such a way that the highest overall distinction is obtained for each disease state in the confusion matrix between clinical diagnosis and the CLASSIF1 classification of the learning set. Data base columns that do not improve the result are omitted during the iterations because their presence in the classification mask deteriorates the overall classification result.

The sum of the percentages in the horizontal lines of the confusion matrices (FIGURE 2) may be higher than 100% when some samples are classified into more than one classification state. This does not, however, affect the values of the correct classifications in the boxed diagonal of the confusion matrices.

The optimized reference classification masks for each disease state are stored for later use by procedure CLASFIND, which prospectively classifies unknown samples. Procedure CLASFIND determines the classification mask for unknown samples by calculation of their triple matrix according to the percentiles of the optimized

CONFUSION MATRIX (% PAT)
DATABASE: THC1MR3U.BI4

CLIN. DIAG.	PAT. n	FLOW-CLASSIF. N	R	D
N	17	100.0	.0	.0
R	97	1.0	95.9	3.1
D	14	50.0	7.1	57.1

N =NORMAL THROMBOS
R =INF.RISK THROMBOS
D =DIABETES THROMBOS
10-90% percentil.of normals

CONFUSION MATRIX (% PAT)
DATABASE: GAC1MRG3.BI4

CLIN. DIAG.	PAT. n	FLOW-CLASSIF. N	O
N	51	96.1	11.8
O	21	14.3	95.2

N =NORMAL
O =OVERTRAINING
10-90% percentil.of normals

CONFUSION MATRIX (% PAT)
DATABASE: KEL4.BI4

CLIN. DIAG.	PAT. n	FLOW-CLASSIF. N	0	1	2
N	6	100.0	.0	.0	.0
0	35	8.6	60.0	37.1	2.9
1	27	.0	7.4	88.9	3.7
2	14	.0	14.3	21.4	71.4

N =NORMAL GRANULOCYTES
0 =NORM.INT.CARE GRAN.
1 =INFECTION
2 =SEPSIS
15-85% percentil.of normals

FIGURE 2. Confusion matrices (see text).

positional pr cautions complet

reference mask. During the subsequent comparison of the resulting sample mask with the optimized reference mask for each disease state, a sample is classified into the disease state with the highest positionwise coincidence with any one of the reference masks. In case of equally frequent coincidences for several reference masks, the program provides several classifications.

RESULTS

Thrombocytes

F3 Thrombocyte list mode files were evaluated with one FSC/SSC window (FIGURE 3A) and three evaluation windows in the FSC/FITC antibody graph (FIGURE 3B). Window 1 comprised antibody negative and positive thrombocytes, window 2 comprised only the antibody negative thrombocytes, and window 3 comprised only the antibody positive thrombocytes. The boundary between windows 2 and 3 was the same for all list mode files and was set to between 5% and 10% of the maximum thrombocyte frequency of the thrombocyte cluster of normal patients. The evaluation procedure assured that small percentages of antibody positive thrombocytes as well as small increases of antibody fluorescence of all thrombocytes were reliably detected. Eleven values, that is, % antibody positive cells and negative cells, mean FSC, ratio SSC/FSC, mean antibody fluorescence, and mean antibody density of all cells, of the antibody positive and negative cells were extracted from each measurement and were data-based.

After the determination of the 10% and 90% values of the normal values of each data base column, the columns with the highest identification rate for abnormal samples were "learned" with the LEARN procedure. The three most significantly different columns for each of the four measurements (CD62, CD63, thrombospondin, IgG control) and for each of the three classification states (normal, risk for myocardial infarction, diabetes) were merged by procedure MERGE into the classification data base, which theoretically should contain $3 \times 4 \times 3 = 36$ data columns. The merged data base, however, contained only 23 data columns because duplicate data base columns were not introduced into the merged data base. They do not provide additional information and thus prolong the optimization process. Only 8 of the 23 data columns of the merged data base were finally used for the reference F4 classification masks (FIGURE 4) during the iterative optimization process of the CLASLERN procedure. The classification masks permit the classification of the learning set as shown in the confusion matrix (FIGURE 2, left panel). The classifica- F5 tion results are given either in the form of an individual letter (FIGURE 5) or as a F6 listing for scientific purposes (FIGURE 6). The reduction of the learning set to 20, 40, 60, and 80 patients and the use of the remaining 77, 57, 37, and 17 patients as unknown samples for a prospective classification indicates that the classifier is stable T1 from a learning set of 40 patients and upwards (TABLE 1).

An interesting aspect of the CLASSIF1 program system is the possibility of standardizing each column of the classification data base onto the respective mean of the normal patients of the learning set. The optimized classification reference mask can then be expressed in a standardized, that is, instrument-independent, way

Clin. Flow. #934 PAGE: 9 SESS: 5 OUTPUT: Wed Oct 28 09:25:15 1992
Books/nyacmath/clfl279/279a22

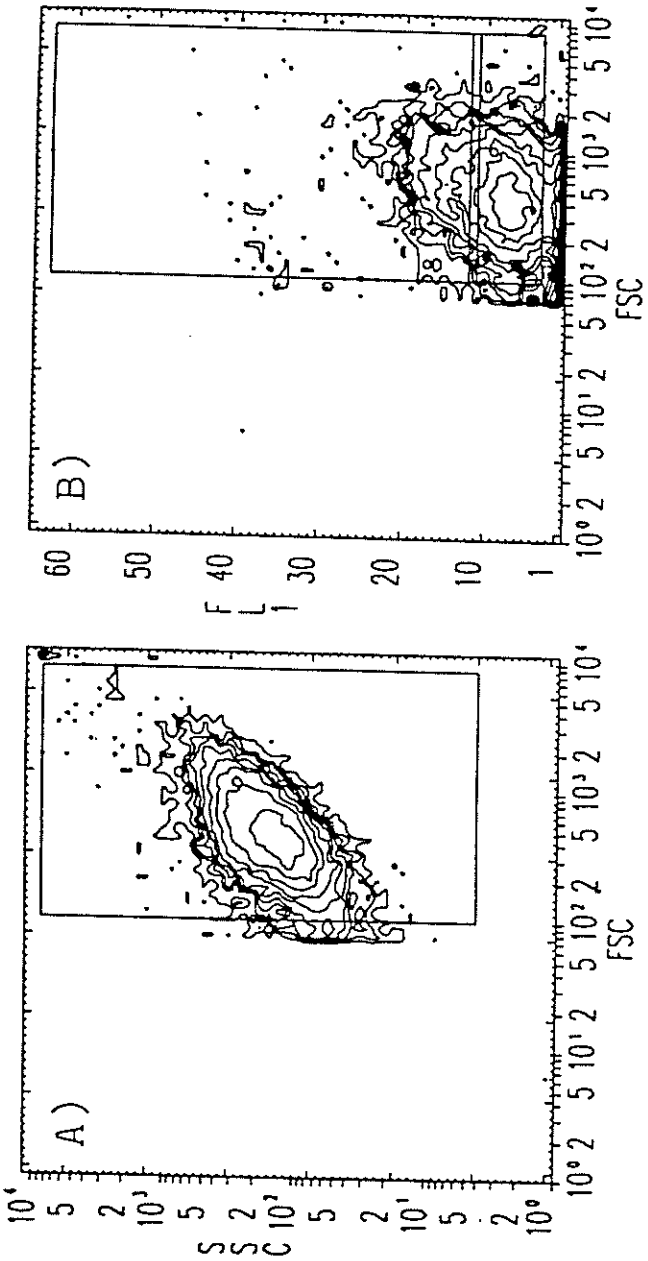

FIGURE 3. Light scatter (A) and fluorescence (B) measurements of anti-CD62 incubated thrombocytes from a patient with high risk for myocardial infarction (TS0051).

din. Flow. #934 PAGE: 10 SESS: 5 OUTPUT: Wed Oct 28 09:25:15 1992
ooks/nyacmath/clfl279/279a22

LEARNING SET DATABASE: THC1MR3U.BI4

MASK PAR.	DB- COL.	PARAMETER EXPLANATION	ORIG COL.	ORIGINAL DATABASE	ORIGINAL REF.FILE	N	R	D
1	2	=MEAN AB POSITIVE CELLS	6	THRMIGGU.BI4	THRNIGGU.RE4	0	+	0
2	4	=AB SURF.DENS.POSITIVE CELLS	9	THRMIGGU.BI4	THRNIGGU.RE4	0	+	0
3	5	=AB SURF.DENS.NEGATIVE CELLS	10	THRMIGGU.BI4	THRNIGGU.RE4	0	0	-
4	8	=MEAN AB POSITIVE CELLS	6	THRM217U.BI4	THRN217U.RE4	0	+	0
5	10	=AB SURF.DENS.POSITIVE CELLS	9	THRM217U.BI4	THRN217U.RE4	0	+	0
6	12	=MEAN RATIO SSC/FSC	4	THRM228U.BI4	THRN228U.RE4	0	+	-
7	17	=AB SURF.DENS.NEGATIVE CELLS	10	THRM228U.BI4	THRN228U.RE4	0	-	-
8	22	=AB SURF.DENS.POSITIVE CELLS	9	THRMP10U.BI4	THRNP10U.RE4	0	+	0

8 OF 23 DATABASE COLUMNS WERE USED FOR MASKS
74 ITERATIONS FOR MASK IMPROVEMENT WERE PERFORMED

FIGURE 4. The merged learning set data base (see text).

Max-Planck-Institut
für Biochemie
Arb.Gruppe Zellbiochemie
Am Klopferspitz
8033 Martinsried
Tel: 49/89/8578-2518, -2525
Fax: 49/89/8678-2563, -3777

Date: Oct. 2, 1992
Time: 15:11:48h

AUTOMATED FLOW CYTOMETRIC CLASSIFICATION

Sample: ?...00224.....R.

QUESTION: NORMAL THROMBOS, INF.RISK THROMBOS, DIABETES THROMBOS

CLASSIFICATION: INF.RISK THROMBOS

Measurement: DIII assay for thrombocyte antigens:
CD62,CD63,thrombospondin +
forward and sideward light scatter
!!! TEST PHASE !!!
- PLEASE, REPEAT ABNORMAL ASSAYS

Classific.database: THC1M3UT.BI6
Learning database: THC1MR3U.BI4
Correct classific: NORMAL THROMBOS : 100.0% n= 17
INF.RISK THROMBOS : 95.9% n= 97
DIABETES THROMBOS : 57.1% n= 14
Signature: Prof.Dr.G.Valet

T2 (TABLE 2), which is an important prerequisite for the laboratory-independent standardization of flow cytometric classifiers.

NR.	CLINICAL DIAGNOSIS	ABBREVIATION	COIN	CLASSIFICATION MASK
1	NORMAL THROMBOS	N	1.00	00000000
2	INF.RISK THROMBOS	R	1.00	++0+++-+
3	DIABETES THROMBOS	D	1.00	00-00--0

REC. NR.	DATAB: THC1MR3U.BI4 DATAB.RECORD LABEL	FLOW-CLASSIFICATION	CLAS COIN	CLASSIFIC.INDICATORS
1	N...00101..... .	N	.88	000000-0
2	N...00102..... .	N	1.00	00000000
3	N...00103..... .	N	.63	+00++000
4	N...00104..... .	N	.63	000++0-0
5	N...00105..... .	N	.88	000000+0
6	N...00106..... .	N	.63	0++000+0
7	N...00107..... .	N	.88	00000+00
8	N...00108..... .	N	.88	+0000000
9	N...00109..... .	N	.50	0--0-00-
10	N...00110..... .	N	.88	0000000+
11	N...00111..... .	N	.75	00+0000+
12	N...00112..... .	N	1.00	00000000
13	N...00113..... .	N	1.00	00000000
14	N...00114..... .	N	1.00	00000000
15	N...00115..... .	N	.88	00000-00
16	N...00116..... .	N	.75	-00-0000
17	N...00117..... .	N	.63	++000+00
36	R...00136..... .	R	.63	++0++000
37	R...00137..... .	R	.88	++0+++0+
38	R...00138..... .	R	.63	+0-++0-+
39	R...00139..... .	R	.75	++-++0-+
40	R...00140..... .	R	.75	++++++0+
41	R...00141..... .	R	.75	++++++0+
42	R...00142..... .	R	.75	++++++++
43	R...00143..... .	R	.75	++-++0-+
44	R...00144..... .	R	.88	++0++0-+
45	R...00145..... .	R	.63	++-+0--+
46	R...00146..... .	R	.75	+00++--+
47	R...00147..... .	R	.75	++-++0-+
48	R...00148..... .	R	.88	++0++0-+
49	R...00149..... .	R	.75	++0++0-+
50	R...00150..... .	R	.75	+00++0-+
51	R...00151..... .	R	.63	+0-++0-+
52	R...00152..... .	R	.75	+00++0-+

FIGURE 6. Classification results given as a listing (see text).

Lymphocytes

F7 F8 The results from five flow cytometric lymphocyte phenotypes and the IgG control were calculated by quadrant evaluation (FIGURE 7) as % positive cells (FIGURE 8A), as relative intensity (FIGURE 8B), and as cell surface density of the antigen expression from the antigen content and the FSC by considering the FSC signal as a cell volume equivalent. The results from each phenotype were introduced into a separate data base. Self-learning on a set of normal and clinically overtrained competition

Clin. Flow. #934 PAGE: 12 SESS: 5 OUTPUT: Wed Oct 28 09:25:15 1992
books/nyacmath/clfl279/279a22

TABLE 1. Predictive Value of the Risk of Myocardial Infarction Classification

Patients (n/n)[a]	Correctness of R (%)[b]
77/20	80
57/40	93
37/60	95
17/80	94

[a]Number of predictive patients/number of learning set patients.
[b]R = risk of myocardial infarction.

TABLE 2. Standardized Classification Formula for Thrombocytes Upon Incubation with Isotype IgG or CD62, CD63, and Thrombospondin Antibodies[a]

Parameters	IgG Mean Ab Pos Cells	IgG Srf Ab Pos Cells	IgG Srf Ab Neg Cells	CD62 Mean Ab Pos Cells	CD62 Srf Ab Pos Cells	CD63 Mean SS/FS Ratio	CD63 Srf Ab Neg Cells	Thrmsp Srf Ab Pos Cells
Upper threshold	1.03	1.12	1.09	1.09	1.12	1.12	1.09	1.10
Lower threshold	0.96	0.88	0.88	0.94	0.86	0.88	0.85	0.86
Normals	0	0	0	0	0	0	0	0
Risk myocard. inf.	+	+	0	+	+	+	−	+
Diabetes	0	0	−	0	0	−	−	0

[a]Standardized thresholds: 10% and 90% of normals, expressed as the ratio of percentile/mean. Terms: Thrmsp = thrombospondin, Ab = antibody, Srf = relative surface density, SS = 90°, FS = forward light scatter, Pos = positive, Neg = negative.

cyclists was then performed. The CLASLERN procedure transferred a total of 25 data base columns from the various lymphocyte phenotype measurements into the classification data base. Only six parameters from the CD45RO/CD4 and CD45RO/CD8 measurements were utilized by the optimized reference classification masks. The confusion matrix (FIGURE 2, middle panel) shows that the overload-induced overtraining syndrome is well recognized. The increased amount (FIGURE 8B) and the relative surface density of CD45RO antigen expression on T lymphocytes, as demonstrated by fluorescent antibody binding, are the most informative parameters.

Granulocytes and Monocytes

F9 Leukocyte function can be estimated by oxidative activity (FIGURES 9A and 9B),
F10 by intracellular calcium levels (FIGURES 9C and 9D), and by protease activity (FIGURES 10A–D). The confusion matrix (FIGURE 2, right panel) of a series of DHR leukocyte measurements of healthy adult persons, of complication-free ICU patients, and of ICU patients with infection or sepsis shows that the oxidative activity of granulocytes and monocytes either alone or under the influence of TNF-α, FMLP, FMLP + TNF-α, and PMA contains a significant degree of information. The CLASLERN procedure transferred 42 data base columns from the five different measurements into the classification data base. The optimized reference classifica-

in. Flow. #934 PAGE: 13 SESS: 5 OUTPUT: Wed Oct 28 09:25:15 1992
oks/nyacmath/clfl279/279a22

FIGURE 7. Lymphocyte immunophenotypes in the peripheral blood of an endurance-trained competition cyclist with overtraining syndrome (GA011).

tion masks contain 32 parameters from all five measurements. Interestingly and

Clin. Flow. #934 PAGE: 14 SESS: 5 OUTPUT: Wed Oct 28 09:25:15 1992
books/nyacmath/clfl279/279a22

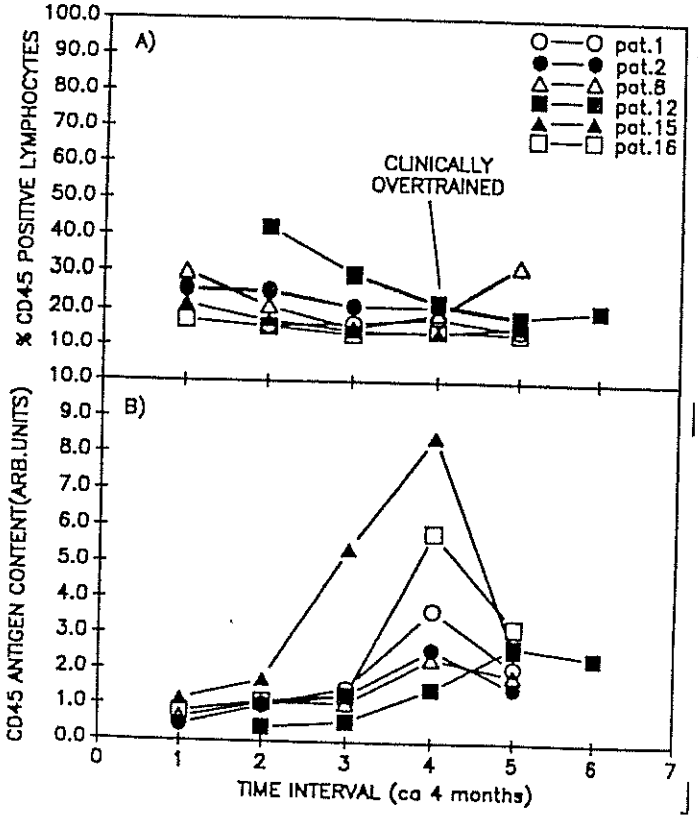

FIGURE 8. Percent CD45RO positive (A) and intensity of antigen expression (B) on peripheral blood lymphocytes of endurance-trained competition cyclists.

unexpectedly, only 17 parameters were selected from granulocytes, whereas 13 parameters were from monocytes and 2 were from lymphocytes.

DISCUSSION

The results show that the CLASSIF1 program system classifies the individual patient status with a high degree of accuracy from list mode data, although the evaluation of the same data by the software of the various flow cytometers was inconclusive at the individual patient level.

The actual performance of the CLASSIF1 program system depends on the speed of the computer and on the complexity and multiplicity of the list mode data, but it remained in all of the aforementioned evaluated cases within 5 to 10 min of learning time for learning sets on the order of 100 to 200 patients derived from 500 to 1000 list mode measurements. In contrast, the prospective classification of unknown samples proceeds at a much higher speed of approximately 100 decisions/s in a computer

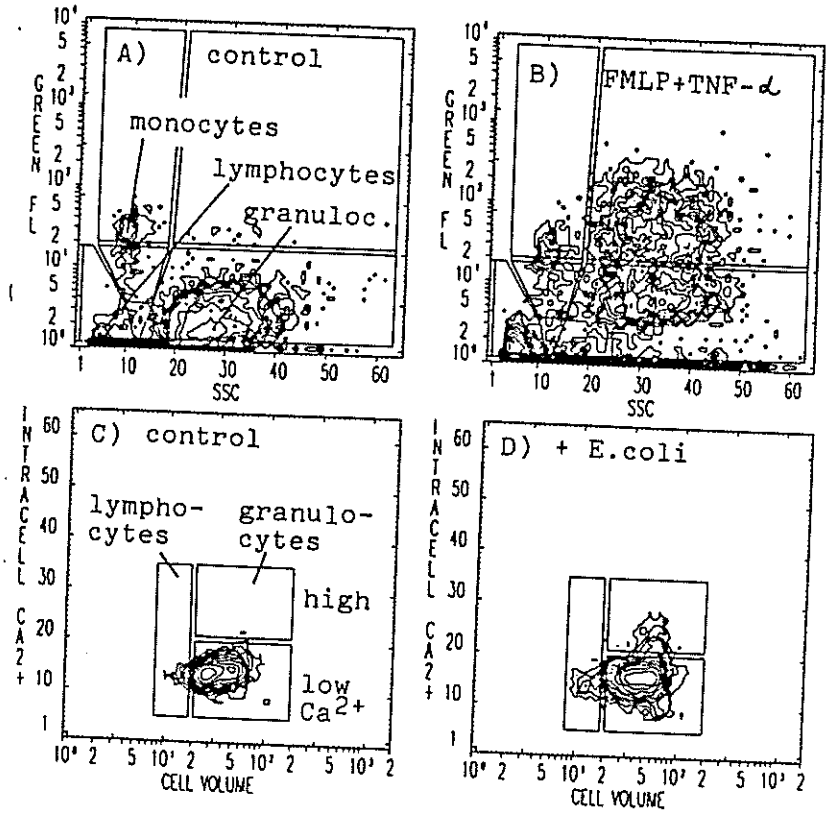

FIGURE 9. Dihydrorhodamine123 (DHR) oxidation in unstimulated (A) and 10^{-7} M FMLP + 10 ng/mL TNF-α stimulated (B) peripheral blood leukocytes of an ICU patient (KE1014) whose monocytes are spontaneously stimulated. The control assay was 0.46% DHR positive (i.e., stimulated granulocytes), TNF-α alone caused an increase to 5.79%, FMLP alone caused an increase to 11.7%, FMLP + TNF-α caused an increase to 41.4%, and 10^{-7} M PMA alone caused an increase to 89.9%. The granulocytes of an infected ICU patient (KE0074) show normal Ca^{2+} levels when incubated in the presence of 20 μM INDO1/AM ester (C), whereas the Ca^{2+} level cannot be restored following 30 min of 37 °C incubation of heparinized blood with *E. coli* K12 bacteria (D).

with an 80486/487 processor at 33-MHz clock frequency. The different list mode calculations that have to be performed by any evaluation program take an additional 50 to 60 s per patient; that is, the CLASSIF1 program can be used in an automatically operating flow cytometer when the list mode data are rapidly (60–80 kbytes/s) transferred, for example, via ethernet communication from the flow cytometer to the evaluation computer and calculated while the flow cytometer measures the next sample.

The establishment of instrument-independent classifiers opens the way to the standardization of flow cytometric classifiers. The standardization depends on a flow cytometer's potential to reproduce the typical histogram patterns for a given application, on the long-term intralaboratory standardization of the measurements

Clin. Flow. #934 PAGE: 16 SESS: 5 OUTPUT: Wed Oct 28 09:25:15 1992
books/nyacmath/clfl279/279a22

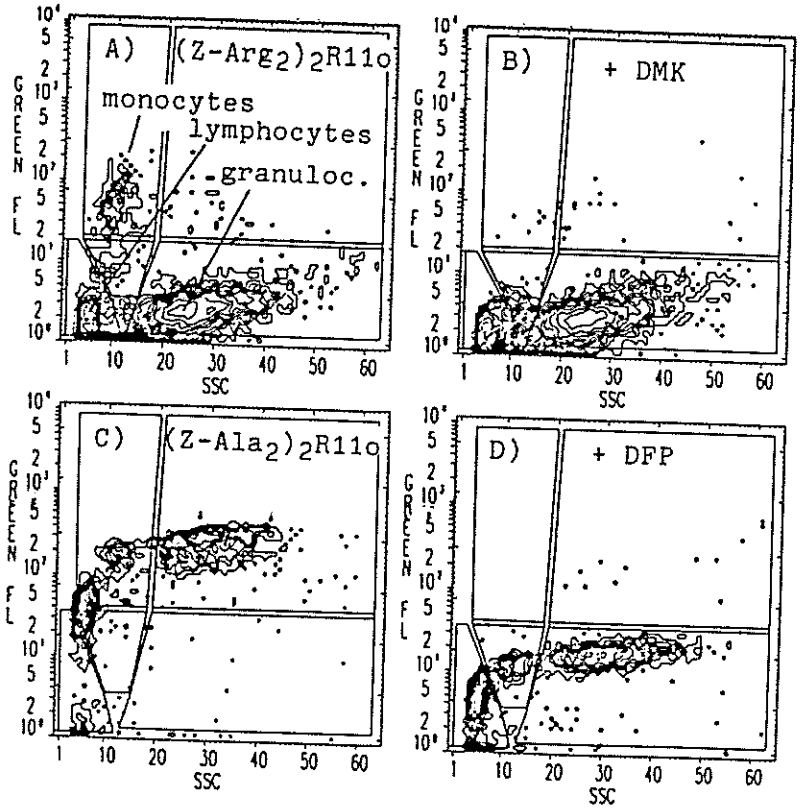

FIGURE 10. Cleavage of the fluorogenic cathepsin L cysteine proteinase substrate $(Z\text{-}Arg_2)_2$-R110 (4 μM) by peripheral human blood leukocytes for 20 min at 37 °C (A) and inhibition of cleavage by preincubation for 10 min at 37 °C with the inhibitor Z-Phe-Ala-CHN_2 (DMK, 10 μM) (B). Cleavage of the fluorogenic cathepsin G serine proteinase substrate $(Z\text{-}Ala_2)_2$-R110 at the same conditions as above (C) and preincubation of the assay with inhibitor DFP (1 mM) as a specificity control (D).

by fluorescent particles, and on reproducibly produced antibodies or biochemical reagents. Expert groups can exchange and classify their standardized data bases to obtain a consensus on the classifier formula (TABLE 2) for a given application. At a new location, only the necessary parameter combinations of a group of normal individuals have to be measured. The standardized data of this patient group are then cross-classified against the expert consensus group's data set of normal individuals in order to certify conformity with the consensus data set. However, the establishment of additional learning sets for abnormal individuals at the new location is unnecessary. This feature of the CLASSIF1 classifiers seems of high practical importance.

The proposed classification concept does not require an absolute numerical coincidence of the unstandardized individual parameters between different flow cytometers in various laboratories because the classification does not depend on

individual parameter values, but on the relative changes of the parameter patterns. Nevertheless, it is clear that standardization trials should bring the numerical values of the individual parameters of flow cytometers in different laboratories as close as possible.

The aforementioned classifications (FIGURE 2) show a close correlation between the biochemical and immunological parameter changes and disease states. Due to the fact that diseases are caused by biochemical deviations in cells and cellular systems, the findings are quite compatible with this general concept. All investigated cell types participate to some extent directly in the disease process, for example, the thrombocytes (FIGURE 2, left panel) in the potential occlusion of narrowed or altered blood vessels preceding the acute event of myocardial infarction or the development of diabetic angiopathy, the lymphocytes (FIGURE 2, middle panel) in the altered defense against infection during an overload-induced overtraining syndrome of competition cyclists, and the granulocytes (FIGURE 2, right panel) of intensive-care-unit patients due to their altered cell functions.

The unexpected use of certain data base columns for the reference emphasizes the need for the invasive self-learning data evaluation of the CLASSIF1 program system, which does not depend on a priori knowledge of the complex parameter interdependences; in fact, this knowledge usually does not exist. Note that this frequent lack of a priori expert knowledge on the interpretation of complex flow cytometric measurements constitutes a significant problem for the use of expert systems[14–17] in flow cytometry, but can be avoided by employing self-learning expert systems.

The execution speed of the triple-matrix classification program is rapid because learning and classification are performed on comparatively few numbers from preestablished data bases. The additional list mode calculations for the data bases of the CLASSIF1 program system are simple and suitable for parallel processing, that is, the data from a sample just measured in an automated flow cytometer can be off-line classified in a second processor during the measurement time of the next sample, leading to a quasi on-line performance of this classification methodology.

In contrast, cluster algorithms,[1,2] principal component/biplot analysis,[9,10] and neural networks[12] are capable of direct on-line list mode classification. This requires substantially more calculations for the classification as compared with the CLASSIF1 program system, but offers the principal advantage of classified on-line cell sorting or of on-line sample classification in automated flow cytometers. However, because efficient classifications require mostly the consideration of data from several multiparameter measurements, a one-step on-line list mode classification is usually not achievable.

Therefore, the on-line classification capacity of a classification method may not represent in practice a decisive advantage because the measurement time rather than the time of computation is the speed-limiting process for the operation of automated flow cytometers. In this situation, some of the CLASSIF1 features like simplicity, easy adaptability to new problems, and generation of instrument-independent and standardized classifiers seem of high practical interest.

Clin. Flow. #934 PAGE: 18 SESS: 5 OUTPUT: Wed Oct 28 09:25:15 1992
/books/nyacmath/clfl279/279a22

REFERENCES

1. BIERRE, P., R. MICKAELS & D. THIEL. 1991. Multidimensional visualization and autoclustering of flow cytometric data. Cytometry 12(suppl. 5): 64.
2. SALZMAN, G. C., S. R. MCLAUGHLIN, S. P. ELLIS & J. F. LEARY. 1991. 3-D autostereoscopic viewing of multidimensional data for guided cluster analysis. Cytometry 12(suppl. 5): 64.
3. MURPHY, R. F. 1985. Automated identification of subpopulations in flow cytometric list mode data using cluster analysis. Cytometry 6: 302–309.
4. BECKMAN, R. J. 1988. Warning: your cluster algorithm may be dangerous to your analysis. Cytometry 9(suppl. 2): 6.
5. SALZMAN, G. C., S. P. PEDERSON, R. J. BECKMAN, R. B. KRALL & C. C. STEWART. 1988. Cluster analysis for flow cytometric data. Cytometry 9(suppl. 2): 84.
6. DEMERS, S., J. KIM, P. LEGENDRE & L. LEGENDRE. 1992. Analyzing multivariate flow cytometric data in aquatic sciences. Cytometry 13: 291–298.
7. VALET, G., S. BAMBERGER, H. HOFMANN, R. SCHINDLER & G. RUHENSTROTH-BAUER. 1979. Flow cytometry as a new method for the measurement of electrophoretic mobility of erythrocytes using membrane charge staining by fluoresceinated polycations. J. Histochem. Cytochem. 27: 342–349.
8. VALET, G. 1990. Graphical representation of three-parameter flow cytometer histograms by a newly developed FORTRAN IV computer program. *In* Flow Cytometry IV. O. D. Laerum, T. Lindmo & E. Thorud, Eds.: 125–129. Universitetsferlaget. Oslo.
9. LEARY, J. F., S. ELLIS, S. HESPELT, S. R. MCLAUGHLIN & J. G. GRAM. 1988. Principal component/biplot analysis for correct identification of rare human fetal cells in maternal blood. Cytometry 9(suppl. 2): 29.
10. LEARY, J. F., S. R. MCLAUGHLIN, M. A. CORIO, L. REMLEY, J. G. GRAM & S. BURDE. 1990. High speed principal component/biplot sorting of rare cells. Cytometry 11(suppl. 4): 19.
11. FRANKEL, D. S., R. J. OLSON, S. L. FRANKEL & S. W. CHISHOLM. 1989. Use of a neural net computer system for analysis of flow cytometric data of phytoplankton populations. Cytometry 10: 540–550.
12. FRANKEL, D. S. & S. L. FRANKEL. 1991. Real time neural network for flow cytometry analysis. Cytometry 12(suppl. 5): 63.
13. REDELMAN, D. 1991. Neural network analysis of flow cytometry data. Cytometry 12(suppl. 5): 63.
14. SALZMAN, G. 1987. A knowledge-based system as a cluster assistant. Cytometry 8(suppl. 1): 12.
15. BAGWELL, C. B. 1988. New horizons: expert systems for flow cytometry. Cytometry 9(suppl. 3): 89–93.
16. MCGUIRE, D., J. P. ROBINSON & G. B. KING. 1991. Automated interpretation of phenotypic data using a multiparameter expert system. Cytometry 12(suppl. 5): 63–64.
17. ROBINSON, J. P., K. RAGHEB, G. LAWLER, S. KELLEY & G. DURACK. 1992. Rapid multivariate analysis and display of cross-reacting antibodies on human leukocytes. Cytometry 13: 75–82.
18. VALET, G., H. H. WARNECKE & H. KAHLE. 1987. Automated diagnosis of malignant and other abnormal cells by flow-cytometry using the DIAGNOS1 program system. *In* Clinical Cytometry and Histometry. G. Burger, J. S. Ploem & K. Goerttler, Eds.: 58–65. Academic Press. New York/London.
19. HABBERSETT, M. C., M. SHAPIRO, B. BUNNAG, I. NISHIYA & CH. HERMAN. 1979. Quantitative analysis of flow microfluorometric data for screening gynecologic cytology samples. J. Histochem. Cytochem. 27: 536–544.
20. TSCHÖPE, D. & B. SCHWIPPERT. 1992. Düsseldorf III Assay: Bestimmung von Thrombozytenmarkern auf Thrombozyten im Durchflußzytometer. *In* Klinische Zytometrie. G. Schmitz, Ed. Schattauer. Stuttgart. In press.
21. TSCHÖPE, D., P. RÖSEN, B. SCHWIPPERT & F. A. GRIES. 1992. Platelets in diabetes: their role in the hemostatic regulation in atherosclerosis. Semin. Thromb. Hemostas. In press.

22. TSCHÖPE, D., H. P. SCHULTHEISS, P. KOLAROV, H. K. NIEUWENHUIS, K. DANEHL, B. STRAUER & F. A. GRIES. 1991. Platelet activation is predictive for an increased PTCA-risk. Circulation 84(suppl. 4): 690.
23. TSCHÖPE, D., J. ESSER, B. SCHWIPPERT, P. RÖSEN, B. KEHREL, H. K. NIEUWENHUIS & F. A. GRIES. 1991. Large platelets circulate in an activated state in diabetes mellitus. Semin. Thromb. Hemostas. 17: 433–439.
24. TSCHÖPE, D., P. SPANGENBERG, J. ESSER, B. SCHWIPPERT, B. KEHREL, P. RÖSEN & F. A. GRIES. 1989. Flow cytometric detection of surface membrane alterations and concomitant changes in the cytoskeletal actin status of activated platelets. Cytometry 11: 652–656.
25. GABRIEL, H., L. SCHWARZ, P. BORN & W. KINDERMANN. 1992. Differential mobilization of leucocyte and lymphocyte subpopulations into circulation during endurance exercise. Eur. J. Appl. Physiol. In press.
26. GABRIEL, H., L. SCHWARZ, W. STEFFENS & W. KINDERMANN. 1992. Immunoregulatory hormones, circulating leucocytes, and lymphocyte subpopulations before and after endurance exercise of different intensities. Int. J. Sports Med. 13: 359–366.
27. FRY, R. W., A. R. MORTON & D. KEAST. 1991. Overtraining in athletes—an update. Sports Med. 12: 32–65.
28. WESTERMANN, J. & R. PABST. 1990. Lymphocyte subsets in the blood: a diagnostic window on the lymphoid system? Immunol. Today 11: 406–410.
29. GABRIEL, H., A. URHAUSEN & W. KINDERMANN. 1991. Circulating leucocyte and lymphocyte subpopulations before and after intensive endurance exercise to exhaustion. Eur. J. Appl. Physiol. 63: 449–457.
30. GABRIEL, H., A. URHAUSEN & W. KINDERMANN. 1992. Mobilization of circulating leucocyte and lymphocyte subpopulations before and after intensive endurance exercise to exhaustion. Eur. J. Appl. Physiol. 65: 164–170.
31. ROTHE, G., W. KELLERMANN & G. VALET. 1990. Flow cytometric parameters of neutrophil function as early indicators of sepsis- or trauma-related pulmonary or cardiovascular organ failure. J. Lab. Clin. Med. 115: 52–61.
32. TSCHÖPE, D., P. RÖSEN, B. SCHWIPPERT, B. KEHREL, S. SCHAUSEIL, J. ESSER & F. A. GRIES. 1990. Platelet analysis using flow cytometric procedures. Platelets 1: 127–133.
33. ROTHE, G., S. KLINGEL, I. ASSFALG-MACHLEIDT, W. MACHLEIDT, CH. ZIRKELBACH, R. B. BANATI, W. F. MANGEL & G. VALET. 1992. Flow cytometric analysis of protease activities in vital cells. Biol. Chem. Hoppe Seyler 373: 547–554.
34. ROTHE, G., A. OSER & G. VALET. 1988. Dihydrorhodamine123: a new flow cytometric indicator for respiratory burst activity in neutrophil granulocytes. Naturwissenschaften 75: 354–355.
35. VALET, G., A. RAFFAEL & L. RÜSSMANN. 1985. Determination of intracellular calcium in vital cells by flow cytometry. Naturwissenschaften 72: 600–602.
36. ROTHE, G. & G. VALET. 1988. Phagocytosis, intracellular pH, and cell volume in the multifunctional analysis of granulocytes by flow cytometry. Cytometry 9: 316–324.
37. ASSFALG-MACHLEIDT, I., G. ROTHE, S. KLINGEL, R. NATI, W. F. MANGEL, G. VALET & W. MACHLEIDT. 1992. Membrane permeable fluorogenic rhodamine substrates for selective determination of cathepsin L. Biol. Chem. Hoppe Seyler 373: 433–440.
38. KACHEL, V., E. GLOSSNER, E. KORDWIG & G. RUHENSTROTH-BAUER. 1977. FLUVOMETRICELL, a combined cell volume and cell fluorescence analyzer. J. Histochem. Cytochem. 25: 804–812.
39. LIEWALD, F., N. DEMMEL, R. WIRSCHING, H. KAHLE & G. VALET. 1990. Intracellular pH, esterase activity, and DNA measurements of human lung carcinomas by flow cytometry. Cytometry 11: 341–348.
40. VALET, G., L. RÜSSMANN & R. WIRSCHING. 1984. Automated flow-cytometric identification of colo-rectal tumour cells by simultaneous DNA, CEA-antibody, and cell volume measurements. Clin. Chem. Clin. Biochem. 22: 935–942.

Experimental Cell Research 163 (1986) 518–524

Flow-cytometric Determination of Glutathione Alterations in Vital Cells by *o*-Phthaldialdehyde (OPT) Staining

J. TREUMER and G. VALET*

Arbeitsgruppe Krebszellforschung, Max-Planck-Institut für Biochemie, D-8033 Martinsried, FRG

A flow-cytometric method for the detection of changes of cellular glutathione content in vital cells is described. The reaction is based on formation of a fluorescent product between *o*-phthaldialdehyde (OPT) and reduced glutathione (GSH). OPT is a more GSH-specific dye than other thiol-specific dyes (e.g., bromobimanes), because it forms a cyclic compound with GSH. Changes of GSH induced by oxidation or thiol-blocking agents are visualized in vital cells after a 5-min staining at room temperature.
© 1986 Academic Press, Inc.

The protection of the intracellular environment against oxidative damage is of major importance in normal cellular metabolism. The main antioxidative defence is provided by the glutathione redox cycle [1], which is present in practically all cells [2]. Under normal conditions the tripeptide glutathione (glu-cys-gly) is mostly present in its reduced form GSH and only to a small degree in oxidized form GSSG [3]. One can distinguish between the intracellular glutathione content and its functional status which is the ratio of GSH to GSSG.

Determination of intracellular glutathione content and its alteration after exposure to oxidative stress mediated by peroxides or diamide [4] are of particular interest for the biochemical characterization of cells. Information about thiol state, redox state and capability of detoxification of xenobiotics like chemotherapeutics in cancer therapy may be obtained in this way. In some instances, correlations between intracellular glutathione concentration and cellular resistance against alkylating agents are apparent [5–9] and even macrophage-mediated tumor cell cytolysis is modulated by cellular GSH content [10].

The objective of this study was to develop a flow-cytometric method for the measurement of GSH in vital cells. Ortho-phthaldialdehyde (OPT), which is a well established reagent for glutathione determination in tissue homogenates [11–13], was used for this purpose. The OPT method is based on reaction with both glutathione amino- and sulfhydryl groups, yielding a cyclic, highly fluorescent product. Since two molecular groups of GSH are involved in the reaction [14], OPT is a more specific glutathione marker than thiol-specific dyes, e.g. bromobimanes [15].

* To whom offprint requests should be addressed.

Copyright © 1986 by Academic Press, Inc.
All rights of reproduction in any form reserved
0014-4827/86 $03.00

MATERIALS AND METHODS

Cells

All incubations and washing steps were performed in 10 mM HEPES-buffered saline pH 7.4 (HBS). Murine Ehrlich ascites tumor (EA2P8, gift from Dr v. d. Mark, Martinsried, FRG) was obtained by puncture of the peritoneal cavity 10 days after inoculation of 0.4 ml ascites fluid (5×10^8 cells/ml) in C57bl mice. The ascites was diluted between 1/10 and 1/50 with HBS prior to staining to obtain appropriate cell counts (5×10^6 cells/ml). A rat mammary tumor cell line (R323ØAC) was grown in 75 ml polystyrene tissue culture flasks by inoculation of 10^5 cells in RPMI-medium with 10% fetal calf serum (FCS) (Paesel, Frankfurt) at 37°C in air with 5% CO_2 for 7–9 days. The cells were harvested by trypsinization (0.025%), washed twice in HBS by centrifugation (10 min at 200 g) and finally passed through a 40-μm nylon mesh to remove cell aggregates.

Chemicals

100-mM stock solutions of *o*-phthaldialdehyde (OPT, Sigma, FRG), monobromobimane (MB, Calbiochem, FRG) and *N*-ethylmaleimide (NEM, Sigma, Taufkirchen, FRG) were prepared in dimethylformamide (DMF, Baker Chemicals, Deventer, The Netherlands). 100 mM stock solutions of mercurydichloride ($HgCl_2$, Merck, Darmstadt), diamide (Sigma), reduced glutathione (GSH, Sigma) and hydrogen peroxide (HPO, Merck) were prepared in HBS. GSH, diamide and HPO were always freshly prepared to avoid decomposition. A 2 mM solution of *p*-chloromercury-phenylsulfonic acid (PCMS, Sigma) in HBS was used in some experiments instead of HBS. Sodium dodecyl sulfate (SDS) was bought from Serva, Heidelberg.

Spectroscopy

Fluorescence-spectrometer LS-5 (Perkin-Elmer Corp., Norwalk, USA) was mounted on-line to a VAX 11/782 computer. The slit setting was 5 nm (excitation) and 2.5 nm (emission) and quartz cuvettes with 10 mm light pass were used. The spectra were measured in 50 mM Tris/HCl buffer, pH 7.4.

Cell Staining

1×10^6 cells were suspended in 500 μl HBS, 5 μl 0.1 M OPT or 0.1 M MB solution was added. The assay was measured in the flow cytometer after 5 min incubation at room temperature.

Flow Cytometry

The Fluvo-Metricell flow cytometer [16] was equipped with a Cytomic 12 microprocessor data acquisition and linked to an Interdata 74 computer (Perkin-Elmer) [17]. List mode data were stored on magnetic tape. The hydrodynamically focused sizing orifice was 95 μm in diameter, 100 μm long and was operated at a constant current of 0.23 mA. Fluorescence was excited by a HBO-100 high-pressure mercury arc lamp between 300 and 400 nm. The cell fluorescence was collected by two light channels between 388 and 440 nm (F1) and between 450 and 700 nm (F2). Data evaluation was performed with FORTRAN programs [18].

HPLC

HPLC separations of lysates of OPT-stained cells were made to discriminate between fluorescence associated with high-molecular and low-molecular fractions. A gel sieve column Ultropak TSK-G 3000SW (LKB, Bromma, Sweden), pump 2150 (LKB) and UV-monitor 2238 (LKB) (260 nm) were used in combination with a 25-μl quartz continuous-flow cell (Hellma, Freiburg) for fluorescence measurement. 5×10^6 cells in 0.5 ml HBS were incubated with OPT as described above, washed twice with HBS by 10 min centrifugation at 200 g and lysed by adding 0.5 ml 50 mM Tris-HCl buffer containing 0.5% SDS. Additional disintegration was obtained by sonification (MSE model 7100, 100 W, microtip, 15 sec, Colora, Lorch, FRG). The sonicated cell lysate was centrifuged (10 min, 3000 g), filtered through a 0.45 μm Millipore filter and loaded onto the molecular sieve column, which was equilibrated and eluted with a 50 mM Tris-HCl buffer, pH 7.2, containing 2 mM EDTA and 0.5% (w/v) SDS. The eluate was monitored for protein by UV absorbance at 260 nm. Simultaneous

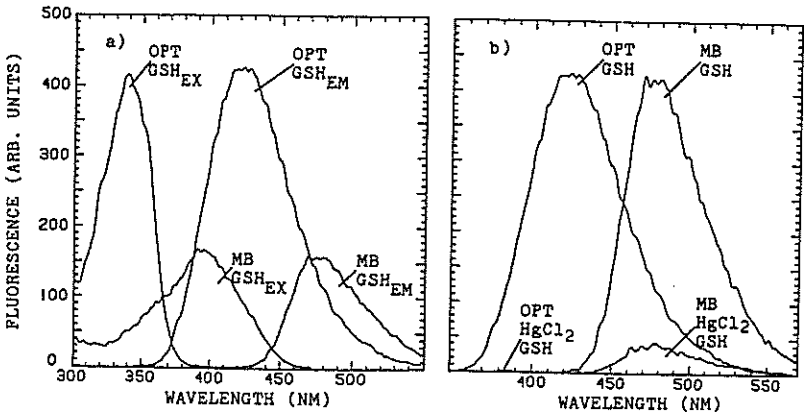

Fig. 1. Excitation- (*EX*) and emission spectra (*EM*) of (*a*) equimolar complexes of glutathione- and thiol-reactive dyes. (*b*) Preincubation with $HgCl_2$ inhibited the reaction completely (*OPT*) or partially (*MB*).

fluorescence detection was performed by the quartz flow cell that was mounted in the fluorescence-spectrometer. The fluorescence was excited at 338 nm and the emission was measured at 420 nm. The fluorimetric data were standardized to the maximum absorbance value of the major protein peak.

RESULTS

Formation of fluorescent adducts between GSH and the thiol-reactive dyes OPT and MB is illustrated in fig. 1*a*. The fluorescence intensity is significantly greater for OPT, thus providing a sensitive detection of GSH. $HgCl_2$ was a potent inhibitor of this reaction (fig. 1*b*): A twofold molar excess of $HgCl_2$ over GSH and OPT reduced fluorescence to 0.5% of the initial intensity. MB, despite a tenfold excess of $HgCl_2$, still showed a residual fluorescence. This fluorescence is probably due to hydrolysis of MB in aqueous media, leading to overestimation of thiol concentration. NEM, a potent thiol-blocking agent, also reduced formation of OPT–GSH fluorescent products, but to a lesser degree (data not shown).

Microscopic observations revealed that OPT stained the entire cell body blue, sometimes superimposed by a quickly bleaching yellow fluorescence. MB-stained cells displayed a uniform turquoise fluorescence.

Analysis of OPT-stained (1 mM) cell lysates by molecular sieve chromatography showed fluorescence linked to both high-molecular protein and low-molecular GSH-containing fractions (fig. 2*a*). Greater variations in either fluorescence distribution or ratio between protein and fluorescence were observed, depending on the type of cells and on the growth conditions. Formation of GSH–OPT low-molecular weight fluorescence was quantitatively abolished in the presence of 2 mM $HgCl_2$, whereas high-molecular weight Protein–OPT fluorescence was only slightly affected (fig. 2*b*). Moreover, GSH–OPT-containing fractions had fluorescence with peak intensity at longer wavelengths than protein–OPT-containing fractions (fig. 3).

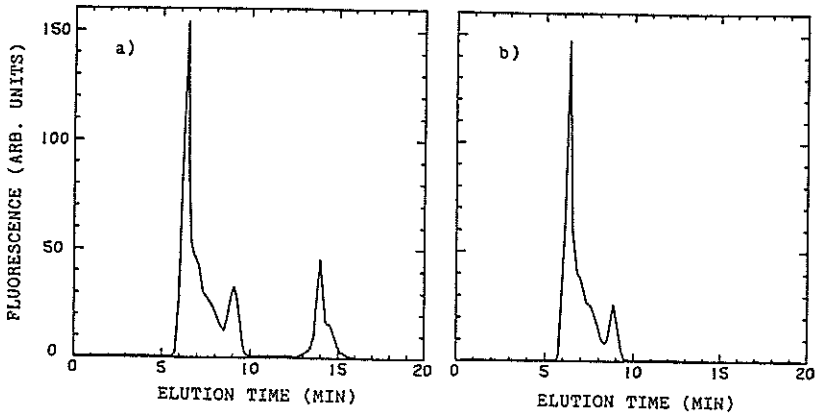

Fig. 2. HPLC molecular sieve separation of OPT-stained cell lysates. (*a*) OPT fluorescence was split into high-molecular protein-containing fractions (6–10 min elution time) and low-molecular GSH-containing fractions (13–15 min elution time). (*b*) Preincubation with 2 mM $HgCl_2$ completely reduced formation of fluorescence in GSH-containing fractions, while protein-containing fractions were significantly less affected.

Analysis of OPT-stained vital cells by flow cytometry is shown in fig. 4*a*. Due to its spectral properties, most of the OPT–GSH fluorescence appears in the green fluorescence channel, whereas the blue fluorescence channel represents mainly protein-bound OPT. Concentration and time-dependent staining experiments recommended incubation of cells in 1 mM OPT for 5 min. Longer staining or higher OPT concentrations gave no increase of blue fluorescence.

Correlation between OPT fluorescence and intracellular glutathione functional status was found, especially after alterations of the cellular free GSH pool:

(*a*) Blocking of the thiol group by incubation of cells in 2 mM $HgCl_2$ prior to OPT staining resulted in significant loss of green fluorescence (fig. 4*b*, table 1).

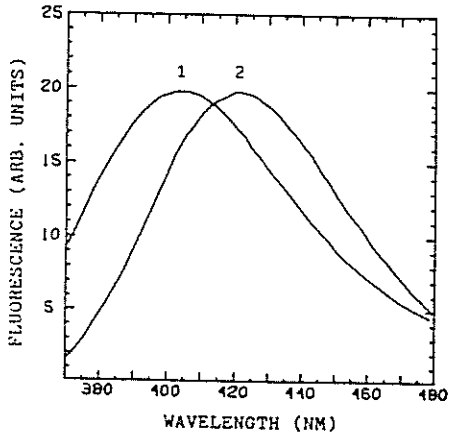

Fig. 3. Emission spectra of *1*, protein-containing; *2*, GSH-containing fractions of OPT-stained Ehrlich ascites cell lysates of fig. 2. Protein-containing fractions exhibited fluorescence at shorter wave fluorescence than the GSH-containing fractions. The spectra were excited at 338 nm.

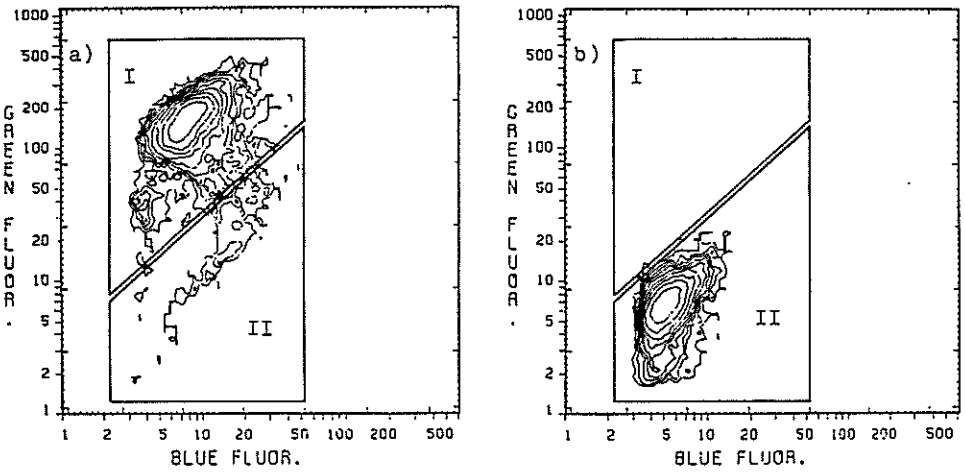

Fig. 4. (*a*) Flow-cytometric analysis of OPT-stained Ehrlich ascites cells. (*b*) Preincubation with 4 mM $HgCl_2$ greatly reduced green fluorescence, while blue protein-fluorescence was only moderately affected.

However, blue protein fluorescence still remained which could not be abolished by exposure to $HgCl_2$ in concentrations up to 20 mM.

(*b*) Incubation with PCMS, a non-permeating thiol-blocking agent, reduced peak intensity of fluorescence in flow-cytometric measurements and HPLC experiments. Only a moderate reduction in attainable fluorescence resulted (table 1), indicating that the OPT fluorescence was located mostly inside the cell.

(*c*) Oxidation of the thiol group by incubation of cells in 2 mM diamide or 2 mM HPO caused a decrease in green GSH fluorescence (table 1).

(*d*) Cellular GSH content was elevated by incubating cells between 0 and 110 min at 37°C in 0.4 mM cysteamine, which leads to an increased glutathione synthesis from precursors. The increase in green OPT fluorescence in vital cells was only moderate (5–10%) (data not shown).

Cells stained with OPT or MB showed similar changes of fluorescence intensity after exposure to $HgCl_2$ or NEM. Treatment with diamide or HPO, however, lead to marked differences: While preincubation with HPO significantly reduced OPT green-fluorescence to levels below those obtained by diamide, MB-stained

Table 1. *Distribution of 1 mM OTP-stained Ehrlich ascites cells between area I (fig. 4) of glutathione-containing cells and area II of glutathione-devoid cells after preincubation of the cells with thiol blocking or oxidizing agents*

Treatment	None	2 mM $HgCl_2$	2 mM HPO	2 mM PCMS
Area I (%)	97.3	0.1	14.0	77.3
Area II (%)	2.7	99.9	86.0	22.7

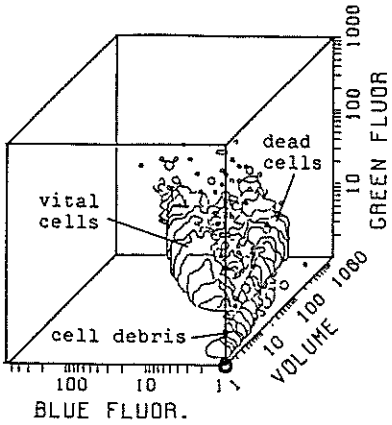

Fig. 5. Cloud display [18] of simultaneous three-parameter measurement of Ehrlich ascites cells stained with 1 mM OPT and 60 μM propidium iodide. Due to their DNA staining with propidium iodide, dead cells become red fluorescent, thus appearing in the green channel. The logarithmic contents of the individual channels of the three-parameter histograms were standardized for this display to the channel with the maximum logarithmic particle content as 100%. Contour lines were plotted at the 10% level of this value to visualize cell- and particle-containing areas. The histogram contains a total of 24 680 particles at a maximum channel content of 184 particles. The contour lines show the positions of all measured cells and particles.

cells showed only a slight decrease in fluorescence. Furthermore, cells stained with 0.5–1 mM MB increased in cell volume. An increasing cell volume was observed with OPT only after pretreatment of cells with $HgCl_2$ or NEM, but not by OPT staining alone.

OPT-stained cells were vital cells, as is shown by simultaneous counterstaining by propidium iodide which stains dead cells (fig. 5).

DISCUSSION

Specific staining of intracellular GSH sulfhydryl groups by thiol-group reactive, fluorescent dyes cannot be accomplished with conventional dyes (e.g., bromobimanes). A widely accepted GSH-staining procedure for tissue homogenates [11–13] was therefore modified for application in flow cytometry. OPT reacts with reduced glutathione yielding a cyclic, highly fluorescent product. OPT is more specific than thiol dyes such as MB because of its simultaneous requirement of amino- and thiol groups for the formation of a fluorescence product [14]. GSH–OPT has a fluorescence emission at higher wavelengths than protein–OPT reaction products (fig. 3), which permits distinction between GSH- and protein fluorescence by flow cytometry (fig. 4*a*, *b*). Staining of protein SH-groups by OPT is a major source of error in fluorimetric cuvette assays with single wavelength fluorescence detection.

Further advantages of the OPT reaction are: no intrinsic fluorescence of free OPT, and stability of OPT in aqueous solutions. Bromobimanes, in contrast, undergo hydrolysis, thereby forming fluorescent products, which causes overestimation of thiol groups. OPT is of low cellular toxicity because no changes in cell volume are observed.

Different information is obtained by bromobimane staining as compared with OPT staining: Bromobimane is reactive towards every thiol group [15], indicating the whole cellular thiol content, whereas OPT stains preferentially GSH. This

was confirmed by experiments influencing the cellular GSH level, e.g. by thiol blocking with $HgCl_2$ (fig. 4*b*, table 1) or NEM, by oxidation with peroxides (table 1) and diamide, or by increased synthesis in the presence of cysteamine. OPT-green-fluorescence in all experiments reflected the occurrence of the expected GSH alterations. Furthermore, the flow-cytometric analysis of OPT-stained cells was in accordance with data obtained by cell homogenization and the standard colorimetric GSH assay [19] on the cell lysates. Especially changes in fluorescence intensity after oxidative stress by HPO reflected highly specific alterations of cellular GSH. HPO lowers GSH enzymatically via GSH peroxidase [20], which is indicated by OPT staining. The blue OPT–protein fluorescence is not affected.

The potential of this new flow-cytometric method for GSH determination is that metabolic changes of GSH and protein thiol groups can be simultaneously observed in different subpopulations of heterogeneous vital cell preparations shortly after removal from the organism.

We wish to thank Drs L. Rüssmann and A. Raffael for helpful and critical discussions during the course of this work.

REFERENCES

1. Kosower, E M & Kosower, N S, Glutathione (ed L Flohe, H C Benoehr, H Sies, H D Waller & A Wendel) p. 287. Academic Press, New York (1974).
2. — Int rev cytol 54 (1978) 109.
3. Jocelyn, P C, Glutathione. Biochemistry Society Symposia (ed E M Crook) no. 17, p. 17. Academic Press, New York (1959).
4. Kosower, E M, Correa, W, Kinon, B J & Kosower, N S, Biochim biophys acta 264 (1972) 39.
5. Green, J A, Vistica, D T, Young, R C, Hamilton, T C, Rogan, A M & Ozols, R F, Cancer res 44 (1984) 5427.
6. Somfai-Relle, S, Suzukake, K, Vistica, B P & Vistica, D T, Cancer treat rev 11 (1984) 43.
7. Suzukake, K, Petro, B J & Vistica, D T, Biochem pharmacol 31 (1982) 121.
8. Ball, C R, Connors, T A, Double, J A, Ujhazy, V & Whisson, M E, Int j cancer 1 (1966) 319.
9. Hamilton, T C, Winker, M A, Louie, K G, Batist, G, Behrens, B C, Tsuruo, T, Grotzinger, K R, McKoy, W M, Young, R C & Ozols, R F, Biochem pharmacol 34 (1985) 2583.
10. Nathan, C F, Arrick, B A, Murray, H W, De Santis, N M & Cohn, Z A, J exp med 153 (1980) 766.
11. Hissin, P J & Hilf, R, Anal biochem 74 (1976) 214.
12. Cohn, V H & Lyle, J, Anal biochem 14 (1966) 434.
13. McNeil, T L & Beck, L V, Anal biochem 22 (1968) 431.
14. Simons, S S & Johnson, D F, Anal biochem 90 (1978) 705.
15. Kosower, N S, Kosower, E M, Newton, G L & Ranney, H M, Proc natl acad sci US 76 (1979) 3382.
16. Kachel, V, Glossner, E, Kordwig, E & Ruhenstroth-Bauer, G, J histochem cytochem 125 (1977) 804.
17. Benker, G, Kachel, V & Valet, G, Flow cytometry (ed O Laerum, T Lindmo & E Thoroud) vol. 4, p. 116. Universitetsforlaget, Bergen, Norway (1980).
18. Valet, G, Flow cytometry (ed O Laerum, T Lindmo & E Thoroud) vol. 4, p. 125. Universitetsforlaget, Bergen, Norway (1980).
19. Tietze, F, Anal biochem 27 (1969) 502.
20. Mills, G, J biol chem 229 (1957) 189.

Received August 9, 1985

FLOW CYTOMETRIC PARAMETERS OF NEUTROPHIL FUNCTION AS EARLY INDICATORS OF SEPSIS- OR TRAUMA-RELATED PULMONARY OR CARDIOVASCULAR ORGAN FAILURE

GREGOR ROTHE,
WOLFGANG KELLERMANN,
and
GÜNTER VALET
Martinsried and Munich, Federal Republic of Germany

From the Mildred-Scheel-Labor für Krebszellforschung, Max-Planck-Institut für Biochemie, Martinsried, and Institut fur Anästhesiologie der Ludwig-Maximilians-Universität, Klinikum GroBhadern, Munich.

Reprinted from
THE JOURNAL OF LABORATORY AND CLINICAL MEDICINE,
St. Louis

Vol. 115, No. 1, pp. 52-61, Jan., 1990
(Copyright © 1990, by The C.V. Mosby Company)
(Printed in the U.S.A.)

Flow cytometric parameters of neutrophil function as early indicators of sepsis- or trauma-related pulmonary or cardiovascular organ failure

GREGOR ROTHE, WOLFGANG KELLERMANN, and GÜNTER VALET

MARTINSRIED AND MUNICH, FEDERAL REPUBLIC OF GERMANY

Flow cytometric parameters of neutrophil function, such as phagocytosis and degradation of *Escherichia coli*, intracellular pH value, esterase activity, and cell volume, were evaluated as risk indicators for sepsis- and trauma-related pulmonary and cardiovascular organ failure in intensive care patients. Serial blood samples (n = 201) were obtained from 47 prospectively identified patients. Each patient's condition was classified daily within four categories: posttraumatic (n = 22) or septic (n = 28) organ failure, transition state (n = 119), and stable organ function after recovery (n = 27). Thirty-two parameters of neutrophil function were automatically calculated for each blood sample from several flow cytometric list mode measurements of cell samples vitally stained with acridine orange for intact and denatured DNA or with 1,4-diacetoxy-2,3-dicyanobenzene for intracellular pH and esterase activity. The DNA of dead cells was simultaneously counterstained with propidium iodide. The cell biochemical parameter pattern was significantly different among samples of patients from the four clinical categories ($p < 0.05$). Hyperergic phagocytosis was observed after trauma, in contrast to hypoergic phagocytosis, increased neutrophil cell volume, and elevated intracellular pH during sepsis. The clinical categories were correctly identified in 82% of the samples by automated classification with the DIAGNOSI/SPSS program system from the flow cytometrically determined cell functions. The course of the disease was correctly predicted 3 days in advance to the clinical manifestation of pulmonary or cardiovascular organ failure in 92% of the samples. The multifunctional analysis of neutrophils by flow cytometry seems of interest for early medical intervention in preseptic and preshock patients. (J LAB CLIN MED 1990;115:52-61)

Abbreviations: AD8 = 1,4-diacetoxy-2,3-dicyanobenzene; AO = acridine orange; DCH = 2,3-dicyanohydroquinone; DMF = N,N-dimethylformamide; *E. coli* = *Escherichia coli*; HBS = 5-mmol/L HEPES-buffered saline (pH 7.35); ICU = intensive care unit; PI = propidium iodide

From the Mildred-Scheel-Labor für Krebszellforschung, Max-Planck-Institut für Biochemie, Martinsried, and Institut fur Anästhesiologie der Ludwig-Maximilians-Universität, Klinikum Großhadern, Munich.

Supported in part by Deutsche Forschungsgemeinschaft Sonderforschungsbereich 0207, project G6.

Submitted for publication March 15, 1989; revision submitted Sept. 1, 1989; accepted Sept. 6, 1989.

Reprint requests: Prof. Dr. Günter Valet, Max-Planck-Institut für Biochemie, Am Klopferspitz 18a, D-8033 Martinsried, Federal Republic of Germany.

5/1/16708

Posttraumatic and septic multiple organ failure are intimately related to changes of neutrophil function. A decreased chemotactic and phagocytic activity of neutrophils leads to bacterial infection, whereas increased activation of neutrophils may induce microvascular endothelial damage.[1] The abundant pulmonary sequestration of neutrophils and the release of large quantities of proteolytic enzymes and reactive oxygen metabolites are associated with the development of the sepsis- and trauma-related adult respi-

ratory distress syndrome.[2,3] Neutrophil functions are altered during infection,[4-7] after thermal injury,[8,9] or after trauma,[10,11] and high neutrophil or band neutrophil counts in peripheral blood are well-known indicators of infectious complications in compromised patients.[12]

The functional analysis of neutrophils is not performed in the routine clinical laboratory because of the lack of fast, sensitive, and reproducible methods for the analysis of variations of neutrophil function.

We recently developed two multiparametric flow cytometric assays for the analysis of neutrophil function.[13] High reproducibility is achieved by minimal sample manipulation, standardized measurement, and automated data evaluation. Buffy coat leukocytes are incubated with viable *E. coli* K12 bacteria in autologous plasma. The phagocytosis and degradation of bacteria, the increase of neutrophil cell volume, and the extent of cell death during phagocytosis are measured after staining with AO and simultaneous counterstaining of dead cells with PI. The esterase activity and the intracellular pH of viable phagocytosing neutrophils are determined after simultaneous staining with ADB and PI.

The goal of this study was to evaluate the potential of these assays as indicators of risk and course of sepsis- and trauma-related pulmonary and cardiovascular organ function in ICU patients.

METHODS

Patients. Patients of an operative ICU with a high risk for pulmonary or cardiovascular organ failure were selected by two criteria: a severe trauma with a trauma score >15[14] or unstable pulmonary or cardiovascular organ function after complicated surgery. Patients with hematologic malignancies, chronic renal failure, liver disease, diabetes mellitus, or during immunosuppressive treatment were excluded from the study. After informed consent, blood samples were drawn serially in 24-hour or 48-hour intervals, until discharge to normal care or patient death.

Control blood samples (n = 24) from 14 healthy individuals were analyzed in parallel to define the normal range.

Research with patients and control persons was carried out according to the principles of the declaration of Helsinki, with approval by the Human Studies Committee of the University of Munich.

Leukocytes. Buffy coat leukocytes were prepared from 5 ml of heparinized (10 U/ml) venous blood by sedimentation at 200 *g* and 4° C for 10 minutes. The leukocytes were collected at the erythrocyte/plasma interface and resuspended in the supernatant plasma at a final concentration of 3.5×10^7 leukocytes/ml. The pH value of the blood plasma rose to pH 7.80 through loss of CO_2 during equilibration of the blood with the ambient air and was readjusted to pH 7.40 by addition of approximately 10 μl of 1 N HCl per ml plasma.

Bacteria. Stationary cultures of *E. coli* K12 (Sigma Chemie, Deisenhofen, FRG) were obtained after 2 days of incubation of the bacteria in HEPES-buffered RPMI-1640 (Gibco BRL, Eggenstein, FRG) at 37° C with 95% air and 5% CO_2. The bacteria (5 ml) were washed twice with 10 ml HBS (0.15 mol/L NaCl, 5 mmol/L HEPES, pH 7.35; SERVA Feinbiochemica, Heidelberg, FRG) and resuspended in HBS at a concentration of 7×10^9 bacteria/ml.

Phagocytosis. The leukocyte suspension in autologous heparinized plasma (50 μl) was incubated with 5 μl of *E. coli* suspension (7×10^9 bacteria/ml HBS) at 37° C. A control sample was incubated with 5 μl HBS in parallel. Aliquots (10 μl) were taken after 0, 30, and 90 minutes, diluted with 1 ml cold HBS and stored on ice for a maximum of 2 hours.

Fluorescent staining. Phagocytosis and degradation of bacteria by neutrophils were measured after staining with AO (Sigma). The diluted cell suspension (250 μl) was incubated for 15 minutes at 4° C with 5 μl of a dye cocktail containing 0.96 mmol/L of AO and 3 mmol/L PI (Sigma) in DMF (E. Merck, Darmstadt, FRG). AO stains the DNA of leukocytes and viable bacteria green and neutrophil granule content, single-stranded nucleic acids, and degraded nucleic acids of dead bacteria red.[13] The increase of AO green fluorescence during phagocytosis of *E. coli* indicates the amount of ingested bacterial DNA. The initial decrease of neutrophil AO red fluorescence at 30 minutes is caused by degranulation and the increase of AO red fluorescence of phagocytosing neutrophils between 30 and 90 minutes is a measure of the intracellular degradation of bacteria. The DNA of dead leukocytes was counterstained by the PI of the dye cocktail.

Intracellular pH and esterase activity were determined after staining with ADB (Paesel, Frankfurt/Main, FRG). The diluted cell suspension (250 μl) was incubated for 15 min at 20° C with 5 μl of a dye cocktail containing 4.1 mmol/L ADB and 3 mmol/L PI in DMF. ADB is cleaved intracellulary by esterases into the fluorescent pH indicator DCH and nonfluorescent acetate. The total fluorescence of the cells is a measure of esterase activity. The ratio of cellular blue to green fluorescence indicates the intracellular pH according to a calibration curve.[15]

Flow cytometry. The electrical cell volume and two fluorescences of more than 2000 leukocytes per sample were measured simultaneously with a FLUVO-II flow cytometer (HEKA-Elektronik, Lambrecht/Pfalz, FRG). The electrical cell volume was measured with HBS as sheath fluid after hydrodynamic focusing of the cells through the center of a cylindrical orifice of 80-μm diameter and 80-μm length at an electrical current of 0.15 mA and a suction of 10^4 Nm^{-2}. Fluorescence was excited with an HBO-100 high-pressure mercury arc lamp (Osram, Augsburg, FRG). The fluorescence of AO was excited between 450 and 500 nm and measured between 500 and 530 nm (AO green fluorescence) and above 550 nm (AO and PI red fluorescence). DCH fluorescence was excited between 340 and 400 nm and the emission was collected between 420 and 440 nm (DCH blue fluorescence) and above 500 nm (DCH green fluorescence and PI red fluorescence). The flow cytometer was calibrated with porous, NH_2-group–bearing particles (Paesel) of 5 μm diameter stained with DCH (Paesel) or fluorescein isothiocyanate (Sigma). The

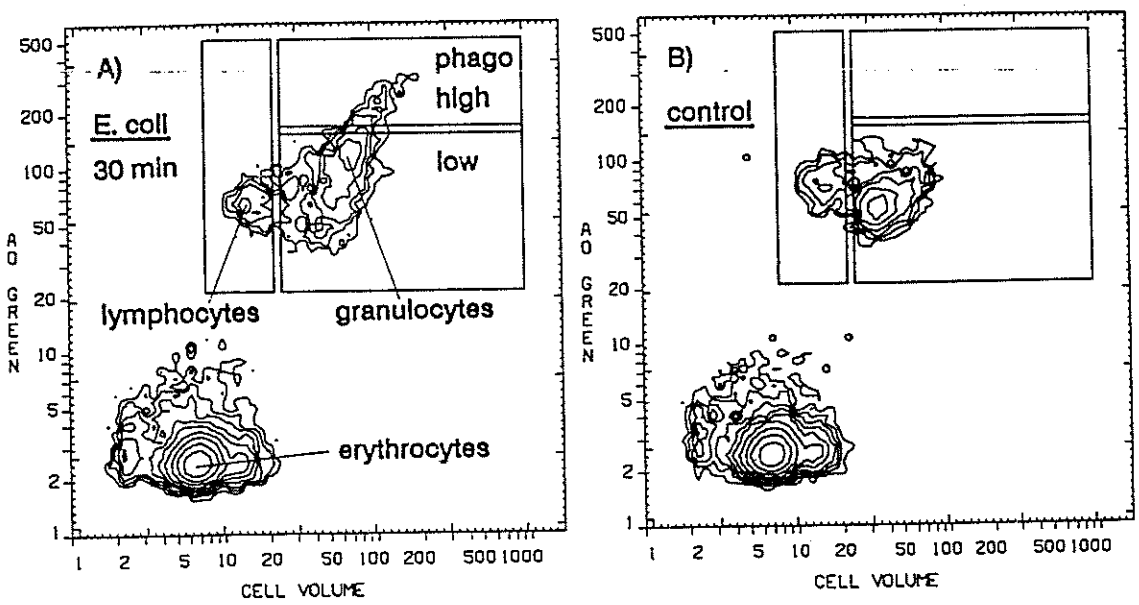

Fig. 1. Increase of neutrophil AO green fluorescence and cell volume as indicators for phagocytosis of bacteria. Buffy coat leukocytes were incubated for 30 minutes, with (A) or without (B) viable *E. coli* at 37° C, followed by staining with AO. Increase of AO green fluorescence is a measure of ingested bacterial DNA. Increase of neutrophil cell volume is a measure of cellular activation during phagocytosis. Dead cells were excluded from the analysis by simultaneous counterstaining with PI.

three signals of each cell were amplified logarithmically, digitized at maximum pulse height by 4096-step analog to digital converters and stored as list-mode data on magnetic tape.

Flow cytometric data evaluation. A graphic representation and a database of 32 parameters per sample were calculated from the flow cytometric list-mode data with the DIAGNOS1 program system[16] (HEKA) on an IBM-AT compatible personal computer. Vital cells and dead cells were analyzed separately by gating the list mode data in a first step for vital cells by their AO green fluorescence or by their DCH blue fluorescence, and in a second step for dead cells by their high PI red fluorescence.[13] The mean values of cell volume (1), AO green (2) and red (3) fluorescence, intracellular pH (4), and esterase activity (5) of viable neutrophils, and the percentage of dead cells (6) were calculated for each of the five incubations (control at 0, 30, and 90 minutes, and *E. coli* at 30 and 90 minutes) from fixed windows in the two parameter histograms obtained after gating on vital or dead cells by the program system giving 30 parameters of neutrophil function. In addition, the percentage of neutrophils was either calculated on the basis of higher AO red fluorescence of neutrophils as compared to monocytes and lymphocytes or on the basis of higher cell volume of neutrophils and monocytes than lymphocytes and the 32 parameters were transferred to the database. Monocyte activity was not evaluated separately because of considerable overlap of the monocyte cluster with lymphocytes and neutrophils.[13]

Clinical data evaluation. Age, sex, diagnosis, trauma score according to Oestern et al.,[14] length of ICU stay, and health status at hospital discharge were recorded for each patient. The patient's current pulmonary and cardiovascular organ function was classified daily into one of four categories: posttraumatic organ failure, septic organ failure, transition state, or normal function after recovery. A patient was classified into the category organ failure when at least one of the following parameters was above or below the following thresholds: a ratio of the arterial oxygen partial pressure to the fraction of inspired oxygen (Pao_2/Fio_2) $\leq$ 280 according to Pepe et al.,[17] a $Fio_2 > 0.5$, mechanical ventilation with a positive endexpiratory pressure > 5 cm H_2O, a mean arterial pressure below 70 mm Hg, or the requirement of positive inotropic support (dopamine hydrochloride $\geq$5 $\mu g\ kg^{-1}\ min^{-1}$) according to Skau et al.[18] If pulmonary and/or cardiovascular organ failure occurred within 6 days after the trauma and in the absence of infection, it was classified as posttraumatic organ failure. Pulmonary and/or cardiovascular organ failure during sepsis as defined by Montgomery et al.,[19] with the additional demonstration of an infectious focus or a positive blood culture, was classified as septic organ failure. The transition state was assumed when the patients did not fulfill the criteria for organ failure, but either required oxygen supply, ventilation, inotropic support, or intravenous volume therapy. A patient was classified as a recovered ICU patient when no pulmonary or cardiovascular support was required.

Statistics. Data are presented as the mean and the standard error of the mean. A statistical analysis of the flow cytometric data was calculated with the SPSS/PC + V2.0 program system for personal computers (SPSS, Chicago, Ill.). Significance of differences between the four clinical groups of patients was tested by the Kruskal-Wallis one-way analysis of

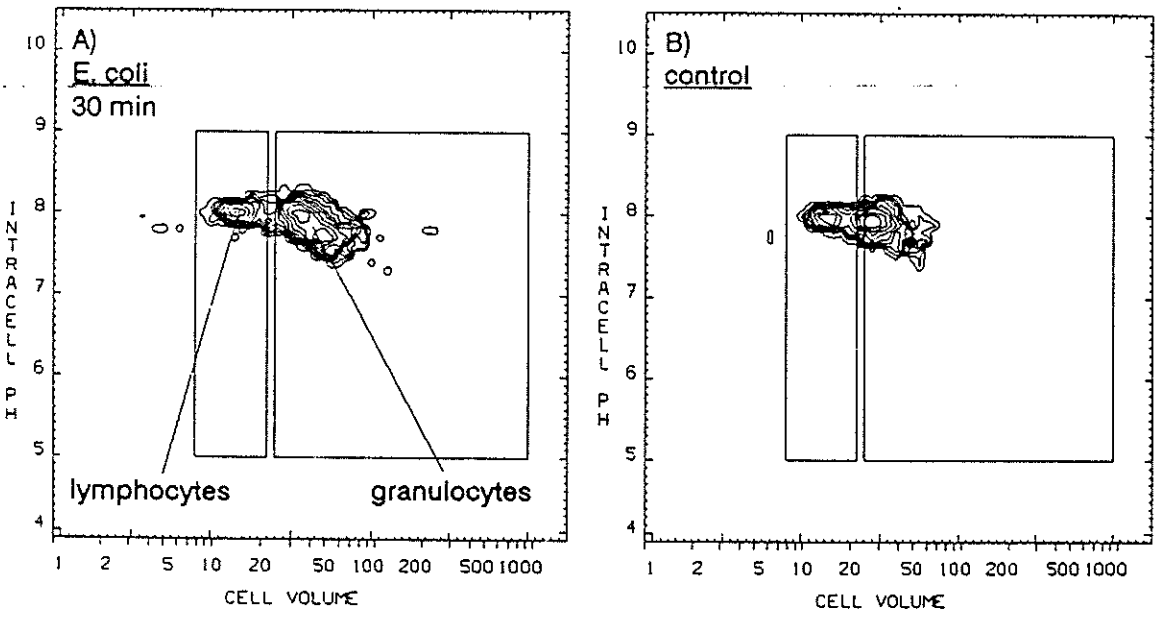

Fig. 2. Decrease of intracellular pH and increase of cell volume of neutrophils during phagocytosis of bacteria. Buffy coat leukocytes were incubated for 30 minutes, with (A) or without (B) viable *E. coli* at 37° C, followed by staining with ADB. ADB is cleaved intracellularly by esterases to the fluorescent pH indicator DCH and acetate. Intracellular pH was calculated from the ratio of cellular blue to green fluorescence, according to a calibration curve in the computer program. Dead cells were excluded from the analysis by simultaneous counterstaining with PI.

Table I. Functional parameters of neutrophils in septic and posttraumatic ICU patients

	Neutrophils			All leukocytes
	AO green fluorescence (arbitrary units)	Intracellular pH	Cell volume (μm^3)	Percentage of neutrophils
Posttraumatic organ failure (n = 22)	1.099 ± 0.067	7.46 ± 0.06	373.5 ± 23.8*	76.8 ± 2.4*
Septic organ failure (n = 28)	0.935 ± 0.049	7.64 ± 0.05*	381.3 ± 13.8*	73.6 ± 1.9*
Transition state (n = 119)	0.981 ± 0.026*	7.56 ± 0.02*	350.4 ± 4.8*	69.9 ± 1.0*
ICU patients after recovery (n = 27)	0.854 ± 0.037	7.37 ± 0.06	305.9 ± 5.7	50.7 ± 2.3
p Value	0.031†	0.001†	< 0.001†	< 0.001†
All ICU patients (n = 201)	0.970 ± 0.020	7.54 ± 0.02	351.1 ± 4.7	68.5 ± 1.0
Healthy normals (n = 24)	1.082 ± 0.067	7.55 ± 0.03	358.6 ± 9.9	34.6 ± 3.2‡

Values are expressed as mean ± SEM.
*$p < 0.05$, significant differences of values of posttraumatic, septic, or transition state patients when compared to values of ICU patients after recovery (Kruskal-Wallis one-way analysis of variance).
†$p < 0.05$, significant differences between values of the four groups of patients (Kruskal-Wallis one-way analysis of variance).
‡$p < 0.05$, significant differences of values between all ICU patients and healthy normal patients (Kruskal-Wallis one-way analysis of variance).

Table II. Effect of *E. coli* on neutrophils of septic and posttraumatic ICU patients and healthy individuals

	Increase of AO green fluorescence (% of control)		Change of intracellular pH (Δ pH)		Increase of cell volume (% of control)	
	30 min	90 min	30 min	90 min	30 min	90 min
Posttraumatic organ failure (n = 22)	125.4 ± 4.9	135.1 ± 6.0	−0.12 ± 0.04	−0.02 ± 0.03	158.9 ± 7.8*	140.3 ± 7.3
Septic organ failure (n = 28)	122.2 ± 5.0	130.4 ± 5.1	−0.04 ± 0.02	−0.07 ± 0.04	140.5 ± 3.5	129.0 ± 4.0
Transition state (n = 119)	122.1 ± 2.1	132.9 ± 2.1	−0.06 ± 0.01	−0.04 ± 0.01	140.6 ± 2.0	127.3 ± 1.9
ICU patients after recovery (n = 27)	129.5 ± 7.8	141.2 ± 5.9	−0.04 ± 0.03	−0.04 ± 0.02	133.3 ± 3.8	122.5 ± 2.6
p Value	0.894	0.411	0.220	0.836	0.026†	0.411
All ICU patients (n = 201)	123.5 ± 1.9	133.9 ± 1.8	−0.06 ± 0.01	−0.04 ± 0.01	141.5 ± 1.7	128.3 ± 1.6
Healthy normals (n = 24)	134.2 ± 5.8	156.9 ± 6.6‡	−0.07 ± 0.02	−0.04 ± 0.02	150.7 ± 3.2‡	160.9 ± 5.0‡

Values are expressed as mean ± SEM.
*$p < 0.05$, significant differences of values of posttraumatic, septic, or transition state patients when compared to values of ICU patients after recovery (Kruskal-Wallis one-way analysis of variance).
†$p < 0.05$, significant differences between values of the four groups of patients (Kruskal-Wallis one-way analysis of variance).
‡$p < 0.05$, significant differences of values between all ICU patients and healthy normals (Kruskal-Wallis one-way analysis of variance).

variance ($p < 0.05$).[20] In a *first classification* scheme, the sensitivity and specificity of the 32-flow cytometric parameter pattern for correct recognition of the *present* clinical state of the patient was analyzed by a discriminant analysis (stepwise reduction of Wilk's lambda).[21] Each cell sample was classified by three discriminant scores using Bayes' rule. The *predictive* sensitivity and specificity of the cell biochemical parameter pattern for the patient's clinical state on the third day after the flow cytometric measurement was tested with a *second classification* scheme, derived from the combination of the flow cytometric data of each sample, with the clinical rating of the patient on the third day after measurement of the sample.

RESULTS

Incidence of pulmonary or cardiovascular organ failure. Posttraumatic (n = 13) or septic (n = 19) pulmonary and/or cardiovascular organ failure occurred in 59.6% of the 47 patients. Sepsis developed in four patients after trauma. A total of 28 of the 201 samples were obtained during episodes of sepsis and 22 samples were obtained during posttraumatic organ failure.

Neutrophil function of normal individuals. The phagocytic response of neutrophils from healthy individuals was characterized by three parameters: increase of cell volume (Fig. 1), increase of AO green fluorescence (Fig. 1), and decrease of the intracellular pH value (Fig. 2). The neutrophil cell volume increased from a mean value of 358.6 μm^3 before incubation (Table I) to 150.7% of this value after 30 minutes of incubation with *E. coli* K12 (Table II). The AO green fluorescence increased from 1.082 arbitrary green fluorescence units in control cells (Table I) to 134.2% of this value after 30 minutes of phagocytosis (Table II). During incubation with *E. coli* for 90 minutes, the cell volume increased to 160.9% and AO green fluorescence to 156.9% of controls. The intracellular pH of normal neutrophils was 7.55 before incubation (Table I) and decreased by 0.07 and 0.04 pH units after 30 and 90 minutes, respectively, of incubation with bacteria (Table II).

Neutrophil function of ICU patients. Significant differences occurred when neutrophils from ICU patients were incubated with *E. coli* bacteria. The ingestion of bacteria and the increase of cell volume were significantly lower in neutrophils from ICU patients than in normal neutrophils. The mean cell volume of ICU patient neutrophils increased to only 141.5% of controls after 30 minutes of incubation with *E. coli* and decreased again to 128.3% after 90 minutes (Table II). The mean AO green fluorescence reached only 123.5% and 133.9% of controls after 30 minutes and 90 minutes, respectively. The intracellular pH during phagocytosis of *E. coli* decreased by 0.06 pH units and 0.04 pH units after 30 minutes and 90 minutes, respectively.

Blood samples from all ICU patients together showed a significantly higher percentage of neutrophils, but the cell volume, AO green fluorescence, or intracellular pH of the neutrophils before incubation with *E. coli* (Table I) was not significantly different from neutrophils of healthy individuals.

Table IIIA. Flow cytometric discriminants of current septic and posttraumatic organ failure

	Posttraumatic organ failure			Septic organ failure		
Rank	Parameter	Incubation	Stand. coeff.	Parameter	Incubation	Stand. coeff.
1	Increase of AO green fluorescence.	*E. coli*, 90 min	1.502	Cell volume	Control, 90 min	0.953
2	Percentage of neutrophils	Control, 0 min	1.225	Percentage of neutrophils	Control, 0 min	0.797
3	Increase of AO green fluorescence.	*E. coli*, 30 min	0.994	Cell volume	Control, 30 min	0.603
4	Cell volume	Control, 0 min	0.513	Increase of AO green fluorescence.	*E. coli*, 90 min	0.549
5	Cell volume	Control, 90 min	0.446	Increase of cell volume	*E. coli*, 90 min	0.337

Table IIIB. Flow cytometric discriminants of imminent septic and posttraumatic organ failure

	Posttraumatic organ failure			Septic organ failure		
Rank	Parameter	Incubation	Stand. coeff.	Parameter	Incubation	Stand. coeff.
1	Percentage of neutrophils	Control, 0 min	1.239	Increase of AO green fluorescence	*E. coli*, 30 min	1.819
2	Cell volume	Control, 90 min	1.124	Cell volume	Control, 90 min	1.436
3	Cell volume	Control, 30 min	0.867	Decrease of intracellular pH	*E. coli*, 90 min	1.307
4	Increase of AO green fluorescence	*E. coli*, 30 min	0.720	Increase of cell death	*E. coli*, 90 min	1.175
5	Intracellular pH	Control, 0 min	0.603	AO green fluorescence	Control, 30 min	0.799

List of five flow cytometric parameters with highest standardized discriminant coefficients in a multifactorial analysis. All 32 flow cytometric parameters were considered for automated discrimination of either current or imminent posttraumatic or septic organ failure. Samples from recovered ICU patients served as control group.

Longitudinal study of neutrophils in individual patients. Typical posttraumatic time courses of the phagocytic response of neutrophils in individual patients showed high increases of neutrophil cell volume during phagocytosis in the early posttraumatic phase, followed by rapid declines of cell volume increase already several days before the onset of septic periods (Fig. 3, *A*). The intracellular pH of control neutrophils and neutrophils incubated with *E. coli* also exhibited a typical pattern with acidic intracellular pH values after trauma and alkaline pH during septic episodes (Fig. 3, *B*).

Significance of disease-related cell biochemical parameter patterns. The grouping of the blood samples according to the daily classification of the patients' pulmonary and vascular organ function revealed significant disease-related parameter patterns for resting (Table I) and phagocytosing (Table II) neutrophils. Blood samples obtained from septic or posttraumatic patients during pulmonary or cardiovascular dysfunction contained neutrophils with a larger mean cell volume and a higher percentage of neutrophils (Table I). An alkaline intracellular pH was associated with sepsis and a high accumulation of AO green fluorescence by neutrophils was observed in the posttraumatic state.

The increase of cell volume during incubation with *E. coli* was significantly higher during posttraumatic organ failure (Table II). The lower phagocytosis of bacteria in septic samples, measured by the increase of AO green fluorescence, and the higher decrease of the intracellular pH in posttraumatic samples were not significantly different from samples obtained from ICU patients after recovery.

Extracellular pH and carbon dioxide tension in ICU patients. In order to correlate intracellular pH values with respiratory acid-base disturbances, the extracellular pH and carbon dioxide tension of arterial blood were determined. The mean arterial pH value in the four groups of patients did not differ significantly, with a range from 7.38 to 7.41 pH units. The arterial carbon dioxide tension had a mean of 41.7 ± 1.0 mm Hg for all patients and was significantly different between the four groups of patients, with the lowest values in recovered ICU patient samples (34.1 ± 1.8 mm Hg), the highest values in transition state samples (43.6 ± 1.4 mm Hg), and intermediate values during posttraumatic (39.8 ± 2.2 mm Hg) or septic organ failure (41.8 ± 1.5 mm Hg).

Automated classification by flow cytometric param-

Table IV. Automated classification of intensive care patients with flow cytometric parameters of neutrophil function for current clinical condition

Clinical diagnosis	n	DIAGNOSI/SPSS-classification*			
		Posttraumatic organ failure	Septic organ failure	Transition state	Normal ICU patients
Posttraumatic organ failure	20	90.0	0.0	10.0	0.0
Septic organ failure	27	0.0	77.8	22.2	0.0
Transition state	113	7.1	14.2	75.2	3.5
ICU patients after recovery	26	0.0	0.0	11.5	88.5

Classification by three discriminant scores was derived by a stepwise minimization of Wilks' lambda from 32 flow cytometric parameters of neutrophils function.
*Values are expressed in percentage.

Table V. Automated three day in advance classification of intensive care patients with flow cytometric parameters of neutrophil function for imminent clinical condition

Clinical diagnosis 3 days later	n	DIAGNOSI/SPSS-classification*			
		Posttraumatic organ failure	Septic organ failure	Transition state	Normal ICU patients
Posttraumatic organ failure	8	100.0	0.0	0.0	0.0
Septic organ failure	12	0.0	91.7	8.3	0.0
Transition state	94	1.1	7.4	87.2	4.3
ICU patient after recovery	23	0.0	4.3	0.0	95.7

Classification by three discriminant scores was derived by a stepwise minimization of Wilks' lambda from 32 flow cytometric parameters of neutrophil function.
*Values are expressed in percentage.

eters. The sensitivity and specificity of the flow cytometric parameters for the identification of the patient's current disease status were analyzed by a discriminant analysis. This stepwise procedure combined the various flow cytometric parameters in increasing number with the aim to improve the discrimination of the four clinical groups of samples (i.e., to minimize the variability of the three discriminant scores within each clinical group, as compared to the variability of the three scores for all patients). The increase of AO green fluorescence during phagocytosis, the cell volume of resting neutrophils, and the percentage of neutrophils were the most significant discriminators when either posttraumatic or septic samples were compared with samples obtained from recovered ICU patients (Table IIIA and IIIB).

Ultimately, the combination of 26 of the 32 determined flow cytometric parameters to three discriminant scores was optimal, with the correct identification of 90.0% of the posttraumatic samples and 77.8% of the septic samples (Table IV). The remainder of the posttraumatic and septic samples were misclassified as transition state. No sample from a recovered ICU patient was misclassified as a posttraumatic or septic sample.

The predictive sensitivity of the flow cytometric patterns of neutrophil function was analyzed by combining the flow cytometric data of each sample with the clinical rating of the same patient on the third day after measurement of the sample. The discriminant analysis of these data led to a second classification algorithm (Tables IIIA and IIIB), which correctly predicted pulmonary or cardiovascular organ failure in posttraumatic or septic patients by 100.0% or 91.7%, respectively (Table V).

DISCUSSION

Flow cytometric parameters of neutrophil function, such as DNA content, intracellular pH, and cell volume during phagocytosis and degradation of *E. coli*, showed significant differences between samples from posttraumatic or septic ICU patients and a healthy con-

trol group (Tables I and II). The combination of several of these parameters to a multifunctional parameter pattern allowed the discrimination of patients with posttraumatic pulmonary or cardiovascular organ failure from patients with septic organ failure and patients in transition state or with stable organ function (Tables IIIA, IIIB, and IV). Furthermore, the course of the disease was predicted 3 days in advance (Table V).

The ingestion and intracellular degradation of bacteria was measured by staining vital cells with the metachromatic dye AO. AO fluoresces green when intercalating into double-stranded nucleic acids and fluoresces red when complexing with single-stranded or denatured nucleic acids.[22] The ingestion of bacterial DNA by neutrophils was lower in blood samples from ICU patients than in blood samples from a healthy reference group (Table II). The four groups of ICU patients did not differ significantly in the increase of AO green fluorescence, indicating no trauma- or sepsis-associated alterations of the capability of neutrophils to ingest bacteria, a property of neutrophils that is already developed at the metamyelocyte state.[23] The incubation of unseparated leukocytes in autologous plasma with a twenty-fold excess of *E. coli* in our assay neither limited phagocytosis by low opsonization nor by low numbers of bacteria.[13]

The vital staining of resting neutrophils with AO also allowed the quantitative analysis of their nuclear structure, as changes of chromatin condensation affect the intercalative binding of AO to DNA.[24] The AO green fluorescence of neutrophils was 29% higher in samples from patients with posttraumatic pulmonary or cardiovascular organ failure than in samples from patients with stabilized organ function (Table I), suggesting significant disease-related alterations of the nuclear structure of neutrophils.

The intracellular pH of resting and phagocytosing neutrophils was analyzed as a parameter of the cellular metabolic activity.[25] The intracellular pH is regulated by an electroneutral Na^+/H^+ exchange in neutrophils and is tightly related to cell activation. An alkaline intracellular pH increases receptor-coupled reactions leading to the expression of NADPH oxidase, which releases superoxide anion in stimulated neutrophils.[26,27] Upon cellular activation, the electron-translocating NADPH oxidase induces an initial cytoplasmic acidification through the generation of large amounts of protons. The protons are transferred to the granules and to the exterior of the cells by Zn^{2+}- or Cd^{2+}-sensitive proton-conducting channels.[28] In addition, the Na^+/H^+ exchange is activated. This leads to a sustained intracellular alkalinization.[29] It also induces chemotaxis[30] and an increase of the cell volume of neutrophils.[31]

The intracellular pH values of resting neutrophils from the four groups of patients were significantly different. Alkaline pH values were observed during septic pulmonary or cardiovascular organ failure and acidic pH values during stable organ function after patients' recovery (Table I). No differences of the extracellular blood arterial pH were observed in the four groups of patients. The alkaline intracellular pH and the large cell volume of neutrophils observed during septic organ failure reflected metabolic activation of the neutrophils because they were accompanied by a normal arterial carbon dioxide tension. Despite the different intracellular pH values of resting neutrophils, the slight acidification of the intracellular pH after phagocytosis was similar in all patient groups (Table II), indicating intact regulation of the acid-balance during the respiratory burst.

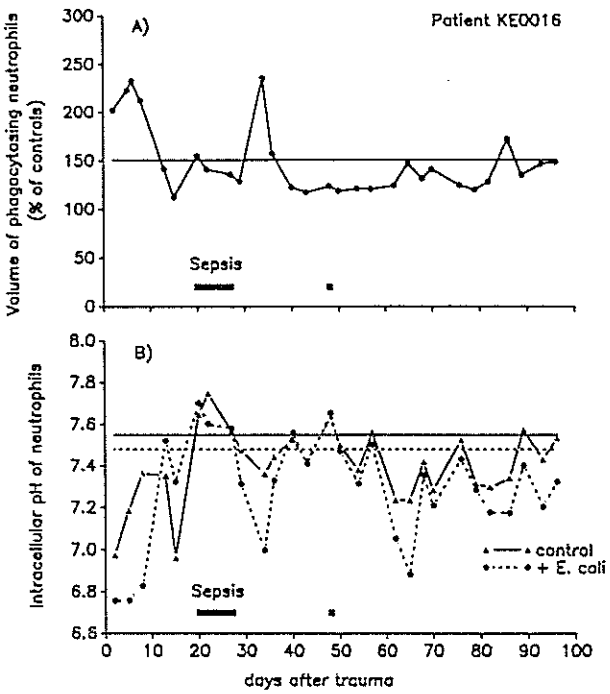

Fig. 3. Longitudinal study of neutrophil function in a posttraumatic patient. A, increase of neutrophil cell volume during phagocytosis of *E. coli*. Buffy coat leukocytes were incubated with *E. coli* for 30 minutes at 37° C, stained with AO, and analyzed as described in Fig. 1. Cell volume of *E. coli*-incubated neutrophils is given as percentage of cell volume of neutrophils incubated without bacteria. B, intracellular pH of neutrophils. Buffy coat leukocytes were incubated with (●--●) or without (▲—▲) *E. coli* for 30 minutes at 37° C, stained with ADB, and analyzed as described in Fig. 2. Straight lines indicate the mean values for a reference group of healthy individuals (n = 14).

The increase of neutrophil cell volume during phagocytosis of *E. coli* was a more sensitive indicator of the activation of the phagocytic process after trauma than the ingestion of *E. coli* as measured by increase of AO green fluorescence (Table II). Furthermore, in all groups of patients—but not in healthy normals—the

increased cell volume of phagocytosing neutrophils declined after 90 minutes of incubation with *E. coli*, despite continuous ingestion of *E. coli* as indicated by increasing AO green fluorescence (Table II). This shows that the change of cell volume during phagocytosis was not only caused by the volume of the ingested bacteria, but in addition indicated active cellular processes, like the reversible cell swelling induced by activated complement,[32,33] phorbol esters, or chemotactic peptides.[31]

The resting cell volume of neutrophils was also a sensitive indicator for both posttraumatic and septic organ failure (Tables I, IIIA, and IIIB). This confirms centrifugal elutriation studies that showed that the resting cell volume of human peripheral blood neutrophils is not correlated with cell age, but associated with increased NADPH oxidase activity,[34] possibly as a consequence of earlier activation of the cell.[35]

The multifunctional flow cytometric analysis of phagocytosing and control-incubated neutrophils revealed two patterns of abnormal neutrophil function in ICU patients (Tables IIIA and IIIB). The posttraumatic activation of neutrophils was associated with an increased functional response to phagocytosis of *E. coli*, as measured by increased cell swelling and increased acidification, whereas neutrophils from septic patients exhibited pre-existing high cell volume and alkaline pH (Table I) and showed low responses when incubated with *E. coli* (Table II). The increase of neutrophil counts and the increase of their resting cell volume and their AO green fluorescence were indicators of neutrophil activation during the transition state of patients.

The activated functional state of neutrophils during posttraumatic pulmonary or cardiovascular organ failure may result from the recruitment of neutrophils from the marginated blood vessel cell pool or from the bone marrow cell pool. Neutrophils derived from the bone marrow have been reported to be functionally different from peripheral blood neutrophils in some studies,[36,37] but not in others.[38] Alternatively, the hyperergic phagocytosis of neutrophils trauma may result from activation of normal peripheral blood neutrophils (e.g., by complement cleavage products). During septic organ failure, bacterial products like endotoxin,[35,39,40] or chemotactic bacterial peptides,[41] or immune-mediators released from monocytes[42] and macrophages[43] like interleukin-1 or tumor necrosis factor alpha[44-46] are liberated and may be responsible for the alkaline pH and large cell volume of neutrophils and their lower responses to incubation with *E. coli*.

The results of this study suggest that systemic alterations of neutrophil function—rather than only an alteration of the local milieu—are associated with the imminence of posttraumatic or septic multiple organ failure. The longitudinal analysis of such alterations of neutrophil function with sensitive multiparametric cell-biochemical techniques is important not only for the early recognition of imminent sepsis, but also for the understanding of the mechanisms of the alterations of neutrophil function during posttraumatic and septic organ failure in ICU patients.

REFERENCES

1. Malech HL, Gallin JI. Current concepts: Immunology. Neutrophils in human diseases. N Engl J Med 1987;317:687-94.
2. Cohen AB, MacArthur C, Idell S, et al. A peptide from alveolar macrophages that releases neutrophil enzymes into the lungs in patients with the adult respiratory distress syndrome. Am Rev Respir Dis 1988;137:1151-8.
3. Zimmerman GA, Renzetti AD, Hill HR. Functional and metabolic activity of granulocytes from patients with adult respiratory distress syndrome. Evidence for activated neutrophils in the pulmonary circulation. Am Rev Respir Dis 1983;127:290-300.
4. Bass DA, Olbrantz P, Szejda P, Seeds MC, McCall CE. Subpopulations of neutrophils with increased oxidative product formation in blood of patients with infection. J Immunol 1986;136:860-6.
5. Ozaki Y, Ohashi T, Niwa Y. Evaluation of neutrophil acetyltransferase activity in patients with inflammatory disorders. Life Sciences 1986;39:2343-50.
6. Barbour AG, Craig CD, Solberg CO, Hill HR. Chemiluminescence by polymorphonuclear leukocytes from patients with active bacterial infection. J Infect Dis 1980;141:14-26.
7. Venge P, Strömberg A, Braconier JH, Roxin LE, Olsson I. Neutrophil and eosinophil granulocytes in bacterial infection: sequential studies of cellular and serum levels of granule proteins. Br J Haematol 1978;38:475-83.
8. Marino JA, Gerding RL, Fratianne RB, Spagnuolo PJ. Neutrophil adhesive dysfunction in thermal injury: the role of fibronectin. J Infect Dis 1988;157:674-81.
9. Davis CF, Moore FD, Rodrick ML, Fearon DT, Mannick JA. Neutrophil activation after burn injury: contributions of the classic complement pathway and endotoxin. Surgery 1987;102:477-84.
10. Dwenger A, Schweitzer G, Regel G. Bronchoalveolar lavage fluid and plasma proteins, chemiluminescence response and protein contents of polymorphonuclear leukocytes from blood and lavage fluid in traumatized patients. J Clin Chem Clin Biochem 1986;24:73-88.
11. Green DR, Faist E. Trauma and the immune response. Immunology Today 1988;9:253-5.
12. Shapiro MF, Greenfield S. The complete blood count and leukocyte differential count. An approach to their rational application. Annal Intern Med 1987;106:65-74.
13. Rothe G, Valet G. Phagocytosis, intracellular pH, and cell volume in the multifunctional analysis of granulocytes by flow cytometry. Cytometry 1988;9:316-24.
14. Oestern HJ, Sturm JA, Tscherne H. Die Klassifizierung der Verletzungsschwere. Hefte Unfallheilk 1983;156:171-6.
15. Valet G, Raffael A, Moroder L, Wuensch E, Ruhenstroth-Bauer G. Fast intracellular pH determination in single cells by flow-cytometry. Naturwissenschaften 1981;68:265-6.
16. Valet G, Warnecke HH, Kahle H. Automated diagnosis of malignant and other abnormal cells by flow-cytometry using the DIAGNOS1 program system. In: Burger G, Ploem JS, Goerttler K, eds. Clinical cytometry and histometry. London: Academic Press, 1987:58-65.
17. Pepe PE, Potkin RT, Reus DH, Hudson LD, Carrico CJ. Clinical

predictors of the adult respiratory distress syndrome. Am J Surg 1987;144:124-30.
18. Skau T, Nyström PO, Carlsson C. Severity of illness in intra-abdominal infection: a comparison of two indexes. Arch Surg 1985;120:152-8.
19. Montgomery AB, Stager MA, Carrico CJ, Hudson L. Causes of mortality in patients with the adult respiratory distress syndrome. Am Rev Respir Dis 1985;132:485-9.
20. Norusis MJ. SPSS/PC+ V2.0 base manual. Chicago: SPSS Inc., 1988.
21. Norusis MJ. SPSS/PC+ V2.0 advanced statistics. Chicago: SPSS Inc., 1988.
22. Darzynkiewicz Z, Traganos F, Kapuscinski J, Melamed MR. Denaturation and condensation of DNA in situ induced by acridine orange in relation to chromatin changes during growth and differentiation of friend erythroleukemia cells. Cytometry 1985;6:195-207.
23. Glasser L, Fiederlein RL. Functional differentiation of normal human neutrophils. Blood 1987;69:937-44.
24. Traganos F, Darzynkiewicz Z, Sharpless T, Melamed MR. Cytofluorometric studies on conformation of nucleic acids in situ. I. Restriction of acridine orange binding by chromatin proteins. J Histochem Cytochem 1976;24:40-8.
25. Frelin C, Vigne P, Ladoux A, Lazdunski M. The regulation of the intracellular pH in cells from vertebrates. Eur J Biochem 1988;174:3-14.
26. Wright J, Maridonneau-Parini I, Cragoe EJ, Schwartz JH, Tauber AI. The role of the Na^+/H^- antiporter in human neutrophil NADPH-oxidase activation. J Leukocyte Biol 1988;43:183-6.
27. Simchowitz L. Intracellular pH modulates the generation of superoxide radicals by human neutrophils. J Clin Invest 1985;76:1079-89.
28. Henderson LM, Chappell JB, Jones OTG. Internal pH changes associated with the activity of NADPH oxidase of human neutrophils: further evidence for the presence of an H^- conducting channel. Biochem J 1988;251:563-7.
29. Weisman SJ, Punzo A, Ford C, Sha'afi RI. Intracellular pH during neutrophil activation: Na^+/H^+ antiport. J Leukocyte Biol 1987;41:25-32.
30. Simchowitz L, Cragoe EJ. Regulation of human neutrophil chemotaxis by intracellular pH. J Biol Chem 1986;261:6492-500.
31. Grinstein S, Furuya W, Cragoe EJ. Volume changes in activated human neutrophils: the role of Na^+/H^+ exchange. J Cell Physiol 1986;128:33-40.
32. O'Flaherty JTO, Kreutzer DL, Ward PA. Chemotactic factor influences on the aggregation, swelling, and foreign surface adhesiveness of human leukocytes. Am J Pathol 1978;90:537-50.
33. Morgan BP. Non-lethal complement attack on human neutrophils: transient cell swelling and metabolic depletion. Immunology 1988;63:71-7.
34. Berkow RL, Dodson RW. Volume dependent polymorphonuclear leukocytes fractions isolated by counterflow centrifugal elutriation: PMN volume does not correlate with PMN age. J Leukocyte Biol 1987;41:518-26.
35. Guthrie LA, McPhail L, Henson PM, Johnston RB. Priming of neutrophils for enhanced release of oxygen metabolites by bacterial lipopolysaccharide: evidence for increased activity of the superoxide-producing enzyme. J Exp Med 1984;160:1656-71.
36. Steele RW, Steele CR, Pilkington NS, Charlton RK. Functional capacity of marginated and bone marrow reserve granulocytes. Infect Immun 1987;55:2359-63.
37. Hetherington SV, Quie PG. Human polymorphonuclear leukocytes of the bone marrow, circulation, and marginated pool: Function and granule protein content. Am J Hematol 1985;20:235-46.
38. Berkow RL, Dodson RW. Functional analysis of the marginating pool of human polymorphonuclear leukocytes. Am J Hematol 1987;24:47-54.
39. Wright GG, Read PW, Mandell GL. Lipopolysaccharide releases a priming substance from platelets that augments the oxidative response of polymorphonuclear neutrophils to chemotactic peptide. J Infect Dis 1988;157:690-6.
40. Moore FD, Moss NA, Revhaug A, Wilmore D, Mannick JA, Rodrick ML. A single dose of endotoxin activates neutrophils without activating complement. Surgery 1987;102:200-5.
41. Hughes V, Humphreys JM, Edwards SW. Protein synthesis is activated in primed neutrophils: a possible role in inflammation. Biosci Report 1987;7:881-90.
42. Koivuranta-Vaara P, Banda D, Goldstein IM. Bacterial-lipopolysaccharide-induced release of lactoferrin from human polymorphonuclear leukocytes: role of monocyte-derived tumor necrosis factor α. Infect Immun 1987;55:2956-61.
43. Movat HZ, Cybulski MI, Colditz IG, Chan MKW, Dinarello CA. Acute inflammation in gram-negative infection: endotoxin, interleukin 1, tumor necrosis factor, and neutrophils. Federation Proc 1987;46:97-104.
44. Sullivan GW, Carper HT, Novick WJ, Mandell GL. Inhibition of the inflammatory action of interleukin-1 and tumor necrosis factor (alpha) on neutrophil function by pentoxifylline. Infect Immunol 1988;56:1722-9.
45. Blanchard DK, Djeu JY, Klein TW, Friedman H, Stewart WE. Protective effects of tumor necrosis factor in experimental *Legionella pneumophila* infections of mice via activation of PMN function. J Leukocyte Biol 1988;43:429-35.
46. Ferrante A, Nandoskar M, Walz A, Goh DHB, Kowanko IC. Effect of tumour necrosis factor alpha and interleukin-1 alpha and beta on human neutrophil migration, respiratory burst, and degranulation. Int Arch Allergy Appl Immun 1988;86:82-91.

Journal of Leukocyte Biology 47:440–448 (1990)

Flow Cytometric Analysis of Respiratory Burst Activity in Phagocytes With Hydroethidine and 2′,7′-Dichlorofluorescin

Gregor Rothe and Günter Valet

Mildred-Scheel-Labor für Krebszellforschung, Max-Planck-Institut für Biochemie, Martinsried, Federal Republic of Germany

Hydroethidine (HE) and 2′,7′-dichlorofluorescin (DCFH) were used for the flow cytometric measurement of reactive oxygen metabolites in leukocytes. Hydroethidine and DCFH were both rapidly oxidized in a cell-free cuvette assay to ethidium bromide (EB) and 2′,7′-dichlorofluorescein (DCF) by H_2O_2 and peroxidase, but not by H_2O_2 alone, while only HE was oxidized by KO_2, a source of O_2^-. Quiescent lymphocytes, monocytes, and neutrophils spontaneously oxidized HE to EB, while DCFH was only oxidized to a low degree. Neutrophils increased 6.9-fold in EB red fluorescence and 12.5-fold in DCF green fluorescence during the respiratory burst induced by phorbol 12-myristate 13-acetate or 6.1-fold and 4.7-fold, respectively, during the respiratory burst induced by *Escherichia coli* bacteria. The HE or DCFH oxidation during the respiratory burst, unlike the spontaneous HE oxidation, was not inhibitable by 10 mM NaN_3 indicating a non-mitochondrial source of cellular oxidants during the respiratory burst such as NADPH oxidase, which produces O_2^-. The oxidation of DCFH, but not of HE, was decreased in stimulated neutrophils, which were simultaneously loaded with HE and DCFH. Intracellular DCFH oxidation induced by incubation of resting neutrophils with extracellular H_2O_2 was not influenced by the presence of HE. This indicates that HE is oxidized at an earlier step in the reactive oxygen metabolism of neutrophils than DCFH, i.e., by early oxygen metabolites like O_2^-, while DCFH is oxidized in part by H_2O_2 and phagosomal peroxidases. The differential oxidation of HE and DCFH during simultaneous cellular staining permits the analysis of up to three functionally different neutrophil populations in septic patients. This is of interest for the determination of disease-related alterations of oxygen metabolism in quiescent and stimulated leukocytes.

Key words: neutrophils, flow cytometry, free radical, reactive oxygen species (ROS)

INTRODUCTION

Phagocytosis or stimulation of neutrophils induces a metabolic burst. The non-mitochondrial oxygen consumption increases, and a variety of reactive oxygen metabolites are released into the phagosome and into the extracellular environment [6]. This respiratory burst is important for the killing of ingested microorganisms [24] but may also be detrimental to the organism through endothelial damage in rheumatic diseases [35], in sepsis [18], and in the adult respiratory distress syndrome [42].

Superoxide anion (O_2^-) is the primary metabolite generated through a one-electron reduction of molecular oxygen by a membrane-bound NADPH oxidase [1,6,36]. It dismutates either spontaneously or via superoxide dismutase (SOD) to H_2O_2, which is converted by myeloperoxidase to hypochlorous acid and chloramines inside the phagosome [37].

Specific biochemical methods for the quantitation of respiratory burst activity are based on the measurement of extracellular oxygen consumption or on the extracellular release of O_2^- and H_2O_2 [2]. A certain part of the O_2^- and H_2O_2 produced during the respiratory burst is reconverted intracellularly to molecular oxygen via SOD or catalase. This part of the O_2^- production is not detectable by extracellular biochemical assays because it leads neither to extracellular release of O_2^- or H_2O_2 nor to extracellular oxygen consumption. The magnitude of the respiratory burst is, therefore, underestimated by extracellular assays. Neutrophils must also be isolated from

Received January 9, 1989; accepted August 15, 1989.

Presented in part at the XIIth International Meeting of the Society for Analytical Cytology, Cambridge, England, August 1987.

Reprint requests: Günter Valet, Max-Planck-Institut für Biochemie, Am Klopferspitz 18a, D-8033 Martinsried, FRG

© 1990 Wiley-Liss, Inc.

whole blood for biochemical bulk assays. This may alter their functional properties [29,34].

Flow cytometric methods for the rapid measurement of intracellular oxidative reaction in single vital cells have been developed as an alternative. The oxidative burst of neutrophils can be measured through the intracellular oxidation of 2′,7′-dichlorofluorescin (DCFH) [5,11] or dihydrorhodamine 123 [33]. Non-fluorescent DCFH is first loaded into vital cells by enzymatic cleavage of the membrane-permeable 2′,7′-dichlorofluorescin-diacetate (DCFH-DA). Intracellular DCFH is oxidized to fluorescent 2′,7′-dichlorofluorescein (DCF) upon activation of the respiratory burst. The oxidation of DCFH is mainly a measure of the phagosomal formation of reactive oxygen metabolites since the fluorescent product DCF is predominantly found inside the peroxidase-containing granules [31]. Soluble stimuli, however, cause the release of O_2^- at the whole plasma membrane and at the phagosomal membrane [9]. Subpopulations of neutrophils with enhanced respiratory burst activity have been detected through DCFH oxidation in patients with bacterial infections [4,11].

The goal of the present study was to develop a flow cytometric method for the direct measurement of oxygen reduction during the respiratory burst of phagocytes. Hydroethidine (HE), the sodium borohydride-reduced derivative of ethidium bromide (EB) [10,38], either alone or in conjunction with DCFH was found useful for this purpose. HE, in contrast to EB, permeates the cell membrane easily and can be directly oxidized to red fluorescent EB, which is trapped in the nucleus by intercalation into DNA, leading to enhancement of EB fluorescence.

MATERIALS AND METHODS

Preparation of Human Leukocytes

Buffy coat leukocytes (200 μl) were prepared from 21 samples of heparinized (10 U/ml) venous blood (5 ml, 9 healthy donors, aged 24–45 years) by centrifugation at 200*g* and 4°C for 10 min. The samples were diluted with approximately 300 μl of the supernatant plasma to obtain a concentration of $3.5 * 10^7$ leukocytes/ml. Six additional blood samples were drawn from 5 septic patients.

Polymorphonuclear and mononuclear cells were separated in some experiments by the one-step method of Ferrante et al. [8,14] using Mono-Poly Resolving Medium (Flow Laboratories, Meckenheim, FRG). The cell fractions were washed once (200*g*, 10 min) with 10 ml HEPES-buffered saline (HBS) (0.15 M NaCl, 5 mM HEPES, pH 7.35, Serva Feinbiochemica, Heidelberg, FRG) and resuspended in 50 to 100 μl of autologous plasma to obtain a concentration of $3.5 * 10^7$ cells/ml. All cell preparations were stored on ice, and the flow cytometric measurements were terminated within 6 hr after removal of the blood from the donors.

Cell Staining

The cell suspension (10 μl) was diluted with 1 ml HBS and stained for 15 min at 37°C with 2.5 μl of a 63.5-mM HE (Polysciences, St. Goar, FRG) solution in N,N-dimethylformamide (DMF) (E. Merck, Darmstadt, FRG) and/or 20 μl of a 0.5-mM DCFH-DA solution (1/20 prediluted with HBS from 10 mM DCFH-DA in DMF, Serva). This corresponds to a final concentration of 160 μM HE or 10 μM DCFH-DA in the cell assay. Sodium azide (Merck) or sodium cyanide (Merck) (20 μl of 500-mM, 50-mM, or 5-mM solutions in HBS) were added together with the dyes in enzyme inhibition experiments. Cyanide, in contrast to azide, was only added after a 15-min prestaining of the cells with DCFH-DA at 37°C to avoid cyanide inhibition of the intracellular DCFH-DA cleaving esterases.

The samples with HE- or DCFH-loaded cells were split into aliquots of 250 μl and further incubated either for 30 min with 5 μl of a 7.5-μM solution of phorbol 12-myristate 13-acetate (PMA) (1/200 prediluted with HBS from 1.5 mM PMA in DMF, Sigma Chemie, Deisenhofen, FRG), or for 15 min with 5 μl of a 65-mM solution of H_2O_2 (Merck) in HBS. The EB fluorescence of dead cells, which was due to contamination of HE with EB, was quenched by addition of 10 μl of 5.2 mM trypan blue (Serva) in HBS immediately prior to flow cytometric measurement. Trypan blue at this concentration did not alter the EB red or DCF green fluorescence of vital cells. The DNA of dead cells was counterstained with 5 μl of 3-mM propidium iodide (PI) (Sigma) solution in HBS 3 min before the measurement in samples stained with DCFH-DA.

Phagocytosis

Escherichia coli K12 bacteria (Sigma) were grown overnight in RPMI-1640 (Gibco BRL, Eggenstein, FRG) at 37°C and 5% CO_2. The bacteria (5 ml) were washed twice with 10 ml HBS and resuspended in HBS to a final concentration of $7 * 10^9$ bacteria/ml. The leukocyte suspension in autologous plasma (100 μl) was incubated with 10 μl of the *E. coli* suspension at 37°C to avoid potential interference of the staining solution with the phagocytosis process. Aliquots (10 μl) were taken every 5 min, diluted with 1 ml HBS, and stained for 15 min at 37°C with 2.5 μl 63.5-mM HE and/or 20 μl of a 0.5-mM DCFH-DA solution corresponding to final concentrations of 160 μM HE and/or 10 μM DCFH-DA.

Fluorescence Spectrometry

Fluorescence spectra were kinetically recorded with a Perkin Elmer LS-5 luminescence spectrometer (Bod-

enseewerk Perkin-Elmer, Überlingen, FRG) connected on-line to a VAX 8550 computer (Digital Equipment, Munich, FRG) using excitation and emission slits of 5 nm nominal band width and quartz cuvettes of 10 mm path length.

Stock solutions of HE (31.75 mM), EB (12.68 mM, Serva), DCFH-DA (50 mM), and DCF (50 mM, Sigma) were prepared in DMF. A 50-mM DCFH solution was prepared by 30-sec hydrolysis of 10 μl of the 50-mM DCFH-DA solution with 20 μl of a 0.1-N NaOH solution followed by addition of 10 ml MOPS-buffer (MBS) (0.2 M MOPS, pH 7.20, Sigma). Horseradish peroxidase (HRP) (Sigma) and SOD (Sigma) were dissolved in MBS at concentrations of 20 and 200 U/ml (HRP), or 20,000 U/ml (SOD). Potassium superoxide (KO_2) (Fluka, Buchs, CH) was directly weighed into the cuvettes at 97.5 μM per cuvette. After addition of 2 ml of the final dye solution in MBS this corresponded to a 48.8-mM KO_2 solution yielding approximately 1.3 mM O_2^- [23].

Spontaneous oxidation of a 10-μM HE solution or of a 0.5-μM DCFH solution in MBS, the oxidation of HE or DCFH in the presence of 48.8 mM KO_2 with or without 1,000 U/ml SOD, and the oxidation of HE and DCFH in the presence of 0, 0.1, 1, 10, and 100 U/ml HRP and of 1.3 mM H_2O_2 were recorded for 40 min at 22°C by measuring the fluorescence intensities at the wavelengths corresponding to the maximum emission and excitation of EB (excitation 473 nm/emission 593 nm) and DCF (excitation 501 nm/emission 521 nm). The residual HE concentration was determined through HE blue fluorescence (excitation 348 nm/emission 421 nm). The residual DCFH concentration was determined as the increase of DCF fluorescence after a second addition of 1.3 mM H_2O_2 and 100 U/ml HRP at the end of the incubation. The oxidation of a 10-μM DCFH solution in MBS by the same amounts of oxidants was measured at its end point after 40 min of incubation, followed by 20-fold dilution with MBS to keep the fluorescence signals within the photomultiplier range.

Flow Cytometry

The electrical cell volume and two fluorescences of more than 2,000 leukocytes per sample were simultaneously measured with a FLUVO-II flow cytometer (HEKA-Elektronik, Lambrecht/Pfalz, FRG). The electrical cell volume was determined by hydrodynamic focusing of the cells through the center of a cylindrical orifice (80 μm diameter, 80 μm length) at an electrical current of 0.15 mA using HBS as the sheath fluid. The fluorescence was excited between 400 and 500 nm with a HBO 100 W/2 high pressure mercury arc lamp (Osram, Augsburg, FRG). The green fluorescence of DCF was collected between 500 and 530 nm, and EB or PI red fluorescence was collected between 590 and 700 nm. The 365-nm line of the mercury arc lamp was used for excitation (350–380 nm) of HE blue fluorescence, which was collected between 418 and 500 nm. The flow cytometer was calibrated with porous, NH_2-group bearing particles (5 μm diameter, Paesel, Frankfurt, FRG) covalently stained with fluorescein isothiocyanate (Serva). The cell volume and fluorescence pulses were amplified by 2.5-decade logarithmic amplifiers. The maximum amplitude of each signal was digitized by 4096-step analog-to-digital converters. The list mode data were evaluated by the DIAGNOS1 program system for display, calculation, and databasing of flow cytometric data [40].

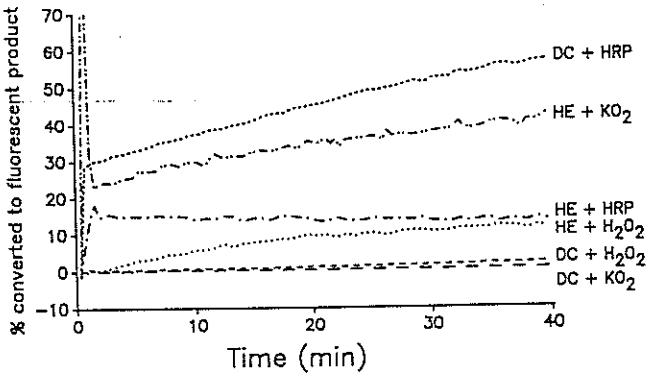

Fig. 1. Oxidation of HE to red fluorescent EB and of DCFH to green fluorescent DCF in a cell-free cuvette assay. Curves represent fluorescence generation from HE or DCFH in the presence of 1.3 mM O_2^- (48.8 mM KO_2) [23], 1.3 mM H_2O_2, or 1.3 mM H_2O_2 and 10 U/ml HRP in MBS at 22°C. Significant fluorescence is generated from DCFH and HE with H_2O_2 and HRP and from HE in the presence of O_2^-. The red fluorescence of EB was measured in intervals of 24 sec fluorimetrically at 593 nm with excitation at 473 nm. The green fluorescence of DCF was measured at 521 nm with excitation at 501 nm. The initial peak of fluorescence following contact of KO_2 with aqueous medium coincided with gas formation.

Statistical Analyses

Data are presented as mean ± standard deviation (SD). The significance ($P < .05$) of the difference of means was tested by the Student t-test.

RESULTS

Oxidation of HE and DCFH by KO_2 and H_2O_2 in a Cell-Free Cuvette Assay

Hydroethidine was only very slowly oxidized by H_2O_2 alone in a cell-free cuvette assay (Fig. 1). Less than 12% of 10 μM HE was oxidized after 40 min of incubation with 1.3 mM H_2O_2. Hydroethidine was, however, completely oxidized in less than 1 min with 1.3 mM H_2O_2 and 1 U/ml HRP as indicated by loss of HE blue fluo-

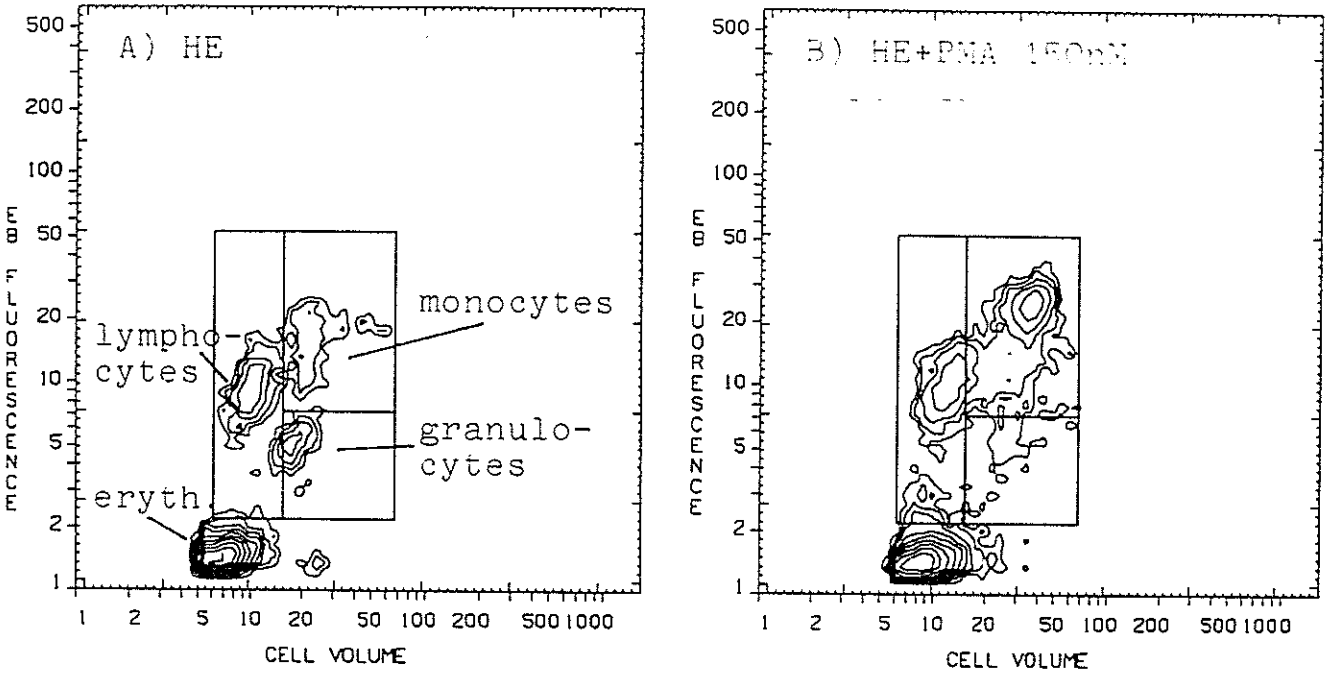

Fig. 2. Cell volume versus EB red fluorescence of buffy coat leukocytes incubated for 15 min with 160 μM HE at 37°C (A). The intracellular oxidation of HE to EB in resting cells is high in monocytes, intermediate in lymphocytes, and low in neutrophils. Following stimulation with 150 nM PMA for a further 30 min at 37°C, the EB fluorescence of neutrophils increased 6.9-fold (B). The graphs are standardized to the maximum logarithmic channel contents (100%). Contour lines were drawn in linear steps of 10% downward. The histograms contain 19,226 (A) and 32,971 (B) cells with 1,981 and 3,507 cells in the maximum channel.

rescence. Between 4.8% (1 U/ml HRP) and 13.6% (10 U/ml HRP) of the product was red fluorescent EB, the remainder being a non-fluorescent oxidation product. Less than 2% of 0.5 μM DCFH was converted after 40 min in the presence of 1.3 mM H_2O_2 alone. Addition of HRP induced the rapid conversion of DCFH to DCF (Fig. 1), and more than 56% of the DCFH was converted to DCF after 40 min of incubation with 10 U/ml HRP and 1.3 mM H_2O_2.

A substantial part (22.9%) of the 10μM HE was converted to EB after 1 min when incubated with 48.8 mM KO_2, a chemical source of O_2^-, but less than 1% of 0.5 μM DCFH was oxidized to DCF (Fig. 1). HE oxidation decreased to less than half of this value (10.5%) when 1,000 U/ml SOD was present together with KO_2 (48.8 mM) for 1 min. This indicates that the KO_2-induced oxidation of HE depended on the presence of O_2^-

The differences in the oxidation of HE and DCFH in the cell-free assay (Fig. 1) were not due to the different concentrations of the substrates (10 μM HE vs. 0.5 μM DCFH) since the degree of oxidation of 10 μM DCFH by 1.3 mM H_2O_2 and 10 U/ml HRP or by 48.8 mM KO_2 after 40 min of incubation followed by 20-fold dilution of the sample did not differ significantly from the results obtained with 0.5 μM DCFH. The dilution of the assay was necessary because the DCF fluorescence of the undiluted sample exceeded the range of the photomultiplier in the fluorimeter.

Intracellular Oxidation of HE and DCFH in Resting and Stimulated Cells

The membrane-permeable blue fluorescent HE rapidly accumulated in the cytoplasm and granules of neutrophils, monocytes, and lymphocytes. Saturation of cellular blue fluorescence was reached with 160 μM HE after a 15-min incubation at 37°C.

Spontaneous oxidation of HE resulted in red EB fluorescence of the cell nucleus. The spontaneous oxidation depended on the cell type (Fig. 2A; Table 1) and was high in monocytes, intermediate in lymphocytes, and low in neutrophils. The identity of the HE-stained cell populations was verified by staining the ficoll/hypaque-isolated mononuclear and the polymorphonuclear cell fraction separately with HE. The monocyte cell cluster was heterogeneous in fluorescence after incubation of unseparated cells for 30 min or more (Fig. 2A) suggesting the presence of two separate monocyte populations. The heterogeneity of monocyte fluorescence was not observed in the isolated mononuclear cell fraction.

Two stimuli, PMA and phagocytosis of *E. coli* bacte-

TABLE 1. Intracellular Oxidation of HE and DCFH in Resting Leukocytes[a]

Cells	EB red fluorescence (arbitrary units)	DCF green fluorescence (arbitrary units)
Neutrophils	0.0325 ± 0.0078	0.0221 ± 0.0042
Monocytes	0.0941 ± 0.0234	ND[b]
Lymphocytes	0.0472 ± 0.0130	0.0156 ± 0.0013

[a]Mean fluorescence ± SD (N = 12 for EB and 9 for DCF) of the different cell populations after 15 min incubation of buffy coat leukocytes of the same preparation with either 160 μM HE or 10 μM DCFH-DA.
[b]Not determined owing to overlap by the neutrophil cell cluster.

TABLE 2. Intracellular Oxidation of HE and DCFH in Stimulated Neutrophils[a]

Incubation	EB fluorescence (% of controls)	DCF fluorescence (% of controls)
PMA	685.3 ± 70.0	1,251.6 ± 135.5
H_2O_2	139.9 ± 7.9	336.1 ± 42.4
E. coli	608.2 ± 115.5	466.3 ± 22.6

[a]Buffy coat leukocytes were prestained for 15 min with 160 μM HE or 10 μM DCFH-DA and subsequently incubated for 30 min with 150 nM PMA or 1.3 mM H_2O_2. In the case of *E. coli*, leukocytes were preincubated for 10 min with bacteria before staining. Data represent means ± SEM (N = 3–15) of the peak fluorescence of neutrophils, expressed in % of the peak fluorescence of controls incubated without the stimulus.

ria, were used to determine whether respiratory burst activity led to an increase of the intracellular oxidation of HE. Stimulation with PMA (150 nM, 30 min, 37°C) induced a 6.9-fold increase of the EB fluorescence of neutrophils as compared to a 2.0-fold increase of the EB fluorescence of lymphocytes in HE-prestained cells (15 min, 37°C) (Fig. 2B; Table 2). Phagocytosis of bacteria similarly increased the EB red fluorescence of neutrophils. The highest EB fluorescence responses (6.1-fold) were obtained after a 10-min preincubation of leukocytes with *E. coli K12* in autologous plasma and subsequent staining of the cells with HE for 15 min (Table 2).

Spontaneous oxidation of DCFH to fluorescent DCF was higher in neutrophils than in lymphocytes (Table 1). The DCF fluorescence of neutrophils increased 12.5-fold upon stimulation with PMA, but only 4.7-fold upon phagocytosis of *E. coli* (Table 2).

The main difference between the intracellular oxidation of HE and DCFH was that HE was oxidized spontaneously to a significant degree not only in neutrophils but also in lymphocytes and monocytes. The spontaneous oxidation of HE was even higher in monocytes and lymphocytes than in neutrophils. This shows that HE was oxidized in resting cells by a mechanism different from respiratory burst activity.

Azide and cyanide as inhibitors of mitochondrial oxygen consumption were used to better characterize the oxidative mechanism. The spontaneous oxidation of HE to EB in resting neutrophils was inhibited through azide (10 mM) or cyanide (1 mM) by 72.4% ± 5.5% (Fig. 3) and 66.9% ± 4.3%, respectively, as compared to control assays (means ± SD). The EB fluorescence of PMA-stimulated neutrophils was reduced by 9.0% ± 0.4% by 10 mM azide (Fig. 3) and 48.6% ± 3.7% by 1 mM cyanide.

Azide (10 mM) inhibited the spontaneous oxidation of DCFH in unstimulated neutrophils. The response was, however, difficult to quantify owing to the low degree of DCFH oxidation in non-stimulated neutrophils. Azide (10 mM) or cyanide (1 mM) increased by 0.6% to 10.3%

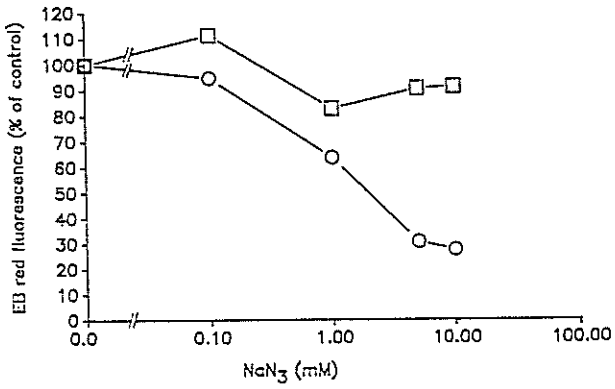

Fig. 3. Influence of sodium azide on the intracellular oxidation of HE in a typical experiment. The EB red fluorescence of neutrophils incubated for 15 min with 160 μM HE was measured with (squares) or without (circles) further stimulation with 150 nM PMA for 30 min. The fluorescence is expressed in percent of control assays incubated without azide.

the intracellular DCFH oxidation by PMA-stimulated neutrophils.

The mechanism of DCFH and HE oxidation was further compared by the addition of H_2O_2 or of KO_2, as a source of O_2^-, to a cellular assay. Addition of 1.3 mM H_2O_2 to dye-loaded cells increased neutrophil DCF fluorescence 3.4-fold, while the EB fluorescence of neutrophils was increased only 1.4-fold as compared to controls (Table 2). The experiments with KO_2 addition were not successful since cell lysis occurred at KO_2 concentrations above 200 μM (data not shown).

Intracellular oxidation of HE in resting cells, or in cells stimulated with PMA or in cells phagocytosing *E. coli*, was not altered by simultaneous presence of DCFH, when compared to cells loaded with HE alone (Fig. 4A). The intracellular oxidation of DCFH in PMA-stimulated or phagocytosing neutrophils was, however, significantly reduced by the presence of HE (Fig. 4B). The decrease of DCFH oxidation in the presence of HE was

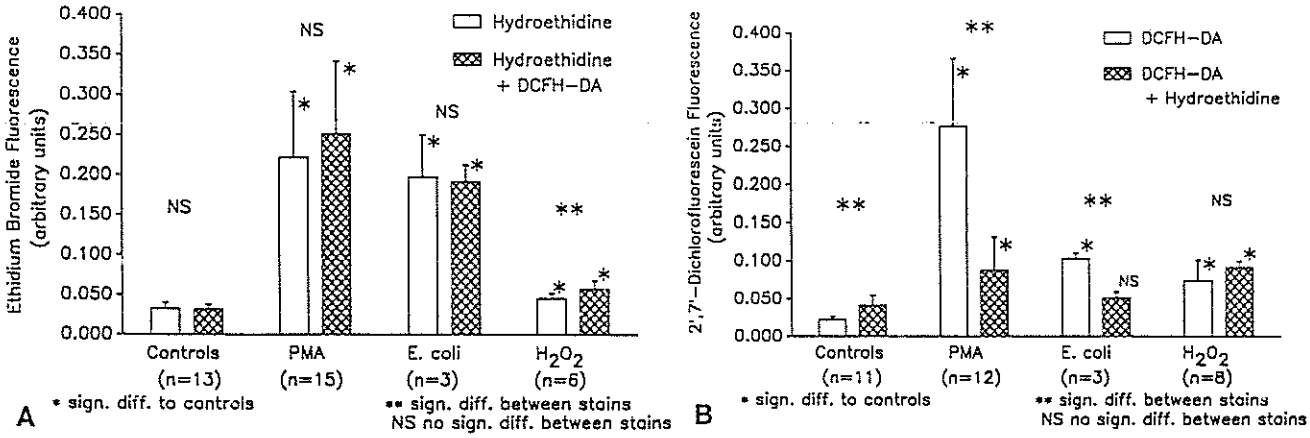

Fig. 4. Flow cytometrically determined EB red fluorescence (A) and DCF green fluorescence (B) of neutrophils in the presence of 150 nM PMA, following phagocytosis of *E. coli K12* or incubation with 1.3 mM H_2O_2. The significance of the difference between samples stained with HE alone (open bars) and samples simultaneously stained with HE and DCFH-DA (cross-hatched bars) (**) or of the results as compared to control assays (*) was evaluated by Student's t-test ($P < .05$).

not observed when 1.3 mM H_2O_2 was added extracellularly to resting neutrophils (Fig. 4B).

The simultaneous staining of different intracellular oxidative processes by HE and DCFH in stimulated neutrophils was used to analyze the functional heterogeneity of neutrophils from septic patients. Up to three subpopulations of neutrophils differing in intracellular oxidation of HE and DCFH were identified in PMA-stimulated blood of septic patients (Fig. 5). Subpopulations of neutrophils that increased only in EB fluorescence but not in DCF fluorescence upon PMA stimulation could be distinguished from neutrophils increasing in oxidation of both substrates and from unresponsive subpopulations, which although viable did not change their EB or DCF fluorescence upon stimulation. The difference between EB and DCF fluorescence in three different neutrophil populations in the blood of septic patients again demonstrated that HE and DCFH indicated different intracellular oxidative processes.

DISCUSSION

The oxidation of HE was significantly different from the oxidation of DCFH both in a cell-free cuvette assay and in cellular experiments with resting and stimulated leukocytes.

The cell-free cuvette assays show that HE and DCFH function as electron donors for peroxidases since they were oxidized by H_2O_2 and HRP but not by H_2O_2 alone (Fig. 1). Hydroethidine was furthermore oxidized by O_2^-, which was generated through the decay of KO_2 in aqueous solution. A substantial part of KO_2-induced HE oxidation was in fact due to O_2^- since addition of SOD, which dismutates O_2^- to H_2O_2, decreased HE oxidation in the cell-free assay. The additional involvement of a singlet oxygen intermediate in the oxidation of HE by O_2^- in aqueous solution cannot be excluded in our experiments [13].

Whether the different behavior of HE and DCFH toward oxidation in the cell-free assay was associated with different mechanisms of HE and DCFH oxidation in the more complex intracellular situation and whether HE and DCFH were useful for the discrimination of different intracellular oxidative pathways of neutrophils was analyzed in a series of cellular experiments.

The results of these experiments show that HE and DCFH are indeed metabolized by cells in different ways. The oxidation of HE in resting cells was substantial and highest in monocytes, followed by lymphocytes and neutrophils (Fig. 2). The oxidation of DCFH in resting cells was overall low by fluorescence. It was very low for lymphocytes and somewhat higher in neutrophils (Table 1) [11]. Furthermore, a separate monocyte cell cluster was not visible [11]. The oxidation of HE in resting leukocytes was sensitive to 10 mM azide (Fig. 3) or 1 mM cyanide, which inhibit the mitochondrial respiration at the cytochrome oxidase level [41]. Oxidation of HE by stimulated neutrophils was not inhibited by azide (Fig. 3) and was only partly inhibited by cyanide. The mechanism of HE oxidation by resting cells is, therefore, different from the HE oxidation during the respiratory burst. It is important to note that the azide and cyanide inhibition experiments are only useful to demonstrate differences in HE and DCFH oxidation between resting and stimulated cells. They do not permit us to obtain more detailed information on oxidative pathways in stimulated neutrophils because the inhibition of multiple heme-enzymes by azide or cyanide induces complex al-

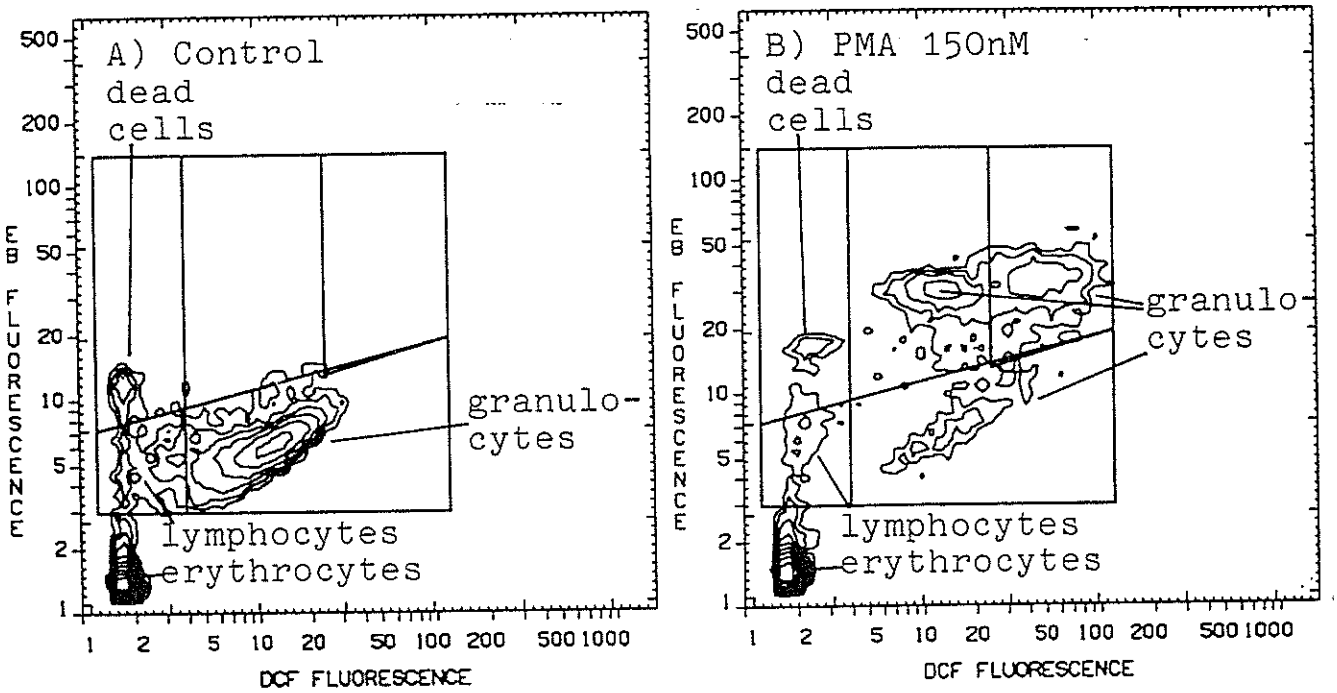

Fig. 5. DCF green and EB red fluorescence of buffy coat leukocytes, obtained from a septic patient, after simultaneous staining with 10 μM DCFH-DA and 160 μM HE for 15 min at 37°C and further incubation without (A) or with (B) 150 nm PMA for 30 min. The DNA of dead cells is counterstained with PI. More than 95% of the leukocytes were neutrophils as judged by morphological analysis of May-Grünwald-Giemsa-stained smears. The simultaneous measurement of peroxidase-dependent DCFH oxidation and NADPH oxidase-dependent HE oxidation revealed three subpopulations of vital neutrophils upon PMA stimulation.

terations of O_2^- production and H_2O_2 metabolism during the respiratory burst. Cyanide causes inhibition of the hexose monophosphate shunt [4], and the precise effect of cyanide on cellular O_2^- production cannot be easily determined in biochemical assays owing to interference of cyanide with SOD-inhibitable ferricytochrome-C reduction [27]. Azide increases oxidation of DCFH by H_2O_2 and myeloperoxidase already in a cell-free assay [4]. Results obtained in cellular experiments with azide or cyanide are, therefore, difficult to interpret.

The significant spontaneous oxidation of HE, but not DCFH, by resting leukocytes may be related to uncoupling of the mitochondrial oxidative phosphorylation by EB [26]. Mitochondria are the major source of O_2^- and H_2O_2 in resting cells. Most of the O_2^- is converted to H_2O_2 inside the mitochondria by a Mn-containing superoxide dismutase, but approximately 20% of the O_2^- escapes to the cytosol [28]. EB specifically binds to a mitochondrial hydrophobic protein and inhibits ATP synthesis but increases respiration [17]. This respiratory uncoupling of the mitochondria should lead to decreased mitochondrial membrane potential and increased intracellular oxidant levels. Incubation of leukocytes with HE in fact caused a 40% decrease of cellular rhodamine 123 fluorescence (data not shown), indicating decreased mitochondrial membrane potential [19], and an increase of the oxidation of DCFH to DCF in cells simultaneously stained with HE and DCFH-DA, indicating increased oxidant levels.

The incubation of resting neutrophils with extracellular H_2O_2, which diffuses into all cellular compartments [30], further confirmed the difference in intracellular HE and DCFH oxidation. Externally added H_2O_2 in neutrophils mainly induces oxidation inside the phagosome because cytoplasmic H_2O_2 is efficiently degraded by catalase and glutathione peroxidase [12]. Addition of H_2O_2 induced a 39.9% increase of EB fluorescence over controls (Table 2). This was less than 7% of the 585.3% increase of EB fluorescence over controls induced by PMA. The 236.1% increase of DCF fluorescence in the presence of H_2O_2, in contrast, corresponded to more than 20% of the 1,151.6% increase of DCF fluorescence in the presence of PMA. The low susceptibility of intracellular HE to oxidation by extracellular H_2O_2 could be due to the non-acceptance of HE as an electron donor by phagosomal or microsomal peroxidases, or to the trapping of non-membrane-permeable EB in the phagosomes where the 20-fold fluorescence increase [22] through binding of EB to nuclear DNA is not obtained.

The use of myeloperoxidase-deficient neutrophils

seems useful to clarify which part of the DCFH or HE oxidation during the respiratory burst and upon addition of external H_2O_2 is due to myeloperoxidase activity. Such experiments are, however, difficult to interpret owing to complex alterations of O_2^- production and H_2O_2 metabolism in myeloperoxidase-deficient neutrophils. They differ in oxygen consumption and in the extracellular release of H_2O_2 and O_2^- from normal neutrophils [27]. The impaired balance of the H_2O_2-metabolizing enzymes in myeloperoxidase-deficient neutrophils also leads to uncharacterized alterations of the H_2O_2 metabolism by other peroxidizing enzymes such as microsomal cytochrome P-450-containing enzymes [25].

To further characterize differences in intracellular HE and DCFH oxidation and to better determine the sequence of oxidation of HE and DCFH, cells were simultaneously loaded with HE and DCFH. The separate reading of the simultaneously generated oxidation products EB and DCF was possible owing to their different fluorescence emission spectra. Neutrophils developed the same EB fluorescence in the presence of DCFH as cells stained with HE alone (Fig. 4A), indicating that HE oxidation was independent of the presence of DCFH. Cellular DCF fluorescence was increased in resting cells in the presence of HE, compatible with increased cytoplasmic oxidant levels caused by uncoupling of mitochondrial respiraton by EB (Fig. 4B). Cellular DCF fluorescence on the contrary was decreased in the presence of HE in PMA-stimulated cells, which produce O_2^- as the primary oxidant. The decrease of intracellular DCFH oxidation in the presence of HE did not occur when extracellular H_2O_2 was added to resting neutrophils. These results are compatible with the view that HE scavenges oxygen radicals, most likely O_2^-, the primary product of oxygen reduction during the respiratory burst, at an earlier step than DCFH. Dichlorofluorescin in this concept would be oxidized by follow-up products of O_2^- dismutation such as H_2O_2 in conjunction with phagosomal peroxidases or through reactive peroxidase metabolites.

Two other oxidants, hydroxyl radical, which can originate from an iron-catalysed reaction of O_2^- with H_2O_2 [3], and singlet oxygen, which is generated from a water-induced dismutation of O_2^- [13], have also been related to the respiratory burst. Recently published results suggest, however, that production of hydroxyl radical [10,21,32,43] or singlet oxygen [20] by neutrophils is unlikely to occur under physiological conditions. No products of free radical- or singlet oxygen-induced oxidation were found in phagocytosing neutrophils [39]. Thus, it is less likely that hydroxyl radical or singlet oxygen are responsible for the intracellular oxidation of DCFH or HE by neutrophils.

The different intracellular oxidation mechanisms of HE and DCFH in PMA-stimulated neutrophils of septic patients simultaneously stained with HE and DCFH permit the functional analysis of up to three subpopulations of viable neutrophils. These subpopulations cannot be discriminated with either HE or DCFH alone (Fig. 5). Our results are compatible with results from other flow cytometric assays, which revealed a functional heterogeneity of peripheral blood neutrophils. Approximately 30% of peripheral blood neutrophils depolarize to the chemotactic peptide N-for-met-leu-phe [15]. On the average only 40% of the neutrophils of patients with infections show enhanced intracellular oxidation of DCFH following stimulation with PMA [4]. These functionally different neutrophil populations do not correspond to morphologically distinguishable subpopulations such as the small amount of band form cells, a morphological subset of functionally immature neutrophils [7,16,44], in normal peripheral blood. The simultaneous HE and DCFH staining method seems of particular interest for the study of the biochemical and phenotypical characteristics and the disease-related significance of these functional subpopulations of neutrophils.

ACKNOWLEDGMENTS

This work was supported by DFG SFB 0207, project G6.

REFERENCES

1. Badwey, J.A., and Karnovsky, M.L. Production of superoxide by phagocytic leukocytes: a paradigm for stimulus-response phenomena. Curr. Top. Cell. Regul. 28,183, 1986.
2. Badwey, J.A., Robinson, J.M., Karnovsky, M.J., and Karnovsky, M.L. Reduction and excitation of oxygen by phagocytic leukocytes: biochemical and cytochemical techniques. In Handbook of Experimental Immunology, Volume 2: Cellular Immunology (Weir, D.M., Ed.). Oxford: Blackwell Scientific Publications, p. 501, 1986.
3. Bannister, J.V., and Bannister, W.H. Production of oxygen-centered radicals by neutrophils and macrophages as studied by electron spin resonance (ESR). Environ. Health Perspect. 64,37, 1985.
4. Bass, D.A., Olbrantz, P., Szejda, P., Seeds, M.C., and McCall, C.E. Subpopulations of neutrophils with increased oxidative product formation in blood of patients with infection. J. Immunol. 136,860, 1986.
5. Bass, D.A., Parce, J.W., DeChatelet, L.R., Szejda, P., Seeds, M.C., and Thomas, M. Flow cytometric studies of oxidative product formation by neutrophils: A graded response to membrane stimulation. J. Immunol. 130,1910, 1983.
6. Bellavite, P. The superoxide-forming enzymatic system of phagocytes. Free Radic. Biol. Med. 4,225, 1988.
7. Berkow, R.L., and Dodson, R.W. Purification and functional evaluation of mature neutrophils from human bone marrow. Blood 68,853, 1986.
8. Bignold, L.P., and Ferrante, A. Mechanism of separation of polymorphonuclear leukocytes from whole blood by the one-step hypaque-ficoll method. J. Immunol. Methods 96,29, 1987.

9. Briggs, R.T., Robinson, J.M., Karnovsky, M.L., and Karnovsky, M.J. Superoxide production by polymorphonuclear leukocytes. A cytochemical approach. Histochemistry 84,371, 1986.
10. Bucana, C., Saiki, I., and Nayer, R. Uptake and accumulation of the vital dye hydroethidine in neoplastic cells. J. Histochem. Cytochem. 34,1109, 1986.
11. Burow, S., and Valet, G. Flow-cytometric characterization of stimulation, free radical formation, peroxidase activity and phagocytosis of human granulocytes with 2,7-dichlorofluorescein (DCF). Eur. J. Cell. Biol. 43,128, 1987.
12. Cohen, H.J., Tape, E.H., Novak, J., Chovaniec, M.E., Liegey, P., and Whitin, J.C. The role of glutathione reductase in maintaining human granulocyte function and sensitivity to exogenous H_2O_2. Blood 69,493, 1987.
13. Corey, E.J., Mehrotra, M.M., and Khan, A.U. Water induced dismutation of superoxide anion generates singlet molecular oxygen. Biochem. Biophys. Res. Commun. 145,842, 1987.
14. Ferrante, A., and Thong, Y.H. Separation of mononuclear and polymorphonuclear leucocytes from human blood by the one-step hypaque-ficoll method is dependent on blood column height. J. Immunol. Methods 48,81, 1982.
15. Fletcher, M.P., and Gasson, J.C. Enhancement of neutrophil function by granulocyte-macrophage colony-stimulating factor involves recruitment of a less responsive subpopulation. Blood 71,652, 1988.
16. Glasser, L., and Fiederlein, R.L. Functional differentiation of normal human neutrophils. Blood 69,937, 1987.
17. Higuti, T., Ohe, T., Arakaki, N., and Kotera, Y. Photoaffinity labeling of a mitochondrial hydrophobic protein by an anisotropic inhibitor of energy transduction in oxidative phosphorylation. J. Biol. Chem. 256,9855, 1981.
18. Holman, J.M., and Saba, T.M. Hepatocyte injury during postoperative sepsis. Activated neutrophils as potential mediators. J. Leukocyte Biol. 43,193, 1988.
19. Johnson, L.V., Walsh, M.L., Bockus, B.J., and Chen, L.B. Monitoring of relative mitochondrial membrane potential in living cells by fluorescence microscopy. J. Cell Biol. 88,526, 1981.
20. Kanofsky, J.R., Wright, J., Miles-Richardson, G.E., and Tauber, A.I. Biochemical requirements for singlet oxygen production by purified human myeloperoxidase. J. Clin. Invest. 74,1489, 1984.
21. Kaur, H., Fagerheim, I., Grootveld, M., Puppo, A., and Halliwell, B. Aromatic hydroxylation of phenylalanine as an assay for hydroxyl radicals: Application to activated human neutrophils and to the heme protein leghemoglobin. Anal. Biochem. 172,360, 1988.
22. LePecq, J.B., and Paoletti, C. A fluorescent complex between ethidium bromide and nucleic acids. Physical-chemical characterization. J. Mol. Biol. 27,87, 1967.
23. Lokesh, B.R., and Cunningham, M.L. Further studies on the formation of oxygen radicals by potassium superoxide in aqueous medium for biochemical investigations. Toxicol. Lett. 34,75, 1986.
24. Malech, H.L., and Gallin, J.I. Current concepts: Immunology. Neutrophils in human diseases. N. Engl. J. Med. 317,687, 1987.
25. McCarthy, M.B., and White, R.E. Functional differences between peroxidase compound I and the cytochrome P-450 reactive oxygen intermediate. J. Biol. Chem. 258,9153, 1983.
26. Miko, M., and Chance, B. Ethidium bromide as an uncoupler of oxidative phosphorylation. FEBS Lett. 54,347, 1975.
27. Nauseef, W.M., Metcalf, J.A., and Root, R.K. Role of myeloperoxidase in the respiratory burst of neutrophils. Blood 61,483, 1983.
28. Nohl, H., and Hegner, D. Do mitochondria produce oxygen radicals in vivo? Eur. J. Biochem. 82,563, 1978.
29. Ogle, J.D., Ogle, C.K., Noel, J.G., Hurtubise, P., and Alexander, J.W. Studies on the binding of C3b-coated microspheres to human neutrophils. J. Immunol. Methods 47,47, 1985.
30. Ohno, Y., and Gallin, J.I. Diffusion of extracellular hydrogen peroxide into extracellular compartments of human neutrophils. Studies utilizing the inactivation of myeloperoxidase by hydrogen peroxide and azide. J. Biol. Chem. 260,8438, 1985.
31. Patel, A.K., Hallett, M.B., and Campbell, A.K. Threshold responses in production of reactive oxygen metabolites in individual neutrophils detected by flow cytometry and microfluorimetry. Biochem. J. 248,173, 1987.
32. Rosen, G.M., Britigan, B.E., Cohen, M.S., Ellington, S.P., and Barber, M.J. Detection of phagocyte-derived free radicals with spin trapping techniques: effect of temperature and cellular metabolism. Biochim. Biophys. Acta 969,236, 1988.
33. Rothe, G., Oser, A., and Valet, G. Dihydrorhodamine 123: a new flow cytometric indicator for respiratory burst activity in neutrophil granulocytes. Naturwissenschaften 75,354, 1988.
34. Seeds, M.C., Parce, J.W., Szejda, P., and Bass, D.A. Independent stimulation of membrane potential changes and the oxidative metabolic burst in polymorphonuclear leukocytes. Blood 65,233, 1985.
35. Shingu, M., Todoroki, T., and Nobunaga, M. Generation of superoxide by immunologically stimulated normal human neutrophils and possible modulation by intracellular and extracellular SOD and rheumatoid factors. Inflammation 11,143, 1987.
36. Tauber, A.I., and Babior, B.M. Neutrophil oxygen reduction: the enzymes and the products. Advances in Free Radical Biology and Medicine 1,265, 1985.
37. Test, S.T., and Weiss, S.J. The generation and utilization of chlorinated oxidants by human neutrophils. Adv. Free Radical Biol. Med. 2,91, 1986.
38. Thomas, G., and Roques, B. Proton magnetic resonance studies of ethidium bromide and its sodium borohydride reduced derivative. FEBS Lett. 26,169, 1972.
39. Thomas, M.J., Shirley, P.S., Hedrick, C.C., and DeChatelet, L.R. Role of free radical processes in stimulated human polymorphonuclear leukocytes. Biochemistry 25,8042, 1986.
40. Valet, G., Warnecke, H.H., and Kahle, H. Automated diagnosis of malignant and other abnormal cells by flow-cytometry using the DIAGNOS1 program system. In Clinical Cytometry and Histometry (Burger, G., Ploem, J.S., and Goerttler, K., Eds.). London: Academic Press, p. 58, 1987.
41. Way, J.L., Cyanide intoxication and its mechanism of antagonism. Annu. Rev. Pharmacol. Toxicol. 24,451, 1984.
42. Weiland, J.E., Davis, W.B., Holter, J.F., Mohammed, J.R., Dorinsky, P.M., and Gadek, J.E. Lung neutrophils in the adult respiratory distress syndrome. Clinical and pathophysiological significance. Am. Rev. Respir. Dis. 133,218, 1986.
43. Winterbourn, C.C. Myeloperoxidase as an effective inhibitor of hydroxyl radical production. Implications for the oxidative reactions of neutrophils. J. Clin. Invest. 78,545, 1986.
44. Zakhireh, B., and Root, R.K. Development of oxidase activity by human bone marrow granulocytes. Blood 54,429, 1979.

Biol. Chem. Hoppe-Seyler
Vol. 373, pp. 547–554, July 1992

Flow Cytometric Analysis of Protease Activities in Vital Cells*

GREGOR ROTHE[a], SVEN KLINGEL[a], IRMGARD ASSFALG-MACHLEIDT[b], WERNER MACHLEIDT[b], CHRISTOPH ZIRKELBACH[a], RICHARD B. BANATI[c], WALTER F. MANGEL[d] AND GÜNTER VALET[a]

[a] Arbeitsgruppe Zellbiochemie, Max-Planck-Institut für Biochemie, W-8033 Martinsried, FRG
[b] Institut für Physiologische Chemie, Physikalische Biochemie und Zellbiologie der Universität München, Goethestr. 33, W-8000 München 2, FRG
[c] Abteilung Neuromorphologie, Max-Planck-Institut für Psychiatrie, W-8033 Martinsried, FRG
[d] Biology Department, Brookhaven National Laboratory, Upton, NY 11973, USA

Summary

The analysis of lysosomal proteases in cell lysates is complicated by pH-dependent and oxidative changes of their activity and complex formation with cytosolic inhibitors. Therefore, new flow cytometric methods were developed for the intracellular measurement of protease activities in viable cells. Intracellular cleavage of substrates such as Z-Arg-Arg-4-trifluoromethylcoumarinyl-7-amide to green fluorescent 7-amino-4-trifluoromethylcoumarin (AFC) in viable neutrophils and monocytes was only detected following phagocytosis of *Escherichia coli*. A measurement of the cysteine or serine proteinase activities in resting human leukocytes was, however, not possible with AFC derivatives as the overlapping blue fluorescence of the substrates reduces sensitivity. Nonfluorescent bis-substituted peptide derivatives of rhodamine 110 (R110), which are intracellularly cleaved to green fluorescent mono-substituted R110 and free R110 proved to be more sensitive substrates. The activity of the lysosomal cysteine proteinases of human monocytes or rat macrophages, i.e. cathepsin B and L, was specifically measured with $(Z\text{-}Arg\text{-}Arg)_2$-R110, $(Z\text{-}Phe\text{-}Arg)_2$-R110, or $(Z\text{-}Ala\text{-}Arg\text{-}Arg)_2$-R110. Fluorescence generation was completely inhibited by Z-Phe-Ala-diazomethane or E-64. The serine proteinases of human neutrophils were analyzed with Elastase-substrates such as $(Z\text{-}Ala\text{-}Ala)_2$-R110 or $(Z\text{-}Ala\text{-}Ala\text{-}Ala)_2$-R110. Specificity was shown by inhibition with diisopropylfluorophosphate.

Introduction

High plasma levels of the lysosomal proteases elastase or cathepsin B are detected during acute inflammatory disorders such as sepsis or posttraumatic shock [1,2]. These proteases together with the oxidants, released by neutrophils, are mediators of the inflammatory tissue destruction [3]. The cellular expression of lysosomal proteases, the mechanism of their intracellular processing, and the mechanisms of their extracellular release are, therefore, of major interest for the development of new thera-

---

*Presented in part at the XIV meeting of the Society for Analytical Cytology, Asheville, NC, USA, March 1990 (Cytometry Suppl. 4: 77, 1990)

Enzymes: Cathepsin B (EC 3.4.22.1); Elastase (EC 3.4.21.37)

Abbreviations: AFC, 7-amino-4-trifluoromethylcoumarin; DFP, diisopropylfluorophosphate; DMF, *N,N*-dimethylformamide; DMSO, dimethyl sulfoxide; E-64, *trans*-epoxysuccinyl-L-leucylamido-(4-guanidino)butane; HBS, HEPES buffered saline (5 mM HEPES, 0.15 M NaCl, pH 7.35); R110, rhodamine 110; Z, benzyloxycarbonyl; -AFC, -4-trifluoromethylcoumarinyl-7-amide; $-CHN_2$, -diazomethane.

Copyright © by Walter de Gruyter & Co · Berlin · New York

peutic approaches. Methods for the analysis of lysosomal proteases in cell lysates depend on the preparation of homogenous cell populations. Furthermore, during cell lysis the activity of proteases may be altered by the interaction with cytosolic inhibitors, pH-changes, or oxidative inactivation [4]. Earlier methods for the intracellular analysis of protease activities were based on the intracellular cleavage of *N*-acyl derivatives of 4-methoxy-2-naphthylamine. The highly diffusible product 4-methoxy-2-naphthylamine was trapped inside the cell by coupling with 5-nitrosalicylaldehyde yielding a yellow fluorescent, crystalline product [5-8]. These methods are restricted to the analysis of proteases with an acidic pH optimum, as incubation at acidic pH is necessary to promote intracellular coupling of the 5-nitrosalicylaldehyde to the product. Furthermore, a high background is induced by the staining of proteins with the coupling reagent. A new method for the intracellular analysis of protease activities in viable cells at physiological pH was developed using either the intracellular conversion of blue fluorescent peptide-AFC substrates [9] to 365-nm excitable green fluorescent AFC or the intracellular cleavage of nonfluorescent R110 derivatives to 488-nm excitable green fluorescent R110 [10,11].

Material and Methods

Cells

Heparinized human peripheral blood was depleted of erythrocytes by 1g sedimentation upon Histopaque-1077 (Sigma, Deisenhofen, FRG) for 30 min at room temperature. The upper half of the supernatant plasma containing 0.4-1.2 x 10^7 leukocytes/ml and thrombocytes was collected and stored on ice.

Peritoneal macrophages were obtained from male Wistar rats either as resident cells or as elicited cells 4 d after intraperitoneal injection of 3 ml of thioglycolate broth solution (Serva, Heidelberg, FRG) by peritoneal lavage with HBS supplemented with 2 mM EDTA. The cells were sedimented at 200g for 5 min, resuspended in HBS with EDTA at 1 x 10^7 cells/ml, and stored on ice.

Fluorescence spectrometry

Fluorescence emission spectra of AFC, Z-Arg-Arg-AFC, R110, Z-Arg-R110, and (Z-Arg-Arg)$_2$-R110 (all stock solutions 20 mM in DMF) in 0.1-M Tris HCl (pH 7.2) were recorded in quartz cuvettes of 10 mm path length on a Perkin-Elmer LS-5 luminescence spectrometer (Bodenseewerk Perkin-Elmer, Überlingen) connected to a VAX 8550 computer (Digital Equipment, Maynard, MA, USA) at 365 nm or 488 nm excitation and with a nominal bandwidth of 5 nm.

Synthesis of bis-substituted rhodamine 110 peptide derivatives

The bis-substituted R110 peptide derivatives (Z-Phe-Arg)$_2$-R110, (Z-Arg-Arg)$_2$-R110, (Z-Ala-Arg-Arg)$_2$-R110, (Z-Ala-Ala)$_2$-R110, (Z-Ala-Ala-Ala)$_2$-R110, and (Z-Ala-Ala-Val)$_2$-R110 were synthesized in analogy to Leytus et al. [10,11] and dissolved 4-mM in DMF. Structure and purity were confirmed by thin layer chromatography, high-resolution mass spectroscopy and NMR spectroscopy.

Cell staining

The human leukocyte or rat peritoneal macrophage cell suspensions (20 µl) were preincubated in 1 ml HBS with 1 µl of DMSO or 1 µl of inhibitor stock solutions (DFP (Aldrich, Steinheim, FRG): 1 M in DMSO; E-64 (Sigma): 100 mM in DMSO; 1,10-phenanthroline (Sigma): 1 M in DMSO; Z-Phe-Ala-CHN$_2$ (Bachem, Heidelberg, FRG): 100 mM in DMSO; Z-Phe-Phe-CHN$_2$ (Bachem): 10 mM in DMSO; pepstatin A (Sigma): 10 mM in DMSO) for the measurement of the intracellular proteolytic activity. The cells were then incubated for 20 min at 37°C with 1 µl of the 10-mM stock solution of Z-Arg-Arg-AFC (Serva), or 1 µl of the 4-mM stock solutions of the R110 peptide derivatives. The incubations were stopped on ice and the samples were analyzed following counterstaining of dead cells with propidium iodide (Sigma).

Phagocytosis

Escherichia coli K12 (Sigma) (*E. coli*) were grown as a stationary culture in RPMI-1640 (Gibco BRL, Eggenstein, FRG). The bacteria were washed and resuspended in HBS at 7 x 10^9 bacteria/ml. For the measurement of proteolytic processes during phagocytosis the leukocyte suspension in autologous plasma (20 µl) was incubated with the *E. coli* suspension (5 µl) at 37°C. After 10 min the cells were diluted with 1 ml of HBS, incubated with the proteinase inhibitors or DMSO, and stained with the fluorogenic substrates as described above.

Flow cytometry

The cellular AFC green fluorescence (420-530 nm) and the red fluorescence of propidium iodide-stained dead cells (550-700 nm) excited (300-400 nm) by a HBO-100 high-pressure mercury arc lamp were analyzed together with electrical determination of the cell volume in a FLUVO-II flow cytometer (Heka Elektronik, Lambrecht/Pfalz, FRG). The cellular R110 green fluorescence (515-545 nm) and the red fluorescence of propidium iodide-stained dead cells (> 650 nm), the cellular forward and side scatter were measured with excitation by an 488-nm argon laser on a FACScan flow cytometer (Becton Dickinson, San José, CA, USA). The list-mode data of 2,000 to 10,000 leukocytes per sample were analyzed with the DIAGNOS1 program system [12].

Results and Discussion

Measurement of the proteolytic digestion of E. coli with Z-Arg-Arg-AFC

Incubation of human peripheral blood leukocytes with Z-Arg-Arg-AFC did result in a low AFC green fluorescence of lymphocytes, neutrophils, and monocytes (Fig. 1a). This was unexpected as monocytes contain signficiantly higher amounts of cysteine proteinases [13,14] compared to neutrophils. Incubation with *E. coli* for 10 min resulted in an 4.36-fold (± 0.45, SEM, n = 3) increase of the fluorescence of neutrophils (Fig. 1b) (Table 1). This was not due to the ingestion of bacterial proteases as no detectable cleavage of Z-Arg-Arg-AFC occurred in *E. coli*, alone. Soluble stimulation by the protein kinase C agonist phorbol 12-myristate 13-acetate (150 nM), the lectin concanavalin A (100 µg/ml), or the bacterial peptide *N*-formyl-Met-Leu-Phe (10^{-6} M) induced similar activation of neutrophils as observed by their oxidative burst response [15] but did not lead to detectable AFC green fluorescence (data not shown). This suggests that in human leukocytes, a high increase of proteolytic acti-

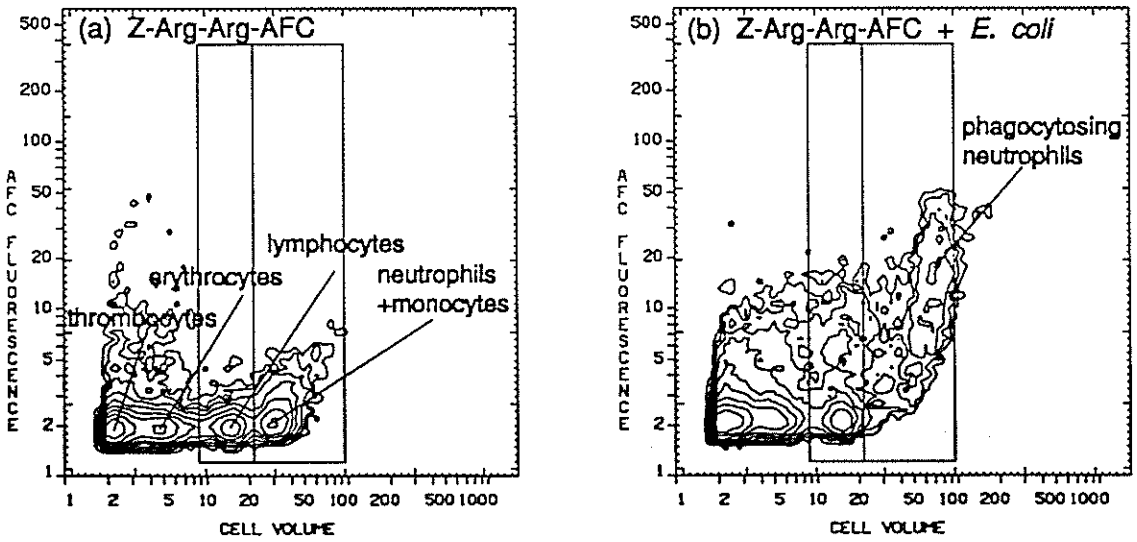

Fig. 1. Intracellular cleavage of Z-Arg-Arg-AFC. Human peripheral blood leukocytes were incubated with Z-Arg-Arg-AFC without stimulation (a) or following preincubation with *E. coli* for 10 min (b).

vity is correlated to the discharge of lysosomal proteases into the phagosome [16,17]. The intracellular generation of AFC was not inhibited by preincubation of the cells with either of the inhibitors E-64, DFP, 1,10-phenanthroline, or pepstatin A (Table 1) [4], alone, suggesting that the activity of neither the serine proteinases, cysteine proteinases, metalloproteinases, or aspartic proteinases was limiting for the observed protease activity.

Table 1. Specificity of the intracellular cleavage of Z-Arg-Arg-AFC by human neutrophils

	Cellular fluorescence during incubation with Z-Arg-Arg-AFC (arbitrary fluorescence units)	
Inhibitor	Nonstimulated cells	Phagocytosing cells
None	.0415 ± .0054	.1847 ± .0154
E-64	.0414	.1905
DFP	.0356	.2131
Pepstatin A	.0439	.1089
1,10-phenanthroline	.0402	.1404

Cells were preincubated without or with *E. coli* for 15 min, followed by an incubation with the inhibitors for 5 min, and 10 μM Z-Arg-Arg-AFC for 15 min. (n = 4 for controls, n = 2 for inhibitor experiments).

The low sensitivity of Z-Arg-Arg-AFC and other *N*-acyl-AFC substrates in an assay of lysosomal cysteine or serine protease activity in non-stimulated human leukocytes may be due to the significant background fluorescence caused by the spectral overlap of the blue fluorescence of the *N*-acyl-AFC substrates (Fig. 2a). This is especially a problem in intracellular assays, where a discrimination between kinetic intracellular substrate accumulation from enzymatic product formation is required.

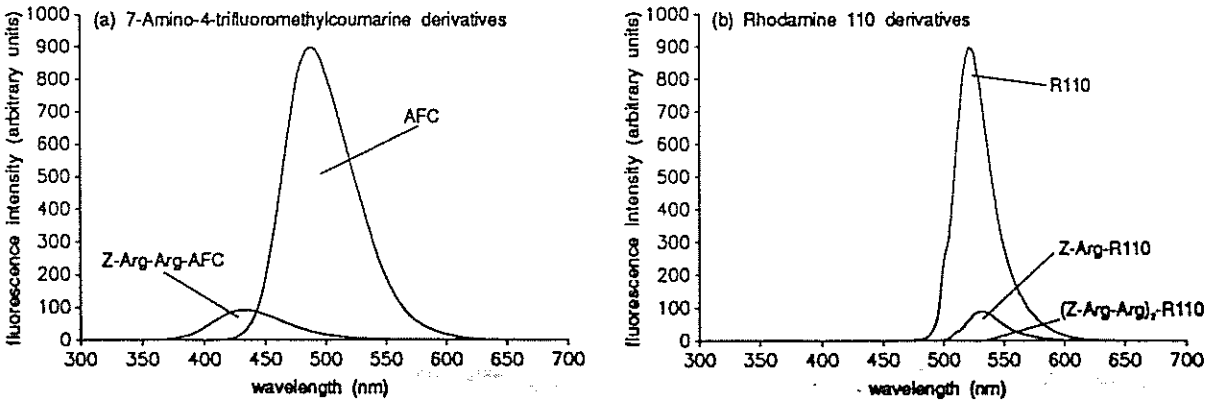

Fig. 2. Fluorescence emission spectra of AFC (a) and R110 (b) protease substrates. Spectra were recorded with 365 nm excitation for 1 μM Z-Arg-Arg-AFC and 1 μM AFC (a) and 488 nm excitation for 200 nM each of $(Z\text{-}Arg\text{-}Arg)_2$-R110, Z-Arg-R110, and R110 (b). This excitation corresponds to the flow cytometric experiments.

Measurement of cathepsin B and L activity with (Z-Phe-Arg)$_2$-R110 or (Z-Arg-Arg)$_2$-R110

N,N'-bis-substituted derivatives of R110 have a more than 10^{-4} lower fluorescence than free R110 [10,11] (Fig. 2b). The 488-nm argon laser excitable green fluorescence generated during the sequential cleavage of bis-substituted R110 to mono-substituted R110 and R110 (Fig. 3) can be, therefore, measured without spectral overlap of the virtually non fluorescent substrates.

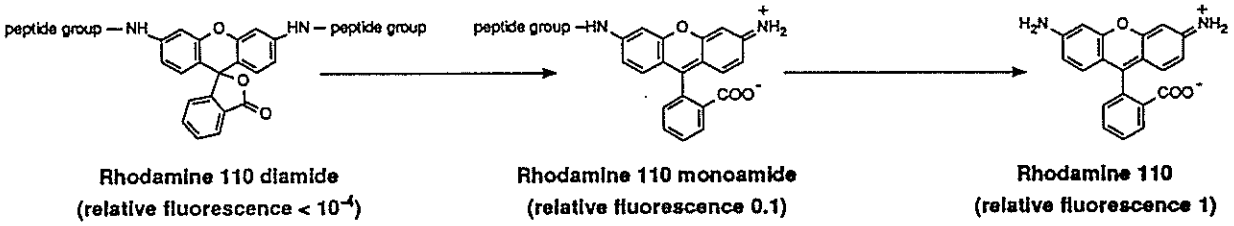

Fig. 3. Sequential generation of fluorescence during cleavage of bis-substituted R110 peptide derivatives.

Incubation of human peripheral blood leukocytes with (Z-Arg-Arg)$_2$-R110 resulted in a 23.6-fold (± 2.6, n=9) higher fluorescence in monocytes than in neutrophils (Fig. 4a), corresponding to the high cysteine proteinase activity in cell lysates of monocytes [13,14]. A specificity of the fluorescence generation for cysteine proteinases was shown by the inhibition of 95.6 % (± 0.5, n=4) of the fluorescence by preincubation of cells with Z-Phe-Ala-CHN$_2$ (Fig. 4b) [19]. Data generated with purified enzymes show that (Z-Arg-Arg)$_2$-R110, in contrast to the cathepsin B substrate Z-Arg-Arg-4-methylcoumaryl-7-amide [18], has a 360-fold higher sensitivity for cleavage by cathepsin L as compared to cathepsin B [13]. A similar specific intracellular cleavage by cysteine proteinases inside human monocytes was found for (Z-Phe-Arg)$_2$-R110 and (Z-Ala-Arg-Arg)$_2$-R110 (data not shown).

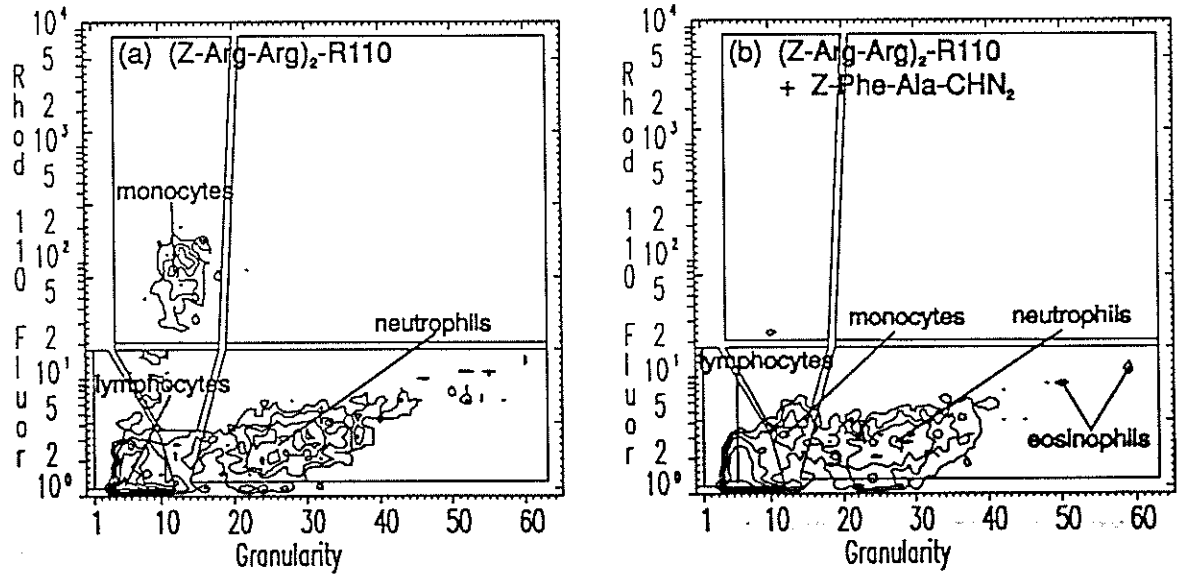

Fig. 4. Intracellular cleavage of the cathepsin B and L substrate (Z-Arg-Arg)$_2$-R110. Human peripheral blood leukocytes were incubated with (Z-Arg-Arg)$_2$-R110 without (a) or with a preincubation with the cysteine proteinase inhibitor Z-Phe-Ala-CHN$_2$ (b).

Resident rat peritoneal macrophages showed a high accumulation of fluorescence during incubation with (Z-Arg-Arg)$_2$-R110 in contrast to the low fluorescence of other intraperitoneal cells, e.g. lymphocytes. (Z-Arg-Arg)$_2$-R110 was cleaved in the resident macrophages at a significant higher rate of 2.05-fold (± 0.24, n=5) over (Z-Phe-Arg)$_2$-R110 (Table 2). Thioglycolate-elicited peritoneal macrophages as macrophages in an activated state, showed a reverse ratio of the intracellular cleavage of the substrates with a decreased intracellular cleavage of (Z-Arg-Arg)$_2$-R110 (53.7 ± 5.0 % of resident cells, n=5) and an increased cleavage of (Z-Phe-Arg)$_2$-R110 (215.8 ± 2.5 % of resident cells, n=5). This suggests that the differential intracellular cleavage of both substrates represents differences in intracellular enzymatic activities rather than a different membrane permeability of the substrates. This may correlate to the differential expression of cathepsin L and cathepsin B during the maturation of mononuclear phagocytes [13,20-24]. Further attempts to differentiate between cathepsin B activity and cathepsin L activity by the selective inhibition of cathepsin L by low amounts of Z-Phe-Phe-CHN$_2$ [25] were unsuccessful since the lower inhibition by Z-Phe-Phe-CHN$_2$ was independent of the substrate or cell type (Table 2).

Table 2. Intracellular cleavage of cysteine proteinase substrates by rat peritoneal macrophages

		Cellular fluorescence (arbitrary fluorescence units)	
Inhibitor	Substrate	Resident macrophages	Elicited macrophages
None	(Z-Arg-Arg)$_2$-R110	.9861	.5341
Z-Phe-Ala-CHN$_2$	(Z-Arg-Arg)$_2$-R110	.2982	.1251
Z-Phe-Phe-CHN$_2$	(Z-Arg-Arg)$_2$-R110	.4586	.2032
None	(Z-Phe-Arg)$_2$-R110	.5563	1.7190
Z-Phe-Ala-CHN$_2$	(Z-Phe-Arg)$_2$-R110	.1295	.1746
Z-Phe-Phe-CHN$_2$	(Z-Phe-Arg)$_2$-R110	.1484	.2034

Cells were preincubated with 10 μM of the inhibitors for 10 min or with 0.1 % DMSO (v/v) as a solvent control, followed by an incubation with the fluorogenic substrates (4 μM) for 20 min at 37°C. (data representative for 2 to 4 experiments).

Measurement of elastase activity with (Z-Ala-Ala)$_2$-R110 or (Z-Ala-Ala-Ala)$_2$-R110

An attempt to measure the lysosomal serine proteinase elastase, which is present in high amounts in the azurophilic granules of neutrophils [26] and in lower amounts in monocytes [27,28], was made by the synthesis of the substrates (Z-Ala-Ala)$_2$-R110, (Z-Ala-Ala-Ala)$_2$-R110, and (Z-Ala-Ala-Val)$_2$-R110 using typical peptide substitutions [29]. (Z-Ala-Ala)$_2$-R110 was cleaved intracellularly at a high rate in human neutrophils while monocytes developed only 25.0 % (± 0.8, n =5) of the fluorescence of neutrophils (Fig. 5a). A selective fluorescent staining of the cellular granules was documented by confocal laser scanning microscopy. Specificity was shown by an inhibition by 97.7 % (± 0.1, n=5) in the presence of DFP. Neutrophils incubated with the tripeptide elastase substrate (Z-Ala-Ala-Ala)$_2$-R110 developed only 4.4 % (± 0.3, n=4) of the fluorescence of (Z-Ala-Ala)$_2$-R110 incubated neutrophils

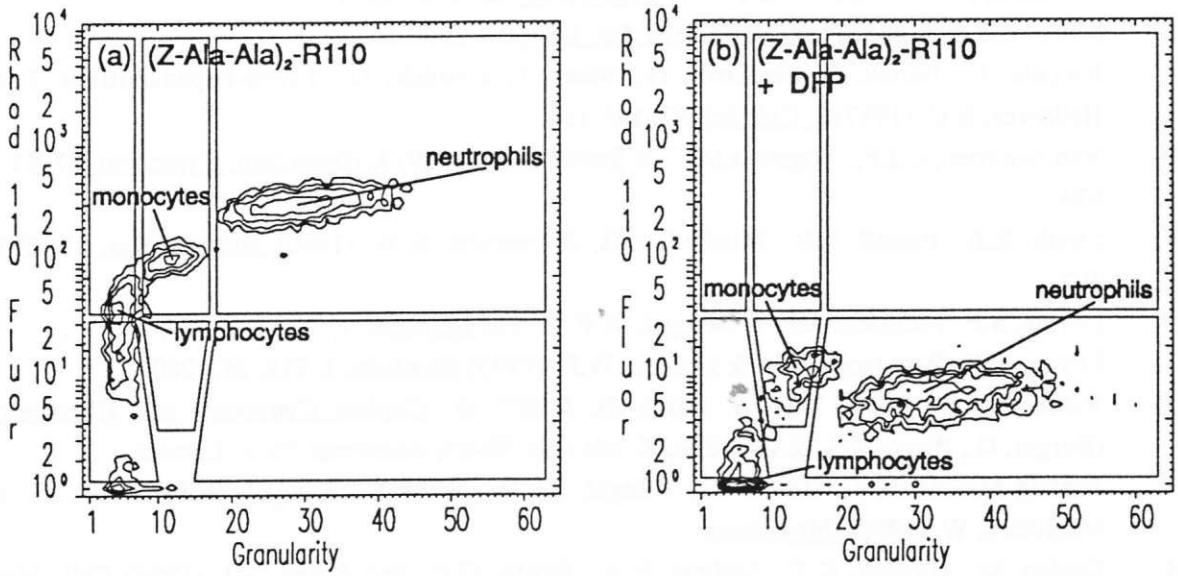

Fig. 5: Intracellular cleavage of the elastase substrate (Z-Ala-Ala)$_2$-R110. Human peripheral blood leukocytes were incubated with (Z-Ala-Ala)$_2$-R110 without (a) or with an preincubation with the serine proteinase inhibitor DFP (b).

and (Z-Ala-Ala-Val)$_2$-R110 did not lead to a significant increase of the cellular fluorescence, suggesting that the very lipophilic substrates do not reach the lysosomes due to trapping in the outer plasma membrane.

In conclusion, bis-substituted R110 dipeptide and tripeptide protease substrates are sensitive substrates for the specific intracellular measurement of lysosomal cysteine and serine proteinases. These methods should be useful for the study of the physiological regulation of the intracellular processing of proteases. Furthermore, they should allow the evaluation of synthetic, membrane-permeable proteinase inhibitors in new therapeutic approaches against inflammatory tissue destruction [3,29-32].

Acknowledgements

We thank Prof. W. Schäfer for high-resolution mass spectroscopy and Prof. J. Sonnenbichler and Dr. I. Zetl for NMR spectroscopy. This work was supported by the Sonderforschungsbereich 207, Universität München (project G-6 and G-1).

References

1. Jochum, M. & Fritz, H. (1989) in: Immune Consequences of Trauma, Shock, and Sepsis (Faist, E., Ninnemann, J. & Green, D. eds.) pp. 165-172, Springer-Verlag, Berlin.
2. Assfalg-Machleidt, I., Jochum, M., Nast-Kolb, D., Siebeck, M., Billing, A., Joka, T., Rothe, G., Valet, G., Zauner, R., Scheuber, H.P. & Machleidt, W. (1990) Biol. Chem. Hoppe-Seyler **371** (Suppl.), 211-222.
3. Weiss, S.J. (1989) N. Engl. J. Med. **320**, 365-376.
4. Kirschke, H. & Barrett, A.J. (1987) in: Lysosomes: Their Role in Protein Breakdown (Glaumann, H. & Ballard, F.J. eds.) pp. 193-238, Academic Press, London.

5. Dolbeare, F.A. & Smith R.E. (1977) Clin. Chem. **23**, 1485-1491.
6. Murphy, R.F. (1985) Proc. Natl. Acad. Sci. USA **82**, 8523-8526.
7. Krepela, E., Bártek, J., Skalková, D., Vicar, J., Rasnick, D., Taylor-Papadamitriou, J. & Hallowes, R.C. (1987) J. Cell Sci. **87**, 145-154.
8. Van Noorden, C.J.F., Vogels, I.M.C. & Smith, R.E. (1989) J. Histochem. Cytochem. **37**, 617-624.
9. Smith, R.E., Bissell, E.R., Mitchell, A.R. & Pearson, K.W. (1980) Thromb. Res. **17**, 393-402.
10. Leytus, S.P., Melhado, L.L. & Mangel, W.F. (1983) Biochem. J. **209**, 299-307.
11. Leytus, S.P., Patterson, W.L. & Mangel, W.F. (1983) Biochem. J. **215**, 253-260.
12. Valet, G., Warnecke, H.H. & Kahle, H. (1987) in: Clinical Cytometry and Histometry (Burger, G., Ploem, J.S. & Goerttler, K. eds.) pp. 58-65, Academic Press, London.
13. Assfalg-Machleidt, I., Rothe, G., Klingel, S., Banati, R.B., Mangel, W.F., Valet, G. & Machleidt, W. (1992) this volume.
14. Davies, M., Hughes, K.T., Andrew, P.W., Smith, G.P., and Peters, T.J. (1984) Cell. Mol. Biol. **30**, 337-343.
15. Rothe, G., Oser, A. & Valet, G. (1988) Naturwissen. **75**, 354-355.
16. Henson, P.M., Henson, J.E., Fittschen, C., Kimani, G., Bratton, D.L., & Riches, D.W.H. (1988) in: Inflammation: Basic Principles and Clinical Correlates (Gallin, J.I., Goldstein, I.M. & Snyderman, R. eds.) pp. 363-390, Raven Press, New York.
17. Jaconi, M.E.E., Lew, D.P., Carpentier, J.L., Magnusson, K.E., Sjögren, M. & Stendahl, O. (1990) J. Cell Biol. **110**, 1555-1564.
18. Barrett, A.J. & Kirschke, H. (1981) Methods Enzymol. **80**, 535-561.
19. Green, G.D.J. & Shaw, E. (1981) J. Biol. Chem. **256**, 1923-1928.
20. Reilly, J.J., Mason, R.W., Chen, P., Joseph, L.J., Sukhatme, V.P., Yee, R. & Chapman, H.A. (1989) Biochem. J. **257**, 493-498.
21. Burnett, D., Crocker, J., Afford, S.C., Bunce, C.M., Brown, G. & Stockley, R.A. (1986) Biochim. Biophys. Acta **887**, 283-290.
22. Murnane, M.J., Phipps, P.M. & Denekmap, D.S. (1988) Exp. Hematol. **16**, 33-37.
23. Ward, C.J., Crocker, J., Chan, S.J., Stockley, R.A. & Burnett, D. (1990) Biochem. Biophys. Res. Comm. **167**, 659-664.
24. Tsukahara, T., Ishiura, S., Kominami, E. & Sugati, H. (1990) Exp. Cell Res. **199**, 111-116.
25. Crawford, C., Mason, R.W., Wikstrom, P. & Shaw E. (1988) Biochem. J. **253**, 751-758.
26. Cramer, E.M., Beesley, J.E., Pulford, K.A.F., Breton-Gorius, J. & Mason, D.Y. (1989) Am. J. Pathol. **134**, 1275-1284.
27. Jensen, H.S. & Christensen, L.D. (1990) Clin. Exp. Rheumatol. **8**, 535-539.
28. Fujisawa, T., Kephart, G.M., Gray, B.H. & Gleich, G.J. (1990) Am. Rev. Respir. Dis. **141**, 689-697.
29. Powers, J.C. (1986) Adv. Inflamm. Res. **11**, 145-157.
30. Van Noorden, C.J.F., Smith, R.E. & Rasnick, D. (1987) J. Rheumatol. **15**, 1525-1535.
31. Baricos, W.H., O'Connor, S.E., Cortez, S.L., Wu, L.T. & Shah, S.V. (1988) Biochem. Biophys. Res. Commun. **155**, 1318-1323.
32. Shaw, E. (1990) Adv. Enzymol. & Related Areas Mol. Biol. **63**, 271-347.

Natur wissenschaften

Kurze Originalmitteilungen

Naturwissenschaften 75, 354–355 (1988) © Springer-Verlag 1988

Dihydrorhodamine 123: a New Flow Cytometric Indicator for Respiratory Burst Activity in Neutrophil Granulocytes

G. Rothe, A. Oser and G. Valet

Mildred-Scheel-Labor für Krebszellforschung, Max-Planck-Institut für Biochemie, D-8033 Martinsried

Granulocytes phagocytose microorganisms and degrade them inside the phagosome by the action of reactive oxygen metabolites, proteases and antibacterial proteins [1, 2]. The production of superoxide anion by a membrane-bound NADPH-oxidase is central for the intracellular oxidative attack of the ingested material. Failure of superoxide anion production during phagocytosis results in severe infection [3]. Extracellular release of superoxide anion and its dismutation product hydrogen peroxide by granulocytes following activation by immune complexes or complement may cause endothelial damage, e.g., in the adult respiratory distress syndrome [4] or in rheumatic diseases [5].

2′,7′-Dichlorofluorescin diacetate (DCFH-DA) has been used for the measurement of intracellular reactive oxygen metabolite production in single granulocytes by flow cytometry [6]. Nonfluorescent 2′,7′-dichlorofluorescin (DCFH) is cleaved from the membrane-permeable DCFH-DA by intracellular esterases and accumulates in vital cells. Stimulation of the respiratory burst by the tumor promotor phorbol 12-myristate 13-acetate (PMA) or phagocytosis of bacteria results in high cellular fluorescence intensities due to intracellular oxidation of DCFH to fluorescent 2′,7′-dichlorofluorescein (DCF). Less potent stimuli, such as the chemotactic peptide for-met-leu-phe (FMLP), however, generate only barely measurable DCF signals. Minor burst stimulation is, however, of great interest for the determination of the effect of physiological stimuli on granulocytes.

It was the goal of the present study to develop a more sensitive method for the flow-cytometric measurement of respiratory burst activity. Dihydrorhodamine 123 (DHR), an uncharged and nonfluorescent derivative of the laser dye rhodamine 123 (R123) was found to be a nontoxic and about threefold more sensitive indicator of granulocyte respiratory burst activity than DCFH-DA. DHR is oxidized intracellulary during the respiratory burst to brightly fluorescent R123.

DHR was synthesized according to [7] and dissolved in N,N-dimethylformamide (DMF) (Merck, Darmstadt, FRG) at 15 mg ml^{-1} (43.3 m*M*). Leukocytes were obtained as supernatant following sedimentation of 3 ml of heparinized (10 U ml^{-1}) venous blood for 40 min at 1 *g* on 3 ml of Ficoll (density *d* = 1.077, Eurobio, Paris, F). Fifty μl of supernatant plasma containing the leukocytes were incubated for 15 min at 37 °C with 5 μl of a suspension of *E. coli* K12 (Sigma, Deisenhofen, FRG). *E. coli* were obtained from stationary cultures in RPMI 1640, washed twice with 50 ml HEPES-buffered saline (0.15 *M* NaCl, 5 m*M* HEPES, Serva, Heidelberg, FRG, pH 7.35) (HBS) and resuspended in HBS at 7×10^9 bacteria per ml. Ten-μl aliquots of the phagocytosis assay were diluted with 1 ml HBS and incubated for a further 15 min at 37 °C with either 1 μl of a 43.3-m*M* DHR-stock solution or 20 μl of a 500-μ*M* working solution of DCFH-DA, obtained by diluting a 10-m*M* stock solution in DMF with HBS. Twenty μl of a 3-m*M* propidium iodide (PI) (Sigma) solution in HBS were added 3 min prior to the flow-cytometric measurement to counterstain the DNA of dead cells.

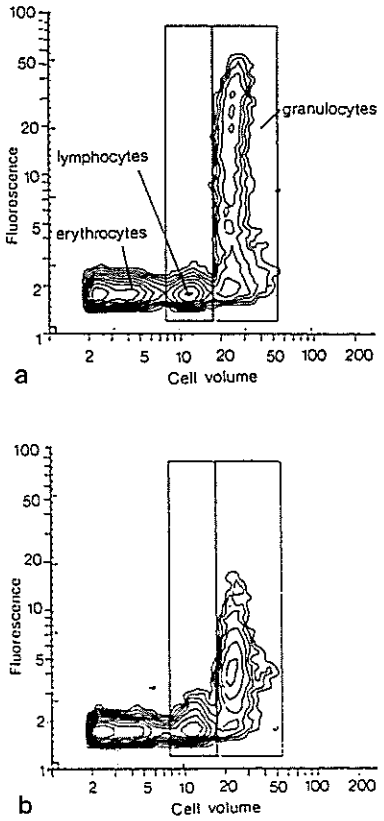

Fig. 1. Cell volume versus R123-fluorescence (a) or DCF-fluorescence (b) of leukocytes stimulated with 10^{-6}*M* N-formyl-met-leu-phe in the presence of 5 μg ml^{-1} cytochalasin B. DHR-stained granulocytes show significantly higher fluorescence (mode = 20 relative fluorescence units) than DCFH-DA-stained cells (four relative fluorescence units). The graphs are standardized to the maximum logarithmic channel contents (100 %). Contour lines were drawn in linear steps of 10 % downwards. The histograms contain 30039 (a) resp. 23690 (b) cells with 2312 and 1633 cells in the maximum channel

The electrical cell volume, the R123 green fluorescence (500 – 530 nm) and PI red fluorescence (590 – 700 nm) of each cell were simultaneously measured in a Fluvo-Metricell flow cytometer (HEKA-Elektronik, Lambrecht/Pfalz, FRG) [8]. The electrical cell volume was determined in a hydrodynamically focused cylindrical sizing orifice of 80 μm diameter and 80 μm length at an electrical current of 0.15 mA using HBS buffer as sheath fluid. Fluorescence was excited between 450 and 500 nm with an HBO-100 high-pressure mercury arc lamp (Osram, Augsburg, FRG). The list mode data were evaluated by the DIAGNOS1 program system for calculation, display and data basing of flow-cytometric data [9].

Granulocytes were strongly stimulated by the phagocytosis of bacteria and showed bright R123 green fluorescence. Their fluorescence was 20-fold higher than that of controls incubated in the absence of bacteria. Only an eightfold increase of fluorescence was observed with DCFH-DA. Lymphocytes, which do not exhibit respiratory burst activity, did not increase their green fluorescence upon stimulation. This showed both the specificity of DHR and the good cellular retention of R123, which was probably due to the intracellular accumulation of R123 at mitochondrial binding sites [10].

The effect of the weakly stimulating chemotactic peptide FMLP on DHR oxidation was studied in a second experiment. Ten μl of the suspension of leukocytes in plasma were diluted with 1 ml HBS supplemented with 1.3 m*M* Ca^{2+}. One μl of a 5-mg ml^{-1} solution of cytochalasin B (Sigma) in DMF was added to enhance the FMLP-induced responses in neutrophils [11]. The cells were stained for 15 min as described above and were incubated for a further 15 min at 37 °C following addition of 10 μl of 10^{-4} *M* FMLP (Sigma) in HBS, which had been prediluted from a 10-m*M* stock solution in dimethyl sulfoxide (Merck). Five μl of a 3-m*M* PI solution were added 3 min prior to the flow-cytometric measurement.

Granulocytes showed an 11-fold increase of R123 green fluorescence (Fig. 1a), when compared to a control without FMLP. This was higher than the threefold increase of DCF fluorescence in a DCFH-DA-stained sample (Fig. 1b). Furthermore, the wide heterogeneity of the FMLP-induced respiratory burst of granulocytes was only visible with the DHR stain.

The DHR method is significantly more sensitive for the flow-cytometric assay of respiratory activity in granulocytes than the DCFH-DA procedure. The described method is of value for the sensitive analysis of granulocyte function with physiological stimuli such as FMLP, activated complement, colony-stimulating factors, platelet-derived growth factor or interferons.

This work was supported by DFG SFB 0207, project G 6.

Received March 24, 1988

1. Weiss, J., et al.: Infec. Immun. *55,* 2142 (1987)
2. Elsbach, P., Weiss, J.: Immunol. Lett. *11,* 159 (1985)
3. Malech, H. L., Gallin, J. I.: N. Engl. J. Med. *317,* 687 (1987)
4. Weiland, J. E., et al.: Am. Rev. Respir. Dis. *133,* 218 (1986)
5. Shingu, M., Todoroki, T., Nobunaga, M.: Inflammation *11,* 143 (1987)
6. Bass, D. A., et al.: J. Immunol. *130,* 1910 (1983)
7. Kinsey, B. M., et al.: J. Med. Chem. *30,* 1757 (1987)
8. Kachel, V., et al.: J. Histochem. Cytochem. *25,* 804 (1977)
9. Valet, G., Warnecke, H. H., Kahle, H.: Clinical Cytometry and Histometry, p. 58 (eds. G. Burger, J. S. Ploem, K. Goerttler). London: Academic Press 1987
10. Johnson, L. V., et al.: J. Cell. Biol. *88,* 526 (1981)
11. Honeycutt, P. J., Niedel, J. E.: J. Biol. Chem. *261,* 15900 (1986)

The incubation of vital cells with DCH in a physiological medium (e. g. 0.15M NaCl, 10 mM TRIS/HCL pH 7.35, (TBS)) shows black dots on a blue fluorescent background under the microscope i. e. the dye is excluded by the cells. Esterification with acetate (Fig. 1a) (1,4-diacetoxy-2,3-dicyano-benzene, ADB, MW 244), butyrate, or an alanyl derivative yields substances which easily permeate the cell membrane (4). The ester molecules are cleaved in vital cells within a few minutes at room temperature by cytoplasmic esterases and the resulting DCH enriches in the cells. The principle of action is similar to the permeation and intracellular cleavage of fluorescein-diacetate by cytoplasmic esterases, followed by the accumulation of free fluorescein in vital cells (5).

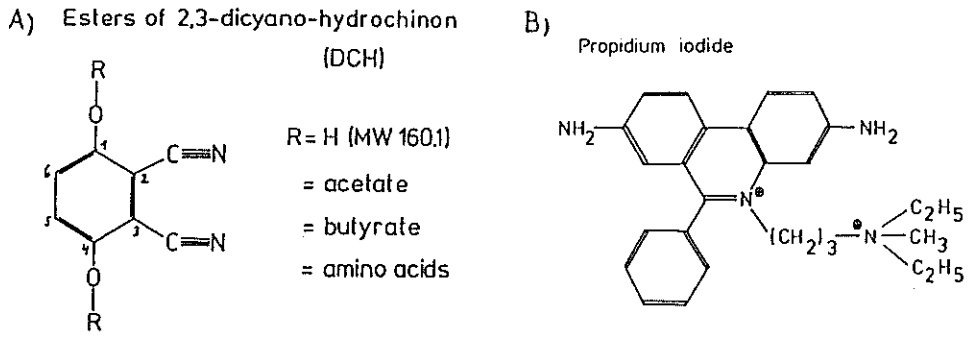

Fig. 1 DCH-Ester (A) and propidium iodide (B)

1.2 Fluorescence spectra

The DCH emission spectra extend from 400 to 550 nm (Fig. 2 a), and the excitation spectra from 300 to 450 nm (Fig. 2 b). The peak of DCH light emission shifts between pH 5 and pH 9 from 445 to 474 nm. ADB is similarly excited as DCH but emits only half of the fluorescence intensity. The peak of ADB light emission remains at 432 nm and is independent of the pH value of the solution. ADB is, therefore, in a strict sense not a fluorogenic substrate as e. g. fluorescein-diacetate which is non fluorescent as an ester. The influence of uncleaved ADB on the results of an intracellular pH-measurement with DCH is, however, small, first: because of the lower molar fluorescence of ADB and second: because of the lack of ADB enrichment in cells. DCH which is cleaved from ADB by intracellular esterases, in contrast, is strongly enriched in vital cells but does not or only weakly accumulate in dead cells.

The fluorescence excitation and emission spectra of propidium iodide (Fig. 1 b) are shown in Fig. 2 c. PI stains the DNA of dead cells but does not stain vital cells. ADB and PI are spectroscopically and chemically compatible dyes. It is, therefore, possible to determine simultaneously the intracellular pH and the esterase activity of vital cells, and the DNA distribution curve of dead cells in fresh cell preparations with a staining cocktail containing ADB and PI.

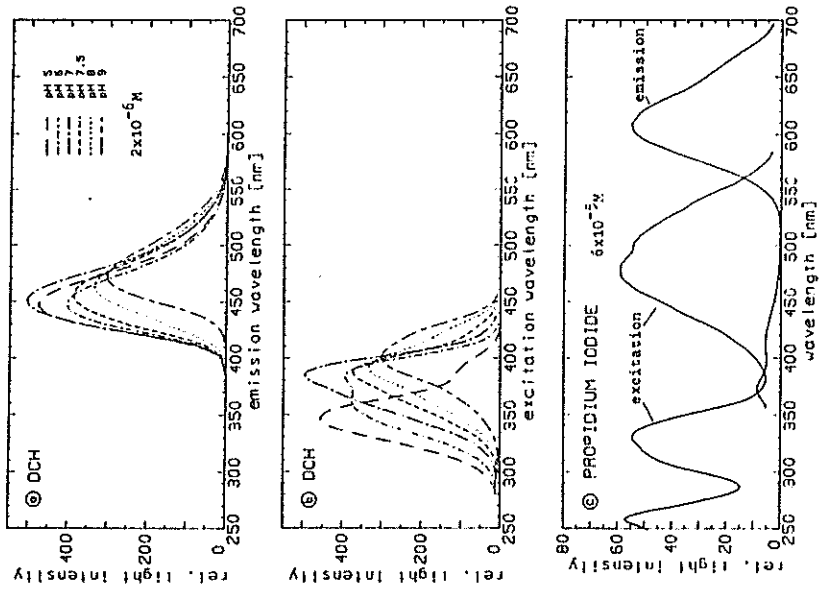

Fig. 2 Emission (a) and excitation (b) spectra of DCH in 0.15 M NaCl, 50 mM PO_4 buffer pH 5 to 9, and of propidium iodide (c) in TBS. The emission spectra were measured by setting the excitation monochromator of the fluorimeter (Perkin-Elmer-LS 5, Überlingen, FRG) to the peak wavelength of the excitation spectrum at each pH-value. The excitation spectra were obtained by setting the emission monochromator to the peak wavelength of the emission spectrum at each pH-value.

1.3 Fluorescence excitation

The fluorescence of DCH and propidium iodide can be excited between 300 and 400 nm with a HBO 100 mercury arc lamp (Fig. 3 a) or with the UV-lines of an argon or krypton laser (Fig. 3 b, 3 c).

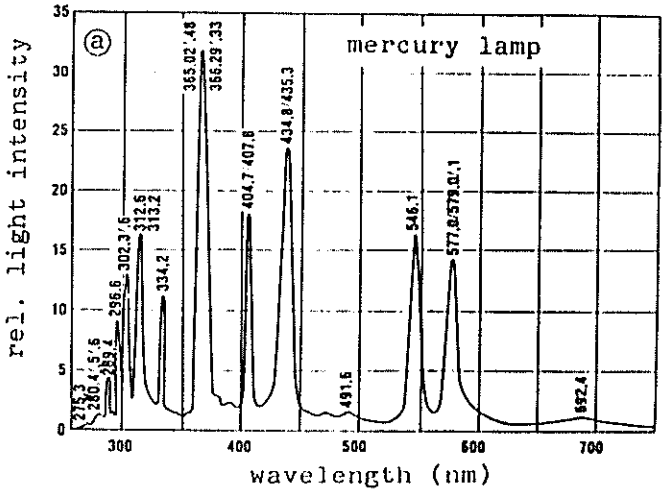

200 Determinations for in vitro Diagnostic use only

World-wide patents pending

Cytostatic Drug Testing Kit for Flow-Cytometry

PAESEL
GMBH & CO

Borsigallee 6
D-6000 Frankfurt/M. 63
FRG
Tel.: 069/422097-98
Tx.: 413202 paesl d

CYTOSTATIC DRUG TESTING ON PATIENT TUMOR CELLS

Explanation of the method and description of the test procedure

1. Determination of intracellular pH and esterase activity in vital cells by flow-cytometry

G. Valet, A. Raffael
Max-Planck-Institut für Biochemie, D-8033 Martinsried

1.1 DCH and ADB dyes

2,3-dicyanohydrochinon (DCH, MW 160) is a fluorescent pH indicator dye (1). The dye changes the colour of fluorescence from blue to green in the pH range 5.0 to 9.0. DCH is particularly useful for flow cytometric studies because first: only one light source is needed for fluorescence excitation, and second: because the intracellular pH determination depends on a fluorescence ratio and not on a fluorescence intensity as with fluorescein (2) or umbelliferone (3) dyes. Intensity changes in living cells are sometimes difficult to interpret. This becomes clear if one considers that fluorescent pH-indicators are brought as esterase substrates into the cell. The intensity of the stain is, therefore, primarily a measure of esterase activity. Intensity changes can only be interpreted as pH changes when changes of esterase activity, cell membrane permeability or cell volume are excluded. The advantage of a fluorescence ratio measurement is that the result is independent of the fluorescence intensity within the range of measurable fluorescences.

The assay can also be measured as a sequence of two parameter histograms (see data evaluation), in case the flow-cytometer or sorter measures only the small angle light scatter and one fluorescence.

1.6 Light-pass in the flow-cytometer

Fig. 4 b indicates the filters and dichroic mirrors (all Zeiss, Oberkochem, FRG) of the FLUVO-METRICELL flow cytometer (6–8) (Fig. 4 a) which was used for the development of this assay. Also indicated is the possibility to use UV-light from an argon or krypton laser for fluorescence excitation (Fig. 4 c).

ADB and PI are both excited between 300 and 400 nm. The blue fluorescence of DCH is collected between 418 and 440 nm (F 1) and the green fluorescence of DCH between 500 and 700 nm (F 2). The red fluorescence of PI is also collected between 500 and 700 nm.

1.7 Signal processing

The maximum amplitude of the volume and the two fluorescence signals of each cell are amplified by 2.5 or 3 decade logarithmic amplifiers. The digitized pulses are collected in LIST-MODE on magnetic tape or disc, or classified ON-LINE in the 64 x 64 x 64 or 32 x 32 x 32 matrix in the memory of a computer and stored permanently on tape or disc at the end of the measurement.

Two parameter histograms are measured, in case no facility for three parameter measurements is available. They are stored in a multichannel analyzer for later analysis with a computer, or they are collected ON-LINE in the memory of a computer and stored on tape or disc as above.

A new and comparatively cheap possibility of measuring and analyzing two parameter histograms without need for a computer is given by the CYTOMIC microprocessor data systems (7, 8) (HEKA, D-6701 Forst/Weinstrasse, FRG).

1.8 Data evaluation

The three parameter matrix is graphically displayed as a cube (Fig. 5 a, optional) for three parameter measurements. This is useful for a quick qualitative visual evaluation. The quantitative calculations is started by projecting the data of the cube onto the esterase/DNA (blue versus yellow fluorescence) plane (Fig. 5 b). The dead (I) and vital (II) cell are distinguishable. The area (II) is used as a gating area to display the cell volume versus esterase activity histogram of the vital cells (Fig. 5 c). The absolute concentration of the cells in the various clusters of Fig. 5 c can be calculated since the one logarithmic volume class corresponds to 13 μm^3. The fluorescence scales are in relative units. The amplitude comprises 3 logarithmic

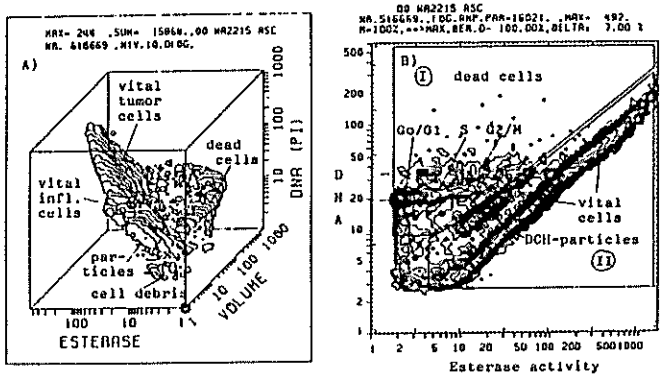

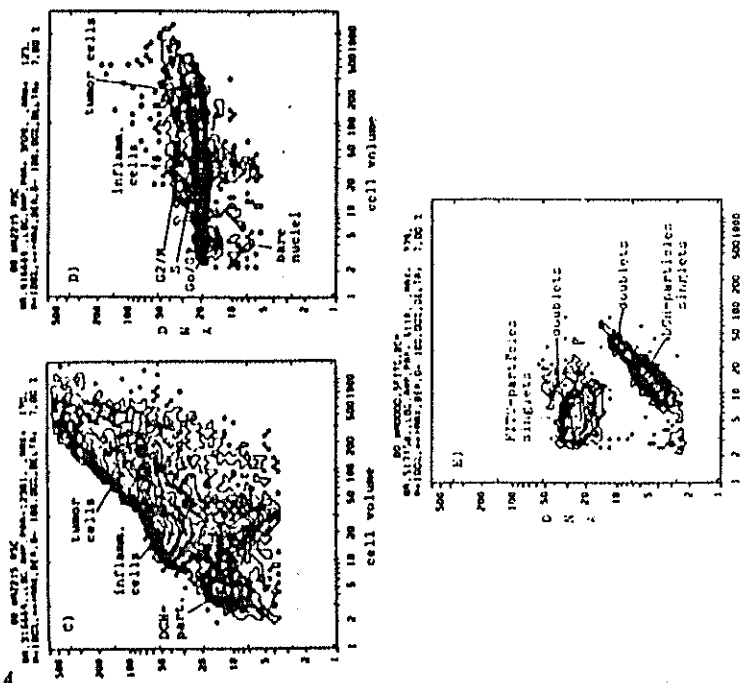

Fig. 5 Three parameter cube display (A) of an ADB/PI stained ascites of an ovarian cancer. The area (II) of the esterase/DNA histogram (B) is used as gating area for the display of the cell volume/esterase histogram of the vital cells (C), and area (I) to gate the cell volume/DNA histogram of the dead cells (D). The position of the clusters of a mixture of FITC or DCH stained calibration particles (E) in the esterase/DNA histogram frame indicates that DCH particles fall within the area of vital cells and FITC particles in the area of dead cells (compare with B).

decades. The logarithm of all channel contents is calculated and the maximum content is set as 100 %. Contour lines are drawn in steps of 7 % downward. The lowest contour line contours channels with a content of one cell.

Concentration of the particles in the assay is known (2 x 10^5/ml). The volume versus DNA histogram of the dead cells (Fig. 5 d) is obtained by using the gating window (I) of Fig. 5 b for the calculation. Fig. 5 e shows the localisation of the FITC-particles and DCH-calibration particles in the esterase/DNA histogram.

The following evaluations of the three parameter cube matrix are used to extract a maximum of information on the vital and dead cells of each measurement. The distribution of the esterase concentration (Fig. 6 a) is calculated by dividing the esterase activity (Fig. 5 c) of each histogram channel by the cell volume of each channel. The intracellular pH distribution (Fig. 6 b) is calculated from the ratio of blue to green fluorescence (F 1/F 2) of each vital cell according to the calibration curve of Fig. 7. The DNA distribution curve of the dead cells (Fig. 6 c) is calculated as projection of Fig. 5 d onto the DNA-axis. Similarly the cell volume distribution curves of vital and dead cells (Fig. 6 d, 6 e) are obtained by projection of Fig. 5 c and Fig. 5 d onto cell volume axis.

If the instrument does not collect three parameter data, one can first measure the cell volume versus esterase activity of vital cells of a sample stained with ADB alone (similar to Fig. 5 c) and in a second measurement determine the blue (F 1) versus green (F 2) fluorescence of the same sample in order to calculate the F 1/F 2 ratios of the cells. The F 1/F 2 ratio is a measure of the intracellular pH (Fig. 7). The cell volume versus DNA histogram (similar to Fig. 5 d) of the dead cells can be determined in an aliquot of the sample by staining the cells with PI alone.

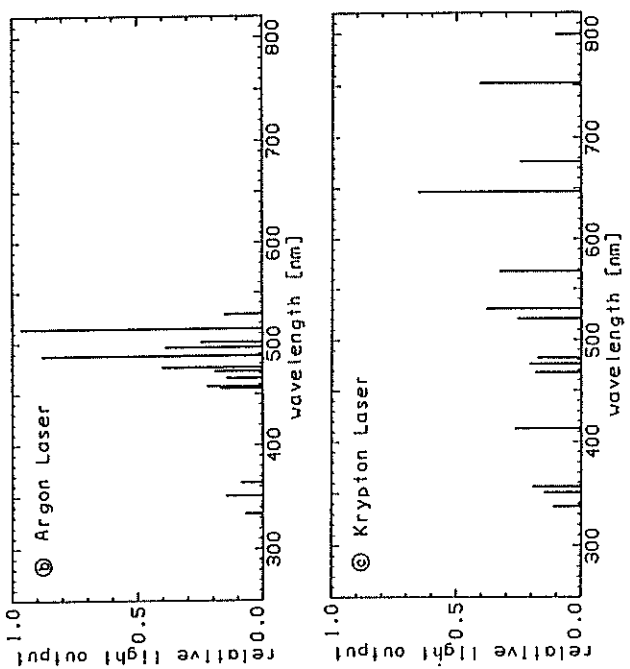

Fig. 3 Light emission spectra of a HBO-100 mercury arc lamp (a) (adapted from Leitz, Wetzlar, FRG), an argon (b) and a krypton (c) laser (adapted from Spectra-Physics, Darmstadt, FRG).

1.4 ADB assay with cells

1.4.1 Material provided

1 ml staining cocktail containing 1 mg/ml ADB and 2 mg/ml PI,
1 ml standard particle suspension, 1 x 10^7 particles/ml (60 μm^3, 4.88 μm diameter).

1.4.2 Assay procedure

250 μl cell suspension (1 x 10^4 to 1 x 10^7/ml) are incubated with 5 μl of a staining cocktail containing 1 mg/ml ADB and 2 mg/ml PI. The solvent of the cocktail is dimethyl-formamide (DMF). 5 μl of monodisperse, 2,3-dicyanohydrochinon (DCH) stained latex particles (1 x 10^7/ml, 60 μm^3, 4.88 μm diameter) as internal standard for cell concentration, cell volume and cell fluorescence are also added. The advantage of DCH-particles is that the extracellular pH of the solution can be monitored together with the intracellular pH in the same measurement.

If two parameter measurements are performed, the cells are either stained with ADB (cell volume versus esterase), with PI (cell volume versus DNA) or with ADB/PI cocktail (esterase versus DNA). DCH particles are added for standardization. The staining time for all assays is 5 min at room temperature.

1.5 Flow-cytometric measurement

The assay is typically measured in a flow cytometer which determines simultaneously the cell volume by an electrical measurement and two cellular fluorescences (Fig. 4 a). The cell volume as measured in an orifice with a diameter between 60 and 100 μm and a 1 : 1 diameter to length ratio. The orifice current is set between 0.2 and 0.5 mA. The fluorescence is excited with a HBO-100 high pressure mercury arc lamp. It is also possible to use flow cytometers or sorters with lasers, provided the laser has UV-capability in the 300 to 400 nm range. The small angle forward light scatter is measured in this case instead of the electrical cell volume.

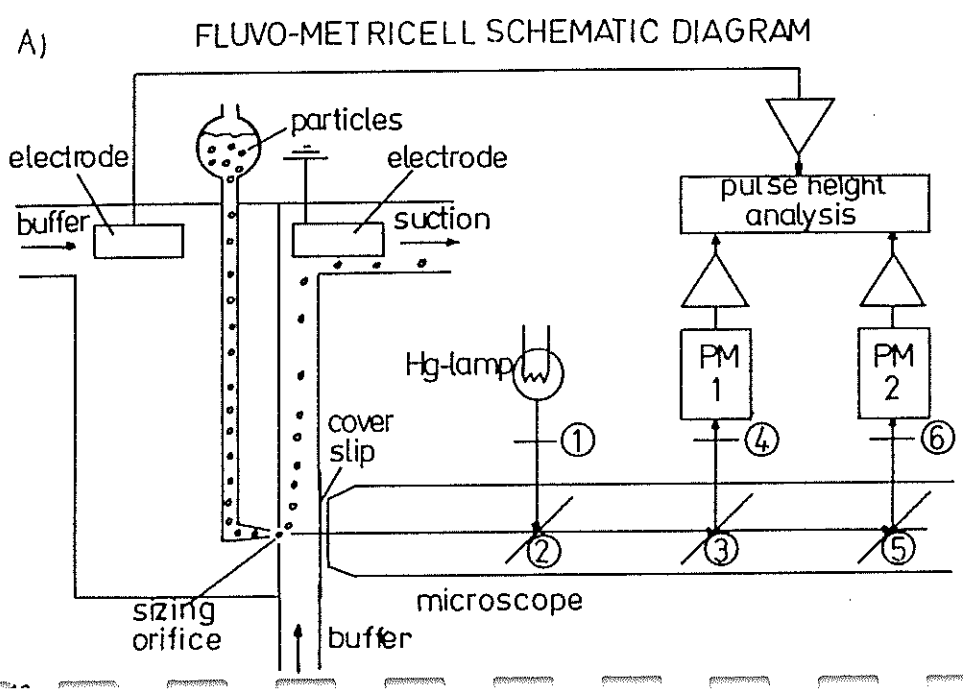

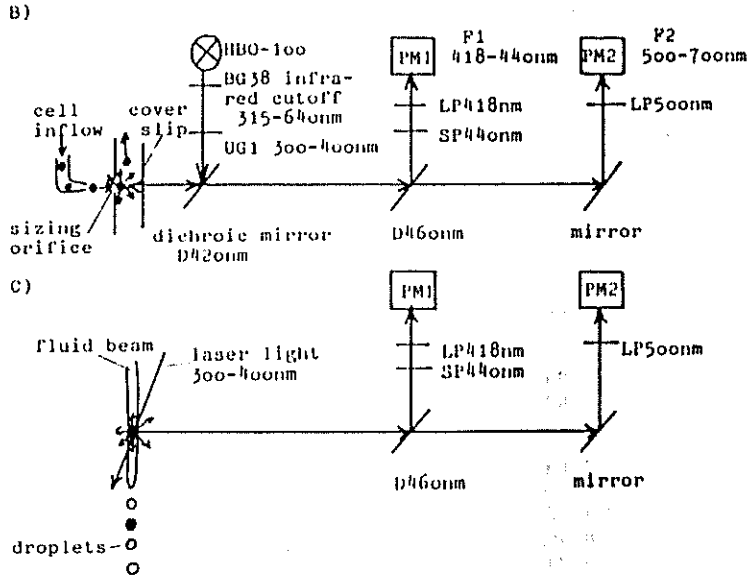

Fig. 4 Schematic diagram of the FLUVO-METRICELL flow cytometer (6) (A) with filters (B), and filter settings for laser excitation (C). PM = photomultiplier, LP = long pass filter, SP = short pass filter, F 1 = blue fluorescence light channel (PM 1), F 2 = green / red fluorescence light channel (PM 2), ① to ⑥ are filters and dichroic mirrors explained in (B) and (C).

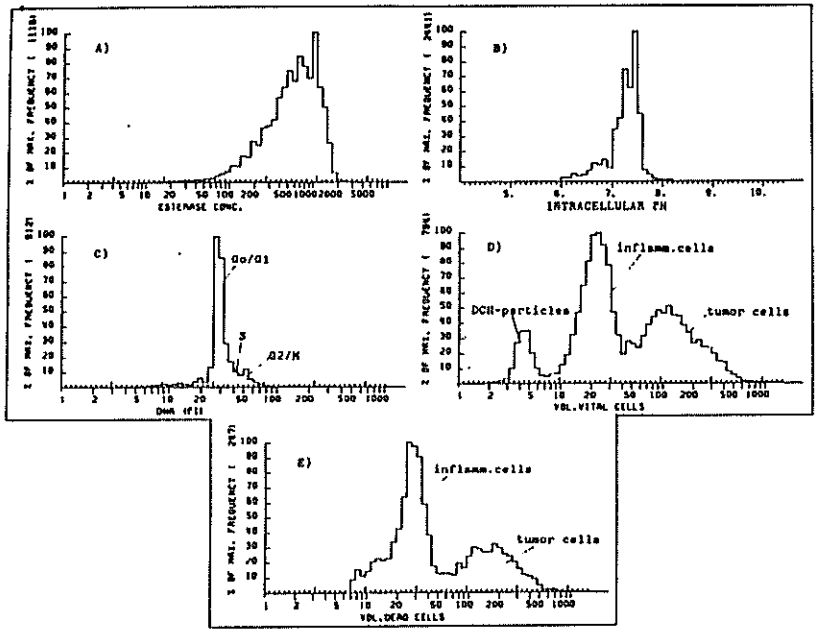

Fig. 6 One parameter distributions calculated from the simultaneous three parameter measurement of Fig. 5 a.

1.9 Calibration of pH-measurement

The calibration of the intracellular pH-measurement is made in two steps:

1.9.1 Instrument calibration

The first step concerns the calibration of the spectral response of the flow cytometer. A 0.15 M NaCl solution is buffered with 50 mM PO_4 and individual buffer samples are prepared with pH-values between pH 5.0 and 9.0 in steps of 0.5 pH units. 250 μl of each buffer are mixed with 5 μl of a DCH solution 1 mg/ml in DMF and introduced into the instrument similarly as a cell sample. Two digital voltmeters are clamped to the analog output of the two photomultiplier tubes of the flow-cytometer. The voltage readings of the photomultipliers prior to the sample input are taken as blank values. Once the fluorescence of the DCH containing sample beam is visible, the readings of the voltmeter increase. The voltage of the blue fluorescence photomultiplier (F 1) and of the green (F 2) fluorescence photomultiplier are measured three times for each buffer. The blank values are subtracted from the readings and the F 1/F 2 ratio of each measurement is calculated. The F 1/F 2 ratios determined experimentally for all 9 buffers in flow-cytometer are then plotted versus the pH of the buffers (Fig. 7). The graph is different for different flow cytometers because other photomultipliers and minor changes in the specification of optical filters and dichroic mirrors influence the result. Once established, the F 1/F 2 versus pH plot represents the permanent calibration curve of the particular flow-cytometer. The calibration curve, according to our experience, is very stable. Spontaneous and repeated measurements with our FLUVO-METRICELL flow cytometer during a period of 3 years yielded virtually superimposable curves, provided no changes of amplifier gain, photomultipliers and filters were made.

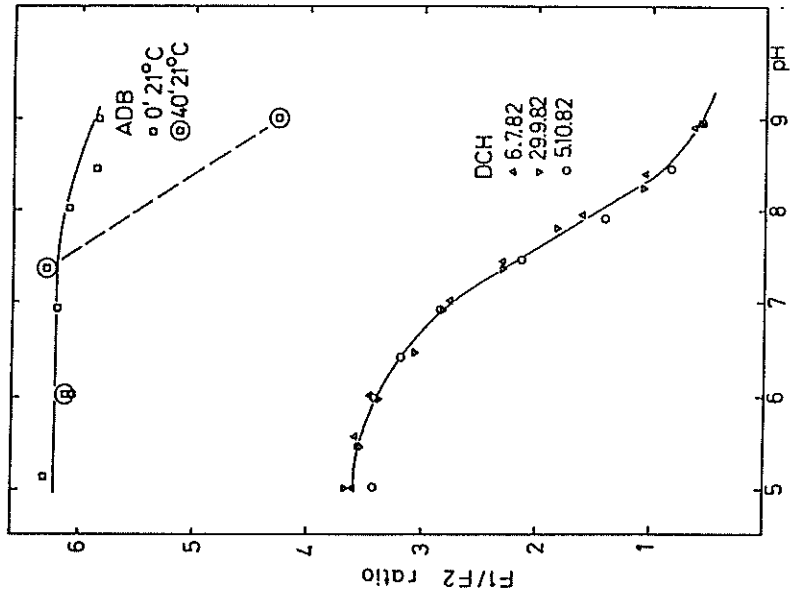

Fig. 7 Blue (F 1) to green (F 2) fluorescence ratio of a DCH and ADB solution measured in a FLUVO-METRICELL (6) flow cytometer. The DCH curve is S-shaped and pH-dependent while the F 1/F 2 ratio of ADB ratio is essentially pH-independent. Prolonged incubation at pH 9.0 leads to partial ADB hydrolysis which decreases the F 1/F 2 ratio.

1.9.2 Cellular calibration

The second step of the calibration procedure consists of the extension of the instrument calibration curve of Fig. 7 to a cellular level. The sequence of the cellular pH-calibration is first: to load the cells with DCH, and second: to expose them to buffers of various pH values in the presence of the H^+-ionophor gramicidin-D and of Na-azide. The H^+-ionophor clamps the intracellular pH to the extracellular pH and the Na-azide inhibits cellular counter regulations by poisoning the cellular energy metabolism.

Assay procedure

250 μl cells (1 x 10^7/ml) are incubated with 5μl ADB 1 mg/ml in DMF for 5 min at room temperature to load the cells with DCH. 10 μ aliquots of the DCH-stained cells are then mixed into 250 μl of buffers of various pH. 5 μl gramicidin-D (2 mg/ml in TBS) solution and 5 μl of a 1 M Na-azide solution are added to each pH-assay. After 20 min incubation at room temperature the blue to green fluorescence histogram of the cells (F 1/F 2) is measured, and the mean F 1/F 2 ratios of all cells is calculated.

Results

The results of a cellular calibration experiment are shown in Fig. 8. It is visible that incubation of the cells with gramicidin-D alone leads between pH 6.5 and 7.5 to a similar calibration curve as the DCH-calibration curve of the flow-cytometer. The curve deviates, however, below and above these pH values. Poisoning of the energy metabolism with Na-azide adapts the lower part of the curve better to the DCH-calibration curve of the flow-cytometer.

The upper part of the curve between pH 7.5 and pH 8.5 remains higher than the DCH-curve. Whether the intracellular pH in this range does not adapt to alkaline

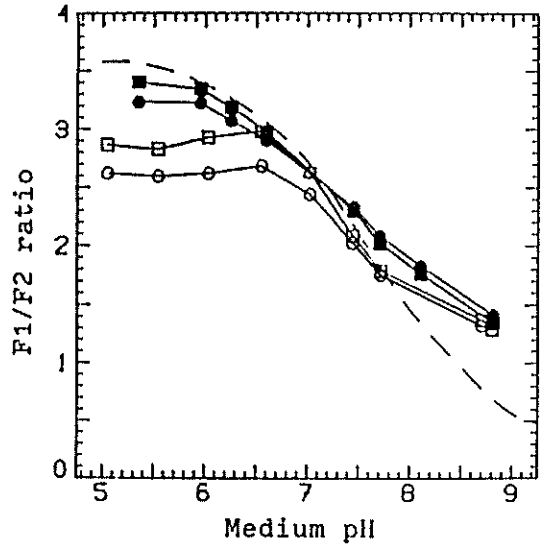

Fig. 8 Intracellular pH calibration of guinea pig macrophages (□, ■) and granulocytes (O, ●) of the peritoneal cavity. The cells were incubated with the H^+-ionophor gramicidin-D (40 µg/ml (□, O) and with gramicidin-D plus Na-azide (20 mM) (■, ●). A cellular calibration curve is obtained in the pH-range 5.5 to 7.5 with gramicidin-D and Na-azide which closely resembles to the dashed DCH curve measured in solution in the flow-cytometer (Fig. 7).

conditions, or whether a particular behaviour of DCH in the cell in this pH range occurs, is not clear. In practice, it is recommended to use the DCH-calibration curve of the flow-cytometer for the calculation of the intracellular pH. This is easier than establishing each time a cellular calibration curve. The approach is reasonable because the DCH-calibration curve of the flow-cytometer and cellular pH-calibration curve coincide well in the pH range 5.5 to 7.5 which is the most important for physiological regulations. Above pH 7.5 the trend of intracellular changes is still correctly indicated but the absolute pH-values calculated from the DCH-calibration curve of the instrument may be slightly lower than the true intracellular pH-values.

Literatures references

1. Weast R. C. (ed.): CRC Handbook of Chemistry and Physics, (1978/79), 59th edition, CRC press, West Palm Beach, p. D-170.

2. Visser J. W. M., Jongeling A. A. M., Tanke H. J., (1979) Intracellular pH-determination by fluorescence measurements. J. Histochem. Cytochem 27, 32-35.

3. Gerson D. F. (1982) Determination of intracellular pH changes in lymphocytes with 4-methylumbelliferone by flow cytometry. In: Nuccitelli R., Deamer D. W. (eds): Intracellular pH: Its measurement, regulation and utilization in cellular functions, Alan R. Liss, Inc., New York, p. 125-133.

4. Valet G., Raffael A., Moroder L., Wünsch E., Ruhenstroth-Bauer G. (1981) Fast intracellular pH-determination in single cells by flow-cytometry. Naturwiss. 68, 265-266.

5. Rotman B., Papermaster B. W. (1966) Membrane properties of living cells as studied by enzymatic hydrolysis of fluorogenic esters. Proc. Natl. Acad. Sci. USA 55, 134-141.

6. Kachel V., Glossner E., Kordwig E., Ruhenstroth-Bauer G. (1977) FLUVO-METRICELL, a combined cell volume and cell fluorescence analyzer J. Histochem. Cytochem. 25, 804-812.

7 Kachel V., Schneider H., Bauer J., Malin-Berdel J. (1983).
Application of the CYTOMIC 12 flow cytometric compact analyzer for automatic kinetic measurements Cytometry 3, 244-250.

8. Kachel V., Schedler K., Schneider H., Haack L. (1984) CYTOMIC data system module, modern electronic devices for flow cytometric data handling and presentation. Cytometry, in press.